European Commission

JRC TECHNICAL REPORTS

In-Vessel Melt Retention (IVMR) Analysis of a VVER-1000 NPP

SANGIORGI Marco, GRAH Aleksander, PASCAL Ghislain (JRC), ZDAREK Jiri, DUSPIVA Jiri, BATEK David, VYSKOCIL Ladislav (UJV Rez, a.s), MELNIKOV Ivan, MERKULOV Valery (NRC KI), FICHOT Florian (IRSN), MATEJOVIC Peter (IVS Trnava Ltd), GRUDEV Pavlin (INRNE-BAS), EZZIDI Alexandre (AREVA), BAJARD Sophie (CEA), BAKOUTA Nikolai, JAMET Mathieu, LE GUENNIC Clémentine (EDF), BUCK Michael (IKE, Stuttgart University), RASHKOV Krasen (Kozloduy NPP), IVANOV Ivan, KALEYCHEV Petar (Sofia Technical University), NIEMINEN Anna (VTT)

2016

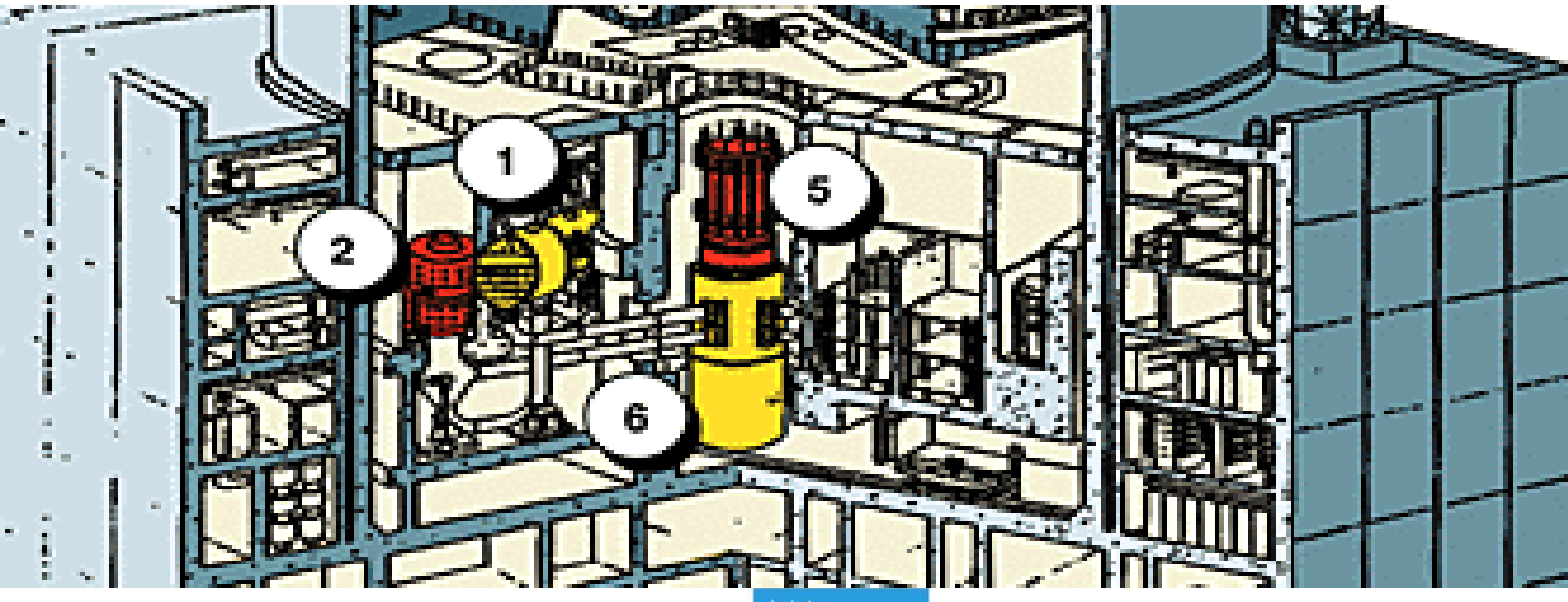

Joint Research Centre

EUR 27951 EN

In-Vessel Melt Retention (IVMR) Analysis of a VVER-1000 NPP

JRC Science Hub
https://ec.europa.eu/jrc

JRC101823

EUR 27951 EN

ISBN 978-92-79-58899-0 (PDF)
ISBN 978-92-79-58898-3 (print)

ISSN 1831-9424 (online)
ISSN 1018-5593 (print)

doi:10.2790/62596 (online)
doi:10.2790/438713 (print)

How to cite: Authors; In-Vessel Melt Retention (IVMR) Analysis of a VVER-1000 NPP; EUR 27951 EN; doi 10.2790/ 62596

Table of Contents

Executive Summary

As part of the outcome of the EU “Stress Tests” in 2012, several areas for further research in the field of Severe Accident Management have been identified for different types of NPPs. One of these areas concerns the feasibility of In Vessel Melt Retention (IVMR) for VVER 1000 reactors. Ensuring that the corium could stay in the RPV (like it happened during the TMI-2 accident) during a Severe Accident would reduce significantly the loads on the last barrier (the containment) and therefore reduce the risk of release of Fission Products to the environment for most of the Severe Accident Scenarios. This type of Severe Accident Management strategy has already been incorporated in the SAMGs of several operating small size Light Water Reactors (reactor below 500 MWe (like VVER440)) and is part of the SAMG strategies for some Gen III+ PWRs like the AP1000.

Starting from 2012, several research institutes and utilities in Europe (and also in the Russian Federation) started some work on this topic. The preliminary results of these first investigations highlighted that large uncertainties (especially in the area of modelling activities) were existing regarding IVMR for VVER1000. This highlighted the need to start an activity supporting the assessment of these uncertainties and one way envisaged was to set up an international benchmark on computer code calculations for “In Vessel Retention for VVER 1000”.

JRC-IET was asked by UJV Rez a.s to organize this international benchmark on computer code calculations for “In Vessel Retention for VVER 1000” with the target of providing preliminary results on the feasibility of this mitigation strategy in case of severe accident for such kind of plants.

This benchmark attracted right from the beginning the interest of many EU partners (UJV Rez - Czech Republic, INRNE-Bulgaria, IVS-Slovakia, CEA-France, IRSN-France, EdF-France) and non EU (Kurchatov Institute –Russian Federation, IPP-Ukraine) partners. Kurchatov Institute provided freely to all partners the necessary data (ASTEC dataset, Severe Accident initial conditions, etc…) to start their own calculations, and to benchmark them with the one already performed at KI.

In the meantime the interested for this topic has continued to grow and several other EU institutions joined this benchmark (VTT-Finland, University of Stuttgart- Germany, Areva – France) especially because the subject of IVMR is also applicable for other types of NPPs, expanding the work as initially planned. A larger project on the topic was prepared in 2014 and proposed to the H2020 call NFRP-01-2014: "Improved safety design and operation of fission reactors”, in order to expand the level of knowledge reached so far.

The report is broken down into seven main Chapters and three appendixes.

- Chapter 1 provides background information for this activity and expected results defined by the participants;
- Chapter 2 provides a general description of In-Vessel Melt Retention (IVMR) principle;
- Chapter 3 provides a short description of the VVER-1000 and VVER-440 design, focussing especially on those details regarding IVMR. It includes general pictures and a detailed picture of the VVER-1000 Lower Head (metallic structure, core barrel, etc…);
- Chapter 4 describes the existing calculations carried out mainly by KI that constituted a starting point of this benchmark, including useful references;
- Chapter 5 is the core of this report, explaining how the calculations were carried out, analyzing and comparing the results. Two kinds of codes were used: CFD (CFX, NEPTUNE CFD, RELAP-3D) and mechanistic / lumped parameters codes (ASTEC, SOCRAT, MAAP, PROCOR, MELCOR);
- Chapter 6 presents existing approaches of IVMR for AP1000 and other NPPs to demonstrate its applicability and summarizes past experiments on the topic;

- Chapter 7 summarizes the findings identified in the benchmark and discusses the remaining open issues;
- Appendix A collects the individual calculation reports by every participant;
- Appendix B describes the first round of calculations;
- Appendix C describes the main models used by every code that lead to the major differences in the results.

The main findings of this benchmark are:

- There are no experimental data available regarding critical heat fluxes for semi-elliptical RPV geometry (like the one of VVER-1000) implying full height scale;
- There are still uncertainties regarding the behaviour of the corium in the lower head until it reaches a more stable state; unfortunately most of the models implemented in all mechanistic codes predicts the bigger heat flux precisely during this initial transient, therefore future experiments should focus on this;
- The way the accident evolves will lead to different degrees of corium oxidation and material relocation and that has a big impact on the heat flux in the lower head;
- A detailed analysis of core degradation and early core meltdown phases is desirable and even necessary for further refinement of the initial conditions for modelling transient phase of IVMR;
- A statistic approach seems to be a good tool to evaluate the probability that the heat flux will exceed a certain value in a certain point of the lower head. Anyway probability calculation requires the estimation of statistical weights w_i for each results that are unknown. The default values w_i =1 require justification since the codes and approaches may be quite different;
- CFD calculations are very time demanding, but seems to be valuable tools for addressing the heat transfer once the corium is stabilized; even though the CFD computations have been performed independently from calculations performed with SA computer codes and are based on different assumptions and techniques, the results displayed considerable similarities, but need further validation;
- CFD calculations are also promising to assess external vessel coolability margins with the use of CHF correlation in post-treatment of the CFD results. If sufficiently validated, these tools would provide assessment of the whole vessel (3D calculations), and hopefully capture some phenomena that cannot be observed in large scale experiments where axisymmetric hypothesis is assumed;
- Future small and large scale experiments fully representing a shape of semi-elliptical lower heads and cylindrical RPV segment will assess the feasibility of IVMR strategy, helping Utilities and Regulatory Bodies in deciding its implementation in existing power plants.

In conclusion this benchmark is an adequate basis for a preliminary assessment of the IVMR strategy and opens a path for future research programmes and experiments which should confirm the applicability of this strategy for large LWRs.

List of Contributors

Lead Author

SANGIORGI Marco	EC-JRC (Netherlands)	marco.sangiorgi@ec.europa.eu

Contributors of the Participating Countries/Organizations:

EZZIDI Alexandre	AREVA	alexandre.ezzidi@areva.com
BAJARD Sophie	CEA	sophie.bajard@cea.fr
BAKOUTA Nikolai	EDF	nikolai.bakouta@edf.fr
JAMET Mathieu	EDF	mathieu.jamet@edf.fr
LE GUENNIC Clémentine	EDF	clementine.le-guennic@edf.fr
BUCK Michael	IKE, Stuttgart University	michael.buck@ike.uni-stuttgart.de
GRUDEV Pavlin	INRNE-BAS	pavlinpg@inrne.bas.bg
FICHOT Florian	IRSN	florian.fichot@irsn.fr
MATEJOVIC Peter	IVS Trnava Ltd.	ivstt@ivstt.sk
GRAH Aleksander	EC-JRC (Netherlands)	Aleksander.GRAH@ec.europa.eu
RASHKOV Krasen	Kozloduy NPP	kprashkov@yahoo.com
MELNIKOV Ivan	NRC KI	corpuskula@gmail.com
MERKULOV Valery	NRC KI	Merkulov_VV@nrcki.ru
IVANOV Ivan	Sofia Technical University	ivec@tu-sofia.bgJ
KALEYCHEV Petar	Sofia Technical University	kaleychev@tu-sofia.bg
BATEK David	UJV Rez a.s.	bae@ujv.cz
VYSKOCIL Ladislav	UJV Rez a.s.	Ladislav.Vyskocil@ujv.cz
ZDAREK Jiri	UJV Rez a.s.	zda@ujv.czJRC
DUSPIVA Jiri	UJV Rez, a.s.	jiri.duspiva@ujv.cz
NIEMINEN Anna	VTT	Anna.Nieminen@vtt.fi

Reviewers

PASCAL Ghislain	EC-JRC (Netherlands)	ghislain.pascal@ec.europa.eu

Secretariat

EUPOPEAN COMMISSION - DG JRC
Institute for Energy & Transport
Nuclear Reactor Safety Assessment Unit
Westerduinweg 3 - P.O. Box 2
1755 ZG Petten - The Netherlands
Tel: +31 (0)224 56 5164
Fax: +31 (0)224 56 5637
E-mail: jrc-iet-nrsa-secretariat@ec.europa.eu

Acronyms

BE	Best Estimates
BWR	Boling Water Reactor
CHF	Critical Heat Flux
EC	European Commission
ERVC	External Reactor Vessel Cooling
EU	European Union
HF	Heat Flux
IVMR	In-Vessel Melt Retention
KI	Kurchatov Institute
LBLOCA	Large Break LOCA
LH	Lower Head (of the RPV)
LOCA	Loss of Coolant Accident
NPP	Nuclear Power Plant
OECD	Organisation for Economic Co-operation and Development
PWR	Pressurized Water Reactor
RPV	Reactor Pressure Vessel
RPV	Reactor Pressure Vessel
SS	Stainless Steel
VVER	Russian Pressurized Water Reactors

1 Introduction

As part of the outcome of the EU "Stress Tests" in 2012, several areas for further research in the field of Severe Accident Management have been identified for different types of NPPs. One of these areas concerns the feasibility of In Vessel Retention (IVMR) for VVER reactors. This type of strategy was already applied or under implementation for VVER 440 at the time of the EU "Stress Tests". Applicability of this strategy to larger NNPs like VVER 1000 started to be investigated just as a result of the EU "Stress Tests". Starting from 2012, several research institutes and utilities in Europe (and also in the Russian Federation) started some work on this topic. The preliminary results of these first investigations highlighted that large uncertainties (especially in the area of modelling activities) were existing regarding IVMR for VVER1000. This highlighted the need to start an activity supporting reduction of these uncertainties and one way envisaged was to set up an international benchmark on computer code calculations for "In Vessel Retention for VVER 1000".

During summer 2013, JRC-IET was asked by UJV Rez (Czech Republic) to organize and to participate in this international benchmark on computer code calculations for "In Vessel Retention for VVER 1000" with the target of providing results before the end of 2014. Following internal discussions within JRC-IET and after having obtained the agreements from JRC hierarchy the benchmark was launched by JRC-IET in September 2013.

The target of this benchmark was to perform analyses of IVMR for VVER1000 with different computer codes (MELCOR, SOCRAT, ASTEC, etc…) and to compare the results. The work to be performed by each partner in the frame of this benchmark is purely based on "in Kind" contributions. To support this benchmark, JRC-IET organized 3 Workshops in its premises in Petten (NL) allowing participants to exchange information and compare results.

The workshops took place during the following dates:

- WS1 28th – 29th November 2013,
- WS2 6th-7th May 2014,
- WS3-Final Meeting the 21-22 October 2014.

On top of workshop organization, JRC-IET also contributed "in kind" by performing severe accident analyses with the ASTEC V2.0 and by distributing necessary data to the partners and by compiling the different partners' contributions to issue a benchmark summary report.

This benchmark attracted right from the beginning the interest of many EU (UJV Rez - Czech Republic, INRNE-Bulgaria, IVS-Slovakia, CEA-France, IRSN-France, EdF-France) and non EU (Kurchatov Institute – Russian Federation, IPP-Ukraine) partners.

During the 1st Workshop it was identified that participants from the Kurchatov Institute (KI) were the more advanced in this topic and KI participants agreed to provide freely to the other partners all the necessary data (ASTEC dataset, Severe Accident initial conditions, etc…) allowing them to start their own calculations for VVER1000 IVMR scenarios and to benchmark their calculations with the one already performed at KI.

In the meantime the interested for this topic has continued to grow and several other EU institutions have also expressed their interest in joining this benchmark (VTT-Finland, University of Stuttgart-Germany, Areva – France) especially because the subject of IVMR is also applicable for other types of NPPs.

A larger project on the topic was prepared in 2014 and proposed to the H2020 call NFRP-01-2014: "Improved safety design and operation of fission reactors" , in order to expand the level of knowledge reached so far.

At the end of the project, the total number of EU and non EU partners who participated to this benchmark was 13.

- UJV Rez (CEZ Republic)
- IRSN (France)
- CEA (France)
- EdF (France)
- Areva (France)
- KI Moscow (The Russian Federation)
- INRNE (Bulgaria)
- TUS (Bulgaria)
- Kozloduy NPP (Bulgaria)
- IPP (Ukraine)
- IVS (Slovakia)
- USTUTT (Germany)
- VTT (Finland)
- JRC-IET (EC)

Some references

ENSREG, “Stress tests performed on European nuclear power plants”, 2012

2 In-Vessel Melt Retention (IVMR)

The in-vessel coolability and retention is based on the idea of flooding the PWR vessel cavity or the BWR drywell with water to either submerge the vessel completely or at least submerge the lower head. The PWR or BWR lower head containing the melt pool is cooled from outside, which keeps the outer surface of the vessel wall cool enough to prevent vessel failure. This concept is employed in the Loviisa VVER-440 in Finland, where it has been approved by the regulatory authority STUK. More recently the IVMR concept was adopted at all VVER-440 units operated in Central Europe. The concept is also employed in the GEN-III PWR designs: AP-600, AP-1000, Korea's Advanced PWR-1400, Mitsubishi's 1700 MW APWR, in the 1000 MWe BWR design of AREVA, and Hitachi's ABWR which was already approved by the US-NRC.

The AP-600 design was analysed with the bounding assumption that the entire core inventory relocated into the lower plenum and forms a convecting melt pool. They found that the heat flux varies with angle, peaking near the equator. Fortunately, the heat removal by the water outside also varied with angle reaching highest value also near the equator. It was found that, for a uniform corium pool for the 600 MWe AP-600 reactor, there was sufficient margin between the critical heat flux (CHF) on the water side and the incident heat flux from the corium pool. This margin of safety, however, may be reduced substantially in case there is a metal layer present on top of the oxidic corium pool. The metal layer results from the steel present in the PWR and the BWR lower heads which is melted by the corium pool and rises to the top of the corium pool, as it is lighter when not mixed with other heavier metal such as Uranium (see Figure 2-1).

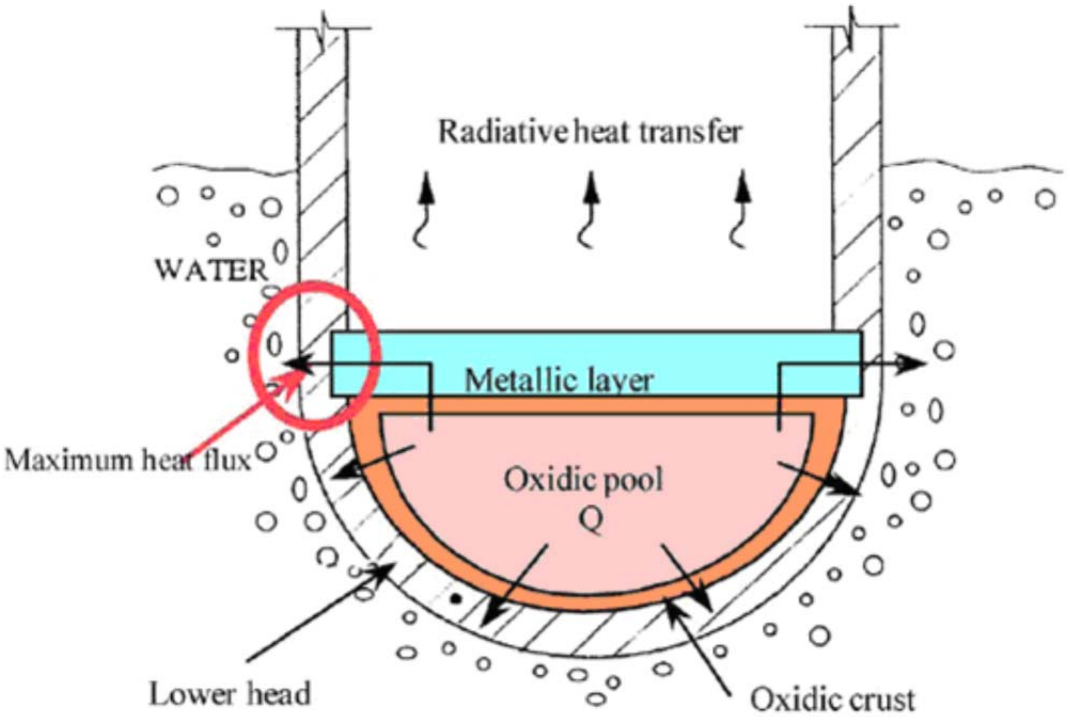

Figure 2-1: In-vessel melt retention

The metal layer receives heat from the corium pool and is subjected to Rayleigh-Bénard convection. Due to a rather low radiative heat transfer from the top of the metal layer, most of the power received is transferred radially to the vessel wall, which is then subject to a very high heat flux. This heat flux focusing is most intense for a thin metal layer since the transverse area for heat transfer is smaller. It was found that for metal layers of < 30 cm thick the focused heat flux could overwhelm the critical heat flux near the equator. For the AP-600, it was found that the metal layer would be thick and there was sufficient margin available between the focused heat flux and the CHF outside.

New research results coming from the OECD sponsored RASPLAV and the MASCA projects indicated the presence of chemical reactions between the melt constituents which may lead to different layer configurations in the melt pool. For example it was found in the RASPLAV project that the presence of even small amounts (<0.3%) of carbon in the system promotes the stratification of the melt pool by separating the oxides from the metals in the melt, thereby forming a light melt layer, rich in metals, and carbides residing on top of the oxide-rich melt pool. A finding from the MASCA project is that steel may extract Uranium and Zirconium from a sub-stoichiometric corium to form a metal compound heavier than the oxidic pool which sinks to the bottom of the oxide-rich melt pool. The condition for this steel-Uranium combination is the unoxidized Zr present in the melt. The mass fraction of U and Zr in the metallic melt and its density are defined by the common amount of steel in the melt and the degree of oxidation of corium relocated from the core. The worst situation would be the one when some of the steel is taken by Uranium metal to the bottom of the pool, while some remains at the top to form a thin metal layer which can result in a strong focused heat flux on the vessel wall. The melt pool composition and configuration of layers is even more complex, since the more recent data obtained in the oxidizing atmosphere (steam) have shown that after Zr oxidation is completed the metal phase releases Uranium and rises back to the top of the pool.

Some references

B. R. Sehgal, Nuclear Safety in Light Water Reactors: Severe Accident Phenomenology. Elsevier/Academic Press, 2012.

V. G. Asmolov, S. S. Abalin, Y. G. Degal'tsev, O. Y. Shakh, E. K. D'yakov, and V. F. Strizhov, "Behaviour of the core melt in a reactor vessel bottom ('RASPLAV' project)," At. Energiya, vol. 84, no. 4, pp. 303–318, 1998.

B. Tourniaire, J. M. Seiler, K. Froment, F. Defoort, F. Fichot, M. Barrachin, and C. Journeau, "The French interpretation of the results of MASCA programme and reactor applications," in Transactions of the American Nuclear Society, 2008, vol. 98, p. 185.

M. Barrachin and F. Defoort, "Thermophysical properties of in-vessel corium MASCA program related results," 2004.

3 VVER-1000 and VVER-440

The Voda Voda Energo Reactor (VVER), or WWER, (from Russian: Водо-водяной энергетический реактор; transliterates as Vodo-Vodyanoi Energetichesky Reaktor; Water-Water Power Reactor) is a series of pressurised water reactor designs originally developed in the Soviet Union, and now Russia, by OKB Gidropress. Power output ranges from 300 MWe to 1700 MWe with the latest Russian development of the design. VVER power stations are used by Armenia, Bulgaria, China, Czech Republic, Finland, Hungary, India, Iran, Slovakia, Ukraine, and the Russian Federation.

The earliest VVERs were built before 1970. The VVER-440 Model V230 was the most common design, delivering 440 MW of electrical power. The V230 employs six primary coolant loops each with a horizontal steam generator. A modified version of VVER-440, Model V213, was a product of the first nuclear safety standards adopted by Soviet designers. This model includes added emergency core cooling and auxiliary feedwater systems as well as upgraded accident localization systems.

The larger VVER-1000 was developed after 1975 and is a four-loop system housed in a containment-type structure with a spray steam suppression system. VVER reactor designs have been elaborated to incorporate automatic control, passive safety and containment systems same way as Western NPPs.

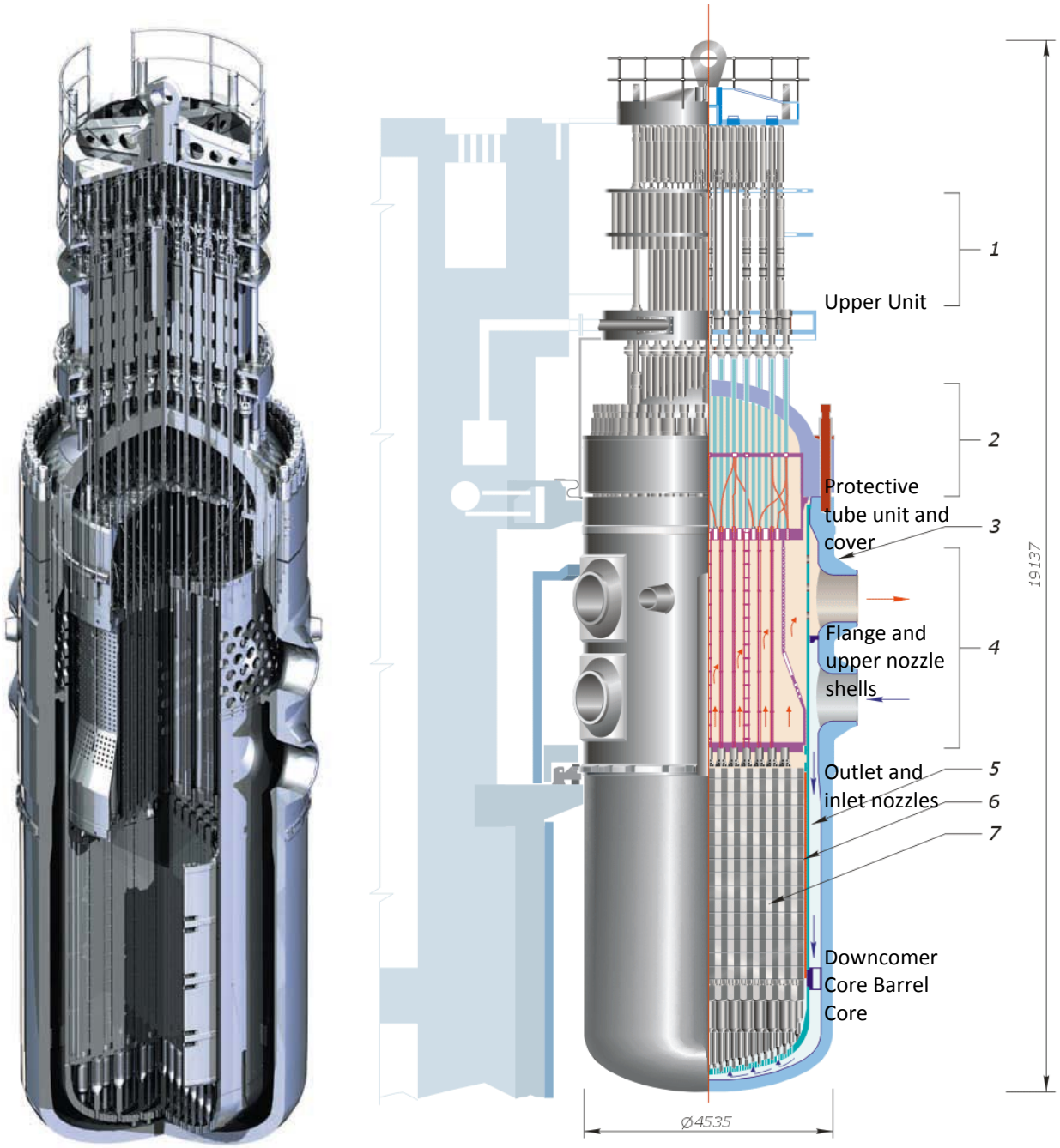

Figure 3-1: VVER-1000/320 scheme

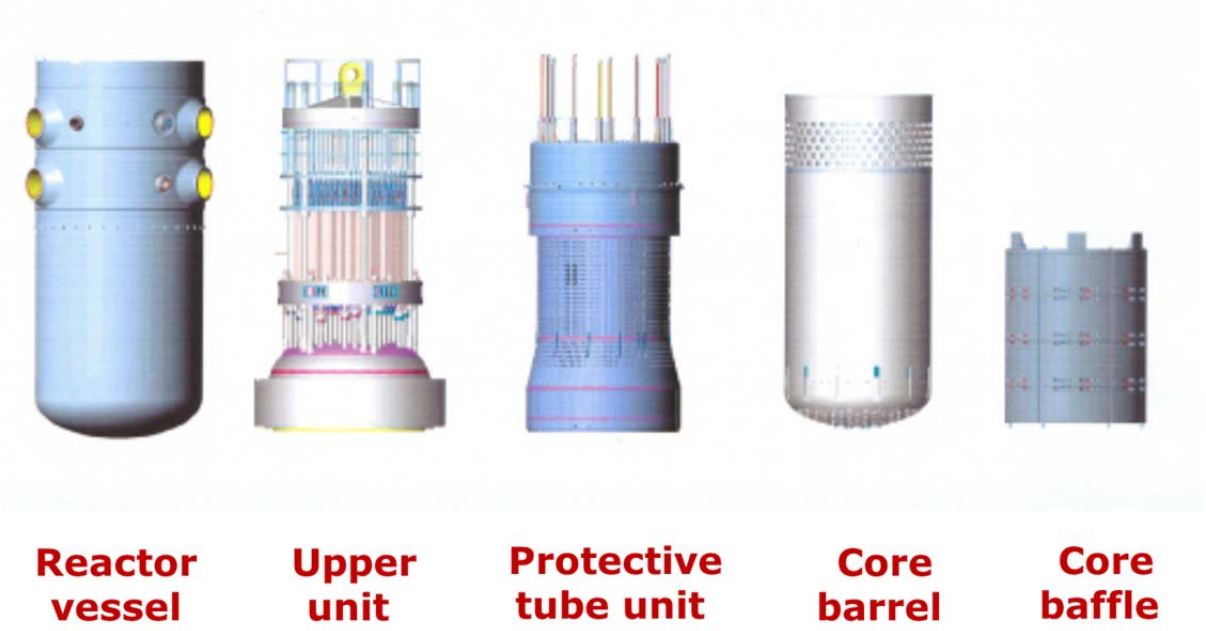

Figure 3-2: VVER-1000/320 main components

Power, MWe	210	365	440	1000
Primary pressure, MP	10,0	10,5	12,5	16,0
Outlet temperature, °C	270	280	300	320
Core heat release rate, kW/l	46	86	84	111
RPV weight, t	223	241	252	304
Reactor weight, t	470	523	573	730

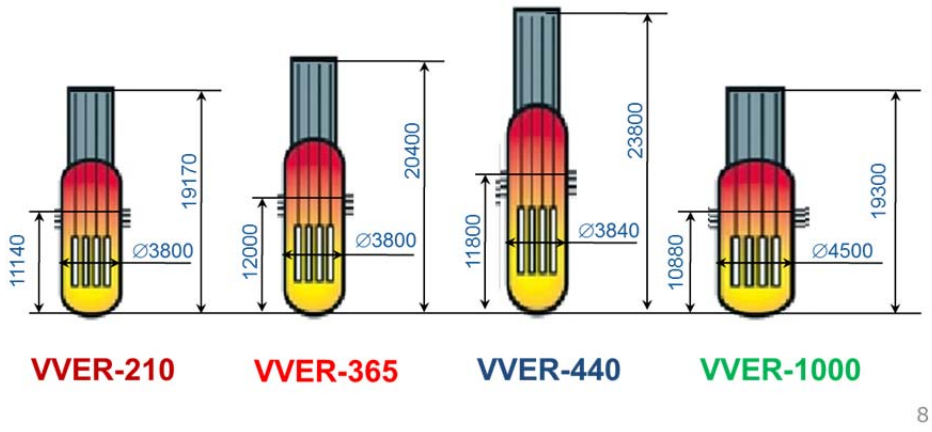

Figure 3-3: VVER RPV main series

There are many differences between the VVER-440 and the VVER-1000, but as far as concerns the IVMR strategy in case of SA, the most relevant difference is the power density: the former has less decay heat to be removed compared to the latter, in spite of being not much smaller. This means that the heat to be removed through the lower head of VVER-440 is smaller making feasible the external cooling solution to keep the melt corium inside the RPV. One more feature of VVER-1000 is the design of its lower plenum (Fig. 3-4): it has a complex structure that makes the analysis more complicated. At the same time, the large amount of steel in the lower plenum, which should be melted, decreases the probability of melt inverse stratification.

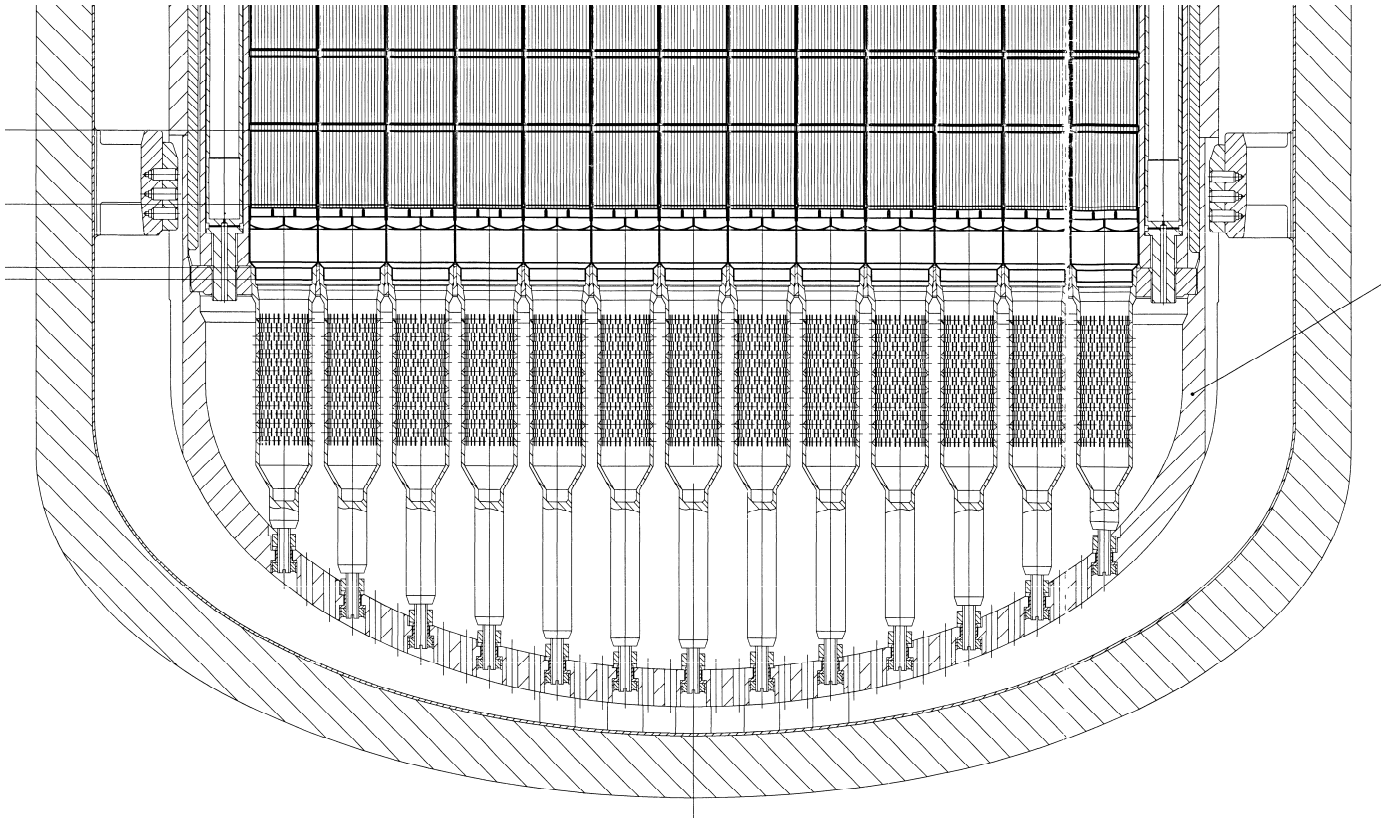

Figure 3-4: VVER RPV lower head draw

4 Existing calculations

The National Research Centre "Kurchatov Institute" in Russia (NRC KI, or KI) has a R&D program on severe accidents to get a sufficient understanding of all major phenomena occurring in case of such accidents in a VVER plant. Further applications of this knowledge allow effective planning of severe accidents management measures. Following this program, KI is conducting experimental programs and code developments in the related fields.

The reference code in Russia is called SOCRAT: System of Codes for Realistic Analysis of Severe Accidents. The main peculiarity of this code from the known computer codes for analysis of severe accidents at NPP such as MELCOR and ASTEC, is a more detailed modelling of core degradation and meltdown processes occurring in beyond design basis accident (including self-consistent modelling both in–vessel and ex–vessel phases). In particular, due to used 2D FEM approach to modelling the lower plenum and RPV, there is no principal limitation on mesh size that allows high spatial resolution combined with high numerical efficiency. The motivation for the development of SOCRAT is driven by the new design requirements to the safety of nuclear power plants with the improved economic factors, by the modernization of existing NPPs, by the development of instructions for accident management and emergency planning. The realistic assessments of Nuclear power plants safety require usage of the best estimate codes allowing description of the melt progression processes accompanying severe accident at the nuclear installation and behaviour of the containment under abnormal condition (in particular, rates of the steam and hydrogen release, relocation of molten materials to the concrete cavity after failure of the reactor vessel). SOCRAT provides self-consistent analysis of in-vessel and ex-vessel processes, including the containment, and the reactor cavity.

KI used the module HEFEST of SOCRAT to perform a best-estimate integral calculation of IVMR with external cooling for a VVER-1000/320, having in mind especially the Temelín NPP located in Czech Republic.

A Large-Break LOCA (LBLOCA) was the postulated SA transient chosen as the most challenging for this type of reactor and the IVMR strategy. In fact in this scenario, the accident evolution is the fastest and the decay heat of the molten corium is the highest. The main assumptions for initial events in this LBLOCA scenario modelled with SOCRAT were the following:

- Double-ended break of the cold leg with equivalent diameter of 850 mm (the broken loop is assumed to be the loop with the pressurizer and the break is located near the reactor inlet).
- Simultaneous off-site loss of the electrical power supply.

The calculation was repeated by KI using the European reference code for severe accidents ASTEC with the same initial events.

Therefore, when this IVMR benchmark was started the following was available:

- LBLOCA integral calculation with SOCRAT, but no open input deck
- LBLOCA integral calculation with ASTEC, with open input deck

More details regarding these calculations can be found in (Zvonarev et al, 2014).

During the 1st Workshop KI agreed to freely provide to other partners all necessary data (ASTEC dataset, Severe Accident initial conditions, etc…) allowing them to start their own calculations for VVER1000 IVMR scenarios and to benchmark their calculations with the one already performed at KI.

These calculations and relative input decks were used as a reference for the benchmark.

Some references

ENSREG, “Stress tests performed on European nuclear power plants.”

B. R. Sehgal, Nuclear Safety in Light Water Reactors: Severe Accident Phenomenology. Elsevier/Academic Press, 2012.

V. G. Asmolov, S. S. Abalin, Y. G. Degal’tsev, O. Y. Shakh, E. K. D’yakov, and V. F. Strizhov, “Behaviour of the core melt in a reactor vessel bottom (’RASPLAV' project),” At. Energiya, vol. 84, no. 4, pp. 303–318, 1998.

B. Tourniaire, J. M. Seiler, K. Froment, F. Defoort, F. Fichot, M. Barrachin, and C. Journeau, “The French interpretation of the results of MASCA programme and reactor applications,” in Transactions of the American Nuclear Society, 2008, vol. 98, p. 185.

M. Barrachin and F. Defoort, “Thermophysical properties of in-vessel corium MASCA program related results,” 2004.

Zvonarev, Yu.& Kobzar, V.& Budaev, M.& Chatelard, P.& Van Dorsselaere, J.P., "ASTEC and ICARE/CATHARE application to simulation of a VVER-1000 Large Break LOCA", Proceedings of the International Conference on Nuclear Energy for New Europe 2009, Bled, Slovenia, September 14–19, 2009.

Y. Zvonarev, V. Kobzar, M. Budaev, P. Chatelard, J.-P. Van Dorsselaere / ASTEC and ICARE/CATHARE application to simulation of a VVER-1000 large break LOCA // Jour. of Energy and Power Engineering. Vol. 4, №3. 2010. pp. 29-37.

Yu. Zvonarev, A. Volchek, V. Kobzar, M. Budaev, A. Konobeev, “Benchmarking between ASTEC and SOCRAT Simulations of In-Vessel Corium Retention Process in a VVER-type Reactor”, Proceedings of the 4th ASTEC User’s Club Meeting, Cologne, Germany, October 11 - 15, 2010.

Yu.A. Zvonaryov, M.A. Budaev, A.M. Volchek, V.A. Gorbaev, V.N. Zagryazkin, N.P. Kiselyov, V.L. Kobzar’, A.V. Konobeev, D.F. Tsurikov. Design Analysis of the Molten Core Confinement within the Reactor Vessel in the Case of Severe Accidents at Nuclear Power Plants Equipped with a Reactor of the VVER Type. Physics of Atomic Nuclei, 2013, Vol. 76, No. 14, pp. 1688–1699.

Y. A. Zvonarev, a. M. Volchek, V. L. Kobzar, and M. a. Budaev, “ASTEC application for in-vessel melt retention modelling in VVER plants,” Nucl. Eng. Des., Jan. 2014.

5 Benchmark results

Due to the complexity of the problem, the benchmark was initially thought to be carried out with mechanistic codes (ASTEC, MAAP, SOCRAT, PROCOR). Anyway JRC developed a model for the CFD code ANSYS CFX and, at the end of the project, other institutions presented also their CFD approach.

5.1 Mechanistic codes

The benchmark was carried out in two calculations rounds: the first calculations were interesting, but it appeared during the first comparison workshop that the data used for performing stand-alone calculations were not properly interpreted and therefore an improved scenario description was given for the second round. Details regarding the first round of calculations can be found in the appendix. According to KI SOCRAT calculation, the conditions for performing ASTEC/ICARE stand-alone calculations were the following:

1. The core starts melting at 1250 s.
2. The core starts to relocate into the elliptic part of the barrel at 3250/3450[1] s. The corium history table refers to corium relocation into the elliptic part of the barrel
3. At 4340/4910[1] s the core barrel fails and the corium relocates all at once into the lower head
4. The FA (Fuel Assembly) supports are inside the barrel
5. The support grid is also inside the barrel
6. When the core barrel fails, all the steel structures inside the barrel AND the barrel itself (elliptic part + some of cylindrical part) also melt and relocates into the lower head
7. We have to add these steel structures (barrel, FA supports and grid) to the corium history at 4340/4910[1] s. when the barrel fails
8. We start the real stand-alone lower head calculation at 4340/4910[1] s. when the barrel fails
9. The initial composition of the corium is the one in Table 1 with averaged temperature T = 2500 K
10. The decay heat must be taken into account from time 4340/4910[1] s when the barrel fails

Table 1: Corium composition for basic calculation (with account of fission products release)

Material	Mass, t	Source
UO_2	85.9	CORE
Zr	15.6	CORE
ZrO_2	17.1	CORE
Steel	34.4	CORE
	12.2	elliptic part of barrel
	9.0	melted cylindrical part of barrel
	12.3	FA-supports
	1.94	support grid

The main inaccuracies of the first round of calculation were:

- The corium history was referring to the corium slumping into the barrel, not into the lower head directly. Most of the participants didn't realize that and calculated the slump directly into the lower head;

[1] The first value is referred to 100% of decay heat; the second value is referred to 80% of decay heat due to volatile FP release out of the RPV.

- On the lower head there are some steel structures that were not taken into account by all participants and would count for additional material when melting.

The codes used by the participants are specified in Table 2.

Table 2: Participants to the second calculations

	Mechanistic Codes						CFD		
	ASTEC integral	ASTEC stand-alone	SOCRAT	MAAP	PROCOR	MELCOR	CFX	NEPTUNE	RELAP
EDF				x				x	
CEA					x				
UJV						x			x
KI		x	x						
INRNE		x							
TUS		x							
JRC		x					x		
IVS	x	x							
VTT		x							

Table 3: Decay heat time dependence, which was used in calculation

Time, s	Decay heat, Wt (per 1 kg of UO_2)
1000	731.6
2000	609.4
3000	542.4
4000	497.1
5000	463.8
6000	437.5
7000	416.6
8000	398.9
9000	384.4
10000	371.6
20000	300.1
30000	268.9
40000	250.5
50000	237.7
60000	227.8
70000	218.9
80000	211.2
90000	203
100000	194.9
200000	166.5
300000	146.3
400000	128.6

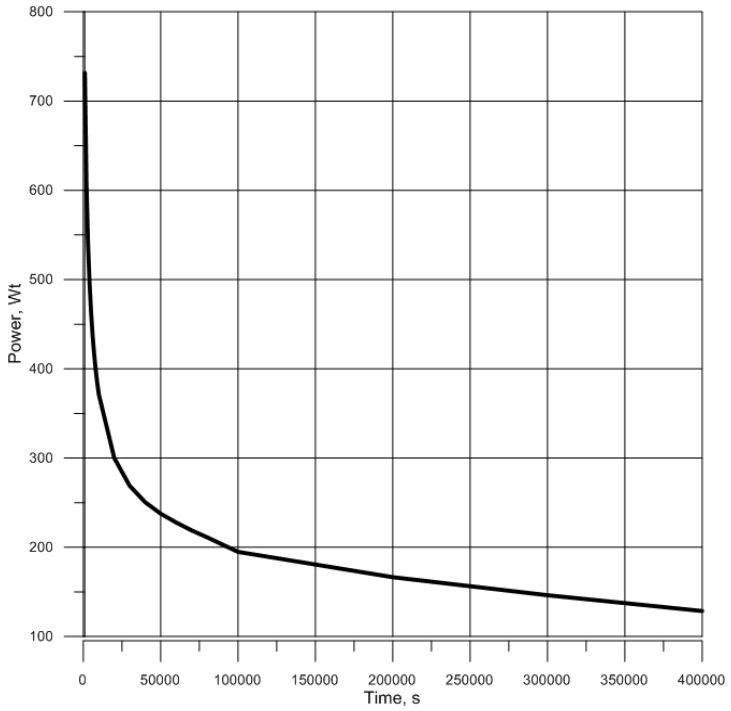

Figure 5-1: Decay heat time dependence

In this second calculation there was an imperfection in the ASTEC input deck distributed as a reference to the participants: the nodalization of the lower head was smaller than the total possible amount of material filling the lower head.

VTT extended the ASTEC lower head nodalization, and even if the peak heat flux was captured with the wrong nodalization, the LH failed in the extended nodalization due to a bigger mechanical stress. EDF and CEA also extended their lower head nodalization.

Another imperfection was found in the definition of the RPV steel: the ASTEC input deck distributed by JRC was considering stainless steel instead of carbon steel. In reality the lower head exact description would have been 7 mm of stainless steel liner + 237 mm of carbon steel measured from inner surface. The thermal conductivity of the carbon steel is higher that stainless steel, but higher values of conductivity should result in higher remaining wall thickness in similar heat flux.

IVS has used its own ASTEC input deck in both, stand-alone ICARE analysis as well as in integral ASTEC analysis.

Figure 5-2 shows the «**max of max**», that is the axial profile of the maximum heat fluxes on the external nodes (heat exchange between water/external vessel) occurring during the whole calculation. This plot is therefore time independent and is a bounding curve. The plot displayed in Figure 5-2 is referred to the best estimate calculations provided by every participant, taking into account a 20% reduction in the decay heat due to volatile fission products release out of the RPV.

The shape of this profile is very dependent on the code used for the calculation.

MAAP and PROCOR predicted their biggest value at a higher elevation compared to ASTEC; MELCOR predicted a peak at a much lower position and SOCRAT predicted a quit flat profile.

If we focus on Figure 5-2 (max of max) it is possible to observe that most of the points are below 1.0 MW/m^2, but there are anyway values exceeding this threshold. The density distribution and cumulated distribution of the max_of_max values are shown in Figure 5-3 and Figure 5-4; if we look at them we can appreciate that the predicted maximum value of the heat flux has a peak around 1.0 MW/m^2 and a probability of 90% to have a lower value.

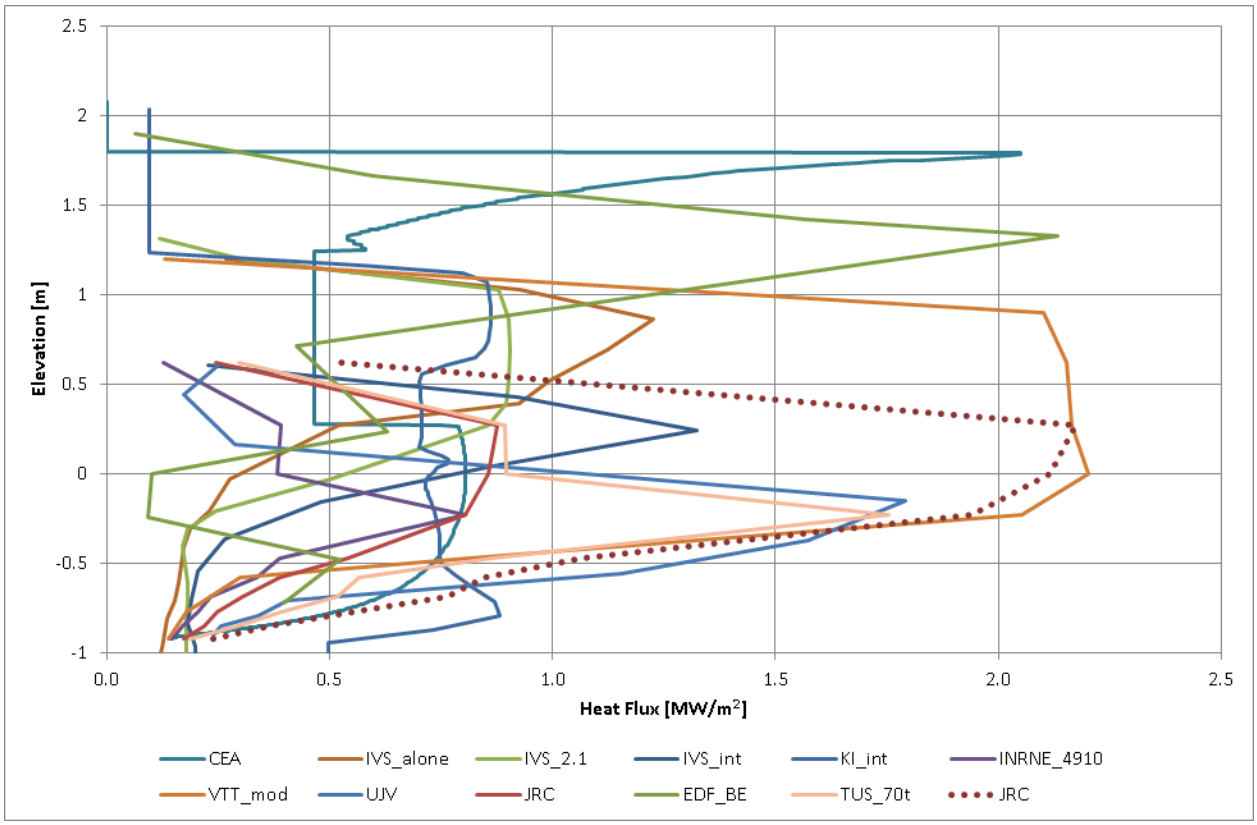

Figure 5-2: Heat flux comparison – "max of max"

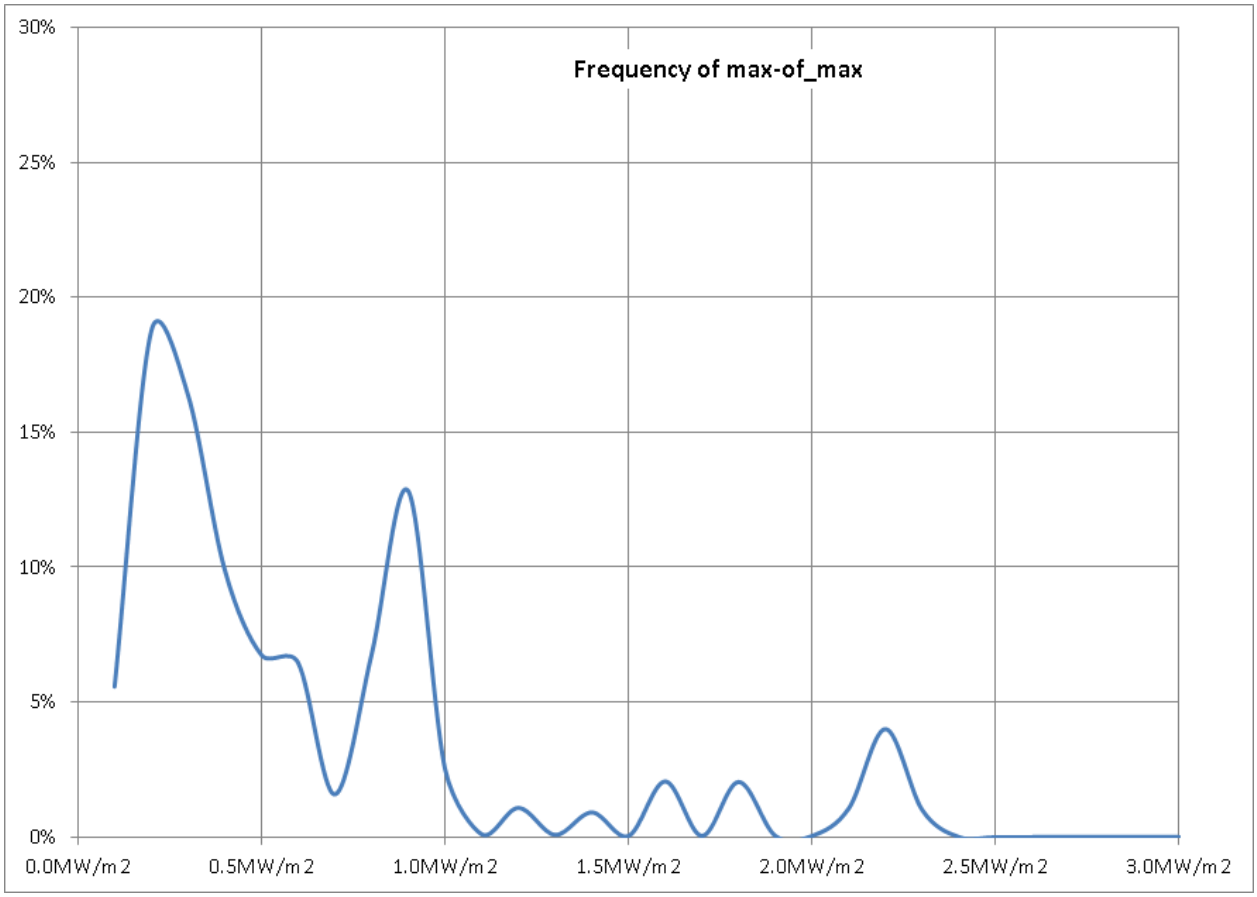

Figure 5-3: Density distributions of the max-of-max

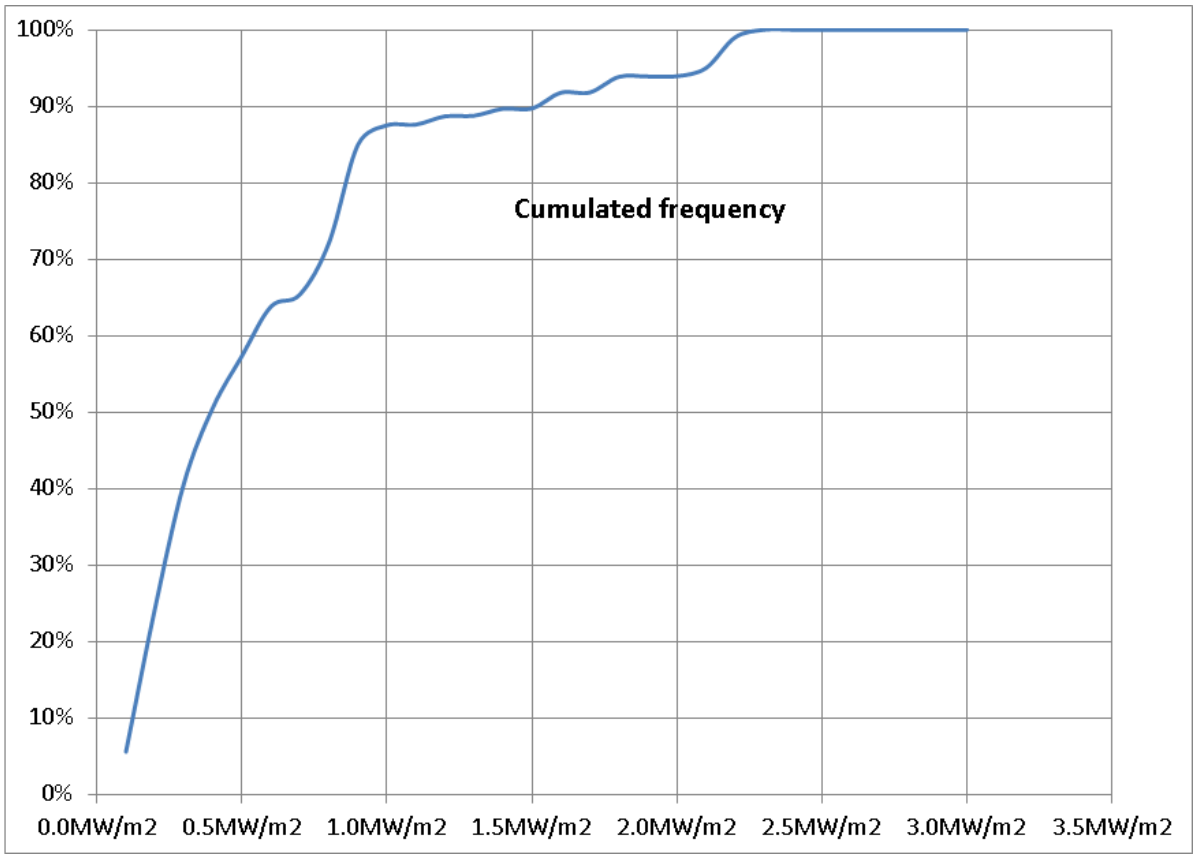

Figure 5-4: Cumulated distribution of max-of-max (second calculation)

The max-of-max plot may be a bit misleading because it doesn't take into account for how long the heat flux was lasting.

Figure 5-5 is interesting because it shows the time evolution of the maximum values of the HF amongst all nodes. This curve was created in the following way: for every calculation and for every time step the maximum HF value all over the LH nodalization was extracted and plotted.

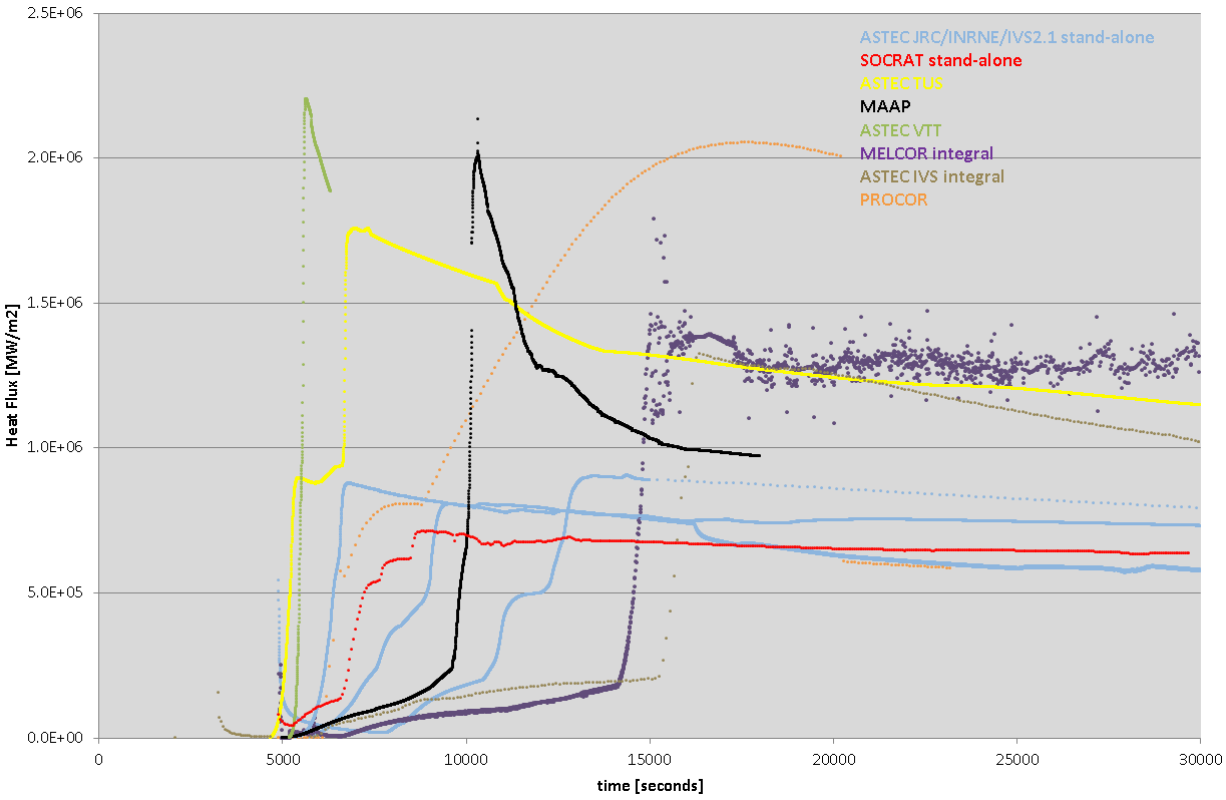

Figure 5-5: time evolution of the max HF values amongst all nodes

The results of Figure 5-5 are also very different from code to code:

- ASTEC ranges between some higher and lower values;
- SOCRAT is similar to ASTEC lower values;
- PROCOR predicts just an almost linear increase in the HF and LH failure after the peak;
- MAAP predicts a big peak similar to ASTEC by VTT (unless the SS is 30 tons or the Zr oxidation is C70, see full report in the appendix);
- MELCOR and ASTEC v2.0 integral calculations are very similar to each other, delaying the peak and then showing a behaviour similar to ASTEC higher values[2];
- VTT is using ASTEC in stand-alone mode, but with special assumptions for the initial state of the melt (overheated) that predicts a HF shape similar to MAAP but at an earlier stage.

PROCOR models two layers in the reference calculation (oxide and metal layers) with a crust surrounding the corium pool. In the SOCRAT reference calculation, the steel coming from the vessel ablation relocates directly in the upper metal layer, with no "focusing effect"; in PROCOR, as the corium pool temperature continues to increase due to the residual power, the vessel wall begins to melt and a third light metal layer (steel from the melted vessel) appears **above the crust**. The thickness of this steel layer increases with the continuous vessel ablation, and a part of it is transferred to the light metal layer under the crust, which is considered as porous. This thin ablated steel layer is the main reason of a higher HF. Besides, PROCOR doesn't model the axial conduction along the vessel wall, therefore it doesn't "spread" the hot points. At the beginning of the SOCRAT reference calculation, the HF peaks in the upper metallic layer and later in the lower oxide layer, whereas in PROCOR the HF related to the oxide layer is always higher than the HF related to the metal layer. This difference may be related to the axial power profile applied in PROCOR to each layer and to the heat exchange correlation used between the two layers of the corium pool.

The HF shape predicted by VTT using ASTEC differs quite a lot from the results of other ASTEC users and is much more similar to MAAP except for a time delay. This time delay is due to the initial state of the melt which was assumed to be overheated. The initial compositions of the layers were defined based on chemical equilibrium states produced by ChemSheet (Hack et al., 1999). In the reference input the starting point was a homogeneous mixture of corium compounds: 85.9 t of UO_2, 15.6 t of Zr, 17.1 t of ZrO_2 and 69.84 t of steel. ASTEC was then responsible for calculating the phase separation together with chemical interactions in the melt pool. The initial thermochemical equilibrium was calculated in the smallest possible temperature when there was no solid phase present, i.e. in the liquidus temperature. In this case the temperature was 2 831 K and it was used also as the initial temperature of the layers. VTT extended the LH nodalization in order to take into account properly the initial amount of melt. In fact ASTEC separates the lower plenum volume from the cylindrical vessel part. If the melt pool volume exceeds 90 % of the lower plenum volume, ASTEC calculates a corrective factor that is applied on volumes of the core melt layers. This affects height of the pool and then vessel wall area that is affected by the intensive heat load. In a case when calculation begins with a melt pool on the lower plenum, the size of the lower plenum should be adjusted so that the corrective factor is as close to 1 as possible on the first time step to achieve realistic results. This is because ASTEC assumes that the melting vessel wall increases the volume of melt pool and the code does not take into account that the initial lower plenum volume is actually increased by the same value as vessel wall is melted. Since the volume of molten steel is approximately the same as for solid steel, the top surface of the pool can assumed to be on the same level all the time.

In MAAP the initial melt temperature is below the eutectic point[3]. The bulk corium pool separates into two layers: oxide and light metal, both surrounded by the crusts. The vessel ablation starts at 8760 s

[2] This follows from the different scenario considered in MELCOR integral analysis (LOCA 200 mm instead of double ended break that was used in SOCRAT analysis; these results were used as input in stand-alone analyses

[3] In eutectic mixtures the solidus and liquidus temperatures are identical, i.e., the mixture melts completely at one temperature, the eutectic point.

and the ablated steel relocates above the horizontal upper crust and forms a top thin layer (like in PROCOR) responsible for the maximum corium-to-vessel heat flux value (2.88 MW/m^2 at 9460 s).

The TUS' calculations were made by ASTECv2.0R3p1 in stand-alone mode with boundary conditions that were not the ones indicated by KI, but those deriving from a previous own ASTEC integral calculation with the scenario of LOCA 200 mm applied to an input deck of VVER-1000. Some results as the obtained temperatures of corium and fluids, as well as the pressure in the vessel were used for calculations with module ICARE by the stand-alone input deck of VVER-1000: steam temperature (400 K), liquid water temperature (365 K) and temperature of the magma relocation (2600 K). TUS made three stand-alone ICARE calculations for 30, 70 and 110 tons of steel; the 70 tons was used as best estimate. For the case LOCA 200 mm, the section of break connection in the input deck was set to 0,03141 m^2 (pi*0,200^2/4). Other assumptions for the stand-alone calculations were:

- full decay power;
- a grid with 9 radial and 10 axial cells for lower plenum;
- the "zero" levels of all components of the model were increased with 0,873 m in correspondence to VVER-1000 RPV bottom head drawing of KI;
- the HFs into the volumes of vessel wall are calculated as sum of the powers, divided by the area of each mesh.

Generalized results presented in Figure 5-6 here show:

- Since the decay heat in the corium is the same but in a smaller volume, the HF profile on the surface corium/vessel in the case of 30 t steel is higher even at 15 000 s in comparison to HF profiles for 70 and 110 t of steel;
- The maximums for external HF have similar values because the different steel masses influence weakly to the maximum of the external peaks and more over the level of the peaks (Figure 5-5);
- The maximums of external HFs versus time - LOCA 200 mm for 30 t, 70 t and 110 t of steel are higher than the one of the initial scenario (green curve, Figure 5-6 right);
- The comparison between TUS-70 t steel at initial scenario and results for full decay heat of other partners (yellow and green curves in Figure 5-6 right) have comparatively same maximums. It shows that the reason for higher peak of HF at cases of LOCA 200 mm is in result of the conditions of this phenomena and also that the mesh modelling is acceptable and true in the cases of LOCA 200 mm calculations.

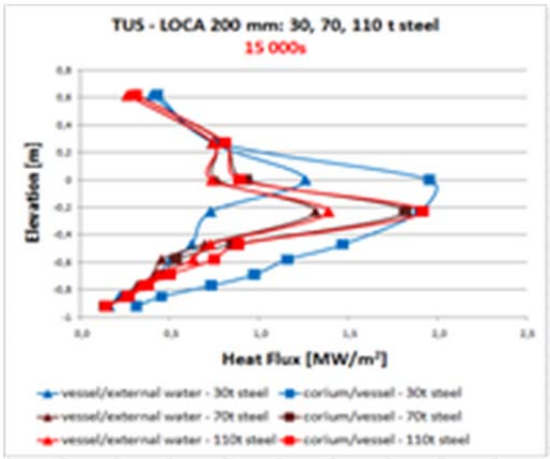

Figure 5-6 HF profiles – 30, 70 and 110 t steel

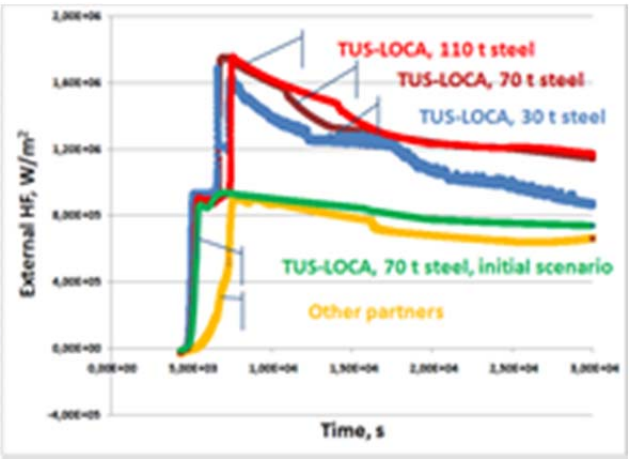

External HF – 30, 70 and 110 t steel / time, s

MELCOR is generally capable to predict focusing effect, but the simulation by UJV is done in the integral manner and it is influenced by whole time progression versus the postulated cases in the ASTEC or SOCRAT modelling of the only behaviour in the lower head. In the simulation the relocation of the corium went to debris cooling due to presence of water in the lower head and the heat up of debris is

relatively slow, also due to the cooling effect of very cool lower head wall, which is in contact with the water in cavity/deflector channel. Due to this configuration, molten pools are formed - first the metallic with lower T_{liq} (MELCOR correctly predicts movement of metallic layer to elevations above oxidic ones) and later the oxidic pool due to higher T_{liq}. But as the crusts are predicted to be formed on sides and on top of oxidic pool, the situation is similar to those predicted in SOCRAT in the very late phase after the impact of corium cooling via RPV LH wall. MELCOR does not produce output for the confirmation from the outputs, as the missing output parameters are: side and top crust thickness and temperatures, and heat transfer between oxidic and metallic layers and so on.

The evolution of maximum heat flux density value predicted in the integral simulation with the MELCOR 1.8.6 integral code is influenced by some reasons:

- Relocation of corium into the lower head is "by pieces" as the code predicts loss of supporting structures, it models the core support plate, but also columns in the lower head of core barrel. Corium relocating below core support plate enters in the inner space of upper part of columns (upper part is hollow, but lower one is solid) where is temporarily hold up, because of presence of water in lower plenum which support of cooling of the columns and delays their loss of integrity and further relocations of corium;
- Due to temporarily hold up of corium it reaches bottom of the RPV as solid particles and their cooling is supported with boil off of remaining water in the lower head of the RPV, then the corium debris are re-heat up and finally re-melted;
- Location of the maximum heat flux is influenced by the accident progression as well as the predicted part of the material already molten (metallic layer is fully molten, but oxidic part includes important contribution of solid debris – in MELCOR terminology "particulate debris"). Generally the location of the highest heat flux density is at elevation of top of oxidic pool. This is typical for cases with reduced heat transfer from the bottom oxidic melt pool to the upper metallic layer – for instance when the top crust at oxidic pool would be formed. But as the crust formation is not modelled in the MELCOR code (see COR-RM-71 on MELCOR Computer Code Manuals, Vol.2), the reason is in the correlation for the heat transfer between molten pools, which depends on Rayleigh number (and the temperature difference between the bulk pool and the interface), which is in case of partly solidified oxidic pool, underestimated (composition of molten material with solid particles).

Time about 5000 s identifies the first relocation of debris to lower head, slow heat up is influenced with heat transfer from solid particles to lower head, which is much higher after re-melting of debris and molten pool formation (about 14 500 s).

Please note that the integral MELCOR calculation returns similar results to the integral IVS ASTEC 2.0r3p2 calculation, possibly due to the presence of water in the lower head when the core relocates.

IVS submitted two ASTEC calculations: an integral scenario with V2.0r3p2, and a stand-alone with v2.1 beta. In the integral analysis performed with ASTEC V2.0 code the whole LB LOCA sequence (LOCA 300 mm on cold leg) is analysed starting from break opening, front-end thermal-hydraulics, core heat-up, melting and relocation, quenching of corium in lower reactor head by residual water, re-melting of debris and developed molten pool formation in lower head. Thus, the mass and composition of molten pool in lower reactor head as well as decay heat generated here is calculated by the code. The residual power was calculated from a defined initial inventory of fission products (FPs) in the core (more than 700 isotopes are defined). During the calculation the code calculates the transmutation and migration of isotopes. When the core starts melting and relocation takes place together with molten UO_2 that is relocated into the RPV lower head, the fraction of decay heat that corresponds to non-volatile FPs contained in relocated mass of uranium follows the corium. When the stratified configuration of molten pool in lower reactor head is formed, redistribution of FPs and decay heat between corium layers is calculated by the code based on chemical affinity of FPs. The magnitude of predicted maximum heat flux is comparable with TUS and MELCOR analyses. However, it should be noted that in integral analysis the radiation from upper corium layer is not modelled and thus, the results are conservative with respect to maximum predicted heat flux. It's worth noting that IVS used in integral calculation a solidus

(T_{sol} = 2550 °K) and liquidus (T_{liq} = 2600 °K) temperature for both UO_2 and ZrO_2 lower than the suggested values of 2850/2900 K.

The stand-alone v2.1beta calculation was based on a nodalization different from the distributed input deck: solid internal structures made of stainless steel (SS) were modelled inside the lower head (using STRU LSTRUCT); the lower head was meshed into 10 equidistant layers through the wall thickness and 19 cells in axial direction; it was assumed that the RPV wall is made of Fe (material properties are predefined in ASTEC code) instead of SS material that was used in distributed input deck, and the thin SS liner on inner surface was not considered but for simplicity replaced by Fe instead (i.e. material with higher thermal conductivity and chemical composition closer to RPV carbon steel). Default values of materials properties that are implemented in ASTEC code (including solidus and liquidus temperatures for UO_2 and ZrO_2) were used; the default values of melting temperatures of UO_2 and ZrO_2 are higher than average initial temperature of UO_2 - ZrO_2 - Zr - SS magma (T = 2500 °K) at the start of calculation. Initial and boundary conditions such as corium mass and composition, time of corium relocation into lower plenum, initial average corium temperature, decay heat generated in corium, were taken from KI calculation. High value of heat flux (~ 0,8 MW/m^2) from upper metallic layer is due to high thermal conductivity between the metallic layer and RPV wall (there is crust between wall and oxidic layer), so most of heat that is generated in oxidic layer is going upward to metallic layer rather than into RPV wall. Furthermore, nearly 30 % of decay heat is generated in metallic layer. Due to presence of metallic U, partial reduction of UO_2 to metallic U was predicted by the code (phase separation model) and IVS allocated decay heat to UO_2 and U.

SOCRAT can run in integral or stand-alone mode. The simplification of corium-slumping increases the heat transfer surface when it runs in stand-alone mode. This means that the local thermal load on the wall is lower compared to integral calculations. Standalone calculation is an ideal case, when corium stratifies immediately (two layers with maximal possible heat transfer surface). Predicted results are not conservative.

Figure 5-7 shows the frequency density of the data shown in Figure 5-5 up to 30.000 seconds, and Figure 5-8 shows its cumulated frequency. Figure 5-7 and Figure 5-8 are time dependent: if the vessel doesn't fail the HF will decrease more and more because the decay heat will be less and less and therefore, the frequency of lower HF will increase more and more.

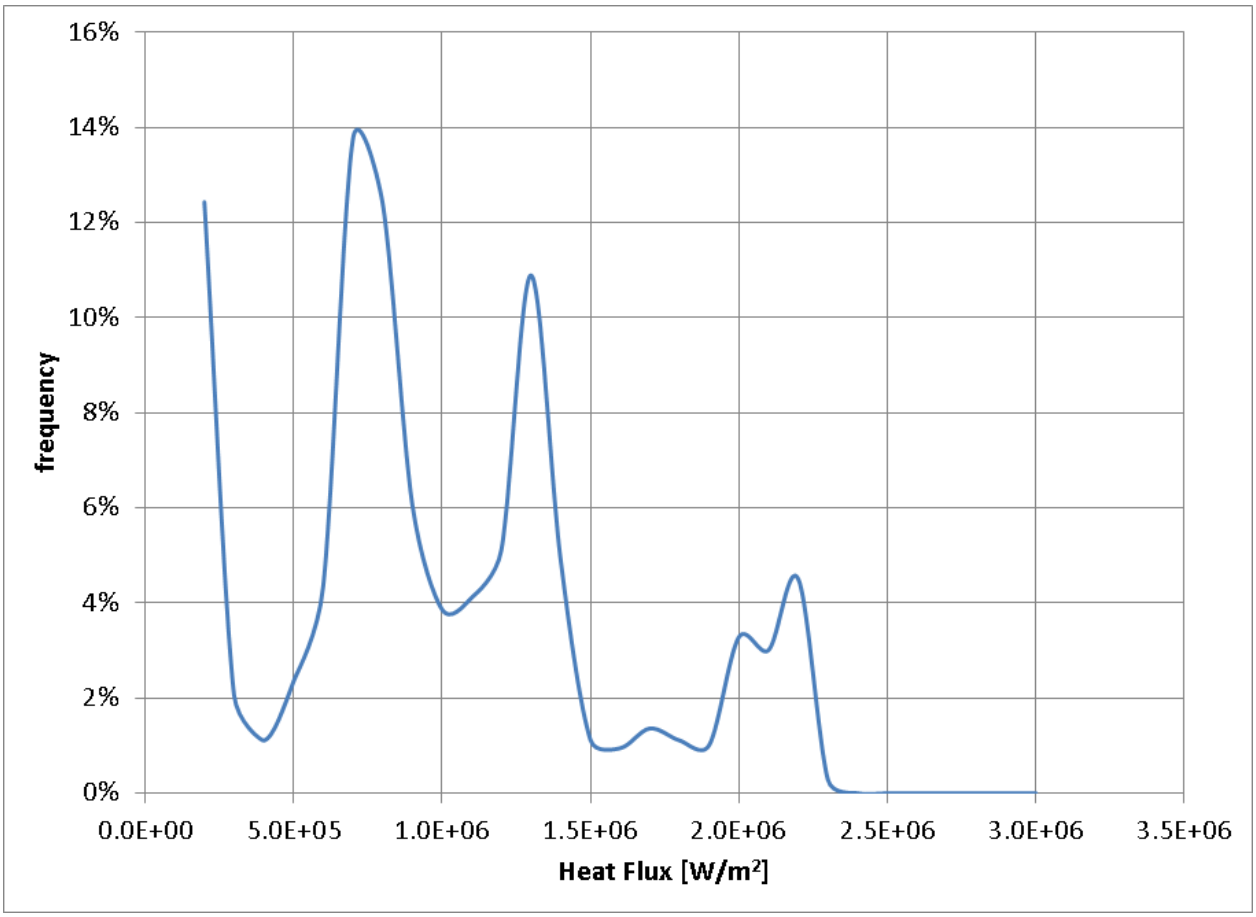

Figure 5-7: density distribution after 30.000 seconds

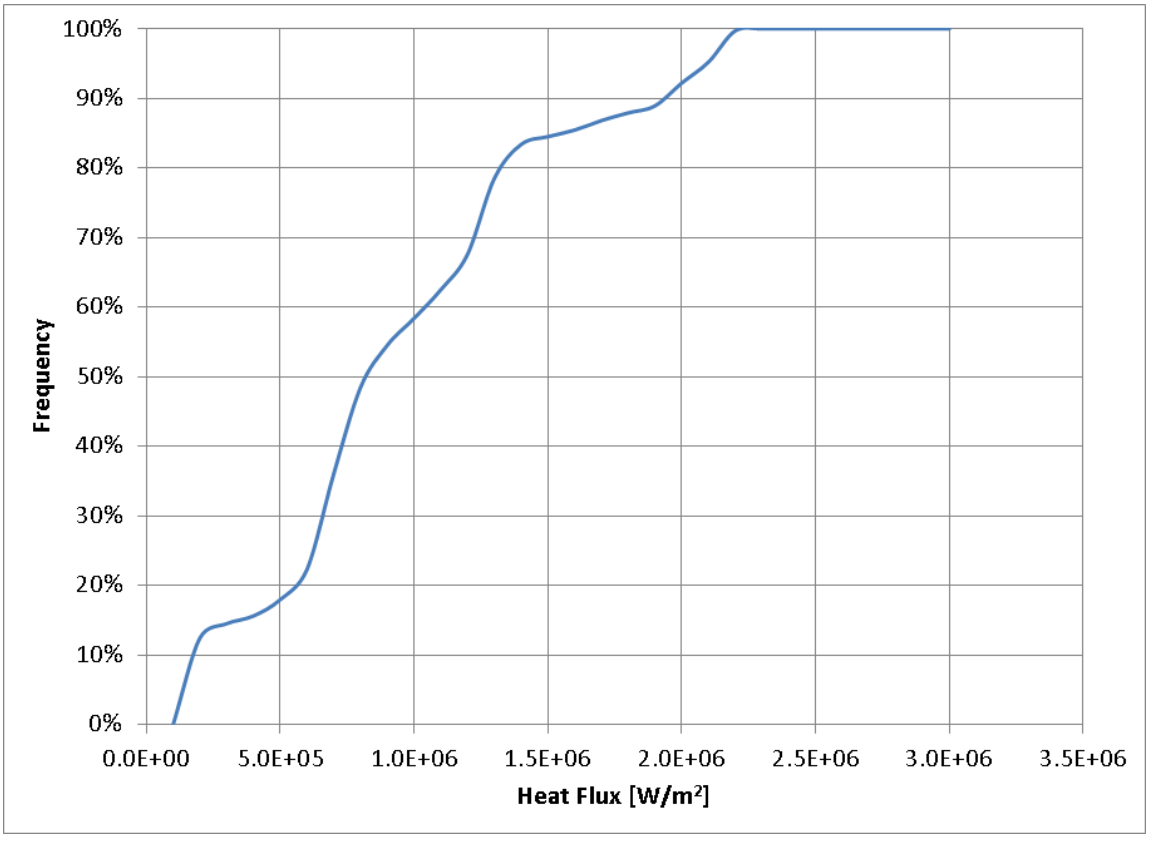

Figure 5-8: cumulated distribution after 30.000 seconds

In Figure 5-5 it was possible to see a problem implicit to all codes: all models for melt stratification are mostly valid for stabilized conditions. Therefore the first part of the transient when the heat fluxes are higher is also the most uncertain.

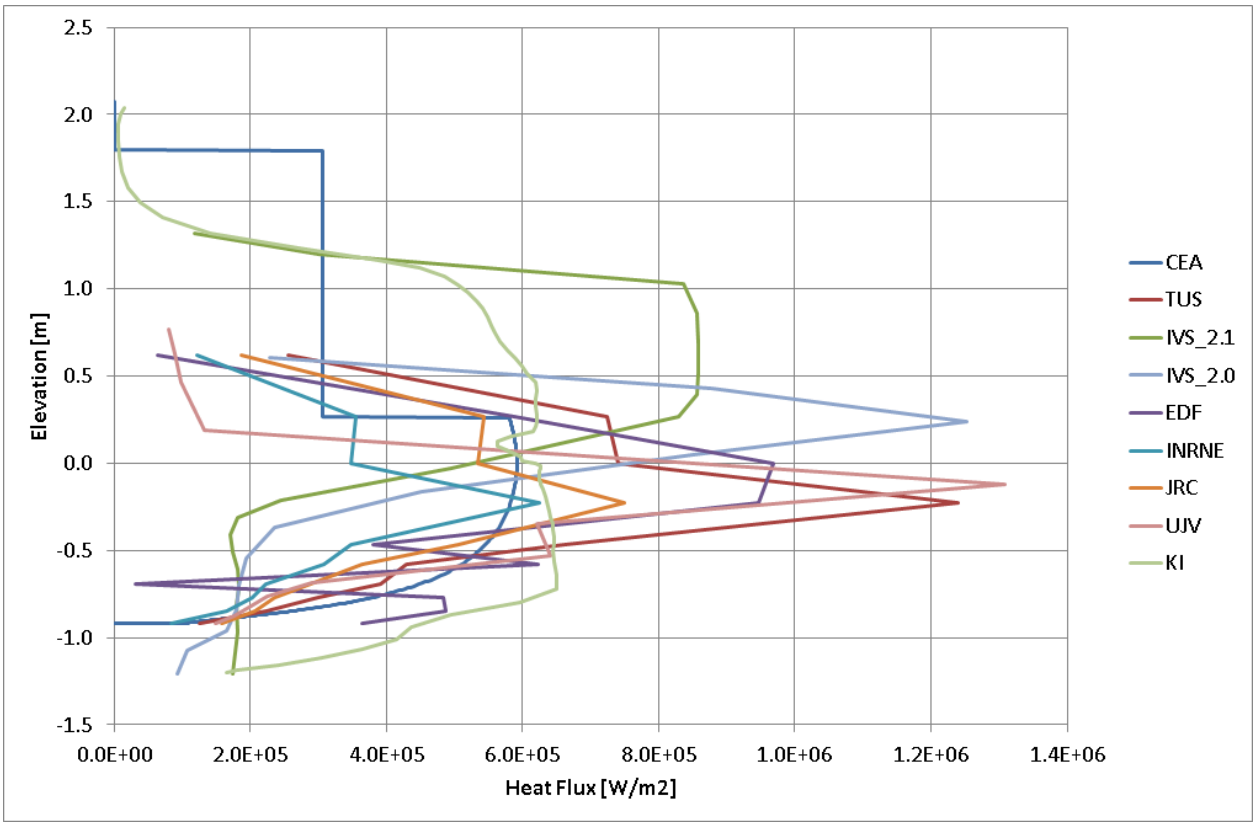

Figure 5-9: Heat flux profile ("max of max") at 20.000 seconds (stable conditions)

Figure 5-9 shows the heat flux profile ("max of max") at 20.000 seconds under more stable conditions. It is possible to observe that all the codes predicted a peak around the transition between the lower oxidic layer and the upper metallic layer.

As a common agreement, for given temperature, $R_{U/Zr}$ and C_{ox}, two possible stratified configurations can be observed at thermodynamic equilibrium, depending on the steel mass proportion in the corium. For the corium inventory considered in this report, when the steel mass in the corium melt becomes greater than the threshold value $\widetilde{m}_0^{steel} \approx 42$ tons, there is a change in stratification: the metal layer density becomes lower than the oxide's one and the oxide layer is situated under the "light metal" layer (see Figure 5-10).

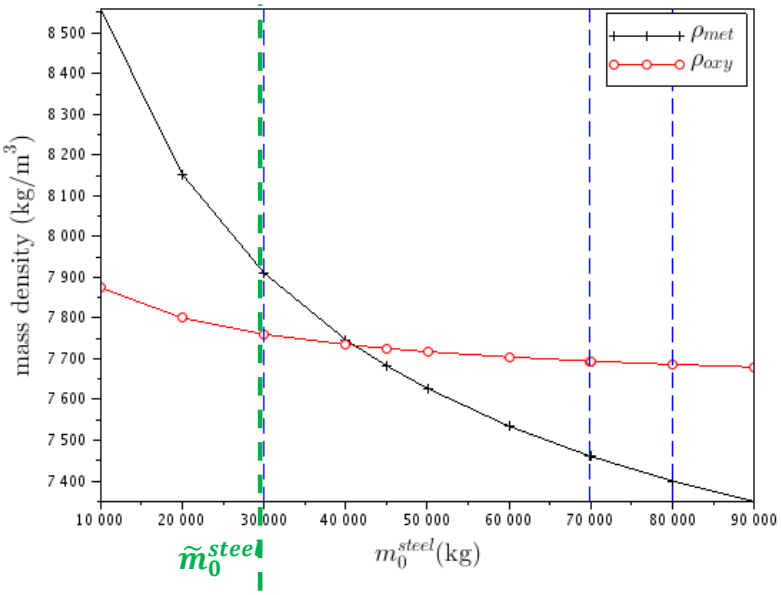

Figure 5-10: Metal and oxide phase densities (ρmet and ρoxy) as a function of m_0^{steel} (initial mass of steel in the corium melt) for T = 2800 K

Effect of steel and structures in the LH:

- According to MAAP (EDF) 30 tons of steel in the bulk pool separation resulted in the formation of a heavy metal layer and an oxide layer. Stratification inversion during the transient leads to the formation of a light metal layer below the crust, while the ablated vessel steel formed another light metal layer above the crust. The HF is bigger compared to the case of 80 tons of steel where there was no stratification inversion. No focusing effect is observed with 30 tons of steel;
- According to IVS ASTEC V2.1 stand-alone calculations, the reduction of SS in upper metallic layer (from 70 to 30 tons) is increasing the maximum heat flux due to focusing effect;
- According to TUS ASTEC calculations, the presence of 30 tons, 70 tons or 110 tons of SS doesn't affect much the maximum HF;
- According to VTT the amount of steel doesn't affect much the final result of the maximum HF, with bigger HF values for bigger amount of steel;
- According to PROCOR, 30 tons of steel in the initial corium bulk leads to a much bigger peak in the HF due to the focusing effect: we have same residual power as before but concentrated in a lower total mass of corium, plus the layer which is under the FE metal layer (separated by a crust) is an oxide layer (stratification inversion), which concentrates more residual power;
- According to KI ASTEC stand-alone calculations (see Appendix 9.1.2) an increase of steel mass doesn't affect significantly the results. Instead a decrease in steel mass leads to a slight increase of max of max heat flux: from 0.855 MW/m^2 in basic calculation with 69 t of steel to 0.923 MW/m^2 (occurs at 6282 s) and 0.911 MW/m^2 (occurs at 6236 s) in calculations with 20 t and 40 t of steel, respectively. Nevertheless this slight increasing is quite enough: heat flux from external surface to water exceeds the critical heat flux at these points.

Effect of the oxidation degree:

- According to VTT the higher the ZrO_2 fraction is the higher are the heat flux maximums. A possible explanation is that the metallic uranium content affects the mass of metal layer and then the heat transfer area. The higher is the ZrO_2 fraction the less metallic uranium there will be and the thinner the metal layer becomes;
- According to EDF/MAAP much lower external HF is predicted for C70 compared to C30[4], while the internal HF is the same for both cases;
- According to PROCOR, increasing the zirconium oxidation degree in the corium inventory (for a fixed $R_{U/Zr}$) tends to delay the vessel failure. There is not a big change in the maximum HF anyway.

[4] C30 means Zirconium oxidation degree NZr/(NZr + $NZrO_2$) C = 30%

Stratification inversion:

In consideration of the cases with inverse stratification of the melt, two essential issues should be commented concerning the mentioned important parameters mass of steel and corium oxidation degree.

- First, the inversion of stratification is predicted in some calculations for the case of 30 ton of steel. It should be noted that this case may be natural for PWRs but seems unrealistic for VVER-1000 because of large amount of steel (about 25 t) in the lower plenum. Together with steel coming from core and lower support plate, the minimal amount of steel participating in the melt during IVMR (developing of the pool directly in RPV) in most cases should be close to 40 t;
- Another essential parameter affecting the inversion is the degree of corium oxidation. Along with the thickness of the metallic layer, it affects the stratification. The investigation of the effect of steel mass and oxidation degree was performed in the paper (J.M. Seiler NED 2007). The results conclude that in the considered case the inverse stratification is unlikely;
- MAAP (EDF) with 30 tons of steel in the bulk pool separation resulted in the formation of a heavy metal layer and an oxide layer;
- According to PROCOR, starting with a bulk core containing 30 tons of steel, when the liquidus temperature is reached (melt liquidus temperature is 2800 K and initial bulk corium temp is 2500 K) and when stratification instantaneously occurs, there is one heavy metal layer (53.09 t) with an oxide layer above (95.51 t), surrounded by a crust.

Ablated steel:

- In PROCOR the vessel wall begins to melt and a third light metal layer (steel from the melted vessel) appears above the crust. This steel is defined as **FE (Focusing Effect) metal layer**. It corresponds to the layer that can be formed during the transient, above the crust (steel coming from the vessel ablation). The upper steel metal layer is considered in the pool inventory for the transient stratification model. This steel layer thickness increases with the continuous vessel ablation. A part of this steel is transferred to the light metal layer under the crust. The mass transfer of steel through the crust is allowed and is managed by a kinetic stratification model. With time this FE metal layer decreases because of the slowing down of the ablation and the continuous transfer of steel below the crust;
- In MAAP by default the ablated vessel steel relocates on top of the pool (above the crust), similar to PROCOR, with a direct influence on the formation of a thin, out-of-equilibrium metallic layer on top of the pool, and on the occurrence of the focusing effect. If the default hypothesis changes and a chemical interaction takes place between the steel and the oxidic crust, then a formation of heavier, uranium-enriched steel that would move downward and ultimately percolate through the crust to be added to the pool (see Figure 5-11). This last configuration leads to much smaller and flat heat flux with a maximum value about 0.4 MW/m^2 located at a lower elevation similar to the ASTEC's;

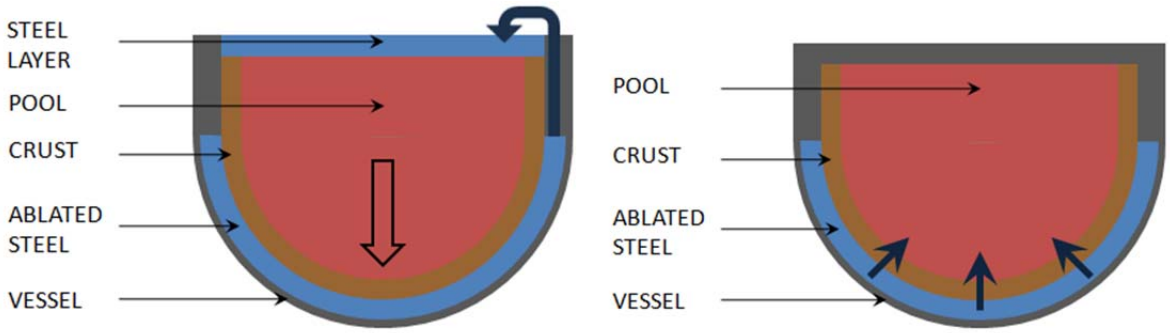

Figure 5-11: two possible ways to treat ablated steel

Transient melting and max-of-max of HF:

- In most calculations the maximum of HF was obtained during transient phase of the melting. That is a consequence of a large heat stored in the melt during previous phases of an accident due to decay heat generation. The importance of transient melting is mentioned in some individual reports but is not commented in details although it is, in fact, most important from the viewpoint of max-of-max of HF. This issue should be studied properly in further investigation (including sensitivity to meshing, which is very important in this problem). It is also important from the viewpoint of relatively moderate values of steady values of HF (Fig. 5-8).

Considered accident scenario:

- Most of users applied nominal initial and boundary conditions proposed by KI (LB DN 850mm). But two calculations were done on the base of another scenario DN 200 (TUS ASTEC and UJV MELCOR), and the obtained results are close to most pessimistic (max-of-max of HF of 1.8 MW/m^2). These results emphasize again the importance of more detailed analysis of first stage of accident scenarios mentioned above and commented in the individual report of UJV.

Separation of the results:

- As it may be seen from Figs. 5-1, 5-4, the calculated values of absolute maximum of HF may be divided on two groups: very large values (more than 1.8-2MW/m^2), most of which are peaked, and moderate values (less than 1.5 MW/m^2). The reason of sharp time peak is in the above mentioned transient melting – the initial heat stored in the melt is quickly transferred to wall, and after that maximum of HF is moderate. The PROCOR result is an exception. The possible reason of its slow increase of max HF may be in some features and details of the modelling: adiabatic heating at first time – the is not spend, heat store is greater than it would be; the absence of axial heat conductivity of RPV wall, which diffuse heat to upper region of the wall and smooth sidewall HF peak. So, the result of PROCOR calculation should be set aside for further precision. The same may be referred to the mentioned cases with DN 200 scenario – additional more consideration is required of the effect of accident first phases. In calculations of EDF MAAP (as it may be seen from the pictures in individual report) the maximum of heat flux is likely due to additional layer of thin steel put above the light metal layer. The coexistence of these two metallic layers separated by thin crust seems not fully justified, hence this result may also be separated for further study and tuning.

To conclude, it may be noted that the "extra high" maxima of HF were mostly obtained in the calculations required additional tuning to converge their conditions to that used as standard in the benchmark. The exception is the result of VTT ASTEC, and the reason of the differences with different results requires careful study.

In the current stage of investigation the value of maximum HF in "residual" results is about 1 MW/m^2 and is not much greater than steady value. Because of above mentioned importance of transient phase and "non-separated" result of VTT ASTEC, the investigations giving the value of 1 MW/m^2 also seem not fully complete. But, likely, they give the low margin of external HF. Essentially, that it is not peaked.

Very preliminary data for experimental investigations may be the following:

– steady thermal loads of 1 MW/m^2 maximum;

– transient peaked loads (200–500s) up to 2 MW/m^2.

5.2 CFD codes

The assumed scenario is a meltdown of a reactor core, similar to the Fukushima event, applied to a VVER1000 reactor and evaluated with CFD tools. The completely molten Reactor core is assumed to be situated in the lower reactor plenum at the beginning. The initial residual heat source is ca. 32 MW, decreasing with time. Furthermore, it is assumed that the operators have flooded the reactor pit around the lower plenum with cooling water. The heat is transferred through the vessel wall into cooling water in the reactor pit.

The goal of this computation is to compare results of different CFD codes and of system codes. Computations have been done for this comparison by JRC, EDF and UJV.

The JRC presents a transient two-dimensional computation for the lower plenum with the software tool ANSYS CFX. The model includes the boiling coolant domain (RPI model[5]), the solid reactor pressure vessel wall, and a fluid stratified two-layer corium domain. Saturated water is inserted at the bottom and a vapour-liquid mixture leaves the domain at the top. Heat transport from the corium through the wall into the evaporating coolant is shown as well as the heat flux density along the wall, temperatures, and velocities for the fluid domains and the volume fractions for the coolant. Typical velocities for the coolant are ca. 3 m/s and at the outlet ca. 7 m/s. Maximum heat flux density is slightly below 0.8 MW/m^2. The computation demonstrates a natural convection effect in the channel, created by a deflector along the wall. A coarse estimation can be done for the ablation of the wall. Based on the temperature field within the wall it can be assumed that a few centimetres (ca. 6.5 cm) of the steal remain below melting temperature, though this estimation is preliminary and not conservative.

The EDF modelling for the VVER1000 is based on a steady-case two-dimensional 15 cm slice for the software package Neptune CFD. The heat flux is imposed at the outside surface of the vessel and the coolant behaviour is studied. The heat flux profile for the boundary condition is obtained by a SOCRAT computation. The water inventory is regulated at the top by recirculation of the liquid fraction. Velocities in the coolant are shown and the natural convection along the wall and a deflector. Peak coolant velocities are in the range from ca. 3 m/s up to ca. 7 m/s. A heat flux density profile along the wall is shown; the maximum value is at ca. 1.3 MW/m^2.

The UJV presents simulations with the Fluent 13 CFD code and the RELAP code. A large break LOCA scenario is considered. The phases of the corium are partly solid, hence melting and solidification effects take place. The Fluent model is two-dimensional and the phases immiscible and the wall do not melt. A heat flux is adjusted at the top surface of the metal phase. Velocities, temperatures, and volume fractions for the corium domain are shown. The presented heat flux densities along the wall show peaks of ca. 1.21 MW/m^2 and ca 1.91 MW/m^2, depending on a variation of the inserted heat. The RELAP model is one-dimensional. Studies with a deflector and without it are performed. The shape of the heat flux boundary is taken from the SOCRAT/HEFEST code. The reactor cavity is either filled with water or the level is varied for sensitivity studies. The resulting heat flux densities peak is in the range 1.2-1.3 MW/m^2 and the maxima of the temperatures at the outer wall surface are about 180 °C. Case studies show that the existence of the deflector enhances the cooling effect; particularly for large heights and low gap width. Further studies show that a certain variation can be shown for the evaluation of the critical heat flux. CFD computations of the melt show profiles for the wall heat flux density which peak at a height of ca. 1.6 m and at ca. 1.05 MW/m^2 and 1.21 MW/m^2.

The EDF simulation with ULPU-V for a Westinghouse AP1000 reactor represents the whole coolant flow between the walls of the reactor pit and the vessel. The model is based on slice geometry of 1/84th for the Neptune CFD with bubbly flows. The void fraction of the coolant is shown for the maximum heat flux of 2.4 MW/m^2. The hydrostatic pressure influences the behaviour of the void fraction. Sub-cooled boiling can be observed and steam re-condensation beyond the heat source. Velocities in the downcomer are well predicted and they are in the range of about 0.5-0.6 m/s.

[5] The wall boiling phenomenon is modelled by the RPI nucleate boiling model of (Kurual and Podowski,1991) and an extended formulation for the departed nucleate boiling regime (DNB) by (Lavieville et al, 2005).

Even though the computations have been performed independently and are based on different assumptions and techniques, the results display considerable similarities: the coolant velocities along the outer vessel wall are typically in the magnitude of slightly above 3 m/s as shown by both JRC (Figure 3 and Figure 6 of the Annex A.11 JRC CFD with Ansys) and by EDF (Figure 2 of the Annex A.12 EDF CFD with NEPTUNE_CFD) and the maximum coolant velocities are computed to be above 7 m/s by both codes. The results for the heat flux density of the three codes display certain differences (Annex A.11 Figure 14, Annex A.12 Figure 4, and Annex A.13 Figure 10); however, the comparison is satisfying considering the differences of the approaches.

Some references

R.O. Gaunt et al., MELCOR Computer Code Manuals, Vol.2 Reference Manuals, Version 1.8.6 September 2005, NUREG/CR6119, SAND 2005-5713, September 2005

N. Kurual and M. Z. Podowski. "On the modelling of multidimensional effects in boiling channels". In Proceedings of the 27th National Heat Transfer Conference, Minneapolis, Minnesota, USA. 1991.

J. Lavieville, E. Quemerais, S. Mimouni, M. Boucker and N. Mechitoua. "NEPTUNE CFD V1.0 Theory Manual". EDF. 2005.

6 Summary of past experiments for IVMR and existing approaches

The purpose of this section is to explain the basic steps of the demonstration and calculation of heat fluxes and the assumptions which are made in almost all of the codes used in the benchmark. It follows the initial methodology of (Theofanous et al., 1997) with minor adaptations. Therefore, it was not intended to make the most accurate evaluation of the heat fluxes in the case of VVER-1000, with the specific shape of the vessel and the specific properties of VVER-steel. The codes used in the benchmark are supposed to provide those accurate results. Therefore, it is not really important if there is 15% less power in the oxide or if the Rayleigh number is twice as large or if the melting temperature of steel is 1750K instead of 1600K. In the end, this will make less than 20% difference in the heat fluxes. It was shown in NUREG/CR-6849, 2004 that the choice of correlations for heat transfers is insignificant compared to other uncertainties like the mass of steel or the release of volatile fission products.

Moreover, there are several uncertainties in material properties and correlations so it is not reasonable to expect that we can estimate the heat fluxes with less than 20-30% error. The choice of "best-estimate" material properties, correlations and assumptions is out of the scope of this section which focuses on the methodology of calculation.

6.1 Presentation of existing approaches

The concept of in-vessel retention of molten corium by external cooling of the vessel lower head was introduced about 20 years ago (Tuomisto and Theofanous, 1994) for the Loviisa reactor (VVER-440). It is represented schematically in Figure 6-1. It was first applied to two designs of reactors: the AP600 (Theofanous et al, 1997) and the VVER-440 (Kymailainen, Tuomisto and Theofanous, 1997). The VVER-440 case has led to a practical application at the Loviisa plant where IVMR is a part of the severe accident management. The AP600 design was not further developed but it was later replaced by the AP1000 design (NUREG/CR-6849, 2004), keeping the option of IVMR.

In parallel, other designs involving IVMR were examined, such as APR-1400 (Rempe et al., 1994, Knudson et al., 1994), SWR-1000 (BWR-type, also known as KERENA)(Schmidt et al, 2001), VVER-640 (Dombrosky et al., 2007) but similar methodology was used, with only slight changes in the basic steps followed but some improvements coming from knew knowledge.

The methodology involves 2 or 3 steps, depending on the reactor power:

1. Identification of accidents sequences with fast and massive relocation of molten corium into the lower plenum (with the associated probability). Typically, those sequences are LBLOCA without availability of safety injections which lead to a complete core uncovery in less than an hour and relocation down to the lower plenum quickly after core uncovery. In such sequences, as the one selected for this benchmark exercise, the residual power in the relocated corium corresponds to approximately 1.5% of the nominal thermal power. Other sequences are less challenging for IVMR because the residual power is lower. For the present case of VVER-1000, that gives a total residual power of approximately 38 MW (at 5000s after scram) which has to be extracted thanks to the external reactor vessel cooling (ERVC) loop. This value is quite high and, for example in (NUREG/CR-6849, 2004), the authors consider that such sequence has a low probability and that the most likely value of residual power would be in the range between 23 MW and 29 MW. We can note that, in the present exercise, the "steady-state" is reached approximately at 20000s after scram, for a residual power of 25MW, which is in the range considered for the AP1000 case.
2. For initial conditions (i.e. mass of corium, its composition, temperature and residual power) corresponding to the sequences identified at the previous step, evaluation the heat flux profile along the vessel, evaluation of the thickness of the vessel (which is significantly reduced at the location of maximum heat flux) and determination of the margin with respect to the expected CHF outside the vessel was carried out. At this point, there are two possibilities:
    a. At any location along the vessel, the heat flux is lower than the local CHF with reasonable margin and the residual vessel thickness is enough to withstand the mechanical load: this demonstrates the possibility of cooling down the corium with external cooling. This is the

case for the Loviisa VVER-440 as demonstrated in (Kymailainen, Tuomisto and Theofanous, 1997).

b. At some locations, the heat flux is higher or very close to the local CHF, or the residual vessel thickness is too low for mechanical resistance: this indicates that vessel failure is likely and the associated probability has to be estimated. This is the case of the AP1000 design, as explained in (NUREG/CR-6849, 2004), where the conditional probability of vessel failure may reach 30%, depending on the assumptions considered.

3. For the cases where vessel failure was considered likely, one should evaluate the consequences of the energetic interaction between molten corium and water outside the vessel. The possibility of steam explosion has to be assessed. The impact on the containment has to be evaluated. It is necessary to demonstrate the containment integrity is preserved even in case of vessel failure leading to corium interaction with water. This part of the methodology is not explained in more details here as it is not the scope of the present benchmark which is dedicated to the assessment of the second step described above.

It is important to keep in mind that the demonstration is probabilistic and that it is not sufficient to demonstrate that the most probable value of the maximum heat flux is lower than the most probable value of the local CHF.

6.1.1 Evaluation of heat fluxes

It is important to realize that the methodology used for the assessment of heat fluxes assumes implicitly that a steady state is reached and all the correlations used are only valid for steady state.

The methodology was established initially for a configuration of materials in the lower plenum where all the corium materials (UO_2, Zr, ZrO_2) were mixed in the "oxide pool" and the "metal layer" contained only steel and was located above the oxide pool because of its lower density. With the knowledge gained after OECD/MASCA program about the possible existence of a heavy metal layer located below the oxide pool, some of the analyses were revised thanks to the introduction of alternative configurations of materials with 3 layers (possibility of co-existence of a heavy metal and a light metal, respectively below and above the oxide pool, considered as an alternative configuration in the AP1000 analysis, as described in (NUREG/CR-6849, 2004). For the sake of simplicity, we will follow here the initial methodology, as described in (Theofanous et al, 1997) and in (Kymailainen, Tuomisto and Theofanous, 1997). This is sufficient to understand the main assumptions governing the evaluation of the heat flux profile along the vessel. We will use the conditions chosen for the benchmark exercise to illustrate the methodology with estimates of the main calculated parameters.

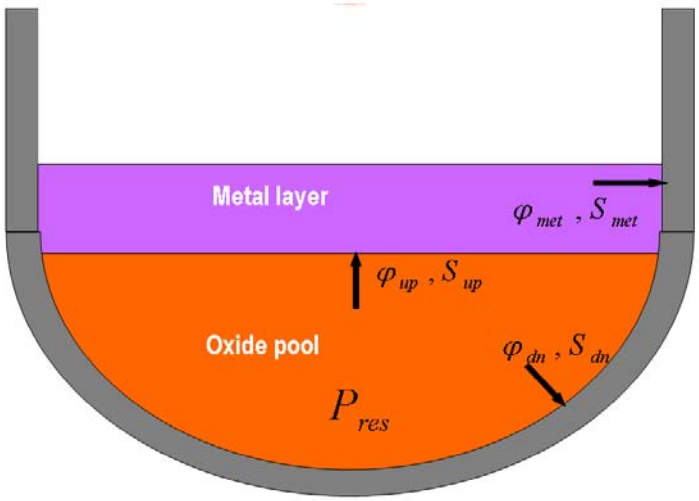

Figure 6-1: Schematic view of the classical configuration and the heat fluxes to estimate

Main steps of the evaluation of the heat flux profile:

Step 1: Determination of the temperature of the oxide pool.

It is assumed that **all the residual power is produced in the oxide pool**. The governing parameter is the internal Rayleigh number:

$$Ra_{ox} = \frac{g\beta_{ox}\dot{Q}_{ox}H^5}{\alpha_{ox}k_{ox}\nu_{ox}}$$

In the present case, the oxide pool would have a height $H \approx 1.15m$. It is reasonable to assume that volatile fission products have escaped which corresponds to a reduction of the residual power in the oxide pool of 20%. Therefore, at the beginning, we have a residual power of 30.4MW corresponding a volumetric power $\dot{Q}_{ox} \approx 2.7MW/m^3$, giving $Ra_{ox} = 8{,}36.10^{14}$. Later, when "steady-state" is reached (approx. 20000s), we have residual power of 20MW, corresponding to a volumetric power $\dot{Q}_{ox} \approx 1.8MW/m^3$, giving $Ra_{ox} = 5{,}5.10^{14}$.

There is a partition of that power and one part is transferred to the vessel wall ($\varphi_{dn}S_{dn}$) and the complementary part is transferred to the top metal layer ($\varphi_{up}S_{up}$).

$$\varphi_{dn}S_{dn} + \varphi_{up}S_{up} = P_{res}$$

Heat fluxes are evaluated thanks to experimental correlations, assuming that **the oxide pool is surrounded by a crust which imposes a uniform boundary condition** at the liquidus temperature of the oxide mixture: T_{liq}^{ox}. With this assumption, both heat fluxes are expressed as a function of the temperature difference $\left(T_{pool}^{ox} - T_{liq}^{ox}\right)$.

$$\varphi_{dn} = \frac{k_{ox}}{H}Nu_{dn}\left(T_{pool}^{ox} - T_{liq}^{ox}\right); \varphi_{up} = \frac{k_{ox}}{H}Nu_{up}\left(T_{pool}^{ox} - T_{liq}^{ox}\right)$$

With:

$$Nu_{dn} = a_{dn}Ra_{ox}^{\ b_{dn}}; Nu_{up} = a_{up}Ra_{ox}^{\ b_{up}}$$

If we choose Mayinger correlation for the bottom and Kulacki-Emara correlation for the top, we get:

$$Nu_{dn} = 0.345Ra_{ox}^{\ 0.2}; Nu_{up} = 0.55Ra_{ox}^{\ 0.2}$$

From that, we directly get the temperature of the oxide pool:

$$T_{pool}^{ox} = T_{liq}^{ox} + P_{res}\frac{H}{k_{ox}}\left(Nu_{dn}S_{dn} + Nu_{up}S_{up}\right)^{-1} = T_{liq}^{ox} + 200$$

where the liquidus temperature of the oxide is variable but may be estimated at $T_{liq}^{\ ox} \approx 2850K$

Step 2: Determination of the partition of power between top and bottom.

One important point is that, with the assumptions chosen, the partition of residual power between bottom and top is independent of the boundary conditions and depends only on the internal Rayleigh number and on the shape of the vessel:

$$\varphi_{up}/\varphi_{dn} = Nu_{up}/Nu_{dn} = \frac{a_{up}}{a_{dn}}Ra_{ox}^{\ \left(b_{up}-b_{dn}\right)}$$

$$\frac{\varphi_{up} S_{up}}{\varphi_{up} S_{up} + \varphi_{dn} S_{dn}} = \frac{Nu_{up} S_{up}}{Nu_{up} S_{up} + Nu_{dn} S_{dn}} = 0.57$$

Therefore, we see that more of 50% of the residual power is transferred to the top metal layer, independently of the boundary conditions. It is also interesting to notice that this partition factor does not change much over the first hours (it varies from 0.57 to 0.56 between 5000S and 20000s).

The bottom and top heat fluxes are:

$$\varphi_{dn} = 0.66 MW/m^2 \rightarrow 0.42 MW/m^2$$

$$\varphi_{up} = 1.29 MW/m^2 \rightarrow 0.85 MW/m^2$$

Step 3: Determination of the maximum heat flux in the bottom part.

Correlations derived from experimental data provide the heat flux profile along the vessel wall.

$$Nu(\theta)/Nu_{dn} = f(\theta)$$

The maximum value is found at the top. This distribution function is difficult to find in the literature for a semi-elliptic vessel. There are data coming from COPO II Lo experiment (Helle et al. 1998) which indicating a "peaking factor" up to 2.5. But these results have not been confirmed by other experiments. If we use the profile proposed by (Theofanous et al, 1997) for a hemispherical vessel, we get a "peaking factor" of 1.8 and, therefore:

$$\varphi_{dn}^{\max} = 1.17 MW/m^2 \rightarrow 0.78 MW/m^2$$

This range of heat flux remains lower than the CHF values that were measured in experiments like ULPU or SULTAN but they are rather close, indicating a limited margin.

Step 4: Determination of the heat flux along the top metal layer.

For the metal layer, natural convection is driven by the contact with the hot oxide pool and the cooling along the side wall and also, possibly, at the top of the metal layer (radiative heat transfer). The standard Rayleigh number is used:

$$Ra_{met} = \frac{g\beta_{met}\left(T_{pool}^{met} - T_{liq}^{wall}\right)H_{met}^{3}}{\alpha_{met}\nu_{met}}$$

The expression of the heat flux along the side wall is:

$$\varphi_{met} = \frac{k_{met}}{H_{met}} Nu_{met}\left(T_{pool}^{met} - T_{liq}^{wall}\right) = \frac{k_{met}}{H_{met}} a_{met} Ra_{met}^{\ b_{met}}\left(T_{pool}^{met} - T_{liq}^{wall}\right)$$

Where, using the Globe-Dropkin correlation, we have the exponent b_{met}=1/3, leading to:

$$\varphi_{met} = a_{met} k_{met}\left(\frac{g\beta_{met}}{\alpha_{met}\nu_{met}}\right)^{1/3}\left(T_{pool}^{met} - T_{liq}^{wall}\right)^{4/3}$$

Here, we assume that there is no heat loss from the top (conservative assumption neglecting radiative heat transfer with upper structures, the calculation with radiative heat transfer is much more complex), the conservation of energy gives:

$$\varphi_{up} S_{up} = \varphi_{met} S_{met}$$

We recall that, because of the partition of energy found previously, this is equivalent, in the present case, to the relation:

$$\varphi_{met} S_{met} = 0.57 P_{res}$$

Therefore we obtain, for the heat flux along the metal layer (for a height of metal layer estimated to 92cm, corresponding to 80t of steel and some Zircaloy):

$$\varphi_{met} = 1.43 MW / m^2 \rightarrow 0.95 MW / m^2$$

The case with 30t of Steel is much more challenging (with a height of metal layer estimated to 44cm):

$$\varphi_{met} = 3.0 MW / m^2 \rightarrow 1.98 MW / m^2$$

We remind here that the case with 30t of Steel is less realistic if we consider SOCRAT calculations as a reference. However, it was decided in this benchmark exercise to include this case as a minimum value for the mass of Steel.

In both cases, the heat flux in the metal layer is higher than in oxide pool, which is the illustration of the focusing effect. But this effect is limited when the thickness of metal is close to 1m. We also have to keep in mind that we have neglected the radiative heat transfer from the top of the layer, making this result quite conservative. The case with 30t of Steel is critical because heat flux exceeds the CHF values that were measured in experiments like ULPU or SULTAN indicating that vessel failure would be likely for that scenario.

The temperature of the metal pool, in the case $\varphi_{met} = 0.95 MW / m^2$, is obtained by:

$$T_{pool}^{met} = T_{liq}^{wall} + \left(\frac{\varphi_{met}}{a_{met} k_{met}} \right)^{3/4} \left(\frac{\alpha_{met} \nu_{met}}{g \beta_{met}} \right)^{1/4} \approx T_{liq}^{wall} + 130$$

where the melting temperature of the wall for VVER carbon steel is usually estimated at $T_{liq}^{wall} \approx 1600\, K$

Step 5: Determination of the minimum thickness of vessel wall.

Along the vessel wall, the identification of the heat flux imposed by the molten pool and the heat flux across the wall provides the wall thickness:

$$\delta_w = \frac{k_w (T_{liq}^{wall} - T_{ext}^{wall})}{\varphi_{met}}$$

In case of a high heat flux of 2 MW/m^2, and taking into account the conductivity of VVER steel which is higher (about 35 W/m/K instead of 19 W/m/K for “standard” steel), we obtain a residual thickness of:

$$\delta_w \approx 2cm$$

Such thickness is sufficient, in principle, to withstand the thermal and mechanical load, as it is demonstrated in (Theofanous et al, 1997), where they indicated that even 5 mm would be enough. Of course, this has to be evaluated carefully as the mechanical resistance depends on the quality of steel, the shape of the vessel, the internal pressure and the temperature gradient across the wall thickness.

6.1.2 Conclusion

The classical methodology, using some conservative assumptions, and neglecting the impact of possible alternative configurations of layers gives the following results, at 20000s after scram, for a total amount of 80t of steel:

$$\varphi_{met} = 0.95 MW / m^2$$

$$\varphi_{dn}^{\max} = 0.78 MW / m^2$$

For 30t of steel, the focusing effect is more important and reaches $\varphi_{met} = 1.98 MW / m^2$, which is likely to be higher than the local CHF.

Immediately after corium relocation (5000s after scram), heat fluxes estimated with the same methodology are even higher. Therefore, it is very important to understand what happens between the instant of massive corium relocation into the lower plenum and the instant when turbulent natural convection is fully established in the oxide pool and in the metal layer.

6.1.3 Additional assumptions and alternative configurations

The methodology described above does not take into account some physical or chemical processes which are known to occur in the corium. Therefore, it is possible to make more accurate calculations by introducing:

- Thermochemical interactions between oxide and metal phases, changing their compositions and possibly leading to the formation of a heavy metal layer located below the oxide pool. This may have a very significant effect on the heat flux in the metal layer.
- Distribution of a fraction of the residual power into the metal phase.
- Radiative heat transfer at the top of the metal layer (less conservative). This effect may be significant for a shallow metal layer on top.
- Alternative heat transfer correlations for natural convection in the oxide pool and in the metal layer. However, their effect is not significant, as shown in (NUREG/CR-6849, 2004).

Some references

Tuomisto H. and Theofanous T.G., "A consistent approach to severe accident management", Nuclear Engineering and Design, 148, 1994

Theofanous T.G., Liu C., Addition S., Angelini S., Kymälainen O. and Salmassi T., "In-vessel coolability and retention of core melt", Nuclear Engineering and Design, 169, 1997

Kymälainen O., Tuomisto H. and Theofanous T.G., "In-vessel retention of corium at the Loviisa plant", Nuclear Engineering and Design, 169, 1997

Esmaili H., Khatib-Rhabar M. and Basu S.., "Analysis of in-vessel retention and ex-vessel fuel coolant interaction for AP-1000", NUREG/CR-6849, ERI/NRC 04-201, 1997

6.2 Summary of Past In-Vessel Retention Experimental Studies

6.2.1 SONATA-IV Program

Korea Atomic Energy Research Institute (KAERI) has been conducting (1997-2001) a large experimental program on in-vessel debris coolability and retention named SONATA-IV (Simulation Of Naturally Arrested Thermal Attack In Vessel). The objective of this research project was to gather proof of the non-adherence of the debris to the lower head of reactor pressure vessel (RPV) and the consequent gap formation between the debris crust and the lower head wall, to investigate the possibility of in-vessel debris cooling through this narrow gap and to evaluate the effect of the gap formation on in-vessel retention. Through the total of 12 LAVA (Lower-plenum Arrested Vessel Attack) tests, the analyses on the melt relocation process, gap formation and the thermal and mechanical behaviours of the vessel were performed. Al_2O_3/Fe thermite melt was used in the tests to simulate an oxide molten pool with upper metallic layer. The corresponding experimental facility is shown in Figure 6-2.

LAVA experimental results confirmed that a continuous gap ranging from 1 to 5 mm was formed and that maximum heat removal capacity through the gap is a key factor in determining the potential of the integrity of the vessel. It was found from the results that the possibility of In-Vessel corium Retention

(IVMR) through gap cooling highly depends on the melt mass relocated into the lower plenum and the gap size.

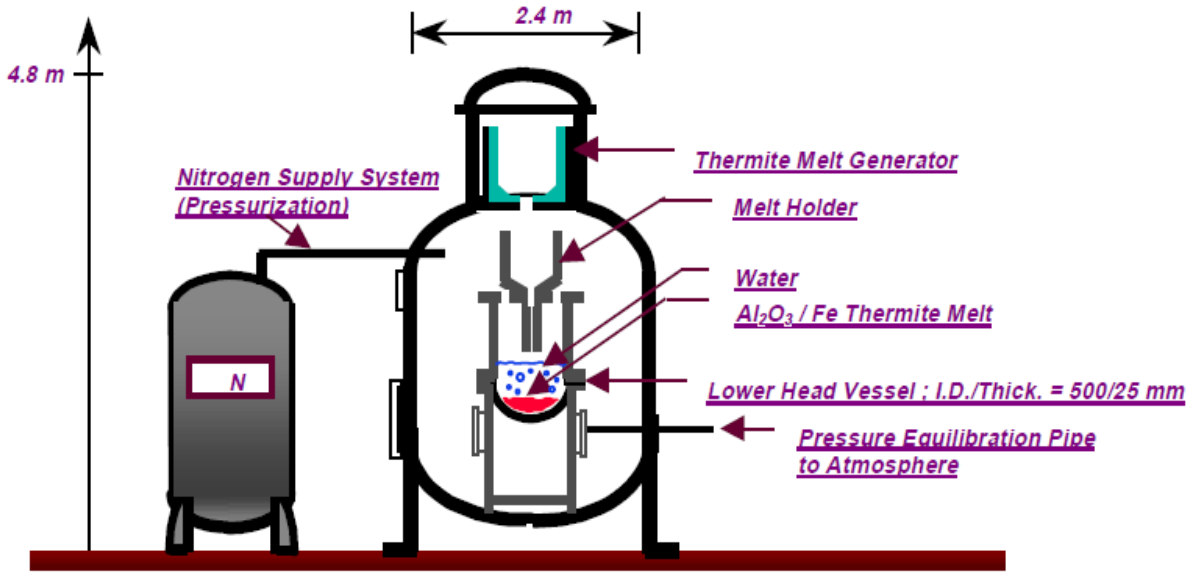

Figure 6-2: LAVA Experimental Facility

Some references

J.H. Kim et al., "Experimental Study on Inherent In-Vessel Cooling Mechanism during a Severe Accident", 7th International Conference on Nuclear Engineering, ICONE-7085, Tokyo, Japan, April 19-23, 1999.

K. H. Kang, et al., ''Evaluations of the coolability through the inherent in-vessel gap cooling in the LAVA experiments,'' Proc. 10th Int. Conf. on Nuclear Engineering (ICONE-10), Arlington, VA, April 14–18, 2002, No. 22230, (2002).

Kang, K. H., R. J. Park, W. S. Ryu, S-B. Kim, K.Y. Suh, F-B. Cheung, and J. L. Rempe, "Thermal and Metallurgical Response of the In-vessel Core Catcher According to the Gap Size with the Lower Head Vessel," International Congress on Advances in Nuclear Power Plants (ICAPP '04), Pittsburgh, PA, USA, June 13-17, 2004.

K. H. Kang et al., "Experimental Investigations on In-Vessel Corium Retention through Inherent Gap Cooling Mechanisms," Journal of Nuclear Science and Technology, Vol. 43, No. 12, p. 1490–1500 (2006).

6.2.2 ALPHA Program

In-vessel debris coolability experiments ALPHA (Assessment of Loads and containment Performance in Hypothetical Accident) have been performed at Japan Atomic Energy Agency (JAEA). In these tests, 30 kg and 50 kg molten aluminium oxide (Al_2O_3) produced by a thermite reaction as a corium simulant was poured into a 0.3 m deep water pool in lower head experimental vessel (LHEV). As indicated in Figure below, the experimental apparatus consisted of a thermite melt generator, a lower head experimental vessel, and water and nitrogen supply systems. The ALPHA containment vessel was pressurized to 1.3 MPa during the experiments, and nearly saturated water was used (450 K at 1.3 MPa). Only the aluminium oxide produced by the thermite reaction between aluminium with iron oxides was delivered into the 0.5-m-diameter carbon steel vessel lined with stainless steel. Figure 6-3 shows the schematic diagram of the ALPHA experimental facility.

Post-test examination with an ultrasonic technique and thermal responses of the LHEV wall showed that the interfacial gap was formed between the solidified Al_2O_3 and the LHEV wall. The LHEV temperature was sharply increased at the beginning of the experiments. The observed temperature increase rate was much smaller than a calculated value based on heat conduction through the LHEV wall. Later, steep temperature decrease was found on the LHEV outer surface while Al_2O_3 was kept at a high temperature. It is supposed that the gap acted as a thermal resistance during the heat-up stage and water subsequently penetrated into the gap resulting in an effective cooling of the LHEV wall. The

maximum heat flux at the inner surface of the LHEV facing to Al_2O_3 was roughly evaluated between 320 kW/m^2 and 600 kW/m^2.

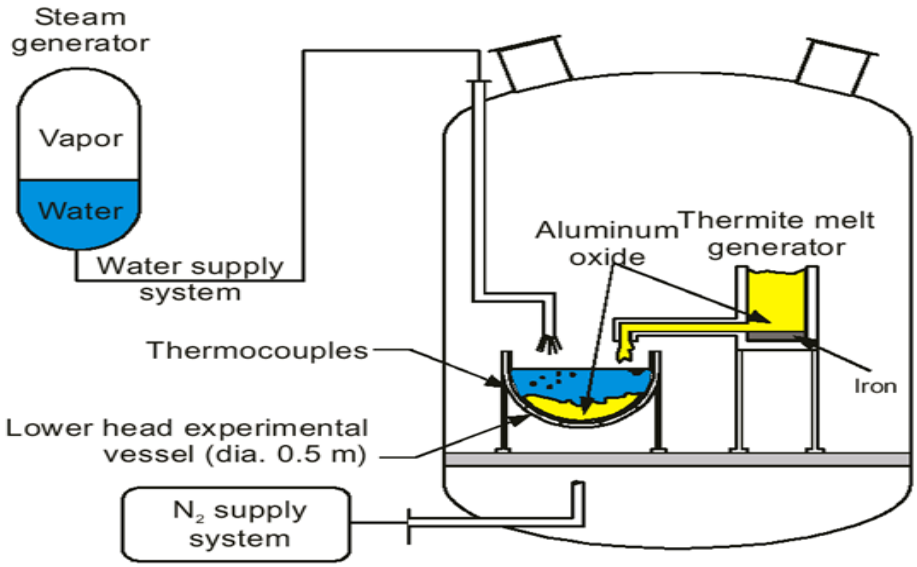

Figure 6-3: ALPHA Experimental Facility

Some references

Y. Maruyama, et al., ‘‘Experimental study on in-vessel debris coolability in ALPHA program,’’ Nuclear Engineering & Design, 187, 241– 254 (1999).

Maruyama, Y., et al., “Analysis of Debris Coolability Experiments in ALPHA Program with CAMP Code,” Ninth International Topical Meeting on Nuclear Reactor Thermal Hydraulics (NURETH-9), San Francisco, California, October 3-8, 1999.

T. Kohriyama, M. Murase, T. Nagae, Y. Okano, and A. Ezzidi, “Validation of heat transfer models in narrow gap for RELAP/SCDAPSIM/MOD3.2,” Nuclear Technology, vol. 147, no. 2, pp. 191–201, 2004.

6.2.3 FAI Limited Scale Integral Experiments

Experiments (6 tests) for IVMR by Ex-Vessel Reactor Cooling (EVRC) were conducted by Henry, et al. (1991) at Fauske & Associates Inc. (FAI), for heat transfer from a downward facing lower head, both with and without vessel insulation. The objective was to investigate the possible limitations to downward facing boiling heat removal due to the insulation, included in the analyses were:

- energy transfer rate potentially imposed on the RPV lower head and cylinder by the accumulated debris;
- ingression of water through the joints between the insulation panels in the lower regions;
- hydrodynamic limitations associated with the two phase heat removal process in the gap region between the insulation and the RPV outer surface;
- steam outflow through the panel junctions in the upper regions of the insulation.

For the experiments, insulation typical of current plants is used to assess this heat removal process for EVRC. The analyses concluded that, for these designs which can submerge the lower head and parts of the vessel cylinder, there is no significant limitation to external heat removal other than heat conduction through the RPV wall. It is also noted that future plants may provide conditions which further reduce any limitations with respect to water availability and removal of the steam produced in the process.

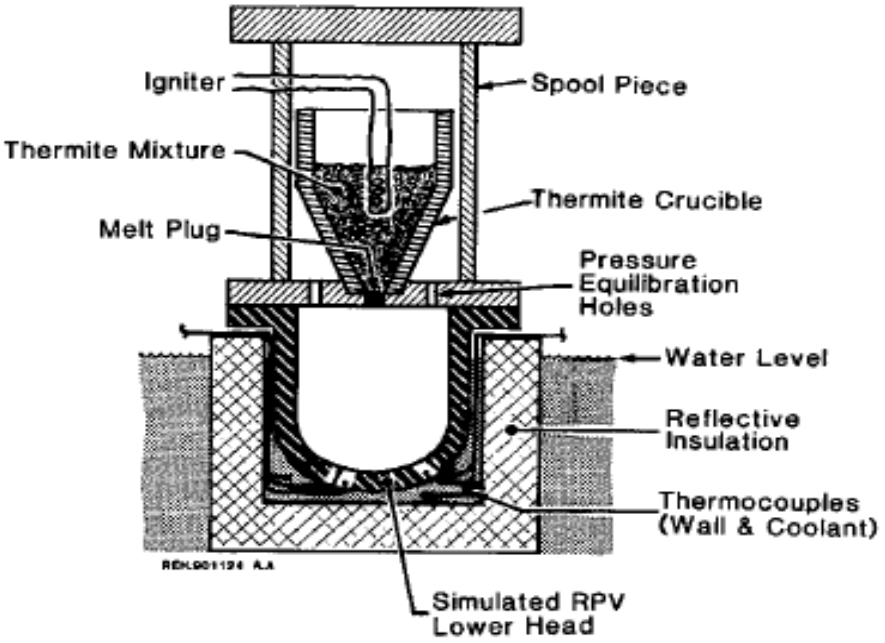

Figure 6-4: Schematic of the experimental apparatus of FAI EVRC

Some references

R. E. Henry and H. K. Fauske, "External Cooling of a Reactor Vessel under Severe Accident Conditions," Nuclear Engineering and Design 139 (1993) 31-43.

R. J. Hammersley, et al., "Experiment to Address Lower Plenum Response under Severe Accident Conditions", PSA International Topical Meeting, Clearwater Beach, FL, pp. 193-198, 1993.

6.2.4 FAI Experimental Study on In-Vessel Cooling Mechanisms

FAI performed several IVMR experiments from 1997 to 2001 in order to investigate in-vessel cooling mechanisms of corium in lower head under different configurations with homogeneous oxide molten pool, an oxide molten pool with upper metallic layer, lower head vessel with penetrations and without penetrations. These experiments were sponsored by different organizations including: EPRI (US), NRC (US), MHI (Japan), Hitachi (Japan), TEPCO (Japan), EDF (France), FKA (Sweden) and ES-konsult (Sweden).

The objectives of these experiments were to examine the non-adherence of debris to vessel wall and the effect on cooling when vessel strain and to address the cooling characteristics when gaps would be formed between reactor vessel and debris crust. Also, effect on cooling characteristics by reflective insulation surrounding the outer surface of the rest vessel and internal structure, and survivability of penetration located at the bottom of the reactor vessel were investigated. This is in order to explain the cooling behaviour observed in TMI-2 with a cooling rate of 10 to 100°C/min after the vessel lower head wall experienced a thermal transient with temperatures reaching values as high as 1100°C.

A total of 9 experiments were performed in two different phases. Phase-1 of the program was called as "Proof-of Principle Test" where a mixture of Al_2O_3 and molten iron were used. In this series of experiments, the primary technical questions to be answered were as follows: (1) when melt (mixture of metallic and oxidic) pours through water, does debris adhere to lower plenum structure?, (2) does the test vessel wall heatup sufficiently to cause vessel strain?, (3) does this influence the cooling rate by the water inside the vessel?, (4) is there any indication of a steam explosion?

Phase-2 experiments used a melt separator to separate molten aluminium oxide from molten iron since molten material in a real reactor should primarily be composed by molten UO_2 and molten ZrO_2. In addition to same objectives as phase-1 experiments, specific objectives of Phase-2 experiments were: (1) is the cooling rate different when the debris is essentially only Al_2O_3 ?, (2) does reflective insulation influence the cooling rate ?, (3) does the configuration of the lower plenum structure influence the

cooling rate ?, (4) does a lower head penetration influence the cooling rate ? Figure below shows the test apparatus used in the experiments.

The major conclusions derived from those nine experiments are summarized as follows:

- Molten debris, whether it is molten iron or molten aluminium oxide, pouring through 30 cm of water and accumulating on the test vessel lower head does not adhere to the vessel wall including the welds of the penetrations;
- Given the significant temperatures that can be achieved when molten material collects on the lower head, the test vessel can undergo strain;
- There was no indication of a steam explosion in any of experiments;
- All the Phase-1 and Phase-2 experiments have detected the existence of small gaps between the test vessel wall and the debris, as well as between the penetration and the debris;
- Phase-1 and Phase-2 experiments detected significant two-phase cooling in the gap between test vessel and debris during quenching process (this is consistent with the observations from the ALPHA experiments of JAEA;
- Configuration of the internal structure in the test vessel has an influence on the cooling mechanisms.

Experiment simulations in different severe accident codes had showed that the codes are either over-predicting the vessel cooling or under-predicting it. The experimental data were to be used by each participant organization to improve or develop its own IVMR boiling heat transfer correlations in its own version of severe accident analysis code (mainly MAAP, MELCOR or SCDAP/RELAP5).

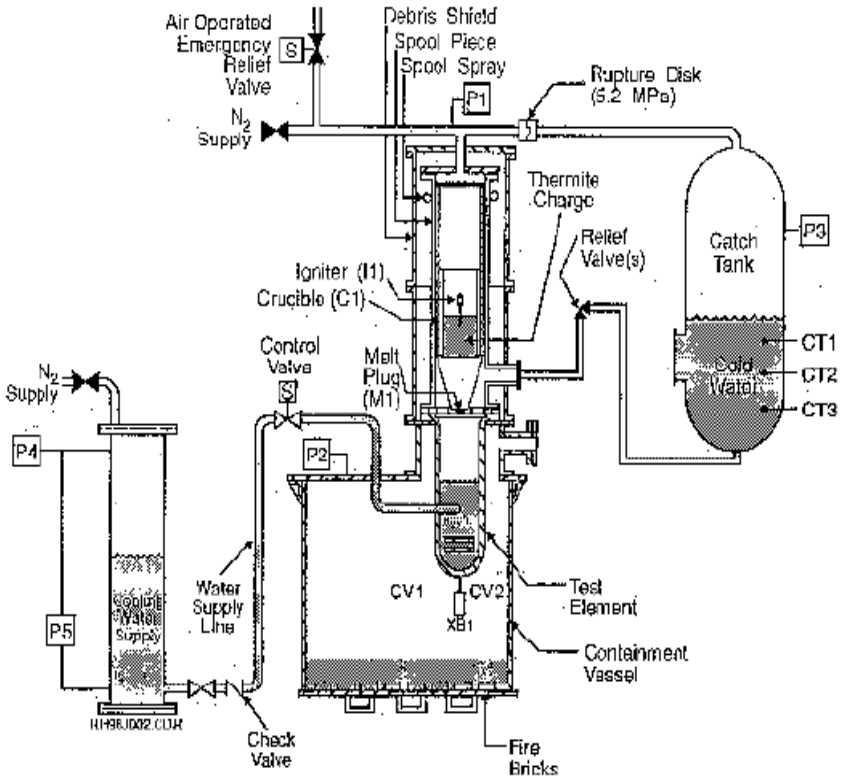

Figure 6-5: Test Apparatus of FAI In-Vessel Cooling Experiment

Some references

J. R. Wolf, et al., TMI-2 Vessel Investigation Project Integration Report, NUREG/CR-6197, TMI V (93) EG10, (1993).

R. E. Henry et al., “Experimental Study on In-Vessel Cooling Mechanisms,” Nuclear Engineering and Design 139 (1993) 31-43.

R. E. Henry et al., “Experimental Study on In-Vessel Cooling Mechanisms,” Nuclear Engineering and Design 139 (1993) 31-43.

R. E. Henry, R. J. Hammersley, ‘‘Quenching of Metal Surfaces in a Narrow Annular Gap,’’ 5th Int. Conf. on Simulation Methods in Nuclear Engineering, (1996).

R.J. Hammersley, R.E. Henry, D.R. Sharp and V. Srinavas, In-Vessel Retention for the AP600 Design during Severe Accidents, presented at the Second Intern. Conference on Nuclear Engineering (ICONE-2), San Francisco, CA, March 21-24, 1993.

R.E. Henry et. al., Cooling of Core Debris within the Reactor Vessel Lower Head, Nuclear Technology, Vol. 101, 385-399 (1993).

K.Y. Suh, R.E. Henry, Debris interactions in reactor vessel lower plena during a severe accident II. Integral analysis, Nuclear Engineering and Design 166, pp.165-178, (1996).

6.2.5 FOREVER Program

Integral scaled coupled melt pool convection and vessel creep failure experiments were performed in the FOREVER program at the Royal Institute of Technology, Stockholm. These experiments were simulating the lower head of a PWR vessel under the thermal load of a melt pool with internal heat sources. Due to the multi axial creep deformation of the three-dimensional vessel with a highly non-uniform temperature field these experiments offered an excellent opportunity to validate numerical creep models.

The hemispherical bottom heads of the experiments considered here (including one made of the French RPV carbon steel 16MND5) had an internal diameter of 188 mm and a wall thickness of 15 mm (Figure 6-6). The applied oxidic melt was a CaO-B_2O_3 mixture (30-70 wt.-%) which had a solidus temperature of Ts=1250 K. To model the internal decay heat generation special designed heater rods fixed to an internal insulation-reflector-lid were immersed into the melt from the top. To initiate the creep process the vessel was pressurized by Argon.

The FOREVER test facility used a 1/10 linear-scaled carbon steel vessel. It was planned to perform experiments with 20 litres binary oxidic melts to study gap formation due to vessel creep. Gap cooling experiments were then performed. Scaling considerations have been investigated and pre-test calculations have been performed with MVITA and ANSYS codes, respectively, for thermal loadings and for creep behaviour.

In these experiments the hemispherical vessels with heated oxide melt, kept at high temperature, were ruptured/cooled. The major findings from these experiments are (1) effectiveness of the gap cooling, (2) a multi-axial creep data base for various vessel steels, (3) effect of penetrations, (4) timing, mode and location of lower head failure, and (5) the fraction of melt discharged to containment.

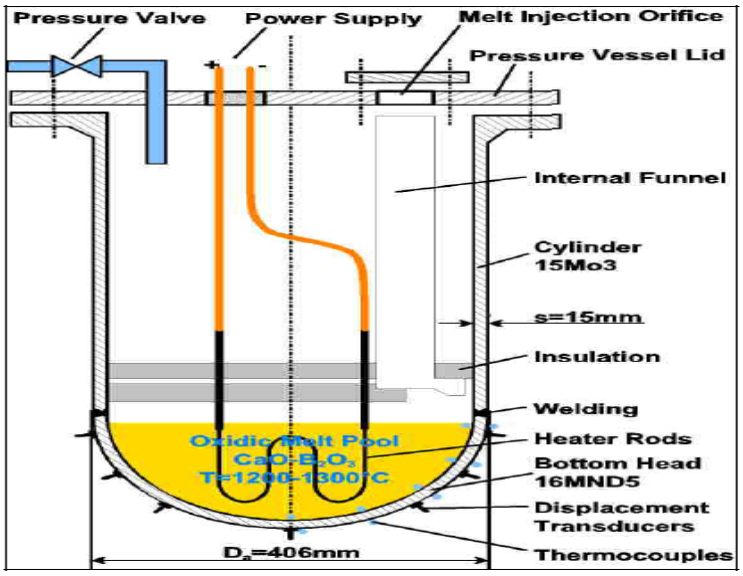

Figure 6-6: Test Apparatus of FOREVER Experiment

Some references

Sehgal, B.R., Nourgaliev, R.R., Dinh, T.N., Karbojian, A., 1999, "FOREVER experimental program on reactor pressure vessel creep behaviour and core debris retention", Proceedings of the 15th International Conference on Structural Mechanics in Reactor Technology (SMiRT-15), Seoul, Korea, August 15-20, 1999.

Willschütz, H.-G., E. Altstadt, B.R. Sehgal, and F.-P Weiss, 2001, "Coupled thermal structural analysis of LWR vessel creep failure experiments", Nuclear Engineering and Design, vol. 208, pp. 265-282.

6.2.6 SULTAN Experiment

This analytical full scale forced convection experiment was performed by French Atomic Energy Agency (CEA) to deal with a wide range of parameters. Critical heat flux (CHF) measurements were made on a large heated plate, which was held at different inclination angles to the horizontal. Data were obtained for different mass flow velocities of cooling water available at different pressures. These data were pertinent to the external cooling of the bottom head, for the scenario of in-vessel melt retention. The obtained CHFs were consistent with those obtained in ULPU experiment.

Based on the measured data a Critical Heat Flux (CHF) correlation was developed, in terms of pressure, mass velocity, steam quality, gap width, and gap inclination. 3-D simulation with the CATHARE code of SULTAN experiment showed the capability of revealing the 3-D effect in the experiment.

The following conclusions were obtained:

- The experiments confirmed high heat transfer coefficients for ex-vessel boiling;
- The plant specific design of RPV, cavity and insulation structure have important impact on the Maximum heat transfer to the external coolant;
- The gravity driven flow is sensitive to steam venting;
- Feasibility studies of ex-vessel cooling must consider the effect of reduced heat transfer due to degradation of insulation, unavailability of flow paths, etc.

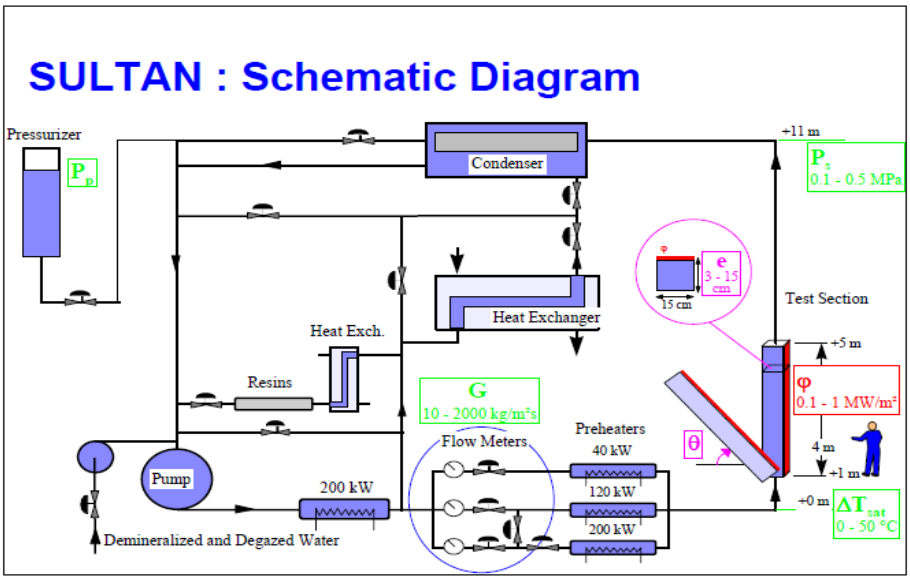

Figure 6-7: SULTAN Schematic Diagram

Some references

Rouge, S., "SULTAN Test Facility for Large-Scale Vessel Coolability in Natural Convection at Low Pressure," Nuclear Engineering and Design, Vol. 169, pp. 185-195, 1997.

Rouge, S., et al.., "Reactor Vessel External Cooling for Corium Retention SULTAN Experimental Program and Modelling with CATHARE Code," Workshop Proceedings on In-Vessel Core Debris Retention and Coolability, NEA/CSNI/R (98) 18, Garching, Germany, 1999.

Theofanous, T. G. et al., "Limits of Coolability in the AP1000-Related ULPU-2400 Configuration V Facility," Paper G00407, Tenth International Topical Meeting on Nuclear Reactor Thermal Hydraulics, NURETH10, October 5-11, 2003, Seoul, Korea.

6.2.7 LIVE Experiment

LIVE test was performed in the frame of the SARNET2 Project for debris melting process in a simulated PWR lower head. It was aimed at providing input data for different debris cooling concepts and general severe accident management.

The LIVE-L8B experiment was performed following many other programs such as POMECO, DEBRIS, PRELUDE, STYX investigated debris cooling effect by top flooding, bottom flooding or flooding with down-comer under various configurations of debris bed and its conditions. The initial debris temperature was considered as one of the parameters which affect the steam generation rate and cooling effect. The cooling effect of debris with homogenous temperature has been investigated in PRELUDE facility. Other studies gave efforts to determine the temperature distribution of a non-homogenous debris bed under water. Therefore the main objective of LIVE-L8B test was to characterize the temperature distribution in debris under boil-off situation. It was also of interest to characterize the crust properties which define the heat transfer boundary condition from crust to vessel during the melting down process of debris bed.

Also, LIVE-L6 experiment was performed in order to clarify the contradictions observed between COPO II and BALI experiments performed in 2D slice geometry on the one side and ACOPO 3D experiments on the other side concerning downward/upward heat fluxes ratio was one of the examples. It was noted that this ratio would be important in the reactor case since it determines the amount of heat transferred to the upper metallic layer and thus the strength of the focusing effect.

LIVE facility consisted mainly of a hemispherical test vessel with a diameter of 1m (see Figure 6-8). The top area of the test vessel was insulated and cooled with a water container. The test vessel was enclosed in a cooling vessel to enable vessel external water cooling. The decay heat of the melt was simulated by 8 planes of heating coils, which could be controlled individually to simulate homogenous

heat generation. The melt was prepared in a separated heating furnace and could be poured into the test vessel either centrally or near the vessel wall. At the end of test a vacuum pump extracted the residual melt back to the heating furnace, thus the crust at the wall remained in the vessel.

The simulant material used for the debris bed in the vessel and the relocating corium was a non-eutectic binary mixture of KNO_3-$NaNO_3$. The debris bed and the corium accounted each 50% of the total core material in the lower head. The temperature distribution of debris bed before melt relocation could be interpreted with a 2D diagram showing the region of the highest temperature and the temperature gradient in the debris bed. After melt relocation into the debris bed, the form and the volume of the liquid region during the melting process were evaluated. Also the timings of some important stages are obtained.

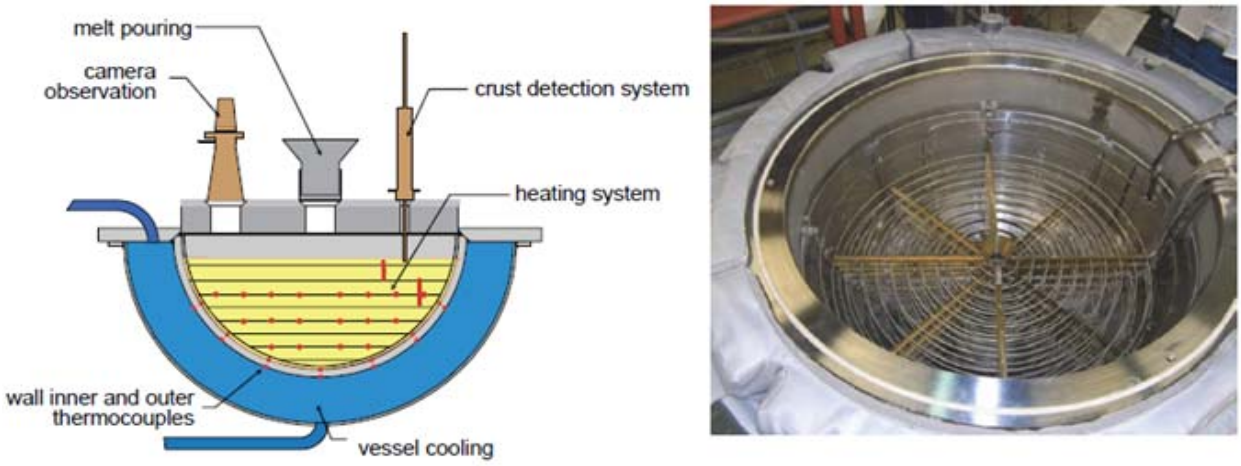

Figure 6-8: LIVE Test Facility with open Vessel with Heating Coils

Some references

J.-P V. Dorsselaere, F. Fichot, J.-M Seiler, Views on R&D needs about in-vessel reflooding issues, with a focus on debris coolability, Nuclear Engineering and Design pp. 236, 1976–1990 (2006).

D. Magallon, et al., European expert network for the reduction of uncertainties in severe accident safety issues (EURSAFE), Nuclear Engineering and Design 235, pp. 309–346 (2005).

M. Bürger, M. Buck, G. Pohlner, S. Rahman, R. Kulenovic, F. Fichot, W.M. Ma, J. Miettinen, Coolability of particulate beds in severe accidents: Status and remaining uncertainties, Progress in Nuclear Energy 52, pp. 61–75 (2010).

I. Lindholm, S. Holmström, J. Miettinen, V. Lestinen, J. Hyvärinen, P. Pankakoski, H. Sjövall, Dryout heat flux experiments with deep heterogeneous particle bed, Nuclear Engineering and Design 236, pp. 2060–2074 (2006).

G. Repetto, T. Garcin, S. Eymery, P. March and F. Fichot, Experimental program on debris refloodin (PEARL), results on PRELUDE facility, The 14th International Topical Meeting on Nuclear Reactor Thermal Hydraulics (NURETH-14), Toranto, Canada, 25-29 September, Nr.126, (2011).

A. PALAGIN et al., “Analysis and Interpretation of the LIVE-L6 Experiment,” 5th European Review Meeting on Severe Accident Research (ERMSAR-2012), Cologne (Germany), March 21-23, 2012.

X. GAUS-LIU, A. MIASSOEDOV, T. CRON, S. SCHMIDT-STIEFEL, T. WENZ., KIT, Karlsruhe (DE), “The Experimental Results of LIVE-L8B - Debris Melting Process in a Simulated PWR Lower Head,” 5th European Review Meeting on Severe Accident Research (ERMSAR-2012), Cologne (Germany), March 21-23, 2012.

M. Helle et al. “Experimental Data on Heat Flux Distribution from a Volumetrically Heated Pool with Frozen Boundaries”, Proceedings of In-Vessel Core Debris Retention and Coolability Workshop, Garching, Germany, March 3-6, pp. 173-183, (1998).

L. Bernaz et al. “Thermal Hydraulic Phenomena in Corium Pools: Numerical Simulation with TOLBIAC and Experimental Validation with BALI”, Proceedings of In-Vessel Core Debris Retention and Coolability Workshop, Garching, Germany, March 3-6, pp. 185-193, (1998).

T. G. Theofanous and S. Angelini, “Natural Convection for In-Vessel Retention at Prototypic Rayleigh Numbers”, Nucl. Eng. Design, 200, pp. 1-9, (2001).

K.Y. Suh, R.E. Henry, Debris interactions in reactor vessel lower plena during a severe accident II. Integral analysis, Nuclear Engineering and Design 166, pp.165-178, (1996).

W.C. Müller, Review of debris bed cooling in the TMI-2 accident, Nuclear Engineering and Design 236, 1965–1975, (2006).

X. Gaus-Liu, B. Fluhrer, A. Miassoedov, T. Cron, J. Foit, S. Schmidt-Stiefel, T. Wenz; Results of the LIVE-L3A Experiment, KIT Scientific reports 7542, ISBN 978-3-86644-505-5, (2010).

X. Gaus-Liu, A. Miassoedov, J. Foit, T. Cron, F. Kretzschmar, T. Wenz, S. Schmidt- Stiefel, LIVE L4 and LIVE L5L experiments on pool and crust behaviour in the RPV lower head, Nr. 26, The 14th International Topical Meeting on Nuclear Reactor Thermal Hydraulics (NURETH-14), Toranto, Canada, September 25-29, Nr.26, 2011.

H. Goodwin, M. R.D. Mailey, “On the density, electrical conductivity and viscosity of fused salts and their mixtures”, Physical review, 26, pp. 28-60, (1908).

M. Kenisarin, High-temperature phase change materials for thermal energy storage”, Renewable and Sustainable Energy Reviews 14, pp. 955-970, (2010).

A. MIASSOEDOV, T. CRON, J. FIOT, S. SCHMIDTSTIEFEL, T. WENZ, I. IVANOV, D. POPOV, “Results of the LIVE-L1 Experiment on Melt Behaviour in RPV Lower Head Performed within the LACOMERA Project at the Forschungszentrum Karlsruhe”, Proceedings of 15th International Conference on Nuclear Engineering Nagoya (ICONE), Japan, April 22-26, 2007.

6.2.8 FARO Experiment

In the FARO experiment (Magallon, et al., 1999) the formation and the cooling of corium debris beds resulting from corium melt jet quenching tests have been investigated. The influence of several parameters has been analysed (such as pressure, water height, corium mass). The interpretation and transposition to the reactor remain to be done.

Data from experiments investigating prototypic material behaviour are consistent with TMI-2 evidence. FARO tests suggest the presence of a gap between relocated corium materials and the test plate and “furrows” and “interconnected porosity” within the solidified corium materials. FARO test data also suggest that gaps are larger in tests with water present. Similar phenomena were also observed in corium materials from the CCM-2 tests (Spencer, 1994). Unfortunately, prototypic material evidence was insufficient to estimate key parameters required to model this cooling. For example, there wasn’t sufficient evidence to estimate the size and density of cracks within solidified corium, the gap sizes that may have formed between the vessel and relocated corium, or the heat transfer from relocated corium materials to coolant flowing in these cracks or gap.

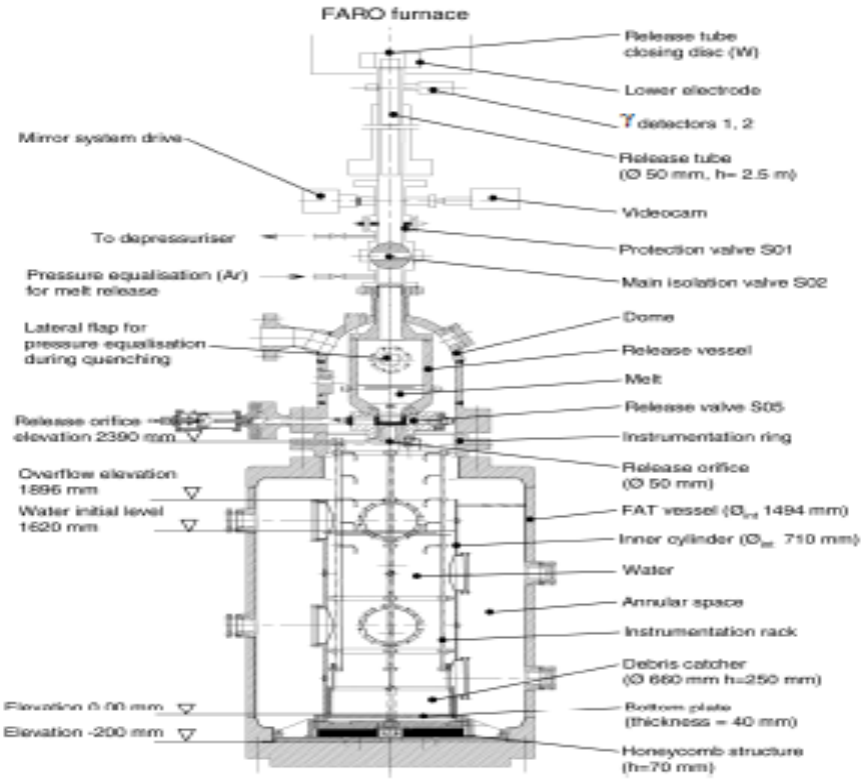

Figure 6-9: Schematic of the FARO Test Facility

Some references

Magallon, D., et al., "Debris and Pool Formation /Heat Transfer in FARO-LWR: L Experiments and Analyses," Proceedings of the OECD NEA Workshop on In-Vessel Core Debris Retention and Coolability, NEA/CSNI/R(98)18, February 1999.

Spencer, B. W., private communication, 1994.

Theofanous, et al., In-Vessel Coolability and Retention of Core Melt, DOE/ID-10460, October 1996.

Theofanous, T. G. and S. Syri, "The Coolability Limits of a Reactor Pressure Vessel Lower Head," Nuclear Engineering and Design, 169, pp. 59-76, 1997.

Theofanous, T. G. et al., "Limits of Coolability in the AP1000-Related ULPU-2400 Configuration V Facility," Paper G00407, Tenth International Topical Meeting on Nuclear Reactor Thermal Hydraulics, NURETH10, October 5-11, 2003, Seoul, Korea.

6.2.9 OECD RASPLAV Project

OECD RASPLAV Project was dealing with experimental study of the behaviour of the molten prototypic material of the core (corium) in the lower head of nuclear reactor. The main objective of the RASPLAV experiments was to study corium melt pool convection in conjunction with the chemical processes in the debris bed/molten pool and at the interface boundaries. During first phase of the Project two large scale experiments with 200 kg of corium were performed. Two smaller tests with corium mass of about 40 kg preceded these large experiments.

The main results of Phase I may be formulated as - technical problems to conduct large scale experiment were resolved - methods of the heating up of core material beyond liquidus temperatures - compatible materials - measurements techniques - new data on corium properties were obtained - analytical tools for corium test analysis were developed - separation of corium melts was observed. The corium consisting of $UO_2/ZrO_2/Zr$ (32% oxidized Zr) stainless steel[6] heated up to temperatures between 2300 and 2700°C which are 50-100°C above the corium liquidus temperature. About 40 tests on

[6] Test wall made from carbon steel was insulated from corium by UO_2 layer. There was no contact corium-steel in RASPLAV project. (in MASCA only)

convection in molten salt pool at different conditions and Ra_i up to 2.10^{13} were also carried out. On Phase 2 of the project two large tests with 200 kg of corium (one test with fully oxidized corium C-100) were done and a row of small tests concerning the melt properties etc.

The RASPLAV experiments showed that the corium melt pool convection flow field may be similar to those that prevail, at equivalent internal Rayleigh numbers Ra_i, in facilities employing simulant materials. The salt and real material tests confirmed that heat transfer correlations established in simulant materials tests can be used for the convection of homogenous corium melt pool at equivalent Ra_i numbers. The experiments, conducted at $Ra_i \leq 10^{11}$~10^{12}, have shown corium melt stratification for prototypic compositions and temperatures. The interpretation of the data obtained with respect to stratification has not been completed so far[7]. If the stratification is found to be stable, and prototypic, for the accident composition and temperatures, it may affect the natural circulation flow fields. The magnitude of the effects of stratification at the prototypic Ra_i numbers (when the flows would have greater turbulence than for those in the RASPLAV tests) has not been determined.

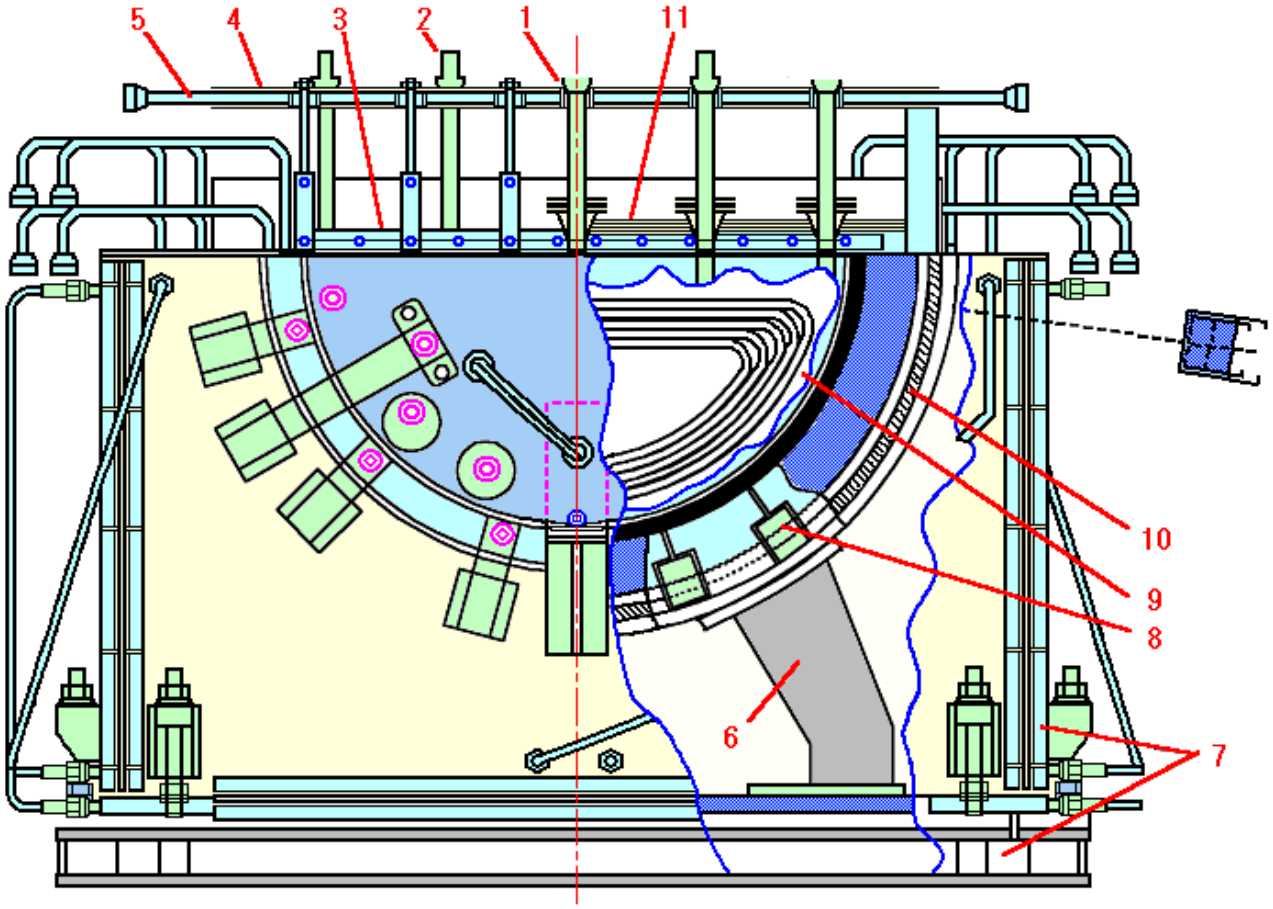

Figure 6-10: Schematic of the RASPLAV Test Facility

Some references

V. G. Asmalov et A. V. Merzliakov, "OECD RASPLAV Project: Phase I results," Proceedings of the workshop on severe accident research held in Japan (SARJ-97), JAERI-CONF--98-009, Yokohama (Japan); 6-8 Oct 1997.

V. ASMOLOV, N. N. PONOMAREV-STEPNOY, V. STRIZHOV, B. R. SEHGAL, "Challenges Left in the Area of In-Vessel Melt Retention", J. Nuclear Engineering and Design, Vol. 209, pp. 87-96, 2001.

V. STRIZHOV, V. ASMOLOV, "Major Outcomes of the RASPLAV Project", RASPLAV Seminar 2000, Munich, November, 2000.

[7] oxide corium stratification occurs for melt compositions not actual for VVER.

6.2.10 POMECO and DEBRIS Experiments

POMECO and DEBRIS are two analytical experiments with debris beds that were performed by KTH and IKE respectively. Their common objective was to address, during degraded core reflooding, debris and molten pool behaviours in reactor vessel lower head to support the quantification of basic laws and coolability behaviour.

Top and bottom flooding (quenching) of hot debris (up to 900°C) were investigated in the DEBRIS facility, also at elevated pressures. POMECO was dedicated to analyses under boil-off conditions with emphasis on basic laws and specific 2D effects (downcomers); more oriented at lower head or ex-vessel situations but it was also addressing basically the situation in the degrading core. Both DEBRIS and POMECO dealt with irregular particles aiming at representing realistic debris.

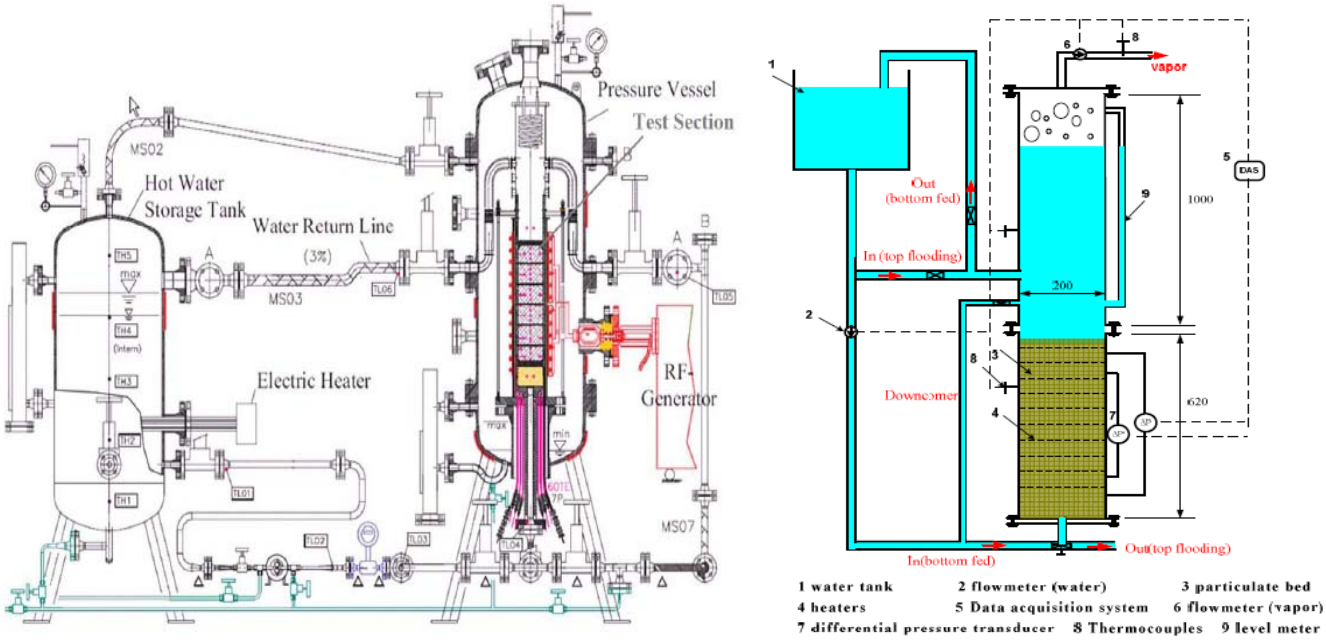

Figure 6-11: Test Facilities POMECO (left) and DEBRIS (right)

Some references

L. Li, S. Thakre, and W. Ma, "An experimental study on two-phase flow and coolability of particulate beds packed with multi-size particles," in Proceedings of the 14th International

Topical Meeting on Nuclear Reactor Thermal Hydraulics (NURETH '11), Toronto, Ontario, Canada, 2011.

M. Rashid, S. Rahman, R. Kulenovic, M. Buerger, and E. Laurien, "Quenching experiments: coolability of debris bed," in Proceedings of the 14th International Topical Meeting on Nuclear Reactor Thermal Hydraulics (NURETH '11), Toronto, Ontario, Canada, 2011.

J-P. Van Dorsselaere et al., "The European Research on Severe Accidents in Generation-II and -III Nuclear Power Plants," Science and Technology of Nuclear Installations Volume 2012, Article ID 686945, 12 pages doi:10.1155/2012/686945.

6.2.11 IRSN Corium and Debris Coolability Experiments

IRSN has performed larger size quenching experiments with 2D porous media, which allows a multidimensional progression of the quench front in the PEARL program. Preliminary reflooding experiments were carried in the PRELUDE facility, involving a debris bed of 4 mm particles inside a 110 mm external diameter and 100 mm height test section, at atmospheric pressure. Investigated parameters were:

- inlet water velocity between 1 and 8 mm/s (4 to 30 $m^3/h/m^2$), in the range foreseen in PEARL test matrix;

- power at 300 W/kg (maintained or not during the reflooding phase)
- initial temperature before reflooding at 420 K, 500 K, 600 K and 1000 K.

Additional PRELUDE experiments were performed to evaluate the power distribution inside a larger debris bed diameter (from 110 to 280 mm) using stainless particles, 2 mm and 4 mm in diameter, up to 300 W/kg.

This program ended with two experiments with a heating sequence of a debris bed (test section diameter 180 mm, particles 4mm) up to 1000 K at about 140 and 200 W/kg before the water injection. Those experiments were well instrumented with thermocouples inside the debris bed at different radial and axial positions to follow the water front propagation with time. The measurements of the injected water flow, as well as the steam flow rate generated during reflooding, were accurately obtained by mean of adapted sensors to reach a very good water/steam balance.

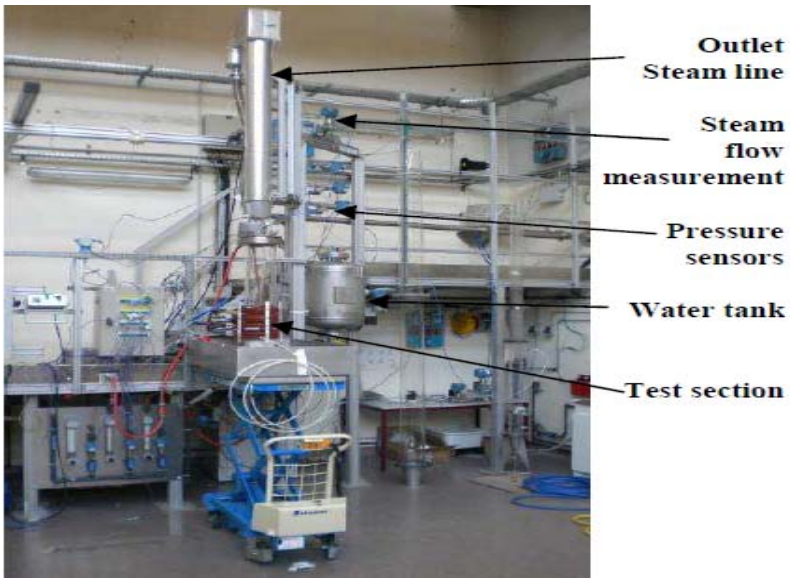

Figure 6-12: PRELUDE Test Facility

Some references

N. Stenne, F. Fichot, and J. P. van Dorsselaere, "R&D on reflooding of degraded cores in SARNET—focus on PEARL new IRSN facility," in Proceedings of the EUROSAFE Forum, Brussels, Belgium, 2009.

G. Repetto, T. Garcin, S. Eymery, P. March, and F. Fichot, "Experimental program on debris reflooding (PEARL) results on PRELUDE facility," in Proceedings of the 14th International Topical Meeting on Nuclear Reactor Thermal Hydraulics (NURETH '11), Toronto, Ontario, Canada, 2011.

J-P. Van Dorsselaere et al., "The European Research on Severe Accidents in Generation-II and -III Nuclear Power Plants," Science and Technology of Nuclear Installations Volume 2012, Article ID 686945, 12 pages doi:10.1155/2012/686945.

6.2.12 Molten Material Heat Transport Tests with Coolant Boiling

Experimental studies on the heat transfer and solidification of the molten metal pool with overlying coolant with boiling were performed at Seoul National University, Republic of Korea. In these experiments, a metal pool was heated from the bottom surface and coolant was injected onto the molten metal pool. As a result, the crust, which was a solidified layer, may have formed at the top of the molten metal pool. Heat transfer was accomplished by a conjugate mechanism, which consisted of the natural convection of the molten metal pool, the conduction in the crust layer and the convective boiling heat transfer in the coolant. This work examined the crust formation and the heat transfer rate on the molten metal pool with boiling coolant. The simulant molten pool material was tin (Sn) with the melting temperature of 232°C. Demineralized water was used as the working coolant. The crust layer thickness was ostensibly varied by the heated bottom surface temperature of the test section, but it

was not much affected by the coolant injection rate. The correlation between the Nusselt number and the Rayleigh number in the molten metal pool region of this study was compared against the crust formation experiment without coolant boiling and the literature correlations. The present experimental results were higher than those from the experiment without coolant boiling, but showed general agreement with the Eckert correlation, with some deviations in the high and low ends of the Rayleigh number. This discrepancy was then attributed to concurrent rapid boiling of the coolant on top of the metal layer.

Some references

J. S. Cho, K. Y. Suh, C. H. Chung, R. J. Park, and S. B. Kim, "Molten material heat transport tests with coolant boiling," Proceedings of the workshop on severe accident research held in Japan (SARJ-97), JAERI-CONF--98-009, Yokohama (Japan); 6-8 Oct 1997.

6.2.13 MASCA Project

The MASCA Project was a follow-up of the RASPLAV Project and investigated in-vessel phenomena during a severe accident. In particular, it addressed the influence of the chemical composition of the molten corium on the heat transfer to the pressure vessel environment. The project addressed this by investigating stratification phenomena of the molten pool, compositions of the two melt layers, and the partitioning of fission products (FP) within the layers. The project was scheduled to be completed in July 2003, but it was continued until 2006 under the MASCA-2 Project, given the experimental needs that still existed and the quality of the experimental work done up to that point. Most of MASCA tests (except RCW-100) were performed with 4 kg or 1.5 kg of corium in cold crucible – in corium tests heat transfer was not studied specially (except planning calculations of RCW-100 and TULPAN-7-8 tests), it was parasitical effect. The heat transfer, declared in project goals, was studied in the experiments with stratified molten salt pools.

The tests aimed to resolve remaining uncertainties about the heat load on the reactor vessel and thus the possibility of retaining the melt in the vessel. These uncertainties are mainly associated with scaling effects and coupling between the thermal-hydraulic and chemical behaviour of the melt. Supporting experiments and analyses – in addition to helping understand key in-vessel phenomena - facilitated a consistent interpretation of the results. The experiments were carried out with corium compositions prototypical of power reactors which use iron and steel materials. The MASCA experimental goal was achieved through corium tests of different scale and was complemented by pre- and post-test analyses and development of computational models. Additional measurements of thermo-physical properties of the melts such as density, thermal conductivity and liquidus-solidus temperatures considerably expanded the material properties data obtained during the RASPLAV Project.

The major goals of the MASCA-1 Project were to:

- Investigate the influence of chemical behaviour on heat transfer in stratified molten pools of prototypical compositions[8];
- Investigate FP behaviour in a molten pool and in particular:
    - Partitioning of FP between layers in case of stratification;
    - Partitioning of FP between phases during melting and solidification;
    - Distribution of FP simulants in the melts
- Expand the material properties database;
- Develop computer models describing the relevant phenomena.

Separate effects were studied in several series of small- and one mid-scale experiment (RCW-100, 100kg of corium). Corium tests were performed in the RASPLAV-2, RCW, TULPAN, TF, STFM, KORPUS, and TIGEL facilities. Salt tests were performed in the RASPLAV-A-Salt-2 facility.

[8] Performance of salt tests to study heat transfer in the stratified molten pool

MASCA-2 aims at providing experimental information on the phase equilibrium for different corium mixture compositions that can occur under severe accident conditions of light water reactor. In this program the influence of an oxidizing atmosphere and the impact of non-uniform temperatures (presence of solid debris) were addressed. The program was also intended to generate data on relevant physical properties of mixtures and alloys that are important for the development of qualified mechanistic models. The main objectives of the MASCA-2 were:

- Study of melt stratification and distribution of major species (U, Zr, O, Fe (SS)) between layers in inert atmosphere for varying iron to corium ratio;
- Study of control rod materials effects on interaction and distribution of major species (U, Zr, O, Fe (SS)) in the inert atmosphere;
- Study of melt stratification and distribution of major species (U, Zr, O, Fe (SS)) between layers in oxidizing atmosphere for varying iron to corium ratio;
- Investigations of molten metal alloys interactions with corium debris bed in the inert and oxidizing atmosphere;
- Extension of material properties database.

MASCA-2 main test results are summarized as follows:

- Inversion of metal and layers,
- Melt oxidation and secondary layers' inversion,
- Influence of control rod materials,
- FP partitioning between layers, and
- Migration of molten metal through debris.

Some references

Russian Research Centre, Kurchatov Institute, “Main Results of the First Phase of MASCA Project,” OECD MASCA Project, Integrated Report, November 2004.

V. G. ASMOLOV, S. V. BECHTA, V. B. KHABENSKY et al., “Partitioning of U, Zr and Fe between Molten Oxidic and Metallic Corium”, Proceeding of MASCA Seminar 2004, Aix-en-Provence, France, 2004.

Russian Research Centre, Kurchatov Institute, “Main Results of the MASCA1 & 2 Projects,” OECD MASCA Project, Integrated Report, June 2007.

6.2.14 Vessel coatings Tests

Under IVMR conditions, the outer surface of the reactor vessel could be altered due to water chemistry, oxidization, and/or aging. Thus, it is necessary to address the potential effect of surface condition on the local CHF limits. From the numerous studies of conventional pool boiling and flow boiling reported in the literature, it is widely recognized that the surface condition could have a significant effect on the CHF. This turns out to be also true for downward facing boiling during ERVC under IVMR conditions. The surface condition could substantially alter the vapour dynamics on the heating surface, thus affecting the local CHF limit at which local dryout would occur.

Theofanous et al. (2003) observed a strong effect of surface condition in their experiments at the UPLU-2400 facility for Configuration V. Test results indicated that the sand particles used to roughen the copper surfaces modified the surface molecules properties, at least temporarily; due to a deposition of aluminium molecules (the sand particles contained aluminium oxide). Because of the surface modification, different CHF limits were obtained. Moreover, they found that the molecular deposition of aluminium could be dissolved by de-ionized water used in some of their tests, leading to a significant reduction in the CHF values in subsequent tests. This degradation effect was not observed in those tests using tap water rather than de-ionized water.

Recently, Dizon et al. (2003) performed an extensive study of the effect of vessel coating on the local CHF limits in the SBLB facility. They developed a spray coating technique to form thin micro-porous

metallic coatings on hemispherical test vessels. Their data clearly revealed that the coated vessels consistently increased the local CHF values from around 40% to more than 110% compared to those obtained under identical boiling conditions on uncoated, plain vessels. Unlike the trend observed for plain vessels, the local boiling curve for coated vessels did not shift monotonically upward and to the right as the angular position was increased from the bottom centre toward the equator of the test vessel. The local CHF limit at the bottom centre was actually higher than the values for adjacent downstream locations up to $\theta = 28^{o}$. The local CHF exhibited a minimum at the $\theta = 14^{o}$ location rather than at the bottom centre.

Some references

J. L. Rempe et al., "In-Vessel Retention – Recent Efforts and Future Needs,"The 6th International Conference on Nuclear Thermal Hydraulics, Operations and Safety (NUTHOS-6) Nara, Japan, October 4-8, 2004.Paper ID. N6P045.

Dizon, M. B., et al., "Effects of Surface Coating on Nucleate Boiling Heat Transfer on a Downward Facing Surface," Proceedings 2003 ASME Summer Heat Transfer Conference, Paper HT2003-47209, 2003.

Theofanous, T. G. et al., "Limits of Coolability in the AP1000-Related ULPU-2400 Configuration V Facility," Paper G00407, Tenth International Topical Meeting on Nuclear Reactor Thermal Hydraulics, NURETH10, October 5-11, 2003, Seoul, Korea.

6.2.15 Research Study in Support of IVMR Program in the Paks NPP

Experimental and analytical studies have been performed to answer the question whether the in-vessel retention of corium can be assured in the Paks nuclear power plant of VVER-440/213 type. For the experimental studies, the CERES facility, the integral type model of the cooling loop was designed and constructed with a volume scale of 1:40 and elevation scale of 1:1. For the analytical studies, a computer code model of the facility was developed for RELAP5/mod3.3. The cooling channel in the reactor and consequently in the modelling has a nominal, narrow, "critical" gap size of 20 mm, for a length of 900 mm, at the elevation where thermal load of vessel wall has its highest value as calculated by the ASTEC code. The gap size is critical from the viewpoint of heat extraction by pool boiling with natural circulation. The question was whether the heat can be extracted from the vessel surface at the highest thermal load without boiling crisis.

Results of the first series of experiments and computer code analyses showed that the vessel wall cooling was effective enough. The external reactor vessel cooling could be applied to the plant.

In the second series of experiments, asymmetric cases have been tested. Three different cooling channels were experimentally investigated, as channel with critical gap size of 10 mm, channel with two-stepped cross section, and channel with five-stepped cross section. In all three cases there is a stable vessel wall cooling, with different peak temperatures of vessel wall.

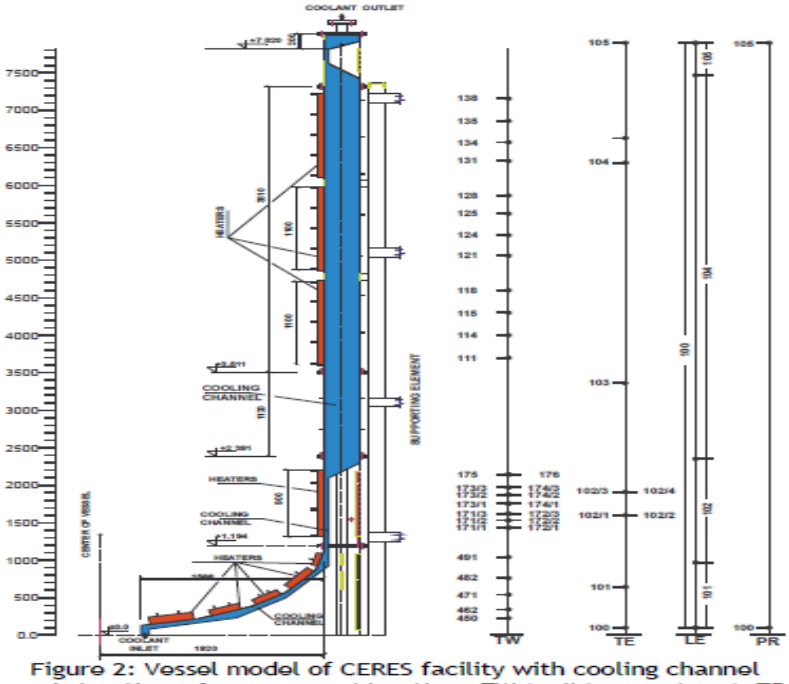

Figure 2: Vessel model of CERES facility with cooling channel
Heaters and elevations of measurement locations: TW (wall temperatures), TE (liquid temperatures), LE (levels), PR (pressures)

Figure 6-13: Vessel model of CERES facility with cooling channel

Some references

L. Szabados, Gy. Ézsöl, L. Perneczky, I. Tóth, Final Report on the PMK-2 Projects. Volume I. Results of Experiments Performed in the PMK-2 Facility for VVER Safety Studies. Akadémiai Kiadó, Budapest, 2007. ISBN 978 963 05846 6.

L. Szabados, Gy. Ézsöl, L. Perneczky, I. Tóth, A. Guba, A. Takács, I. Trosztel, Final Report on the PMK-2 Projects. Volume II. Major findings of PMK-2 test results and validation of thermohydraulic system codes for VVER safety studies. Akadémiai Kiadó, Budapest, 2009. ISBN 978 963 05 8810 2.

6.2.16 Other Experimental Studies

While early studies of melt pool convection were conducted with isothermal boundary conditions without phase change, during the 1990s and early 2000s, several other experimental programs were performed with phase change, ranging from real corium tests (RASPLAV and MASCA), to simulant salt tests (RASPLAV-SALT, SIMECO and LIVE) and tests using water as the corium simulant (COPO II and BALI).

The SIMECO experiment was performed to investigate the effect of boundary crusts and mushy layers on natural convection heat transfer. The experiment showed that the upward Nusselt number is close to that determined from the Steinberner-Reineke correlation.

The SIMECO experiments were conducted in a slice type facility (Figure 6-15) which includes a semi-circular section and a vertical section. The diameter, height and width of the test section are 620x530x90 mm. Binary salt mixtures were employed as a melt simulant, both eutectic (50%- 50%) and non-eutectic (20%-80%) mixtures of KNO_3- $NaNO_3$ were used.

The COPO II and BALI experiments were performed in large 2D slice geometry to study the thermal-hydraulics of a corium pool, the simulant used was water. The boundaries of the pool were cooled till freezing so truly isothermal boundaries were established. The measured values of the COPO II showed that the upward Nusselt numbers are consistent with BALI results. However, they are slightly higher than predicted by the widely used correlation of Steinberner and Reineke, and also higher than measured in 3D ACOPO experiments which did not have crusts at the boundaries. For the side and bottom boundaries, the COPO II and BALI experiments showed clearly higher heat transfer coefficients (20-30%) than those in the ACOPO and those predicted by the Steinberner-Reineke correlation, particularly regarding the vertical boundary. The reason for this discrepancy may be the effect of water

density reversal at 4°C on heat transfer of the pool. The other potential reason is the ice crust surface roughness which intensifies turbulence mixing of the pool, particularly along the boundary layers. The third reason is that in the COPO II and BALI experiments, the pool boundaries are frozen, causing a large temperature difference between the pool boundary and the bulk of the fluid. Therefore the fluid properties are non-uniform, raising a question of the reference temperature at which the fluid properties are applied in the heat transfer correlations.

Nevertheless, a unifying trend derived from the experimental studies is that the experimental heat transfer correlations built on data from simulant fluid experiments under isothermal boundary conditions are applicable to a melt pool with phase change.

The SIMECO experiments were conducted in a slice type facility (Figure 6-15) which includes a semi-circular section and a vertical section. The diameter, height and width of the test section are 620x530x90 mm. Binary salt mixtures were employed as a melt simulant, both eutectic (50%- 50%) and non-eutectic (20%-80%) mixtures of KNO_3- $NaNO_3$ were used. For the PECM validation we use the experiment with a eutectic mixture (the experiment number

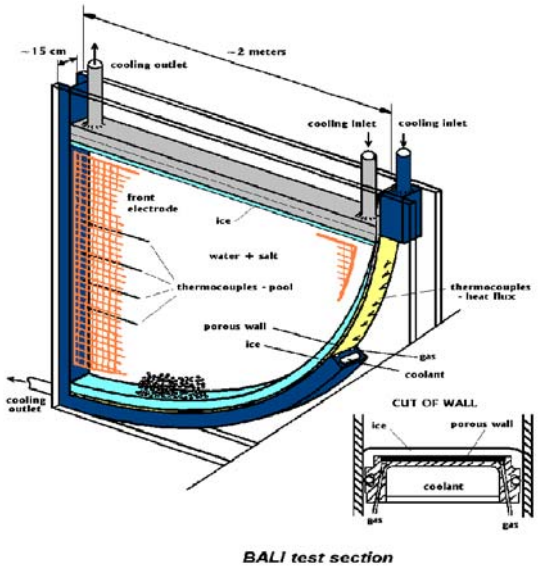

Figure 6-14: BALI In-Vessel Test Section

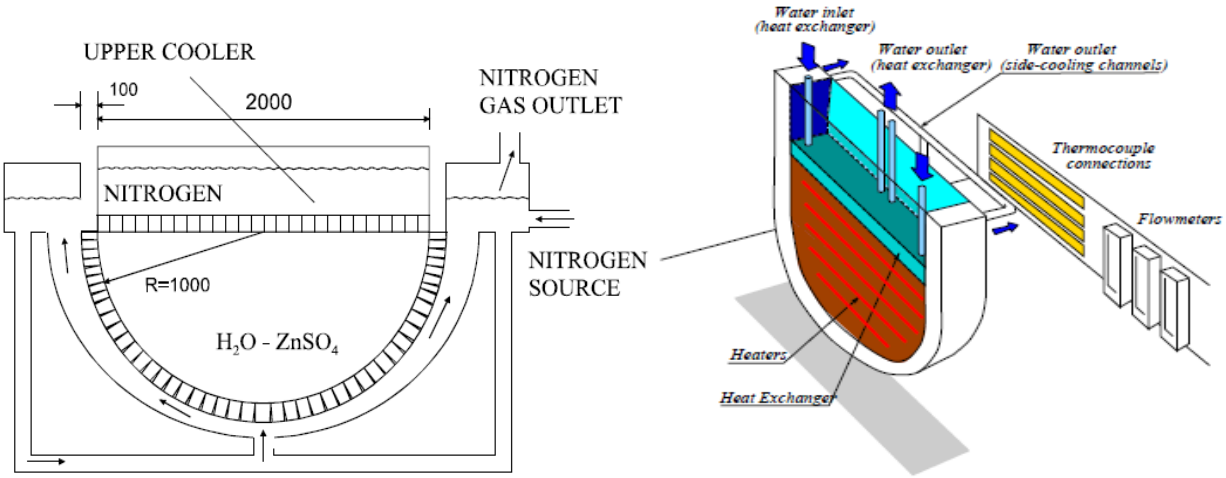

Figure 6-15: Schematic of the COPO II-AP (left) and SIMECO (right) Test facilities

Some references

V. ASMOLOV, N. N. PONOMAREV-STEPNOY, V. STRIZHOV, B. R. SEHGAL, "Challenges Left in the Area of In-Vessel Melt Retention", J. Nuclear Engineering and Design, Vol. 209, pp. 87-96, 2001.

V. G. ASMOLOV, S. V. BECHTA, V. B. KHABENSKY et al., “Partitioning of U, Zr and Fe between Molten Oxidic and Metallic Corium”, Proceeding of MASCA Seminar 2004, Aix-en-Provence, France, 2004.

V. STRIZHOV, V. ASMOLOV, “Major Outcomes of the RASPLAV Project”, RASPLAV Seminar 2000, Munich, November, 2000.

B. R. SEHGAL, V. A. BUI, T. N. DINH, J. A. GREEN, G. KOLB, “SIMECO Experiments on In-Vessel Melt Pool Formation and Heat Transfer with and without a Metallic Layer”, Proceedings of In-Vessel Core Debris Retention and Coolability Workshop, Garching, Germany, March 3- 6, pp. 205-213, 1998.

A. MIASSOEDOV, T. CRON, J. FIOT, S. SCHMIDTSTIEFEL, T. WENZ, I. IVANOV, D. POPOV, “Results of the LIVE-L1 Experiment on Melt Behaviour in RPV Lower Head Performed within the LACOMERA Project at the Forschungszentrum Karlsruhe”, Proceedings of 15th International Conference on Nuclear Engineering Nagoya (ICONE), Japan, April 22-26, 2007.

M. HELLE, O. KYMALAINEN and H. TUOMISTO, “Experimental Data on Heat Flux Distribution from a Volumetrically Heated Pool with Frozen Boundaries”, Proceedings of In-Vessel Core Debris Retention and Coolability Workshop, Garching, Germany, March 3-6, pp. 173-183, 1998.

L. BERNAZ, J.- M. BONNET, B. SPINDLER, C. VILLERMAUX, “Thermal Hydraulic Phenomena in Corium Pools: Numerical Simulation with TOLBIAC and Experimental Validation with BALI”, Proceedings of In-Vessel Core Debris Retention and Coolability Workshop, Garching, Germany, March 3-6, pp. 185-193, 1998.

B. R. SEHGAL, V. A. BUI, T. N. DINH, J. A. GREEN, G. KOLB, “SIMECO Experiments on In-Vessel Melt Pool Formation and Heat Transfer with and without a Metallic Layer”, Proceedings of In-Vessel Core Debris Retention and Coolability Workshop, Garching, Germany, March 3-6, pp. 205-213, 1998.

7 Future research needed

Based on cumulative knowledge, it would be very useful having a final heat flux distribution along the semi-elliptical lower head and above in a form of histogram which will identify occurrence of maximum heat flux at different angular positions along the whole perimeter of the lower head and RPV cylindrical part. This was not possible to be done in a straightforward way because the participants used different nodalization.

The histogram distribution was selected due to common agreement of all participants, based on thorough assessment of all provided results which indicated different results in terms of reached maximum value, position and time of the CHF.

There is no doubt of very high quality of all performed calculations, however without thorough and highly representative experimental verification of results the IVMR strategy will be not accepted, neither by Utilities as well as Regulatory Bodies.

A proposal on future experimental work could be the following:

- Perform small and large scale experiments fully representing shape of the semi-elliptical lower head and cylindrical RPV segment. Until now all small and large scale experiments (including ULPU experiments) were performed with cooling Cu surface of the heater. We need to perform tests with several different RPV surface conditions (it means RPV steel not Cu), including possible surface improvements (e.g. cold spray with high porosities) and without any doubt also with different cooling media (there are several options and not only demi water, H_3BO_3 concentration, but definitely all impurities which are already on the RPV surface and at the RPV cavity).
- In general we would like to generate set of CHF curves for different RPV surface status and for each RPV surface also CHF curve with different cooling media and not only one CHF curve as it is the case for MASCA and ULPU experiments.
- Due to very extensive programme, with lot of modifications needed, we will first perform matrix of small scale experiments under different above described conditions and then based on those results perform large scale experiments fully representing shape and scale for selected boundary conditions experiments.

Other Areas for further investigation and modelling of IVMR by ASTEC could be:

- Influence of cooling water over external surface, as flooding periods, water quantities, temperature, etc., over HF distribution for VVER 1000.
- Influence of in-vessel parameters as temperature, quantity and location of the melt over HF distribution.

8 Conclusions

As part of the outcome of the EU "Stress Tests" in 2012, several areas for further research in the field of Severe Accident Management have been identified for different types of NPPs. One of these areas concerns the feasibility of In Vessel Retention (IVMR) for VVER 1000 reactors.

Starting from 2012, several research institutes and utilities in Europe (and also in the Russian Federation) started some work on this topic.

JRC-IET was asked to organize an international benchmark on computer code calculations for "In Vessel Retention for VVER 1000" with the target of providing preliminary results on the feasibility of this mitigation strategy in case of severe accident for such kind of plants. This benchmark attracted right from the beginning the interest of many EU partners (UJV Rez - Czech Republic, INRNE-Bulgaria, IVS-Slovakia, CEA-France, IRSN-France, EdF-France) and non EU (Kurchatov Institute –Russian Federation, IPP-Ukraine) partners. Kurchatov Institute provided freely to all partners the necessary data (ASTEC dataset, Severe Accident initial conditions, etc…) to start their own calculations, and to benchmark them with the one already performed at KI.

In the meantime the interested for this topic has continued to grow and several other EU institutions joined this benchmark (VTT-Finland, University of Stuttgart- Germany, Areva – France) especially because the subject of IVMR is also applicable for other types of NPPs, expanding the work as initially planned.

The principles of this international benchmark are the following:

- The target of this benchmark is to perform analyses of IVMR for VVER1000 with different computer codes (MELCOR, SOCRAT, ASTEC, etc…) and to compare the results
- The work to be performed by each partner in the frame of this benchmark is purely based on "in Kind" contributions to support this benchmark,

JRC-IET organized 3 Workshops in its premises in Petten (NL) (to allow participants to exchange information and compare results.

- The workshops took place at the following dates:
    - WS1 28th – 29th November 2013,
    - WS2 6th-7th May 2014
    - WS3-Final Meeting the 21-22 October 2014

On top of workshop organization, JRC-IET also contributed "in kind" by performing severe accident analyses with the ASTEC V2.0 and by distributing necessary data to the partners and by compiling the different partners' contributions to issue a benchmark summary report.

The main findings of this benchmark are:

- There are no experimental data available regarding critical heat fluxes for semi-elliptical RPV geometry, (like the one of VVER-1000);
- There are still uncertainties regarding the behaviour of the corium in the lower head until it reaches a more stable state; unfortunately most of the models implemented in all mechanistic codes predicts the bigger heat flux precisely during this initial transient, therefore future experiments should focus on this;
- The way the accident evolves will lead to different degrees of corium oxidation and material relocation and that has a big impact on the heat flux in the lower head

- A statistic approach seems to be a good tool to evaluate the probability that the heat flux will exceed a certain value in a certain point of the lower head
- CFD calculations are very time demanding, but seems to be valuable tools for addressing the heat transfer once the corium is stabilized; even though the CFD computations have been performed independently from calculations performed with SA computer codes and are based on different assumptions and techniques, the results displayed considerable similarities;
- Future small and large scale experiments fully representing a shape of semi-elliptical lower heads and cylindrical RPV segment will assess the feasibility of IVMR strategy, helping Utilities and Regulatory Bodies in deciding its implementation in existing power plants.

In conclusion this benchmark is an adequate basis for a preliminary assessment of the IVMR strategy and opens a path for future research programmes and experiments which should confirm the applicability of this strategy for large LWRs.

APPENDIX

A Individual reports

A.1 EDF MAAP

The purpose of this bench is to compute a realistic flux profile on the inner side of the vessel, which will help for the conception of UJV's upcoming IVMR test section. The first phase of the accident (from the initiating event up to the corium relocation to the lower head) was not computed by MAAP. A stand-alone calculation was conducted based on the KI's givens:

- corium history : instantaneous relocation of sub-oxidized (C-45) corium (M = 188.4t, T = 2500K);
- decay heat law (Wt per 1kg of UO_2);
- geometry of the reactor vessel bottom head. The semi-elliptical bottom part is joined to a cylindrical part. The two parts have different thicknesses.

A.1.1 Calculation setup

A.1.1.1 Decay heat law approximation

Time, s	Heat Wt/kg
4910	**373,44**
5000	371,04
6000	350
7000	333,28
8000	319,12
9000	307,52
10000	297,28
20000	240,08
30000	215,12
40000	200,4
50000	190,16
60000	182,24
70000	175,12
80000	168,96
90000	162,4
100000	155,92
200000	133,2
300000	117,04
400000	102,88

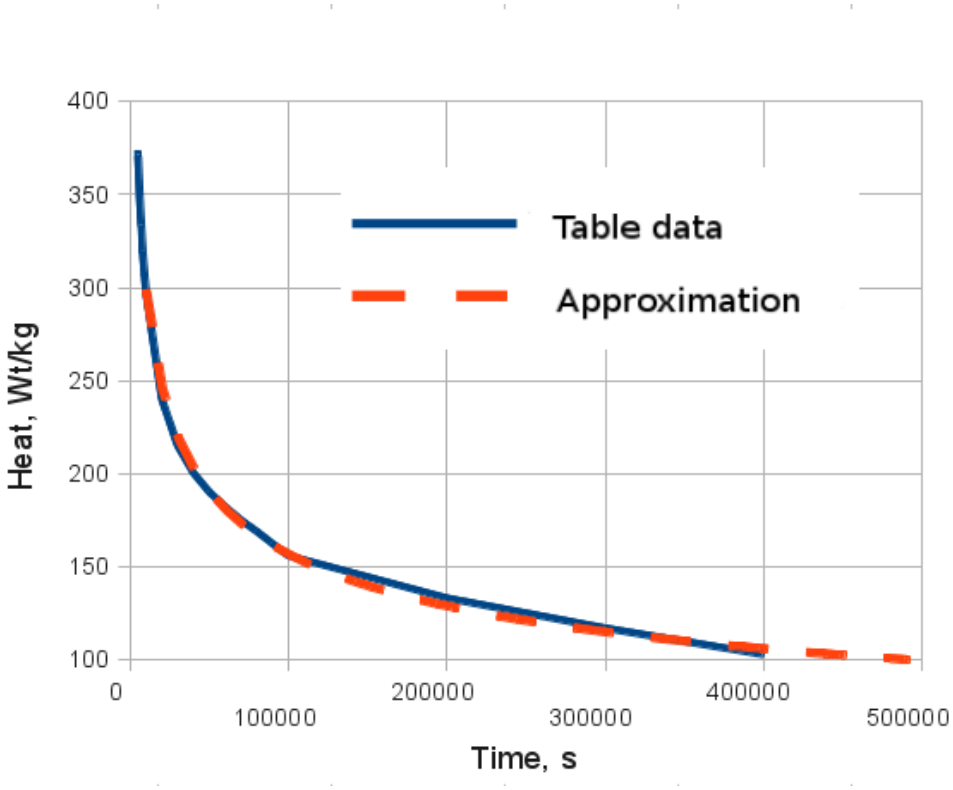

A.1.1.2 MAAP lower head mesh establishment

The elliptical part is modelled as half of an ablated spheroid whose semi-radiuses are b = 0.967 m and a = 2.2675 m; its thickness is 0.244 m. The radius of the cylindrical part is 2.068 m, and its thickness is 0.2 m.

There are 20 axial meshes in the semi-elliptical part, 50 axial meshes in the cylindrical part and 5 radial meshes; the outermost and innermost radial meshes are only half as thick as the three other radial meshes.

The zero level is set at the junction, as shown in Figure A.1.1 below.

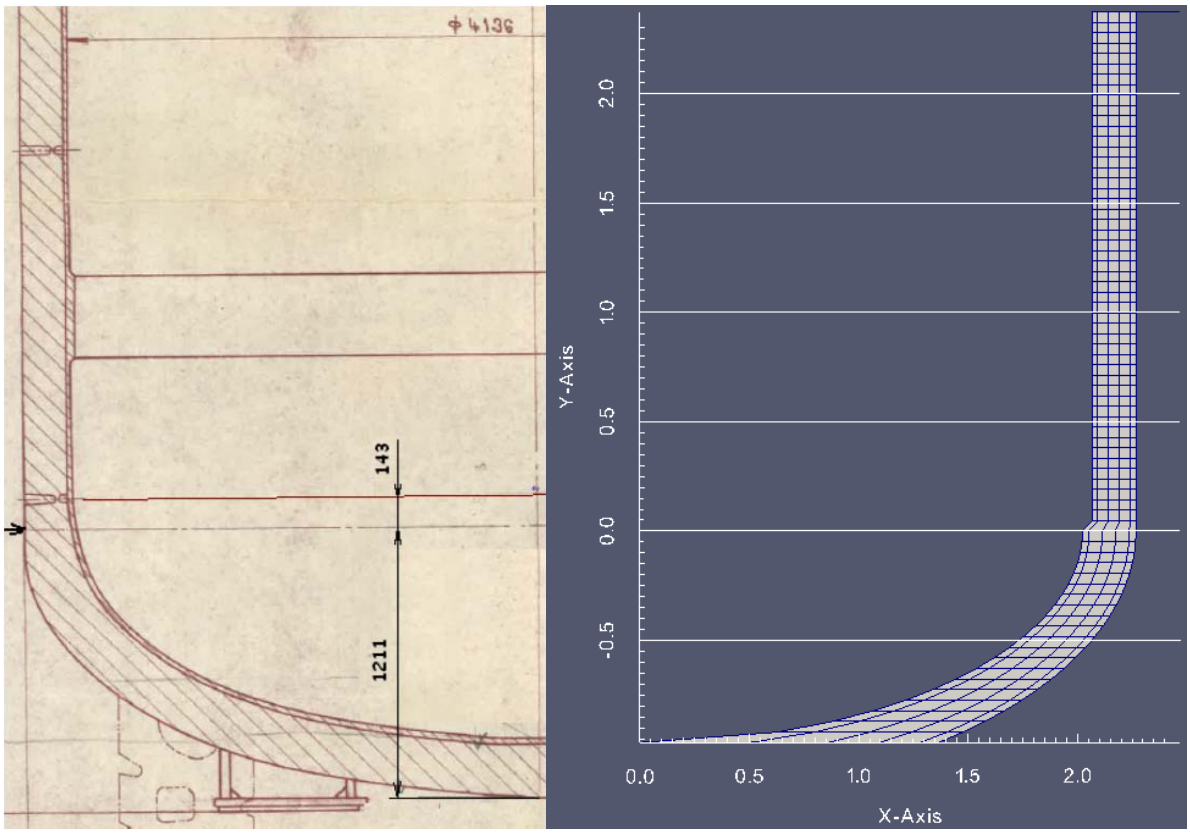

Fig. A.1.1 VVER-1000 RPV Bottom head drawing and MAAP lower head mesh

A.1.1.3 Other assumptions

The reactor pit is initially flooded. The reactor vessel is initially drained. The water-in-pit injection system is fully operational and is activated upon detection of a low water level. The vessel wall and the water in the pit are initially in thermal equilibrium at 322 K. In-vessel and in-pit pressures are close to 1 bar even if 2 bars could be more realistic, but with scarce impact on the results. We used prototypic vessel steel: T_{fusion} = 1800K, Cp = 530 J/kg/K, K = 35W/m/K.

The heat exchange coefficient between the vessel wall and the water is calculated using Rohsenow's correlation for the saturated nucleate boiling as a function of the average temperature of the outer vessel wall.

A.1.2 Best estimate calculation

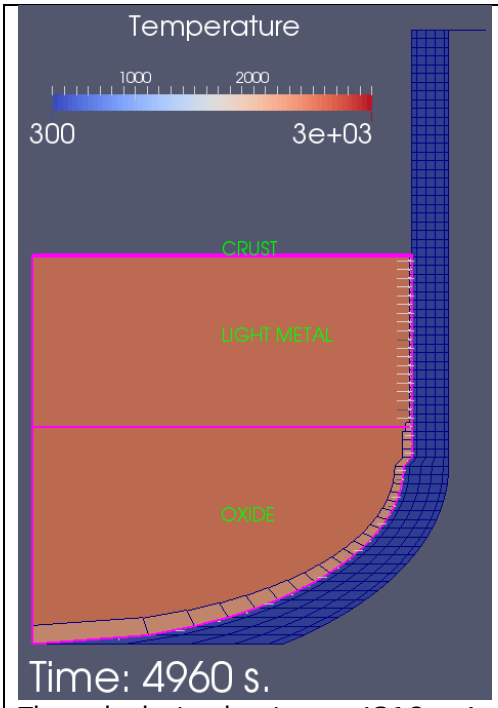

The calculation begins at 4910 s. At 4960 s, the bulk corium pool separates into two layers: oxide and light metal, both surrounded by the crusts.

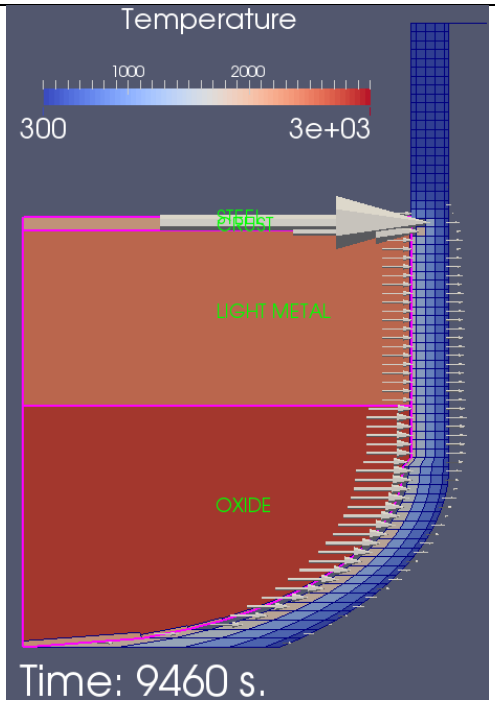

The vessel ablation starts at 8760 s. The ablated steel relocates above the axial crust and forms a top layer. The maximum corium-to-vessel flux value is 2.88 MW/m^2 at 9460 s.

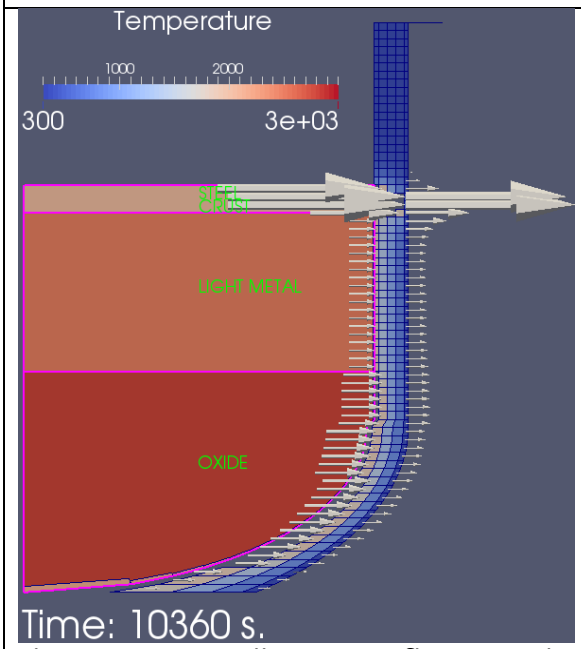

The maximum wall-to-water flux is reached at 10360 s. At that time, the flux value is 2 MW/m^2.

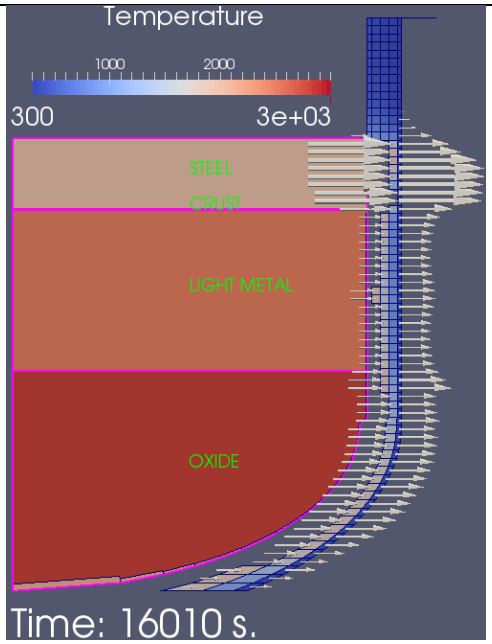

The quasi-steady state is reached at 16000 s with both fluxes about 1 MW/m^2.

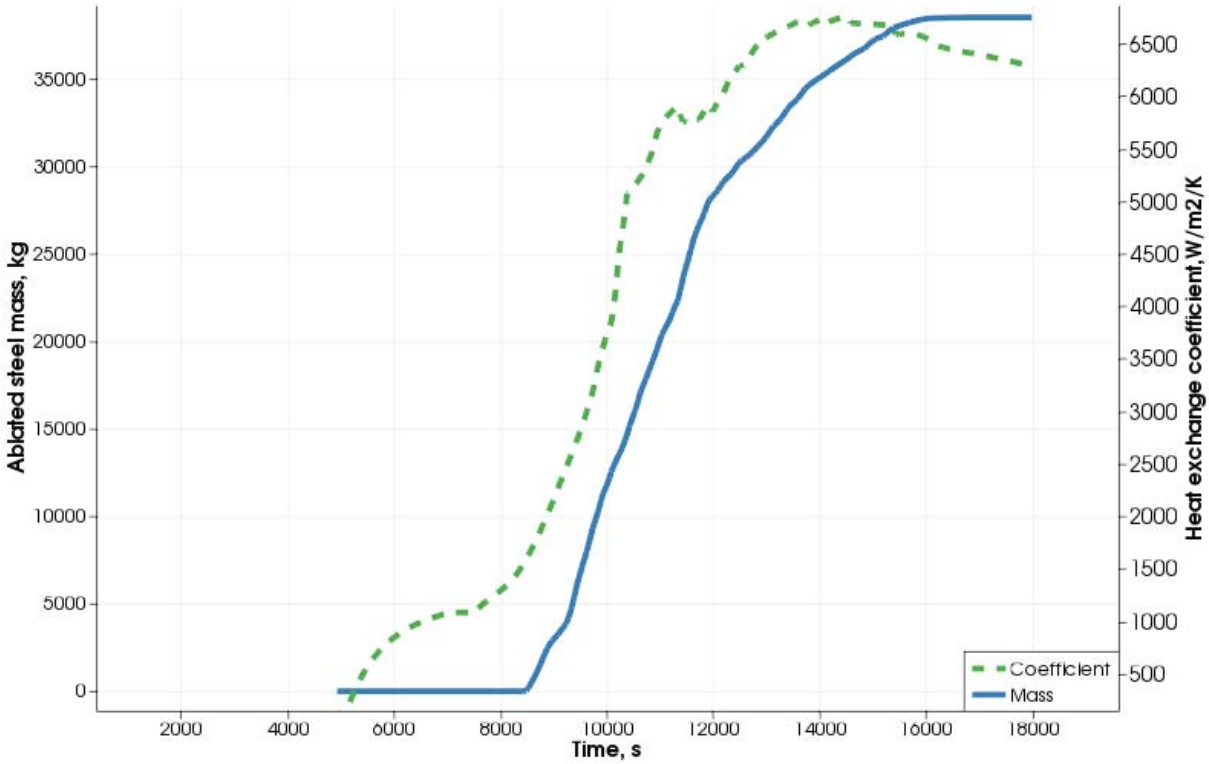

Fig. A.1.2 Ablated steel mass and vessel-to-water heat exchange coefficient.

Once the quasi-steady state has been reached at 16000 s, the flux stabilizes at about 1 MW/m^2. The ablated steel mass is 38.5t and the minimum residual thickness is 2 cm. However, one should note that this value corresponds to the thickness of the last radial mesh, and is therefore not necessarily significant; a lower residual thickness would most likely be observed with a more refined mesh. A calculation with a more specialized code (such as Code_Aster for instance) could potentially yield more realistic results on this issue.

A.1.3 Sensitivity study

The calculation was realized for various masses of steel in the initial corium, and various corium oxidation degrees. An additional calculation was performed with a constant wall-to-water heat exchange coefficient.

A.1.3.1 Initial steel mass = 30 t

In this case, the bulk pool separation resulted in the formation of a heavy metal layer and an oxidic layer. Stratification inversion during the transient lead to the formation of a light metal layer below the crust, while the ablated vessel steel formed another light metal layer above the crust. This resulted in a transient 4-layer configuration, as shown in the screenshots below.

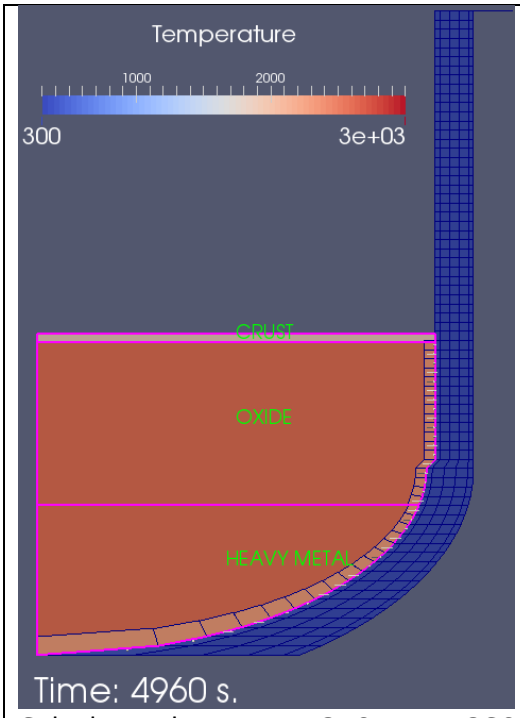

Calculation begins at 4910 s. At 4960 s, the bulk corium pool separates into two layers: oxide and heavy metal, both surrounded by the crusts.

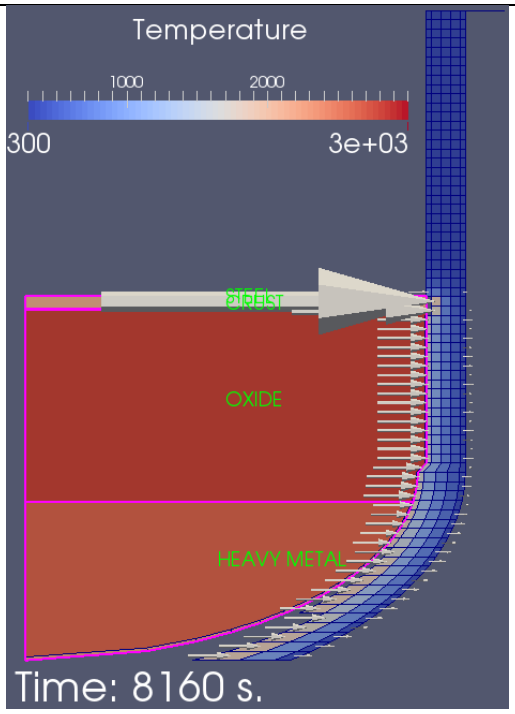

The vessel ablations starts at 5910 s. The ablated steel forms a top layer above the crust. The maximum corium-to-vessel flux value is 3.5 MW/m^2 at 8160 s.

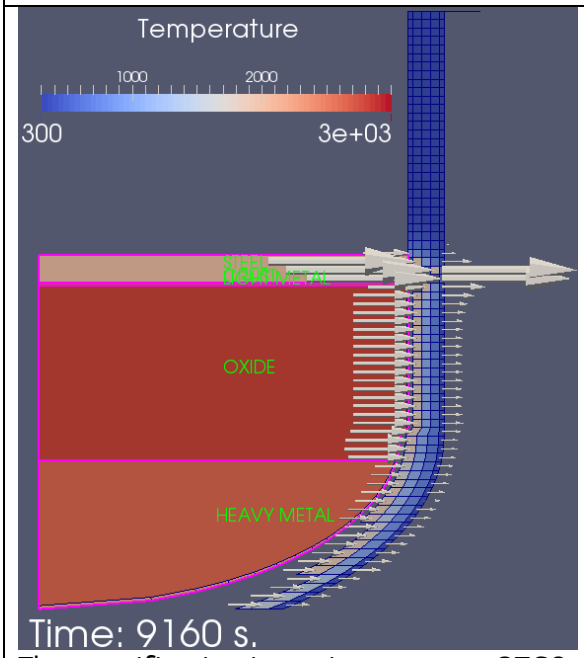

The stratification inversion starts at 8760 s. The maximum value 1.7 MW/m^2 is reached at 9160 s for the wall-to-water flux.

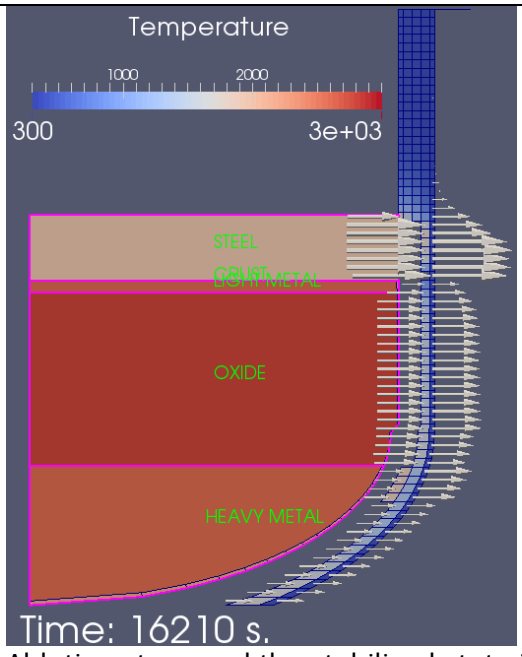

Ablation stops and the stabilized state is reached at 16210 s with both fluxes about 0.8 MW/m^2. Stratification inversion is not yet finished at this time.

The stabilized state parameters are the following:

- fluxes about 0.8 MW/m^2;
- the ablated steel mass is 37.7t;
- the minimum residual thickness is 2 cm (the same remark as before applies).
- the maximum vessel-to-water heat exchange coefficient is H = 7.8 kW/m^2/K.

A.1.3.2 Initial steel mass = 80 t

The simulation progress and the layers configuration for this case are similar to the best-estimate calculation. The key stages of the case are presented below:

- The calculation begins at 4910 s. At 4960 s., the bulk corium pool separates into two layers: oxide and light metal, both surrounded by the crusts.
- The vessel ablation starts at 8560 s. The ablated steel forms a layer above the axial crust. The maximum corium-to-vessel flux value is 3.4 MW/m^2 at 9410 s.
- The maximum vessel-to-water flux value is 2.3 MW/m^2 at 10360 s.
- The stabilized state (no more ablation) is reached at 17760 s. with fluxes about 0.9 MW/m^2.

The stabilized state parameters are the following:

- internal and external fluxes about 0.9 MW/m^2;
- the ablated steel mass is 38.7 t;
- the minimum residual thickness is 2 cm (last solid radial mesh thickness);
- the maximum vessel-to-water heat exchange coefficient is H = 6.5 kW/m^2/K

A.1.3.3 Zirconium oxidation degree NZr/(NZr + NZrO$_2$) C = 30%.

To achieve this oxidation degree, we considered the following initial masses for Zr and ZrO_2 :

- M_{Zr} = 19.8t,
- M_{ZrO2} = 11.47t.

Reminder: in the best-estimate calculation, the initial masses were M_{Zr} = 15.6t and M_{ZrO2} = 17.1t.

The simulation progress and the layers configuration for this case are similar to the best-estimate calculation. The key stages of the case are presented below:

- The calculation begins at 4910 s. At 4960 s, the bulk corium pool separates into two layers: oxide and light metal, both surrounded by the crusts.
- The vessel ablation starts at 8510 s. The ablated steel forms a layer above the axial crust. The maximum corium-to-vessel flux value is 3.1 MW/m^2 at 9510 s.
- The maximum vessel-to-water flux value is 2.5 MW/m^2 at 10360 s.
- The stabilized state (no more ablation) is reached at 17410 s with fluxes about 1.2 MW/m^2.

The stabilized state parameters are the following:

- fluxes about 1.2 MW/m^2;
- the ablated steel mass is 38.7 t;
- the minimum residual thickness is 2 cm;
- the maximum vessel-to-water heat exchange coefficient is H = 6.6 kW/m^2/K.

A.1.3.4 Zirconium oxidation degree C = 70%.

To achieve this oxidation degree, we considered the following initial masses for Zr and ZrO_2:

- M_{Zr} = 8.49t,
- M_{ZrO2} = 26.76t.

The simulation progress and the layers configuration for this case are similar to the best-estimate calculation. The key stages of the case are presented below:

- The calculation begins at 4910 s. At 4960 s, the bulk corium pool separates into two layers: oxide and light metal, both surrounded by the crusts.

- The vessel ablation starts at 8410 s. The ablated steel forms a layer above the axial crust. The maximum corium-to-vessel flux value is 2.4 MW/m^2 at 9110 s.
- The maximum vessel-to-water flux value is 1.2 MW/m^2 at 12260 s.
- The stabilized state (no more ablation) is reached at 17810 s with fluxes about 0.9 MW/m^2.

The stabilized state parameters are the following:

- fluxes about 0.7 MW/m^2;
- the ablated steel mass is 38 t;
- the minimum residual thickness is 2 cm;
- the maximum vessel-to-water heat exchange coefficient is H = 6.3 kW/m2/K

A.1.3.5 Constant vessel-to-water heat exchange coefficient H_{ext} = 10kW/m^2/K.

The code calculated value of the coefficient has been substituted by the recommended value.

The simulation progress and the layers configuration for this case are similar to the best-estimate calculation. The key stages of the case are presented below:

- The calculation begins at 4910 s. At 4960 s, the bulk corium pool separates into two layers: oxide and light metal, both surrounded by the crusts.
- The vessel ablation starts at 8460 s. Ablated steel forms a top layer. The maximum corium-to-vessel flux value is 3 MW/m^2 at 9460 s.
- The maximum vessel-to-water flux value is 2.3 MW/m^2 at 10460 s.
- The stabilized state (no more ablation) is reached at 17060 s. with fluxes about 1 MW/m^2.

The stabilized state parameters are the following:

- fluxes about 0.7 MW/m^2;
- the ablated steel mass is 38.2 t;
- the minimum residual thickness is 2 cm.

A.1.4 Conclusions

The best-estimate calculation and the sensitivity study yielded:

- maximum corium-to-vessel flux values that range from 2.5 to 3.5 MW/m^2;
- maximum vessel-to-water flux values that range from 1 to 2.5 MW/m^2.

The focusing effect always takes place in the cylindrical part of the vessel, at an approximate height of 1.8 m.

We do not observe a significant variation of the ablated steel mass or minimum residual wall thickness between the calculations.

The results have been summed up in Table 3 and Table 5.

Table 4 Summary of the key parameters

Case	Best estimate	Steel 30 t	Steel 80 t	C30	C70	H10
Initial layer configuration	LM over oxidic layer	HM under oxidic layer	LM over oxidic layer	LM over oxidic layer	LM over oxidic layer	LM over oxidic layer
Maximum corium-to-vessel flux (MW/m^2)	2.88	3.5	3.4	3.1	2.4	3.0
Maximum vessel-to-water flux (MW/m^2)	2.0	1.7	2.3	2.5	1.2	2.3
Stabilized flux (MW/m^2)	1.0	0.8	0.9	1.2	0.9	0.7
Ablated steel mass (t)	38.5	37.7	38.7	38.7	38	38.2
Maximum vessel-to-water heat coefficient ($kW/m^2/K$)	6.6	7.8	6.5	6.6	6.3	10 .0 (constant)

Table 5 Key events chronology

Case	Best estimate	Steel 30 t	Steel 80 t	C30	C70	H10
Ablation beginning (s)	8760	5910	8560	8510	8410	8460
Maximum corium-to-vessel flux (s)	9460	8160	9410	9510	9110	9460
Maximum vessel-to-water flux (s)	10360	9160	10360	10360	12260	10460
Ablation end (s)	16000	16210	17760	17410	17810	17060

A.2 IVS ASTEC V2.0r3p2 integral calculation

General modelling approach: The LB LOCA scenario (break 300 mm on cold leg) without availability of active emergency core cooling system and without availability of feedwater was considered. Due to fast core heat-up, melting and molten pool formation in lower reactor head this kind of scenario represents bounding case regarding the thermal load acting on reactor wall. An integral analysis was performed using all ASTEC modules that are responsible for in-vessel phenomena (CESAR, ICARE, ISODOP, ELSA, SOPHAEROS). In addition, simple confinement model was used (CPA module). The whole sequence was analysed starting from break opening, front-end thermal-hydraulics, core heat-up, melting and relocation, quenching of corium in lower reactor head by residual water, re-melting of debris and vessel internals presented here, and finally, developed molten pool formation in lower head. Thus, the mass and composition of molten pool in lower reactor head as well as decay heat generated here was calculated by the code. Consequently, the obtained thermal load acting on the RPV wall is time dependent.

Decay heat calculation: the residual power was calculated from a defined initial inventory of fission products (FPs) in the core (about 700 isotopes were defined). In the course of calculation the code calculates transmutation of isotopes and decay heat (ISODOP module), release of volatile FPs from core after cladding failure (gap release) and from fuel matrix (ELSA module), chemistry, transportation and retention of FPs within primary system (SOPHAEROS module), release of FPs from break (and corresponding part of decay heat) into confinement. The thermal-hydraulic response of confinement and transport of FPs is calculated by CPA module. When the core melting and relocation took place, together with molten UO_2 that is relocated into the RPV lower head, the fraction of decay heat that corresponds to non-volatile FPs contained in relocated mass of uranium followed the corium. When the stratified configuration of molten pool in lower reactor head is formed, distribution of FPs between corium layers is calculated by the code based on chemical affinity of FPs.

Molten pool modelling features: The Lower Plenum model of ICARE module enables simulation of corium relocation into lower reactor head, interaction of corium jet with residual water and vessel internals that are located here. Stratified pool configuration was considered assuming "detailed" (SEPA_ACT = 1) phase separation model and uniform composition and temperature within each corium layer. Radiation from upper corium layer was not modelled (not possible in integral calculation). Thus, heat flux through RPV wall is overestimated.

Material properties. The same solidus (T_{sol} = 2550 °K) and liquidus (T_{liq} = 2600 °K) temperature was used for both, UO_2 and ZrO_2. Other material properties were taken from built in characteristics of ASTEC code. Composition and physical properties of generic stainless steel (alloy of Fe, Cr and Ni) are predefined in ASTEC code.

Confinement and external RPV cooling: In parallel with the in-vessel phenomena the confinement response was analysed. Coolant balance in confinement sump was calculated based on the initial inventory, contributions of coolant from primary leak and steam condensed on confinement walls. When the core outlet temperature reached 750 °C the pump taking suction from confinement sump was switched on and the reactor cavity was flooded. At that time the “dry cavity” (nearly adiabatic) boundary condition applied on the RPV outer surface was replaced by “wet cavity” condition and the HTC equal to 10 $kW.m^{-2}.K^{-1}$ and actual coolant temperature in flooded cavity were applied. This allows simulation of heat transfer from molten pool through RPV wall into coolant in cavity. When water in the riser part of flooded cavity around RPV became saturated, steam generated here was vented into confinement. Simple controller that preserves water level in reactor cavity was used.

Results: The core heat up started about 30 min from the beginning of the accident. Shortly later the cladding burst occurred and volatile FPs started to escape from the core to primary system and hence through break into confinement. Reactor cavity was flooded shortly before 1 hour from the beginning of the accident. After start of core melting and relocation a temporary molten pool was formed on the core support plate. Failure of core barrel followed by side relocation of the corium into lower reactor head occurred at t ~ 1 hour 30 min. At this time more than 100 tons of molten corium was collected on core support plate (Fig. 4). Nearly 80 tons of this mass was suddenly relocated into lower reactor head and

interacted with residual water here (Fig. 1). Due to the corium jet erosion by residual water about 50% of corium was fragmented and quenched into solid debris (Fig. 5). Second, smaller corium slump (~15 tons of molten corium) took place after 2 hours from the beginning of the accident.

Temporary molten pool configuration was formed in lower reactor head with SS structures (still solid in this phase) plunged inside liquid corium and with debris layer on the top. This configuration consisted of heavy metallic layer (containing some oxides) at the bottom, massive layer of oxides (containing relatively high mass of metals) and finally, layer of debris on the top.

Shortly after t ~ 4 hours the core support structures and debris in lower reactor head were melted and new developed molten pool configuration was formed here. The original pool arrangement was reconfigured and new light metallic layer was formed on the top. At the same time mass of lowermost heavy metallic layer was reduced significantly and crust was formed between oxidic layer and upper metallic layer. Since this time the bulk of decay heat was removed from corium pool through RPV wall (Fig. 3) into coolant in flooded reactor cavity. At the elevation of hot metal layer on the top of pool corium pool wall ablation took place. Ablated steel resulted in further increase of Fe component and gradual increasing of thickness of upper metallic layer.

Light metal that appeared in newly created upper layer during phase separation process was initially highly overheated. Thus, maximum heat flux on the outer RPV surface (~ 1,35 MW/m^2, Fig. 2) was reached at t ~ 4 hrs 30 min shortly after creation of upper metallic layer when the metal was hottest and the metallic layer was still relatively thin. In the further course of the accident total energy removed through RPV wall was higher than the heat generated inside the reactor vessel (Fig. 3). Thus, the temperature of upper metallic layer was dropping gradually (Fig. 1) whereas the temperature of oxidic pool that was separated by solid crust was kept constant.

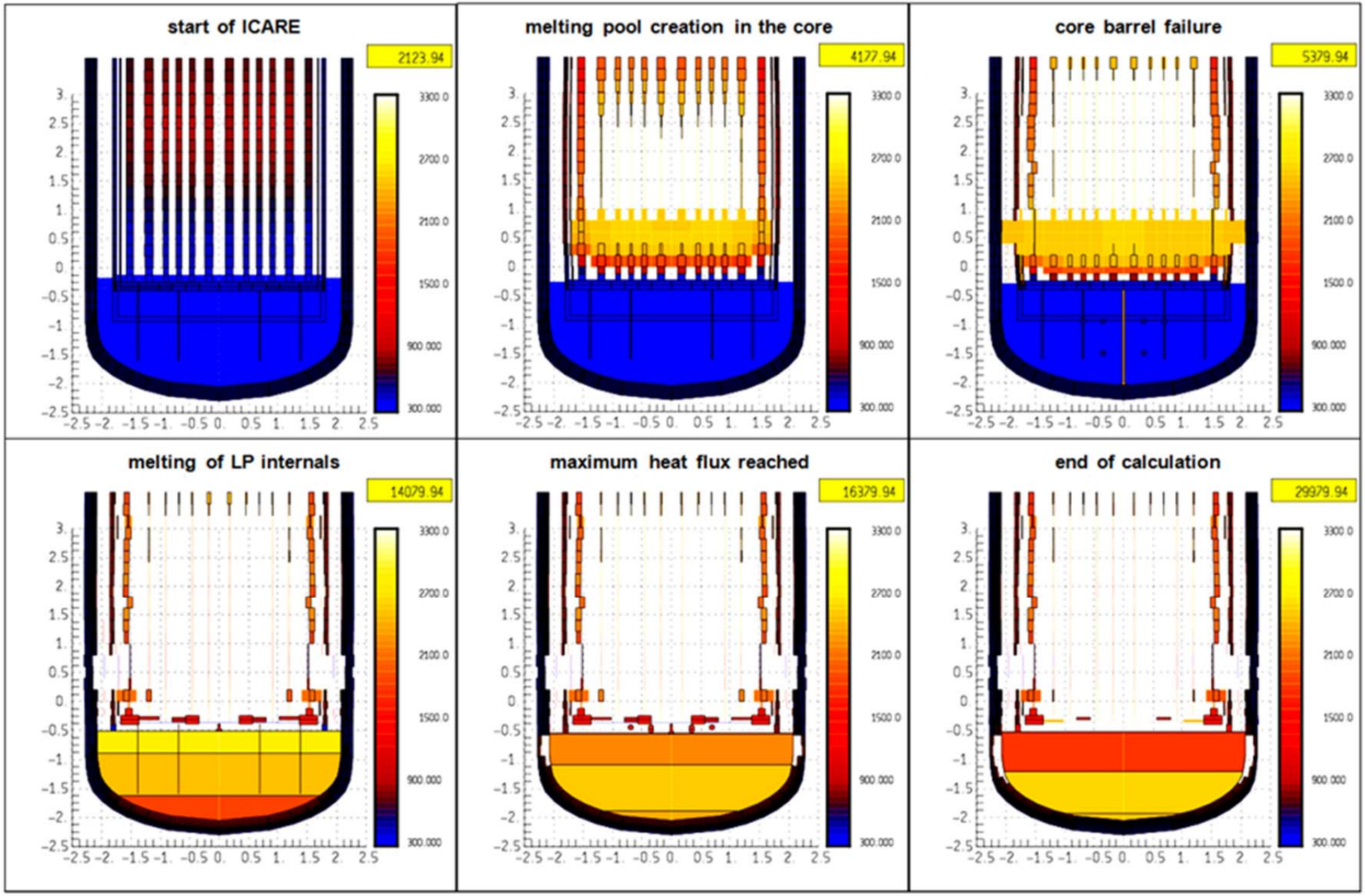

Fig. 1. Temperature field in corium pool and RPV wall

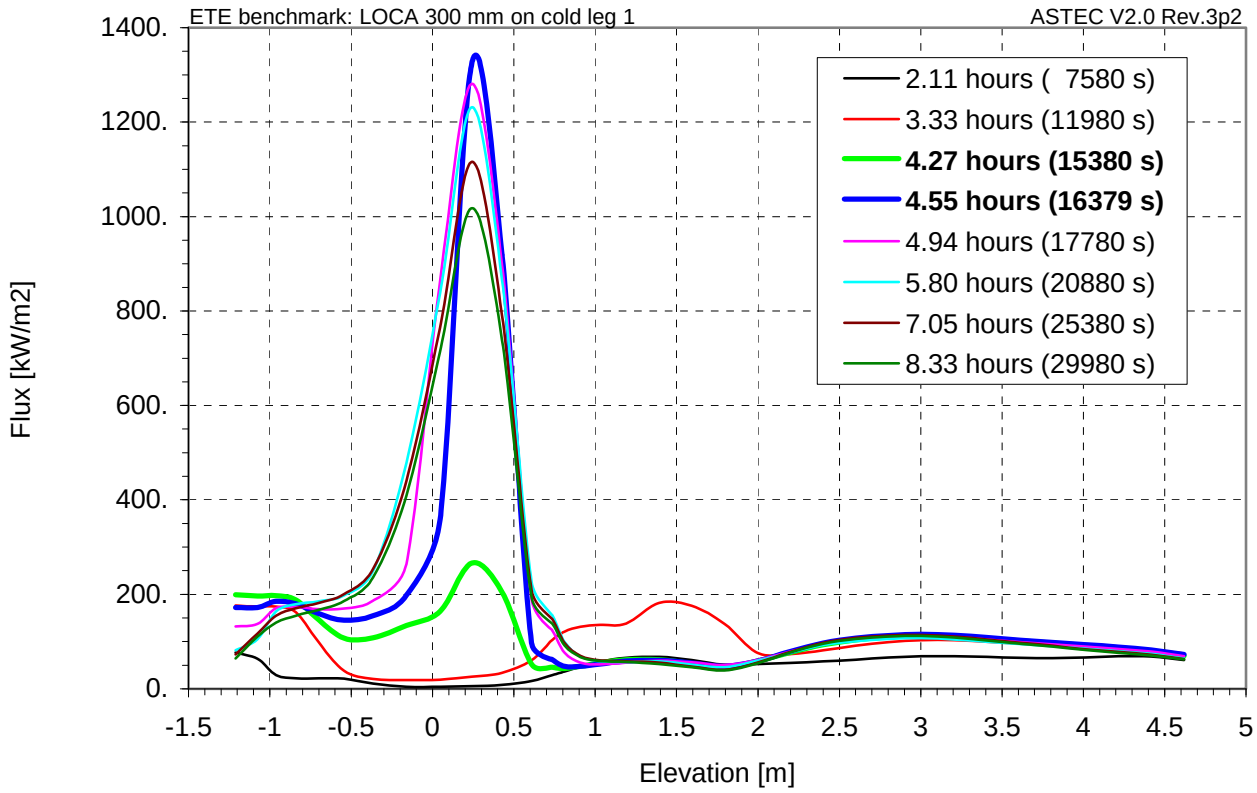

Fig. 2. Heat flux profiles on outer RPV surface at different times

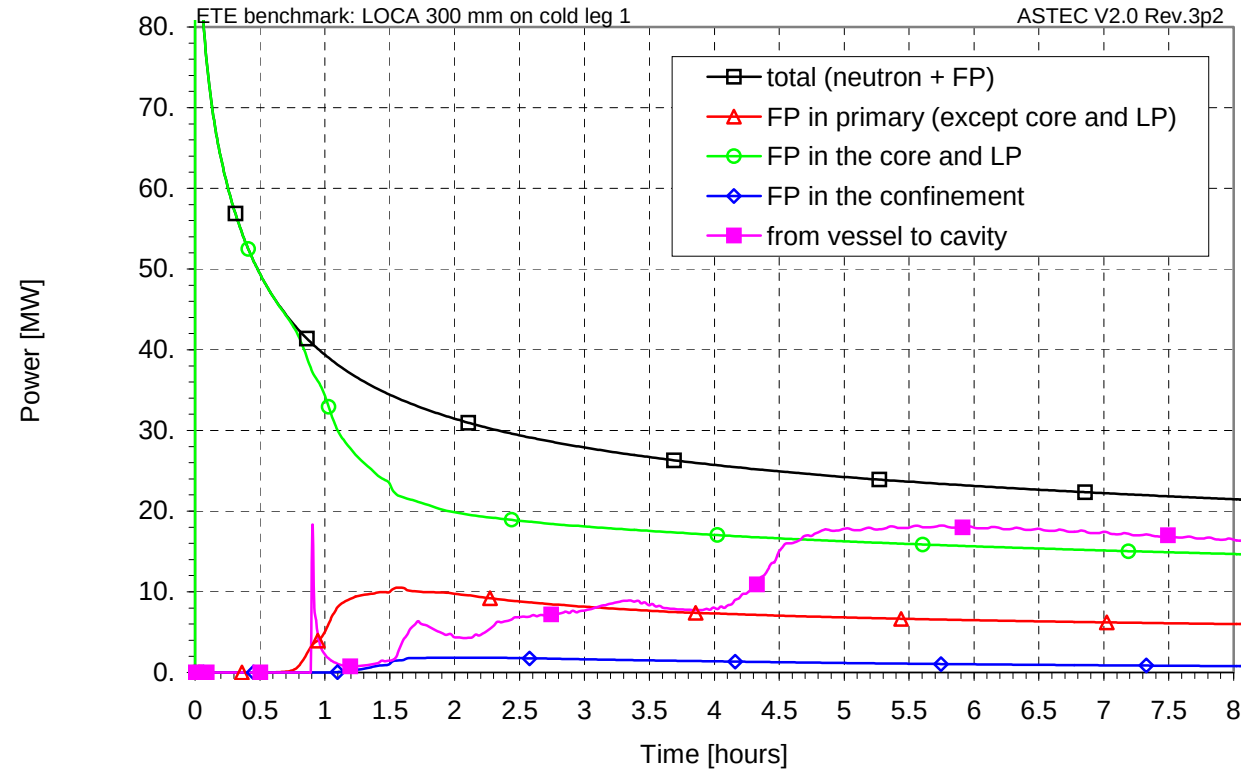

Fig. 3. Power balance of FPs and heat transfer through RPV wall

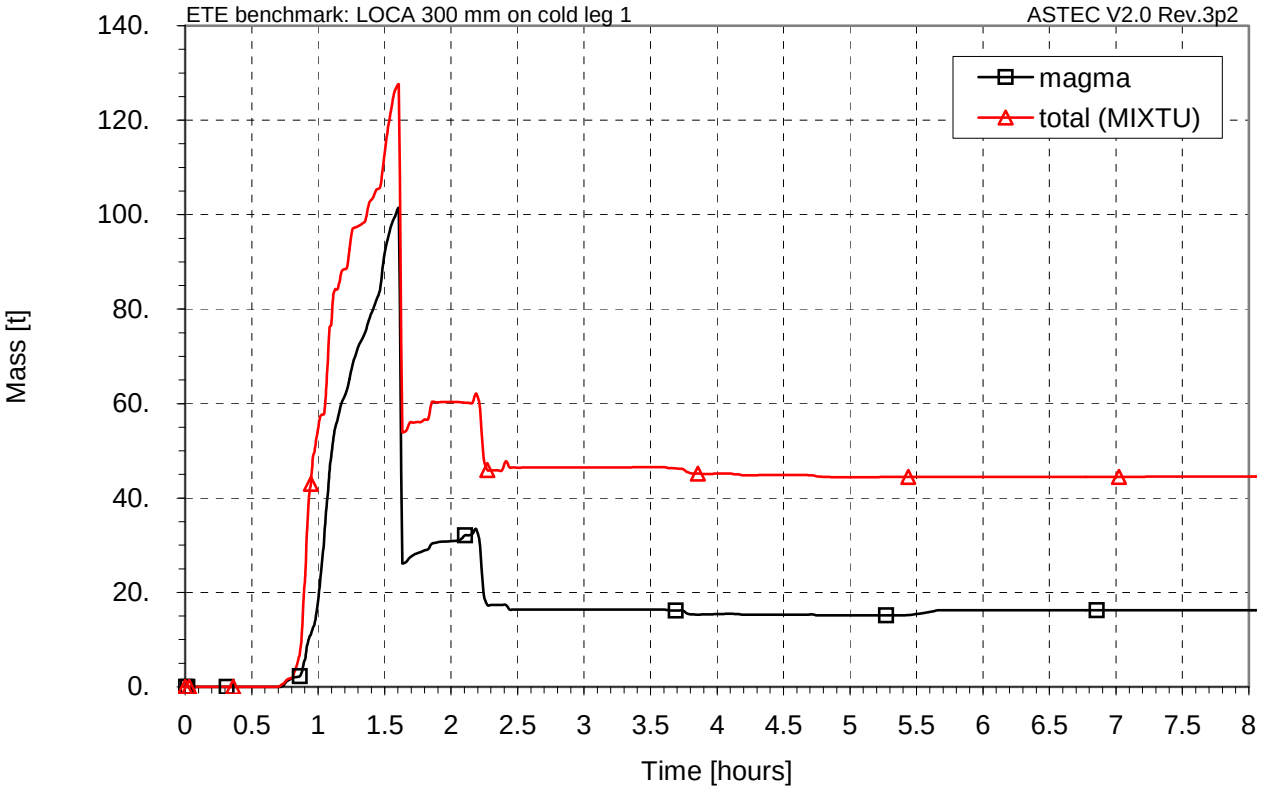

Fig. 4. Masses of magma and degraded core materials on core support plate.

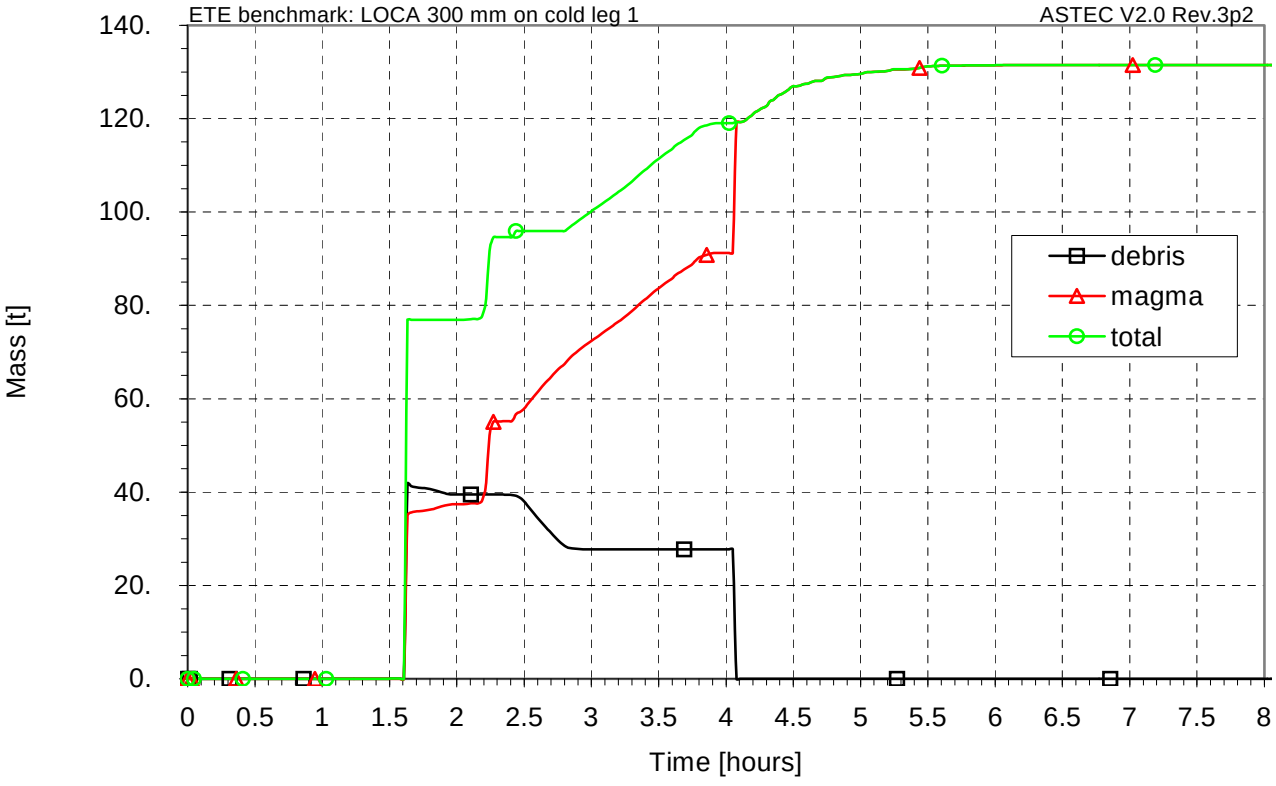

Fig. 5. Masses of magma and debris in lower plenum.

A.3 IVS ASTEC V2.1beta stand-alone calculation

General modelling approach: The ICARE stand-alone analysis starts at t = 4910 s of overall transient assuming core barrel melt trough followed by corium relocation into dry lower reactor head, where solid internal structures made of stainless steel (SS) were modelled. The relocation phase was not modelled; sudden presence of corium in lower head was assumed instead.

The transient than continues with heat-up and melting of solid vessel internals, formation of volumetrically heated molten pool, reactor wall heat up and ablation, formation of developed molten pool assuming heat transfer through reactor wall into water in flooded reactor cavity and radiation from upper pool surface. Heat transfer on outer reactor surface and radiation from upper pool surface were modelled as boundary conditions.

Nodalization: Lower plenum model that is part of ICARE module was used in the analysis. The lower head was meshed into 10 equidistant layers through the wall thickness and 19 cells in axial direction. It was assumed that the RPV wall is made of Fe (material properties are predefined in ASTEC code). Actual shape of RPV was modelled. The SS liner on inner surface was not considered but replaced by Fe instead.

Lower head internals: solid support structures at the beginning of transient were modelled using (STRU LSTRUCT). Total mass of these solid structures was 26400 kg. These structures are made of SS. Composition and physical properties of generic SS (composed of Fe, Cr, Ni) are predefined in ASTEC code. Initial temperature of RPV wall and internals in lower head was equal to 227 °C.

Initial and boundary conditions such as corium mass and composition, time of corium relocation into lower plenum, initial average corium temperature, decay heat generated in corium, were taken from KI calculation and definition of benchmark scenario that was agreed before. Constant internal pressure 0.2 MPa was assumed.

Decay power. Reduction of total decay heat by 20% was assumed in all calculations (accounting for release of volatile fission products). It was assumed that the decay heat is generated in both, UO_2 and U. Thus, during the phase separation in corium pool when the reduction of ceramic UO_2 to metallic U takes place, the total power generated in corium pool is preserved according to decay curve Furthermore, this means that when the stratified arrangement of corium layers takes place, bulk of the decay heat is produced in oxide layer and the remaining fraction is generated in metallic layer.

External RPV cooling was modelled as boundary condition assuming constant value of heat transfer coefficient 10 kW/(m^2. K) at the outer RPV surface and ambient coolant temperature 120 °C (saturation at 200 kPa abs.). This boundary condition was applied since the beginning of analysis (t = 4910 s).

Material properties: Default values of materials properties that are implemented in ASTEC code (including solidus and liquidus temperatures for UO_2 and ZrO_2) were used. The default values of melting temperatures of UO_2 and ZrO_2 are higher than average initial temperature of UO_2 - ZrO_2 - Zr - SS magma (T = 2500 °K) at the time t = 4910.

Radiative heat transfer from upper corium layer was considered assuming the temperature of upper vessel structures that have not been relocated yet close to melting point of SS (boundary condition T_{plate} = 1700 °K, i.e. close to melting point of SS).

Stratification of originally homogeneous pool was calculated by the code assuming detailed model of phase separation (STRU SEPA_ACT = 1). This means that the number, arrangement and composition of corium layers were predicted by the ASTEC code. Besides base case with ~70 tons of SS sensitivity study regarding the mass of SS in corium pool was performed (analysed margin 30 - 80 tons of SS).

Results: The course of energy balance in molten pool for the base case is shown on Fig. 1. Since ~20000 s the pool stratification is completed and power generated in pool and heat transferred through reactor wall are nearly in equilibrium (the difference corresponds to radiation). Final pool configuration and heat flux profiles on outer reactor surface for 30, 70 and 80 tons of SS is shown on Fig. 2.

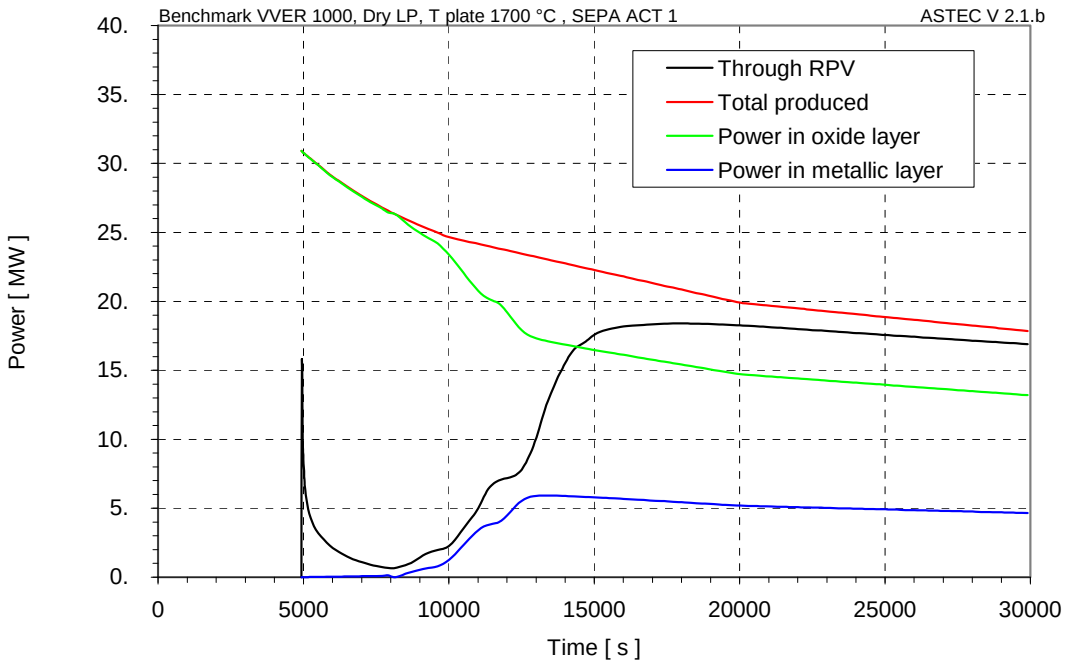

Fig. 1. Balance of power in lower reactor head.

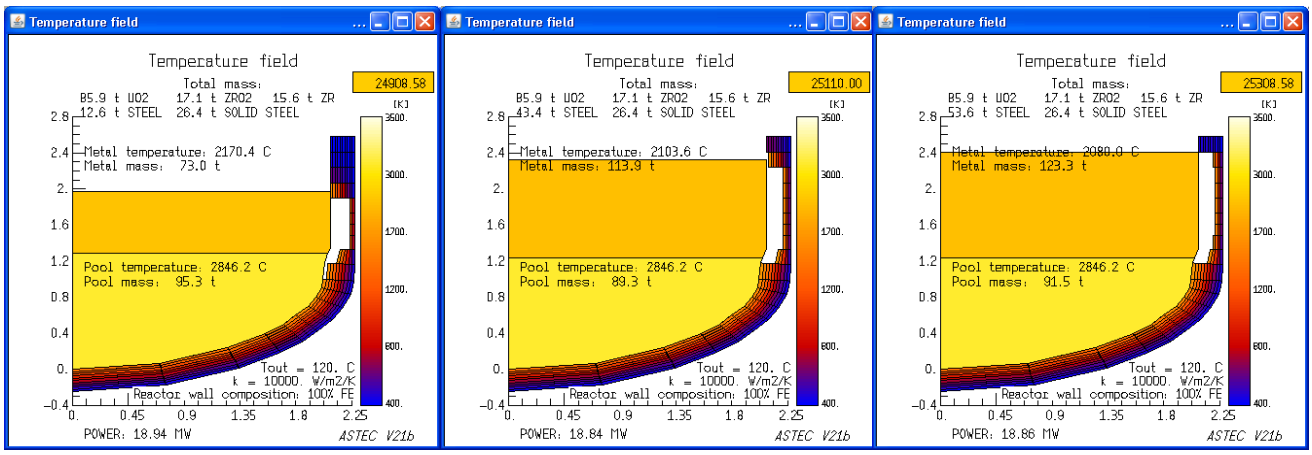

Fig. 2. Stratified configuration: Effect of SS mass 30, 70 and 80 tons, comparison of final pool configurations at t ~ 7 hours (above) and maximum heat flux profile reached during transient (right).

Heat fluxes on RPV outer surface.

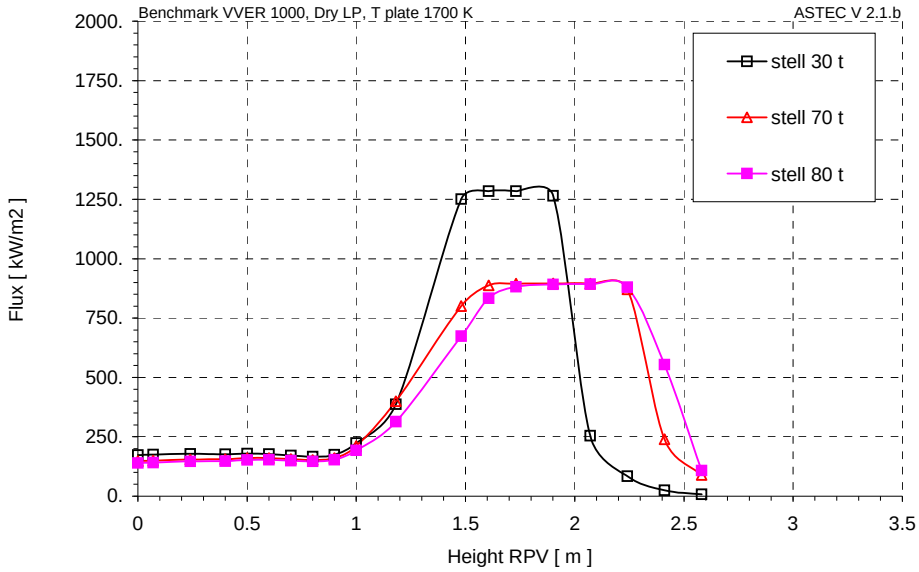

A.4 INRNE ASTEC v2r3 stand-alone calculation

A.4.1 Introduction

Hereafter is presented in-vessel melt retention investigation with external vessel water cooling in case of severe accident (SBO with LBLOCA).

The analyses have been performed as stand-alone calculations with ICARE/ASTECv2.0r3 model for VVER1000 design.

Two “best estimate” calculations have been done: “Initial calculation” and “Basic calculation (fission products release, -20%)”

The “Initial calculation” started at time 4340 s after the beginning of severe accident (Large Break LOCA (2 ´850 mm) with full SBO) in VVER1000. This is the moment of core barrel melting-through and corium relocation into the bottom of lower head vessel.

The “Basic calculation” started at 4910 s after the beginning of the same SBO scenario but with assumption for decay heat power reduction with 20%.

A.4.2 Basic model assumptions

An ICARE/ASTECv2r3 model for VVER 1000 vessel without internals and without coolant has been developed. An elliptical bottom of the lower plenum has been modelled.

The elliptical part of the lower head vessel has been divided into 5 radial rings (MESR 5) and 7 axial segments (summary 35 meshes) as it is shown in Figure 1.

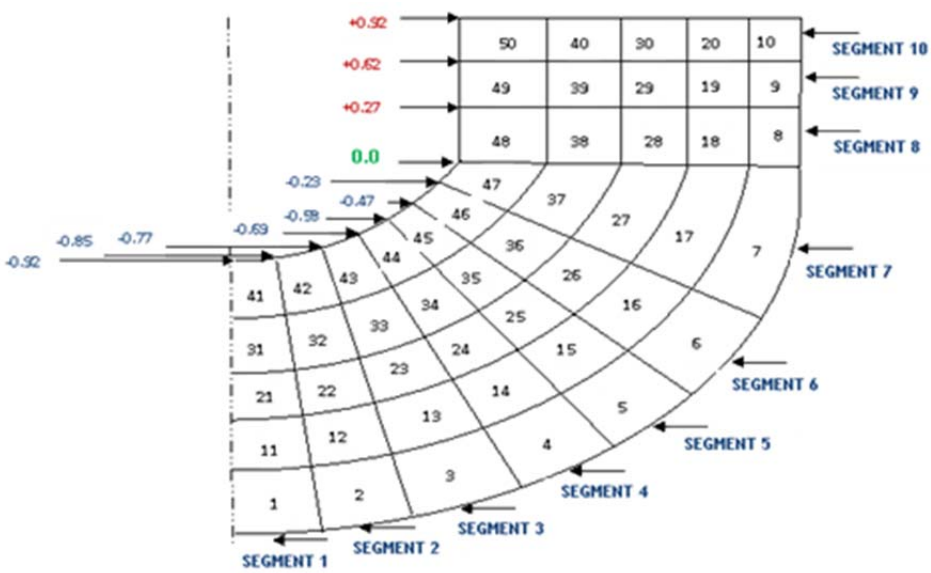

Figure 1: Segmentation of the reactor vessel in the model

The cylindrical part of the lower plenum has been modelled as 5 rings and 3 axial segments (summary 15 meshes).

The cylindrical part of the vessel from elevation “0” to elevation “0.8” has been modelled as 1 ring and 3 axial segments (summary 3 meshes).

It have been performed calculation, where external water cooling has been simulated by a constant value of heat exchange coefficient **H=10000. [W/m²/K]**

Initial and boundary conditions

(Pout = 1.5D+05) ! out pressure

(Tout = 425.) ! out temperature [K]= 152 ^{0}C

(Time_beg = 4340. and 4910. ! calculations beginning

(platetmp=1500.) ! support plate fictive temperature for heat losses due to radiation

(T1 = 2500.) ! initial corium temperature

The slump in the lower plenum has been modelled.

The slumps of corium into the lower plenum in the both calculations have been performed at the beginning of the calculations. The corium is composed by UO_2, ZrO_2, Zr and Stainless Steel. Initial corium composition is shown in Table 1.

Table 1: Initial corium composition

Material	**Mass, t**	**Source**
UO_2	85.9	CORE
Zr	15.6	CORE
ZrO_2	17.1	CORE
Steel	34.4	CORE
	12.2	elliptic part of barrel
	9.0	melted cylindrical part of barrel
	12.3	FA-supports
	1.94	support grid

Melting temperatures of oxides:

As eutectic point of the UO_2 and ZrO_2 it was used in the model 2850 K.

It was also assumed that corium arrives from the core to the bottom head with temperature 2800 K.

```
STRU MATE NAME UO2
        TBEG  2800.  TEND 2850. HEAT 7.4D4  TYPE  L
END
STRU MATE NAME ZRO2
        TBEG  2800.  TEND 2850. HEAT 9.0D4  TYPE  L
END
```

Other model assumptions:

SEPA_ACT 1 ! separation model is applied

NCONFG 3 !the corium is modelled in 3 layers

STRU RUPTURE ! The structure “Rupture” uses “Fusion” and “Mechanic” criteria.

CRIT 'FUSION'

CRIT 'MECHANIC'

END

Decay heat for the both calculations: “Initial calculation” and “Basic calculation”

Decay heat time dependence used in the calculations is presented in Table 2:

Table 2: Decay heat history

Time from the accident start, s	**Decay heat, Wt (per 1 kg of UO_2)**	
	Initial calculation	**Basic calculation (account of fission products release, -20%)**
1000	731.6	585.28
2000	609.4	487.52
3000	542.4	433.92
4000	497.1	397.68
4910	-	**373.44**
5000	463.8	371.04
6000	437.5	350
7000	416.6	333.28
8000	398.9	319.12
9000	384.4	307.52
10000	371.6	297.28
20000	300.1	240.08
30000	268.9	215.12
40000	250.5	200.4
50000	237.7	190.16
60000	227.8	182.24
70000	218.9	175.12
80000	211.2	168.96
90000	203	162.4
100000	194.9	155.92
200000	166.5	133.2
300000	146.3	117.04
400000	128.6	102.88

A.4.3 Main results from analyses

A.4.3.1 Initial calculation:

The calculations continue till 30000s. Till this time the lower head vessel failure doesn't occur.

There are presented below the temperature field figures and the temperature diagrams of the different rings versus elevation.

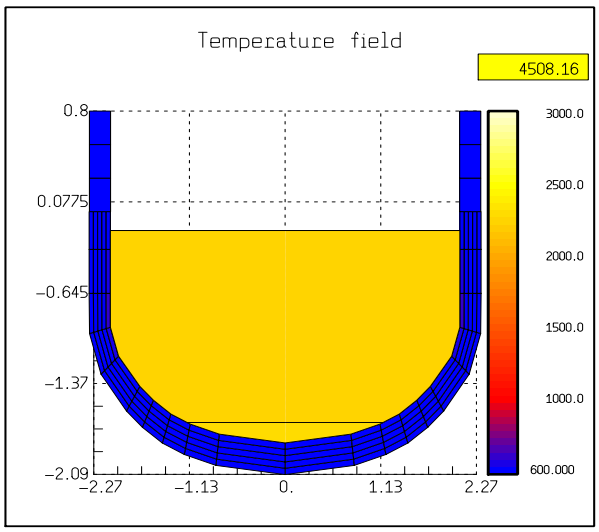

Figure 2: Temperature field at 4508s

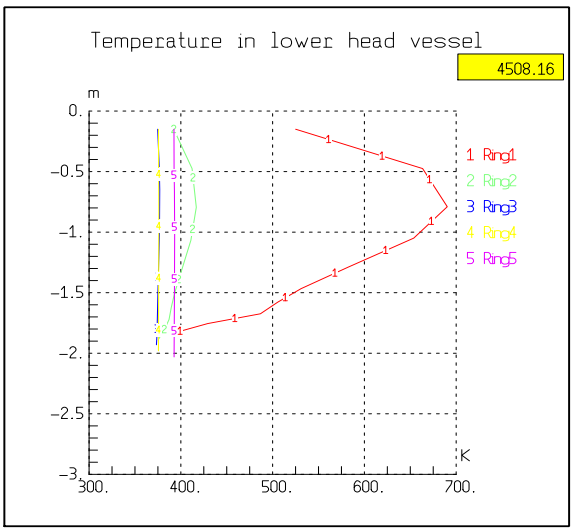

Figure 3: Rings temperature diagram at 4508s

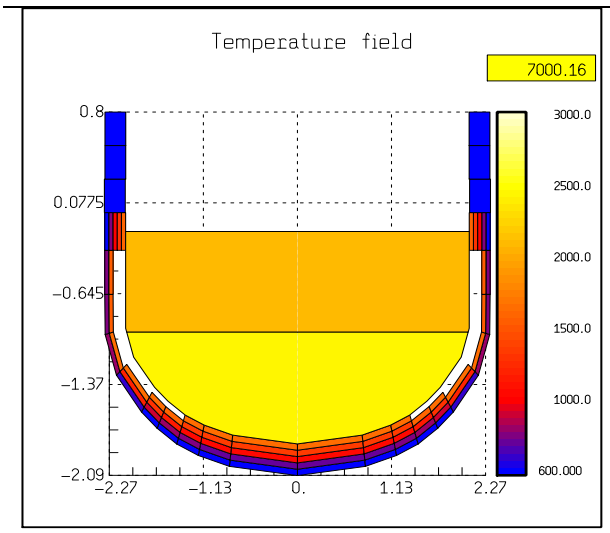

Figure 4: Temperature field at 7000s

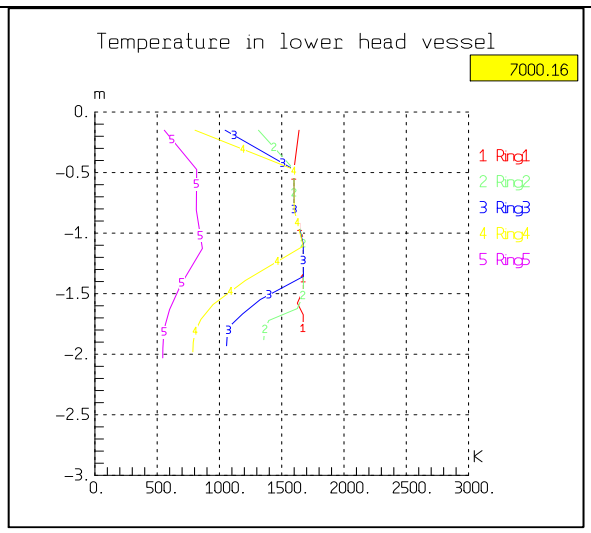

Figure 5: Rings temperature diagram at 7000s

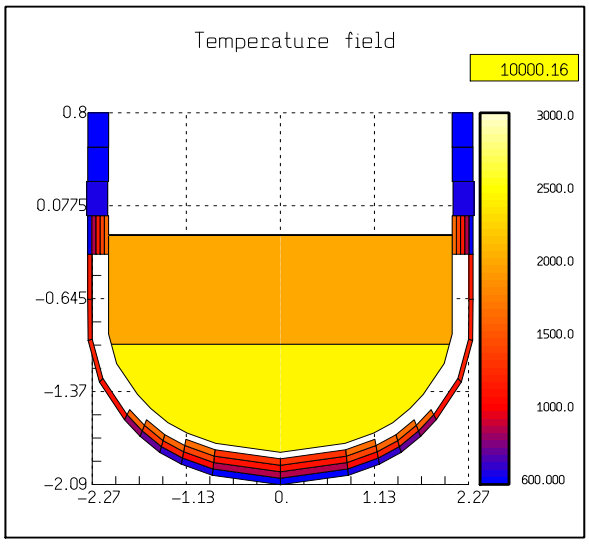

Figure 6: Temperature field a 10000s

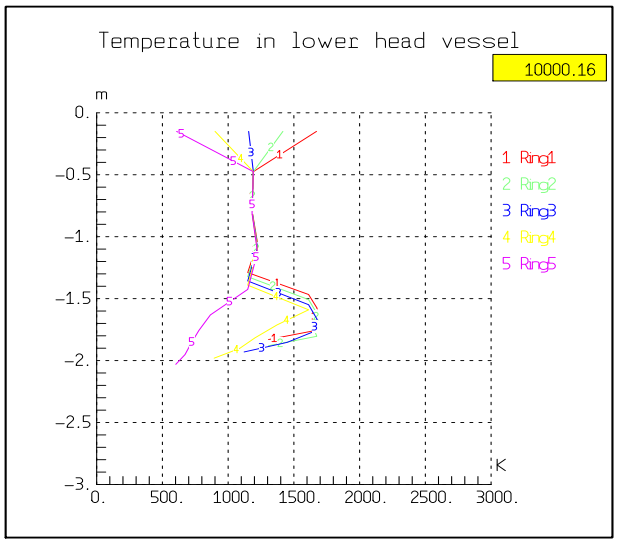

Figure 7: Rings temperature diagram at 10000s

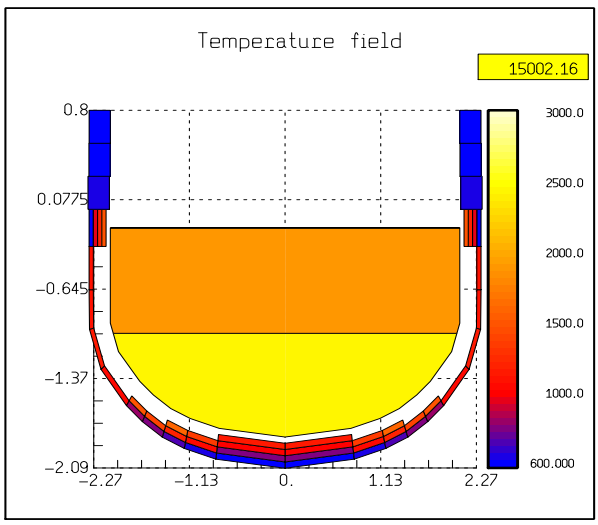

Figure 8: Temperature field at 15002s

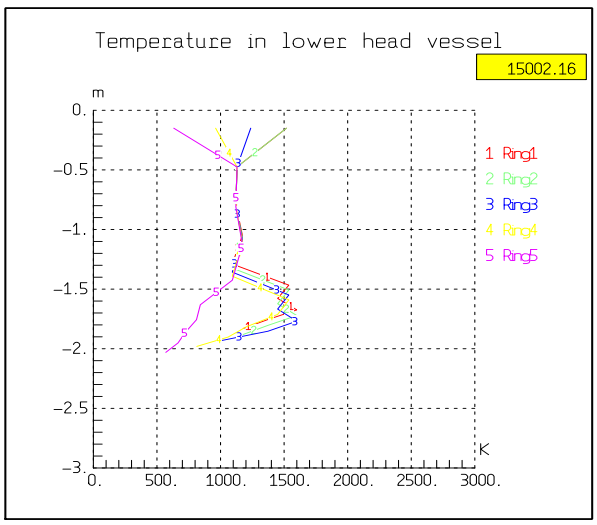

Figure 9: Rings temperature diagram at 15002s

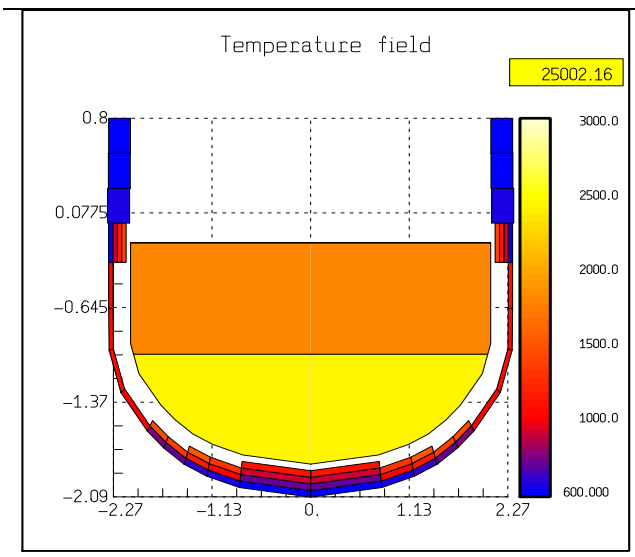

Figure 11: Temperature field at 25002s

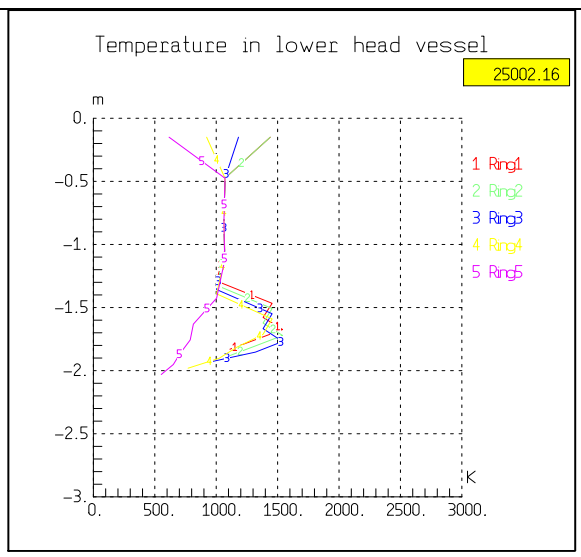

Figure 12: Rings temperature diagram at 25002s

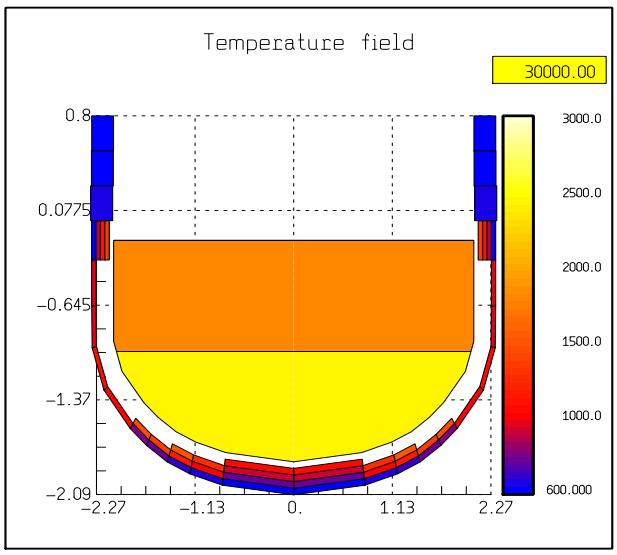

Figure 13: Temperature field at 30000s

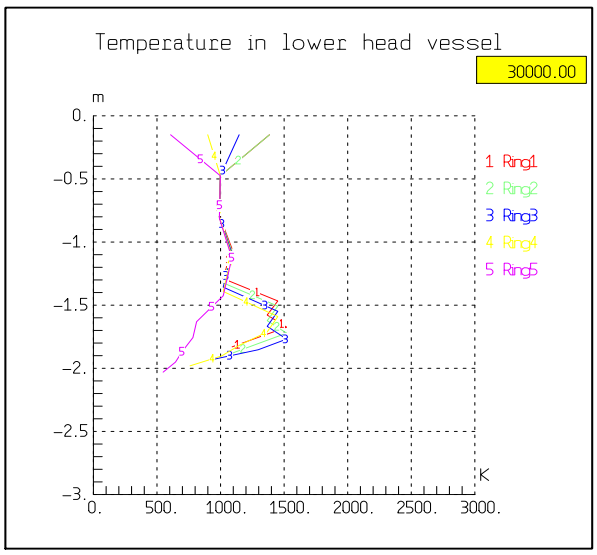

Figure 14: Rings temperature diagram at 30000s

There are presented below (Figure 15) the heat fluxes from the vessel to the water for H=10000 [W/m^2/K] for different elevations. They were calculated for the most external meshes of the lower head vessel (the surfaces of the external meshes were used). In the input the external mashes have numbers from 1 to 10 (from elevation "-0.92" to elevation "+0.62"). It was assumed that the elevation "0" corresponds to border between elliptical part and cylindrical part of the lower head.

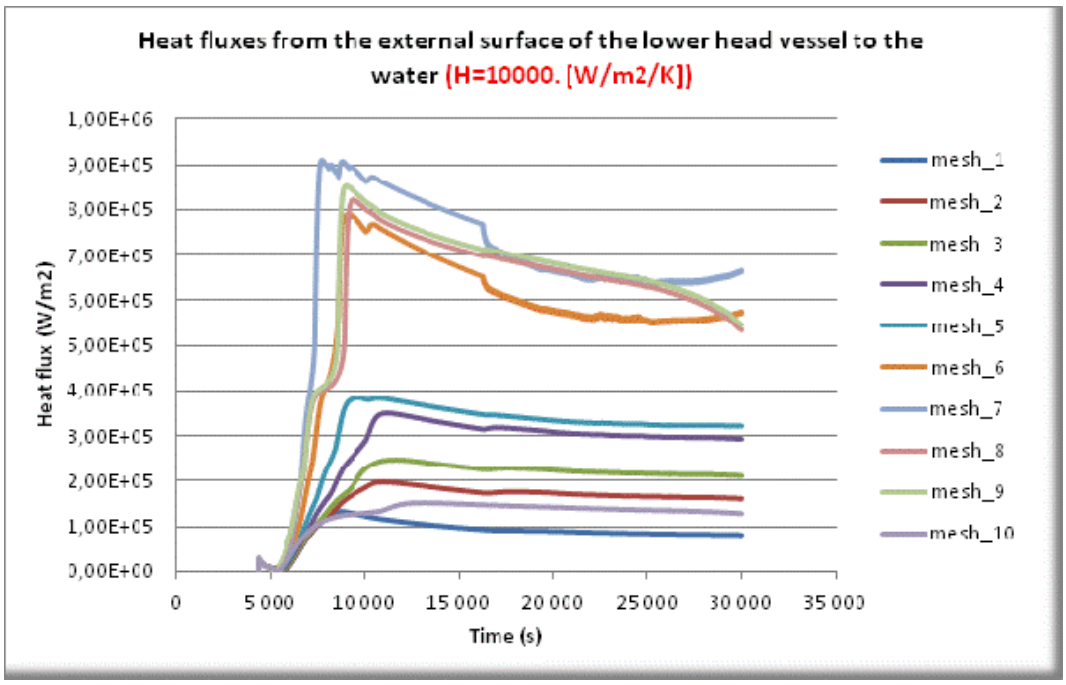

Figure 15: Heat flux from the external surface of the lower head vessel to the water

The maximal heat fluxes from the melt pool to each internal segment (for H=10000. [W/m^2/K] calculation) are presented at Figure 16 below.

This maximum value corresponds to the mesh in contact with the pool.

Primary in the input the internal mashes have numbers from 41 to 50 (from elevation "-0.92" to elevation "+0.62"). Once the mesh melts it disappears and the maximum heat flux corresponds then to the neighbor mesh.

The maximal heat fluxes are determined for each internal mesh by equation: $\varphi=(POWE+PCON)/S_{int\_mesh}$, where:

- PCON (W) is the convective power exchanged on the internal face of the mesh;
- POWE (W) represents the other powers exchanged on the internal face of the mesh;
- S_{int_mesh} is internal face of the mesh in contact with the pool.

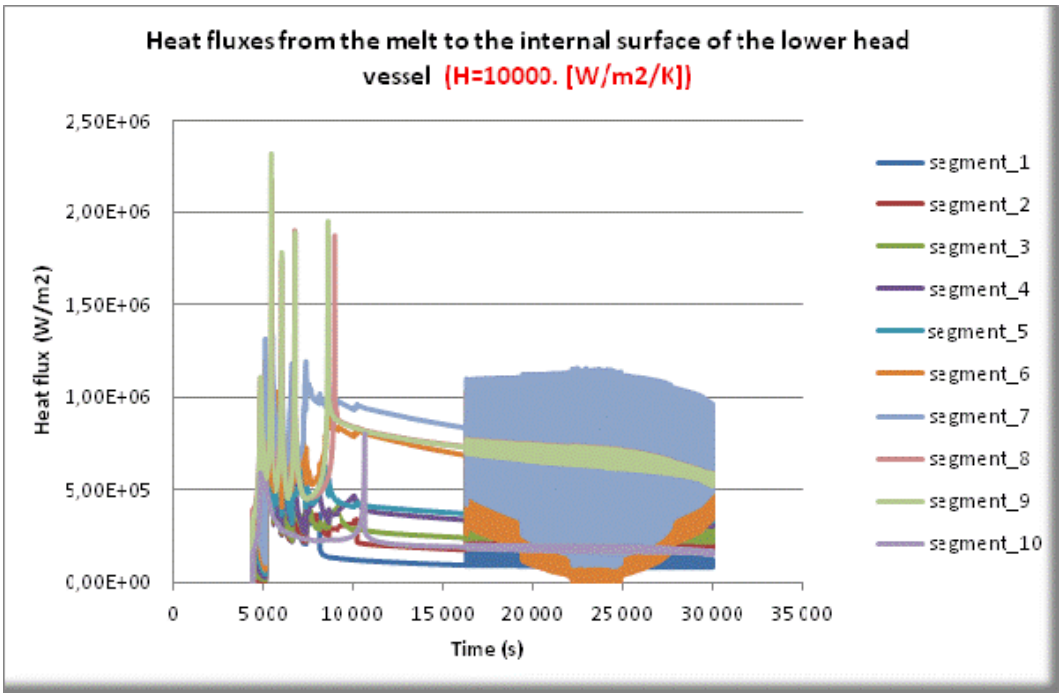

Figure 16: Heat fluxes from the melt to the internal surface of the lower head vessel

The maximum HF axial profile given looking at each external and internal point during the whole time at all elevations are presented at Figure17. All those maximum values defining a bounding curve.

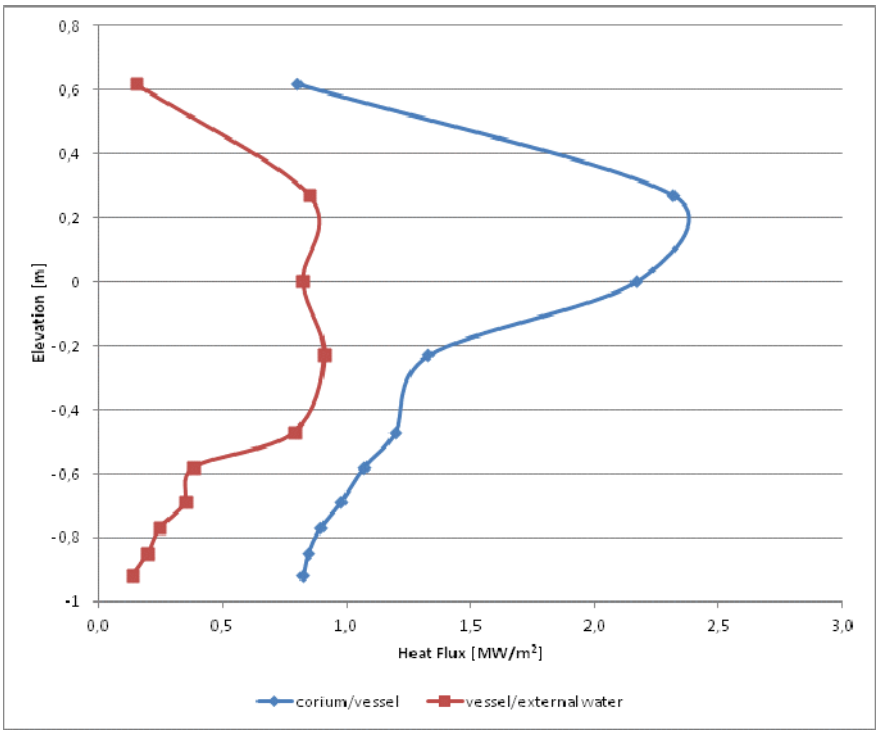

Figure 17: Bounding curve of maximal heat fluxes

A.4.3.2 Basic calculation:

The calculations continue till 30000s. Till this time the lower head vessel failure doesn't occur.

There are presented below the temperature field figures and the temperature diagrams of the different rings versus elevation.

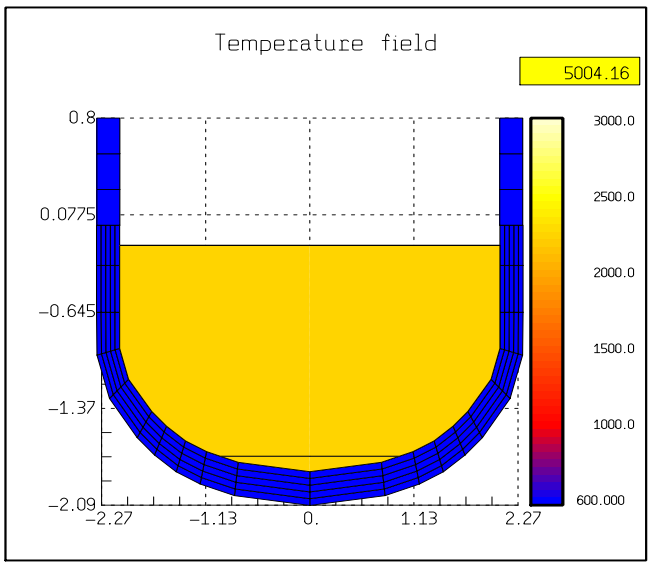

Figure 18: Temperature field at 5004s

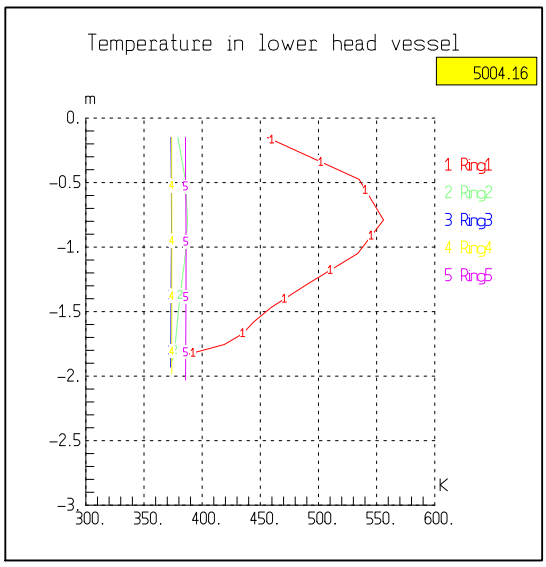

Figure 19: Rings temperature diagram at 5004s

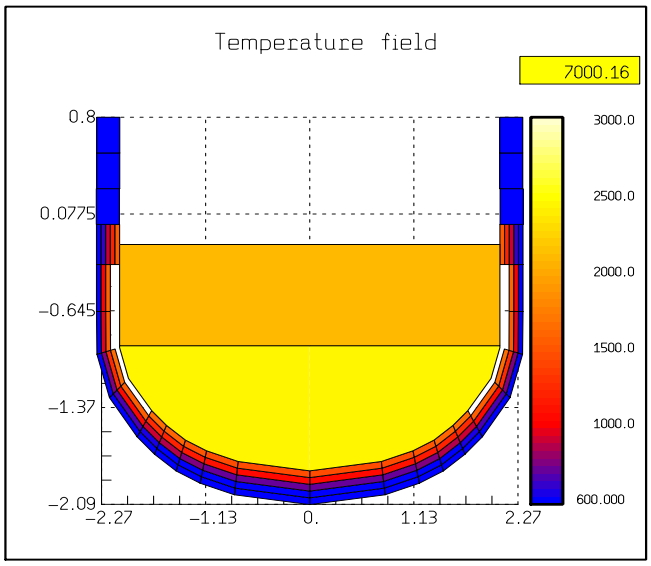

Figure 20: Temperature field at 7000s

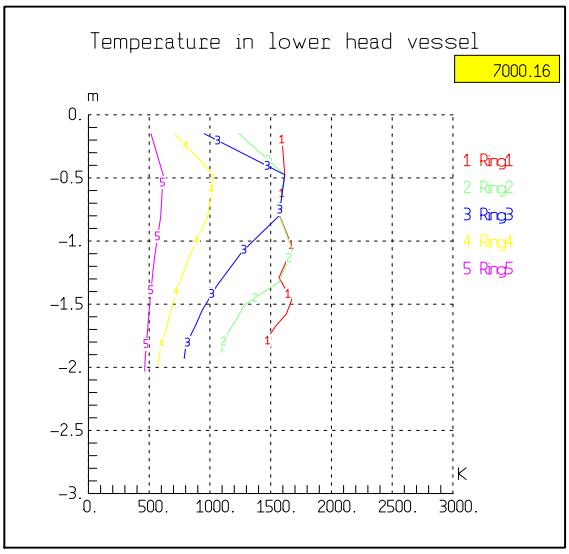

Figure 21: Rings temperature diagram at 7000s

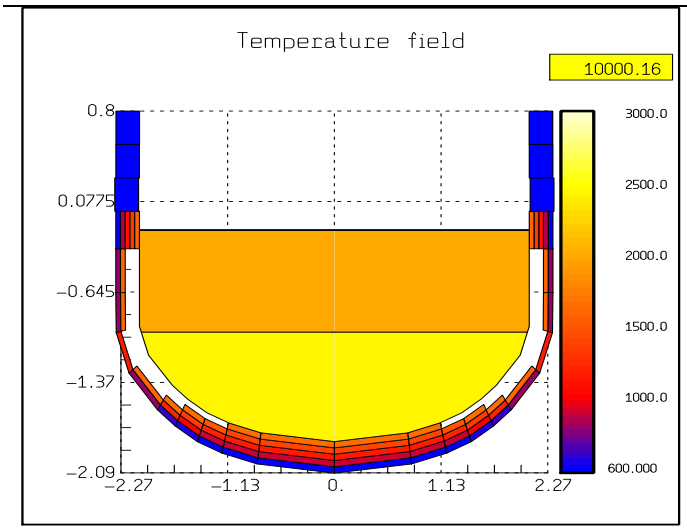

Figure 22: Temperature field at 10000s

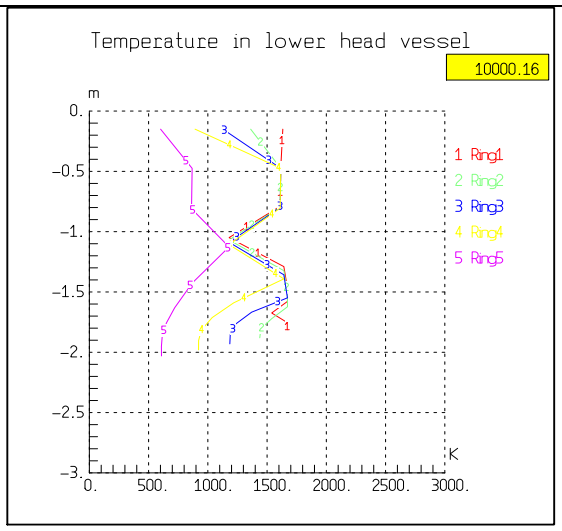

Figure 23: Rings temperature diagram at 10000s

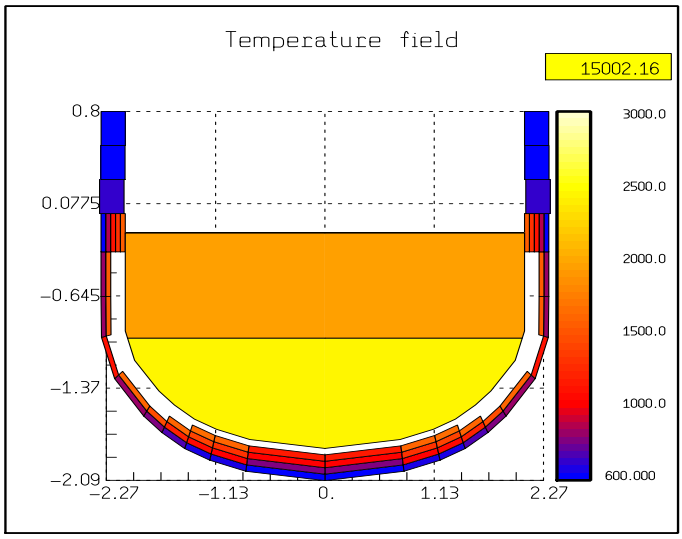

Figure 24: Temperature field at 15002s

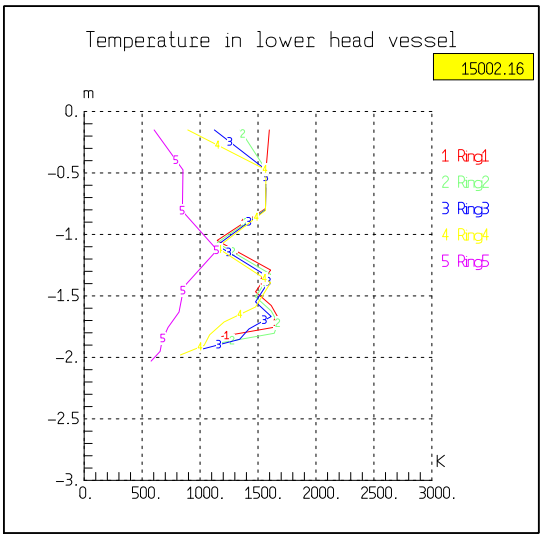

Figure 25: Rings temperature diagram at 15002s

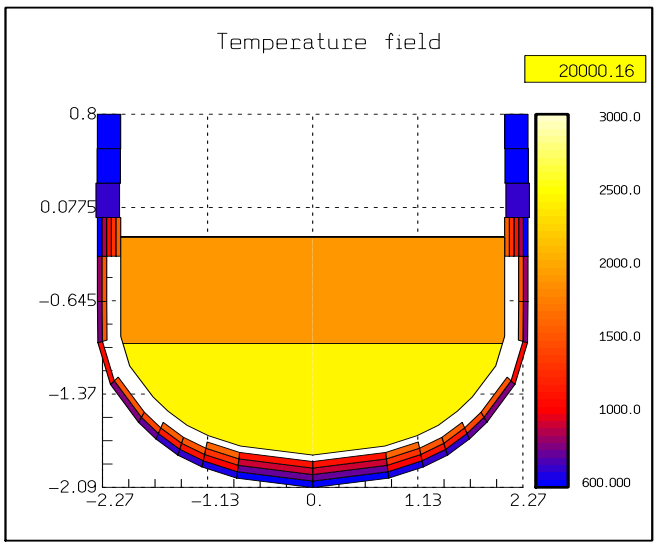

Figure 26: Temperature field at 20000s

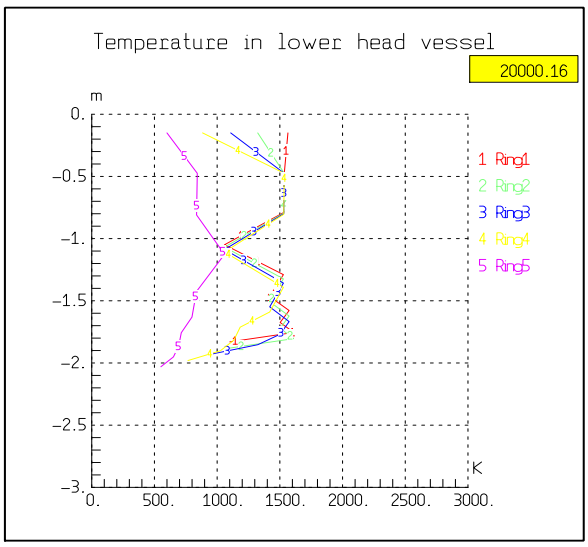

Figure 27: Rings temperature diagram at 20000s

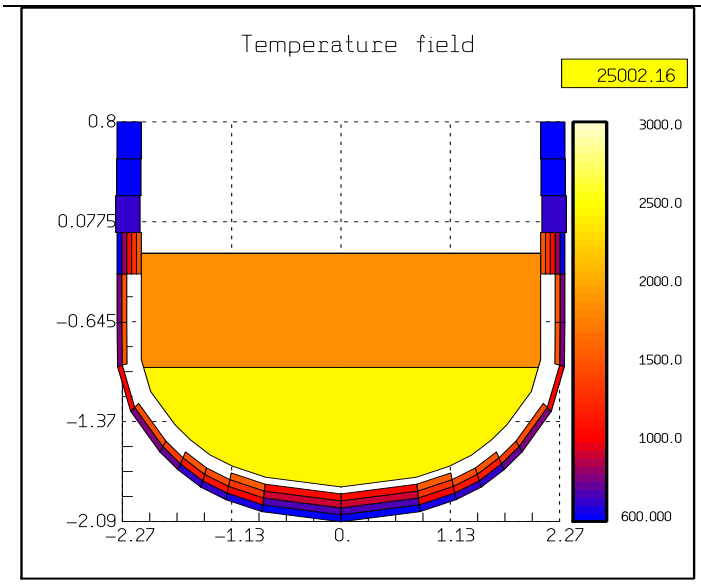

Figure 28: Temperature field at 25002s

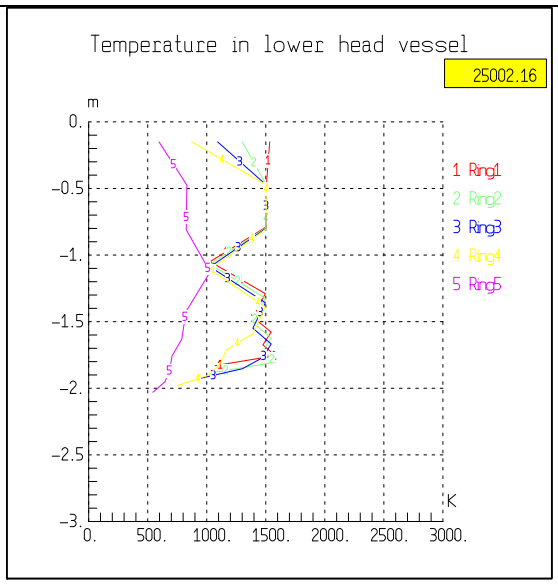

Figure 29: Rings temperature diagram at 25002s

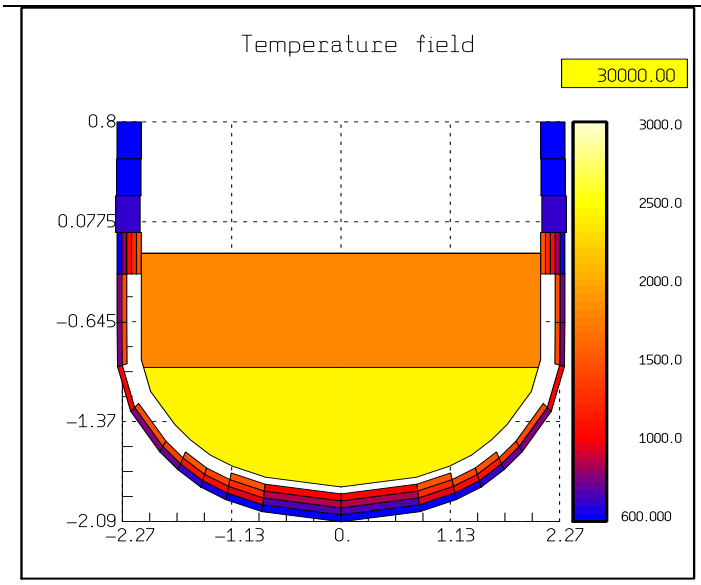

Figure 30: Temperature field at 30000s

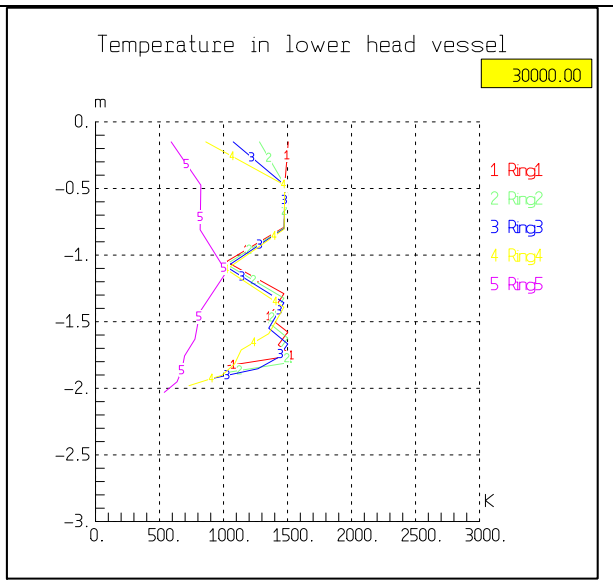

Figure 31: Rings temp diagram at 30000s

There are presented below (Figure 32) the heat fluxes from the vessel to the water for H=10000 [W/m^2/K] for different elevations.

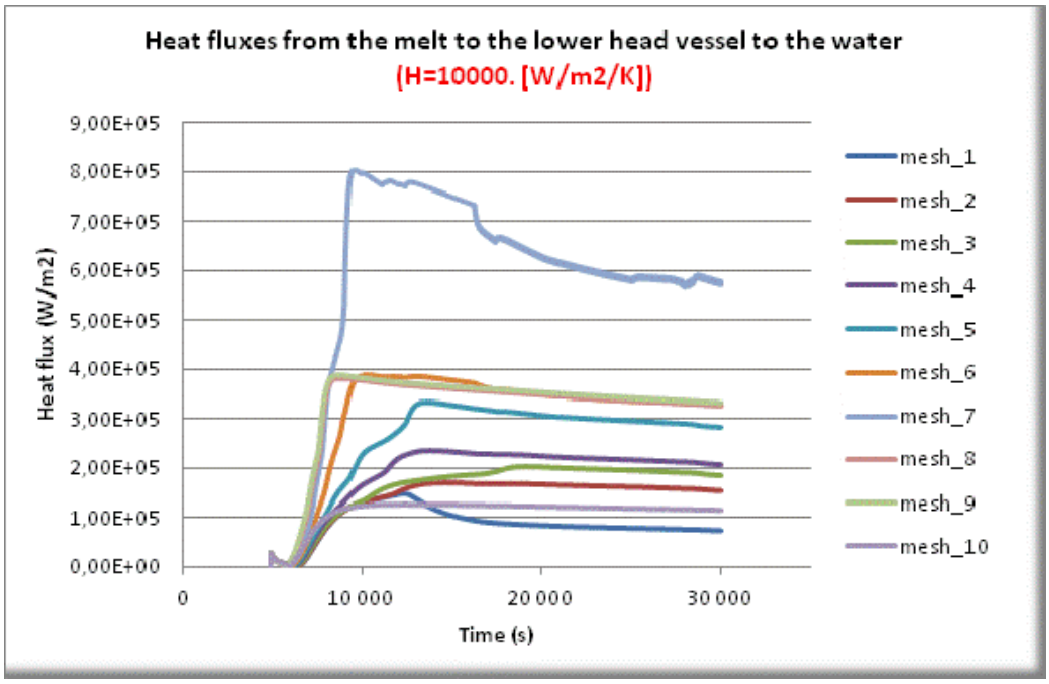

Figure 32: Heat flux from the external surface of the lower head vessel to the water

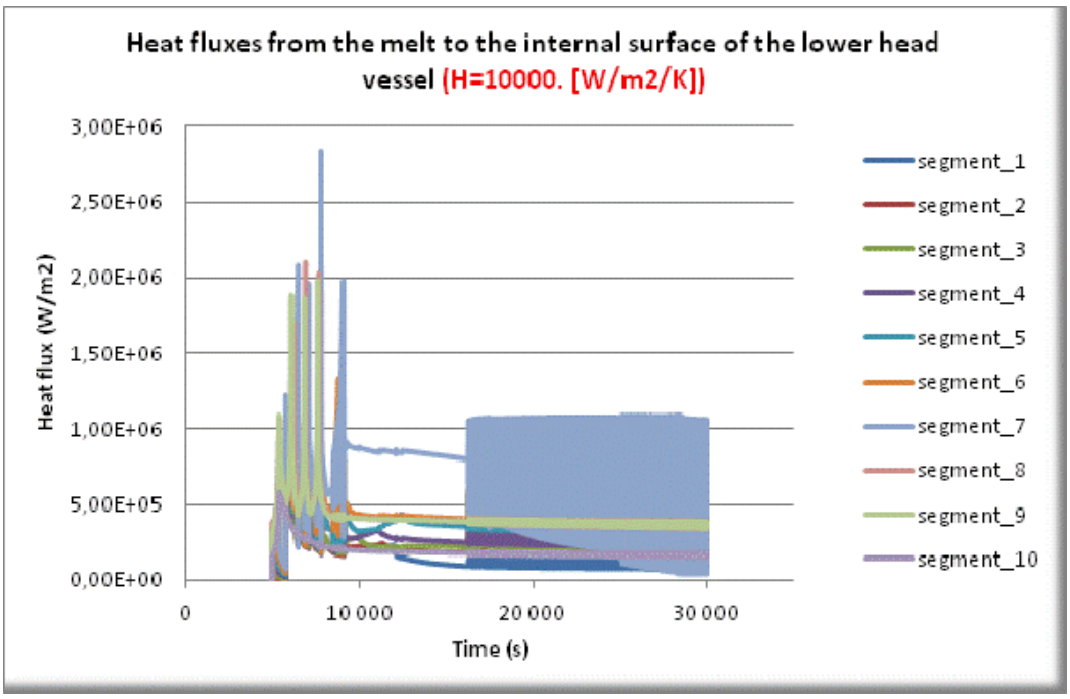

Figure 33: Heat fluxes from the melt to the internal surface of the lower head vessel

The maximum HF axial profile given looking at each external and internal point during the whole time at all elevations are presented at Figure17. All those maximum values defining a bounding curve.

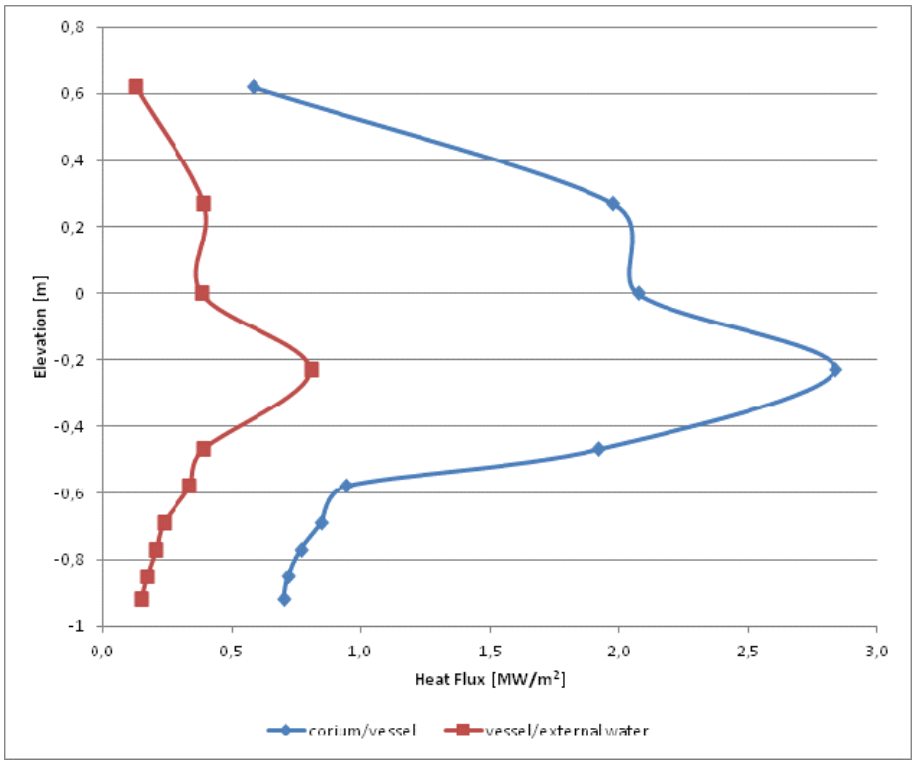

Figure 34: Bounding curve of maximal heat fluxes

A.4.4 Conclusions

<u>The conclusion could be summarized based on the heat balance as follows:</u>

In the “Initial calculation” the maximal heat flux of 2.32 MW/m^2 occurs at 5360.16s. It happens at segment number 9 between the elevations “+0.27” and “+0.62”.

In the “Basic calculation” the absolute maximum of heat fluxes (2.84 MW/m^2) occurs at 7754.16s at segment 7 (between elevations “-0.23” and “0.0”.

A.5 CEA PROCOR

A.5.1 Executive summary of PROCOR "best-estimate" calculation

The corium flow falls in "one initial bulk layer" into the lower head at 4911 s. This bulk layer is not yet completely liquid (T_{corium} = 2500 K < $T_{liquidus\_corium}$ = 2800 K). In this initial fusion phase, PROCOR crude modelling considers that the residual power heats the corium pool adiabatically. At 6011 s, the liquidus melt temperature (2800 K) is reached and the associated stratification at thermodynamic equilibrium is imposed. In accordance with the hypothesis of "two layers", there is one oxide layer (90.86 t) with a light metal layer above (97.58 t), surrounded by a crust.

The corium pool temperature continues to increase due to the residual power. Around 6200 s, the vessel wall begins to melt and a third light metal layer (steel from the melted vessel) appears **above the crust**. This steel layer thickness increases with the continuous vessel ablation. A part of this steel is transferred to the light metal layer under the crust, which is considered as porous.

After ~ 8011 s, the FE metal layer (i.e. the steel layer above the crust) thickness begins to decrease due to:

- The slowing down of vessel ablation. The lateral HF from the corium pool layers to the vessel wall begins to stabilize and slightly decrease around 8000 s. So a stationary wall thickness is nearly reached (the vessel wall ablation is nearly stopped) until the HF transmitted by the FE metal layer increase again (due to its thinning).
- And to the continuous transfer of steel from the FE metal layer downward, through the upper crust. Indeed, the corium pool stratification (under the crust) is still far from thermochemical equilibrium.

During this upper steel layer decreasing, the associated lateral HF increases until 2.05 MW/m^2. Then it decreases until 1.9 MW/m^2, when the corium pool is stabilized. This HF is associated to a FE metal layer of 1.18 mm (residual thickness). This "high value" is related to the PROCOR model which has no "HF limiter", related to a layer height threshold.

Considering that the CHF on the cylindrical part of the vessel is equal to 2.175 MW/m^2 (input data given to PROCOR), the vessel does not fail.

Main differences with the reference calculation and analysis:

- *There are two layers in the reference calculation (oxide and metal layers) without a crust surrounding the corium pool.*
- *The steel coming from the vessel ablation relocates directly in the upper metal layer in the reference calculation. As this layer thickness is important, there is no "focusing effect" at this elevation. Indeed, a thin metallic layer would concentrate the energy on a thin elevation range of the vessel wall. That's why the maximum lateral HF values (~ 0.6 MW/m^2) remain low in the reference calculation. Moreover, there is no axial conduction modelled in PROCOR in the vessel wall (no "spreading" of the hot points). But the effect of axial conductivity in the vessel should be moderate as the characteristic time associated with this phenomenon is greater than the characteristic time of the vessel melting by focusing effect (hundreds of seconds).*
- *In the beginning of the reference calculation, the HF is peaked in the upper region (metal) and later in the lower region (oxide), whereas in PROCOR the HF related to the oxide layer is always higher than the HF related to the metal layer. This difference may be related to the axial power profile applied in PROCOR to each layer and to the heat exchange correlation used between the two layers of the corium pool.*

A.5.2 "Best-estimate" calculation with PROCOR

A.5.2.1 Input data

For this "best-estimate" calculation, the **input data** used are the updated information transmitted by the Kurchatov Institute. The basic calculation, with account of fission products release (-20 % subtracted to the residual power), is used here.

The LWR vessel Lower Head application of PROCOR was used in the present study. For this application, the input data required by the code are:

- The corium flow (inventory, temperature and chronology) from the core to the lower head.
- The decay power chronology.

The PROCOR calculation begins at time = 4910 s = time when the core barrel melts through (see §5.1). The corium is supposed to relocate in the lower plenum in 1 s, from 4910 s to 4911 s.

The corium composition is given in §5.1. All the different materials fall in the lower head at the same time. The total mass of materials is equal to 188.44 tons.

The decay power chronology is given in §5.1. The initial value for the decay heat is taken at 4340 s as recommended in §5.1, in the PROCOR calculation (when the barrel fails).

A.5.2.2 Model and complementary hypotheses

A.5.2.2.1 Glossary

FE metal layer = Focusing Effect metal layer. It corresponds to the layer that can be formed during the transient, above the crust (steel coming from the vessel ablation). This term will be used in the following text and figures.

$R_{U/Zr} = \frac{N_U}{N_{Zr}^{total}}$ and $C_{ox} = \frac{N_{ZrO_2}}{N_{Zr}^{total}}$ with N_U : the total number of atoms of U

N_{ZrO_2} : the number of molecules of ZrO_2

N_{Zr}^{total} : the total number of atoms containing Zr

The crust is not represented on the following figures.

A.5.2.2.2 Input data common to all the codes of the benchmark

- The average temperature of the corium is equal to 2500 K.
- The calculation starts with all the corium material in the lower head, in one initial bulk layer before stratification.
- The melt liquidus temperature = 2800 K. When the corium temperature increases until 2800 K, stratification of the corium in several layers occurs.
- The initial pressure (internal and external to the vessel) = 2 bars.
- The VVER1000 geometry specificity is taken into account, with a semi-elliptical lower head of thickness = 244 mm and a cylindrical part of thickness 200 mm. The junction between these two parts of the vessel is smooth.

A.5.2.2.3 PROCOR Model parameters

- Water temperature (internal and external to the vessel) = 385 K.
- Vessel failure minimum thickness threshold: 1 cm. When the RPV wall thickness becomes less than 1 cm, the vessel is considered as failed.
- Vessel mesh height = 3 m (0 being the internal point at the bottom of the lower head).
- Number of meshes on the vessel wall = 500. There is no axial conduction in the wall (between the different meshes) considered in PROCOR; each mesh is treated as a 1D slab considering a plane fusion front.
- Heat transfer coefficient considered on the vessel wall (constant value on wall height) for external boundary condition = 10000 $W/m^2/K$.
- Steel fusion temperature = 1750 K.
- The “fictive upper plate” temperature is equal to 1750 K: it represents the boundary condition for the FE metal layer located above the crust. As this temperature is not lower that the steel fusion temperature and that PROCOR calculates radiation between this grey body and the FE metal layer, this one is totally liquid (no possible solid part).

A.5.2.2.4 PROCOR Model hypothesis

Figure 1 hereunder shows the available possibilities of PROCOR for the stratification. Considering a corium pool composed of one oxidic layer and possibly two metallic layers (one heavier, one lighter), the transient stratification model is a generalization of the OD mass transfer model obtained from a phenomenological analysis of the MASCA-RCW experiment and is based on the thermodynamic equilibrium associated to the corium pool inventory that gives the stationary state that the corium pool will eventually reach. In this calculation, the addition of steel is related to the vessel ablation, so it is «pure steel». The steel coming from the core structures is located in the “light metal” layer with the corium pool model (which gives the thermodynamics equilibrium).

- A corium pool surrounded by a refractory crust is modelled with **up to three layers during the transient**; the associated kinetics stratification model leads at steady-state, to a two-layer configuration that corresponds to the thermodynamic equilibrium of the system (it can be oxide + light metal or oxide + heavy metal as calculated by the model. One more layer can be formed during the transient above the crust (steel coming from the vessel ablation).The horizontal crust separating this steel from the corium pool is supposed to be unstable in such a way that this “FE metal layer” is considered in the pool inventory for the transient stratification model (parameter “mass transfer through upper crust” set to “yes”).

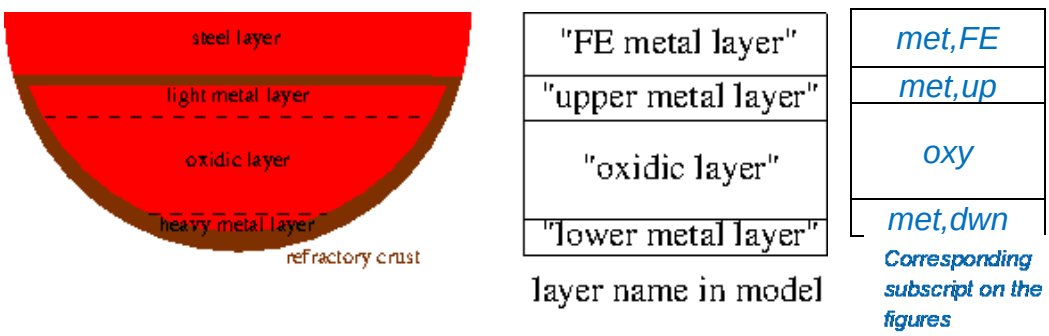

Figure 1 : Corium pool stratification

- The initial state corresponds to an adiabatic heating and an instantaneous total fusion of the corium. The obtained configuration is directly the two-layer one that corresponds to the thermodynamic equilibrium of the system U-O-Zr-steel.
- An analytical and normalised heat flux profile (which can be constant, linear or based on MAAP4 heat flux profile) is applied to the mean lateral heat flux (calculated with the 0D model of mass and energy conservation) of each corium pool layer.
- The critical heat flux correlation used in the vessel ablation model is based on the ULPU profile. The axial profile taken into account is the ULPU one, but the values are multiplied by a factor large enough for the vessel not to fail. As a matter of fact :
    - The ULPU correlation is valid for spherical lower head and specific conditions. It may not be applicable to a semi-elliptical lower head.
    - The aim of this calculation is to evaluate a "penalizing" heat flux profile on the vessel.

  In PROCOR, a critical value ϕ_i^{crit} (based on the experimental program ULPU) is associated to each mesh i of the vessel wall (see Figure 2). The ULPU heat flux profile is multiplied by 1.45, so the maximum value (on the cylindrical part) is equal to 2.175 MW/m^2 instead of 1.5 MW/m^2 (ULPU value).

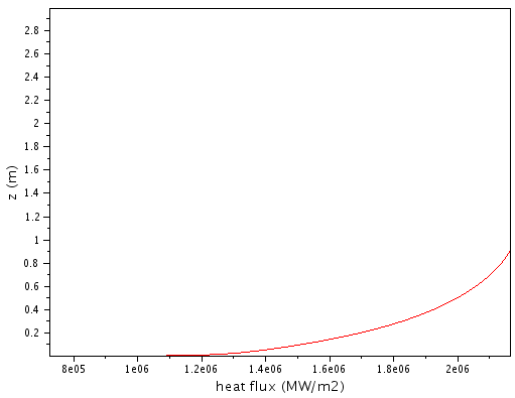

Figure 2: Critical heat flux profile on the vessel wall

At each time step of the PROCOR calculation, the internal heat flux ϕ_i^{in} (transmitted by the internal layers of the corium pool to the vessel wall) is compared to this critical value:

- While $\phi_i^{in} < \phi_i^{crit}$, the plane fusion equation, with an established conduction heat flux in the solid wall, is solved.
- When $\phi_i^{in} \geq \phi_i^{crit}$, the conduction in the wall is supposed to be zero and $\boldsymbol{\phi_i^{out} = 0}$, with ϕ_i^{out} = external heat flux going out from the vessel wall, on the "wet" side. In this case, all the internal heat flux is used for the vessel wall fusion.

A.5.3 PROCOR "best-estimate" results – CHF_{max} = 2.175 MW/m^2

When the corium flow falls into the lower head at 4911 s, the corium average temperature is equal to 2500 K and there is one initial bulk layer, as shown on Figure 3. This bulk corresponds to a solid (T_{corium} = 2500 K < $T_{liquidus\_corium}$ = 2800 K). In this initial fusion phase, PROCOR crude modelling considers that the residual power heats the corium pool adiabatically. At 6011 s, the liquidus melt temperature (2800 K) is reached and the associated stratification at thermodynamic equilibrium is imposed. There is one oxide layer (90.86 t) with a light metal layer above (97.58 t), surrounded by a crust (note that the crust is not represented on these pictures).

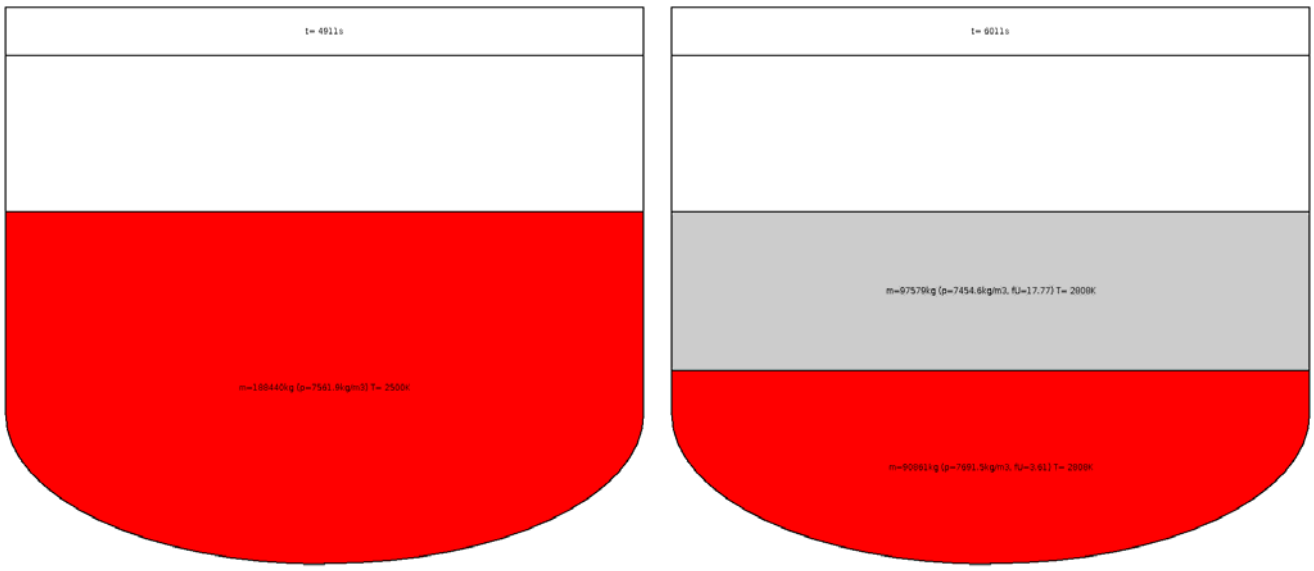

- red = oxide layer under the crust
- light grey = light metal layer under the crust

Figure 3: Vessel photos at t = 4011 s with one "bulk" corium layer (left picture) and t = 6011 s just after total fusion in thermodynamic equilibrium (right picture)

Figure 4 shows the evolution of the metal and oxide densities as a function of the steel mass in the system U-O-Zr-steel, calculated using (Salay et al., 2005). For a given temperature, two possible stratified configurations can be observed depending on the steel mass proportion in the corium. When the steel mass in the corium melt becomes greater than the threshold value $\widetilde{m}_0^{steel}$ ≈ 42 tons, there is a change in stratification: the metal layer density becomes lower than the oxide's one and the oxide layer is situated under the "light metal" layer.

So, the configuration on Figure 3 is observed because the steel mass proportion, over the total mass of corium, is very important in the initial corium inventory (m_0^{steel} = 69.84 tons corresponding to the second blue line on Figure 4).

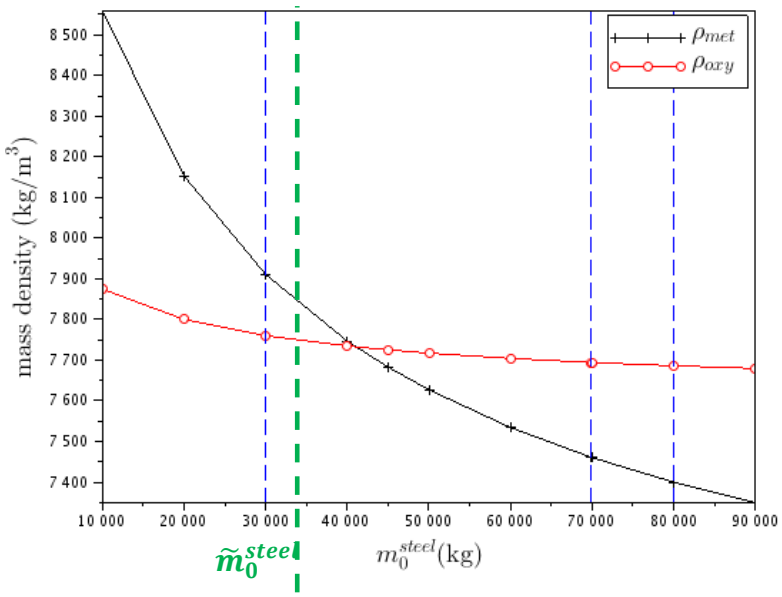

Figure 4 : Metal and oxide phase densities (ρ_{met} and ρ_{oxy}) as a function of m_0^{steel} (initial mass of steel in the corium melt) for T = 2800 K

The results of J.M.Seiler [NED 2007] exhibits only the cases where R_U/Zr = 1.2 and R_U/Zr = 1.45 whereas here: R_U/Zr = 1.027 and Cox = 44.8 % (see table 1). The paper says (p. 1756): "The reduction of the U/Zr ratio leads clearly to a significant increase of the maximum mass of steel that stratifies below the oxidic corium." These density curves also depend on the temperature considered and strongly depend on the density law rho(T) used for the different species.

The corium pool temperature continues to increase due to residual power. Around 6300 s, the vessel wall begins to melt and a third light metal layer (steel from the melted vessel) appears above the crust as shown on Figure 5. The upper steel metal layer is considered in the pool inventory for the transient stratification model.

This steel layer thickness increases with the continuous vessel ablation as the melted steel from the wall relocates above the upper crust. A part of this steel is transferred to the light metal layer under the crust. The mass transfer of steel through the crust is allowed (see PROCOR calculation hypotheses) and is managed by a kinetic stratification model.

After ~ 8011 s, the FE metal layer thickness begins to decrease due to:

- the slowing down of vessel ablation. The lateral heat fluxes from the corium pool layers to the vessel wall begin to stabilize and slightly decrease around 8000 s as shown on Figure 9 (left picture). So a stationary wall thickness is nearly reached (see Figure 12, left picture where the vessel wall ablation is nearly stopped) until the heat flux transmitted by the FE metal layer increase again (see Figure 9, left picture),
- and to the continuous transfer of steel from the FE metal layer downward, through the upper crust. Indeed, the corium pool stratification is still far from thermochemical equilibrium.

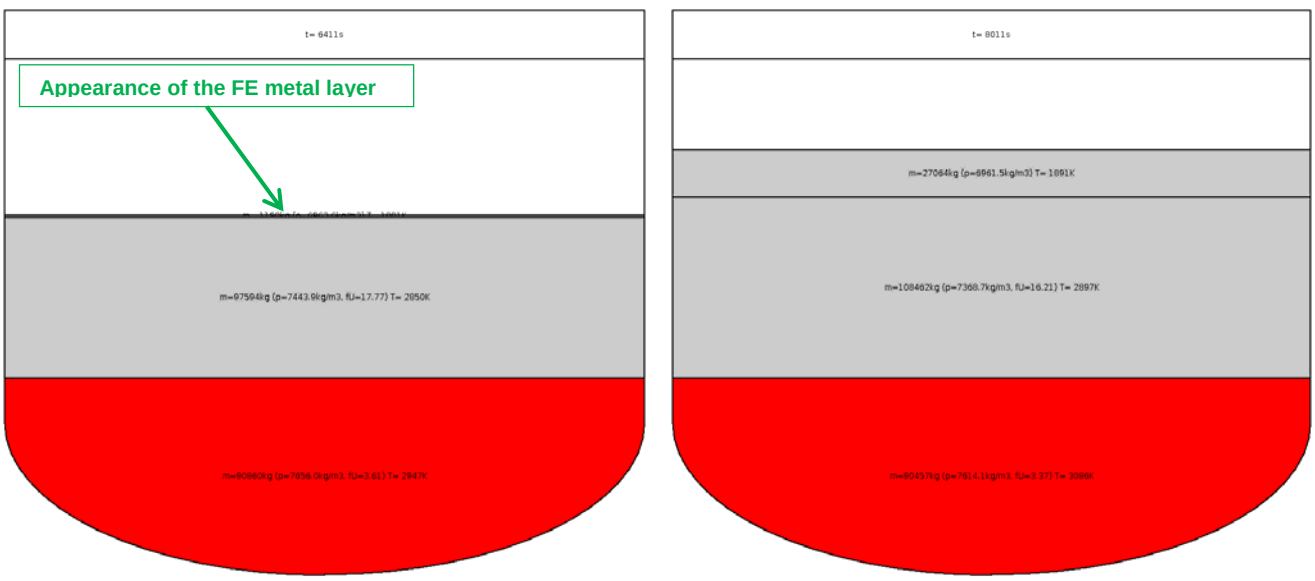

- red = oxide layer under the crust
- light grey (lower rectangle) = light metal layer under the crust
- light grey (upper rectangle) = FE metal layer, above the crust (steel coming from the vessel ablation)

Figure 5: Vessel photos at t = 6411 s with the appearance of the FE metal layer (left picture) and t = 8011 s when the FE metal layer thickness is maximum (right picture)

Despite a "focusing effect", the vessel does not fail during the FE metal layer formation (thickening) or during its thinning. Figure 6 shows the vessel state during the FE metal layer thinning and at the end of the calculation (23211 s), when the corium pool is stabilized in the lower head.

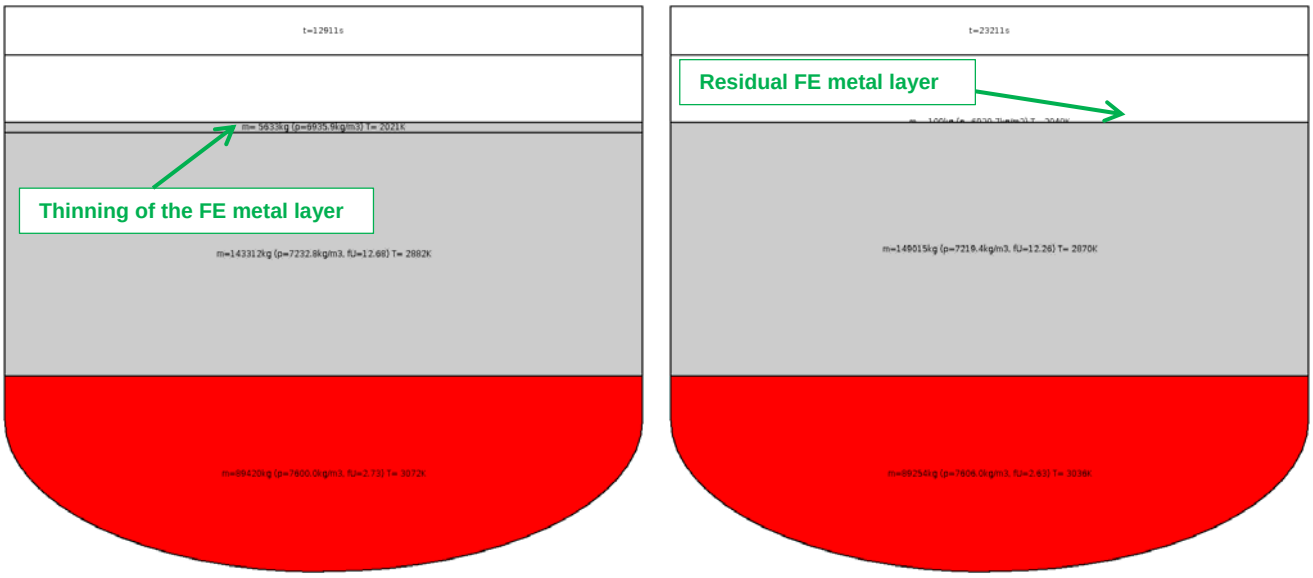

- red = oxide layer under the crust
- light grey (lower rectangle) = light metal layer under the crust
- light grey (upper rectangle) = FE metal layer, above the crust (steel coming from the vessel ablation)

Figure 6: Vessel photo at t = 12911 s during the FE metal layer thinning (left picture) and t = 23211 s when the corium pool is stabilized in the vessel (right picture)

Figure 7 shows the mass increasing of the light metal layer under the crust (black curve) linked to the mass transfer from the FE metal layer (blue curve). Its increase followed by a decrease is clearly seen on Figure 7. The oxide mass nearly doesn't vary (90.86 t just after stratification and 89.25 t at the stabilized state, 23211 s).

Let's recall that, even if it is represented on the figure (with a null value), there is no solid part in the FE metal layer, related to the chosen boundary conditions (see PROCOR calculation hypotheses).

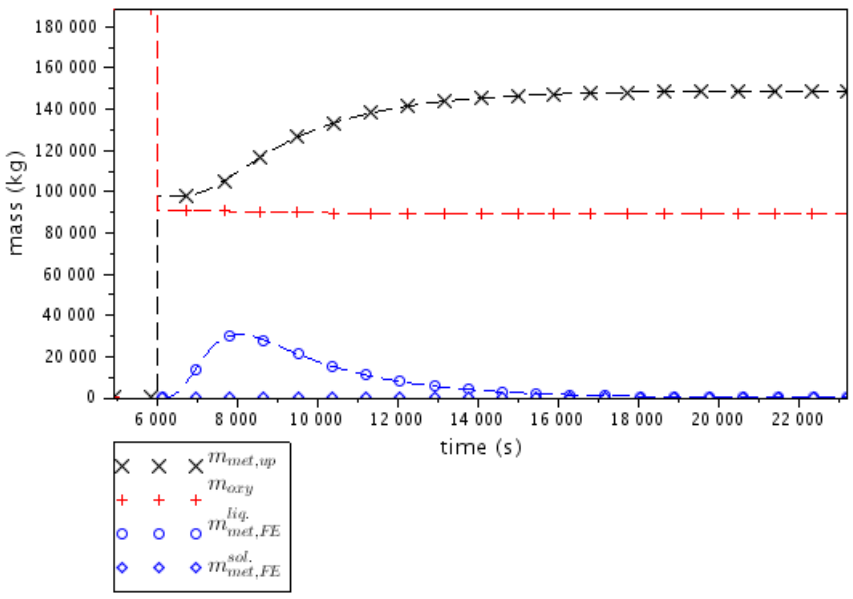

$m_{met,up}$: mass of the upper metal layer of the corium pool
m_{oxy}: mass of the oxidic layer of the corium pool
$m^{liq.}_{met,FE}$: liquid mass of the FE metal layer of the corium pool
$m^{sol.}_{met,FE}$: solid mass of the FE metal layer of the corium pool

Figure 7: Evolution of the layers mass of the corium pool

Figure 8 shows the mass increase of steel coming from the vessel ablation, until about 8000 s. Then it stops whereas the steel layer mass transfer through the crust continues. It results in a decrease of the FE metal layer.

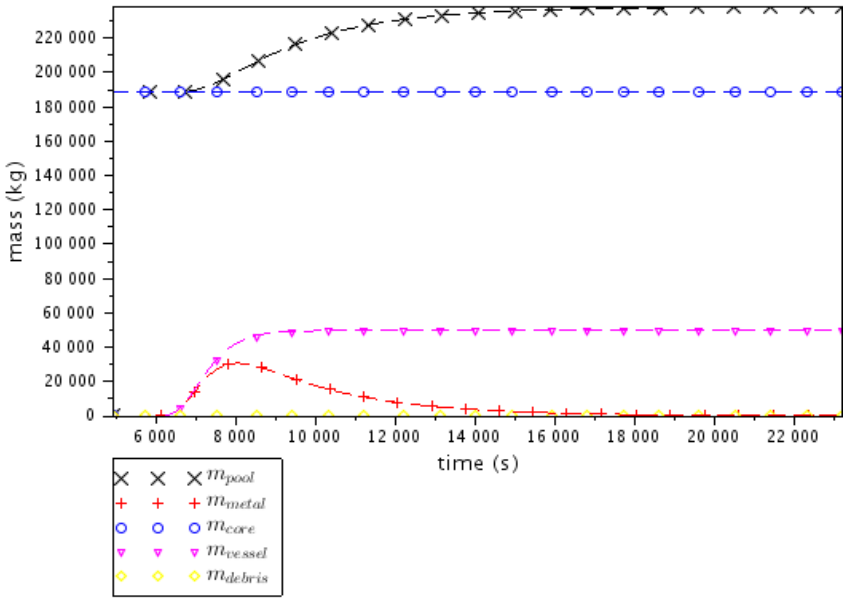

$m_{pool} = m_{met,up} + m_{oxy}$: mass of the corium pool

$m_{metal} = m_{met,FE}^{liq} + m_{met,FE}^{sol}$: mass of the FE metal layer of the corium pool

m_{core}: cumulative mass of liquid corium transferred from the core to the lower head

m_{vessel}: cumulative mass of ablated vessel wall transferred to the corium pool

m_{debris}: cumulative mass of melted debris transferred to the corium pool

Figure 8: Evolution of in-vessel related masses

A first small peak is observed during the early formation of this upper steel layer.

When the FE metal layer thickness decreases, the lateral heat flux associated to this layer increases until 2.05 MW/m^2 (see Figure 9). Then it decreases slightly around 1.9 MW/m^2.

The heat flux transmitted by the upper metal layer (under the crust) through the lateral surface of the vessel wall is always lower than the one transmitted by the oxidic layer (see Figure 9).

The heat flux transmitted by the upper metal layer (under the crust) through the upper surface is greater than the one transmitted by the oxidic layer during the first part of the transient, before ~ 8000 s. Then the heat flux transmitted by the upper metal layer upward is decreasing until a value which is below the one relative to the oxidic layer.

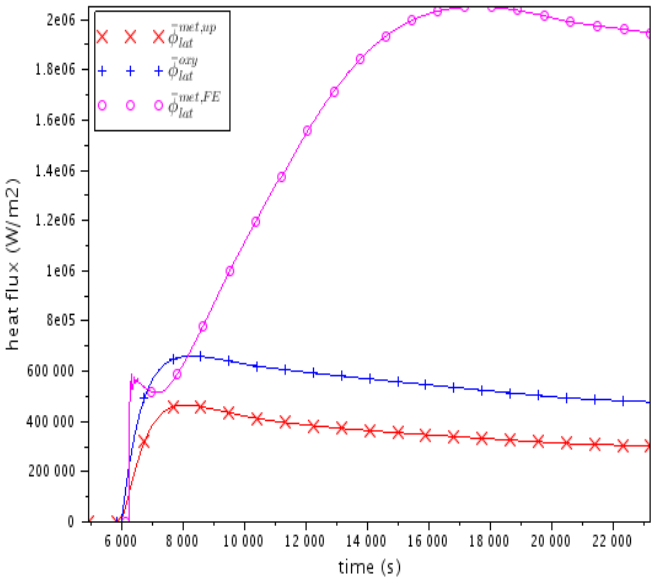

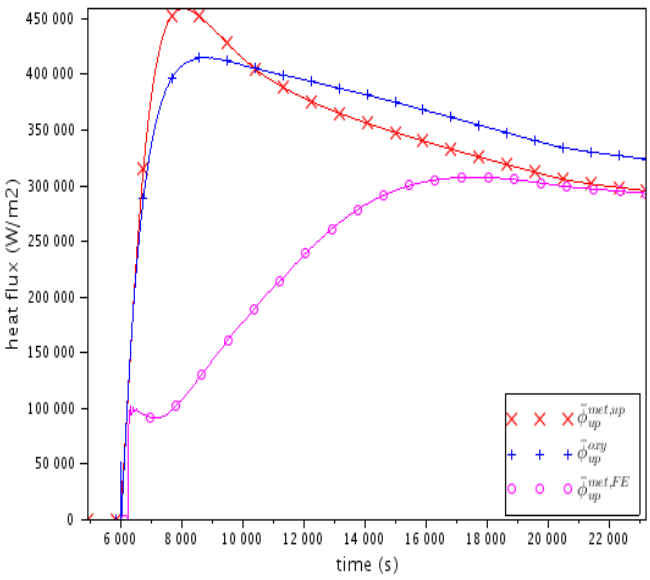

$\bar{\phi}_{lat}^{met,up}$: lateral heat flux for the upper metal layer

$\bar{\phi}_{lat}^{oxy}$: lateral heat flux for the oxidic layer

$\bar{\phi}_{lat}^{met,FE}$: lateral heat flux for the FE metal layer

$\bar{\phi}_{up}^{met,up}$: upper heat flux for the upper metal layer

$\bar{\phi}_{up}^{oxy}$: upper heat flux for the oxidic layer

$\bar{\phi}_{up}^{met,FE}$: upper heat flux for the FE metal layer

Figure 9: Evolution of in-vessel corium layer of the corium pool mean lateral and upper heat fluxes (W/m²)

These results must also be related to the thickness evolution of the FE or "out of equilibrium" steel layer, given in Figure 10. The maximum lateral heat flux of ~ 1.9 MW/m² when the corium pool is stabilized is associated to a FE metal layer of 1.18 mm. This represents a residual thickness and a so high value for the lateral heat flux can't reasonably be associated to a so thin "residual layer".

When the maximum lateral heat flux (2.05 MW/m²) is reached, ~ 17611 s, the FE metal layer thickness is around 0.97 cm. Let's recall that the PROCOR model does not limit the lateral heat flux value in the case of an infinitely thin layer. This modelling issue associated with the thermalhydraulics of a thin steel layer is complex because it highly depends on the boundary conditions at the top (free interface with the gaseous atmosphere) and the bottom (interface with an unstable thin crust on top of the oxidic pool). R&D work will start on 2015 at CEA regarding this point.

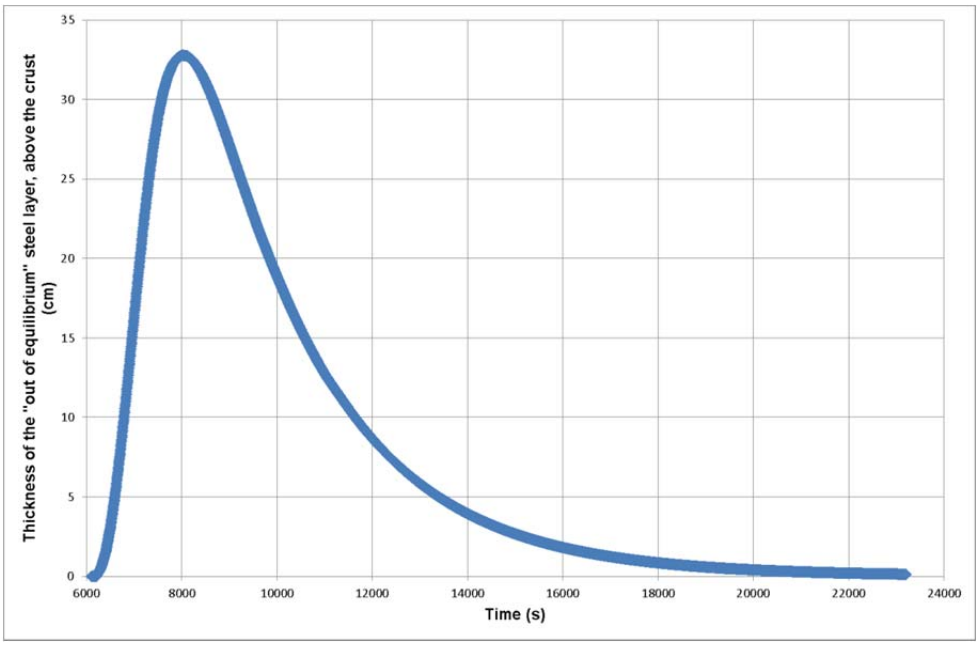

Figure 10: Evolution of the thickness of the FE metal layer as a function of time

Figure 11 (left figure) shows that the heat flux profile is very “peaked” at 17611 s due to the small thickness of the FE metal layer. After 21011 s (right figure), the FE metal layer thickness becomes so small that the high value for the lateral heat flux associated to this layer is “averaged” over the mesh height.

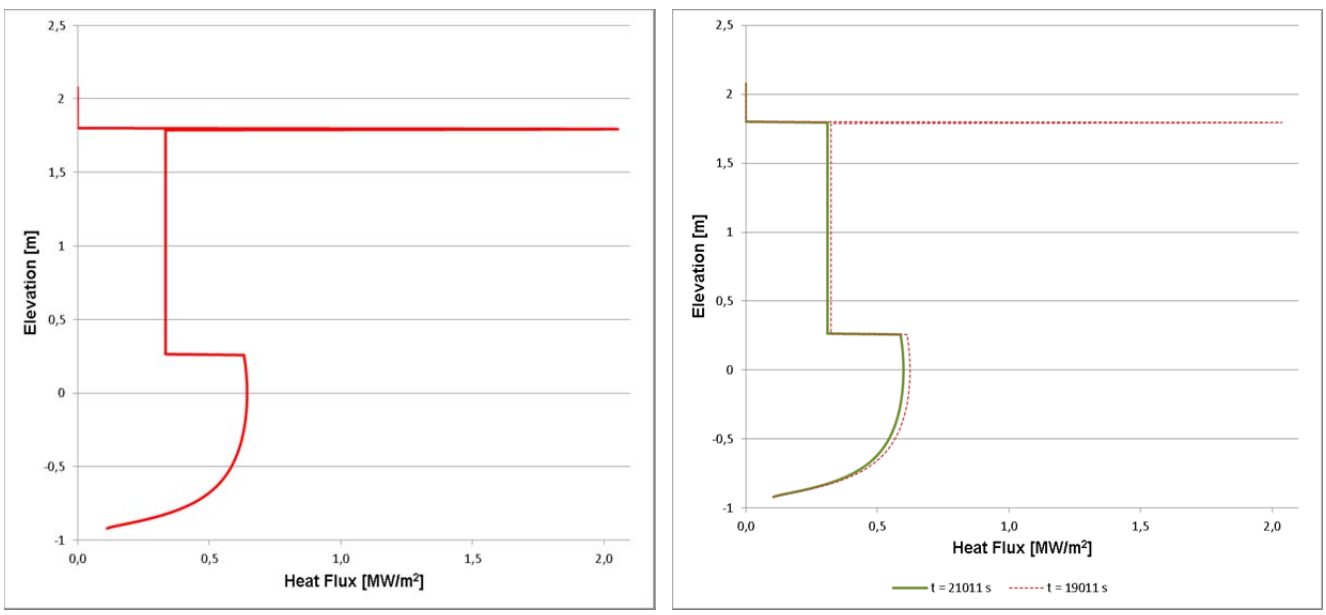

Figure 11: Heat flux profile at the 17611 s, when the lateral heat flux is maximum (on the left) and heat flux profiles at 19011 s and 21011 s, after stabilization (on the right)

Figure 12 shows axial profiles evolutions versus time. The very lower part of the vessel (facing the bottom oxide layer) and its upper part (facing the FE metal layer) are the most ablated. Vessel wall ablation is important in the oxide layer and in the upper steel layer areas. The lower heat flux of the upper light metal layer under the crust is related to a lower temperature of the layer, compared to the oxide layer mean temperature; there is quickly ~ 100 K of difference at 6411 s and then ~ 200 K of difference from ~ 7000 s (the layer temperature is shown on figures representing the corium pool layers like Figure 5). This is related to uranium concentration in the

oxide layer, but also to the upward, downward and lateral heat transfer correlation between the different layers.

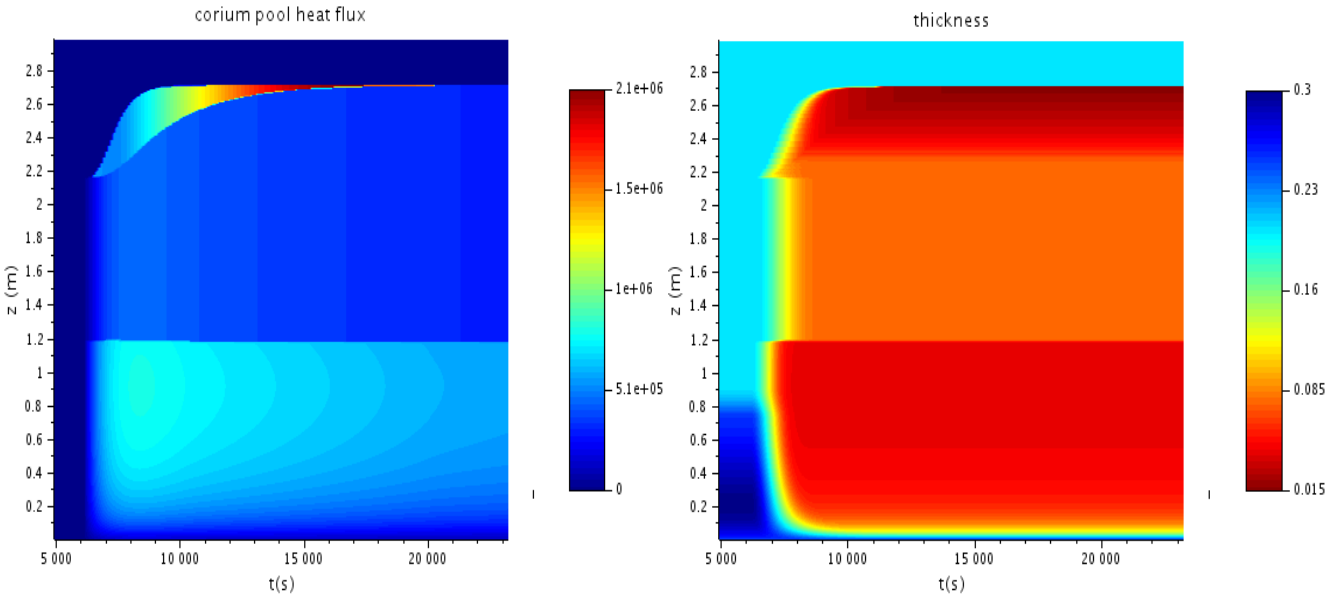

Figure 12: Evolution of the axial profiles: of internal heat flux transmitted to the vessel wall (MW/m²) (left figure) and of residual vessel thickness (m) (right figure)

This difference of temperature between the layers is related to uranium concentration in the oxide, but also to the upward, downward and lateral heat transfer correlation between the different layers.

The heat flux transmitted to the vessel wall increases quickly in the upper area of the wall, with the thinning of the upper steel layer. The **vessel minimum thickness is equal to ~ 1.49 cm**. The vessel median thickness is around 7.74 cm.

A.5.4 Sensibilities and other calculations– CHF_{max} = 1.5 MW/m²

In this part, the maximum value for the CHF on the cylindrical part of the vessel is taken equal to 1.5 MW/m² (ULPU value).

A.5.4.1 PROCOR results with CHFmax = 1.5 MW/m²

In this part, the same input data as for the "best-estimate" case are taken into account, except the value of the maximum CHF.

The initial phenomenology and stratification is exactly the same as for the "best-estimate" case (see Figure 3). The kinetics related to the FE metal layer thickening then thinning is exactly the same as for the "best-estimate" case (see Figure 5).

In this case, the "focusing effect" and the vessel failure were avoided during the FE metal layer formation, but **the vessel fails during its thinning at 11827 s**. This related to the smaller value of the maximum CHF : as soon as the lateral heat flux transmitted by the corium pool to the vessel wall is higher than 1.5 MW/m², all the energy is used for vessel ablation and no more conduction supposed in this case ⇒ no heat flux evacuation through the vessel wall).

Figure 13 showing the evolution of in-vessel related masses is exactly the same as Figure 8 until 11827 s (vessel rupture in this case). Similarly, all the figures showing the transient evolution are similar to the ones of the "best-estimate" case, excepted that they stop at 11827 s.

So, in the present case, the maximum lateral heat flux transmitted by the FE metal layer to the vessel wall is equal to 1.51 MW/m² (recall: the CHF margin is lowered to 1.5 MW/m² in this chapter) and occurs at the end of the transient. The vessel failure occurs on the cylindrical part of the vessel, at 1.7 m (the reference being the junction between the semi-elliptical and cylindrical parts). It happens at the level of the FE metal layer and during the thinning of this one.

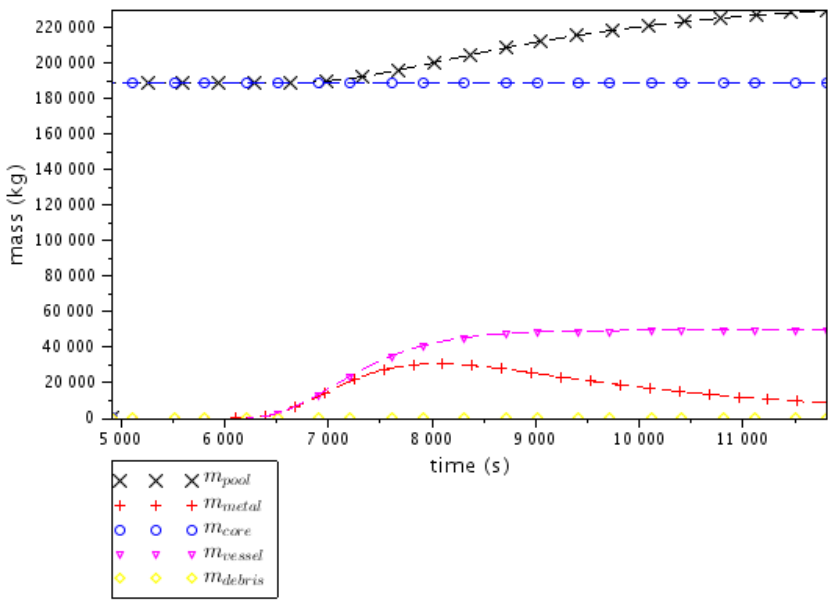

$m_{pool} = m_{met,up} + m_{oxy}$: mass of the corium pool

$m_{metal} = m^{liq}_{met,FE} + m^{sol}_{met,FE}$: mass of the FE metal layer of the corium pool

m_{core}: cumulative mass of liquid corium transferred from the core to the lower head

m_{vessel}: cumulative mass of ablated vessel wall transferred to the corium pool

m_{debris}: cumulative mass of melted debris transferred to the corium pool

Figure 13: Evolution of in-vessel related masses

A.5.4.2 Sensibility on the initial steel mass: 30 t instead of 69.84 t

The aim of this calculation is to test the sensibility to the initial mass inventory and instantaneous stratification (see Figure 4).

In this calculation, all the hypotheses of the “best-estimate” calculation are kept. The initial steel mass in the corium melt is reduced to 30 t instead of 69.84 t before. The initial total mass is also reduced from 188.44 t to 148.6 t.

This initial corium melt composition corresponds to the first blue line on the left on Figure 4, which is before the change in stratification. As expected, when the liquidus temperature is reached at 5710 s and when stratification instantaneously occurs, there is one heavy metal layer (53.09 t) with an oxide layer above (95.51 t), surrounded by a crust, as shown on Figure 14. With the increase of corium pool temperature, the vessel wall begins to melt and a third layer (steel from the melted vessel) appears above the crust.

Vessel failure occurs then quickly during the beginning of the FE metal layer formation, at **6279 seconds**.

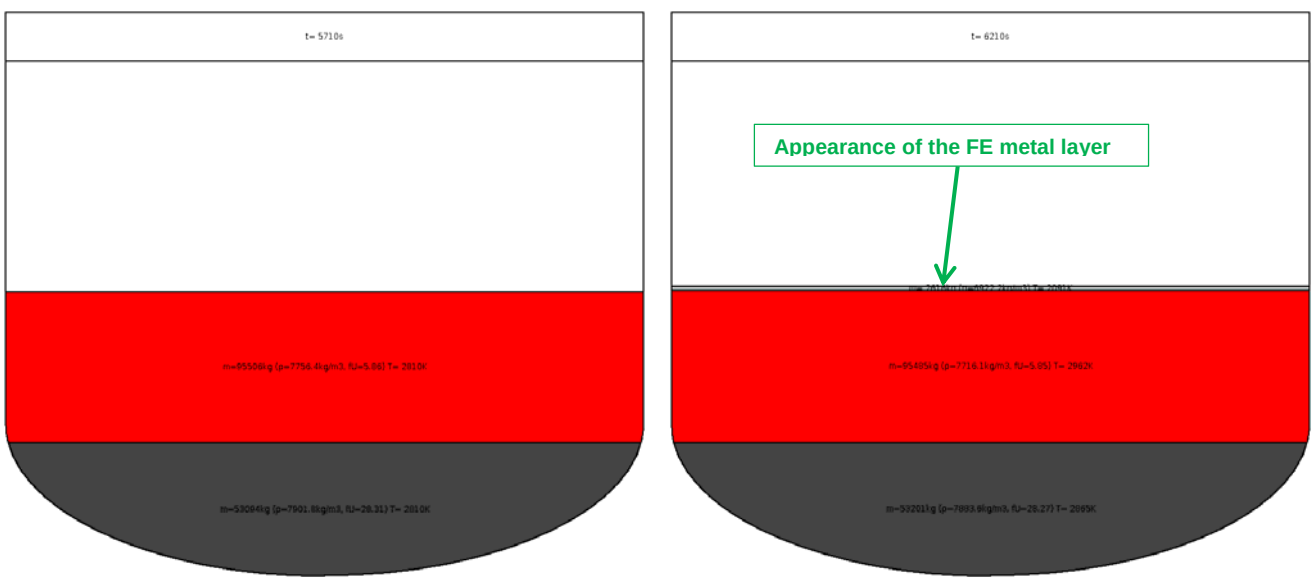

- dark grey = heavy metal layer, under the crust
- red = oxide layer, under the crust
- light grey = FE metal layer, above the crust (steel coming from the vessel ablation)

Figure 14: Vessel photos at t = 5710 s just after total fusion in thermodynamic equilibrium (left picture) and t = 6210 s with the appearance of the FE metal layer (right picture)

Figure 15 shows the mass increase of steel coming from the vessel ablation, until about 6200 s, just before vessel failure: the FE metal layer mass is about 2.5 tons.

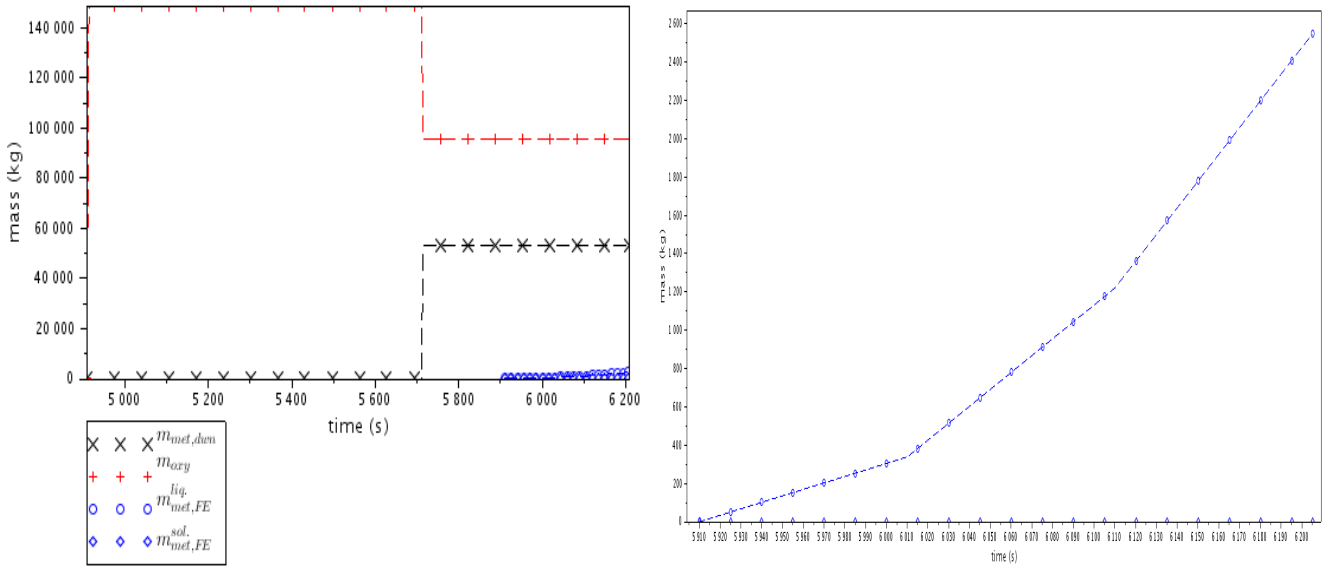

$m_{met,dwn}$: mass of the lower metal layer of the corium pool m_{oxy}: mass of the oxidic layer of the corium pool

$m^{liq.}_{met,FE}$: liquid mass of the FE metal layer of the corium pool

$m^{sol.}_{met,FE}$: solid mass of the FE metal layer of the corium pool

Figure 15: Evolution of corium pool masses (global picture on the left and ZOOM on the right)

Figure 16 shows the lateral heat flux transmitted by the FE metal layer to the vessel wall reaches a peak of 6.77 MW/m² around 6000 s. This peak must be related to the upper heat flux transmitted by the oxide layer under the crust at that time: $\bar{\phi}^{oxy}_{up} \approx 0.55$ MW/m². **It is 3.7 times higher than in the "best-estimate" calculation** (with an initial steel mass of 69.84 t) where the first peak was lower (around 1.5 MW/m²). This difference can be related to three points:

- The same residual power as before is concentrated in a lower total mass of corium here.
- The layer which is under the FE metal layer (separated by a crust) is an oxide layer here, which concentrates more residual power, relatively to the light metal layer (which was located under the upper crust in the "best-estimate" calculation.
- The upward, downward and lateral heat transfer correlation between the different layers as well as the lateral profile applied on each layer differ between the two calculations, because the order of the different layers is not the same.

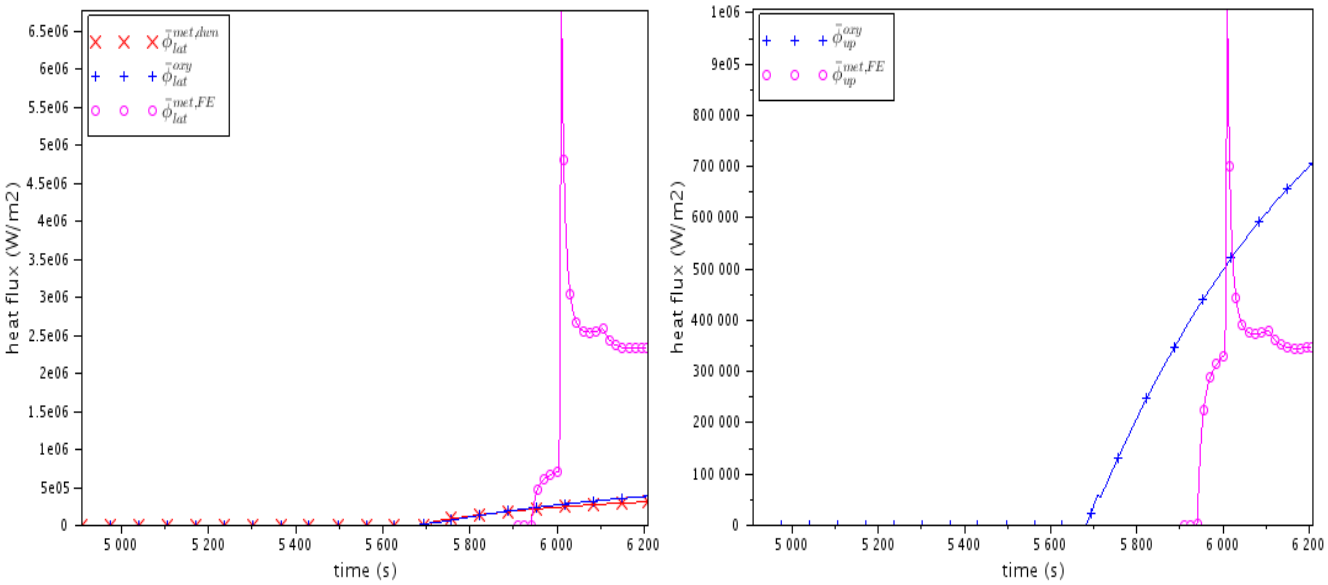

$\bar{\phi}_{lat}^{met,dwn}$: lateral heat flux for the heavy metal layer

$\bar{\phi}_{lat}^{oxy}$: lateral heat flux for the oxidic layer

$\bar{\phi}_{lat}^{met,FE}$: lateral heat flux for the FE metal layer

$\bar{\phi}_{up}^{oxy}$: upper heat flux for the oxidic layer

$\bar{\phi}_{up}^{met,FE}$: upper heat flux for the FE metal layer

Figure 16: Evolution of in-vessel corium layer of the corium pool mean lateral and upper heat fluxes (W/m²)

Figure 17 shows axial profiles evolution versus time. The vessel ablation is localized in its upper part (facing the FE metal layer). **Vessel failure occurs at 6268 s** on the cylindrical part of the vessel, at 1.73 m from the internal bottom of the lower head (or **0.81 m** if we consider that elevation 0 corresponds to the junction between ellipsoidal and cylindrical parts of the vessel). It happens at the level of the FE metal layer and during the thickening of this one.

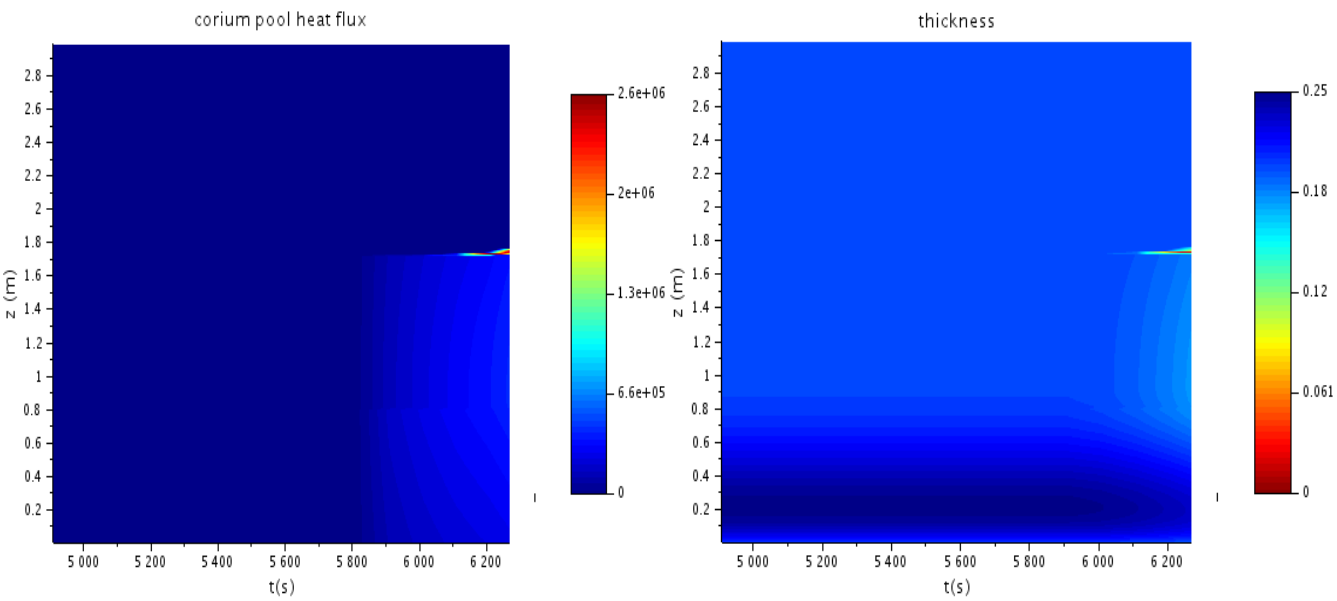

Figure 17: Evolution of the axial profiles: of internal heat flux transmitted to the vessel wall (MW/m²) (left figure) and of residual vessel thickness (m) (right figure)

A.5.4.3 Sensibility on the initial steel mass: 80 t instead of 69.84 t

The aim of this calculation is to test the sensibility to the initial mass inventory and instantaneous stratification (see Figure 4).

In this calculation, all the hypotheses of the “best-estimate” calculation are kept. The initial steel mass in the corium melt is increased to 80 t instead of 69.84 t before. The initial total mass is also increased from 188.44 t to 198.6 t.

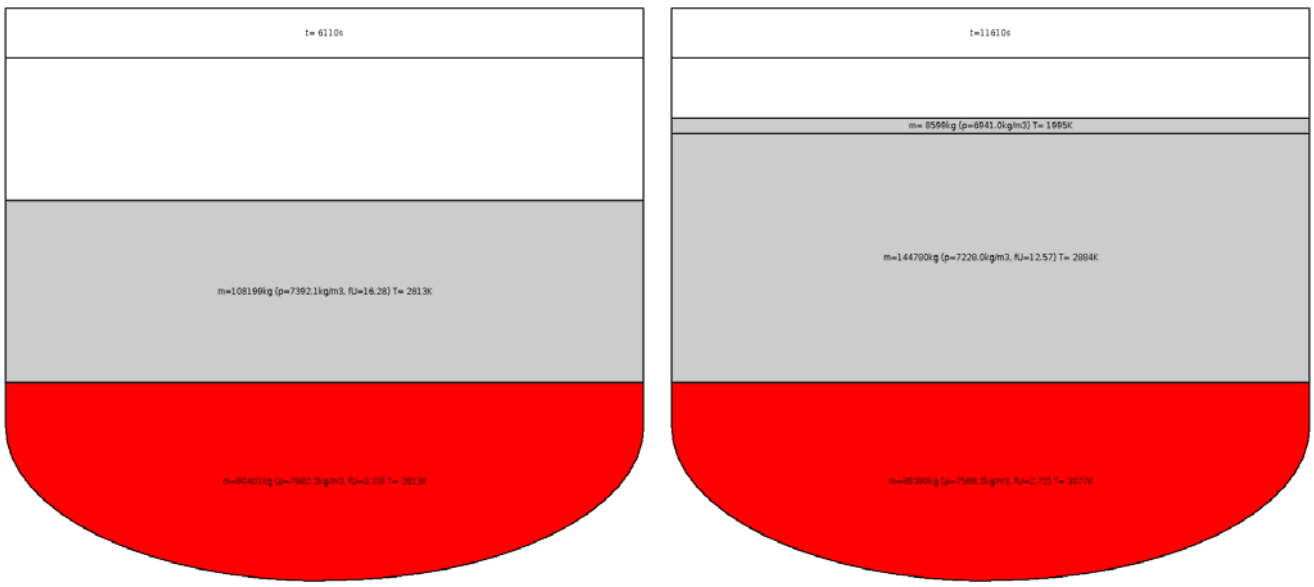

- red = oxide layer under the crust
- light grey (lower rectangle) = light metal layer under the crust
- light grey (upper rectangle) = FE metal layer, above the crust (steel coming from the vessel ablation)

Figure 18: Vessel photos at t = 6110 s just after total fusion in thermodynamic equilibrium (left picture) and t = 11610 s just before vessel failure (right picture)

This initial corium melt composition corresponds to the third blue line on the right on Figure 4, which is after the change in stratification. As expected, when the liquidus temperature is reached at 6110 s and when stratification instantaneously occurs, there is one oxide layer (90.4 t) with a lighter metal layer above (108.2 t), surrounded by a crust, as shown on Figure 18. With the increase of corium pool temperature, the vessel wall begins to melt and a third layer (steel from the melted vessel) appears above the crust.

The transient is very similar to the main calculation (with an initial steel mass of 69.84 t). The FE is thickening in a first time and then thinning in a second time. **Vessel failure** finally occurs during the thinning of the FE metal layer, at **11627 s**. The final state is shown on Figure 18 (right picture).

Figure 19 shows the mass increasing of the light metal layer under the crust linked to the mass transfer from the upper steel layer. The oxide mass nearly doesn't vary (90.4 t just after stratification and 89.4 t just before vessel failure). It is very similar to Figure 7 (case where the initial steel mass layer = 69.84 t).

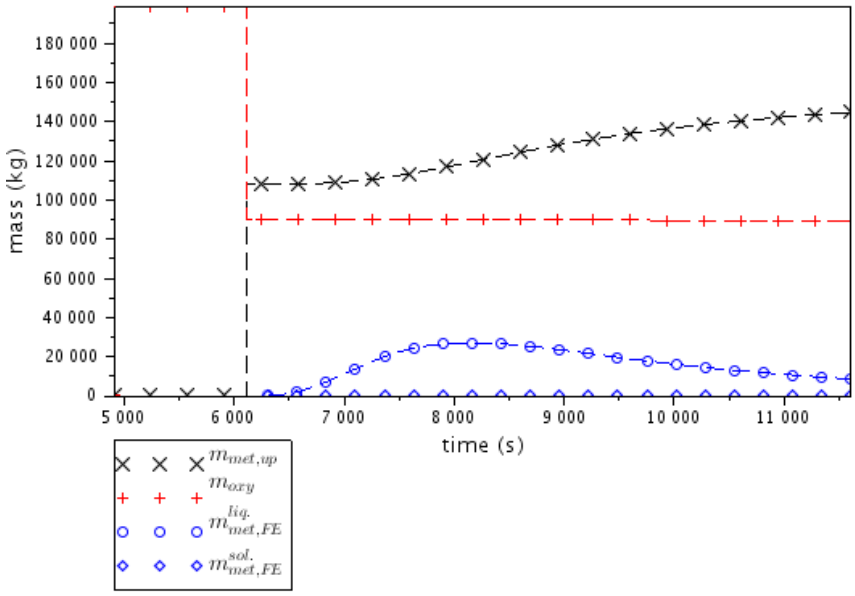

$m_{met,up}$: mass of the upper metal layer of the corium pool
m_{oxy}: mass of the oxidic layer of the corium pool
$m^{liq.}_{met,FE}$: liquid mass of the FE metal layer of the corium pool
$m^{sol.}_{met,FE}$: solid mass of the FE metal layer of the corium pool

Figure 19: Evolution of the layers mass of the corium pool

Figure 20 hereunder is similar to Figure 9 related to m_0^{steel} = 69.84 t. The vessel failure occurs a little later here (11627 s instead of 11127 s before), because the residual power is the same but the corium pool mass is more important (about 10 t more of steel). The maximum lateral heat flux of 1.5 MW/m² is also obtained during the thinning of the FE metal layer.

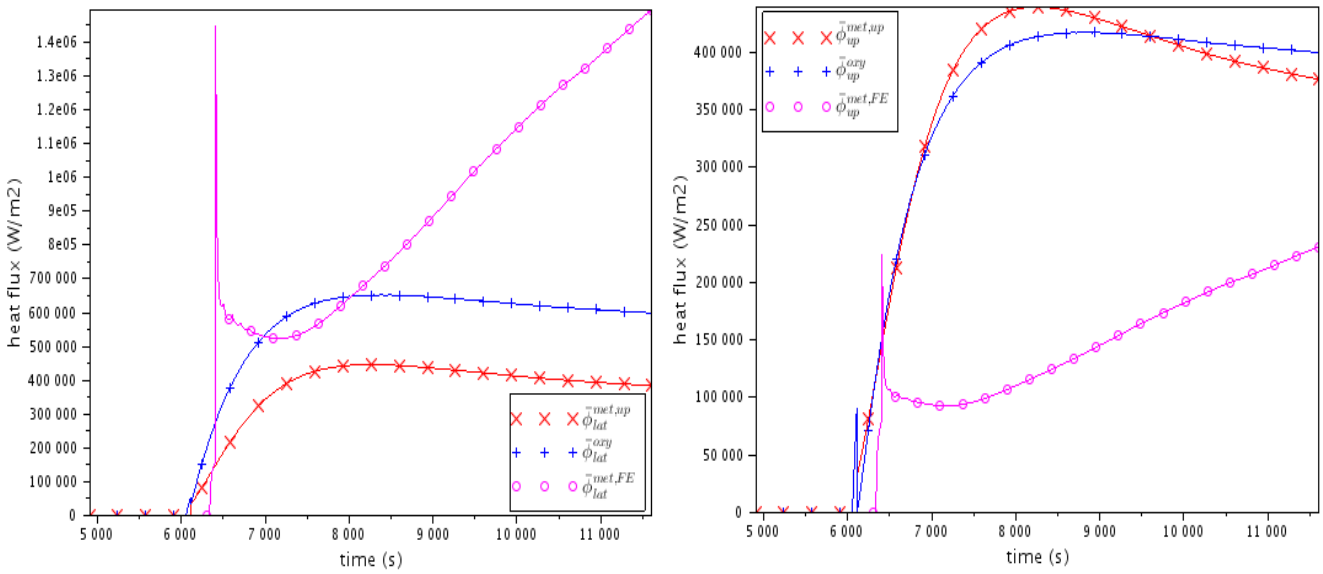

$\bar{\phi}^{met,up}_{lat}$: lateral heat flux for the upper metal layer
$\bar{\phi}^{oxy}_{lat}$: lateral heat flux for the oxidic layer
$\bar{\phi}^{met,FE}_{lat}$: lateral heat flux for the FE metal layer
$\bar{\phi}^{met,up}_{up}$: upper heat flux for the upper metal layer
$\bar{\phi}^{oxy}_{up}$: upper heat flux for the oxidic layer
$\bar{\phi}^{met,FE}_{up}$: upper heat flux for the FE metal layer

Figure 20: Evolution of in-vessel corium layer of the corium pool mean lateral and upper heat fluxes (W/m²)

In the same way, Figure 21 is similar to Figure 12. The **vessel failure occurs at 11627 s** (11127 s for the "best-estimate" case) on the cylindrical part of the vessel, at 2.68 m from the internal bottom of the lower head (or **1.76 m** if we consider that elevation 0 corresponds to the junction between ellipsoidal and cylindrical parts of the vessel). It happens at the level of the FE metal layer and during the thinning of this one.

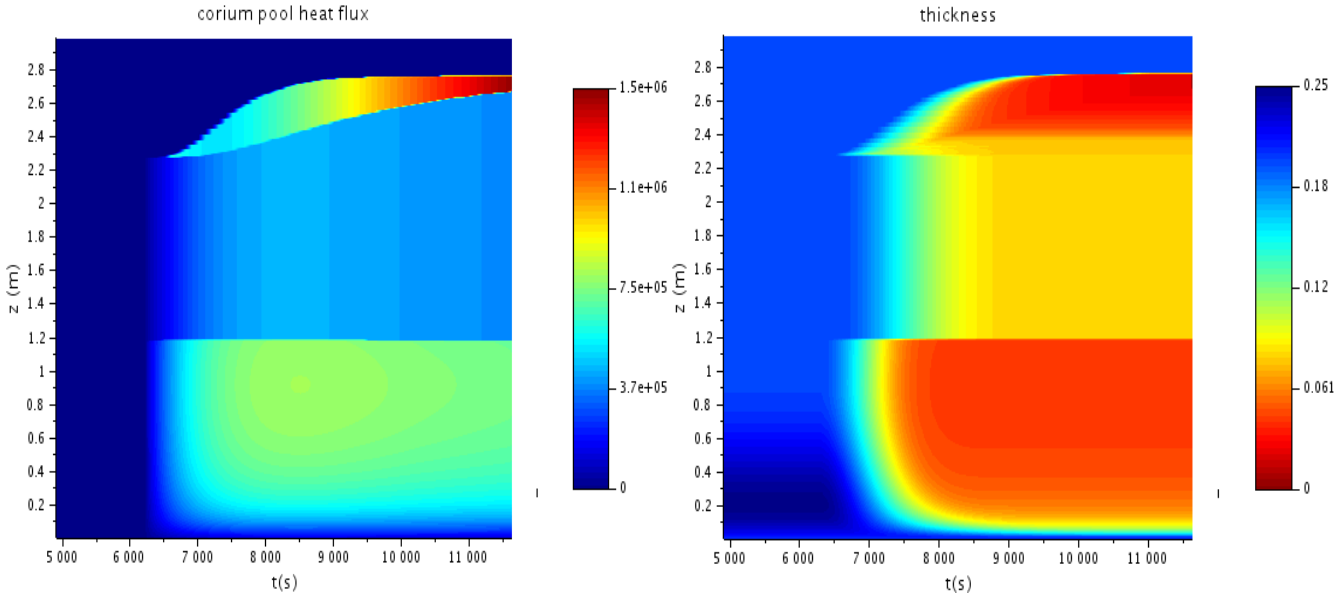

Figure 21: Evolution of the axial profiles: of internal heat flux transmitted to the vessel wall (MW/m²) (left figure) and of residual vessel thickness (m) (right figure)

A.5.4.4 Sensibility to the corium (zirconium) oxidation degree: Cox = 30% and Cox = 70%

The steel mass in the corium inventory doesn't change here and remains equal to 69.84 tons. Here, there is only a variation of C_{ox}, $R_{U/Zr}$ remains constant (see Table 1). In the reference or "best-estimate" calculation, C_{ox} = 44.8 %.

From the change of stratification point of view, these two calculations will represent two points more on the right part ($\rho_{oxy} > \rho_{met}$) of Figure 4. So, the physical phenomena of these transients will be similar to the one of the "best-estimate" case.

Table 1: Corium composition for reference calculation, and sensibility calculations with C_{ox} = 30% and C_{ox} = 70%

C_{ox}	m_{ZrO2} (kg)	m_{Zr} (kg)	m_{UO2} (kg)	m_{steel} (kg)	m_{totale} (kg)	$R_{U/Zr}$
Reference : 44,8%	17100	15600	85900	69840	**188440**	*1,027*
30%	11470	19800	85900	69840	**187010**	*1,026*
70%	26760	8490	85900	69840	**190990**	*1,025*

The initial total mass doesn't vary a lot: ~ 2% maximum.

When the liquidus temperature is reached at 6010 s for C_{ox} = 30%, respectively 6110 s for C_{ox} = 70%, and when stratification instantaneously occurs, there is one oxide layer (80.7 t for C_{ox} = 30%, respectively 107.6 t for C_{ox} = 70%) with a lighter metal layer above (106.3 t for C_{ox} = 30%, respectively 83.4 t for C_{ox} = 70%), surrounded by a crust, as shown on Figure 22.

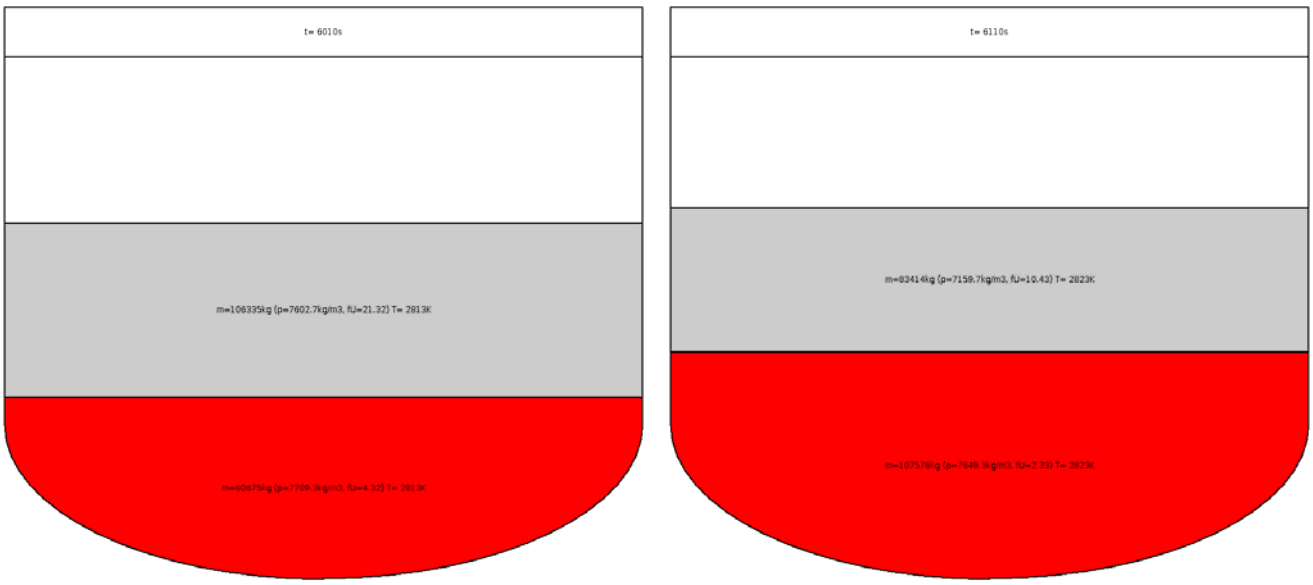

- red = oxide layer under the crust
- light grey = light metal layer under the crust

Figure 22: Vessel photos at t = 6010 s on the left (C_{ox} = 30%) and at t = 6110 s on the right (C_{ox} = 70%), just after total fusion in thermodynamic equilibrium

With the increase of corium pool temperature, the vessel wall begins to melt and a third layer (steel from the melted vessel) appears above the crust.

The transient is very similar to the reference calculation. The FE is thickening in a first time and then thinning in a second time. **Vessel failure** finally occurs during the thinning of the FE metal layer, at **10227 s for C_{ox} = 30%, respectively 13526 s for C_{ox} = 70%**.

Figure 23 shows the mass increasing of the light metal layer under the crust linked to the mass transfer from the FE metal layer. The oxide mass nearly doesn't vary:

- 80.7 t just after stratification and 79.5 t just before vessel failure for C_{ox} = 30%,
- 107.6 t just after stratification and 106.8 t just before vessel failure for C_{ox} = 70%.

It is very similar to Figure 7 (reference case with the same initial steel mass layer = 69.84 t).

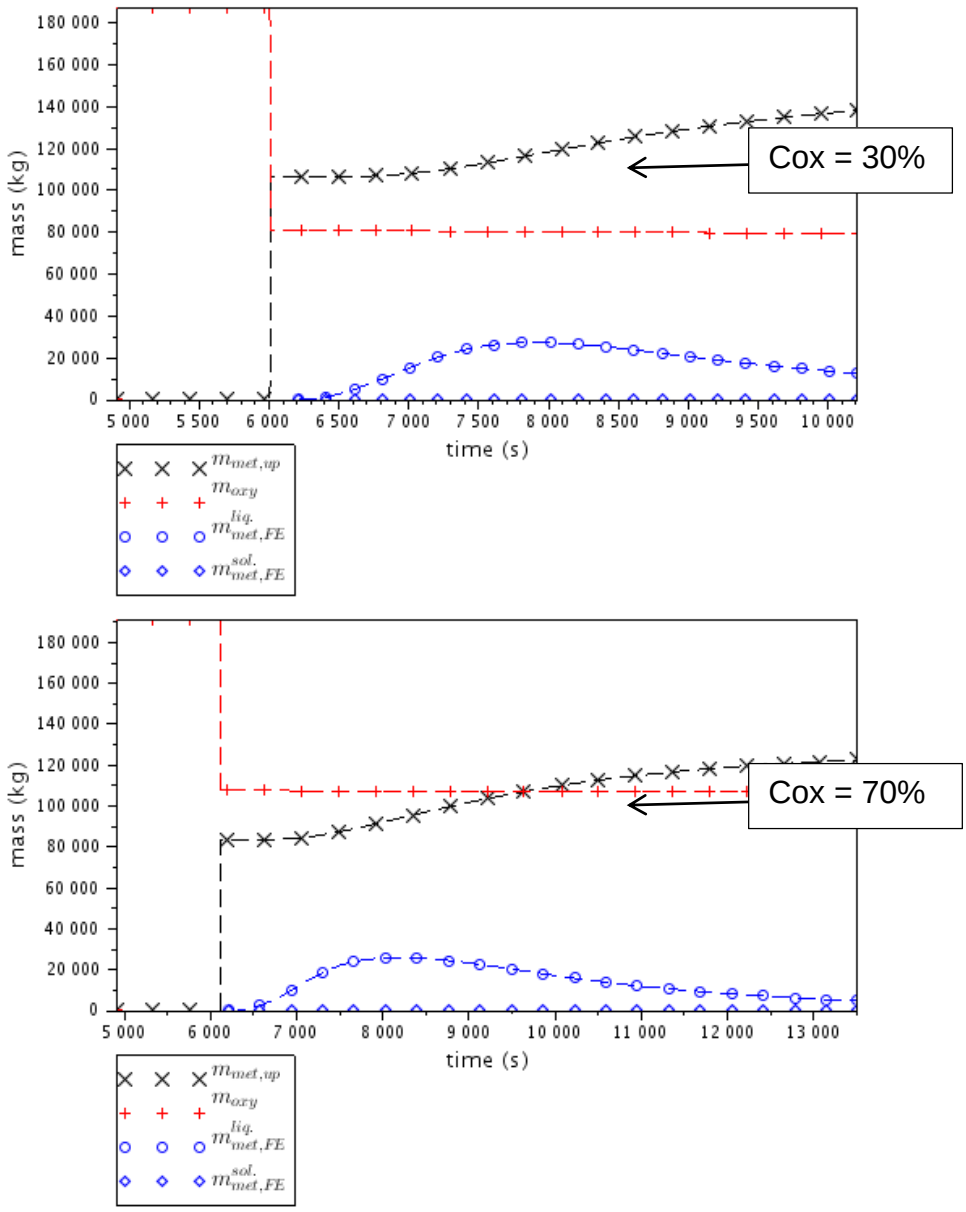

$m_{met,up}$: mass of the upper metal layer of the corium pool
m_{oxy}: mass of the oxidic layer of the corium pool
$m^{liq.}_{met,FE}$: liquid mass of the FE metal layer of the corium pool
$m^{sol.}_{met,FE}$: solid mass of the FE metal layer of the corium pool

Figure 23: Evolution of the layers mass of the corium pool for C_{ox} = 30% (upper figure) and C_{ox} = 70% (lower figure)

Figure 24 and Figure 25 hereunder are similar to Figure 9 related to the reference case (with m_0^{steel} = 69.84 t). The vessel failure occurs a little earlier for C_{ox} = 30%: 10227 s instead of 11127 s for the reference case. This must be related to the residual power which is the same, but associated to a corium pool mass a little less important for C_{ox} = 30% (1.43 t less according to Table 1). On the contrary, for C_{ox} = 70%, the vessel failure occurs a little later: 13526 s (2.55 t more for the corium pool mass according to Table 1).

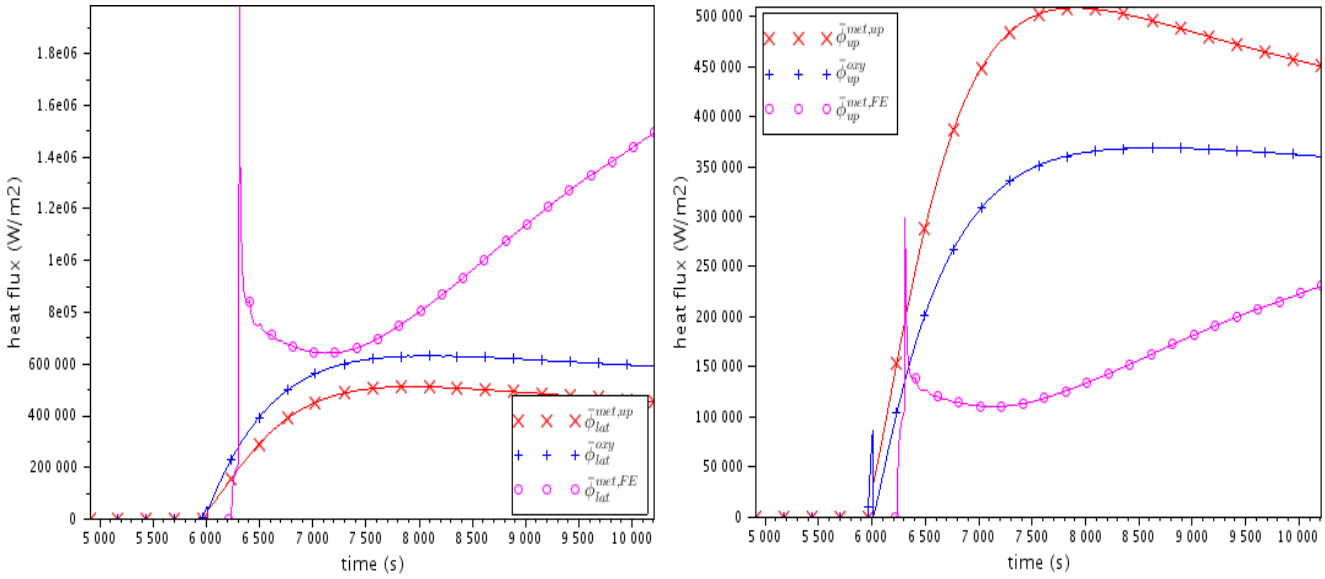

$\bar{\phi}_{lat}^{met,up}$: lateral heat flux for the upper metal layer

$\bar{\phi}_{lat}^{oxy}$: lateral heat flux for the oxidic layer

$\bar{\phi}_{lat}^{met,FE}$: lateral heat flux for the FE metal layer

$\bar{\phi}_{up}^{met,up}$: upper heat flux for the upper metal layer

$\bar{\phi}_{up}^{oxy}$: upper heat flux for the oxidic layer

$\bar{\phi}_{up}^{met,FE}$: upper heat flux for the FE metal layer

Figure 24: Evolution of in-vessel corium layer of the corium pool mean lateral and upper heat fluxes (W/m²) for C_{ox} = 30%

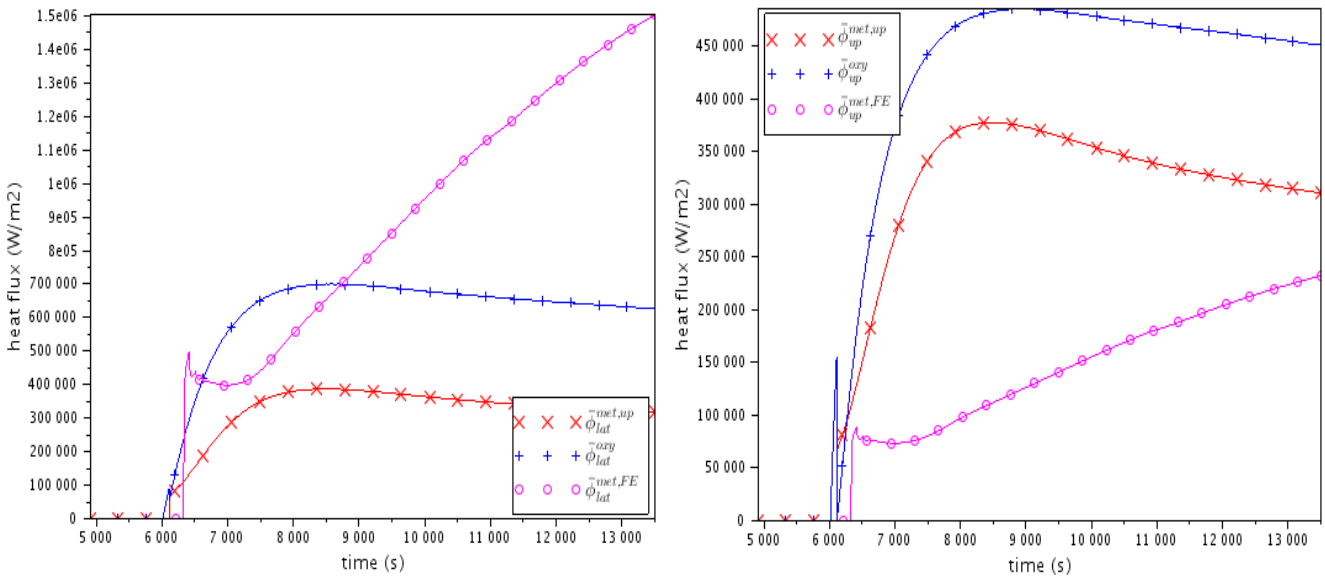

$\bar{\phi}_{lat}^{met,up}$: lateral heat flux for the upper metal layer

$\bar{\phi}_{lat}^{oxy}$: lateral heat flux for the oxidic layer

$\bar{\phi}_{lat}^{met,FE}$: lateral heat flux for the FE metal layer

$\bar{\phi}_{up}^{met,up}$: upper heat flux for the upper metal layer

$\bar{\phi}_{up}^{oxy}$: upper heat flux for the oxidic layer

$\bar{\phi}_{up}^{met,FE}$: upper heat flux for the FE metal layer

Figure 25: Evolution of in-vessel corium layer of the corium pool mean lateral and upper heat fluxes (W/m²) for C_{ox} = 70%

For C_{ox} = 30%, the maximum lateral heat flux of 1.99 MW/m² is obtained during the formation of the FE metal layer, at 6310 s.

For C_{ox} = 70%, the maximum lateral heat flux of 1.51 MW/m² is obtained during the thinning of the FE metal layer, at the end of the calculation when the vessel fails, at 13526 s. This is similar to the reference case as shown on Figure 9. But in the reference case, the value of the lateral heat

flux reached during the FE metal layer formation is very close to the maximum value, reached at the end of the calculation, at vessel failure. These differences are related to the mass repartition evolution in the different layers: it impacts the associated value for the power transmitted in the axial and radial (inter-layers) directions.

In the same way, Figure 26 and Figure 27 are similar to Figure 12: the vessel failure occurs on its cylindrical part.

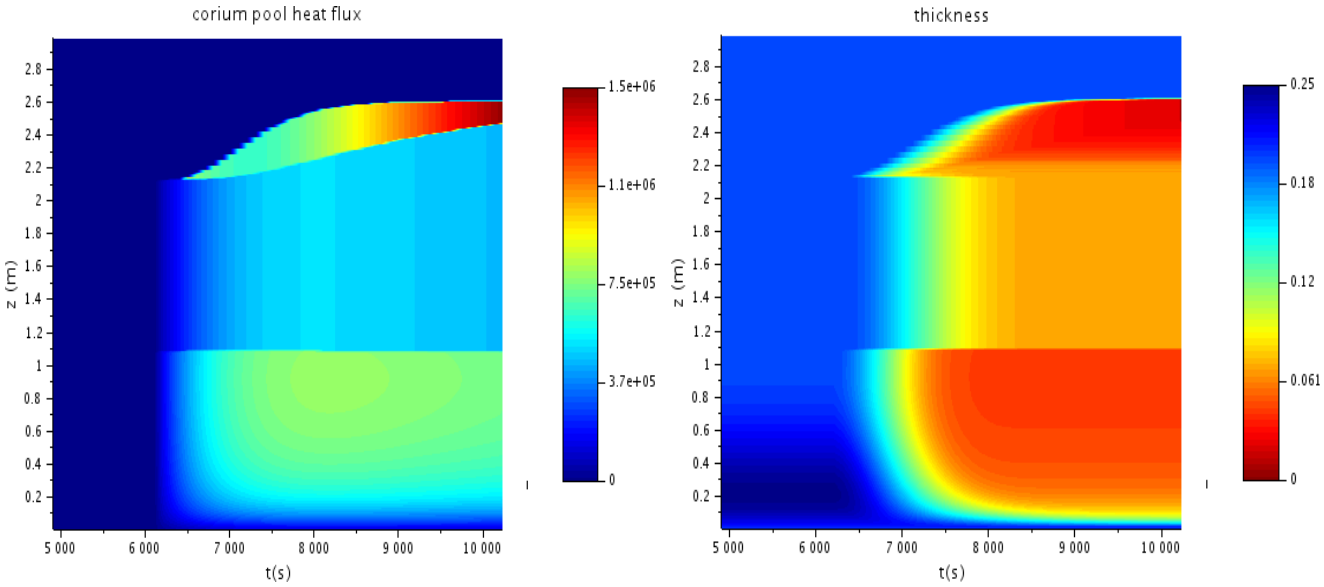

Figure 26: Evolution of the axial profiles: of internal heat flux transmitted to the vessel wall (MW/m²) (left figure) and of residual vessel thickness (m) (right figure) –for C_{ox} = 30%

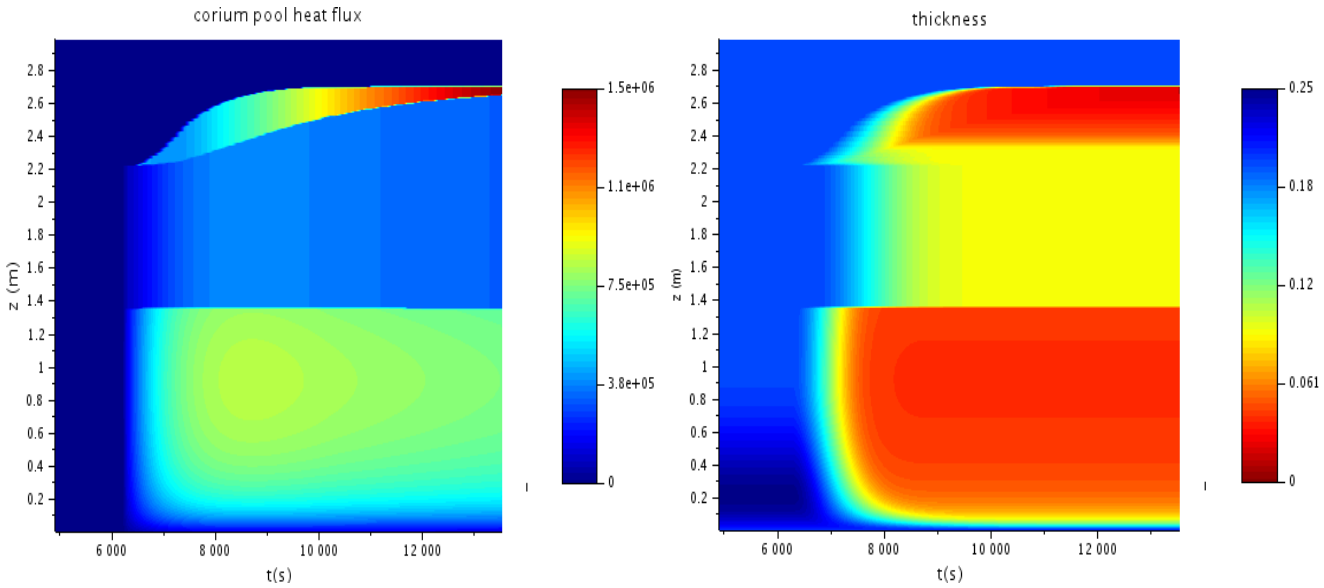

Figure 27: Evolution of the axial profiles: of internal heat flux transmitted to the vessel wall (MW/m²) (left figure) and of residual vessel thickness (m) (right figure) –for C_{ox} = 70%

The **vessel failure occurs at 10227 s for C_{ox} = 30%, respectively 13526 s for C_{ox} = 70%** (11127 s for the "best-estimate" case) on the cylindrical part of the vessel:

- at 2.47 m from the internal bottom of the lower head (or **1.55 m** if we consider that elevation 0 corresponds to the junction between ellipsoidal and cylindrical parts of the vessel) for C_{ox} = 30%,

- at 2.66 m from the internal bottom of the lower head (or **1.74 m** if we consider that elevation 0 corresponds to the junction between ellipsoidal and cylindrical parts of the vessel) for C_{ox} = 70%.

For C_{ox} = 30%, C_{ox} = 70% and for the reference case, vessel failure happens at the level of the FE metal layer and during the thinning of this one.

A.5.4.5 Conclusion on the sensitivity to the steel mass and to the zirconium oxidation degree in the corium inventory

Steel mass

Increasing the steel mass proportion in the corium inventory tends to delay the vessel rupture. It may be possible to increase the steel mass until a threshold level which would permit to avoid the vessel failure.

But this strong quantity of steel in the corium inventory (at least greater than 80 t according to the PROCOR calculations) may not be real regarding a VVER1000 core inventory.

Zirconium oxidation degree

Increasing the zirconium oxidation degree in the corium inventory (for a fixed $R_{U/Zr}$) tends to delay the vessel failure. It may be possible to increase the zirconium oxidation degree until a threshold level which would permit to avoid the vessel failure.

But this strong quantity of oxidized zirconium (at least greater than 70% according to the PROCOR calculations) may be overestimated regarding a VVER1000 severe accident.

A.5.4.6 Results summary for the reference ("best-estimate") and for the sensitivity calculations

The results of the PROCOR calculations of the former paragraphs have been summarized in Table 2 hereunder.

Table 2: Summary of the key results (with 3 layers maximum during the transient)

Case	"Best estimate" M_steel = 69,84 t	M_steel = 30t	M_steel = 80t	M_steel = 69,84t	
	Cox = 44,8 %			Cox = 30 %	Cox = 70 %
Initial layer configuration	**LM over oxidic layer**	HM under oxidic layer	LM over oxidic layer	LM over oxidic layer	LM over oxidic layer
Maximum-to-vessel heat flux (MW/m²)	**1,50**	6,77	1,50	1,99	1,50
Instant of maximum-to-vessel heat flux (s)	**11127**	*6010*	11626	6310	13526
Ablated steel mass from vessel (t)	**43,33**	2,70	44,17	43,18	43,16
Ablation beginning (s)	**6311**	6010	6410	6310	6310
Vessel-to-water heat coefficient (kW/m²/K)	10				
Vessel failure time (s)	**11127**	6268	11626	10227	13526
Vessel failure height (m)	**1,62**	0,81	1,76	1,55	1,74

Corium inventory ⇒ AFTER change of stratification

Corium inventory ⇒ BEFORE change of stratification

A.5.5 PROCOR calculation with 3 layers at initial stratification – same input data as "best-estimate" calculation

The result obtained for any calculation performed with any code is strongly dependent on the considered hypotheses. This part shows that a modification of the number of layers in the corium pool (by hypothesis) has an important impact on the results.

In this part, the maximum value for the CHF on the cylindrical part of the vessel is taken equal to 1.5 MW/m² (ULPU value).

A.5.5.1 Test 1: 3 layers at initial stratification (+ possible stratification inversion)

Here, all the input data and model hypotheses of the "best-estimate" calculation are kept, except the following one:

- At initial stratification (when $T_{corium} = T_{liquidus}$), a configuration with three layers is used considering, under the crust, the two layers at equilibrium corresponding to the steel mass threshold (see Figure 4) at the stratification inversion and, above the crust, the remaining steel in the system.

As in the "best-estimate" case, the stratification inversion is possible here. The formation of an upper light metal layer (under the crust) by migration of metal from the heavy metal layer upward, through the oxide layer, can occur with the inter-layers mass transfers. The mass transfer of all the elements in the metal phases is proportional to the Uranium mass transfer (U is the species limiting the transfer kinetics).

So the configuration shown on Figure 1 with <u>up to four layers</u> (three under and one above the crust) can be obtained during the transient.

Figure 28 (left picture) shows this initial configuration obtained after stratification, when $T_{corium} = T_{liquidus}$. There is a heavy metal layer (66.04 t) with an oxide layer above (93.18 t), surrounded by a crust and a FE metal layer (29.22 t) above. The following figure summarizes the models used for inter-layers mass and heat transfer.

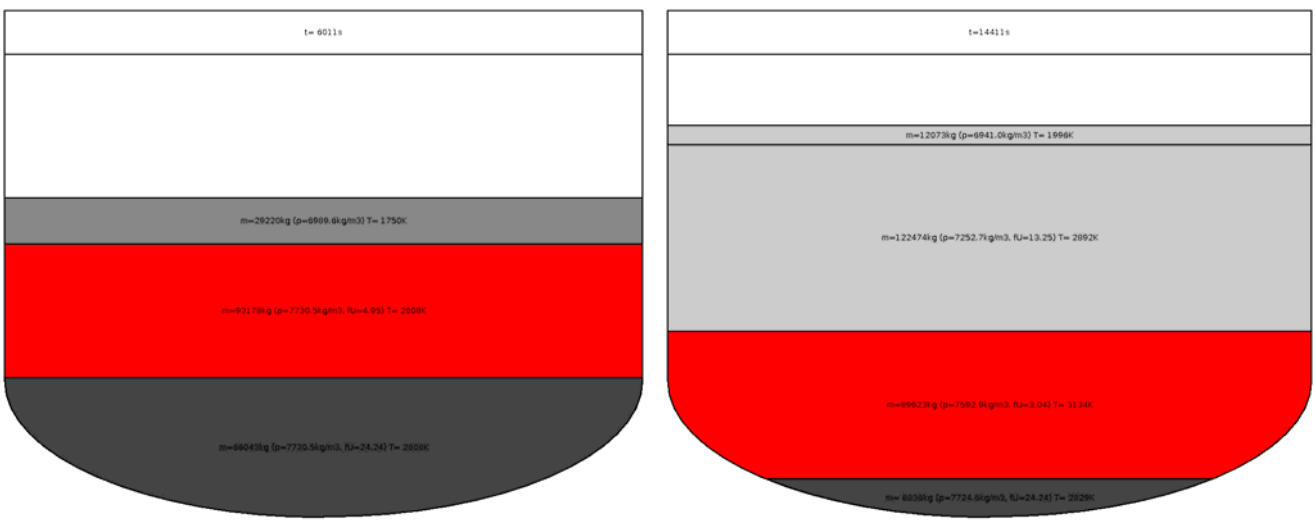

- dark grey = heavy metal layer, under the crust
- red = oxide layer, under the crust
- *mid grey (on left picture only) = FE metal layer above the crust, at stratification time (the "exceeding" steel compared to the proportion at the "stratification inversion point" is put in this layer)*
- light grey (lower rectangle) = light metal layer, under the crust
- light grey (upper rectangle) = light metal layer, above the crust (steel coming from the vessel ablation)

Figure 28: Vessel photos at t = 6011 s just after total fusion in thermodynamic equilibrium (left picture) and t = 14411 s just before vessel failure (right picture)

Figure 28 (right picture) shows the final configuration, just before vessel rupture.

Here, the stratification inversion is possible, so a third "upper light metal layer" is formed just under the crust. This third layer is thickened by the heavy metal layer and the FE metal layer thinning (mass transfer of light metal). This transient is similar to the "best-estimate" transient: the vessel rupture occurs during the thinning of the FE metal layer.

Figure 29 shows that the FE metal layer mass decreases, and in parallel the lateral heat flux imposed by the FE metal layer to the vessel wall increases continuously until 1.5 MW/m^2.

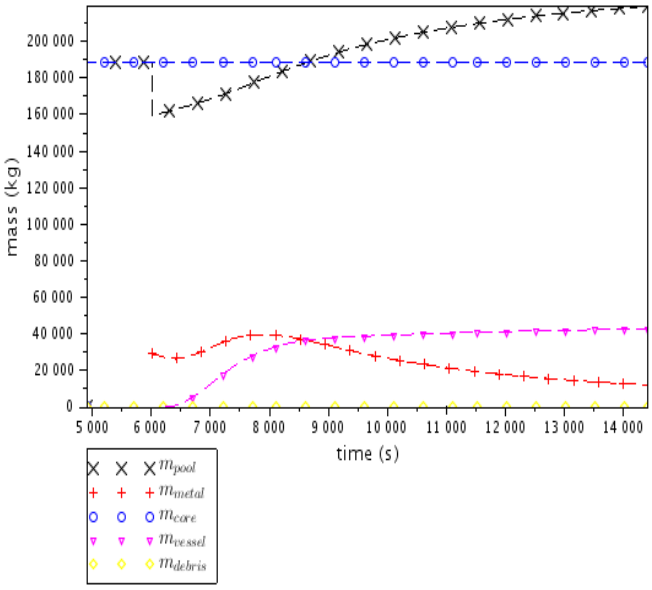

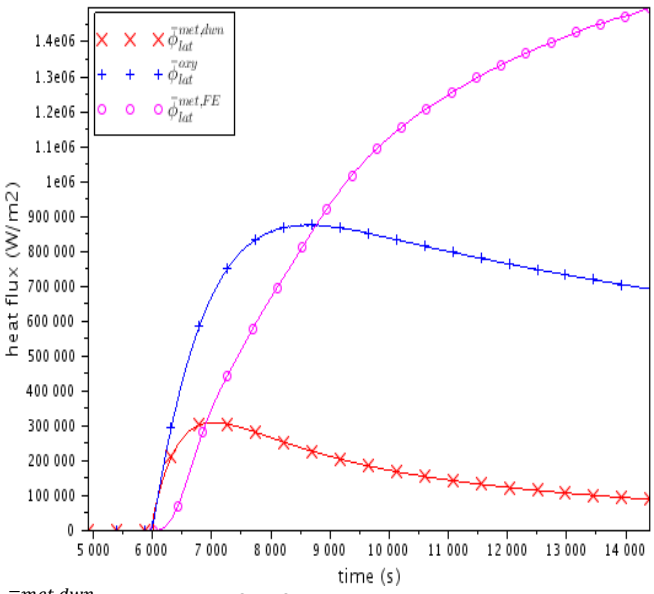

$m_{pool} = m_{met,dwn} + m_{met,oxy} + m_{met,up}$: mass of the corium pool

$m_{metal} = m_{met,FE}^{liq} + m_{met,FE}^{sol}$: mass of the FE metal layer of the corium pool

m_{core}: cumulative mass of liquid corium transferred from the core to the lower head

m_{vessel}: cumulative mass of ablated vessel wall transferred to the corium pool

m_{debris}: cumulative mass of melted debris transferred to the corium pool

$\bar{\phi}_{lat}^{met,dwn}$: lateral heat flux for the heavy metal layer

$\bar{\phi}_{lat}^{oxy}$: lateral heat flux for the oxidic layer

$\bar{\phi}_{lat}^{met,FE}$: lateral heat flux for the FE metal layer

Figure 29: Evolution of in-vessel related masses of the corium pool and mean lateral heat fluxes

Figure 30 shows axial profiles evolutions versus time. The median part of the vessel (facing the upper light metal layer) is the less ablated part of the vessel wall. The **vessel failure occurs at 14427 s** on the cylindrical part of the vessel, at 2.51 m from the internal bottom of the lower head (or **1.59 m** if we consider that elevation 0 corresponds to the junction between ellipsoidal and cylindrical parts of the vessel). It happens at the level of the FE metal layer and during the thinning of this one.

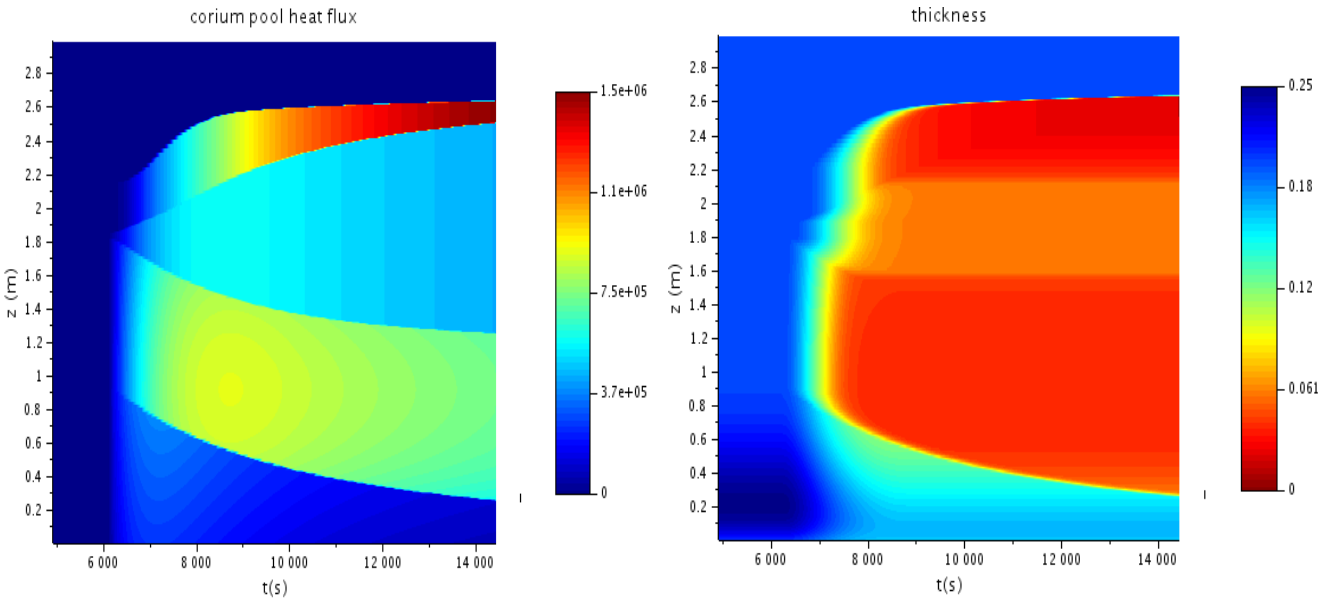

Figure 30: Evolution of the axial profiles: of internal heat flux transmitted to the vessel wall (MW/m²) (left figure) and of residual vessel thickness (m) (right figure)

A.5.5.2 Test 2: idem Test 1 with impossible stratification inversion

Here, all the input data and model hypotheses of the "best-estimate" calculation are kept, except the following ones:

- At initial stratification (when $T_{corium} = T_{liquidus}$), a configuration with three layers is used considering, under the crust, the two layers at equilibrium corresponding to the steel mass threshold (see Figure 4) at the stratification inversion and, above the crust, the remaining steel in the system. This is modification is similar to test 1 (§A.5.5.1).

- In the kinetic model of stratification, the mass transfer inter-layers is supposed to be infinitely slow. As a consequence, the stratification inversion is not possible. As a matter of fact, it has been observed in experiences that the configuration where the light metal layer is above the oxide layer (right zone where $\rho_{met} < \rho_{oxy}$ on Figure 4) is reached after a transient which can take some time. This is the **only modification between test 1 (§A.5.5.1) and test 2.**

As the kinetics of upward migration of the metal is infinitely slow here, the upper metal layer under the crust can't exist.

The initial stratification is exactly the same as for test 1, as shown on Figure 31 (left picture). There is a heavy metal layer (66.04 t) with an oxide layer above (93.18 t), surrounded by a crust and a FE metal layer (29.22 t) above.

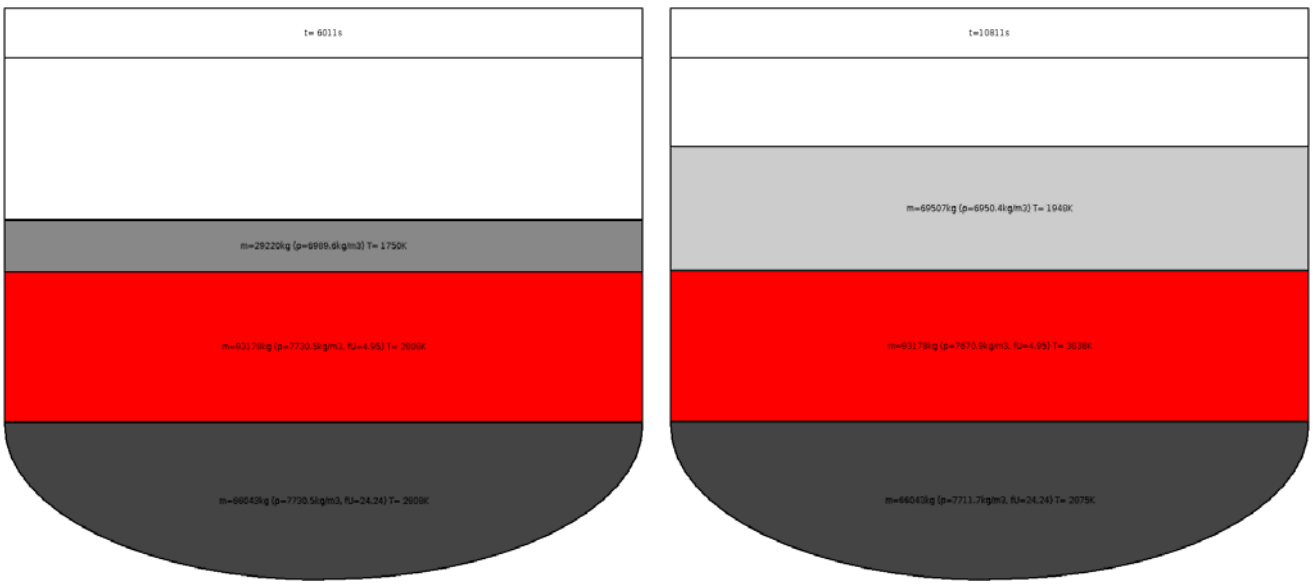

- dark grey = heavy metal layer, under the crust
- red = oxide layer, under the crust
- *mid grey (on left picture only) = FE metal layer above the crust (steel coming from the vessel ablation) at 1750 K (T_{fusion} of steel), just after formation*
- light grey = FE metal layer above the crust (steel coming from the vessel ablation)

Figure 31: Vessel photos at t = 6011 s just after total fusion in thermodynamic equilibrium (left picture) and t = 10811 s after corium stabilization in the vessel (right picture)

As the stratification inversion is not possible (inter-layers mass transfers infinitely slow by hypothesis), there is no upper light metal layer formation under the crust and the FE metal layer doesn't penetrate through the crust. So the steel from the melted vessel wall will thicken this FE metal layer.

The first “mode of failure” does not exist because there is enough steel mass in the FE metal layer at the initial state of the corium pool, to avoid it. The FE metal layer mass is thickening during all the transient because the thermochemistry is blocked (infinitely slow inter-layers mass transfers ⇒ no formation of a third light metal layer under the upper crust ⇒ no migration of steel from the FE metal layer through the upper crust).

Consequently, there is no vessel failure in this case as illustrated on Figure 32. The final amount of steel in the FE metal layer above the crust is about 70 t and the maximum lateral heat flux imposed by the FE metal layer to the vessel wall is 1.14 MW/m².

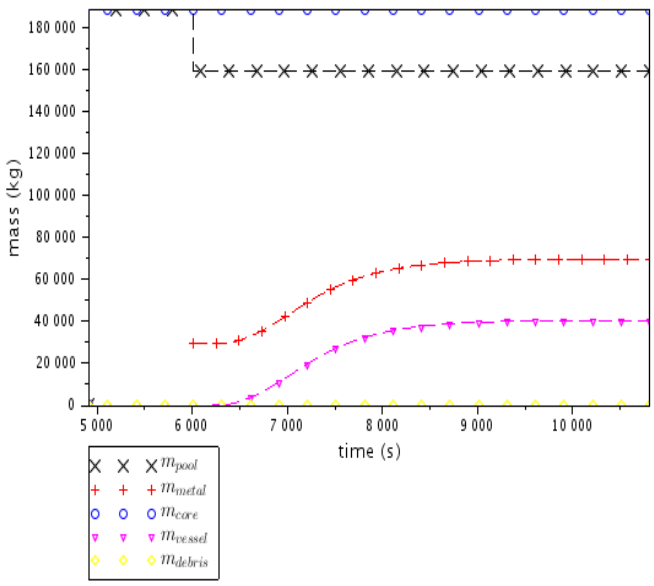

$m_{pool} = m_{met,dwn} + m_{met,oxy}$: mass of the corium pool

$m_{metal} = m_{met,FE}^{liq} + m_{met,FE}^{sol}$: mass of the FE metal layer of the corium pool

m_{core}: cumulative mass of liquid corium transferred from the core to the lower head

m_{vessel}: cumulative mass of ablated vessel wall transferred to the corium pool

m_{debris}: cumulative mass of melted debris transferred to the corium pool

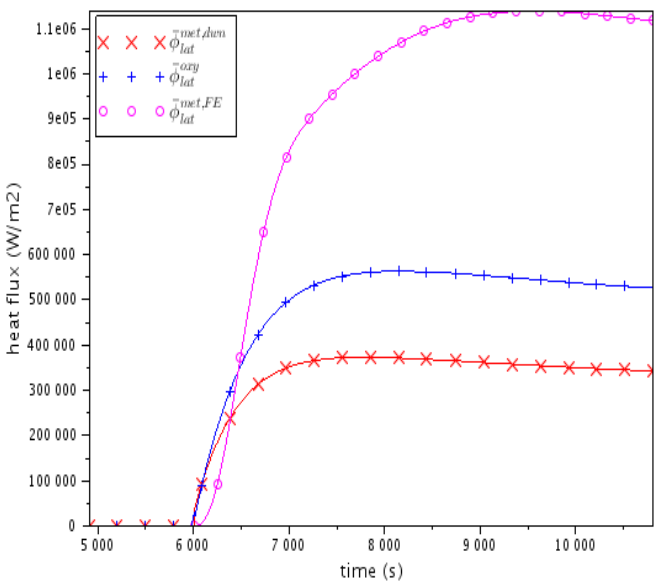

$\bar{\phi}_{lat}^{met,dwn}$: lateral heat flux for the heavy metal layer

$\bar{\phi}_{lat}^{oxy}$: lateral heat flux for the oxidic layer

$\bar{\phi}_{lat}^{met,FE}$: lateral heat flux for the FE metal layer

Figure 32: Evolution of in-vessel related masses of the corium pool and mean lateral heat fluxes

Figure 33 shows axial profiles evolutions versus time. The middle part of the vessel (facing the oxide layer) and its upper part (facing the FE metal layer) are the most ablated parts of the vessel wall. The **wall minimum residual thickness is 2.89 cm**.

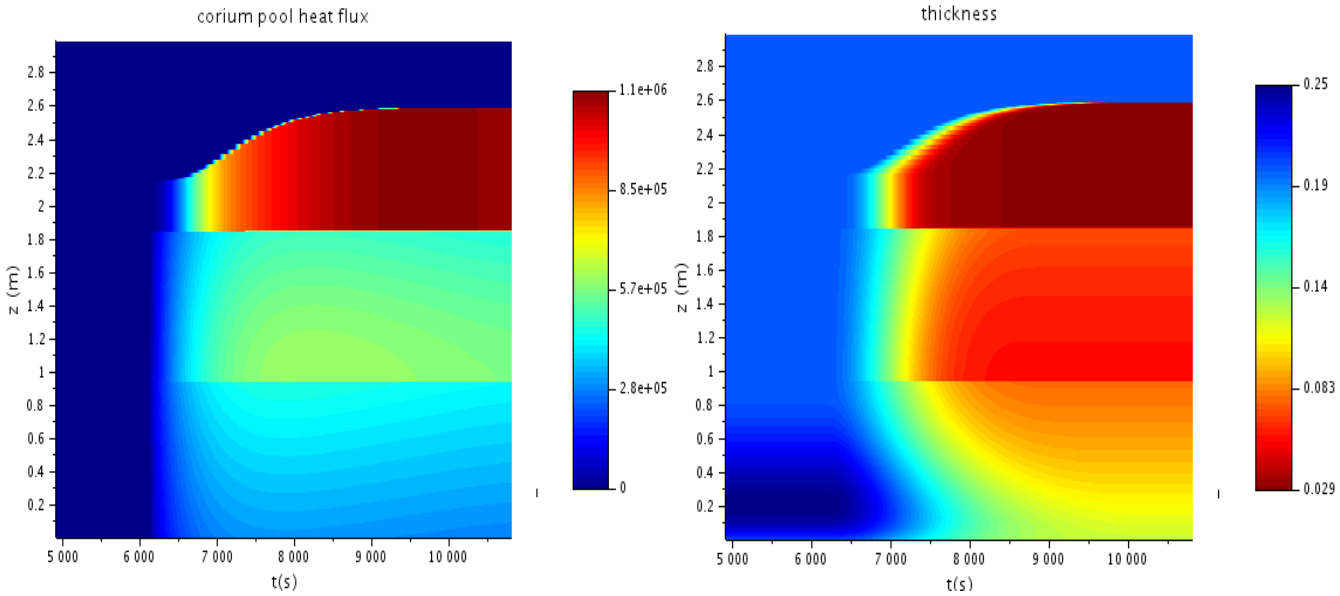

Figure 33: Evolution of the axial profiles: of internal heat flux transmitted to the vessel wall (MW/m²) (left figure) and of residual vessel thickness (m) (right figure)

A.5.6 Conclusion

Finally the important hypotheses that can strongly modify the calculation results are:

- The hypotheses related to the initial stratification, related to the numbers of layers in the corium pool and their order.
- The permeability of the upper crust, which permits steel mass transfer or not.
- The kinetics related to the mass transfers in the corium pool (inter-layers) and through the upper crust, also related to the stratification inversion.

A.5.7 Some references

R. Le Tellier, L. Saas, S. Bajard, “Transient stratification modelling of a corium pool in a LWR vessel lower head”, to be submitted to Nuclear Engineering and Design

M. Salay, F. Fichot, Modelling of metal-oxide corium stratification in the lower plenum of a reactor vessel, in: Proc. of Int. Topical Meeting on Nuclear Thermal-Hydraulics (NURETH-11), Avignon, France, 2005

T.N. Dinh, J.P. Tu, and T.G. Theofanous, “Two-Phase Natural Circulation Flow in AP-1000 In-Vessel Retention-Related ULPU-V Facility Experiments”, in: Proceedings of ICAPP ’04 Pittsburgh, PA USA, June 13-17, 2004 - Paper 4242

1) Appendix 1: input data transmitted by Kurchatov Institute

1. Updated information of the corium history

The new basic calculation includes fission products release.

Table 1 - Chronology of main events of simulated accident

Event	**Time, s**	
	Initial calculation	**Basic calculation (account of fission products release, - 20%)**
Accident initiation	0	0
Injection of water from safety injection tanks	5.5-54	5.5-54
Core heat up onset	700	700
Fuel cladding burst	1050-1280	1050-1280
Hydrogen generation onset	1160	1160
Fuel cladding melting onset	1250	1250
Melt transfer onset	1350	1360
Full core dryout	2290	2340
Beginning of corium relocation into the core barrel	3250	3450
Core barrel melting-through	4340	4910
Reactor vessel failure	8900	14000

Core barrel melting-through at time 4910 s. Right at this moment corium relocates into lower plenum instantly. Corium relocates as one big portion with averaged temperature T = 2500 K.

Table 2 - Corium composition for basic calculation (with account of fission products release)

Material	**Mass, t**	**Source**
UO_2	85.9	CORE
Zr	15.6	CORE
ZrO_2	17.1	CORE
Steel	34.4	CORE
	12.2	elliptic part of barrel
	9.0	melted cylindrical part of barrel
	12.3	FA-supports
	1.94	support grid

Table 3 - Decay heat time dependence

Time from the accident start, s	Decay heat, Wt (per 1 kg of UO_2)	
	Initial calculation	Basic calculation (account of fission products release, -20%)
1000	731.6	585.28
2000	609.4	487.52
3000	542.4	433.92
4000	497.1	397.68
4910	-	**373.44**
5000	463.8	371.04
6000	437.5	350
7000	416.6	333.28
8000	398.9	319.12
9000	384.4	307.52
10000	371.6	297.28
20000	300.1	240.08
30000	268.9	215.12
40000	250.5	200.4
50000	237.7	190.16
60000	227.8	182.24
70000	218.9	175.12
80000	211.2	168.96
90000	203	162.4
100000	194.9	155.92
200000	166.5	133.2
300000	146.3	117.04
400000	128.6	102.88

It should be noticed, that time countdown was started from the accident start. For calculations in stand-alone mode, it's necessary to use decay heat dependence from the time 4910 s. This time corresponds to core barrel melting through (for basic calculation with fission products release account). Thus, initial value for decay heat will be 373.44 Wt (per 1 kg of UO_2).

2. Recommended parameters for sensitivity study

- Steel mass (30 t, 80 t)
- Corium (zirconium) oxidation degree (30%, 70%)
- Account of heat yielded by the metallic layer (15%)

We recommend 2 layers stratification model for corium pool.

Composition of metal layer bases on MASCA experiments and includes metal Uranium and ZrO_2.

We also recommend the follow heat transfer coefficient $H=10^4$ $W/(m^2.K)$ for reactor vessel surface.

A.6 TUS ASTEC hybrid integral/stand-alone

A.6.1 First report

The TUS' calculations aimed to analysis the conditions of in-vessel melt retention and the influence of steel mass was made by ASTECv2.0R3p1 (and the results are used as input data for ASTECv2.0 for HF calculations) with the scenario of LOCA 200 mm applied in the integral input deck of VVER-1000. The sequence of events is as follow:

1/ 0 s: opening of the break, reactor scram, stop of pumps

2/ 10 s: turbine isolation

3/ 11 s: loss of feed water to steam generator

4/ 135 s: spray system in direct mode

Some results as the obtained temperatures of corium and fluids, as well the pressure in the vessel for the interval 0 – 5000 s are presented in Fig.1 and 2. These are used for calculations with module ICARE by the stand-alone input deck of VVER-1000. After LOCA 200 mm at 4340 s the calculations' results for heat fluxes (HF) - internal (over the surface corium/vessel) and external (vessel/external water) are obtained and compared at different steel mass.

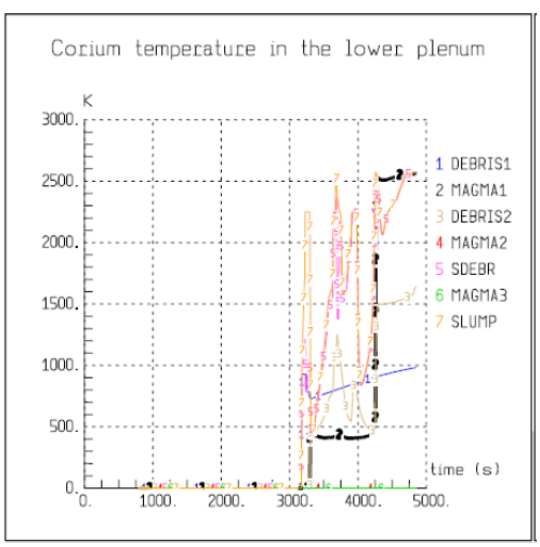

Fig.1 Temperature of the melt (curve 2) – LOCA 200 mm

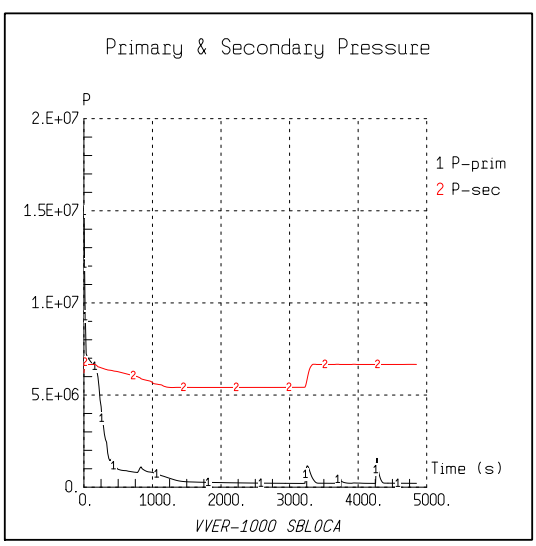

Fig.2 Pressure in the vessel

In TUS there are implemented 4 calculations as the levels of the lower plenum are changed, in correspondence to VVER-1000 RPV bottom head drawing distributed between participants of the project. In the Fig.3 and Fig. 4 are presented the temperature fields of initial scenario steel mass in the corium composition and in the case of calculations for LOCA 200 mm for VVER-1000 with 70 t steel in the corium composition. The fields are very similar.

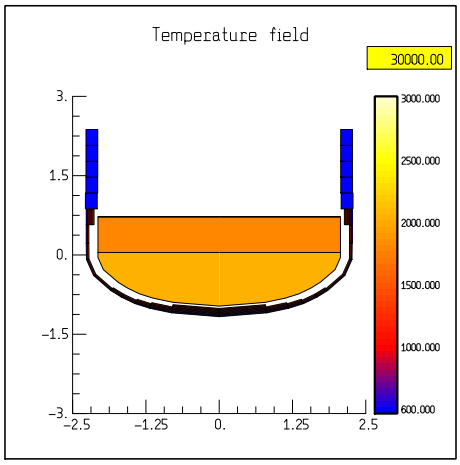

Fig.3 Temperature field in the vessel – 70 t steel steel in the melt (Initial scenario)

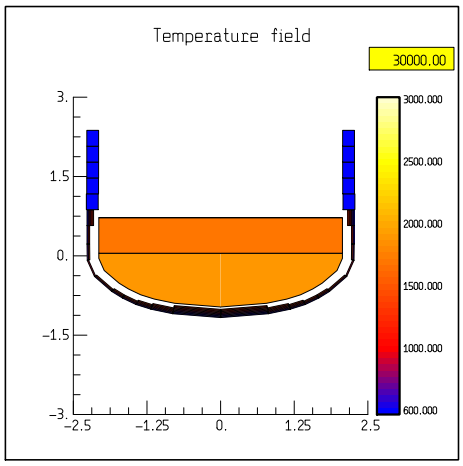

Fig.4 Temperature field in the vessel – 70 t in the melt (LOCA-200 mm)

To analyze the influence of steel mass, TUS implements also calculations with 30 t and 110 t of steel. The obtained results for HF in that case are compared with the results of JRC with calculation for decay power reduction of 20%. The other events for TUS calculations as decay heat, etc., are in correspondence to scenario and tables in the document "Updated information of the corium history".

1) TUS' results for HF - 3 calculations for LOCA 200 mm in the case of VVER-1000 with 30, 70 and 110 t of steel in the corium composition, with the ICARE stand-alone input deck

The comparative analysis of HF obtained for LOCA200 for 30 t, 70 t and 110 t steel is on the basis of the main results, presented in Fig. 5.

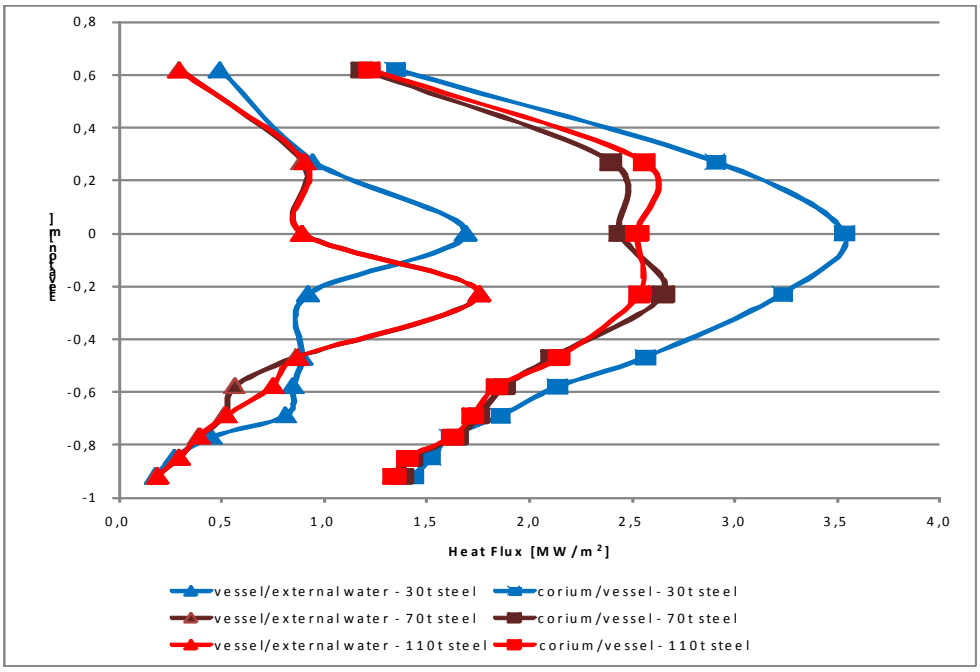

Fig.5 Comparison of HF obtained of TUS for LOCA200 for 30, 70 and 110 t steel mass

In the case of 30 t steel, around level 0 there are a higher peaks of HF on the internal (over the surface corium/vessel) and external (vessel/external water). In the cases of 70 t and 110 t of steel the HF on the surface corium/vessel is producing in larger volume (-0.2 until 0.23 m) but with smaller values (than in the case of 30 t steel) in result of distribution of the same energy in bigger

lower volume of corium. The HF on the external (vessel/external water) for the both cases (70 t and 110 t) has the same value as for 30 t but on -0.2 m.

2) Comparison of the results for HF calculations of TUS and JRC for VVER-1000 with 70 t of steel in the corium composition, with the ICARE stand-alone input deck

The comparison is shown in the Fig. 6 as results of TUS (at initial scenario) and JRC (at decay power reduction of 20%). There is comparatively similar internal HF in the both cases. On other hand the internal and external HFs are also similar, because of the conditions of the both scenarios.

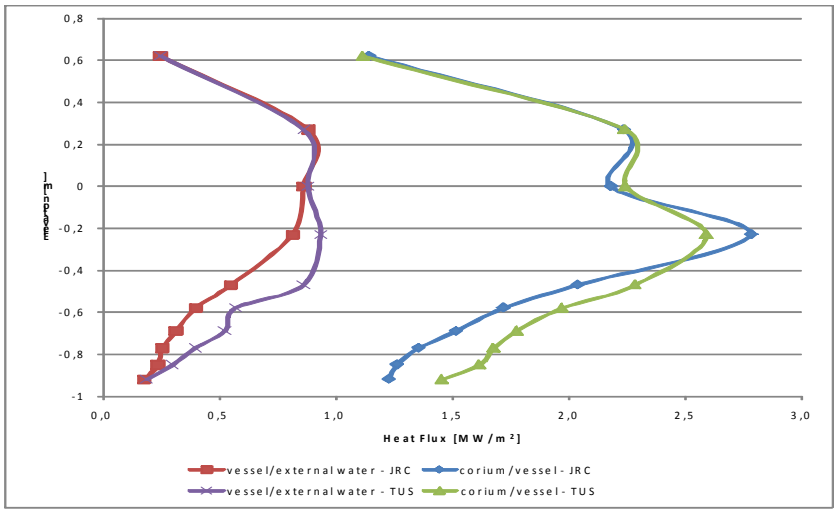

Fig.6 Comparison of the results of TUS (initial scenario) and JRC (decay power reduction of 20%)

3) Comparison of the results for power balance for calculations of TUS for initial scenario for 70 t steel and LOCA 200 mm

In the Fig.7 and Fig.8 are shown the power balance in lower plenum in the cases of initial scenario for 70 t steel and LOCA 200 mm. The heat loss in the interval 7000 s - 10000 s in the case of LOCA 200 mm is higher (Fig.7), in comparison to initial scenario (Fig.6) at same conditions of water cooling.

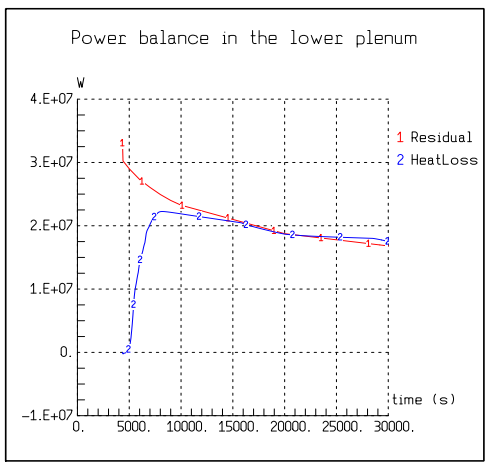

Fig.7 TUS – initial scenario (70 t steel), changed levels

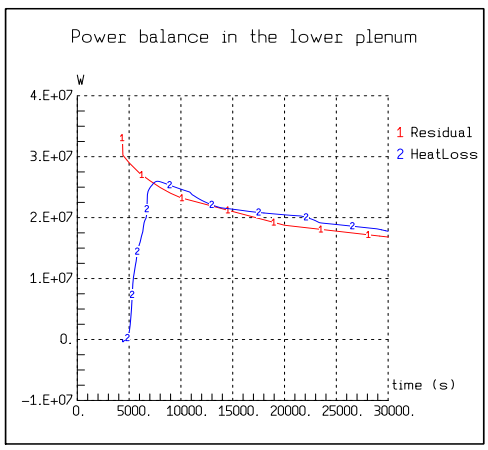

Fig.8 TUS – 70 t steel, LOCA 200 mm

Conclusion

There are presented results of TUS from calculations for initial scenario and for conditions of LOCA 200 mm in the case of VVER-1000, and there is analysed of the influence of the steel mass in the

melt to HF. In the conditions of LOCA 200 mm there are higher peaks of the external flux in comparison to initial scenario (Fig.6 and Fig.7).

The mass of the steel influences the internal HF distribution – the higher HF in the cases of 70 t and 110 t is at significant lower values in comparison of 30 t steel melt. In the case of LOCA 200 mm, the different steel mass influences weakly to the maximum of the external peaks, but influences over the value of the peaks.

A.6.2 Second report

With aim to analyze the phenomena "in-vessel melt retention", TUS implemented series of calculations with ASTEC. The calculations and obtained results for internal and external heat fluxes (HF) are taking into account:

- *The conditions of LOCA 200 mm;*
- *The influence of steel mass in the corium.*

In initial calculation, for the conditions of LOCA 200 mm, by ASTECv2.0R3p1 are obtained basic variables as temperatures of corium and fluids, the pressure in the vessel, etc. The implemented scenario was based on the input deck of *VVER 1000* in *ASTEC*.

TUS implemented 3 basic calculations: with 30 t, 70 t and 110 t steel in the melt pool at the follow conditions:

- The temperatures of corium and fluids, pressure in the vessel, etc., are for condition of LOCA 200 mm in the case of VVER-1000.
- The calculations start from 4340 s till 30 000 s, by the of LOCA 200 mm conditions.
- It was used the stand-alone input deck of VVER-1000 for the module ICARE.
- The levels of lower plenum are changed, in correspondence to VVER-1000 RPV bottom head drawing distributed from NRC (KI) between participants of the project.
- Other conditions for these calculations such as decay heat, material properties, etc., are in correspondence to scenario and tables of NRC KI in the document "Updated information of the corium history" sent from JRC to all participants.
- Obtained results by the ASTEC calculation are used as input data for calculation with ASTECv2.0 by the stand-alone input deck of VVER-1000, which was distributed to the participants of the project.

The main results of TUS calculations are presented as follow:

1) ***LOCA 200 mm at VVER-1000 – 30 t, 70 t and 110 t steel and HF profiles in the times of max/max***

In the case of 30 t steel around level 0 there are higher peaks of HF on the both surfaces - internal (corium/vessel) and external (vessel/flooding water), Fig.1.

In the cases of 70 t and 110 t of steel, the HF on the surface corium/vessel is producing in larger volume (-0.2 until 0.2 m) but with smaller values (than in the case of 30 t steel) in result of distribution of the same energy in bigger lower volume of corium. Therefore HFs for 70 and 110 t steel have smaller peaks in comparison to 30 t.

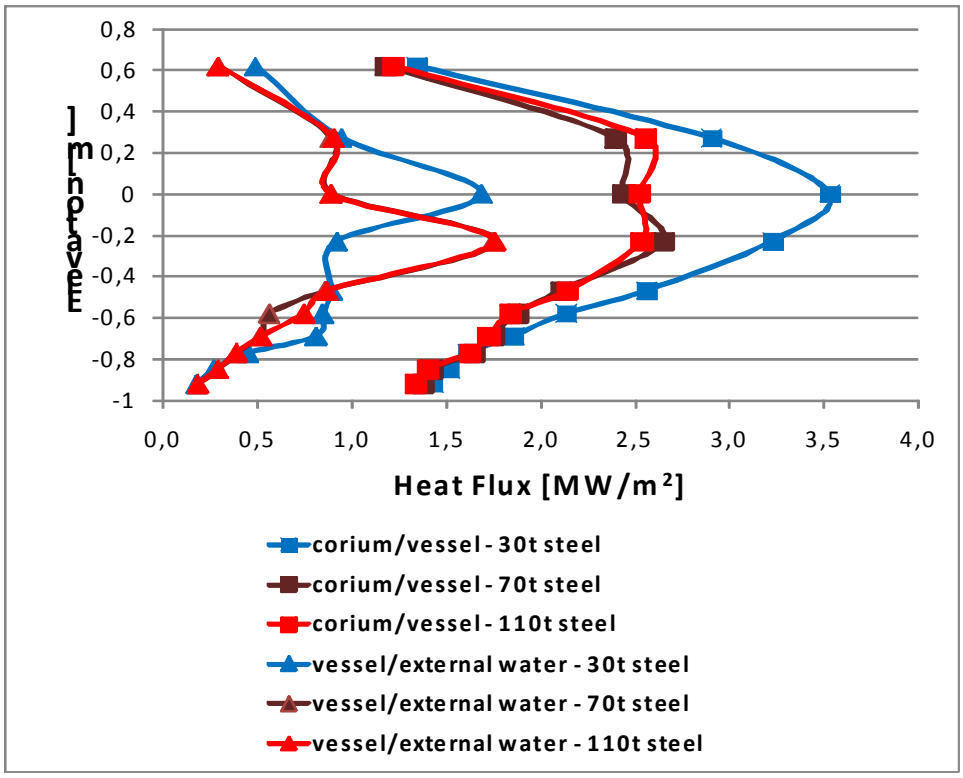

Fig.1 HF profiles for LOCA 200 mm – 30, 70 and 110 t steel

The HF on the external (vessel/water) for the cases 70 t and 110 t has the same value as for 30 t - but on level -0.2 m, not on the level 0 m. These results shown that the different steel masses influence weakly to the maximum of the external peaks and more over the level of the peaks. In the table 1 are presented the discrete values for HFs, used in Fig.1.

Table 1 Heat fluxes at LOCA 200 mm

	corium/vessel - 70t steel	*vessel/external water - 70t steel*	*corium/vessel - 30t steel*	*vessel/external water - 30t steel*	*corium/vessel - 110t steel*	*vessel/external water - 110t steel*
Elevation	MW/m2	MW/m2	MW/m2	MW/m2	MW/m2	MW/m2
-0,92	1,38	0,19	1,43	0,18	1,34	0,19
-0,85	1,42	0,29	1,52	0,27	1,40	0,30
-0,77	1,65	0,39	1,62	0,45	1,62	0,39
-0,69	1,75	0,52	1,86	0,81	1,72	0,52
-0,58	1,88	0,57	2,14	0,85	1,84	0,75
-0,47	2,11	0,86	2,56	0,89	2,14	0,87
-0,23	2,65	1,75	3,23	0,92	2,54	1,76
0	2,44	0,90	3,53	1,69	2,53	0,89
0,27	2,40	0,89	2,91	0,95	2,56	0,91
0,62	1,18	0,30	1,35	0,49	1,22	0,30

For the aims of investigation of IVMR TUS applied:

i. *Initial scenario for 70 steel without modelling of LOCA*

ii. *Stand-alone ID calculation with LOCA 200 and 30 t, 70 t and 110 t steel*

In comparison with the initial scenario (Fig.2) the results by the LOCA 200 mm conditions (Fig.3) by same conditions of water cooling shown higher heat loss in the interval 7000 s – 10 000 s. That confirms also the peak of the HF on the surface vessel/water at levels 0 and -0,23 in the cases of LOCA for 30 t, 70 t and 110 t steel (Fig.1).

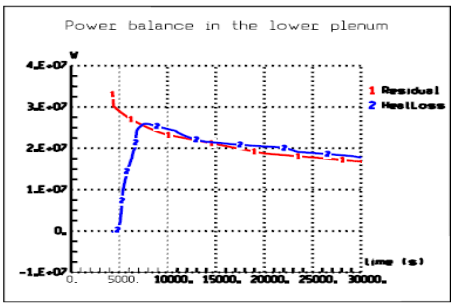

Fig.2 Power balance – 70 t steel (Initial scenario)

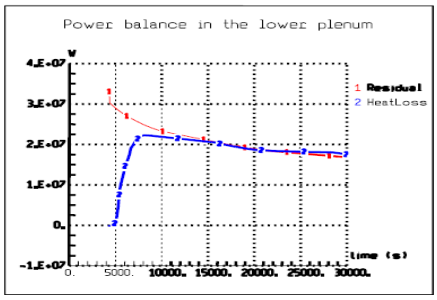

Fig.3 Power balance - 70 t steel (LOCA-200 mm)

2) Comparison of results of TUS with results of some other participants

2a) The comparison shown in the Fig.4 presents the results of TUS (at initial scenario at full decay power) and JRC (at decay power reduction of 20%). The internal and external HFs are similar, because of the near conditions of the both scenarios.

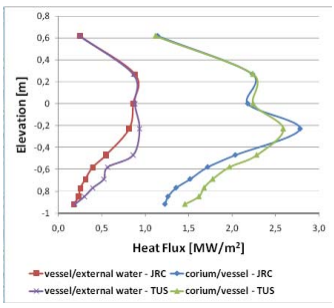

Fig.4 Comparison-TUS and JRC

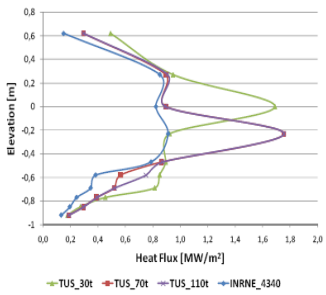

Fig.5 Comparison at full decay power

2b) Only TUS and INRNE *(in the second comparison preview delivered by JRC)* have results for full heat flux, but the TUS case is with LOCA 200 mm. This comparison (Fig.5) shown the influence of LOCA 200 mm.

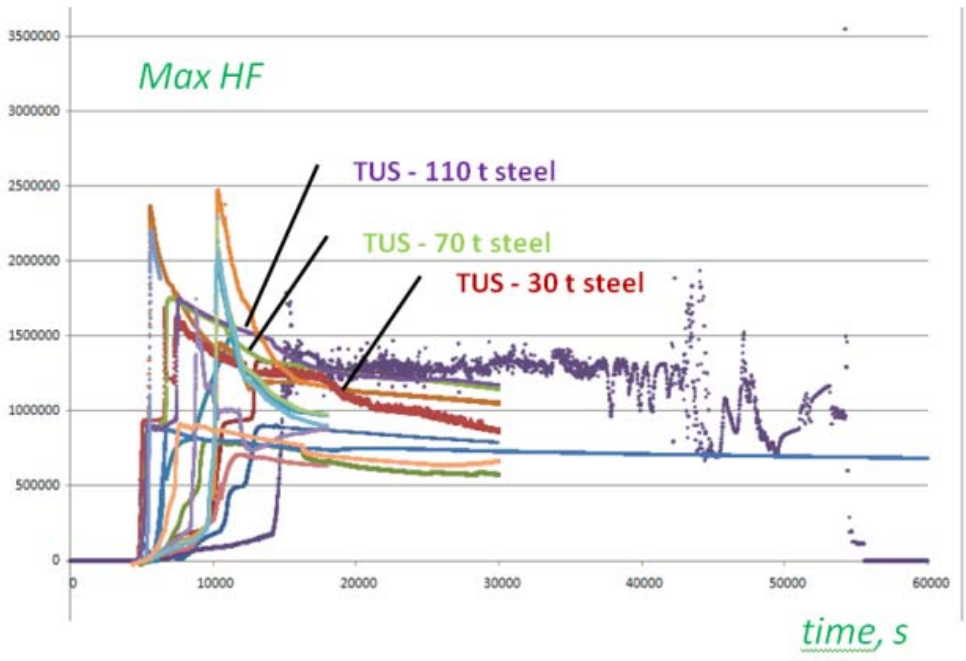

Fig.6 Comparison – all participants

2c) The calculations of TUS with different steel mass show that TUS' calculations for 70 t have similar time of Max HF, as all other organizations which have calculations only for 70 t (Fig.6).

Conclusions

For the conditions of LOCA 200 mm:

- In comparison to initial scenario there are higher peaks of the external flux in different levels (0 m for 30 t steel mass and -0.2 m for 70 and 110 t steel mass) of the 3 basic calculations, defined above;
- The mass of the steel influences the internal HF distribution – the higher HF in the cases of 70 t and 110 t is significant at lower levels (-0.2 m), in comparison to 30 t steel melt (0.0 m);
- The different steel mass influences weakly on the maximum of the external peaks, but significant on the level of the peaks.

A.7 VTT ASTEC stand-alone

A.7.1 Introduction

When a hypothetical severe accident proceeds into the late-phase of the in-vessel part, a large melt-pool may be formed to the bottom of a pressure vessel. This will impose the vessel wall under a massive thermal load. Flooding the cavity with water to submerge the vessel completely, or at least submerge the lower head, has proven to be effective in-vessel melt retention (IVMR) strategy in the Loviisa VVER-440 plant. However, it is uncertain if this method can be applied to larger reactors firstly due to higher decay heat levels and secondly due greater melt masses. The analyses presented in this report related to VVER-1000 IVMR were performed as ICARE stand-alone calculations with ASTEC V2.0rev3p2 (Chatelard et al., 2009).

A.7.2 The basic principles of modelling

As starting point was used the reference input prepared by IRSN especially for this benchmark. The most important modifications made to the input related to the definition of the decay heat and to the definition of melt pool configuration initial state. The initial compositions of the layers were defined based on chemical equilibrium states produced by ChemSheet (Hack et al., 1999). In the reference input the starting point was a homogeneous mixture of corium compounds: 85.9 t of UO_2, 15.6 t of Zr, 17.1 t of ZrO_2 and 69.84 t of steel. Once the initial melt composition was set-up, ASTEC was in charge of calculating the phase separation together with chemical interactions in the melt pool.

Table 6. Predefined composition of the layers at T = 2 831 K.

Compound	**Oxide layer** M_{tot} = 92 322.44 kg ρ = 7 508.7 kg/m³ m/M_{TOT}	**Metal layer** M_{tot} = 96 118.56 kg ρ= 6 944.3 kg/m³ m/M_{TOT}
Cr	0.002520639	0.12834823
Cr_2O_3	2.53182E-05	2.64E-06
Fe	0.000657742	0.522147292
FeO	0.000411311	8.21913E-05
Fe_2O_3	5.61538E-06	1.41327E-07
Ni	0.000815431	0.071876765
NiO	2.91313E-07	6.64662E-08
UO_2	0.676861076	0.009190091
ZrO_2	0.283919853	0.011714644
U	0.024679392	0.182890955
Zr	0.010103104	0.07374698

In *Table 6* is presented the composition produced by ChemSheet thermochemical equilibrium calculation. The equilibrium was calculated in the smallest possible temperature when there was no solid phase present, i.e. in the liquidus temperature. In this case the temperature was 2 831 K and it was used also as the initial temperature of the layers. Despite predefinition of phase

separation, detailed separation model was activated (SEPA_ACT = 1) to achieve wanted behaviour for melting steel from vessel wall. It can be assumed, that this additional steel migrates mostly to metal phase.

The decay heat level was assumed to be reduced by 20 % due to gaseous fission product release in the early-phase. In the reference input deck the decay heat was given in W_{th}/kg_{UO2} (STRU POWE TYPE MASS) and it was indicated that UO_2 is producing the decay heat (MATE UO2). However, part of the UO_2 in the melt pool is reduced to metallic uranium in the presence of metallic zirconium. When this chemical reaction has occurred, the level of decay heat defined as described is smaller than it should be since there is less UO_2. But in reality, the fission products producing the decay heat are still present in the oxidic layer

In the analyses presented in this paper, the decay heat is defined in W_{th} (STRU POWE TYPE TOTAL). Also in this case has to be selected the material that is so called producing the decay heat. But now the material can be selected so that the division between metal and oxide layer is within correct limits. In this case the Cr_2O_3 was defined to produce the decay heat (MATE CR2O3). In (Seiler et al., 2007a) is mentioned that typically 5-10 % of the decay heat is produced in the metal layer. In all analysed cases the amount of Cr_2O_3 in metal layer was fixed so, that 9.5-9.9 % of it remained in metal layer. Typically this meant 15-150 g reduction or addition of Cr_2O_3 to the metal phase. This was assumed to have no effect to thermochemical equilibrium since the masses of metal layers were 55-110 tons.

A.7.3 The results

The results are presented as heat fluxes from the melt pool to the vessel wall and from vessel wall to the external coolant. In calculating the heat flux for each level is taken into account he convective power exchanged on the faces (PCON) and the other powers exchanged on faces (POWE). The sum represents the total power and dividing it by the area of the face (S) the result is the heat flux. All values are given both for internal and external face of each lower plenum mesh levels.

A.7.3.1 The base case with comparison to modified lower plenum nodalization

ASTEC separates the lower plenum volume from the vessel part cylindrical volume. If the melt pool volume exceeds 90 % of the lower plenum volume, ASTEC calculates a corrective factor that is applied on volumes of the core melt layers. This affects height of the pool and then vessel wall area that is affected by the intensive heat load.

In a case when calculation begins with a melt pool on the lower plenum, the size of the lower plenum should be adjusted so that the corrective factor is as close 1 as possible on the first time step to achieve realistic results. This is because ASTEC assumes that the melting vessel wall increases the volume of melt pool and the code does not take into account that the initial lower plenum volume is actually increased by the same value as vessel wall is melted. Since the volume of molten steel is approximately the same as for solid steel, the top surface of the pool can assumed to be on the same level all the time.

In *Figure 1-1* is presented the difference between (a) lower plenum nodalization in the reference input deck and (b) modified lower plenum nodalization where the size is adjusted as described above.

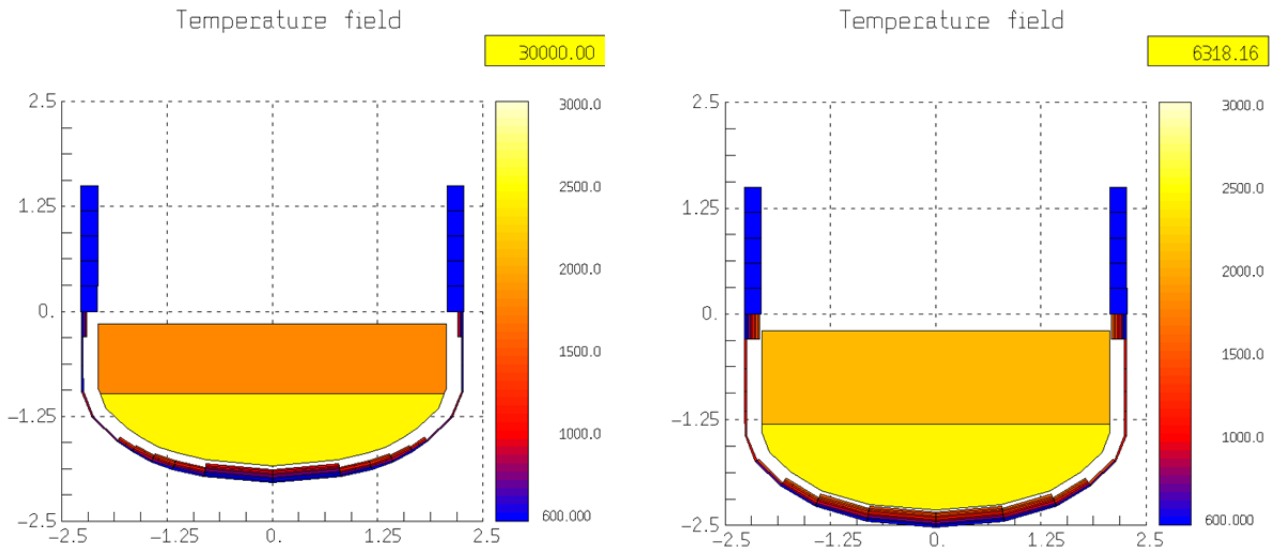

(a) (b)

Figure 1-1. (a) Lower plenum nodalization in reference input and (b) in modified lower plenum case.

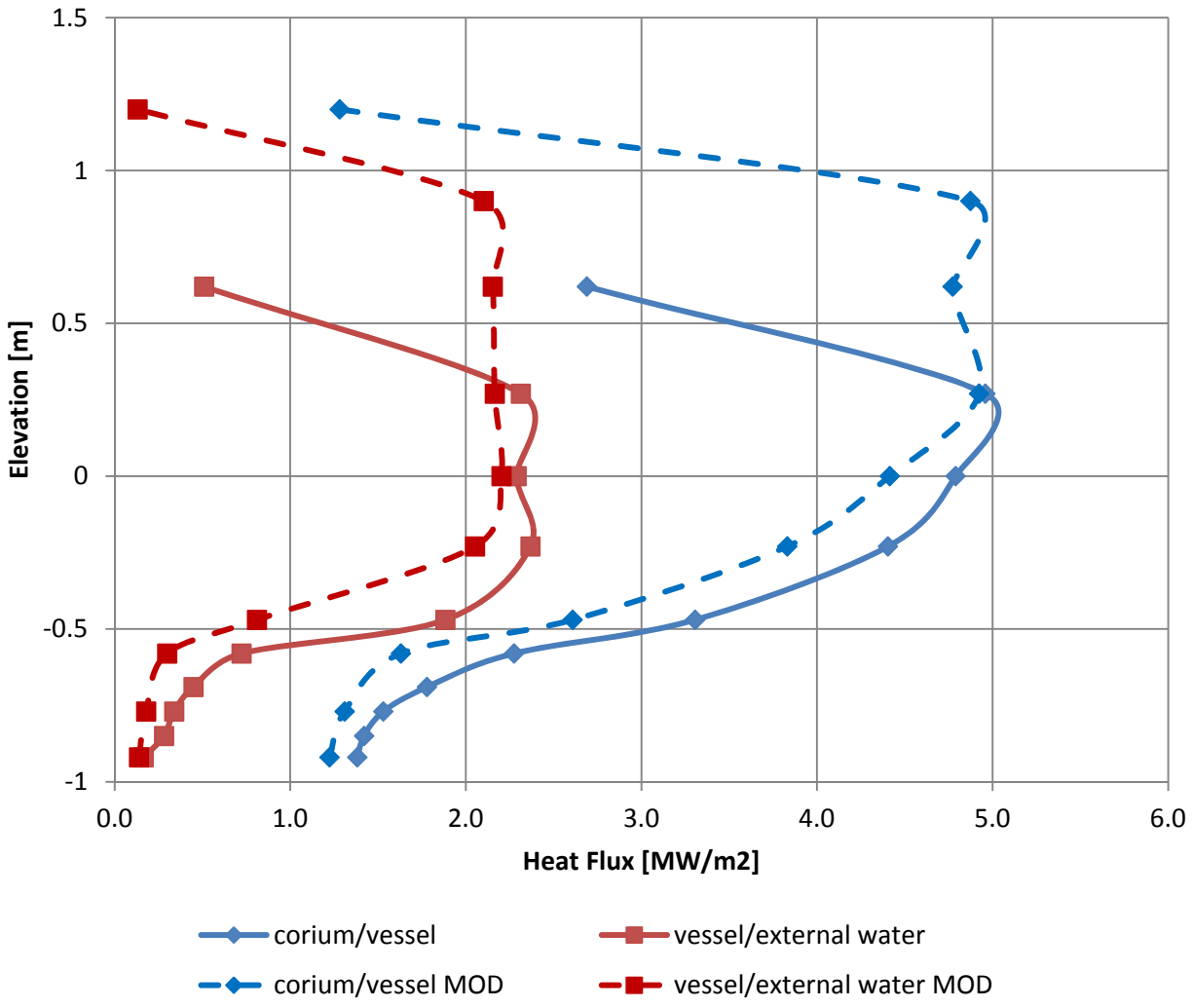

Figure 1-2. Maximum heat fluxes inside and outside the vessel with reference lower plenum nodalization and with modified nodalization (MOD).

The maximum heat fluxes for each mesh level are presented in *Figure 1-2* for both lower plenum nodalizations. As expected, heat flux is spread higher in the case of modified nodalization.

Surprising though was that the vessel did fail because plastic failure criterion was reached in the case of modified nodalization but not in the case of reference nodalization.

This is assumed to be because the vessel wall area next to melt pool is bigger and then more steel is melted to increase the weight of the pool effecting mechanic stress. Notable also is that the maximum heat fluxes are smaller in the case of modified nodalization. This probably results from early failure of the vessel after which the calculation ended and the heat fluxes did not yet reach their maximum values.

A.7.3.2 Results on sensitivity studies

The core melt in the lower plenum will form a chemical system that drives towards equilibrium. The system is affected by its thermal conditions as well as by chemical processes. When defining if three-layer pool configuration is possible to be formed the most important parameters are firstly the level of zirconium oxidation and secondly the amount of steel present in the system. Basically the smaller the level of zirconium oxidation is the more uranium will be reduced and then the density of metal phase will be higher. Then it is more probable that the metal phase will stratify below the oxide phase and additional light metal layer could be formed on top of oxide phase.

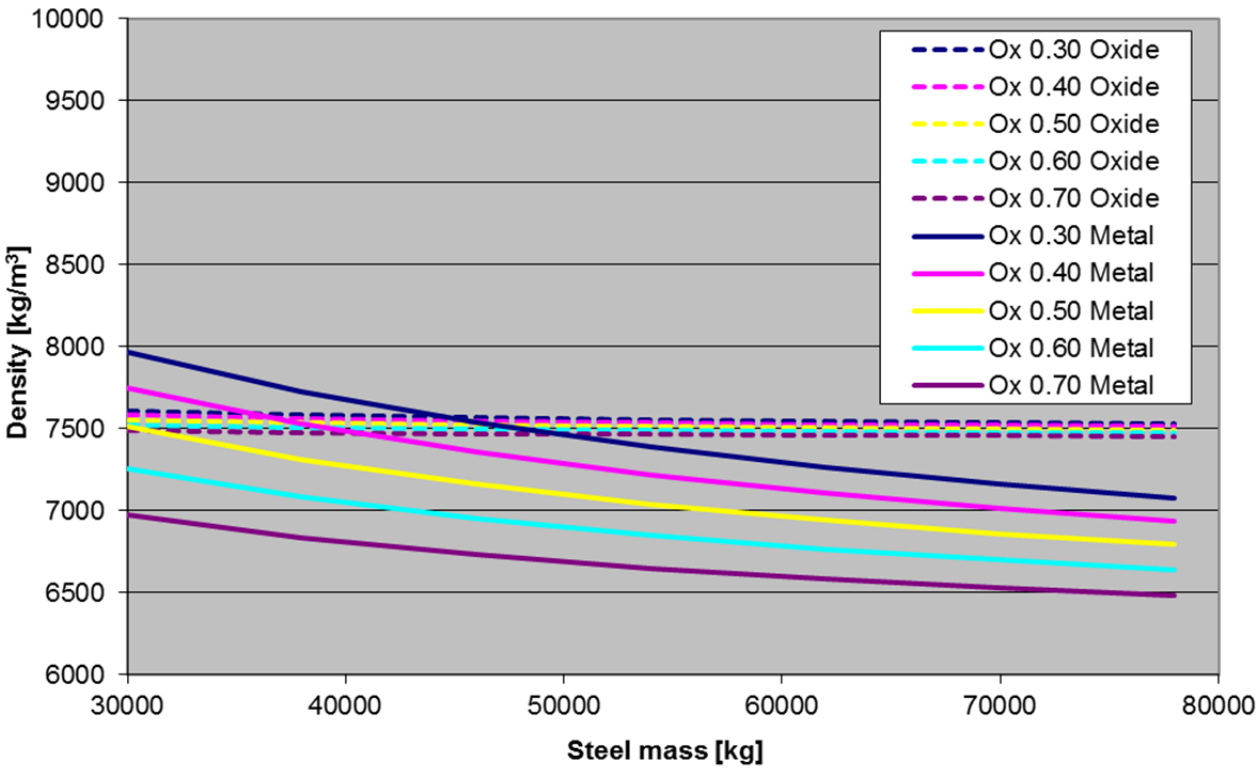

Figure 1-3. The results of the thermodynamical equilibrium calculations with ChemSheet.

The effect of these parameters, i.e. oxidation fraction and steel amount, to possible pool configurations can easily be analysed by a method used also by Seiler et al., (2007b). There is given for a fixed uranium dioxide (UO_2) and zirconium (Zr) masses different values for the zirconium oxidation level and steel amount. After calculating the thermodynamical equilibriums for different cases, the densities of the metal and oxide phases are plotted as a function of steel amount. This will result a set of trend curves for the densities of metal and oxide phases.

This method was utilized for analysing the melt pool behaviour of VVER-1000 reference reactor and the result can be seen in *Figure 1-3*. The initial UO_2 amount was 85 900 kg and Zr amount 28 260 kg. The thermodynamical equilibriums were defined for five different Zr oxidation levels (30 %, 40 %, 50 %, 60 % and 70 %) for which each was given seven different masses of steel (30

000 kg, 38 000 kg, 46 000 kg, 54 000 kg, 62 000 kg, 70 000 kg and 78 000 kg). All in all 35 different cases were analysed.

From *Figure 1-3* can be seen that within given limits (30-80 tons of steel and ZrO_2 fraction 30-70 %) three-layer pool configurations are highly improbable. They are theoretically possible only with zirconium oxidation fractions below 40 %. With 40 % ZrO_2 fraction the mass of steel in the system need to be below 36 500 kg and with 30 % ZrO_2 fraction below 44 500 kg.

A.7.3.2.1 The steel effect

The effect of steel mass in the melt pool to the heat fluxes was analysed with selecting four cases with steel masses of 30 t, 46 t, 62 t and 78 t and with fixed ZrO_2 fraction of 40 %. The compositions resulted by ChemSheet thermochemical equilibrium calculations for these cases can be seen in Table 7 together with corresponding phase densities and mixture liquidus temperatures. These values were directly used in ASTEC inputs as initial state values. The maximum heat fluxes produced in these four analysed cases can be compared in *Figure 1-4*.

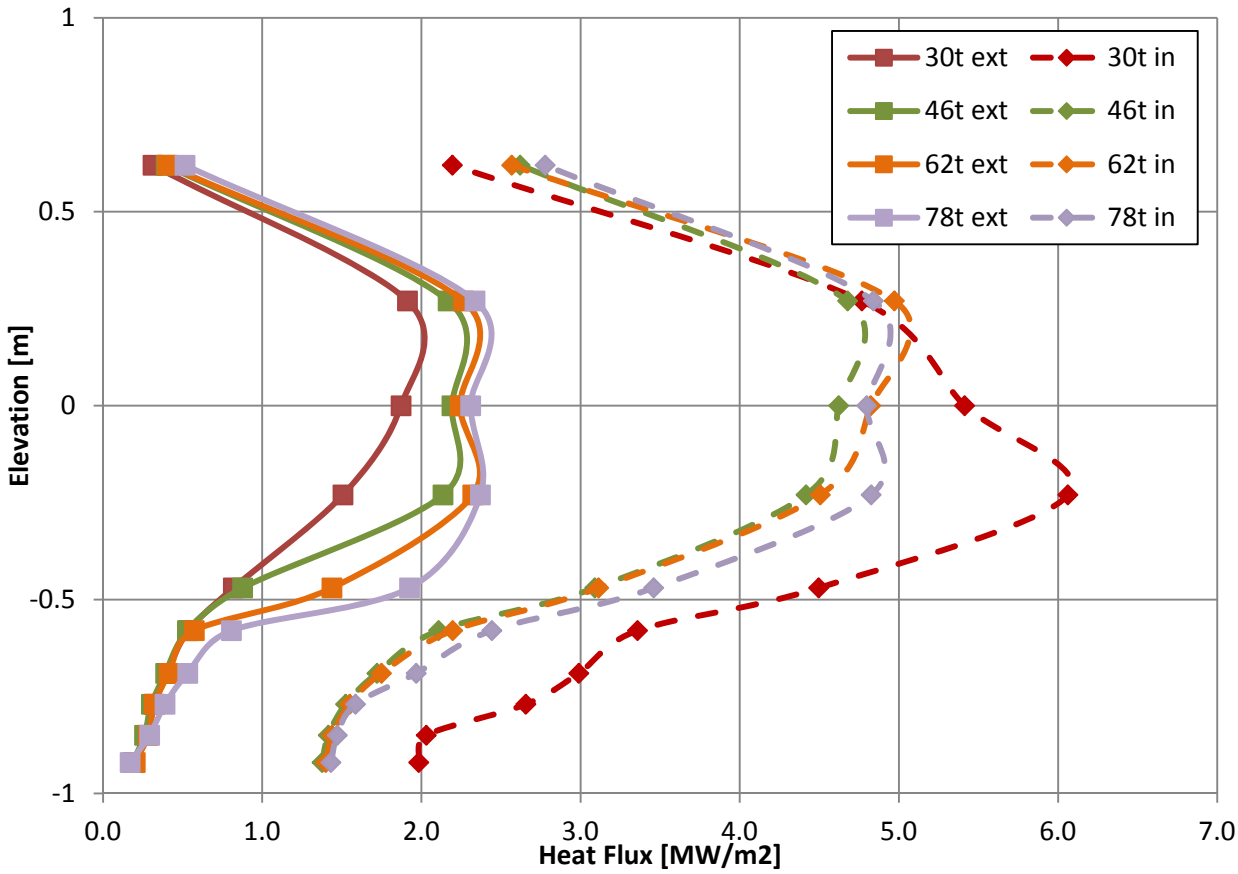

Figure 1-4. Maximum heat fluxes from the melt to the vessel wall (in) and from vessel wall to external coolant (ext). Fixed ZrO_2 fraction of 40 % and four different initial steel amounts: 30 t, 46 t, 62 t and 78t.

Table 7. Initial composition of the layers for analysing the effect of steel amount.

	30 t of steel, T = 2 814 K		**46 t of steel, T = 2 824 K**	
Compound	**Oxide layer** M_{tot} = 93 411.76 kg ρ = 7 581.3 kg/m³ m/M_{TOT}	**Metal layer** M_{tot} = 54 713.54 kg ρ= 7 749.7 kg/m³ m/M_{TOT}	**Oxide layer** M_{tot} = 91 340.84 kg ρ = 7 545.0 kg/m³ m/M_{TOT}	**Metal layer** M_{tot} = 72 784.43kg ρ= 7 356.6 kg/m³ m/M_{TOT}
Cr	0.002547977	0.094334423	0.002542364	0.110556067
Cr_2O_3	8.99752E-06	1.63105E-06	1.4677E-05	2.0224E-06
Fe	0.000692035	0.393354611	0.000676463	0.453900418
FeO	0.000167698	2.9498E-05	0.000259115	4.84868E-05
Fe_2O_3	1.54934E-06	3.83026E-08	2.88105E-06	7.16832E-08
Ni	0.000623896	0.053765747	0.000712251	0.062306318
NiO	7.97201E-08	1.57497E-08	1.49984E-07	3.18196E-08
UO_2	0.6531813	0.009839531	0.665446148	0.009533454
ZrO_2	0.275438451	0.011591863	0.279643163	0.011627247
U	0.045975592	0.313761888	0.035269726	0.251535659
Zr	0.021362317	0.123320752	0.015432907	0.100490223
	62 t of steel, T = 2 829 K		**78 t of steel, T = 2 832 K**	
Compound	**Oxide layer** M_{tot} = 89 999.50 kg ρ = 7 525.0 kg/m³ m/M_{TOT}	**Metal layer** M_{tot} = 90 125.71 kg ρ= 7 109.0 kg/m³ m/M_{TOT}	**Oxide layer** M_{tot} = 88 990.88 kg ρ = 7 512.5 kg/m³ m/M_{TOT}	**Metal layer** M_{tot} = 107 134.24 kg ρ= 6 937.5 kg/m³ m/M_{TOT}
Cr	0.002533416	0.121281336	0.002526233	0.128934925
Cr_2O_3	2.02843E-05	2.22424E-06	2.57452E-05	2.3512E-06
Fe	0.000664657	0.494324377	0.000655777	0.523320231
FeO	0.000341764	6.65169E-05	0.000416634	8.33066E-05
Fe_2O_3	4.29503E-06	1.07463E-07	5.72747E-06	1.43895E-07
Ni	0.000773606	0.068020064	0.000818738	0.072125523
NiO	2.23739E-07	4.96144E-08	2.96842E-07	6.78293E-08
UO_2	0.67301944	0.00934975	0.67827327	0.009229227
ZrO_2	0.281752403	0.01165988	0.282922319	0.011684647
U	0.028793125	0.210738264	0.024401815	0.181736556
Zr	0.012096591	0.084557428	0.009953215	0.072883019

As is visualized in *Figure 1-3* and mentioned also in Table 7, in the case of 40 % zirconium oxidation fraction and 30 tons of steel the density of metal layer is higher than the density of oxide layer in the thermochemical equilibrium state. In this calculation, the layer arrangement was set to match this equilibrium state, i.e. the metal layer was defined to be stratified below oxide layer and also third layer was allowed to be created on top of the oxide layer.

However, since detailed separation model was activated, the melting steel from the vessel wall migrated mostly to metal phase. This resulted that the density of metal phase decreased and it did ascended on top of the oxide phase after a while. *Figure 1-4* demonstrates that in the case when this additional phase stratification occurred, the peak of the heat flux from the melt pool to the vessel wall is notably larger than it probably otherwise would be.

A.7.3.2.2 ZrO_2 fraction effect

The effect of zirconium oxidation fraction to the heat fluxes was analysed with selecting four cases with different ZrO_2 fractions (30 %, 40 %, 50 % and 60 %) and with fixed 38 ton initial steel mass in the pool. In *Table 8* is presented the compositions of the layers in thermochemical equilibrium for the four cases together with other relevant information needed in the ASTEC inputs. The effect of ZrO_2 fraction to maximum heat fluxes inside and outside the vessel is illustrated in *Figure 1-5*.

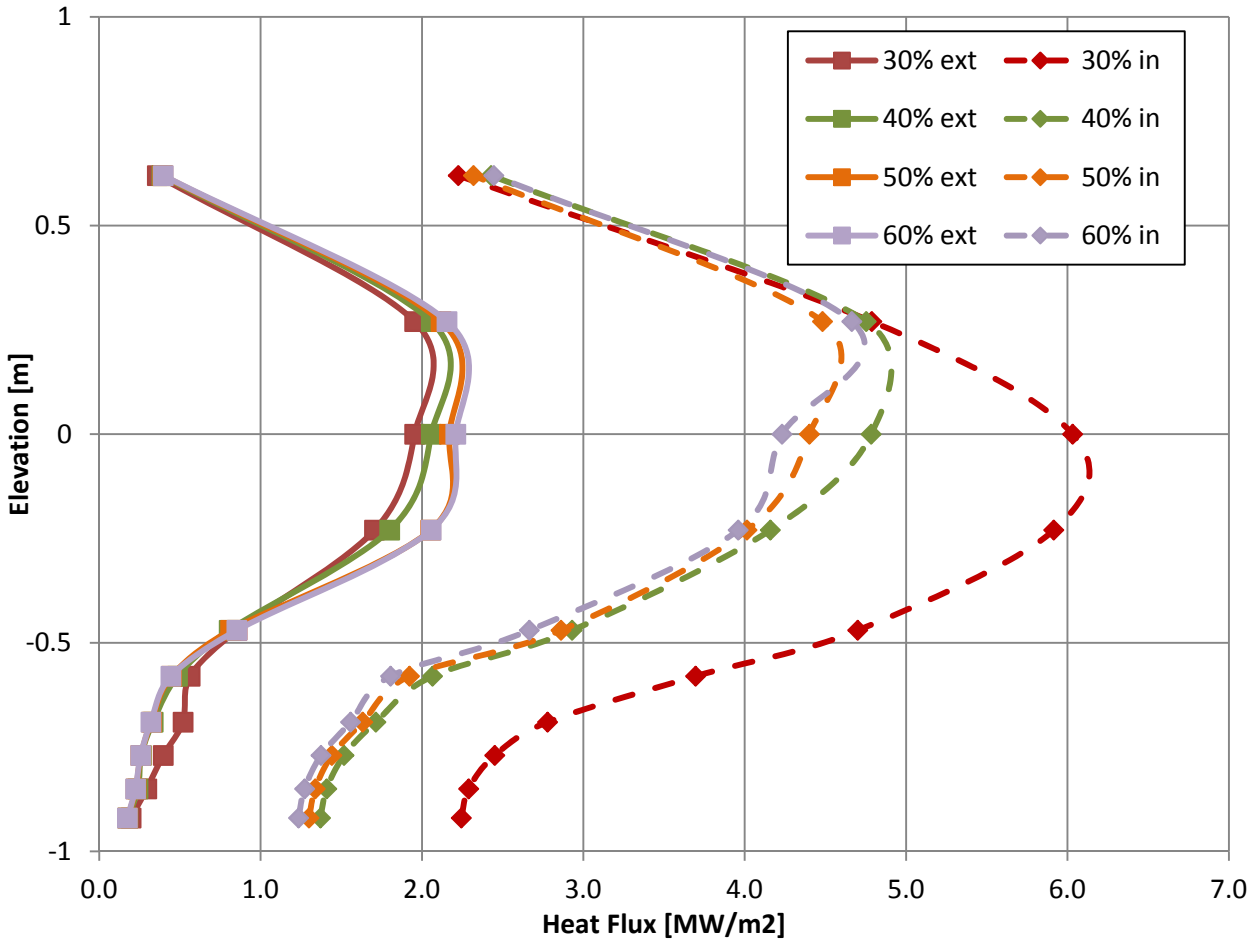

Figure 1-5. Maximum heat fluxes from the melt to the vessel wall (in) and from vessel wall to external coolant (ext). Fixed initial steel amount of 38 tons and four different ZrO_2 fractions: 30 %, 40 %, 50 % and 60 %.

Also in this analysis one of the cases produced initially inverse stratification for metal and oxide phases. With zirconium oxidation fraction of 30 % and 38 ton steel amount, the density of metal

phase in thermodynamical equilibrium is bigger than the density of oxide phase. Also in this case the metal phase restratified on top of the oxide phase and similar behaviour of the heat flux was observed as in analysing the steel effect.

Table 8. Initial composition of the layers for analysing the effect of ZrO_2 fraction.

	ZrO_2 fraction 30 %, T = 2 815 K		**ZrO_2 fraction 40 %, T = 2 819 K**	
Compound	**Oxide layer** M_{tot} = 86 359.31 kg ρ = 7 585.0 kg/m³ m/M_{TOT}	**Metal layer** M_{tot} = 68 774.65 kg ρ= 7 725.8 kg/m³ m/M_{TOT}	**Oxide layer** M_{tot} = 92 238.94 kg ρ = 7 560.1 kg/m³ m/M_{TOT}	**Metal layer** M_{tot} = 63 886.34 kg ρ= 7 527.6 kg/m³ m/M_{TOT}
Cr	0.00257098	0.09621796	0.002546559	0.103375637
Cr_2O_3	9.43134E-06	1.24175E-06	1.18365E-05	1.82782E-06
Fe	0.000688113	0.396762253	0.000683791	0.426999936
FeO	0.000173635	3.05864E-05	0.000214499	3.90644E-05
Fe_2O_3	1.63115E-06	4.01416E-08	2.1982E-06	5.4515E-08
Ni	0.000631782	0.054459504	0.000672476	0.058509564
NiO	8.41364E-08	1.66994E-08	0.660155063	2.34452E-08
UO_2	0.65579559	0.00991338	0.27794119	0.009664791
ZrO_2	0.274254207	0.011566805	0.039857631	0.011608884
U	0.04507469	0.309769115	0.017914512	0.278992238
Zr	0.020799744	0.121279097	0.002546559	0.110807977
	ZrO_2 fraction 50 %, T = 2 823 K		**ZrO_2 fraction 60 %, T = 2 827 K**	
Compound	**Oxide layer** M_{tot} = 97 951.61 kg ρ = 7 533.9 kg/m³ m/M_{TOT}	**Metal layer** M_{tot} = 59 165.02 kg ρ= 7 313.9 kg/m³ m/M_{TOT}	**Oxide layer** M_{tot} = 103 492.24 kg ρ = 7 506.2 kg/m³ m/M_{TOT}	**Metal layer** M_{tot} = 54 615.74 kg ρ= 7 083.6 kg/m³ m/M_{TOT}
Cr	0.002520252	0.111417734	0.002492959	0.120486453
Cr_2O_3	1.52221E-05	2.77471E-06	2.02596E-05	4.14823E-06
Fe	0.000678052	0.460923454	0.000670808	0.499116527
FeO	0.000269132	5.082E-05	0.000345147	6.77563E-05
Fe_2O_3	3.03537E-06	7.59846E-08	4.33611E-06	1.09709E-07
Ni	0.000718997	0.063036564	0.000772528	0.068112766
NiO	1.5795E-07	3.3754E-08	2.25463E-07	5.01734E-08
UO_2	0.664517452	0.009400121	0.668934571	0.009118589
ZrO_2	0.281880522	0.011672886	0.286055496	0.011759389
U	0.034388367	0.24482096	0.028618661	0.206793295
Zr	0.015008655	0.098674575	0.012084817	0.084540914

A.7.4 Conclusions

To achieve as realistic results as possible with ASTEC calculation beginning with a melt pool on the lower plenum the size of the lower plenum is suggested to be adjusted to the melt volume so that the corrective factor is as close 1 as possible on the first time step. However, the sensitivity analyses presented in this report were performed without this step. The adjusted lower plenum seems to result more probably vessel failure when the maximum heat fluxes may not be caught.

Within given limits for ZrO_2 fraction and initial steel mass it seems to be highly improbable a three-layer pool configuration to be formed. This hypothesis is actually reinforced when taking into account that steel melting from the vessel wall migrates mostly to metal phase reducing its density. In the cases where metal phase was supposed to be initially stratified below oxide phase according to thermochemical equilibrium state was observed a restratification. These cases produced the highest heat fluxes from the pool to the vessel wall. This indicates the importance of analyses of transient conditions.

The effect of zirconium oxidation fraction and initial steel fraction to the maximum heat fluxes outside the vessel was straightforward at the level of metal layer: the higher the steel mass is the higher is also the heat flux. This is a result from high thermal conductivity of steel since heat transfer occurs at a higher rate across materials of higher thermal conductivity. And also, the higher the ZrO_2 fraction is the higher are the heat flux maximums. This is probably a result from the metallic uranium content that effects to the mass of metal layer and then to heat transfer area. The higher is the ZrO_2 fraction the less metallic uranium there will be and the thinner the metal layer becomes. The behaviour of maximum heat fluxes inside the vessel is not that consistent. This is assumed to be because the transient effect is more intensive inside the vessel.

A.7.5 Some references

Chatelard, P., Chikhi, N., Cloarec, L., Coindreau, O., Drai, P., Fichot, F., Ghosh, B. & Guillard G. 2009. ASTEC V2 code ICARE physical modelling. IRSN Institut de radioprotection et de sûreté nucléaire, Direction de la prevention des accidents majeurs. 668 p. SEMCA-2009-148.

Hack, K., Petersen, S., Koukkari, P. & Penttilä, K. 1999. CHEMSHEET an Efficient Worksheet Tool for Thermodynamic Process Simulation. Microstructures, Mechanical Properties and Processes, Bréchet Y., Wiley (Ed.), EUROMAT, Vol. 3, pp 323-330.

Seiler, J.M., Fichot, F., Barrachin, M., Tourniaire, B., Defoort, F. & Journeau, C. 2007a. A cea irsa synthesis on the main lessons from MASCA programme and related reactor applications. OECD/CSNI MASCA 2 seminar, Cadarache, France, 11th-12th October.

Seiler, J.M., Tourniaire, B., Defoort, F. & Froment, K. 2007b. Consequences of material effects on in-vessel retention. Nuclear Engineering and Design 237, pp 1752-1758.

A.8 UJV MELCOR 1.8.6

A.8.1 Introduction

The UJV Rez contributed to the benchmark on IVMR strategy for the VVER-1000/320 with the integral calculation using the MELCOR code. The term “integral calculation” means that the analysis of the plant response on the events and actions is performed using the one complex input model, which describes the whole unit - core, RPV, primary and secondary circuits, containment, and systems they are used during the accident progression and mitigation – like RCS depressurization, hydrogen recombination, cavity reflooding and consequent water supply to cavity, hydroacumulators, but also reactor protection systems. Description of the input models is included in the chapter 1, chapter 2 summarizes performed calculations, and chapter 3 describes main results of selected calculations.

A.8.2 Input model description

As mentioned in the Introduction, the analyses were performed with the integral model, which is described in this chapter using some logical parts – RPV plus core, primary and secondary circuits, containment with specific attention to cavity modelling, and other parts.

A.8.2.1 RPV and core models

Model of the RPV and core is shown at Figure 1, where the left figure shows subdivision of the RPV into thermal-hydraulics nodes (called in the MELCOR as Control Volumes – CV) with red borders and definition in the COR package, which solves behaviour of intact and degraded core including behaviour of corium in lower plenum. Nodalization in COR package is visualized by blue lines at left figure which is relevant for the first set of analyses (later in this document named as LOCA_v03 for example), but for the second set the center and right figures are relevant, as their difference is mainly in the simplification of modelling of core bypass, which is at left figure indicated as CV031, but this is not present at right and center ones as it was merged with CV030. Analyses with identification of differences in core degradation prediction confirmed that such simplification is acceptable and it does not influence results in non-acceptable manner.

Model of the COR package is shown at center and right figure of Figure 1, and these two differ in visualized components – center one visualizes fuel pallets (UO_2 – brown, FU component), cladding and spacer grids (Zr alloy – green, CL component), upper and lower fuel assembly nozzles (stainless steel – blue, SS component – this is mean supporting structure), structures in lower plenum – core support plate, columns, and lower head of core barrel (stainless steel – blue, SS component), lower head of RPV modelled in the COR package (carbon steel – grey, Segments of lower head), and CVs of different colors of background. The right figure visualize modelling of control rods using component non-supporting structure (NS), which consists of absorbtion material (boron carbide, light red color), stainless steel cladding (grey color), and stainless steel top nozzle of clusters (blue). Background colors are identical as they represent identical CVs.

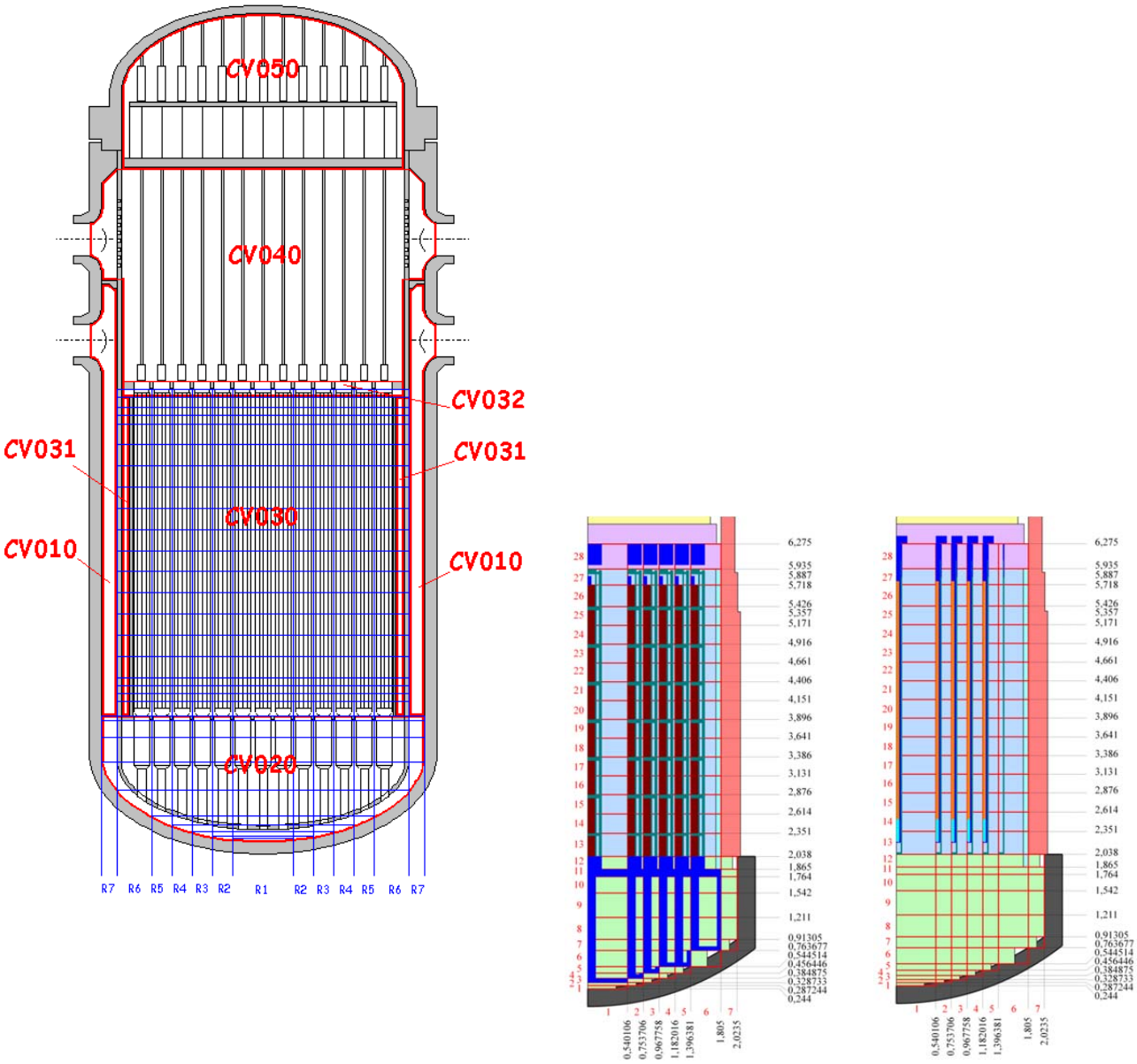

Figure 1 Nodalization of RPV and core – CVs and COR nodalization for MELCOR 1.8.6

A.8.2.2 Primary and secondary circuit models

Model of primary and secondary circuits is based on basic assumption of number of modelled loops – loop no. 1 (see Figure 2 - left) is modelled as independent, loops no. 2 and 3 are merged into double model loop, and loop no. 4 with connection to pressurizer via surge line is modelled as independent.

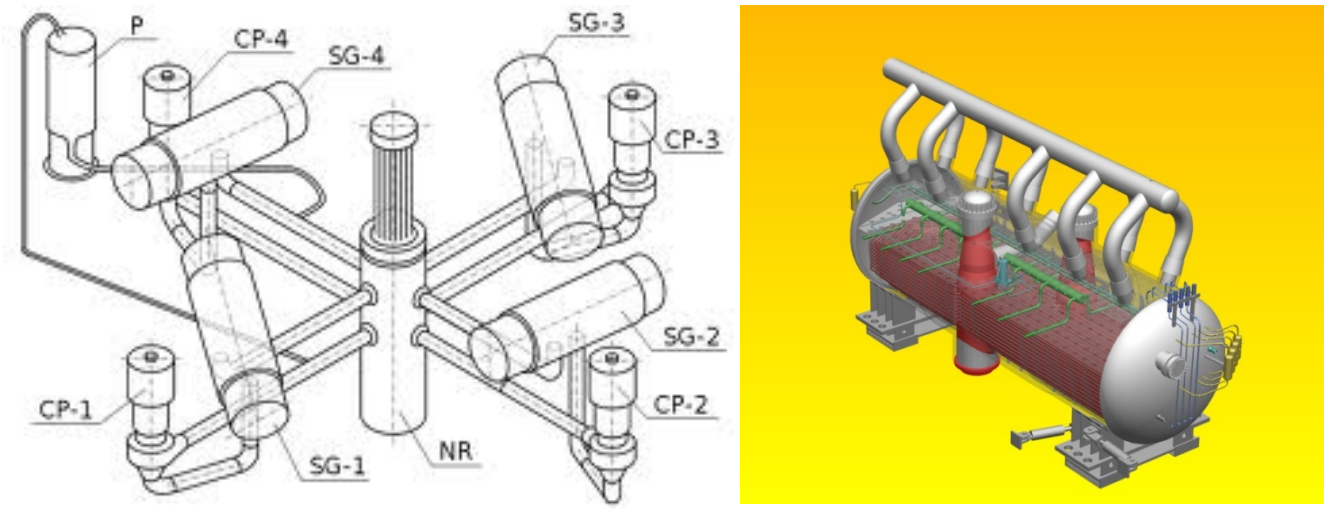

Figure 2 Overview of primary circuit loops of the VVER-1000/320 (generally numbering can be different unit by unit, this numbering is representative for unit 1 of Temelín NPP, for example) and detail of horizontal steam generator

Nodalization of primary circuit loops are identical, Figure 3 shows model loop no.4 with connection to pressurizer and its nodalization plus buble tank. Numbering of CVs, FLs and HSs is in basic format concerning numbers of modelling loops, so number n has to be substituted with 1 for loop no.1, 2 for merged loops no. 2 and 3, and 4 for loop no.4. Figure 3 has also part of secondary side of steam generator, but its components are in red color. The same colors are used also on Fig. 4, where nodalization of secondary circuit is shown.

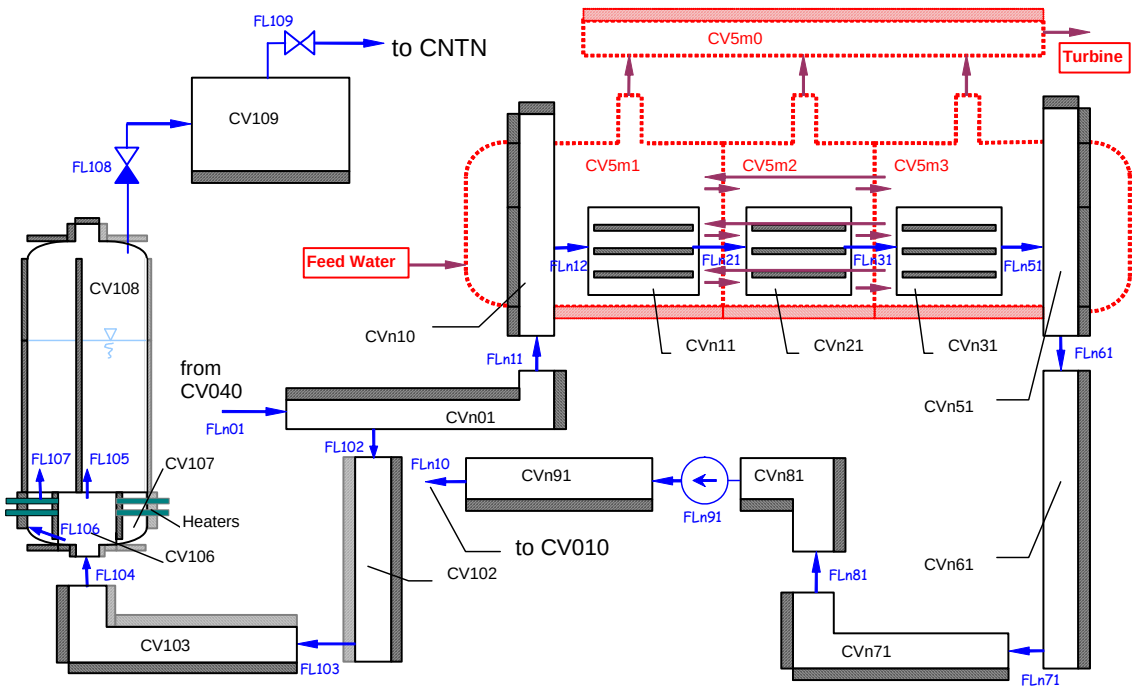

Figure 3 Nodalization of primary circuit loop of the VVER-1000/320

(black – CV and HS of primary circuit, blue – FL of primary circuit, red – CV and HS of secondary circuit, and bordeaux – FL of secondary circuit)

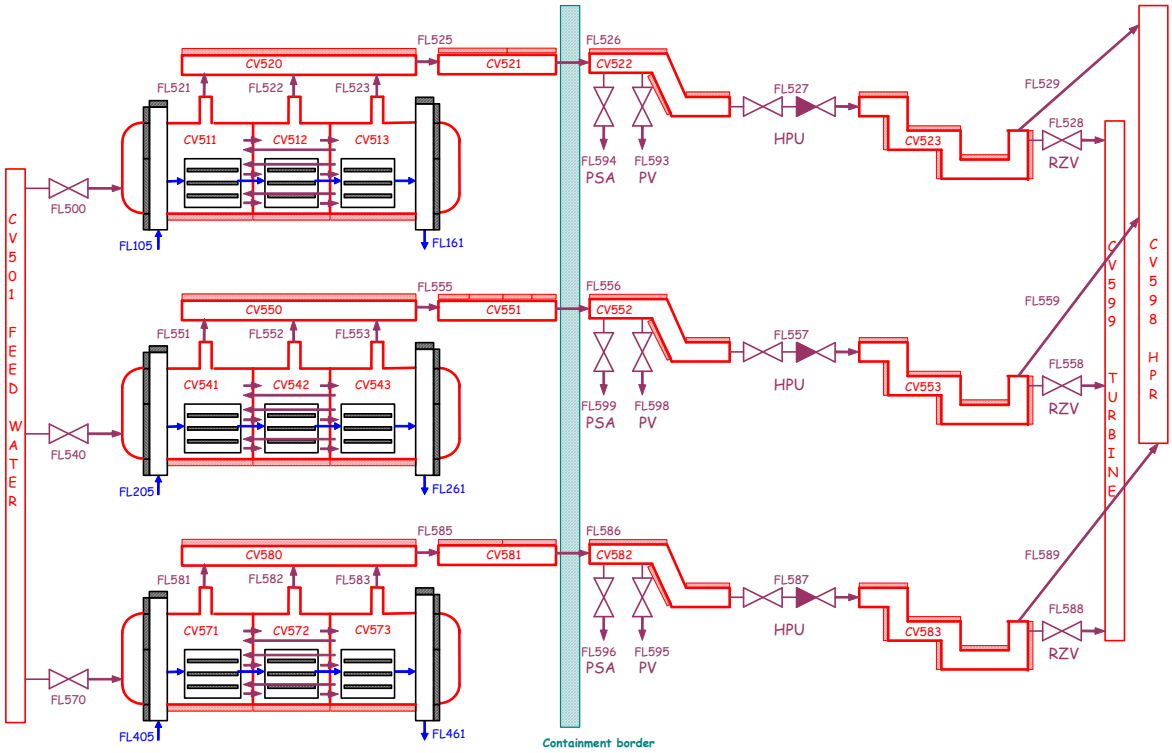

Figure 4 Nodalization of secondary circuit loops of the VVER-1000/320

(black – CV and HS of primary circuit, blue – FL of primary circuit, red – CV and HS of secondary circuit, and bordeaux – FL of secondary circuit)

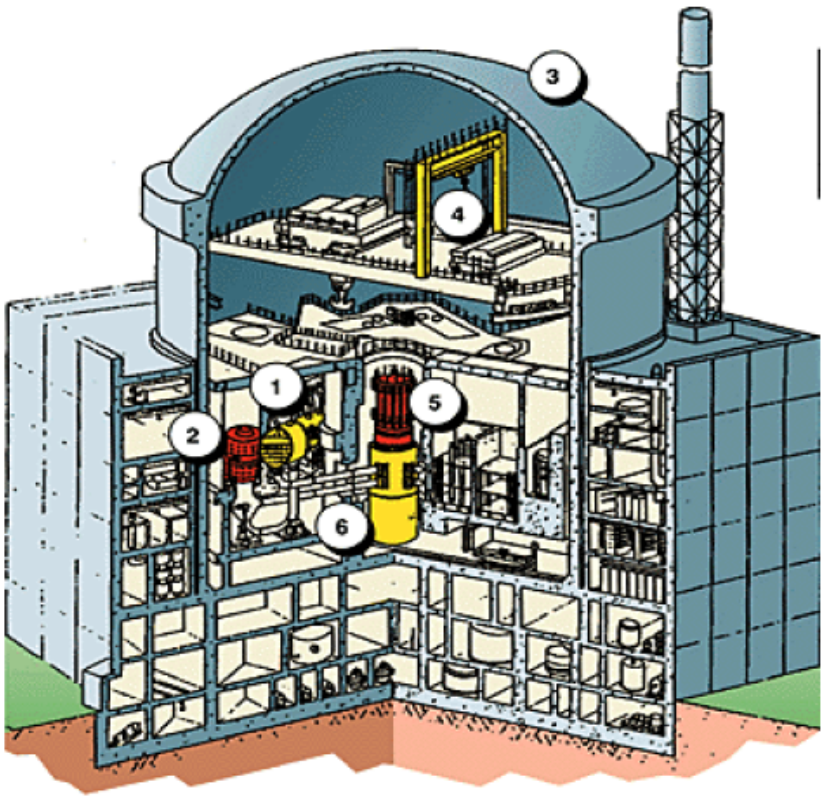

Figure 5 Cut through the Containment of the VVER-1000/320

(1 – horizontal SG, 2 – MCP, 3 – Dome of containment, 4 – polar craine, 5 – spent fuel pool, 6 - RPV)

A.8.2.3 Containment model

Model of containment includes all parts of hermetic rooms, but rooms below containment base-mate are not modelled (Fig.5) in the version used for the IVMR strategy simulation. Surrounding rooms to cylindrical part are merged into one CV together with rooms below base-mate. Generally containment can be subdivided into two parts – reactor hall (upper part) and lower rooms. Reactor hall is one huge space, which is in the model subdivided into xx CVs virtually due to need of flow pattern modelling, but lower part is modelled using nn CVs as some rooms are merged into common CV, but main parts/rooms of the containment are modelled independently – like SG boxes or cavity or recirculation sump. Figure 6 shows a basic nodalization of the VVER-1000/320 containment, but the figure represents in 2D the CVs which represent 3D configuration, so some technique of visualization had to be applied. This nodalization is used for the typical analyses of the severe accidents, but in case of the application of the IVMR strategy original CV810 (reactor cavity) is subdivided into more CVs to model implemented deflector.

Concerning a possibility to apply the IVMR strategy for the VVER-1000/320 reactor, it is necessary to mention couple of limiting conditions. The principle limitation to this strategy is that the recirculation sump of the containment is one floor below the reactor cavity, and all drainage of water inside of the containment is directed to recirculation sump. It is fully impossible to manage redirection of water drainage to reactor cavity, so the only external reflooding and water long term supply systems have to be added. The second limitation is in the design conditions of the cavity with very thick wall, so the only possible solution of connection of water supply is via. venting lines. Next limitation is related to the power of the reactor, which is relatively high (1000 MWe with assumptions of future power uprate in range of few percent) and heat flux density profiles and their maxima to be removed. As these values seems be very high (it has to be confirmed and the benchmark is one of activities for the confirmation), it is assumed that boiling in free water pool is not sufficient and intensification is needed. One of such possible solution is an application of a deflector. Figure 7 shows two design solutions of the deflector. Left part shows flow-through variant without a possibility of intensive internal water circulation inside of the containment. Right one, with short deflector, enables formation of the internal coolant circulation in the cavity, which results in the faster flow inside of the deflector and increase of the CHF profile along the RPV surface. Nodalizations of those two solutions are on Figure 8, and both variants were applied in analyses (code v0x is later used in definition of assumptions of each of analyses performed) with the MELCOR code.

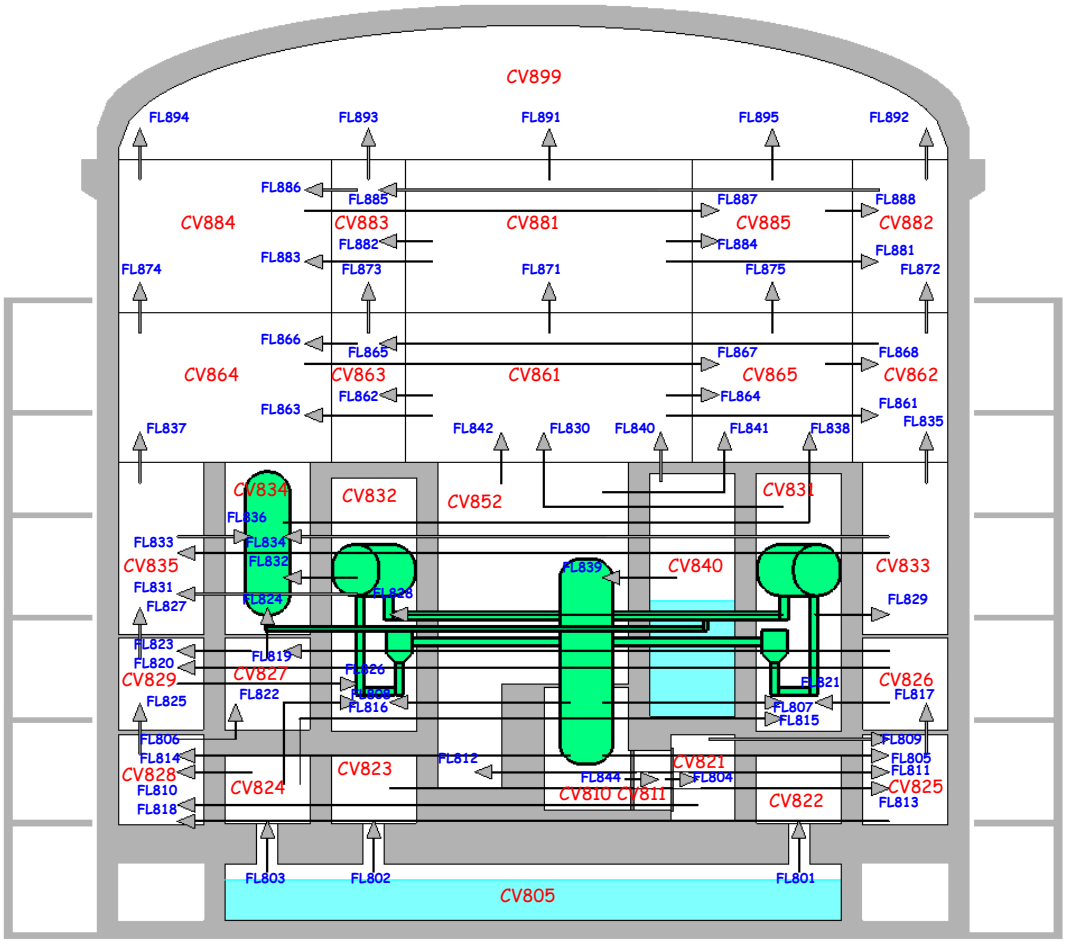

Figure 6 Nodalization of Containment of the VVER-1000/320

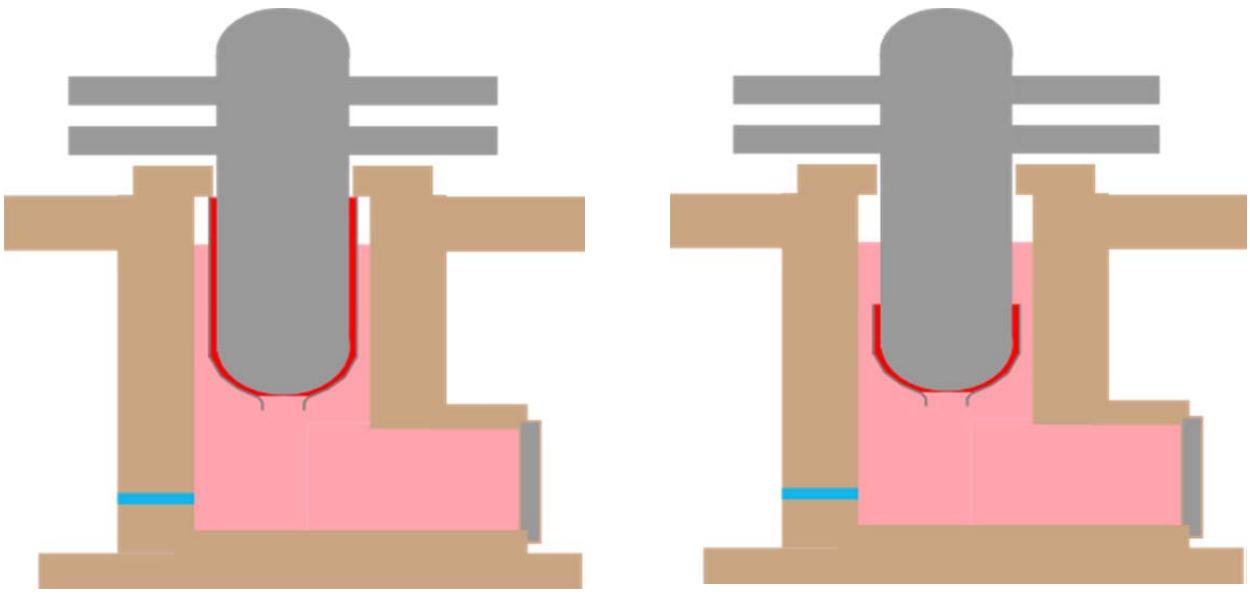

Figure 7 Variants of deflector design in reactor cavity of the VVER-1000/320 containment (left with full height deflector and right with short deflector)

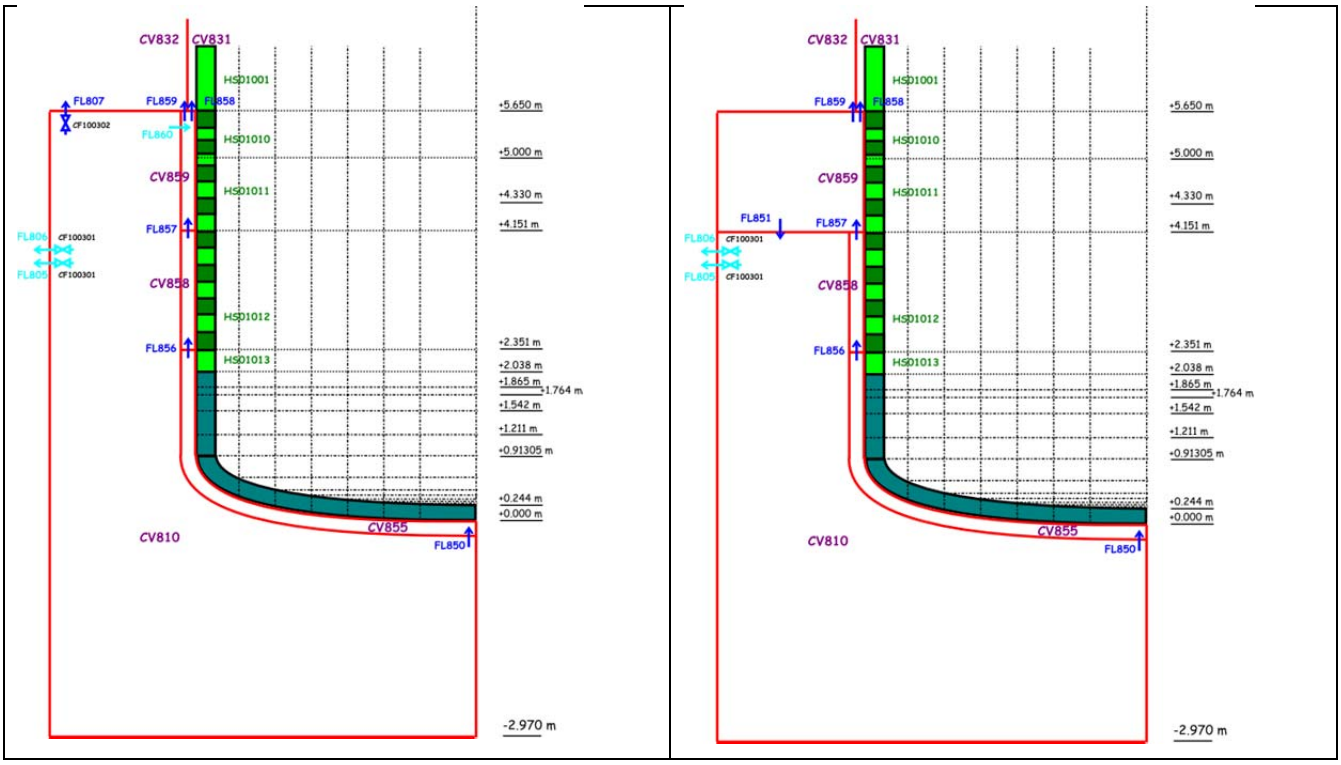

Figure 8 Nodalization of reactor cavity of the VVER-1000/320 containment with two variants of deflector design (left (v05) with full height deflector and right (v06) with short deflector)

A.8.2.4 Other models

This chapter briefly describes other important models concerning the application of the IVMR strategy mainly. Generally there are many additional models included in the whole plant model starting with reactor protection system modelling, modelling of safety systems – hydroaccumulators, LPI, HPI, containment spray systems, SG feed water system and emergency FW systems, heater in pressurizer, PORV and SV of pressurizer, membrane of the bubble tank, steam dump to condenser and atmosphere systems, SG safety valves and others. Concerning the severe accident phenomena, the hydrogen removal system is expected, which at the Temelin NPP consists of two parts – DBA part with 25 PAR AREVA FR-1/150 and severe accident one (recently under implementation, full functionality will be after outages in 2015 for both units) which consists of 14 PAR NIS22 and 41 PAR NISS44. Next systems related to the severe accident modelled are related to possibility of operator full opening of all pressurizer valves to depressurize RCS in case of the high pressure scenario (like SBO) and activation of cavity reflooding and consequent water supply to keep chosen water level in the cavity. Those systems are based on the source CV (time independent CV full of water) and FL with valve which activates (open) for initial reflooding based on a signal of the entry to the SAMG plus predefined (with possibility of user choice of duration) delay and for the control of water level which open or close the flow path for water supply. Based on the amount of water added into the cavity during water supply phase, the same amount is removed from recirculation sump to prevent overfilling and overpressure of the containment.

A.8.3 Calculations performed

As mentioned in the Introduction, the analyses were performed with the integral model and two main initiating events were simulated leading into two different severe accident scenarios.

The first initiating event is LBLOCA (D_{eq} = 200 mm on cold leg between MCP and RPV) and additional events resulting into the progress into the severe accident are loss of all active ECC

systems (LPI, HPI, FW, EFW, Containment Spray), the only functional systems are passive ones (hydroaccumulator, PORV or SV) and systems dedicated for severe accident management – PARs, reflooding of cavity and water supply to the cavity.

The second initiating event is station blackout (SBO), which results in loss of all active systems – from the point of modelling it means loss of LPI, HPI, FW, EFW, Containment Spray, the only functional systems are passive ones (hydroaccumulator, PORV or SV) and systems dedicated for severe accident management – PARs, depressurization of primary circuit (opening of all PORV and SV at pressurizer), reflooding of cavity and water supply to the cavity.

Calculation of both scenarios was initiated with the full height configuration of the deflector (left figure on Figures 7 and 8) using the MELCOR 1.8.6 (release 3481, later 4073). The calculations were very unstable with many termination due to non-convergence mainly in the COR package, but also heat structure package contributed with some terminations. Generally, terminations resulting from the HS package were possible to overstep using some repair measures in the input file, but many of the termination causes from the COR package were fatal. Regardless of those troubles, the first results were presented at the May 2014 meeting (LBLOCA_v02), but with remark that some user faults in definition of input for the deflector were identified (RPV wall segments were in contact with CV810 – main volume of reactor cavity – instead of the CV855 – volume between deflector and RPV, se Fig.8 left). These cases were re-run, but only LBLOCA (in version v05) was successful for sufficient time to make any conclusion, as another user fault in the definition of water supply system model was identified, which caused termination of water supply after certain time. So this case is an example how the unit would behave in case of loss of water feed into cavity during fully developed molten pools within the IVMR strategy application.

The case with short deflector was successfully calculated for the LBLOCA (v06 case) using the MELCOR 1.8.6 and predicted the most important results, regardless the run was again terminated due to trouble in COR package, but several thousand seconds after the full development of molten pool configuration and quasi steady situation of the IVMR strategy.

The cases of the SBO initiating events were not successful as they were usually terminated during the formation of molten pools and any reasonable results were not possible to extract. Such activity need more time and it is expected to continue in activities in this branch in future.

Another activities were focused on the conversion of the input from the MELCOR 1.8.6 to version MELCOR 2.1 and running both scenarios with this latest version, which is expected as upcoming production version of the MELCOR code. All cases, they were run with many sub-released versions (MELCOR 2.1 rel. 4206, 5026, 6220, 6312, 6330, and 6342) resulted in the practically identical terminations during very early phase of core degradation (during initial formation of particulate debris in centre part of the core – axial level 22 of 28, but lower 12 levels represent lower plenum). Two subcases were analysed as the original modelling with the advance B4C model was terminated due to problem in this advance B4C models, the version with the simple B4C model was always terminated at practically same time due to non-convergence in COR package (CORRN1 routine time step cutting). These troubles were reported to the developers (Sandia National Labs), input were passed for the identification of causes during the MCAP meeting in September 2014, but no answer received up to the middle of November 2014. So the activities in the branch of MELCOR 2.1 are now temporarily frozen.

Summarizing the activities with the MELCOR code, results to be presented in this report come from two calculations LBLOCA_v05 (case with full height deflector and later loss of water supply into cavity) and LBLOCA_v06 (case with short deflector).

A.8.4 Results of UJV MELCOR calculations

The chapter 2 summarized calculations and identified three main cases of the LBLOCA scenario – v02 (first case from May 2014 meeting with wrong definition of CV in contact with RPV lower

head), corrected case v05 and case v06 with short deflector. Table 1 compares timing of main events and shows that the initial progression is in very good agreement, the only difference between case v02 and cases v05 and v06 is in the inverted order of the first cladding rupture and fulfilment of the SAMG entry criterion ($T_{CORE-EXIT}$ > 650 °C). This difference can be cause either by modifications in the cooling of RPV or application of different release of the MELCOR 1.8.6 as the v02 was run with release 3481, but v05 and v06 with release 4073. Concerning of all three cases the formation of convective molten pool in the lower head was predicted in similar time at about 15 000 s.

Table 1 Timing of main events in analyses of LBLOCA simulations with MELCOR 1.8.6

Event	Time [s]		
	v02	v05	v06
Initial Event Occured	0.00	0.00	0.00
REACTOR SCRAM	0.11	0.11	0.11
HYDROACCUMULATOR YT12B01 - First Injection	153.47	153.41	153.57
HYDROACCUMULATOR YT13B01 is Empty	289.49	291.98	297.64
Core Exit T > 650 deg C - Entry to SAMG	1832.36	1988.10	1889.54
Cladding rupture due to overheating	1910.45	1844.12	1827.21
Change of FL911 Status - CAV Reflooding initiation	2012.48	2168.19	2381.68
Failure of Core Support Plate - relocation to LH	5560.26	5433.55	5060
Switching to continuous water supply to Cavity	6563.17	6762.93	6710.9
Calculation terminated by : COREU3 T CONVERGENCE	16476.10	14551.50	12705
LHF in Segment 6 by creep rupture	-	19265.30	-
Calculation terminated by : COREU3 T CONVERGENCE	-	-	21934

As the MELCOR code is the integral code and its treatment of the IVMR strategy modelling is simplified and influenced by user nodalization assumptions, the main purpose of the code is in identification of time dependence of debris/melt relocation to the lower plenum, their temperature and general behaviour (passing through lower head internals), melting of remaining intact lower head internals, identification of the decay power history in the corium and indicative identification of general behaviour. As addition the impact of the strategy to the containment response and estimation of external source term can be also calculated. On other hand, it is obvious that the code can't be used as the only tool for proving of applicability of such strategy for the NPP, it has to be confirmed using additional and more detailed analyses of corium behaviour inside of the RPV lower head and cooling outside of RPV wall including comparison with the specific CHF profile. The activities of UJV with the MELCOR code within the benchmark were focused mainly on identification of corium composition and identification of decay power history in the debris/corium in lower plenum. Global evolution of scenario was also evaluated, but as indicative results only.

Table 2 shows the final composition of materials in the lower plenum in case LBLOCA_v06 and their evolution is shown on Figure 9. Data shows that at the end of simulation total mass of corium is 163.63 ton, the oxidic part (sum of UO2, ZrO2 and SSOX) is 95 ton and metallic materials (steel and Zr) is 68.681 ton. The ratio of Zr oxidation is 20.5 % calculated from the masses of ZrO2 and remaining Zr, recalculated to the initial mass of Zr. This ratio identifies that for the LBLOCA oxidation is not very intensive, as expected because due to the low pressure in primary circuit, the content of steam in the core is also low and conditions are favorable for steam starvation.

Table 2 Final composition of material in lower plenum (case LBLOCA_v06, MELCOR 1.8.6)

Component/material	Mass [kg]
Steel total	4.5486E+04
SSOX total	1.0122E+03
UO_2 total	8.5885E+04
Zr total	2.3195E+04
ZrO_2 total	8.1015E+03
Total	**1.6368E+05**

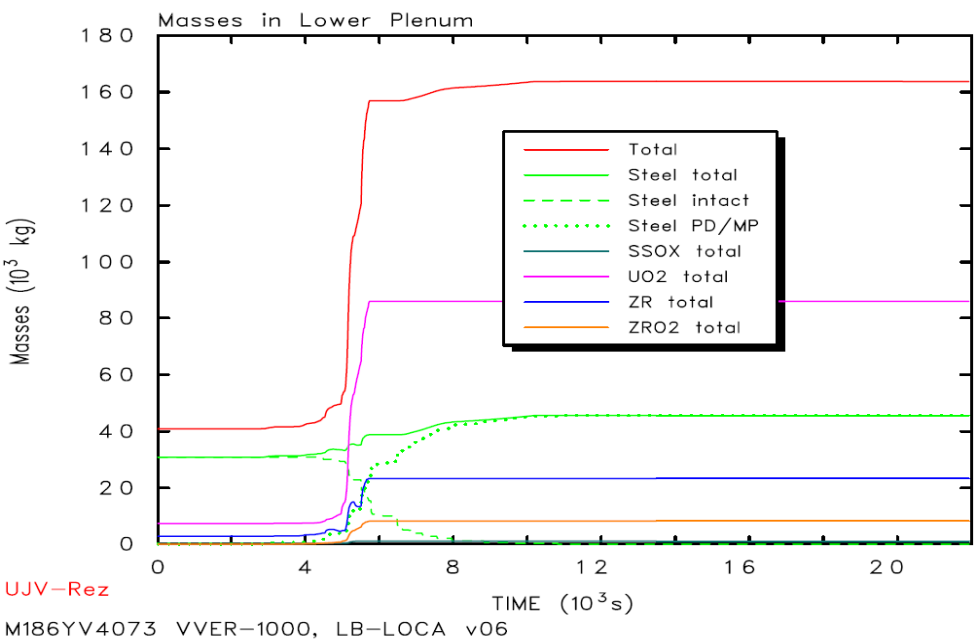

Figure 8 Evolution of component masses in lower plenum in case LBLOCA_v06

Figures 9, 10, and 11 summarize a comparison of evolutions of masses of various components in cases LBLOCA v02, v05 and v06. It is shown that the trends are very similar, mainly cases v05 and v06. Figure 10 shows that mass of UO_2 particulate debris in the lower plenum is increasing first, but later decreases as UO_2 is melted and mass of UO_2 is thus converted from PD component to molten pool. Very interesting is Figure 11, which presents evolution of masses of convecting molten pools. It is very well visible that the mass, mainly of oxidic pool, is increasing during debris heat up/melting phase (14 000 to 17 000 s), but later, probably due to cooling of the corium in the lower head, masses of molten pool oscillate as the criteria for inclusion to the convecting melt pool are fulfilled or not. Comparison of Figures 10 and 11 shows that the modelling in the MELCOR is quite complicated, as the mass in component molten pool does not means mass of convecting melt pool. Moreover the only mass of convecting melt pool is available output variable, but not mass of melt pool component in each of cell, so it is not possible to create a figure of evolution of molten material in lower plenum as sum of all lower plenum COR cells. The only indirect way could be used to subtract mass of PD from total mass, but it is a little user non-friendly.

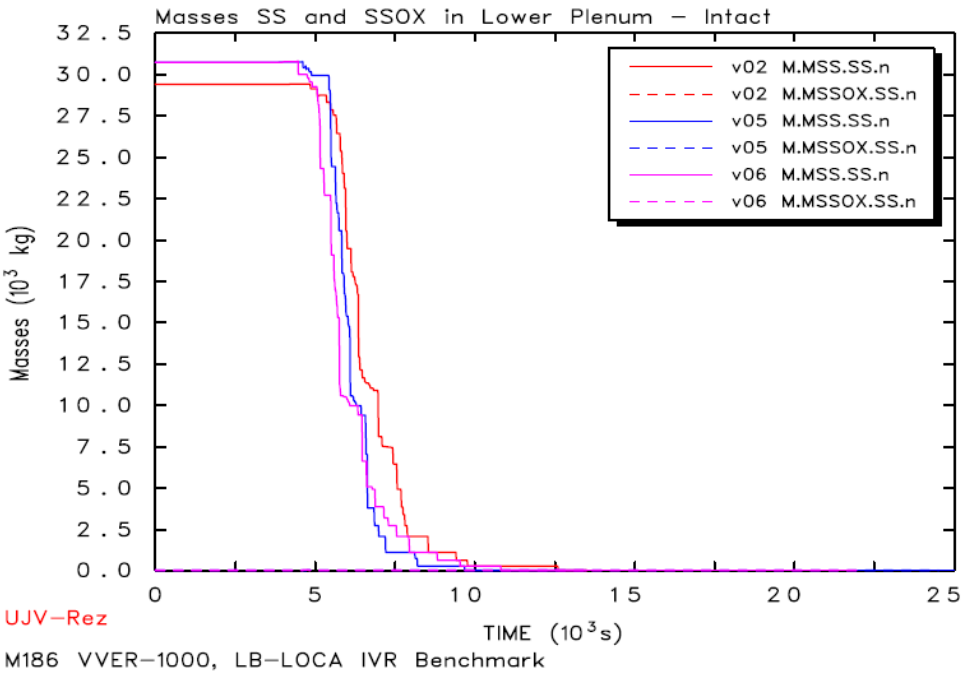

Figure 9 Evolution of steel intact mass in lower plenum – comparison of LBLOCA cases v02, v05 and v06

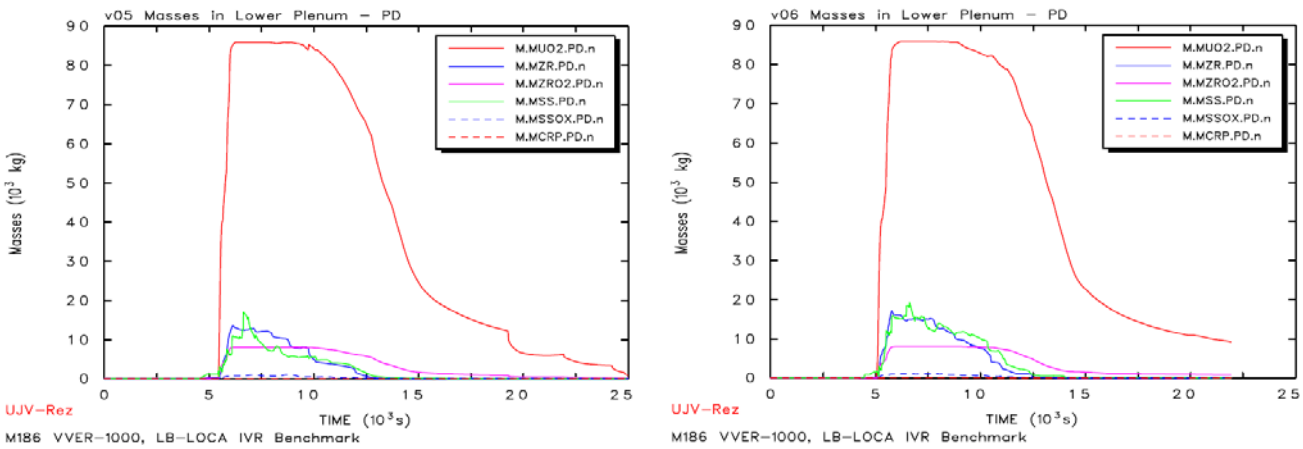

Figure 10 Evolution of PD masses in lower plenum – comparison of LBLOCA cases v05 and v06

As mentioned above, one of the important outputs from the integral analysis is evolution of decay power releasing in debris/melt in lower plenum. Figure 11 compares evolution of total decay power (solid line) and decay power releasing in core (dashed line) – it means decay power releasing in all component of core package in all cells, i.e. in core region as well as in lower plenum. To identify what is decay power in lower plenum, it is necessary to sum data per component and cell from the listing formatted output, which is available only for predefined times. This is source of green bullets on Fig 11 and it shows that very quickly after the start of material relocation, the total decay power is releasing in lower plenum location.

In any case, this integral simulation shows that the approach of the stand-alone simulation which assumes that total mass and total decay are available in the lower plenum immediately after the initiation of the corium relocation to the lower plenum is not fully correct and corium mass and decay power have to be treated with their histories of evolutions.

Concerning the results of corium behaviour in the lower head, set of figures was prepared using the postprocessor ATLAS (developed by GRS). The screen used visualizes temperatures and

presence of decries/melt (box with border line of colour based on temperature colour scale in lower left corner) in lower plenum COR nodes, but also intact components (boxes with black border line), temperatures of lower head segments and nodes of segment, but also temperature of atmosphere/water outside of RPV, but using different colour scale table (in upper right corner) and water level as blue line (solid for swollen level and dashed for collapsed). The same screen was used for both cases v05 and v06, but it is fully representative for nodalization in v05 case and in case v06 the behaviour in upper part of cavity is not correctly visualized (compare with Fig. 8), but it is possible to make some imagination of cavity response also for this v06 case.

Generally it is possible to say that the progression of accident in the lower took a lot of time, mainly concerning the time needed for melting of remaining intact component in lower head – but it is influenced by presence of water in lower head during corium/debris

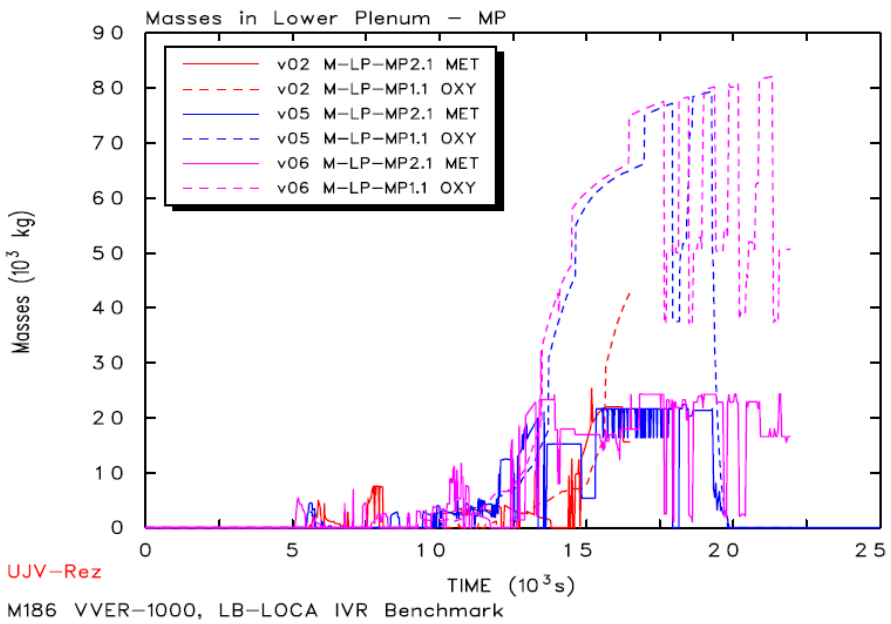

Figure 11 Evolution of convective pool masses in lower plenum – comparison of LBLOCA cases v02, v05 and v06

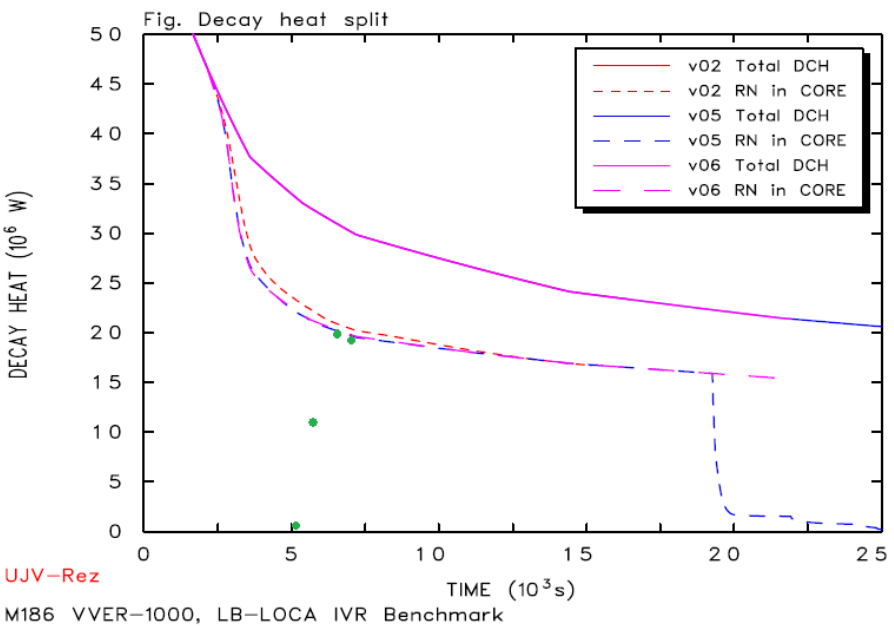

Figure 12 Evolution of decay power distribution – comparison of LBLOCA cases v02, v05 and v06 (green dots represents decay power in releasing in lower plenum in case v06)

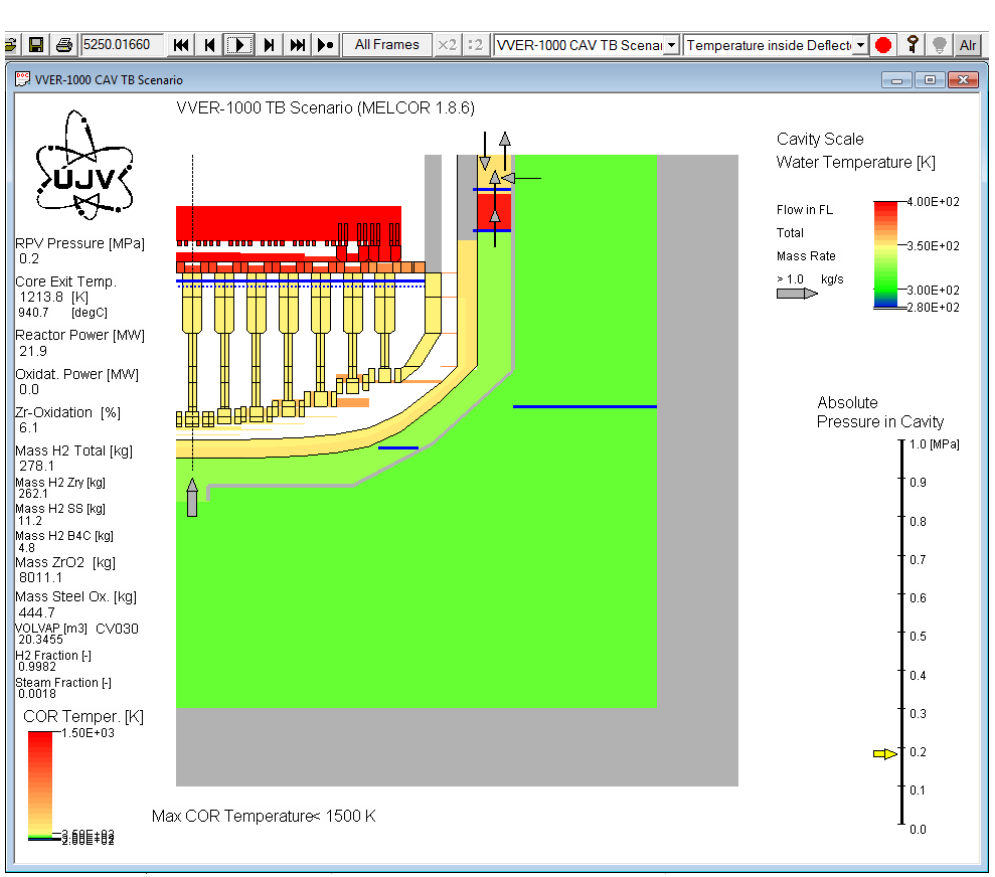

LBLOCA v05

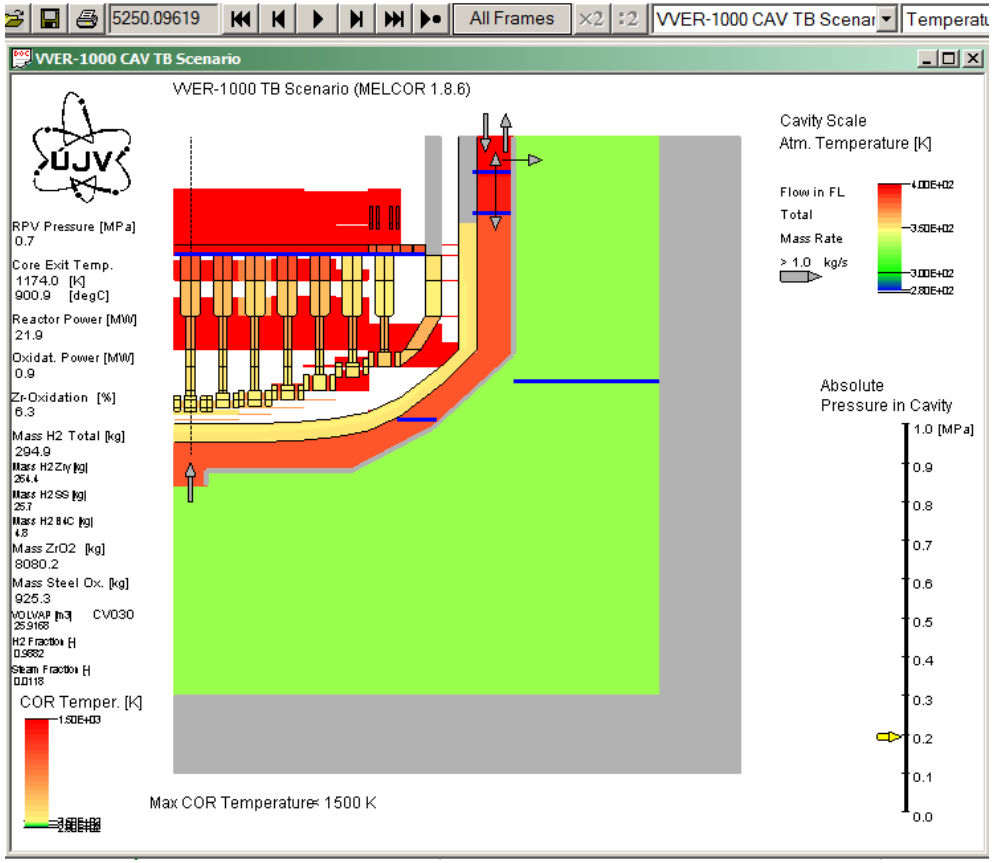

LBLOCA v06

Figure 13 Visualization of lower plenum temperature spatial distribution, location of intact component and corium and coolant outside of RPV wall - Comparison of cases LBLOCA v05 and v06, time 5250 s

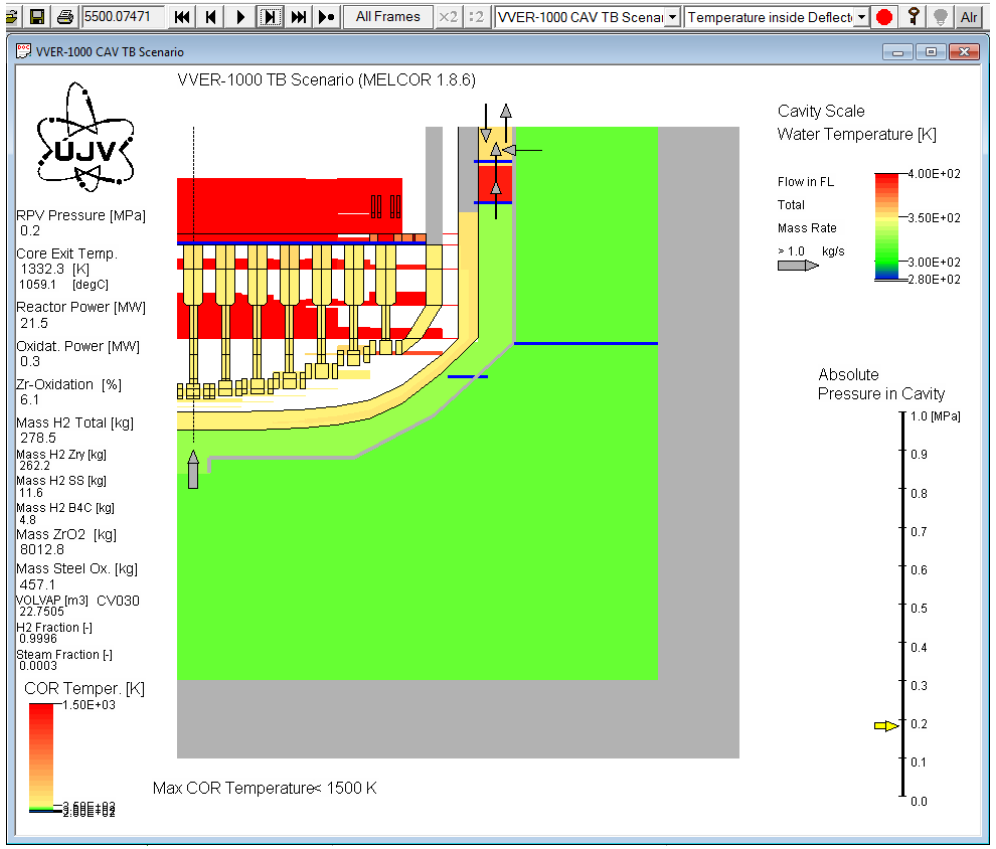

LBLOCA v05

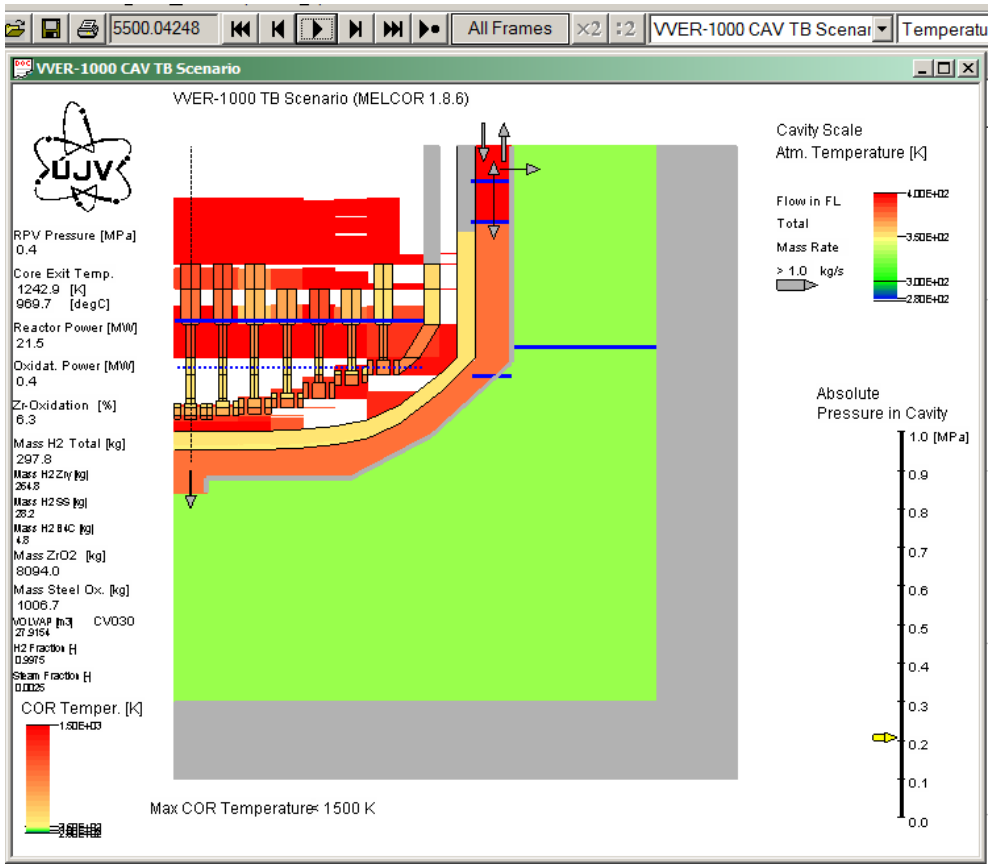

LBLOCA v06

Figure 14 Visualization of lower plenum temperature spatial distribution, location of intact component and corium and coolant outside of RPV wall - Comparison of cases LBLOCA v05 and v06, time 5500 s

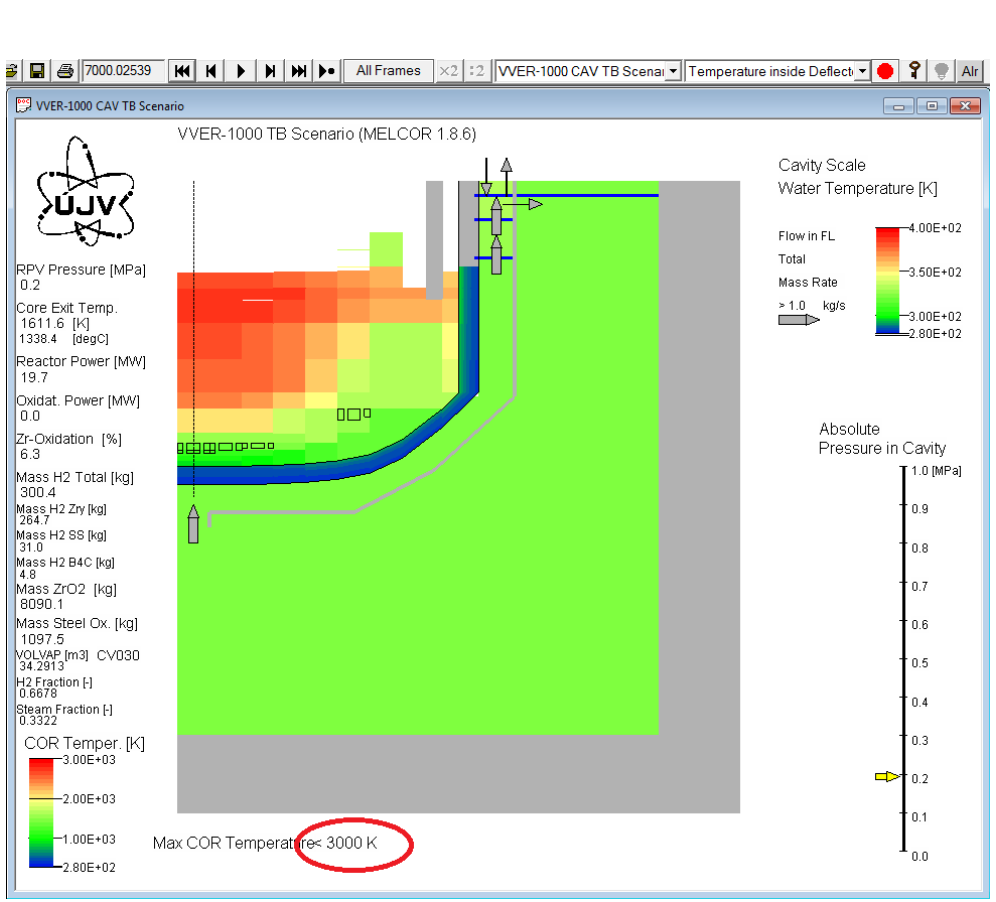

LBLOCA v05

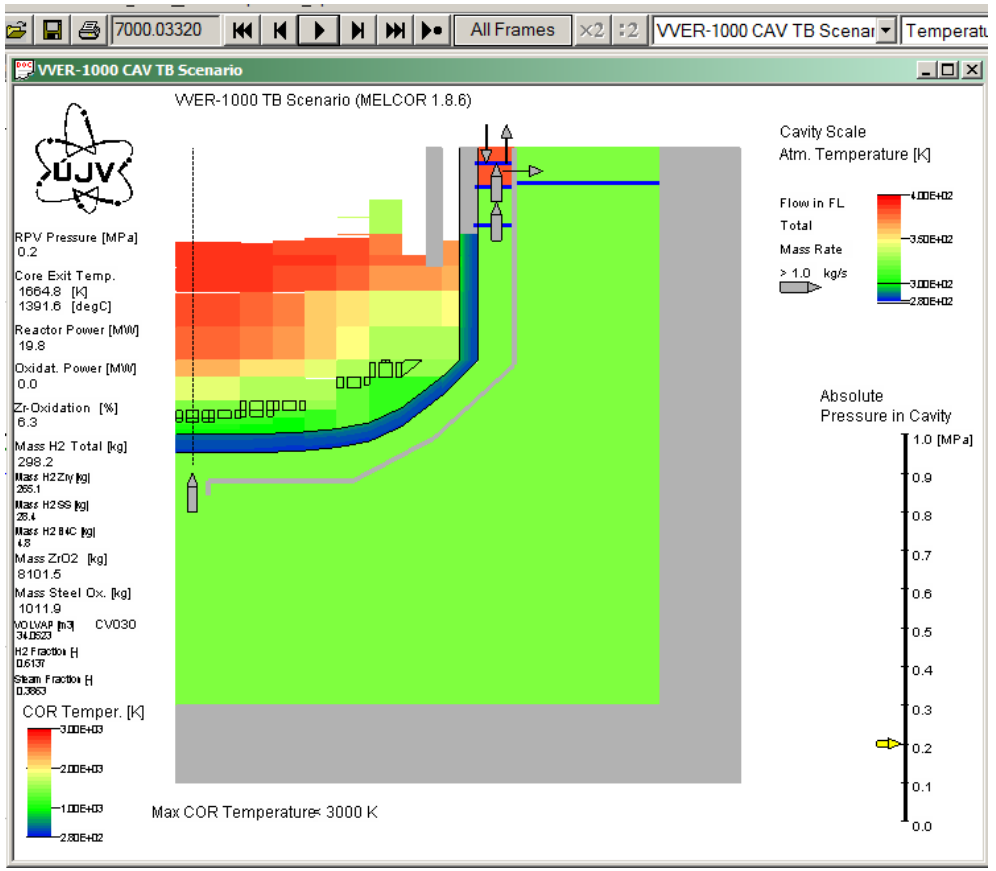

LBLOCA v06

Figure 15 Visualization of lower plenum temperature spatial distribution, location of intact component and corium and coolant outside of RPV wall - Comparison of cases LBLOCA v05 and v06, time 7000 s

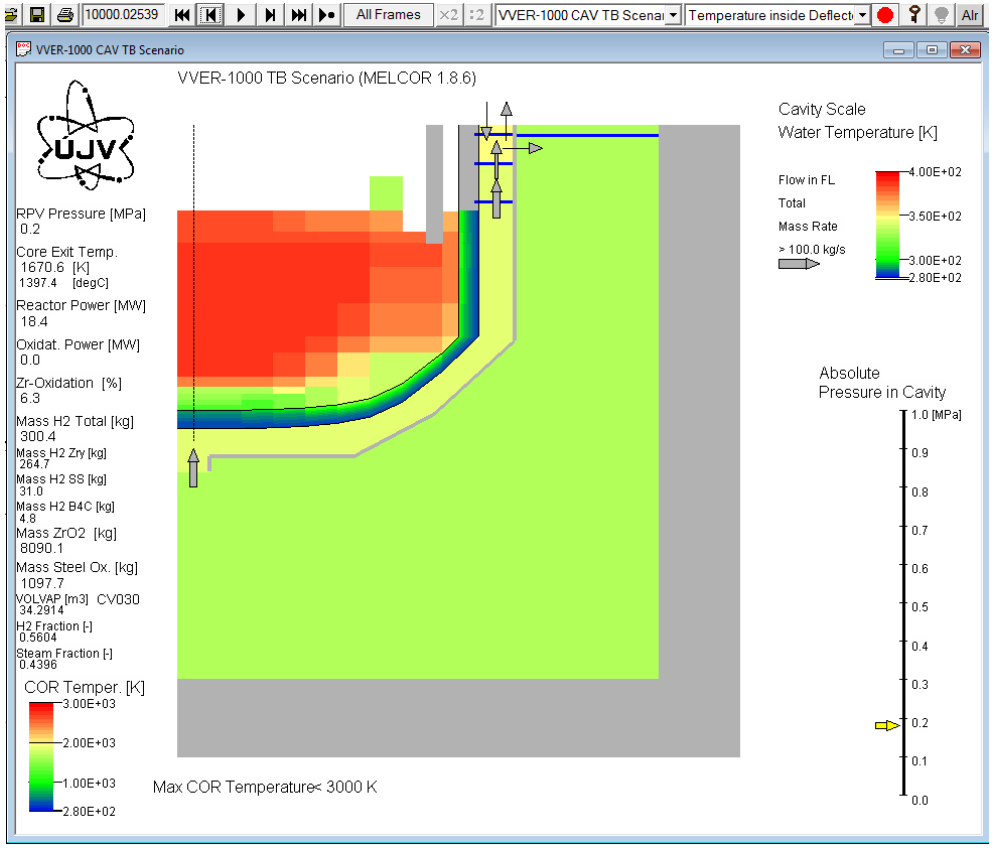

LBLOCA v05

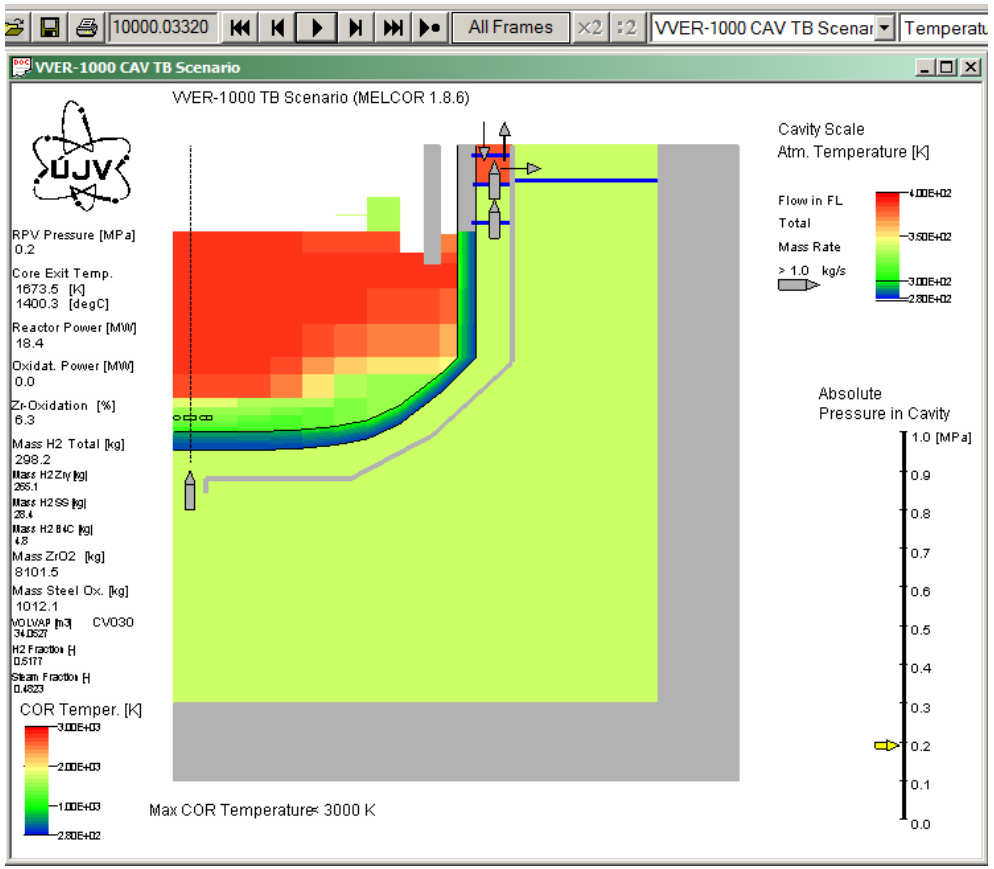

LBLOCA v06

Figure 16 Visualization of lower plenum temperature spatial distribution, location of intact component and corium and coolant outside of RPV wall - Comparison of cases LBLOCA v05 and v06, time 10 000 s

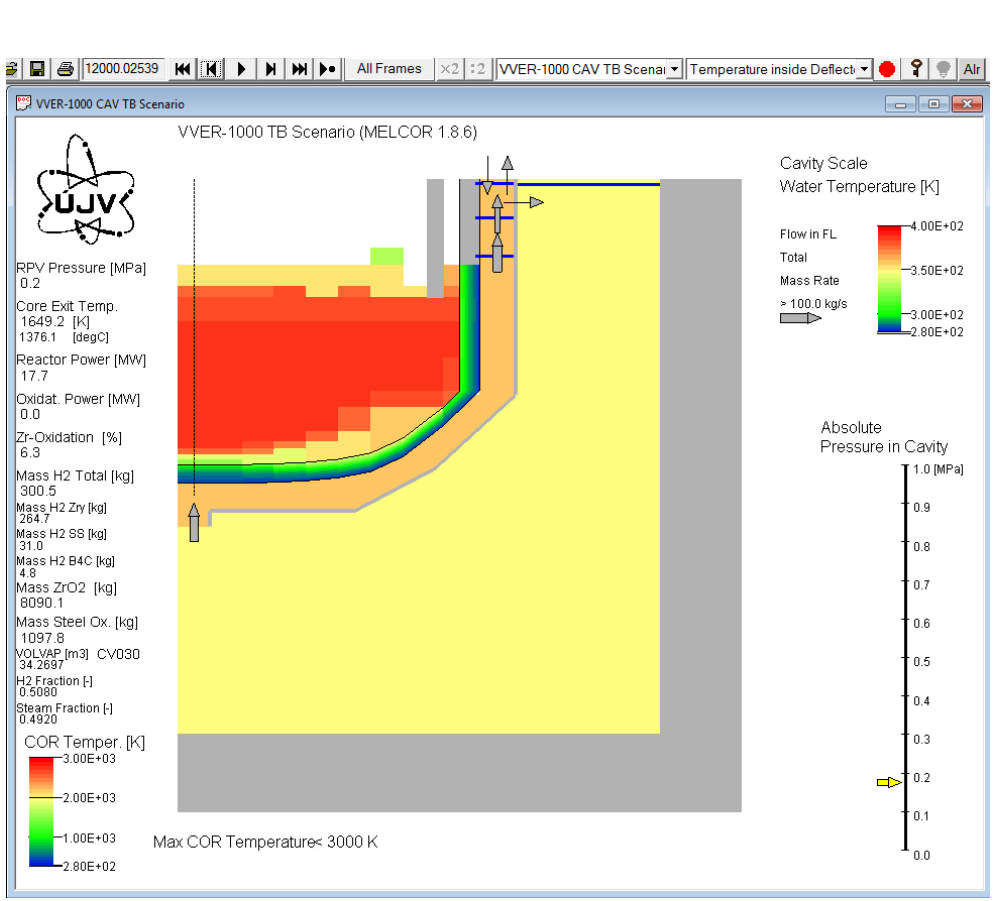

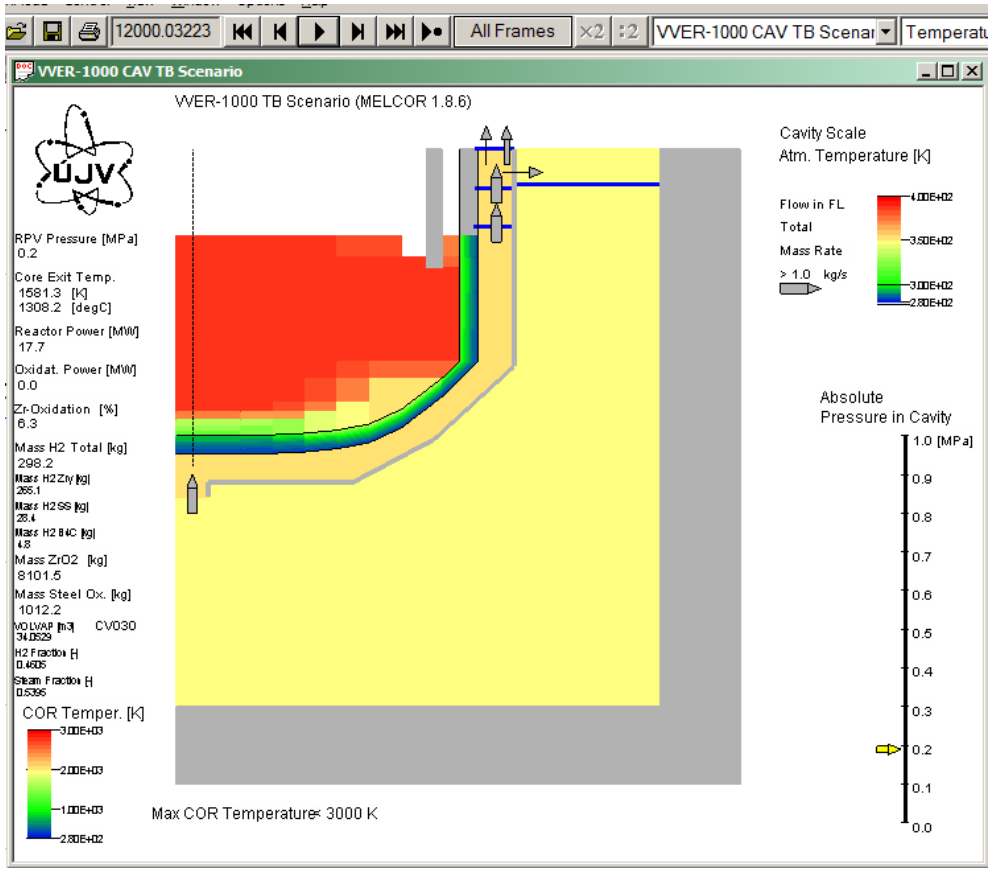

LBLOCA v05 **LBLOCA v06**

Figure 17 Visualization of lower plenum temperature spatial distribution, location of intact component and corium and coolant outside of RPV wall - Comparison of cases LBLOCA v05 and v06, time 12 000 s

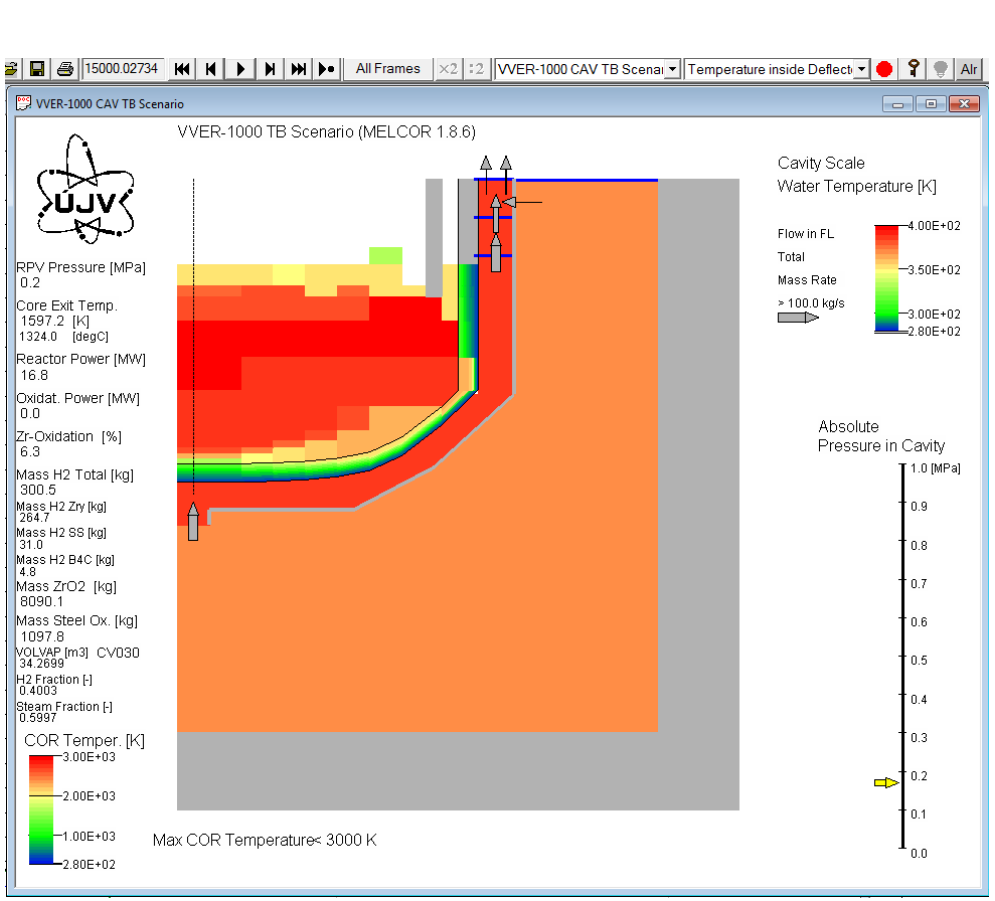

LBLOCA v05

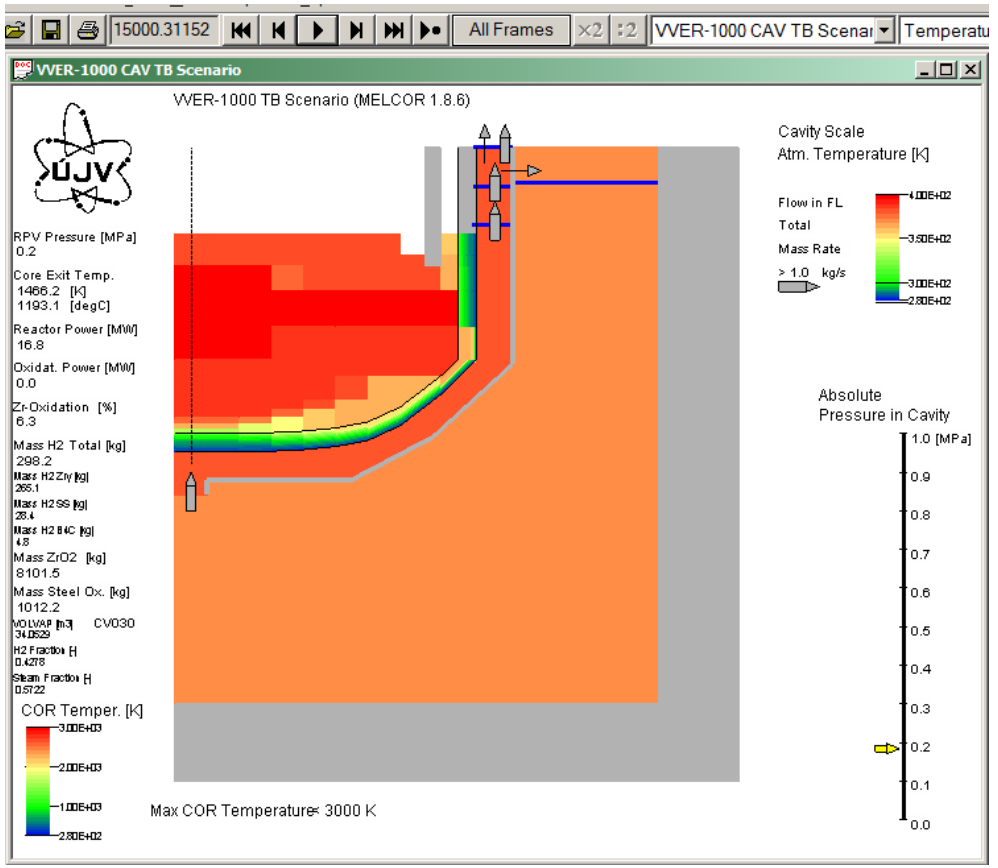

LBLOCA v06

Figure 18 Visualization of lower plenum temperature spatial distribution, location of intact component and corium and coolant outside of RPV wall - Comparison of cases LBLOCA v05 and v06, time 15 000 s

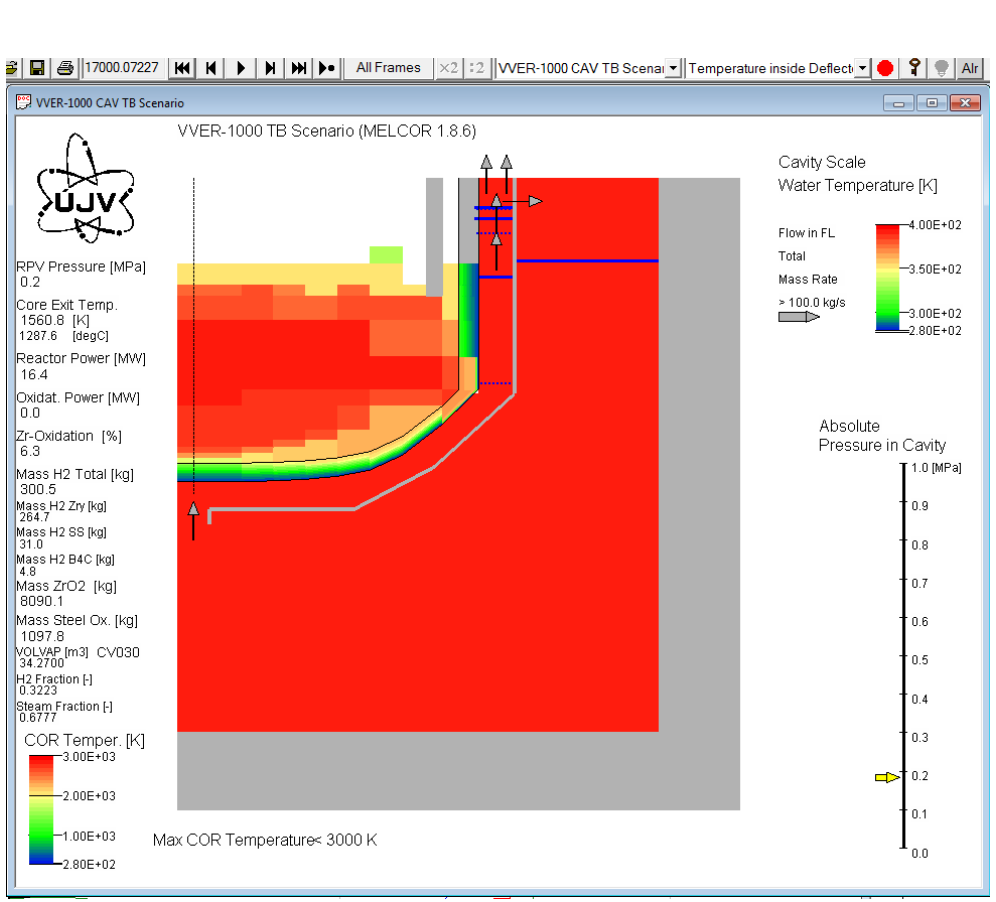

LBLOCA v05

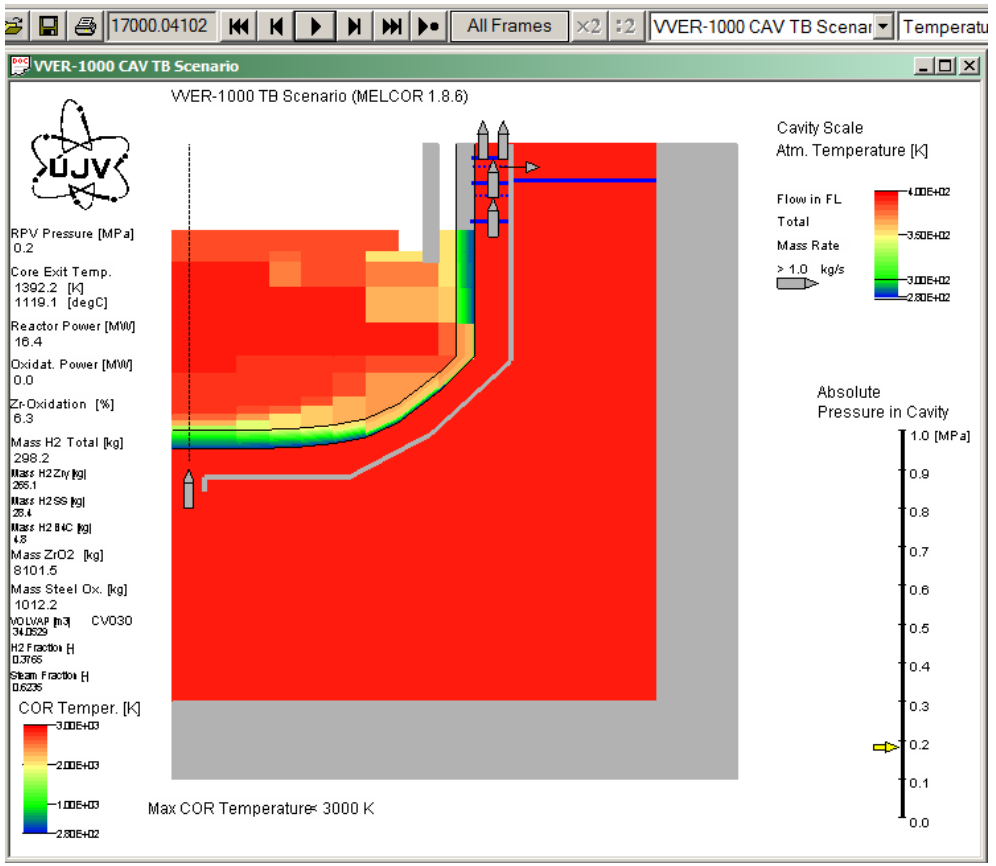

LBLOCA v06

Figure 19 Visualization of lower plenum temperature spatial distribution, location of intact component and corium and coolant outside of RPV wall - Comparison of cases LBLOCA v05 and v06, time 17 000 s

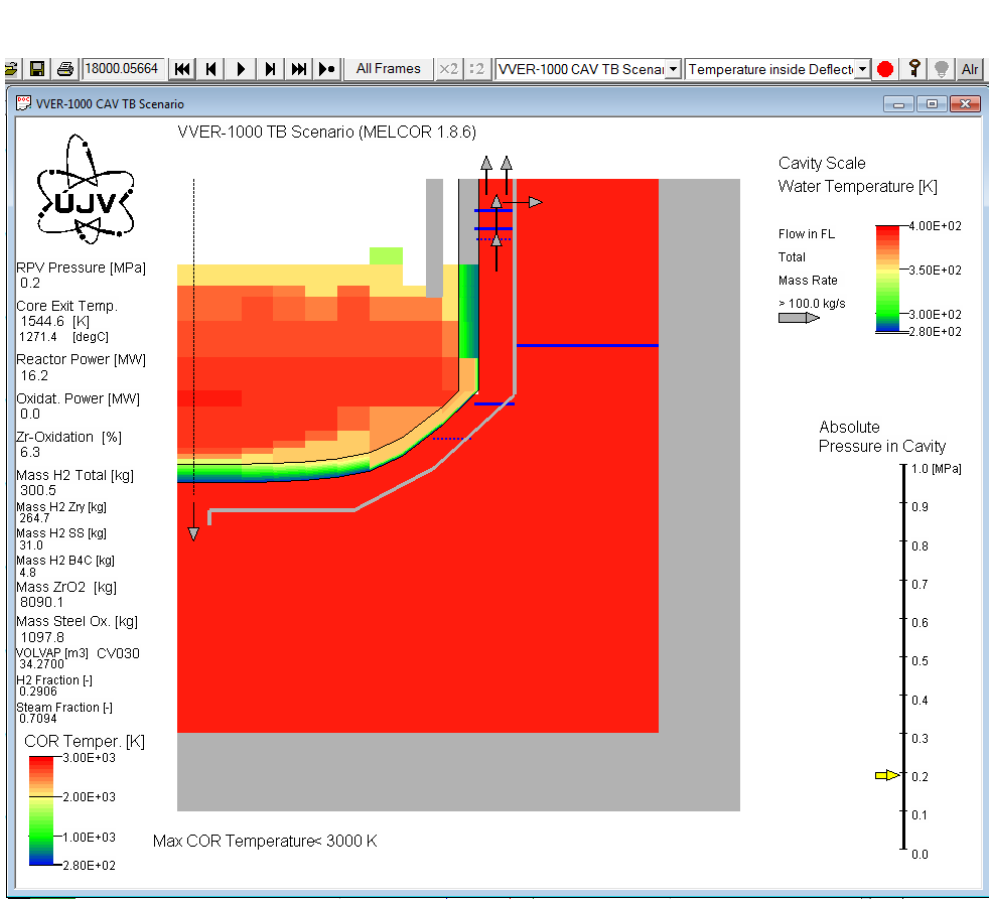

LBLOCA v05

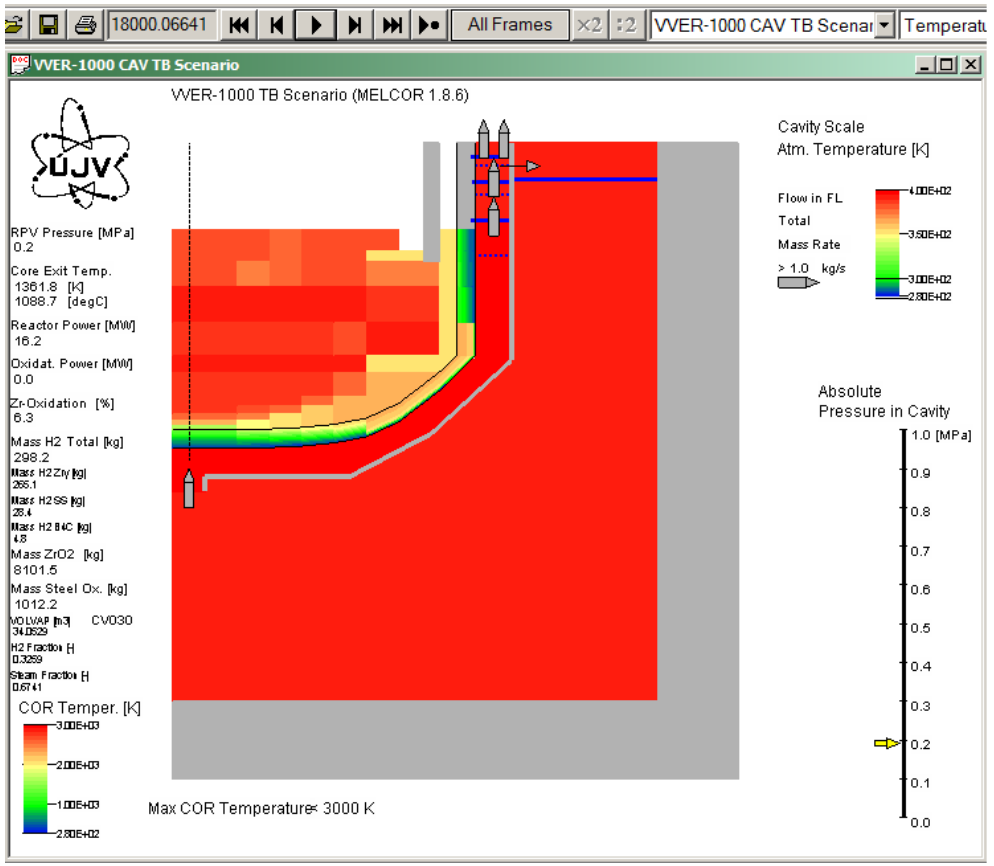

LBLOCA v06

Figure 20 Visualization of lower plenum temperature spatial distribution, location of intact component and corium and coolant outside of RPV wall - Comparison of cases LBLOCA v05 and v06, time 18 000 s

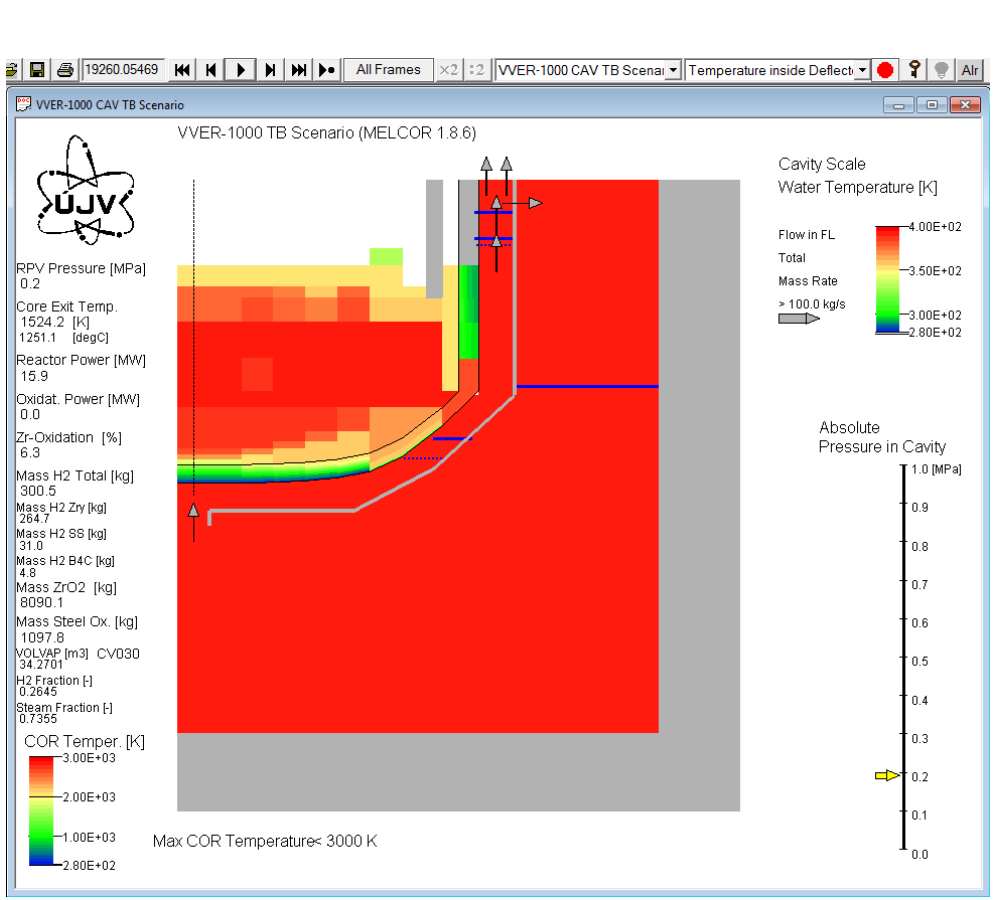

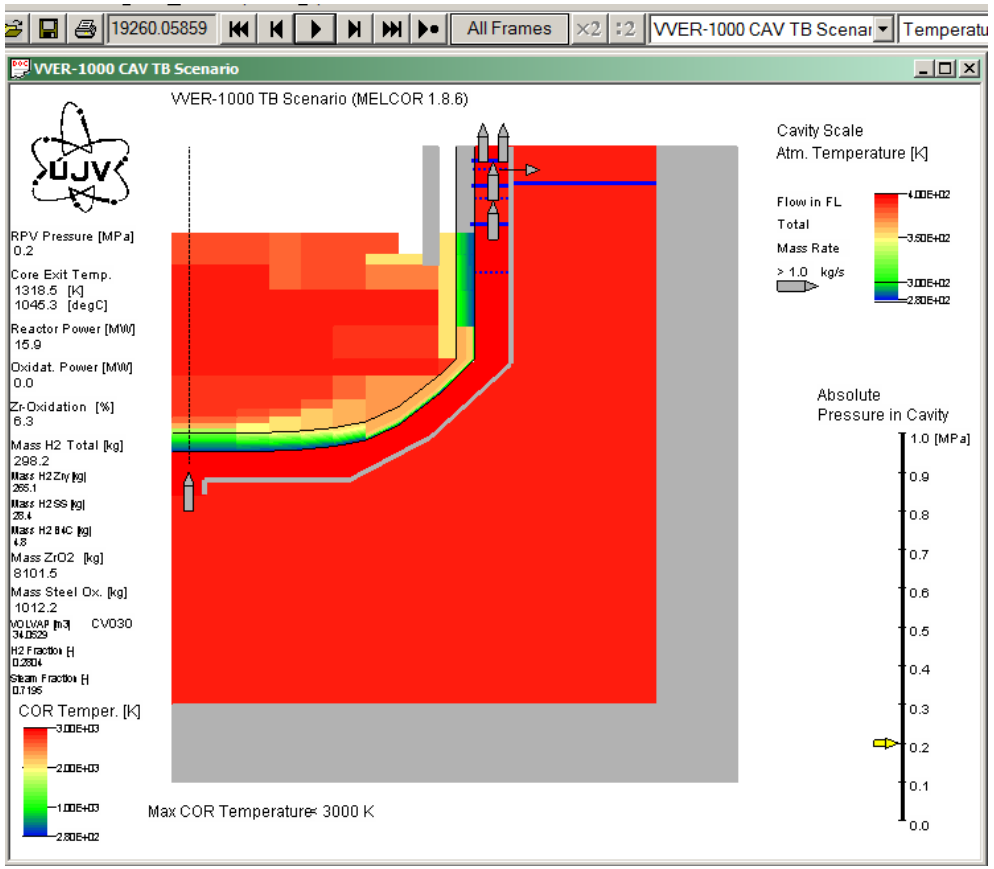

LBLOCA v05 **LBLOCA v06**

Figure 21 Visualization of lower plenum temperature spatial distribution, location of intact component and corium and coolant outside of RPV wall - Comparison of cases LBLOCA v05 and v06, time 19 260 s

relocation process, which caused significant subcooling of debris, below melting temperature of steel. Generally periphery of lower head was significantly subcooled and it was necessary to heat up it. This is a reason, why the principal heat removing to water is in case of integral analyses predicted with significant delay in comparison with stand-alone calculations.

During the description of scenario calculated (chapter 2), it was mentioned that in case v05 the loss water supply happened due to fault in the water supply model. At Fig. 18 you can see that the cavity is full of water, but at Figure 19, water level dropped and at Fig 20 and 21 it very well visible that water level at the end of simulation is below the location with the highest heat flux (transition between semielliptical lower head and cylindrical part of the vessel). The drop is visible inside and also outside of the deflector, very intensive boiling causes that the entry of water is not sufficient and water level inside is below the outside one.

The most interesting output from the analyses is the axial profile of heat flux densities. Figure 22 shows profiles for selected times and also maximum values of all times for each of levels. It is obvious that the highest values are reached at top of oxidic pool. The evolution of maximum heat flux density value predicted in the integral simulation with the MELCOR 1.8.6 integral code is influenced by some reasons

- Relocation of corium into the lower head is "per partes" as the code predicts loss of supporting function of supporting structures they model the sore support plate, but also columns in the lower head of core barrel. Corium relocating below core support plate enters to the inner space of upper part of columns (upper part is hollow, but lower one is solid) where is temporarily hold up, because of presence of water in lower plenum which supports cooling of the columns and delays their loss of integrity and further relocations of corium.

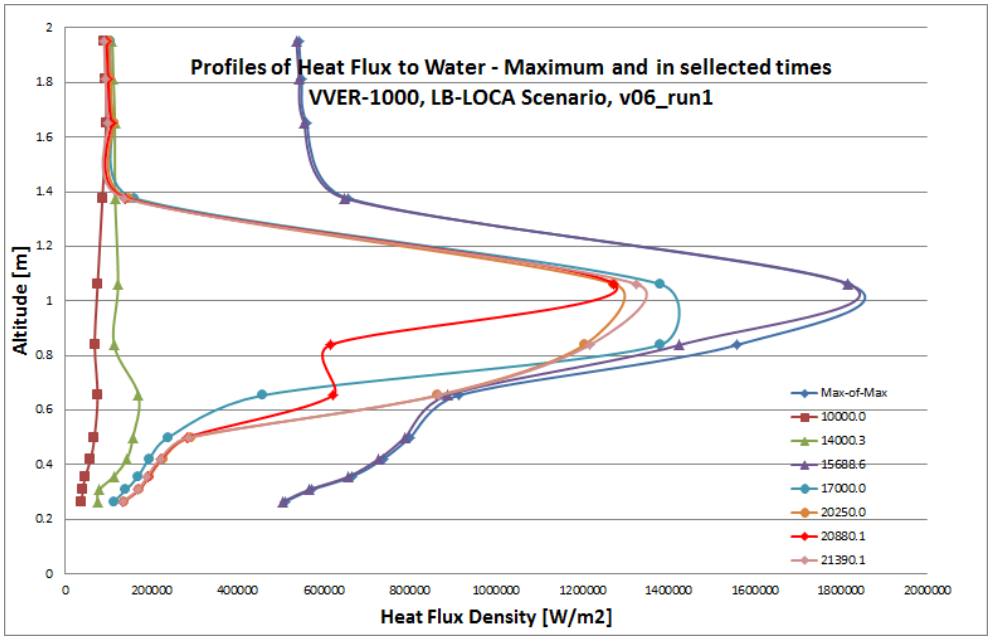

Figure 22 Profile of heat flux densities from RPV surface to water in selected times plus selected maximal values in all times for each of location (MELCOR calculated for LB LOCA (200 mm) scenario points highlighted by bullets, curves were generated as smooth lines in Excel, so they don't represent real profile) (case LBLOCA_v06)

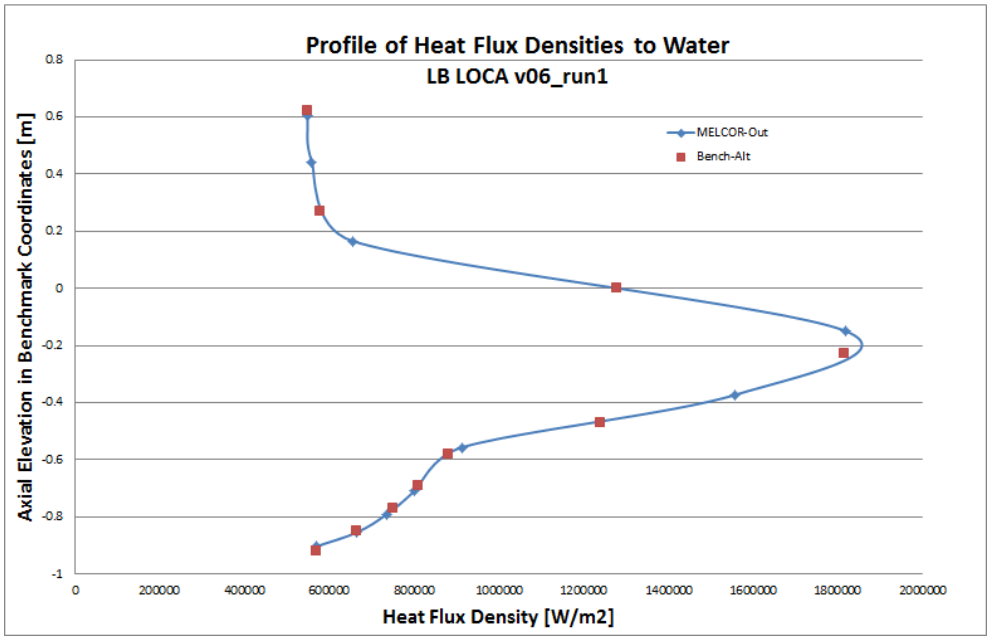

Figure 23 Profile of maxima from MELCOR results at the MELCOR model elevations and at elevations required by benchmark organizers (case LBLOCA_v06)

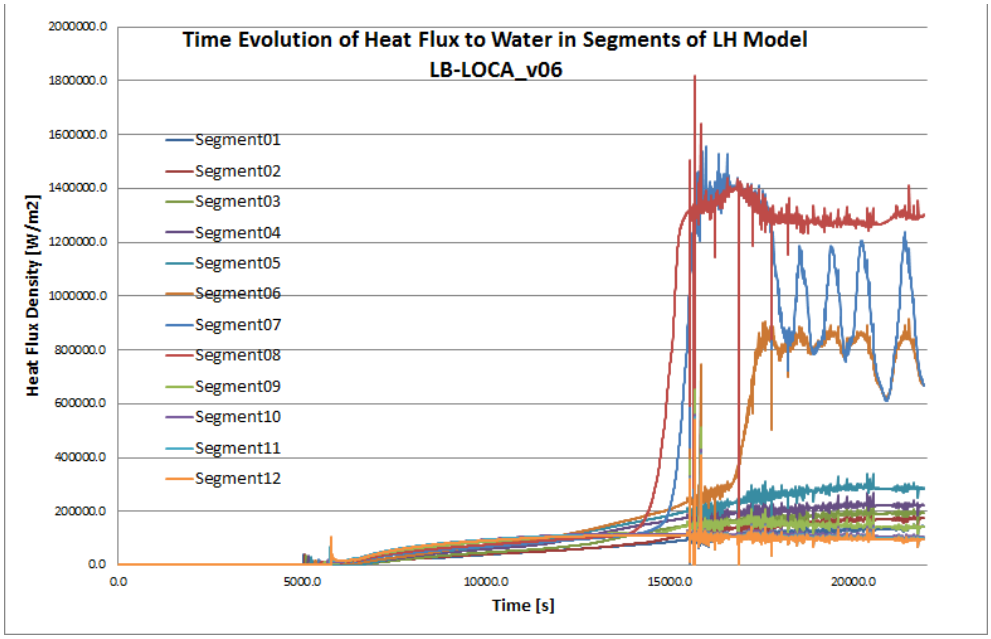

Figure 24 Evolution of heat flux densities in segments of MELCOR 1.8.6 LBLOCA_v06 case

- Due to temporarily hold up of corium it reaches bottom of the RPV as solid particles and their cooling is supported with boil off of remaining water in the lower head of the RPV, then the heat up of corium debris are re-heat up and finally re-melted.
- Location of the maximum heat flux is influenced by the accident progression as well as the predicted part of the material already molten (metallic layer is fully molten, but oxidic part includes important contribution of solid debris – in MELCOR terminology "particulate debris"). Generally the location of the highest heat flux density is at elevation of top of oxidic pool. This is typical for cases with reduced heat transfer from the bottom oxidic melt pool to the upper metallic layer – for instance when the top crust at oxidic pool would be formed. But as the crust formation is not modelled in the MELCOR

code (see COR-RM-71 page of MELCOR manual), the reason of maxima in heat flux located in upper part of the oxidic pool is in correlation for the heat transfer between molten pools, which depends on Rayleigh number (and the temperature difference between the bulk pool and the interface), which is in case of partly solidified oxidic pool underestimated (composition of molten material with solid particles).

For the purpose of possibility to compare profiles from different codes, the organizers of the benchmark required to submit a profile for exactly defined elevations, so Figure 23 shows a relation between curve and points of maximum values from Figure 22 to required elevations (red squares). But also the evolution of the points is very interesting Figure 24, because it shows real values of maxima, because some just only peak values has to be eliminated from the real profile, so the maximum heat flux density in the MELCOR 1.8.6 simulation of the LBLOCA in v06 case is 1.4 MW/m^2 for short time period, long term maximum is slightly below 1.3 MW/m^2.

A.8.5 Conclusions

The UJV Rez contributed to the benchmark on IVMR strategy for the VVER-1000/320 with the MELCOR 1.8.6 calculation of the LB LOCA initiated scenario. Although it was expected to submit also simulations of SBO initiated scenario and calculations preformed with the MELCOR 2.1, those case were not succeeded in passing through calculation of reasonable part of scenario, to be able to submit results. It is expected to continue in this effort in future[9].

The predictions of a severe accident progression with the integral model showed an importance of simulation of some phenomena which participants with stand-alone model neglected – like boil off of remaining water in lower plenum together with blockage of debris relocation to RPV bottom with the internals and their needs for heat up and melt-through. These phenomena result in significant delay in prediction of start of intensive heat transfer thorough lower head to the water. Although the capability of the integral code for the modelling of IVMR strategy are not the best one, it is very useful tool which can confirm many information needed for stand-alone simulation definition and results confirmation, including maxima of heat fluxes concerning their approximate value.

A.8.6 Abbreviations

B4C ... Boron Carbide

CHF ... Critical Heat Flux

CL ... Cladding, component in COR Package

COR ... Package of MELCOR code which solves fuel behaviour and its degradation

CV ... Control Volume

DBA ... Design Basis Accident

DCH ... Decay heat

ECC ... Emergency Core Cooling

EFW ... Emergency Feed Water System

FL ... Flow Path

[9] DN850 was not calculated as it was agreed at the kick off meeting that the Large break LOCA, but in range from DN200 to 300 is better.

FU ... Fuel, component in COR Package

FW ... Feed Water System

HPI ... High Pressure Injection System

HS ... Heat Structure

GRS ... Gesellschraft für Anlagen- und Reaktorsicherheit mbh (Germany)

IVMR ... In-Vessel Retention

LOCA ... Loss of Coolant Accident

LPI ... Low Pressure Injection System

MCAP ... MELCOR Cooperative Assesment Program

MCP ... Main Coolant Pump

NPP ... Nuclear Power Plant

NS ... Non-Supporting Structure, component in COR Package

PAR ... Passive Autocatalytic Recombiner

PD ... Particulate Debris, component in COR Package

PORV ... Pressure Operted Relieve Valve

RCS ... Reactor Cooling System

RN ... Radionuclide Package

RPV ... Reactor Pressure Vessel

SA ... Severe Accident

SAMG ... Severe Accident Management Guidelines

SBO ... Station Blackout

SG ... Steam Generator

SS ... Supporting Structure, component in COR Package

SSOX ... Steel Oxide

SV ... Safety Valve

A.8.7 Some references

R.O. Gaunt et al., MELCOR Computer Code Manuals, Vol.2 Reference Manuals, Version 1.8.6 September 2005, NUREG/CR6119, SAND 2005-5713, September 2005

Beraha D. at al., “ATLAS Postprocessor for analytical tool”, http://www.grs.de/arbeitsfelder/reaktorsicherheit/transienten_und_leckereignisse/atlas.html, (1998)

A.9 NRC “Kurchatov institute” calculations

A.9.1 SOCRAT integral and stand-alone

A.9.1.1 Scenario

Guillotine rupture of the main circulation pipeline’s cold leg near the reactor inlet is supposed to have occurred at zero moment of time, causing two-way primary coolant leakage through DN850. Loss of all AC sources coupled with diesel generators’ failure is also supposed to have taken place in parallel with the pipe rupture, resulting in the shutdown of all systems supplying water to the reactor (except the passive ECCS part). Reactor shuts down due to the loss of power. Furthermore, this accident is supposed to proceed without operator interference.

Water supply from ECCS tanks only is supposed. Actuation of ECCS tanks is insufficient to prevent core overheating, since the borated water from them gets spent in less than a minute. Thus, irretrievable losses of primary coolant cause the core to dry out and heat up, and the severe phase of accident to develop. Fission product release during core degradation is taken into account.

This sequence of events forms a severe accident scenario with the shortest time interval between the reactor shutdown and the ingress of molten corium into the lower part of the RPV. Consequently, it’s this scenario that provides for the highest possible temperature of corium contacting the RPV. In such a case, the task of preserving the RPV integrity is the most challenging.

The RPV is cooled down on the outside with water naturally circulating in the reactor pit.

A.9.1.2 Main Events

A major leak in one of the main circulation pipeline loops causes massive ingress of coolant into containment and drastic deterioration of primary circuit parameters. Reactor scram occurs. At the same time, main circulation pumps run out and turbine stop valve close due to power failure. Secondary makeup system switches off.

Milestone event	Time, s
Accident begins	0
ECCS tanks operate	5.5–54
Core heat-up starts	700
Fuel rod cladding fails	1050-1280
Intensive hydrogen generation in the core starts	1160
Fuel rod cladding meltdown starts	1250
Corium flowdown starts	1360
Total core dryout occurs	2340
Core materials start getting to the lower plenum	3450
Barrel melts through	4910

The initial phase of the accident is characterized by extremely large flow through the leak and rapid drop of primary pressure, which in about 20 seconds falls from its nominal value to the one close to the containment pressure. The pressurizer dries out in less than 10 seconds. Water in the core starts boiling virtually at once after the leak has occurred and as early as 5.5 seconds after the beginning of accident,

when water supply from ECCS tanks starts, the core already contains virtually no water. Then the core is refilled with water from ECCS tanks for several minutes.

Once the water level in the core gets below the top of heated part of fuel rods (approximately 12 minutes since the beginning of accident), the core starts to heat up. The code predicts fuel claddings to start failing from 1050th second. Fuel rod cladding meltdown starts at 1250 s. After fuel melting corium slumps into barrel. At time 4910 s barrel melts through and the corium relocates into lower plenum.

Total mass of slumping into lower plenum materials, tons:

UO_2	**ZrO_2**	**Zr**	**Steel**
85.9	17.1	15.6	69.84

A.9.1.3 Reactor nodalization scheme

From the hydraulic viewpoint, the computational reactor model distinguishes the following areas:

- inlet nozzles (mixing the coolant from loops with ECCS water);
- downcomer;
- lower area (between elliptical lower heads of RPV and barrel);
- fuel assembly supports (including the hydraulic profiling zone);
- support spacer grid;
- fuel assemblies;
- protective tubing, including barrel plates and penetrations;
- outlet nozzles.

Minimal possible number of ten sections was selected for representative description of fuel rods situated in the heated part of VVER-1000 core, due to low lengthwise heat conductivity of fuel rods and to high steam-quality gradient in some modes. Code requirements necessitate the same height-wise distribution to apply to all other structures (guide channels, CPS, baffle and barrel). Reactor model meeting these conditions is shown in Figure 1.

Reactor inlet chamber is presented by VESSEL_INLET element, which simulates the upper part of the annulus between the vessel and the barrel (inlet nozzles area). Lower plenum downcomer is presented by VESSEL_DOWN1 simulating the annulus between the vessel and the barrel from the cold nozzles area to the level of the core support spacer and VESSEL_DOWN2 simulating the cylindrical area between the vessel and the barrel below the core support spacer. VESSEL_LP simulates the volume limited by elliptical lower heads of the vessel and the barrel. Volume inside the barrel to the lowest core mark is simulated by VESSEL_LP-NKS and VESSEL_NKS (upper part of fuel assembly supports).

The core, together with unheated parts of fuel assemblies, is divided into three parallel vertical hydraulics flows (CORE_73, CORE_54 and CORE_36) presented by series-connected channels and chambers intended for hooking up the quasi-channels, which simulate coolant cross-flows. CORE_BYPASS simulates the area of coolant leaks from lower to upper reactor regions bypassing the core: baffle channels and leakages between barrel and baffle. CORE_NKBP is a zone of leaks through guide channels.

The code presents fuel rods as multilayer cylindrical structures simulating individual pellets and claddings with account of gaps between them. Respective temperature profile is calculated for eight points, evenly distributed along the radius: from zero to the external cladding surface.

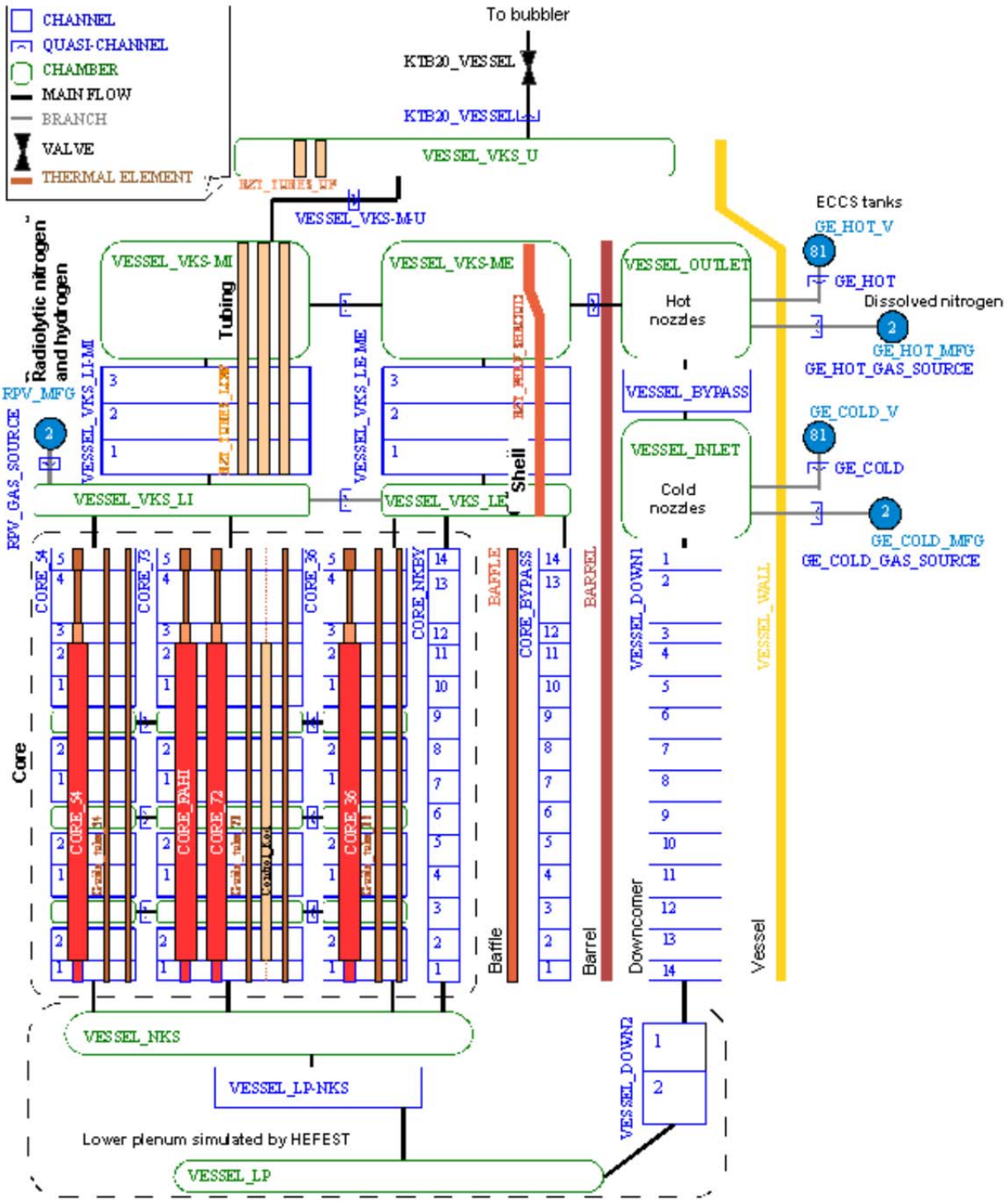

Figure 1: Reactor Nodalization Scheme

The reactivity control system is simulated by seven thermohydraulic elements. VESSEL_VKS-LI and VESSEL_VKS-LE account for coolant mixing just above the bottom plate of protective tubing. VESSEL_VKS-L-M* and VESSEL_VKS-M* simulate the volume between the bottom plate and the central plate of protective tubing, with VESSEL_VKS-L-M* situated at the inlet nozzles area level and VESSEL_VKS-M* at the outlet nozzles area level. VESSEL_VKS-U simulates the amount of coolant between the central plate of protective tubing and the reactor lid.

Reactor outlet chamber is presented by VESSEL_OUTLET, which simulates the zone between the perforated part of the barrel and the vessel (outlet nozzles area). VESSEL_VKS-ME-OUTLET orifice corresponds to the summary size of barrel perforations.

Water tanks are simulated with special boundary conditions (Type=81). Volume and temperature of water in the tank, as well as parameters of connecting pipes and cutoff and check valves are preset using special boundary condition parameters. GE_COLD_V boundary condition applies to two tanks supplying water to the reactor pressure chamber (in the cold nozzles area). GE_HOT_V boundary condition applies to two tanks supplying water to the reactor collecting chamber (in the hot nozzles area). Water tanks are connected to lower plenum and to reactivity control system via quasi-channels. “Water tank” boundary condition includes both direct and check valve. Hydraulic losses in pipes are converted into additional local losses.

SOKRAT/V1 software describes corium behaviour in the lower plenum using its HEFEST module. The mesh simulating lower plenum structures is divided into relatively small finite elements (Figure 2). This finite element mesh sets the boundaries of basic structural elements, such as the reactor vessel, the barrel and fuel assembly supports (Figure 3). To simulate the zone to be filled with incoming material, the mesh provides for sub-areas with respective boundaries (fill-in layers).

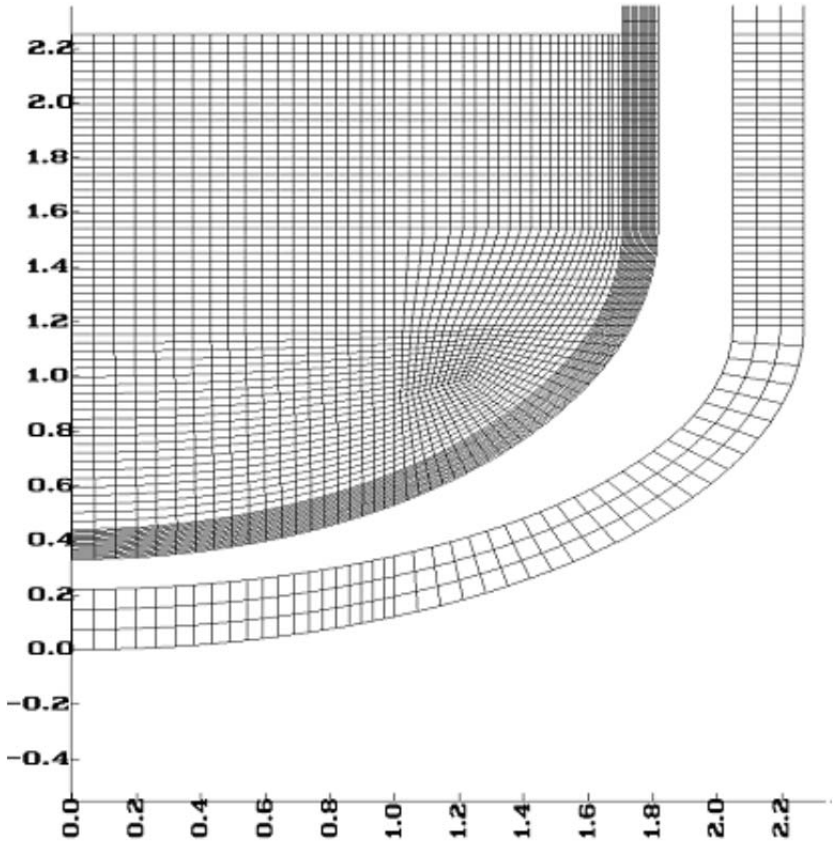

Figure 2: Mesh for simulation of initial stage of processes in the lower plenum

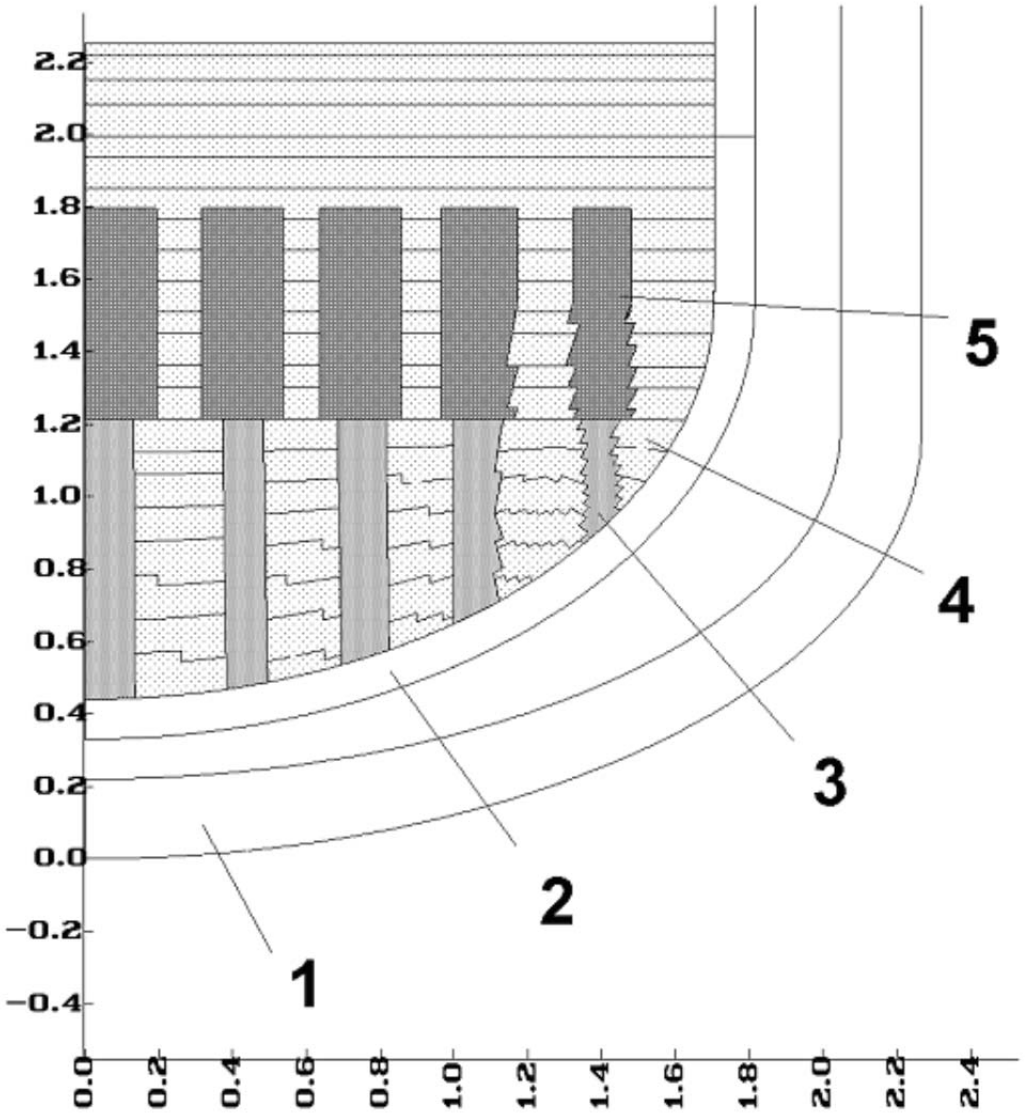

1 – RPV, 2 – barrel wall, 3 – steel supports,

4 – fill-in layers, 5 – tubular fuel assembly supports filled first of all

Figure 3 – Lower plenum divided into layers by receipt of incoming materials

Every mesh sub-area is linked to a specific material having its respective properties preset in the input data array. Division (into sub-areas) of the lower plenum containing fuel assembly supports accounts for the masses of steel structures it also contains. Lower plenum and RPV sub-areas were presented in form of ellipsoids mated with cylinders.

Pool-boiling heat removal from external surface of the reactor vessel is assumed.

Upper sub-area boundaries are subject to radiation boundary conditions accounting for heat exchange with the core. Convective heat exchange between corium and water inside the reactor vessel is also simulated.

Figure 4 shows the computational layout of an intact circulation loop. From hydraulic viewpoint, loop pipes are presented by cells (each from one to ten diameters long); horizontal and vertical tube sections consist of at least two cells before their vertical bend. Symmetrical model is assumed for the loops to avoid numeric effects. Steam generator is presented as three layers of tubes, in order to properly describe the heat transfer area reducing in proportion to the amount of boiling water. Considerable non-uniformity of water temperature in the primary tubing made it necessary to divide each tube into six lengthwise cells.

Each loop includes: hot leg, steam generator and cold leg with the main circulation pump. Computational model of the main circulation pipeline is the same for all loops; this makes it possible to minimize the nodalization impact on the results of their calculated behaviour.

The pressurizer is presented by a tank consisting of five cells necessary for proper level indication and a connecting pipe with horizontal and vertical sections.

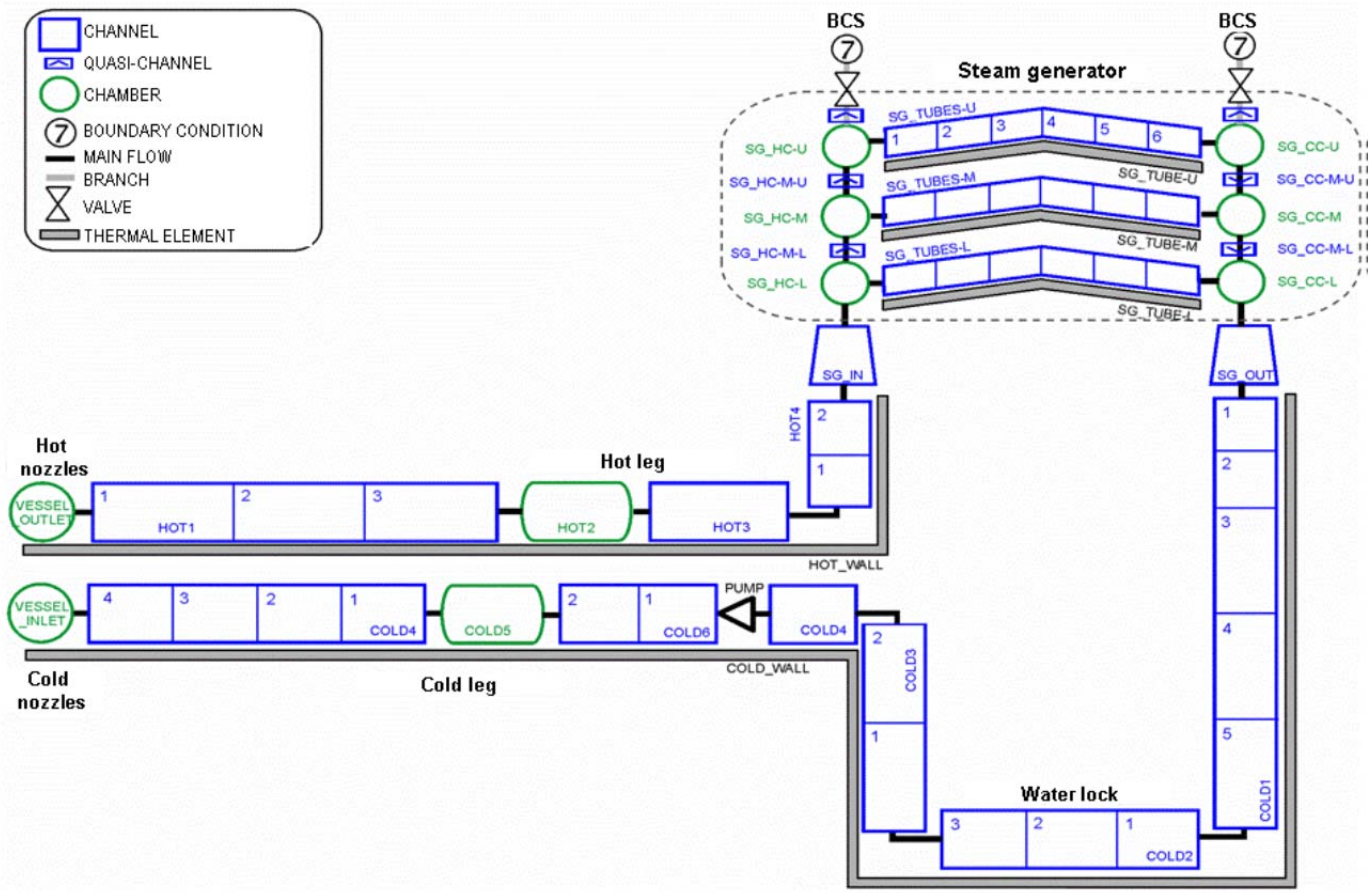

Figure 4 - Circulation loop nodalization

The leak nod is simulated by one or two (for two-way leakage) zero-length channels (quasi-channels) of respective diameters.

Figure 5 shows the computational layout of the steam generator. On secondary side, steam generator is presented by a model including recirculation and distinguishing the riser and the downcomer. Height-wise distribution of geometry volumes and heat-exchange surfaces is based on design dependences of heat-exchange surface and steam-water mixture volume on the level of steam-water mixture in the steam generator. Secondary circuit of the steam generator is divided into eleven height-wise areas and presented by eight volumes simulating:

- SG_FW chamber - feedwater supply zone;
- SG_DC channel - downcomer including channels containing no heat-exchange tubes and adjacent to steam generator shell on the inside together with corridors between tube banks;
- SG_BOTTOM channel - volume between the bottom generatrix of SG shell and the bottom row of the tube bundle;
- SG_RISER channel - tube bundle divided into four layers. Three lower layers are divided in accordance with the primary circuit: the bottom layer is a space containing 1580 heat-exchange tubes, the

intermediate layer contains 3140 tubes and the upper layer contains 6258 tubes. The fourth layer is a space between the upper row of heat-exchange tubes and the submerged perforated plate;

- SG_SEP channel - simulates the submerged perforated plate;
- SG_UP chamber - volume above the submerged perforated plate, where the main separation of steam-water mixture occurs;
- SG_TOP channel - upper steam volume of the steam generator;
- SG_STEAM chamber - SG steam discharge tubes and steam header.

Feedwater is supplied via SG_FW_IN quasi-channel subject to SG_MFW boundary condition. SG shell wall is presented by SG_WALL thermal element, including heat insulation, to account for external heat losses.

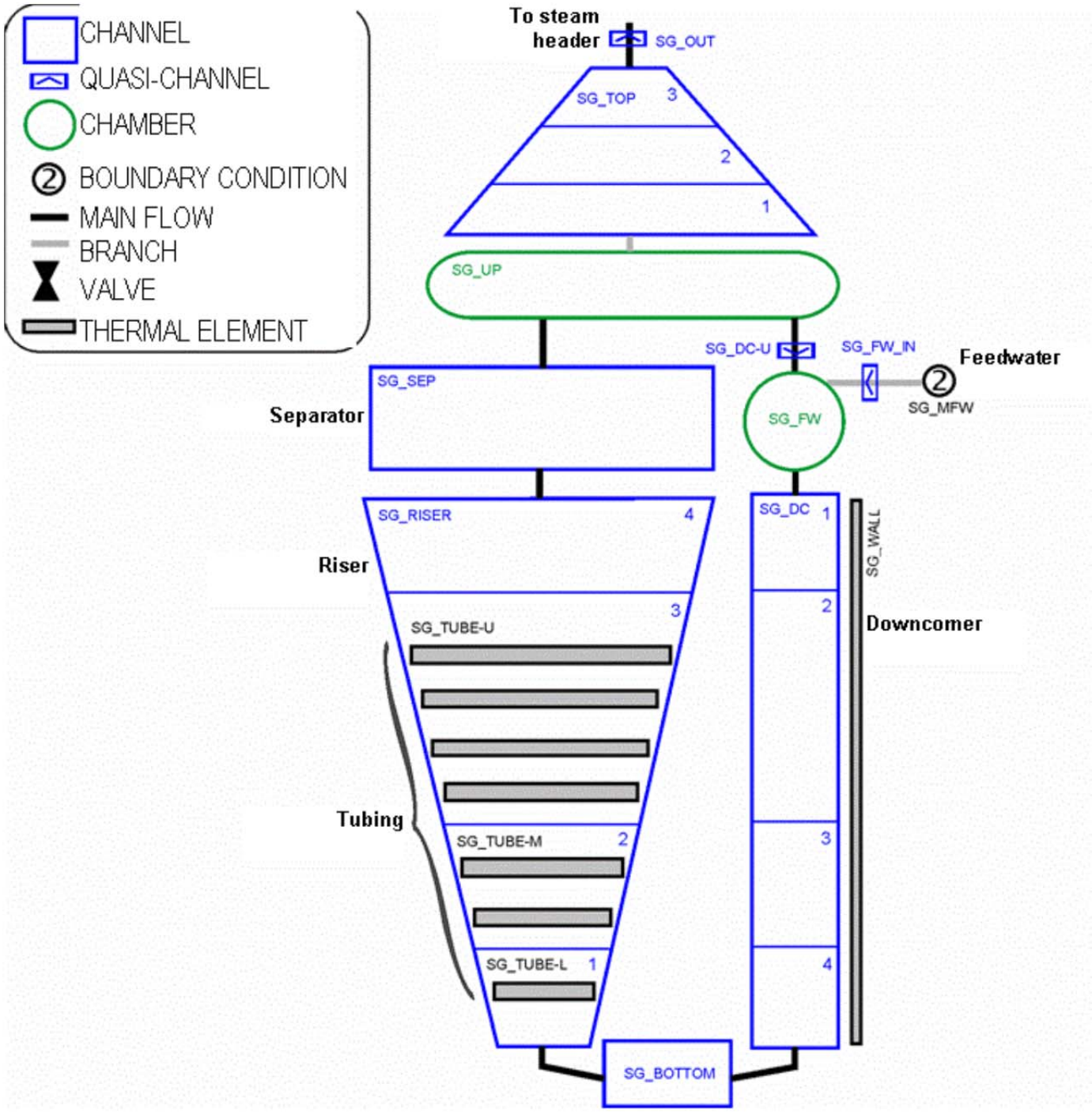

Figure 5 - Nodalized steam generator secondary side layout

A.9.1.4 Results overview

Two types of calculations were performed.

1. Integral calculation. Two stage corium slumping into lower plenum. The first stage: corium slumps into barrel. The second stage: Corium relocates into lower plenum after barrel melting. (Figure6, a)

2. Standalone calculation. Corium slumps into lower plenum directly as one portion with fixed averaged temperature. (Figure6, b)

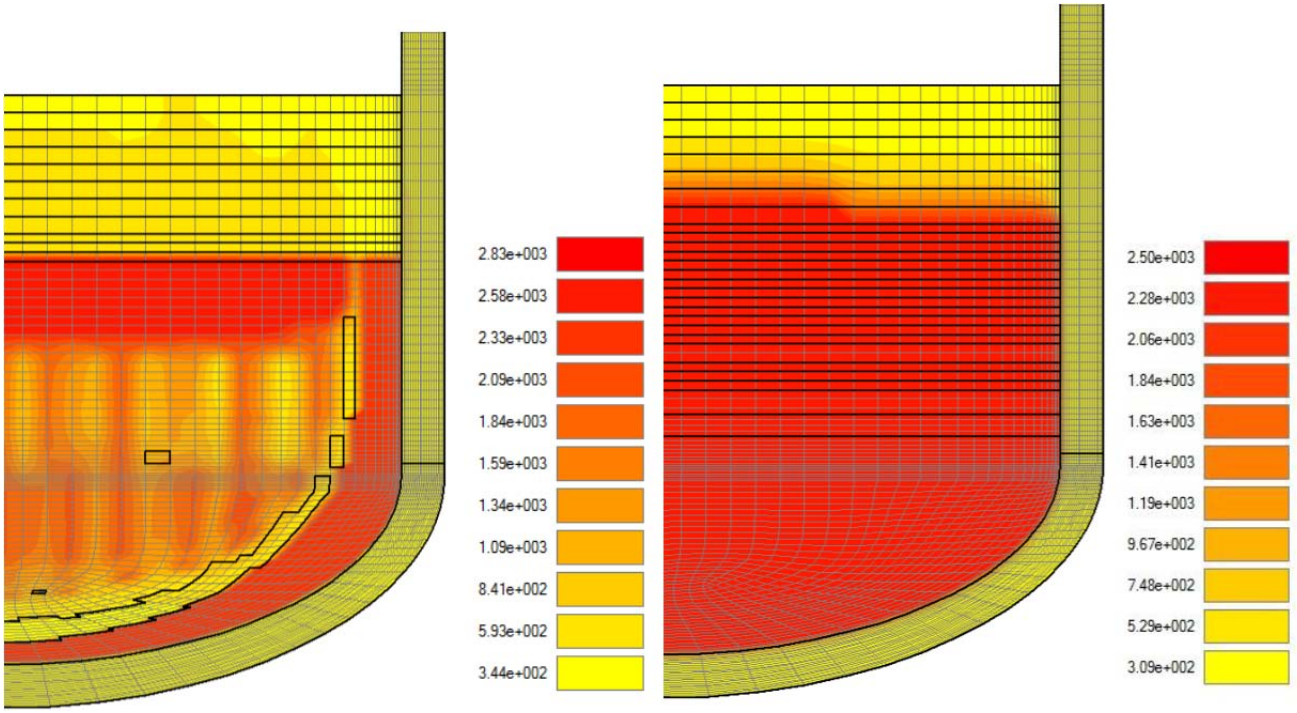

a) Integral calculation

Here you can see unmelted parts of barrel and FA supports

b) Standalone calculation

Simplifying of corium slumping

Figure 6 - Initial configuration. Temperature field (time=4910sec)

For the analysis of the case failure, we control two criteria:

1 Mechanical criterion. We calculate the residual wall thickness and the temperature distribution in the wall. Obtained results show that the critical values do not exceeded.

2 Thermal load on the wall. One of the most important values is the heat flux density on the outer wall. This value defines the margin to heat transfer crisis (HTC). HTC leads to the case failure.

Analyses of heat flux distribution allow defining complex thermal load on the wall. Very helpful is max of max heat flux distribution (Figure8). Every point of figure matches maximum heat flux value for all timestamps for current elevation.

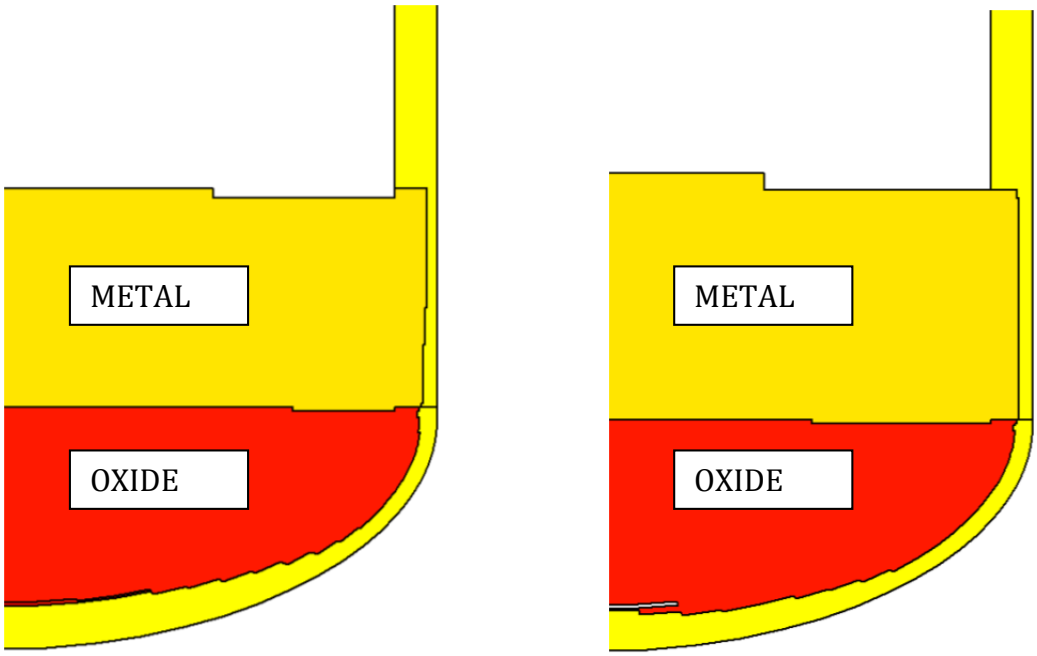

Integral calculation Standalone calculation

Figure 7 - Corium pool structure (time~10000 sec)

For the analysis of the case failure, we control two criteria:

1 Mechanical criterion. We calculate the residual wall thickness and the temperature distribution in the wall. Obtained results show that the critical values do not exceeded.

2 Thermal load on the wall. One of the most important values is the heat flux density on the outer wall. This value defines the margin to heat transfer crisis (HTC). HTC leads to the case failure.

Analysis of heat flux distribution allows defining complex thermal load on the wall. Very helpful is max of max heat flux distribution (Figure 8). Every point of figure matches maximum heat flux value for all timestamps for current elevation.

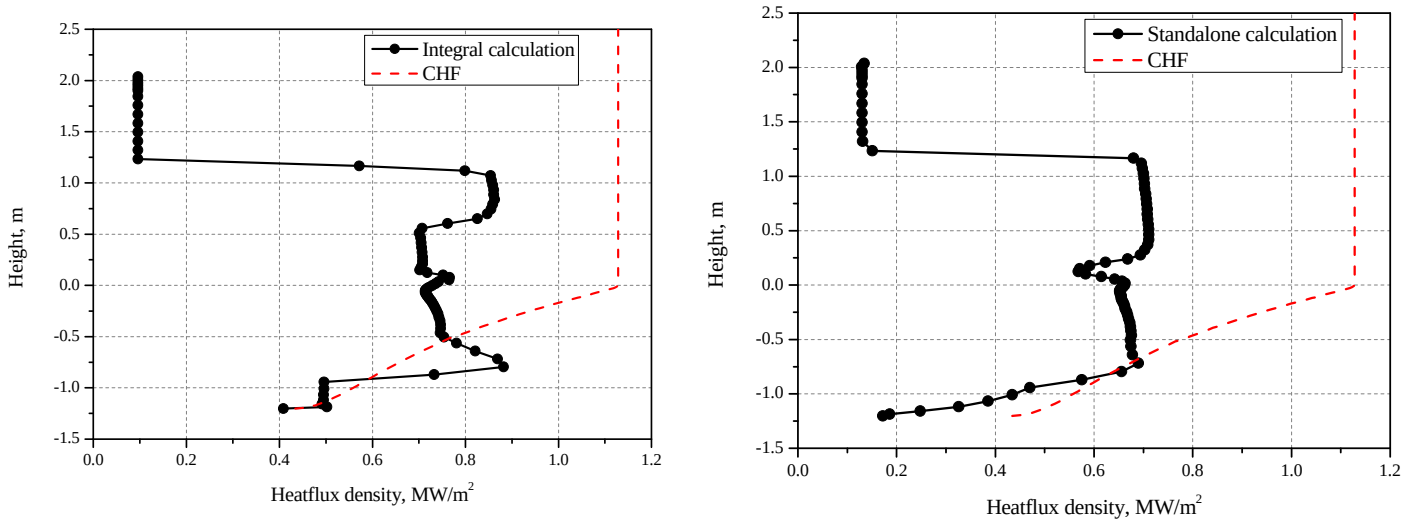

Integral calculation Standalone calculation

Figure 8 - Heatflux distribution on external wall (max of max)

A simplification of corium slumping increases the heat transfer surface. It means that the local thermal load on the wall is lower. Standalone calculation is an ideal case, when corium stratifies immediately (two layers with maximal possible heat transfer surface). Predicted results are not conservative. Comparison max of max heat flux distribution for integral and standalone calculations is presented on Figure 9.

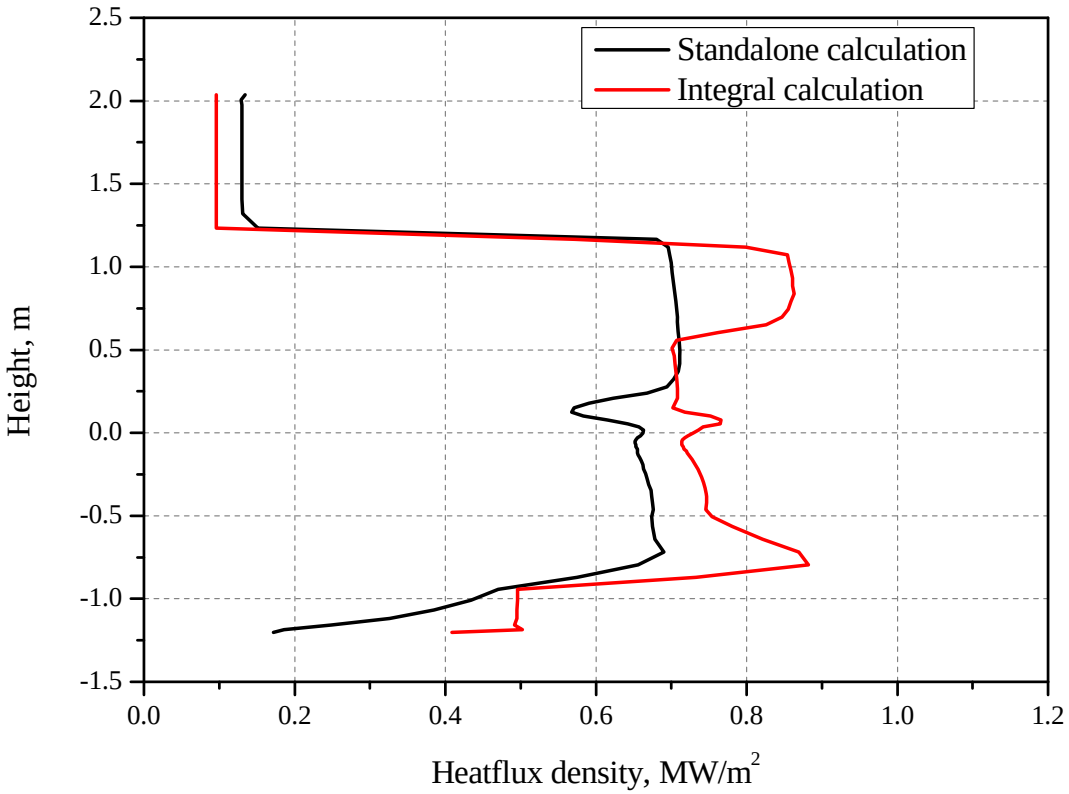

Figure 9 – Heat flux distribution on external wall (max of max)

There are two curve families of “Max of max” distribution, which describe wall burning by each layer. Heat flux profiles for standalone calculation at different moments are presented on Figure 10.

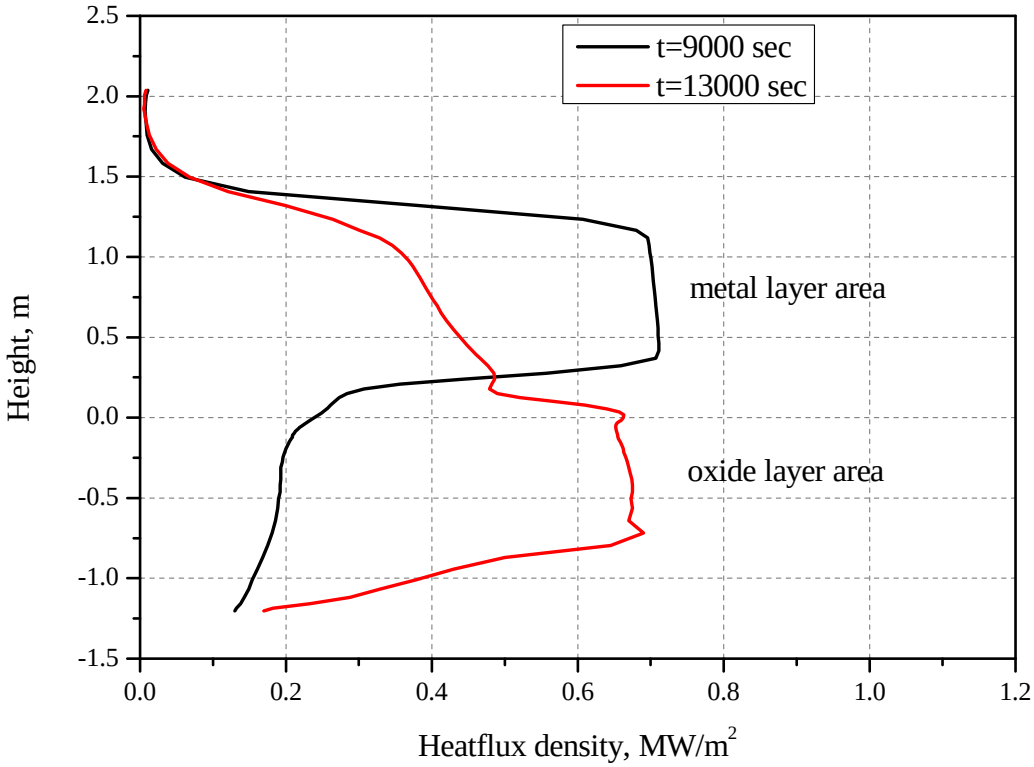

Figure 10 – Heat flux profiles at different moments. Standalone calculation

Corium-wall interaction is complex: it is characterized by two peaks of heat flux. And these peaks occur at different time. That's why max of max heat flux distribution is very helpful during margin to heat transfer crisis obtaining.

A.9.1.5 Conclusions

Complex numerical simulations were performed by SOCRAT – HEFEST code including deep sensitivity analysis. Simplifying of corium slumping leads to difference in transient state. However, no significant changes were obtained in steady values of slidewall heat flux. There are largest peaks on transient phase. The reason is unsteady melting of RPV wall by the metal layer.

During our calculations were detected:

- ✓ Critical dependence on stratification procedure (stratification sequence, layers, options)
- ✓ Critical dependence on metal layer thickness
- ✓ High dependence on initial conditions. Initial conditions could be optimized for this task.
- ✓ Mesh effects - insufficiently mesh density leads to result distortion

A.9.2 ASTEC V2.1 stand-alone

Hereafter is presented in-vessel melt corium retention calculations, which were performed by NRC "Kurchatov institute" with ASTEC V2.1 stand-alone. Modified by JRC-IET ASTEC input deck was used.

A.9.2.1 Basic calculation

ASTEC stand-alone basic calculation is based on the SOCRAT integral calculation results for .the severe accident with double-ended guillotine Large Break LOCA 850 mm and station blackout. The chronology of main events of the accident is represented in Table 1.

Table 1 - Chronology of main events of the accident

Event	Time, s
	Basic calculation (fission products release account, -20%)
Accident initiation	0
Injection of water from safety injection tanks	5.5-54
Core heat up onset	700
Fuel cladding burst	1050-1280
Hydrogen generation onset	1160
Fuel cladding melting onset	1250
Melt transfer onset	1360
Full core dryout	2340
Beginning of corium relocation into the core barrel	3450
Core barrel melting-through	4910
Reactor vessel failure	14000

Core barrel melting-through at time 4910 s. Right at this moment corium relocates into lower plenum instantly. Corium relocates to the lower plenum as one big portion.

Table 2 - Corium composition for basic calculation (with account of fission products release)

Material	Mass, t	Source
UO_2	85.9	CORE
Zr	15.6	CORE
ZrO_2	17.1	CORE
Steel	34.4	CORE
	12.2	elliptic part of barrel
	9.0	melted cylindrical part of barrel
	12.3	FA-supports
	1.94	support grid

It was assumed that corium relocates from the core to the lower plenum as one big slump with average temperature 2500 K. ASTEC calculation starts at 4910 s. This time corresponds to core barrel melting-

through. It is assumed, that corium is homogenous. Initial corium composition for this moment is presented in Table 2.

Eutectic point of the UO_2 and ZrO_2 in the calculation was 2850 K.

Detailed phase separation model was used: SEPA_ACT = 1

Number of corium layers allowed: up to 3.

Support plate fictive temperature for heat losses due to irradiation: 1700 K.

External water cooling was simulated by setting heat exchange coefficient H = 10000 $W/m^2/s$ on the external surface of the reactor pressure vessel.

Decay heat time dependence was used with fission products release account (Table 3).

The calculation continues till 30000s.

Table 3 - Decay heat time dependence

Time from the accident start, s	Decay heat, Wt (per 1 kg of UO_2)
	Basic calculation (account of fission products release, -20%)
1000	585.28
2000	487.52
3000	433.92
4000	397.68
4910	373.44
5000	371.04
6000	350
7000	333.28
8000	319.12
9000	307.52
10000	297.28
20000	240.08
30000	215.12
40000	200.4

A.9.2.2 Basic calculation results

There are presented below the temperature field figures.

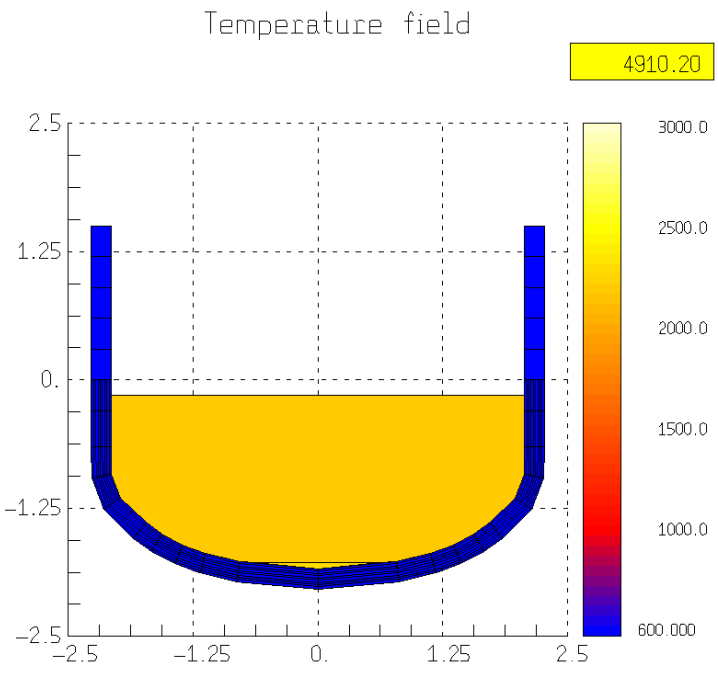

Figure 1. Temperature field at 4910 s

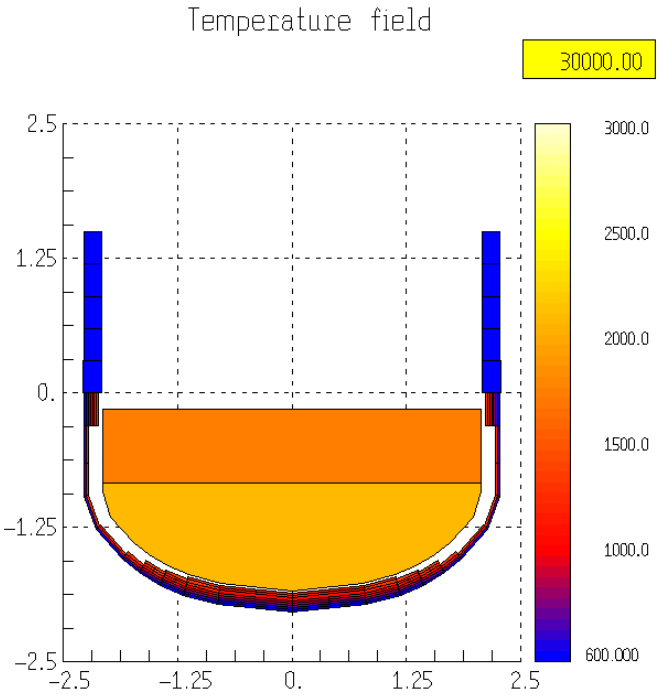

Figure 2. Temperature field at 30000 s

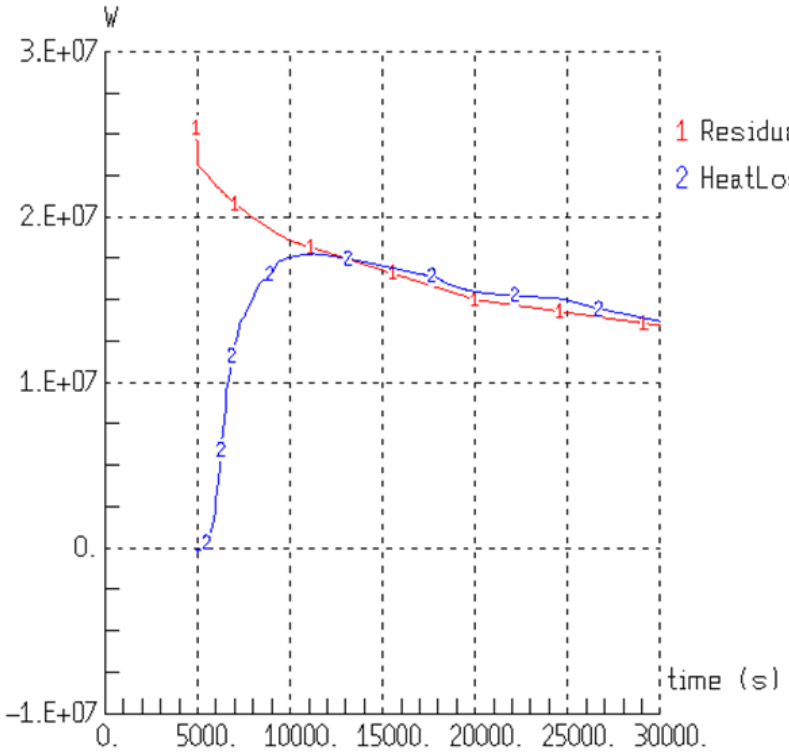

Figure 3. Power balance in the lower plenum

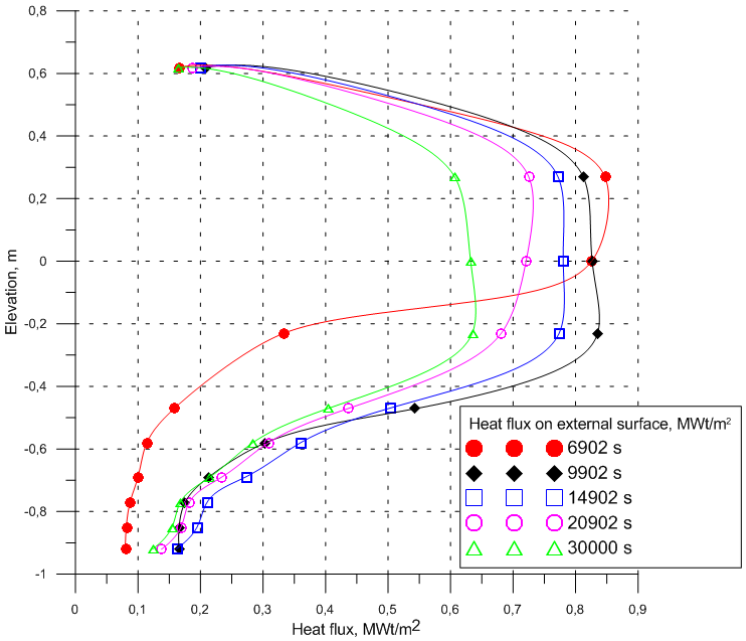

Figure 4. Heat flux from external surface to water at different times

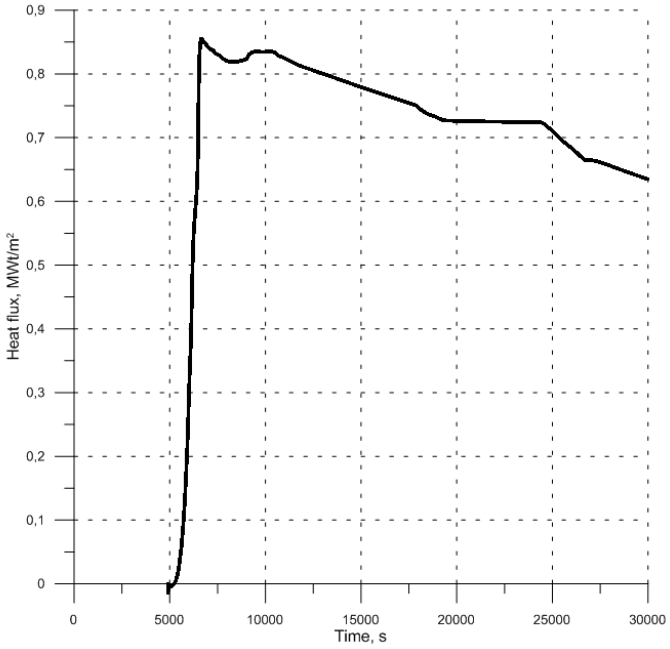

Figure 5. Full time evolution of the max heat flux among all external surface nodes

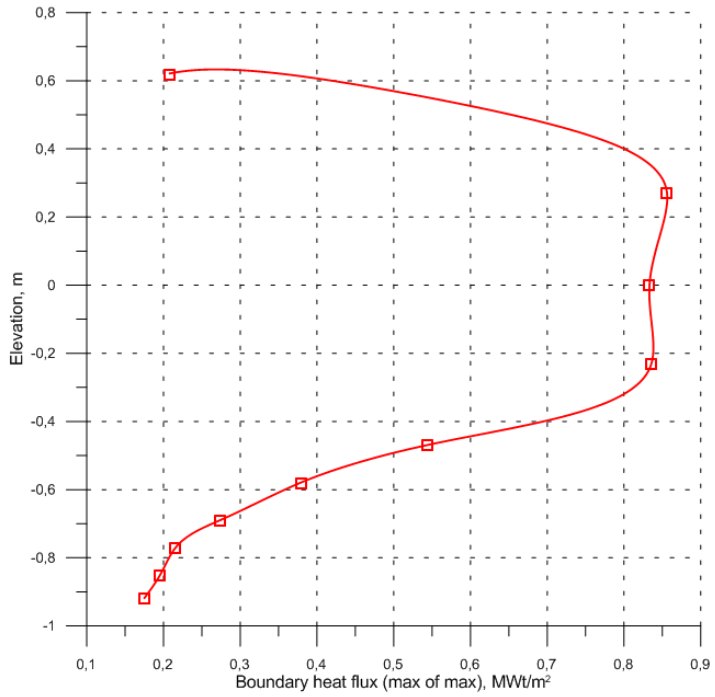

Figure 6. Minimal residual vessel thickness

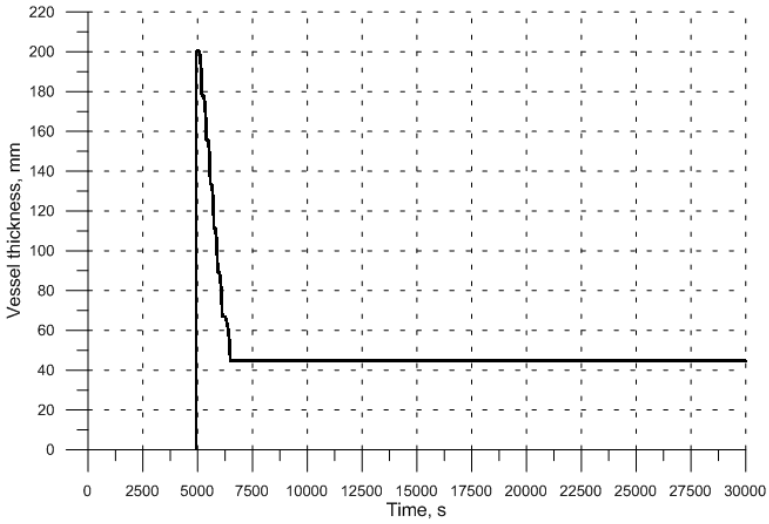

Figure 7. Boundary heat flux (max of max)

A.9.2.3 Conclusions

In the basic calculation the maximal heat flux value is 0.855 MW/m². It occurs at 6674 s and corresponds to 9 axis mesh (elevation is 0.27 m). Residual reactor pressure vessel thickness is 0.0444 m (2 radial meshes left). Vessel failure doesn't occur till the end of the calculation.

A.9.3 Sensitivity studies. Steel mass

Some additional calculations were performed. The varying parameter was steel mass: 20 t, 40 t, 50 t, 80 t, 100 t. Other calculation options are fully complied with basic calculation.

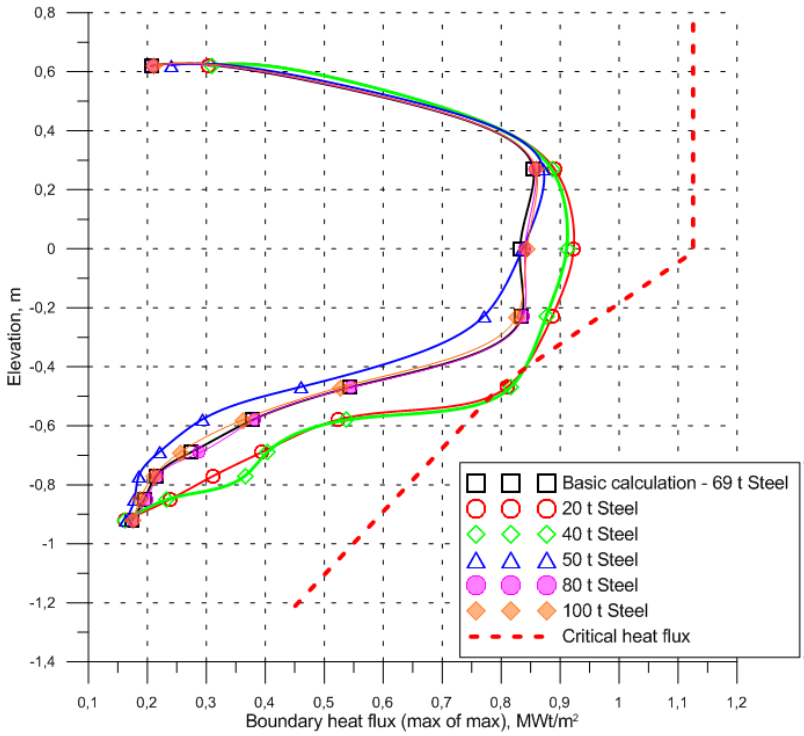

Figure 8. Boundary heat flux (max of max)

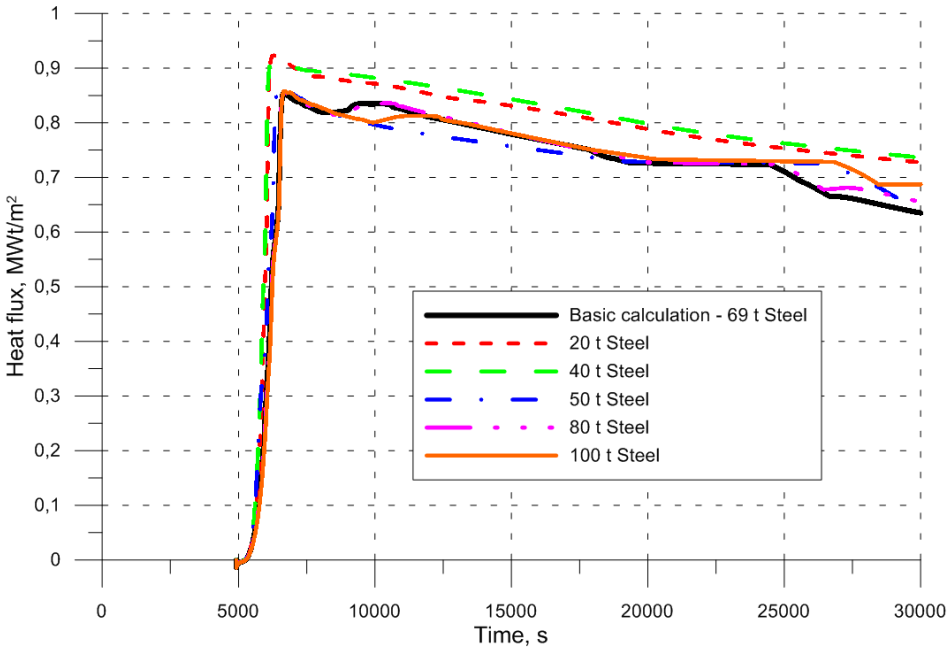

Figure 9. Full time evolution of the max heat flux among all external surface nodes

According to calculations steel mass increasing doesn't affect significantly the results. But steel mass reduction leads to slight increasing of max of max heat flux: from 0.855 MW/m^2 in basic calculation with 69 t of steel to 0.923 MW/m^2 (occurs at 6282 s) and 0.911 MW/m^2 (occurs at 6236 s) in calculations with 20 t and 40 t of steel, respectively. Nevertheless this slight increasing is quite enough for vessel failure: heat flux from external surface to water exceeds the critical heat flux. But only for one axial mesh (-0.47 m).

A.9.4 Sensitivity studies. Initial corium temperature

Also calculations with different initial corium temperature were performed: Tcorium = 2200 K and 2800 K (initial corium temperature in basic calculation was 2500 K). Other options are fully complied with basic calculation.

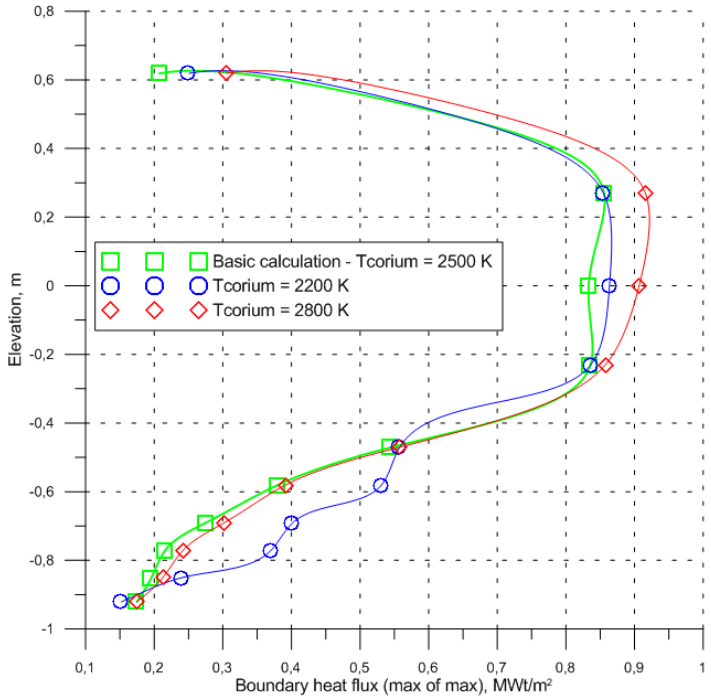

Figure 10. Boundary heat flux (max of max)

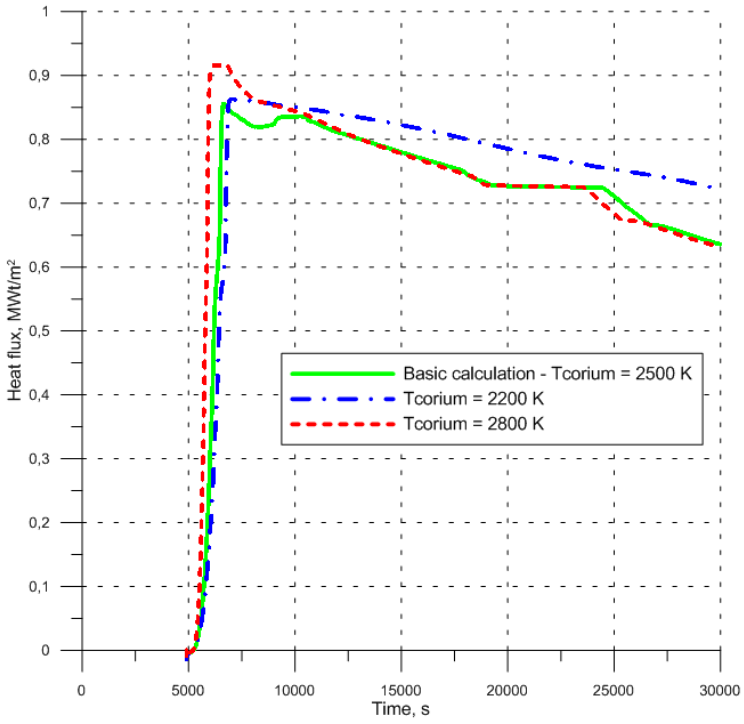

Figure 11. Full time evolution of the max heat flux among all external surface nodes

Initial corium temperature doesn't affect much the results. In all calculations vessel failure doesn't occur. Max of max heat flux slightly increases, but doesn't exceed the critical one. Minimal residual vessel thickness is 0.0444 m.

A.9.5 Sensitivity studies. Phase separation model

There are three phase separation models in ASTEC: without separation, detailed and simple phase separation model. Using of simple model leads to unexpected results.

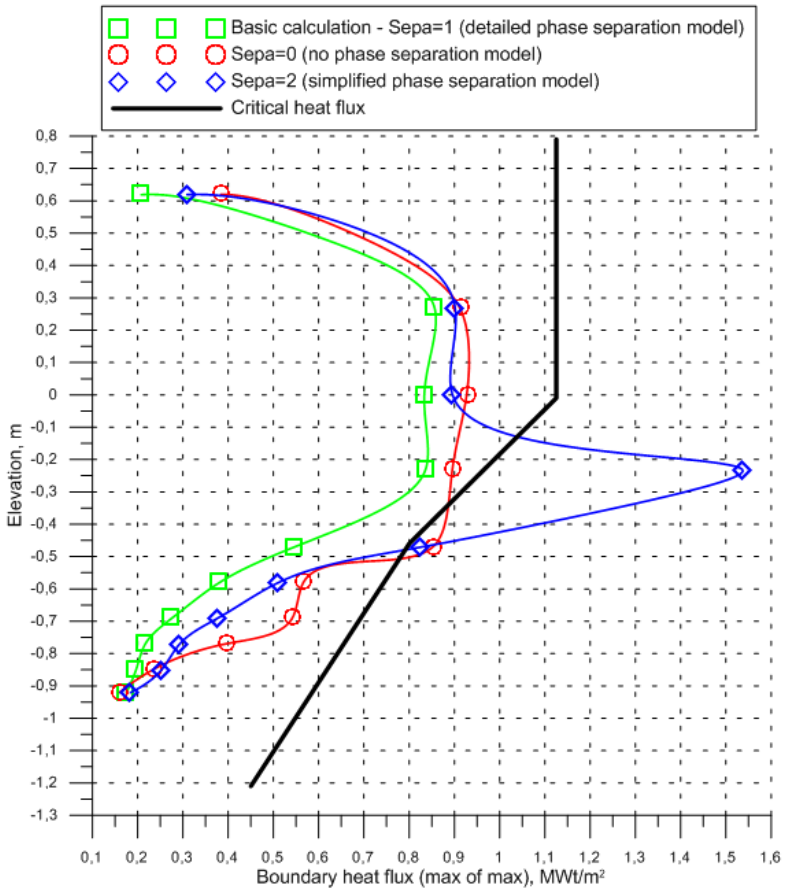

Figure 12. Boundary heat flux (max of max)

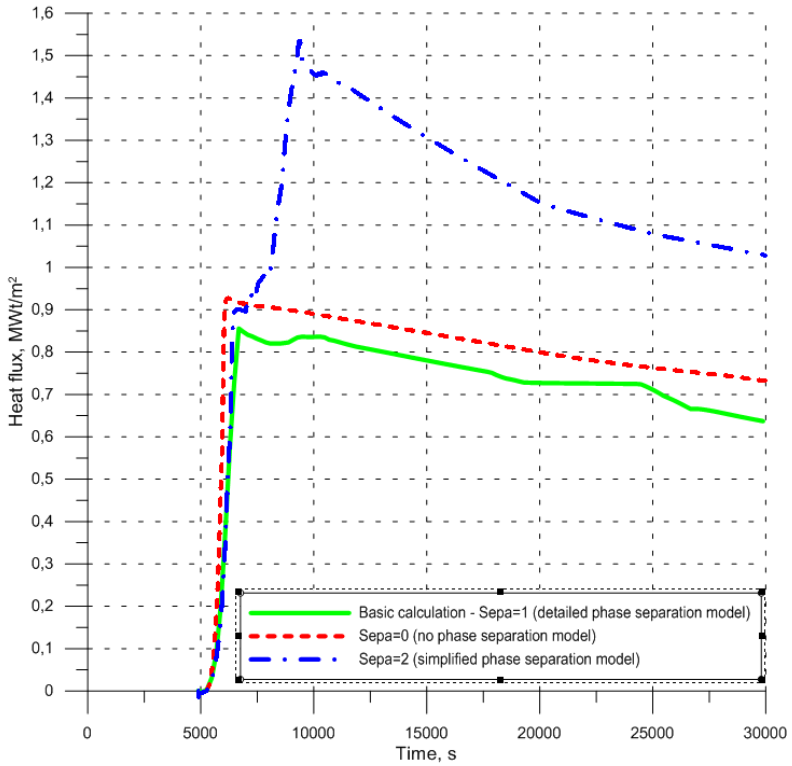

Figure 13. Full time evolution of the max heat flux among all external surface nodes

Extremely large heat flux for Sepa=2 calculation corresponds to -0.27 m elevation (7th external surface axial mesh). At this height vessel thickness decreased to 0.022 m (radial meshes left).

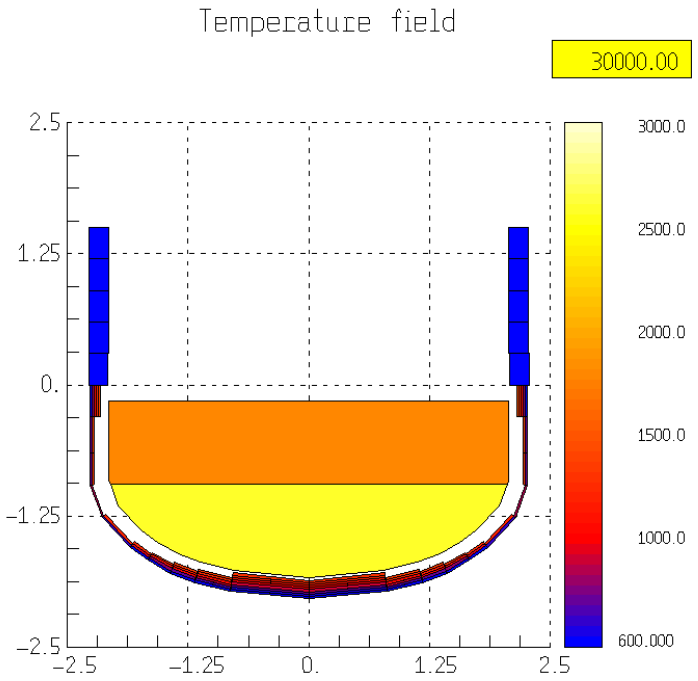

Figure 14. Temperature field at 30000 s

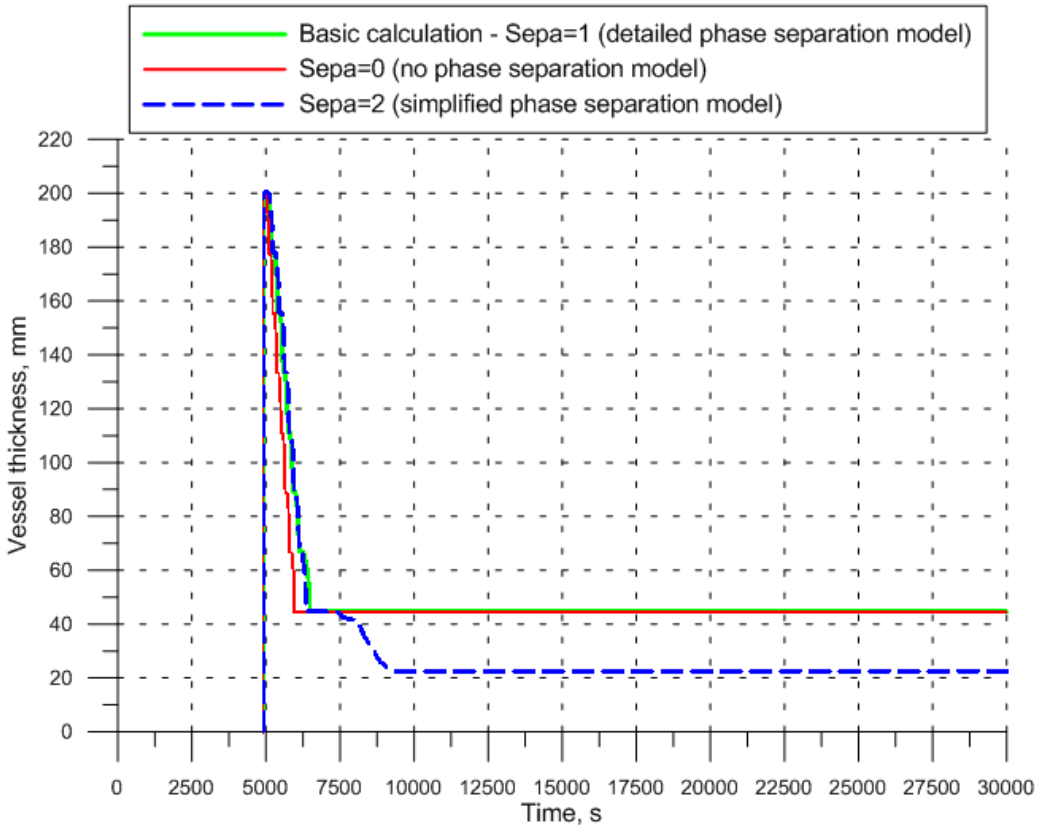

Figure 15. Minimal residual vessel thickness

A.9.6 Sensitivity Studies' Conclusions

Phase separation model change significantly affects the results. Max heat flux increases almost twice: from 0.855 MW/m^2 at 6674 s in basic calculation (Sepa = 1) to 1.535 MW/m^2 at 9398 s (Sepa=2). Oxide layer temperature increases too. Minimal residual vessel thickness decreases to 0.022 m.

A.9.7 Future needs

Calculations

A new SOCRAT version will be released soon. It will better describe the heat exchange processes during in-vessel retention. Also it will be more consistent with the available experimental data. Therefore, it will be useful to perform the calculations with new SOCRAT version.

It's necessary to check and analyse carefully balances, initial and boundary conditions, etc., to understand discrepancies between available calculations with different codes, which were used for the benchmark.

For codes with low mesh density (especially, for ASTEC) it's necessary to perform sensitivity calculations with different mesh to clarify how mesh affects the results. It's possible to set in SOCRAT the same mesh, which was set in ASTEC. It is expected, that new SOCRAT results will be differ from old ones with large number of meshes.

During benchmark it was found that initial conditions for calculations are quite tough\conservative (initial corium temperature, uranium dioxide and steel mass). It's necessary to reduce conservatism that will help to increase the in-vessel retention possibility.

Experiments

It's definitely necessary to get experimental data on critical heat flux for VVER-1000 reactor pressure vessel. It's impossible to truly substantiate the possibility of in-vessel melt corium retention without such data.

Also it's necessary to carry out new experiments on interface oxide melt-metal melt composition and interaction processes at this interface.

It's necessary to obtain new experimental data on the melts density temperature dependence. Such data will allow defining melts temperature coefficients of volume expansion and the intensity of convection in metallic phase.

Liquidus temperature for the metallic melt was obtained from the thermodynamic model. Parameters of this model were evaluated on the basis of double phase diagrams. Liquidus temperature experimental investigation will clarify parameters values and will verify thermodynamic model.

Vessel steel dissolution in molten metallic corium phase has never been studied experimentally. Dissolution kinetics experimental data will allow to get dissolution process constants. Prediction possibilities will be extended.

A.10 JRC ASTEC v2.0 stand-alone

A.10.1 First calculations

The initial conditions to run ASTEC/ICARE stand-alone calculations were extracted from the SOCRAT integral calculation and distributed to all participants. These initial conditions included:

- Melt history: mass, temperature and composition of corium arriving into elliptical part of the barrel
- Decay heat

The first calculations were based on the assumption described hereunder, but before proceeding further on with the reading, it is important to know that some assumptions were misunderstood:

- The corium history was referring to the corium slumping into the barrel, not into the lower head directly. Most of the participants didn't realize that and calculated the slump directly into the lower head.
- On the lower head there are some steel structures that were not taken into account by all participants and would count for additional material when melting.

Said this, the assumptions for the first calculations were the following:

Table 1 Corium history provided by KI for the 1st calculations

Time, s	Mass of UO_2, t	Mass of ZrO_2, t	Mass of Zr, t	Mass of SS, t	Total mass, t	Temperature, °K
3251.5	0	0	0	0.1108	0.1108	1851
3280.5	0	0	0	1.0426	1.0426	1874
3509.6	0.7874	0.2769	0.694	1.0527	2.811	2745
3531.5	15.643	6.0004	8.8717	3.0852	33.6003	2787
3540.5	77.5435	12.434	8.9465	9.5945	108.519	2846
3548	81.4016	12.518	8.9469	10.7901	113.657	2853
3954.4	81.6538	13.0472	10.5921	14.6109	119.904	2960
3957.4	81.7304	13.218	11.179	15.9999	122.127	2964
4703.3	81.7304	13.218	11.179	16.1732	122.301	2885
4709	82.7726	13.5081	11.786	20.3003	128.367	2891

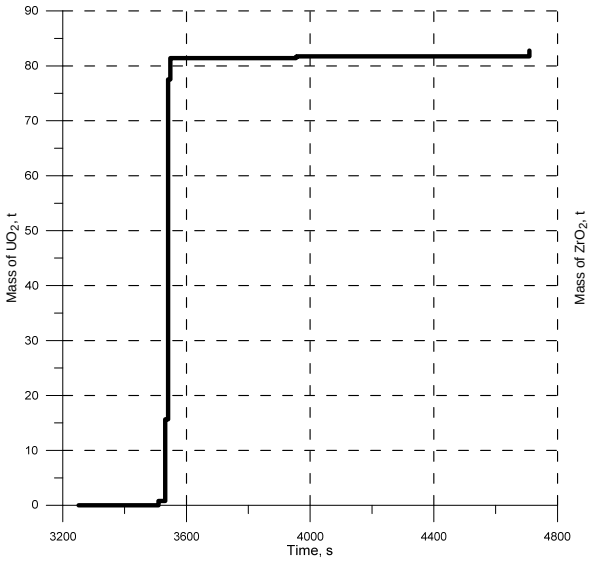

Figure 1: UO_2 accumulation in lower plenum

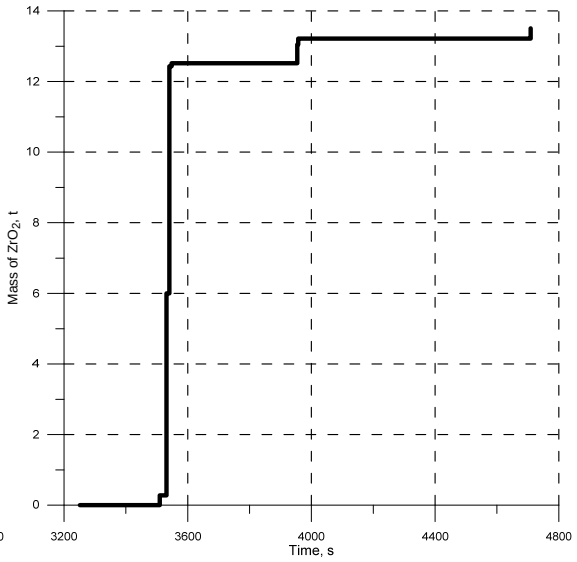

Figure 2: ZrO_2 accumulation in lower plenum

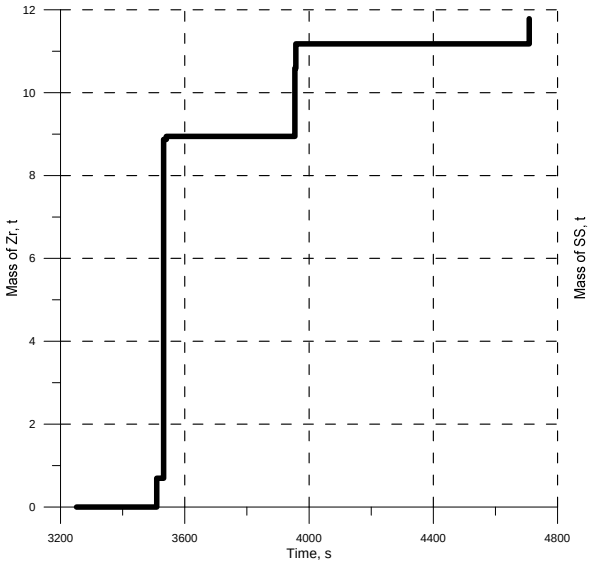

Figure 3: Zr accumulation in lower plenum

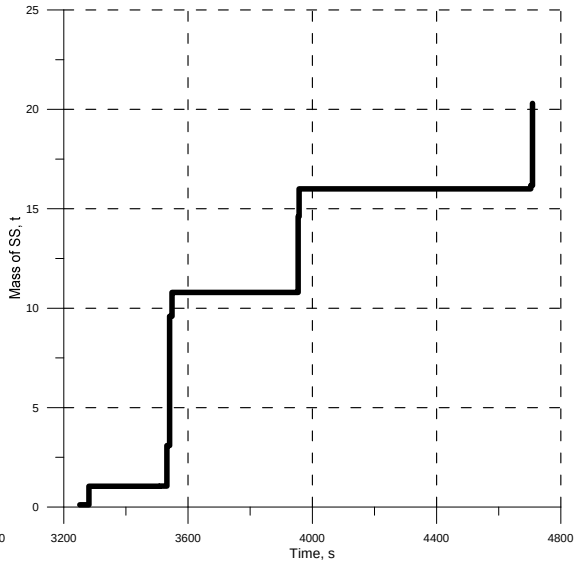

Figure 4: SS accumulation in lower plenum

Table 2: Decay heat time dependence, which was used in calculation

Time, s	Decay heat, Wt (per 1 kg of UO_2)
1000	731.6
2000	609.4
3000	542.4
4000	497.1
5000	463.8
6000	437.5
7000	416.6
8000	398.9
9000	384.4
10000	371.6
20000	300.1
30000	268.9
40000	250.5
50000	237.7
60000	227.8
70000	218.9
80000	211.2
90000	203
100000	194.9
200000	166.5
300000	146.3
400000	128.6

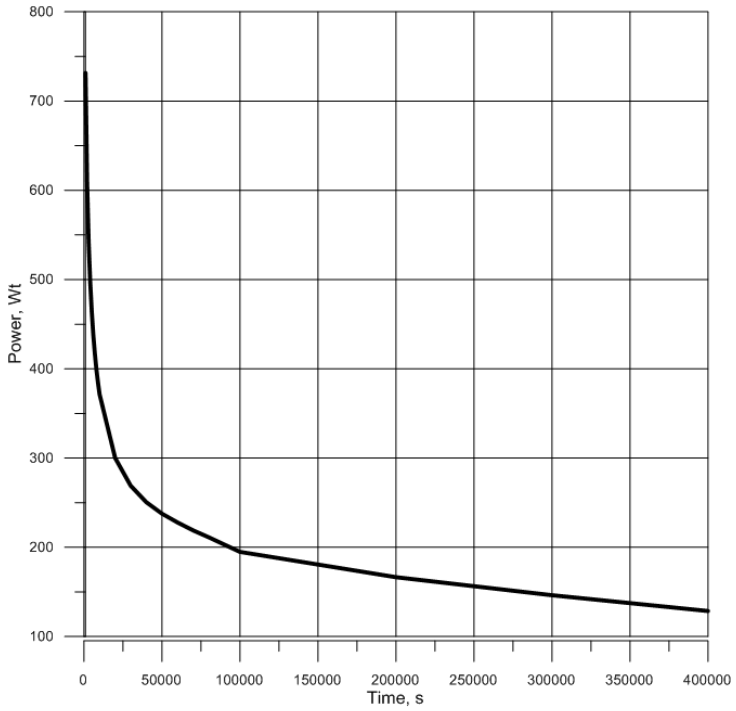

Figure 5: Decay heat time dependence

The main initial assumptions were the following:

- To simplify the calculation, one magma injection was used, with a total melt according to Table 1.
- The corium slump temperature was initially set to 2960. K
- The materials melting points were the default ones: UO_2/ZrO_2 TBEG 2800. TEND 2850.
- the lower head was supposed to be dry
- RPV pressure 10 bars

The RPV rupture criteria took into consideration were two:

- Simple approach based on temperature and mechanical stress
- A more detailed approach called LOHEY

The LOHEY, developed by IBRAE, was already available in past ICARE2 versions and can be used for both hemispherical and half-ellipsoidal lower heads. When the original LOHEY model is selected, it is necessary for the users to define precisely themselves the creep properties of the stainless steel alloy to be considered in the ICARE2 simulation (this requires the definition of a dedicated CREE sub-blockdata within the LOHEY rubric). All the properties which were assigned in this CREE sub-blockdata corresponded to the SA533B1 carbon steel used in the LHF tests steel (prototype material for US PWRs).

The LOHEY model is very sensitive to the pressure difference between the inside and the outside of the RPV, predicting sometimes rupture.

The very first calculation was performed in order to compare the three ASTEC corium models:

- with a simple no phase separation model, that is the simplest case, one dense corium layer will be formed, no differentiation between oxidic and metallic layers;
- a model based just on material density and using a user-defined time constant. This model allows the separation of corium in two (or three) layers predominantly constituted of oxides or metals, irrespective of any thermodynamic equilibrium between those layers;
- a detailed phase separation model, in which the phases migrate themselves into layered structures, the dynamics of which depends on their relative density and related dynamic effects. The overall process of phase separation is thus the result of interaction of thermochemical separation of phases and hydrodynamic formation of layered structures.

A comparison of the three models is shown in Figure 6, where the internal heat flux (between the corium and the lower heat) is depicted in stabilized conditions. The detailed 2 layers model predicted RPV rupture, so the HF shown in Figure 6 is not stabilized, but the one corresponding to the failure time.

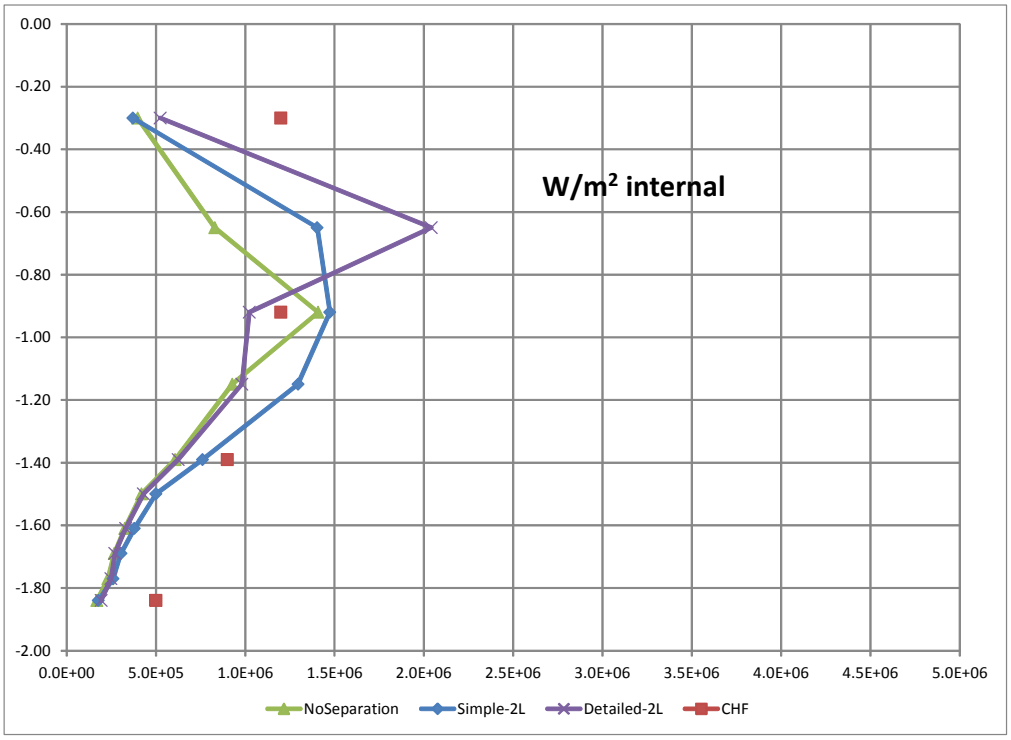

Figure 6: Decay heat time dependence

The detailed phase separation model showed to be very sensitive to the melting point of the eutectic UO_2-ZRO_2, presenting a layer inversion with a lower melting point of 2550. K (Tbeg = 2550.K) , Figure 7.

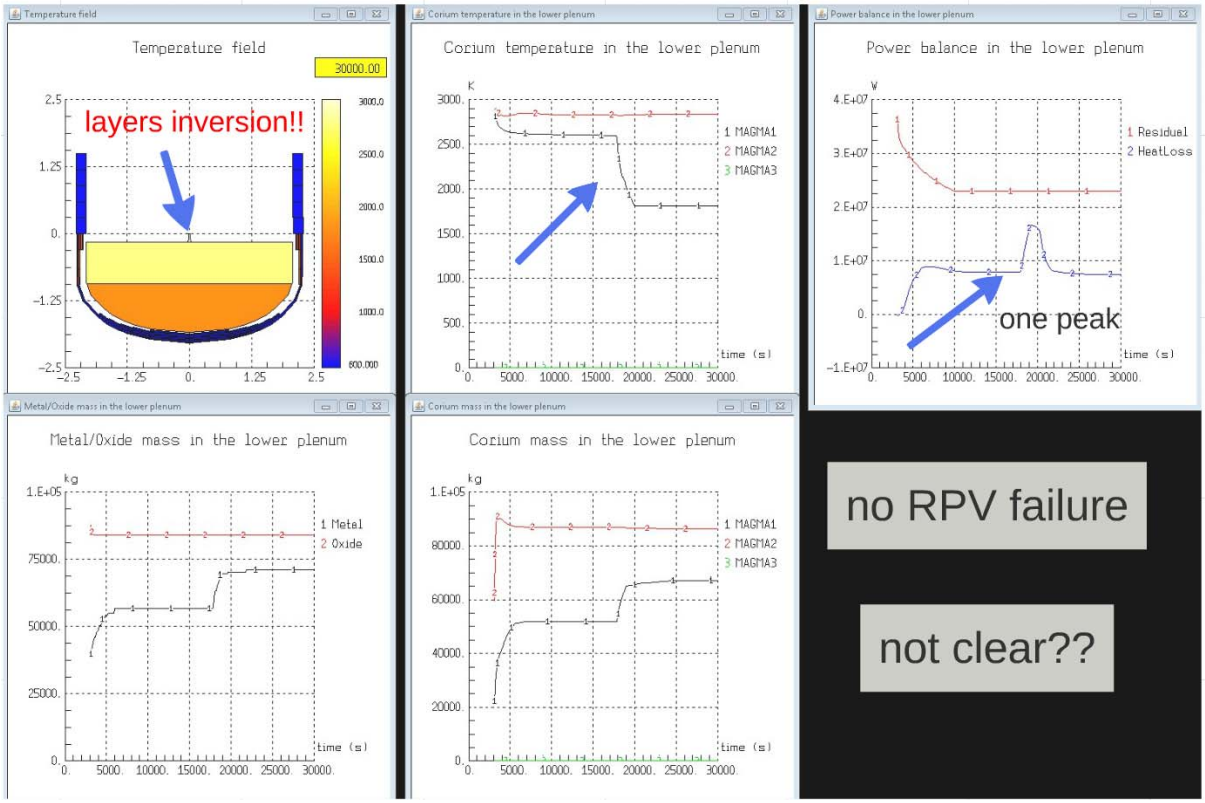

Figure 7: Calculation with a melting point of the eutectic UO_2-ZrO_2 of 2550 K

After these first preliminary calculations, whose intention was to create a first base case study, some rough sensitivity analysis was carried out on the following topics, just to observe how much they could affect the results:

- ZrO_2 / Zr proportion (oxidation degree)
- Material melting temperature
- Magma temperature
- Slump time constant
- Power decay
- Heat losses radiation upper plate
- Water and pressure

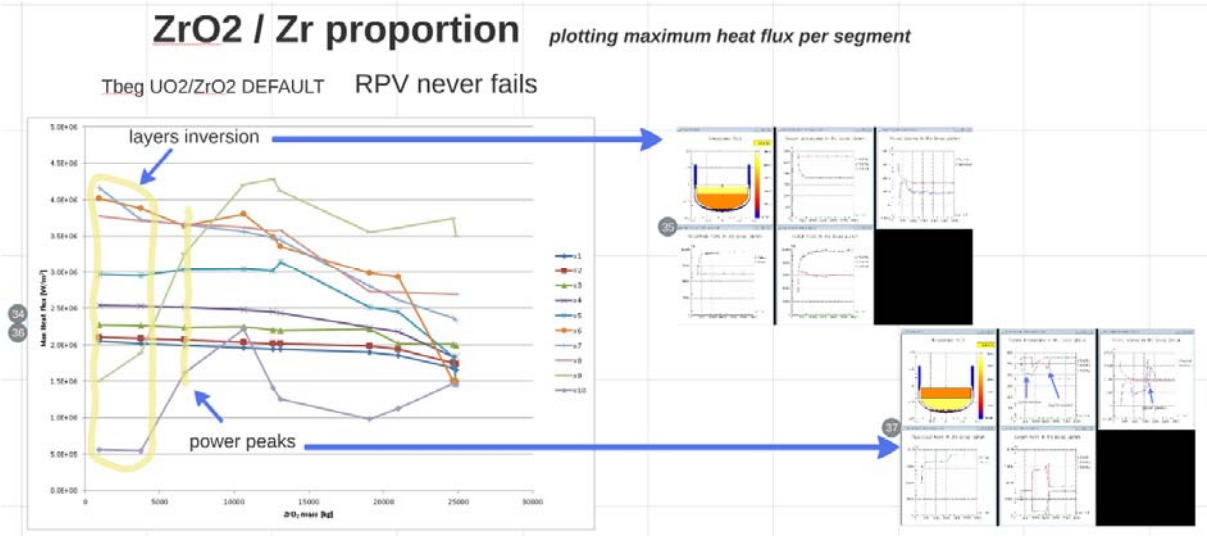

Figure 8: Calculation changing the ZrO_2 / Zr proportion (oxidation degree)

ZrO_2 / Zr proportion (oxidation degree), Figure 8, revealed to be very important, giving place to layer inversion and power peaks.

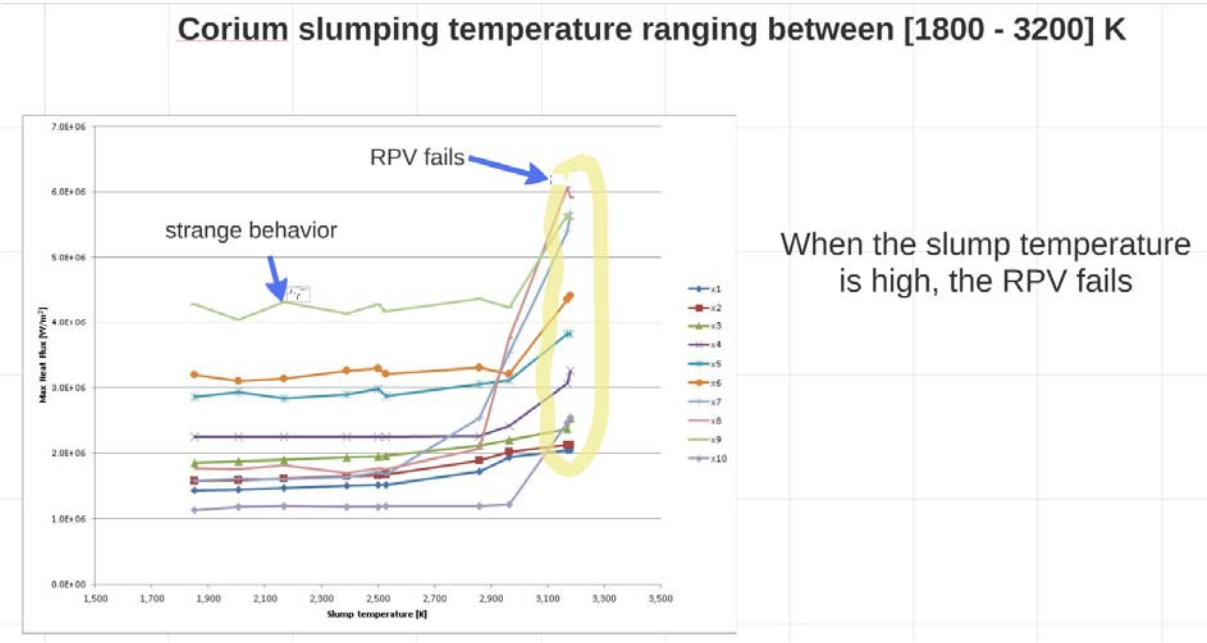

Figure 9: Calculation changing the corium slumping temperature

The temperature of the slumping corium is also very important: when the corium is overheated (temperature above the liquidus point) the heat flux is much higher and can lead to RPV failure.

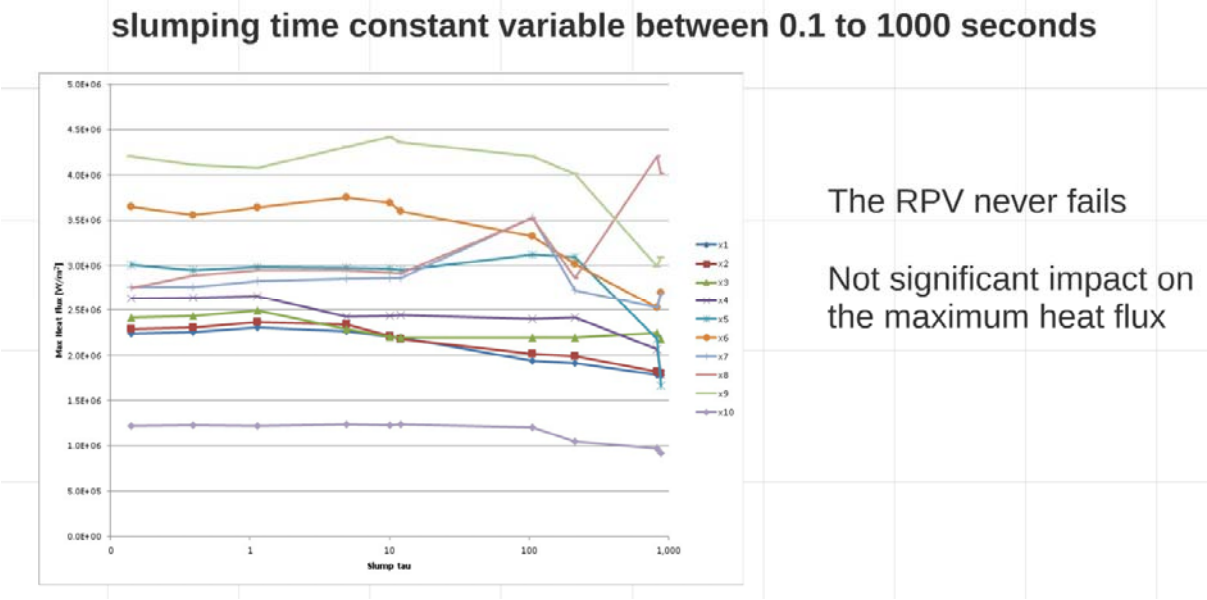

Figure 10: Calculation changing the slumping time constant

This is a time constant related to the slumping model of ASTEC; it's more a numerical than physical variable and doesn't affect much the results.

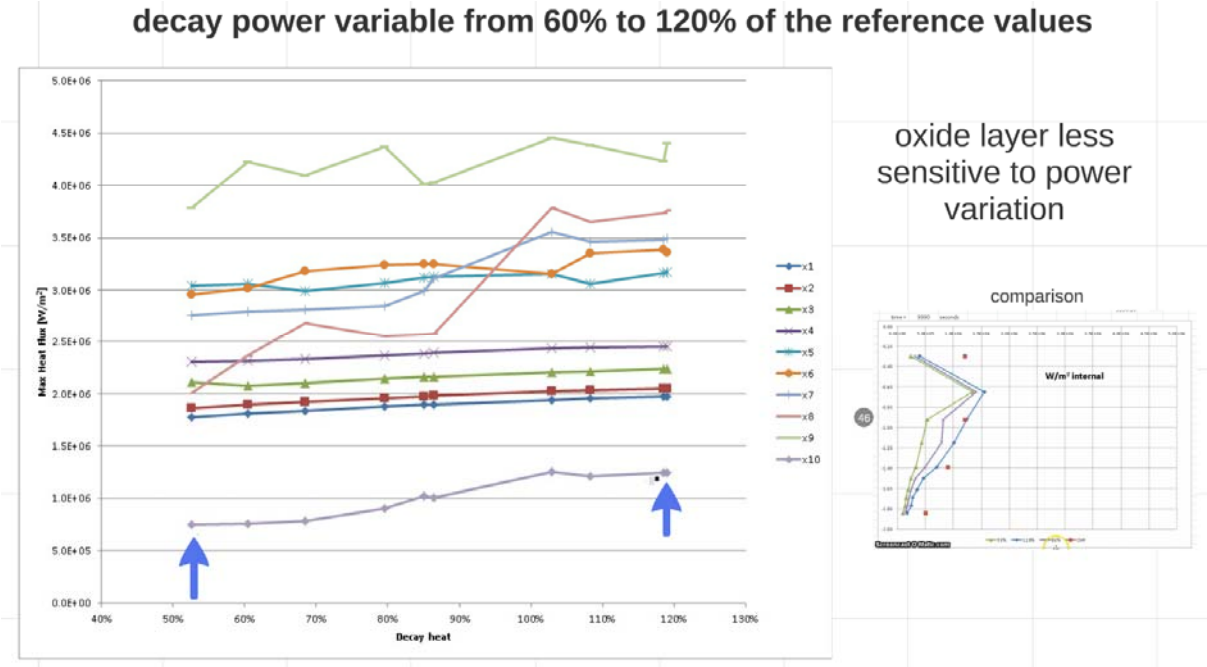

Figure 11: Calculation changing the decay power

The decay power obviously affects the results, but once the corium is stabilized, the maximum heat flux doesn't change much. A possible explanation to that is because all the power is assumed to be generated in the oxidic layer and the thin metallic layer above it generates a focusing effect.

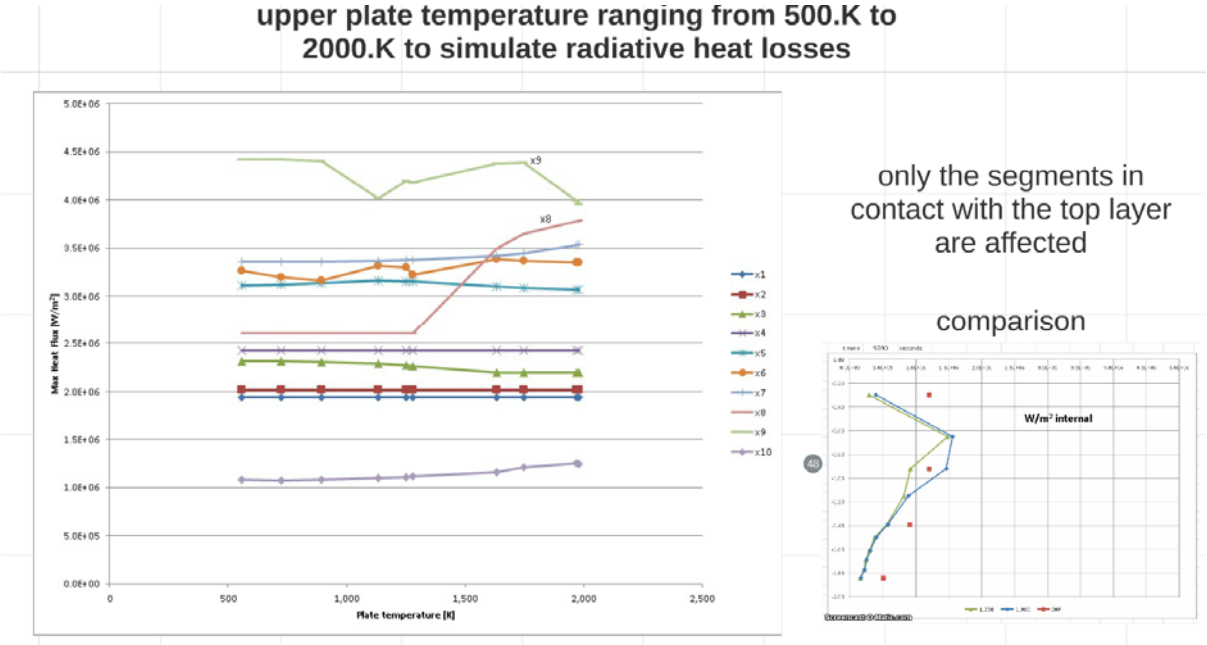

Figure 12: Calculation changing the upper plate temperature

In order to take into account the heat losses due to radiation, ASTEC uses a fictive upper plate temperature. Once the corium is stabilized, there is not a big difference in the heat flux.

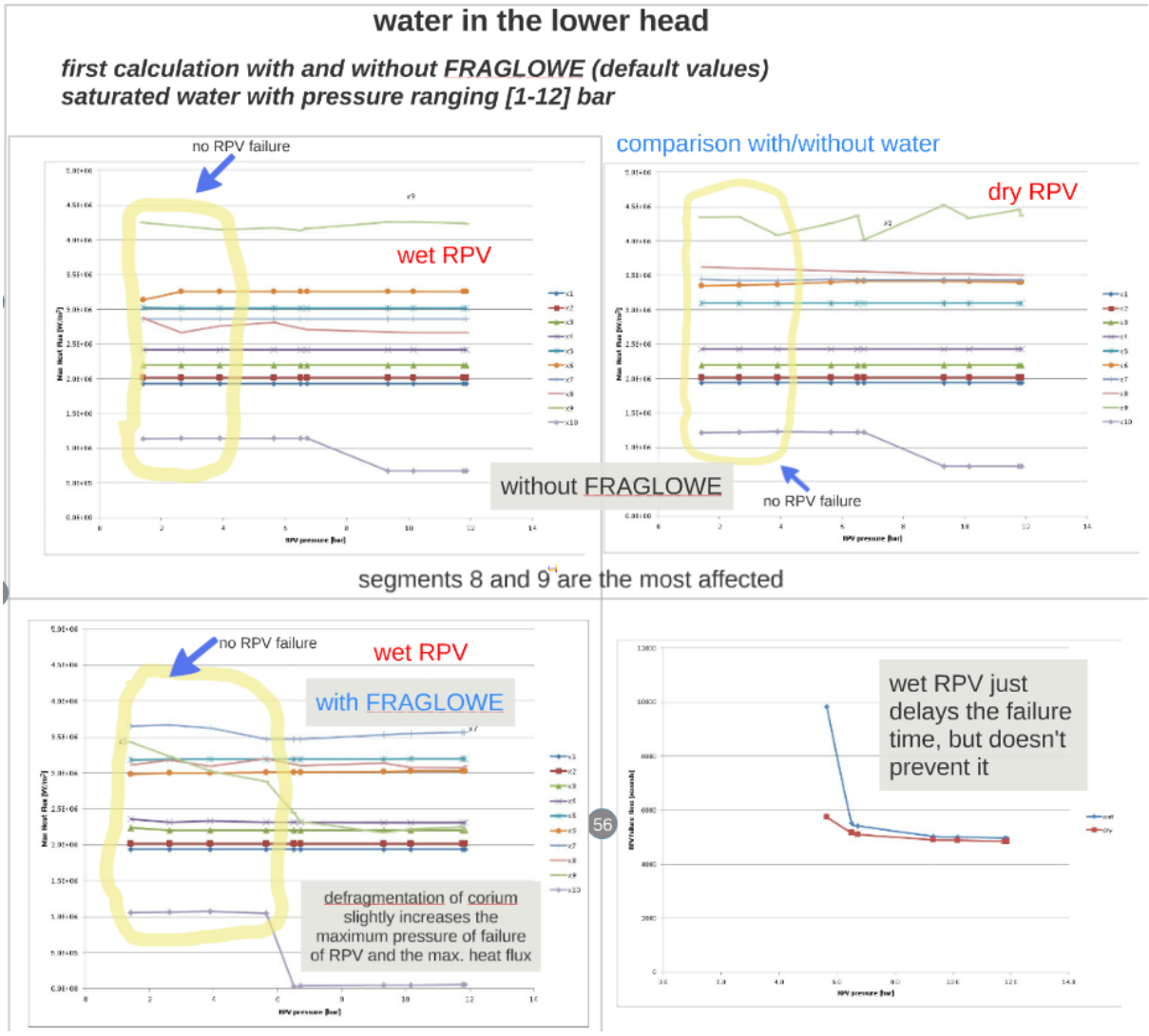

Figure 13: Presence of water in the lower head

The presence of water in the lower head doesn't affect the results, but it just shifts them in time, delaying the RPV failure or the peak in the heat flux.

effect of water level in the lower head

RPV pressure set to 2 bar

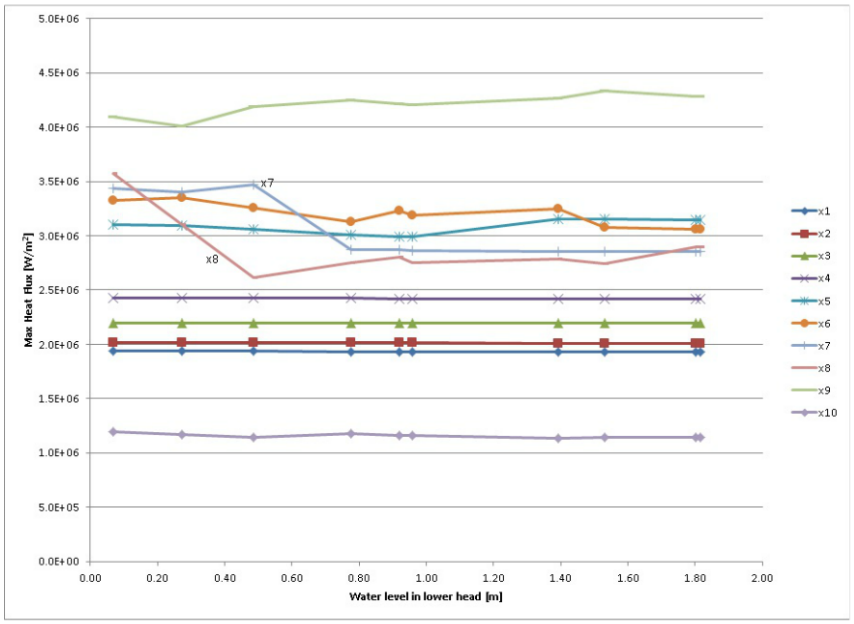

almost no effect when the water level is higher than 1 meter

Figure 14: Amount of water in the lower head

The amount of water in the lower head has almost no effect on the results.

variable diameter of the fragmented corium particles

range between 2 and 20 mm - water level 1 meter

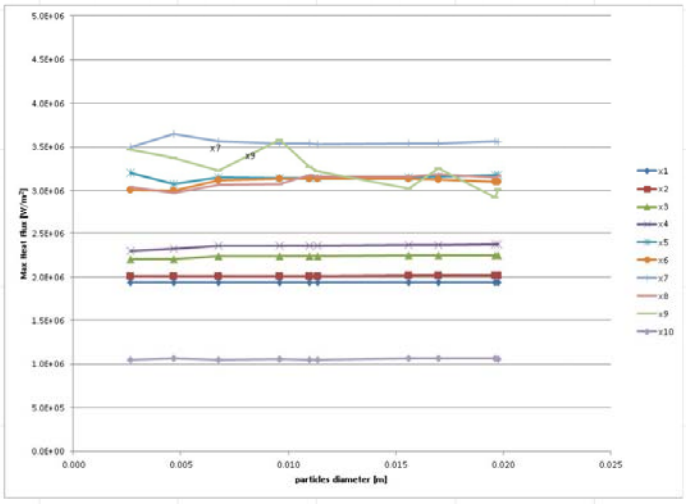

the diameter of the fragmented corium particles doesn't affect much the maximum heat flux.

Figure 15: Effect of changing the diameter of the fragmented corium

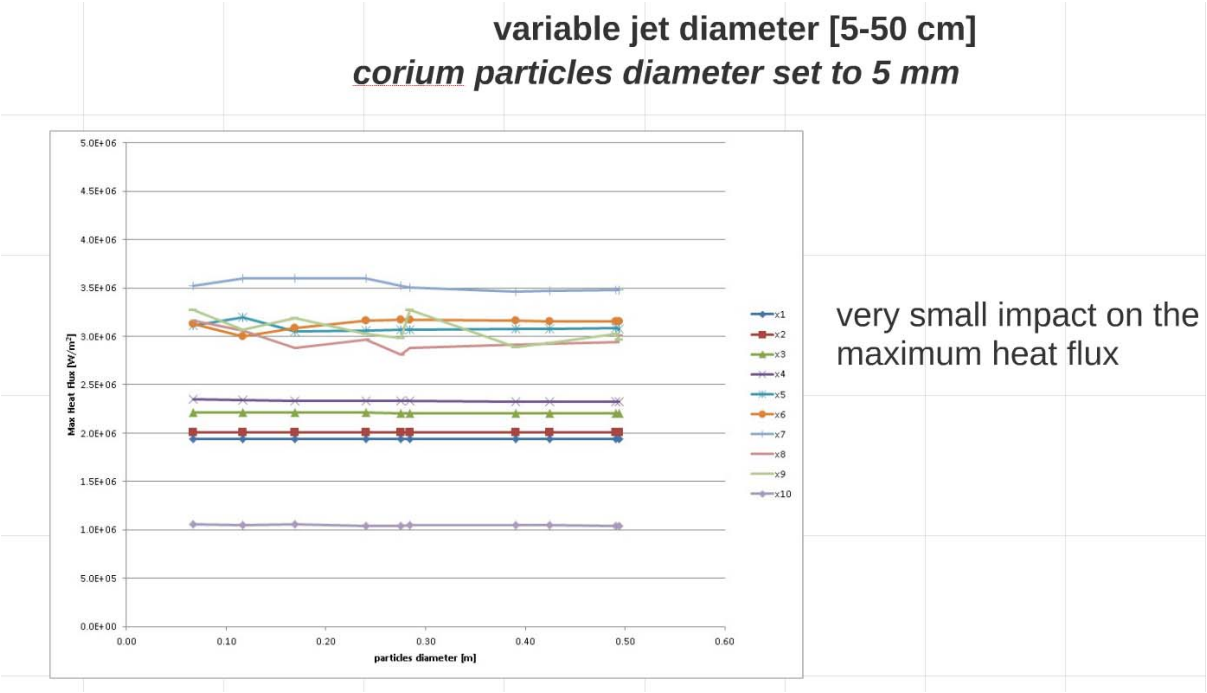

Figure 16: Effect of changing the diameter of the corium jet

Changing the diameter of the fragmented corium particles and jet doesn't affect much the results.

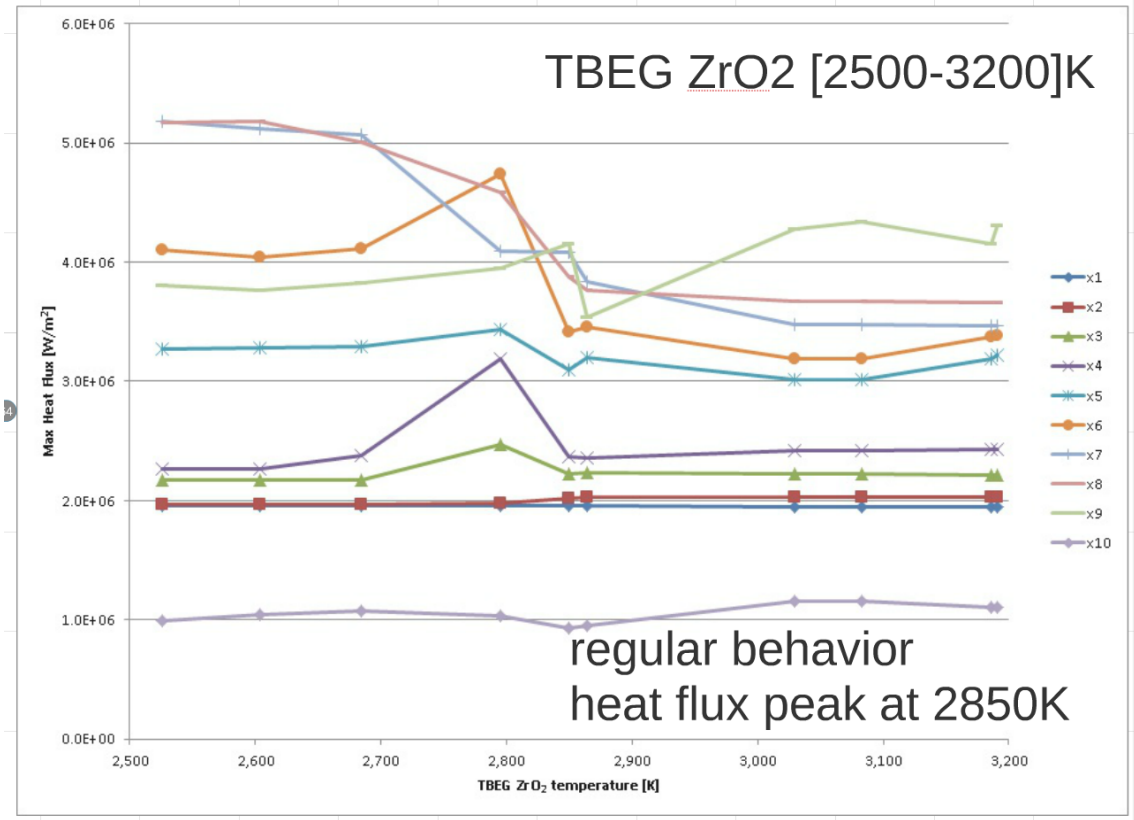

Figure 17: Effect of changing the melting temperature of ZrO_2

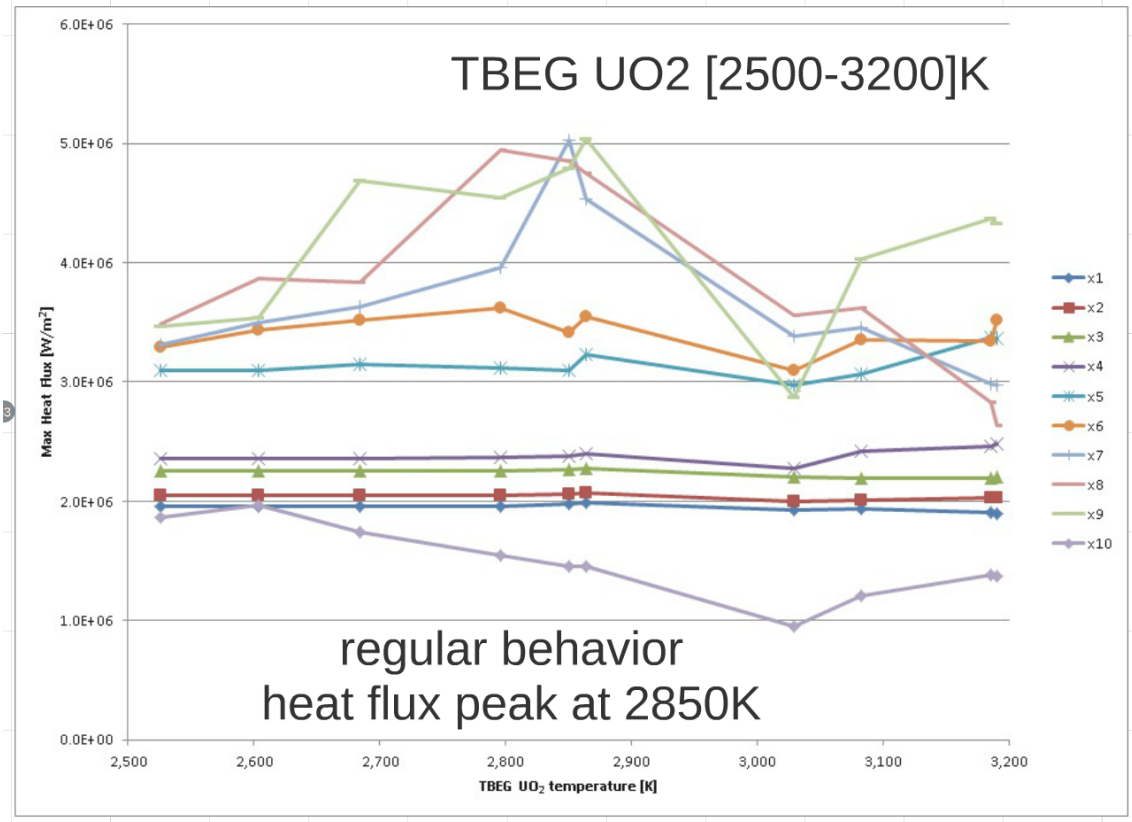

Figure 18: Effect of changing the melting temperature of UO_2

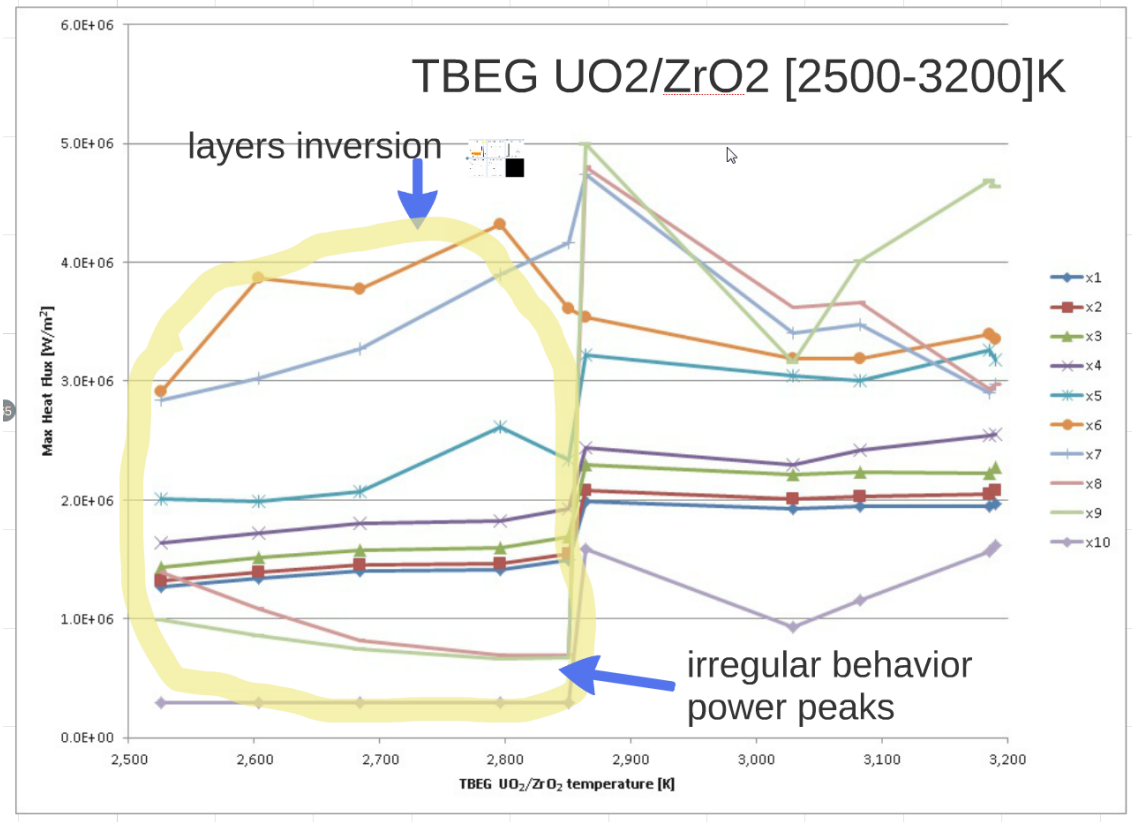

Figure 19: Effect of changing the melting temperature of ZrO_2 and UO_2

Playing with the eutectic liquidus/solidus temperatures has a big impact on the final results, especially coupled to the corium slumping temperature.

A.10.2 Second calculations

The first calculations were interesting, but it appeared during the first comparison workshop that the data used for performing stand-alone calculations were not properly interpreted and therefore in this second round an improved scenario description was given. According to KI SOCRAT calculation, the conditions for performing ASTEC/ICARE stand-alone calculations are the following:

11. The core starts melting at 1250 s.
12. The core starts to relocate into the elliptic part of the barrel at 3250/3450[10] s. The corium history table refers to corium relocation into the elliptic part of the barrel
13. At 4340/4910[1] s the core barrel fails and the corium relocates all at once into the lower head
14. The FA supports are inside the barrel
15. The support grid is also inside the barrel
16. When the core barrel fails, all the steel structures inside the barrel AND the barrel itself (elliptic part + some of cylindrical part) also melt and relocates into the lower head
17. We have to add these steel structures (barrel, FA supports and grid) to the corium history at 4340/4910[1] s. when the barrel fails
18. the real stand-alone lower head calculation starts at 4340/4910[1] s. when the barrel fails
19. The initial composition of the corium is the one in Table 1 with averaged temperature T = 2500 K
20. The decay heat must be taken into account from time 4340/4910[1] s when the barrel fails

Table 9: Corium composition for basic calculation (with account of fission products release)

Material	Mass, t	Source
UO_2	85.9	CORE
Zr	15.6	CORE
ZrO_2	17.1	CORE
Steel	34.4	CORE
	12.2	elliptic part of barrel
	9.0	melted cylindrical part of barrel
	12.3	FA-supports
	1.94	support grid

Additional assumptions for the calculation were:

- Dry lower head
- Sepamode = 1
- Number of corium layers = up to 3
- Solidus/liquidus temperature of the UO_2/ZrO_2 eutectic = 2850/2900 K
- Fictive upper plate temperature = 1700 K
- Decay heat reduced to 80%

[10] The first value is referred to 100% of decay heat; the second value is referred to 80% of decay heat due to volatile FP release out of the RPV.

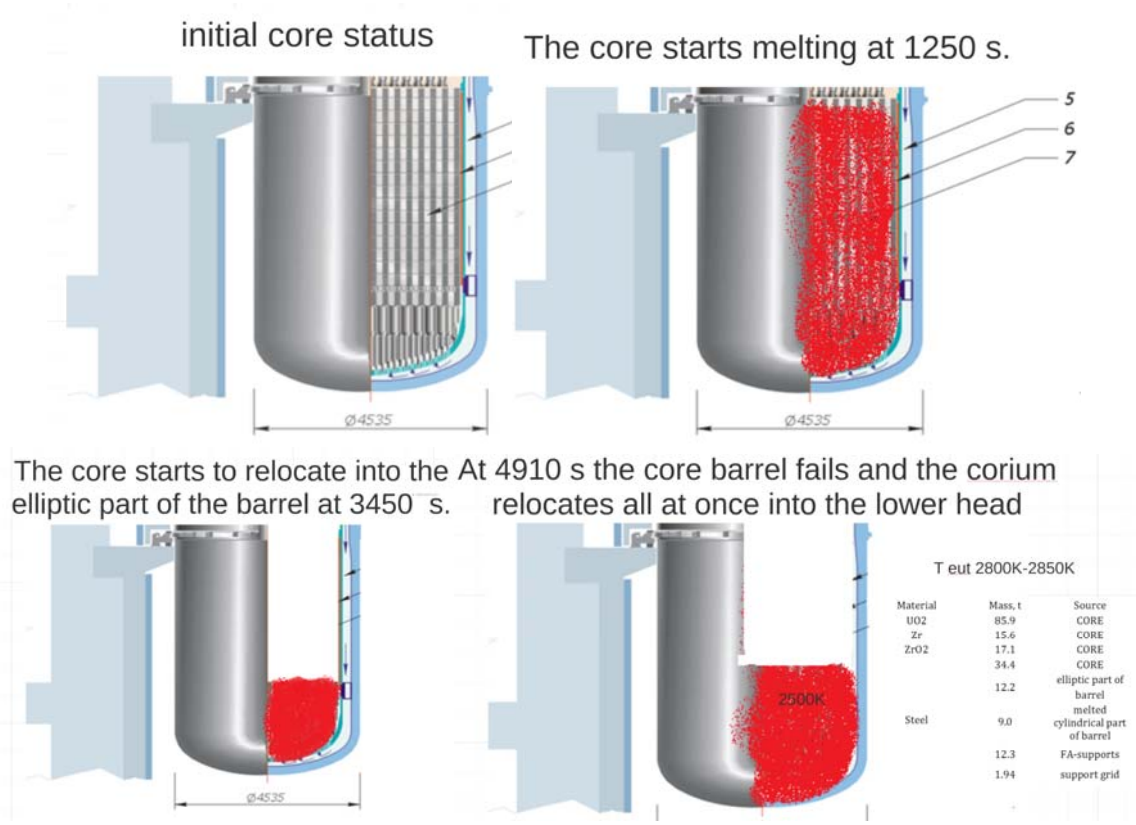

Figure 20: Sequence of core degradation and corium relocation

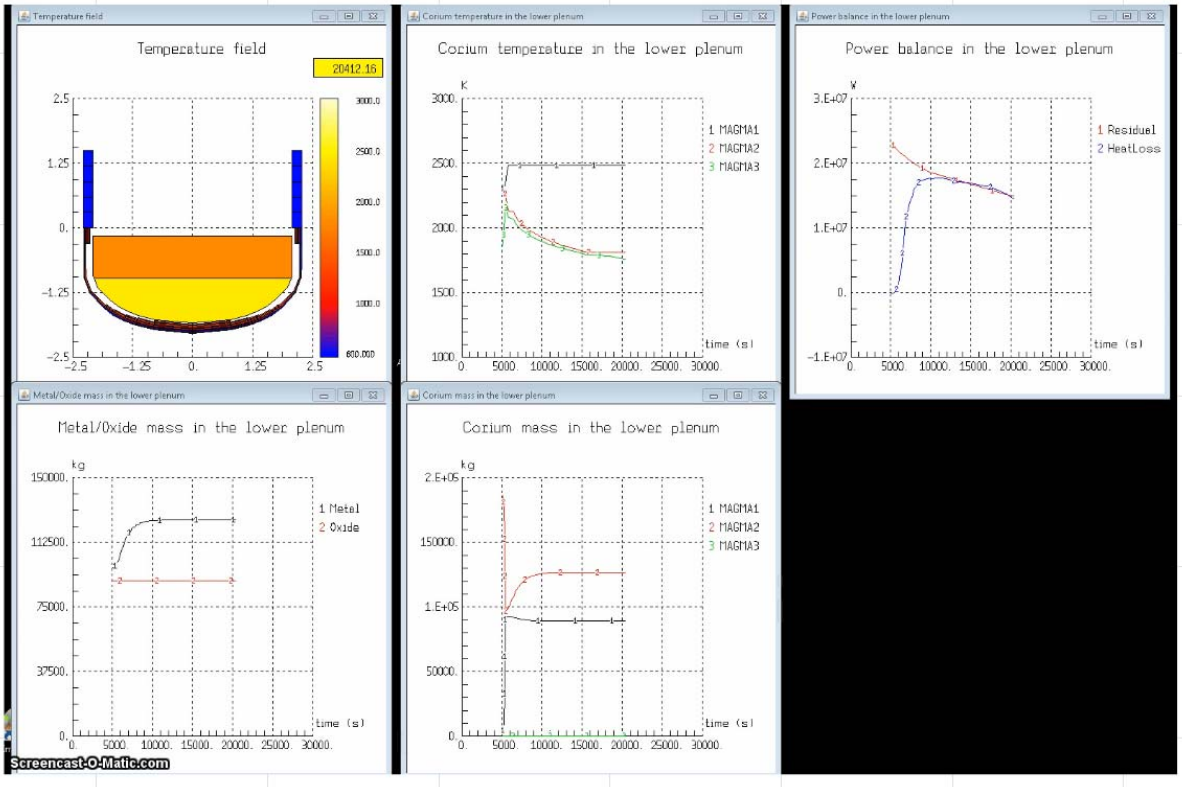

Figure 21: ASTEC calculation

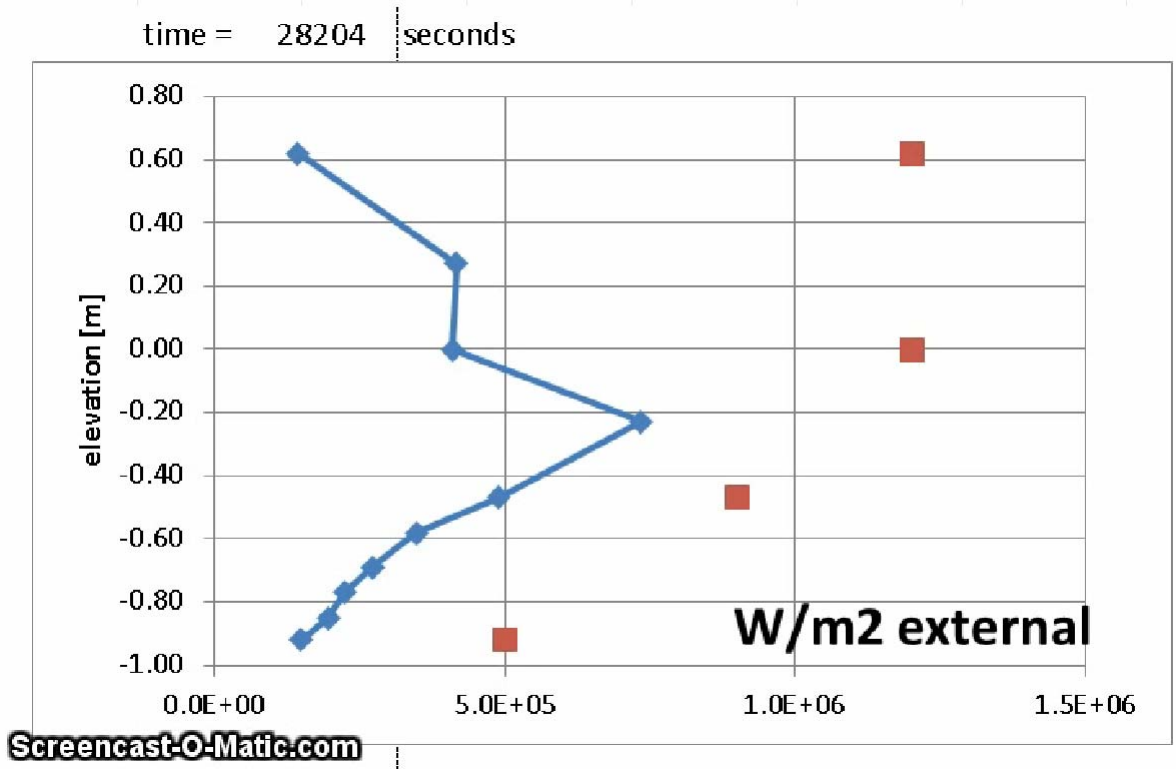

Figure 22: External heat flux with corium stabilized

The calculation was very smooth and the heat flux predicted was below the critical values.

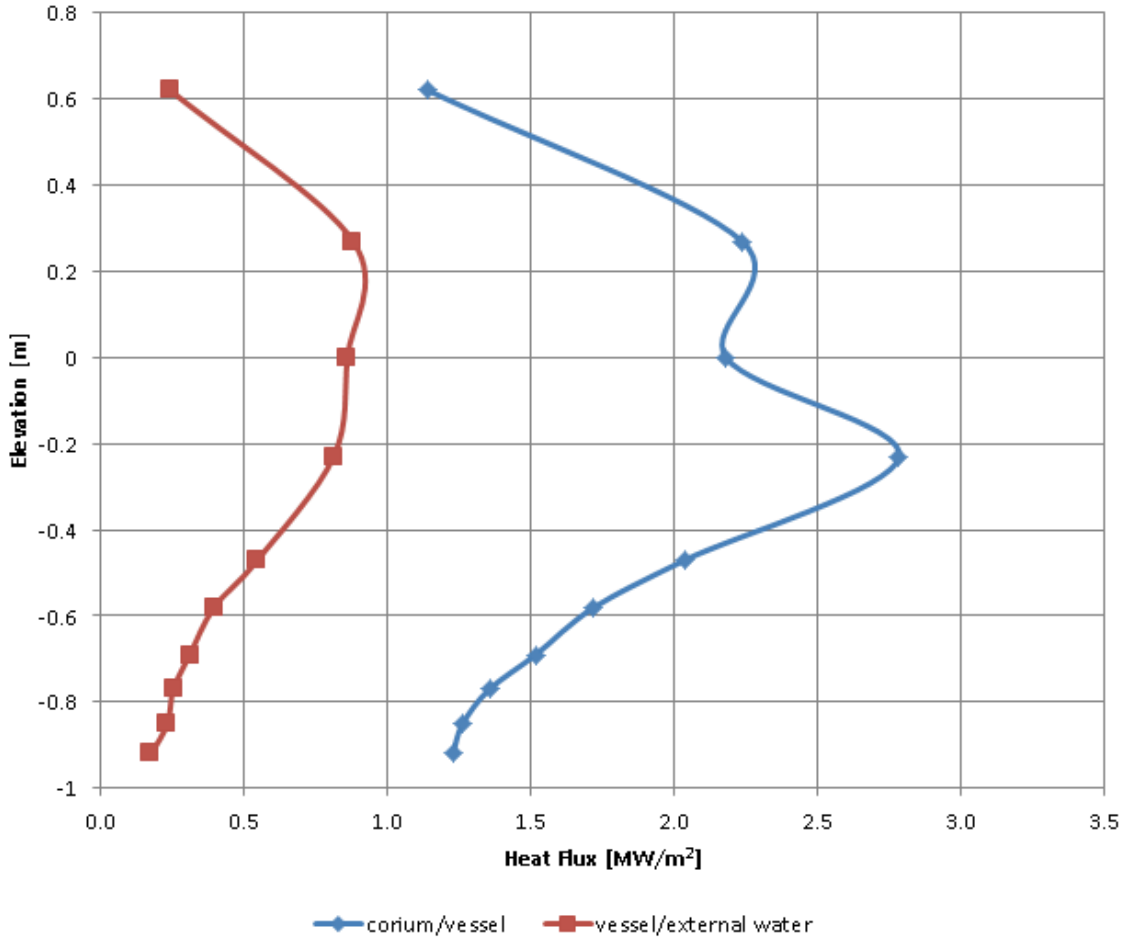

Figure 23: max of max

A.11 JRC CFD with Ansys CFX

A.11.1 Setup

The transient computations have been performed with the code Ansys CFX, version 15.0. The modelling includes the molten corium represented by two stratified layers (a metallic layer and an oxide layer), the solid vessel wall, and the reactor pit flooded with water. Along the outer side of the wall there is a deflector, creating a channel in vertical direction. The buoyancy of the heated water at the wall is expected to result in considerable vertical flow velocities and to increase the heat transfer coefficient. The geometrical properties, assumed for the modelling, are shown in Figure 6. Cooling water is inserted at the bottom (ca. 200 l/s) at saturation temperature of 120 °C. A mixture of water and vapour leave at the top of the coolant domain. Other outer surfaces are assumed to be adiabatic. At the beginning of the computation the core is already molten and corium is situated in the lower plenum in stratified layers; the coolant and the reactor wall have saturation temperature. The modelling of the lower plenum of the reactor pressure vessel is realized as a two-dimensional slice of One degree and a combination of structured and unstructured mesh with over 27800 cells.

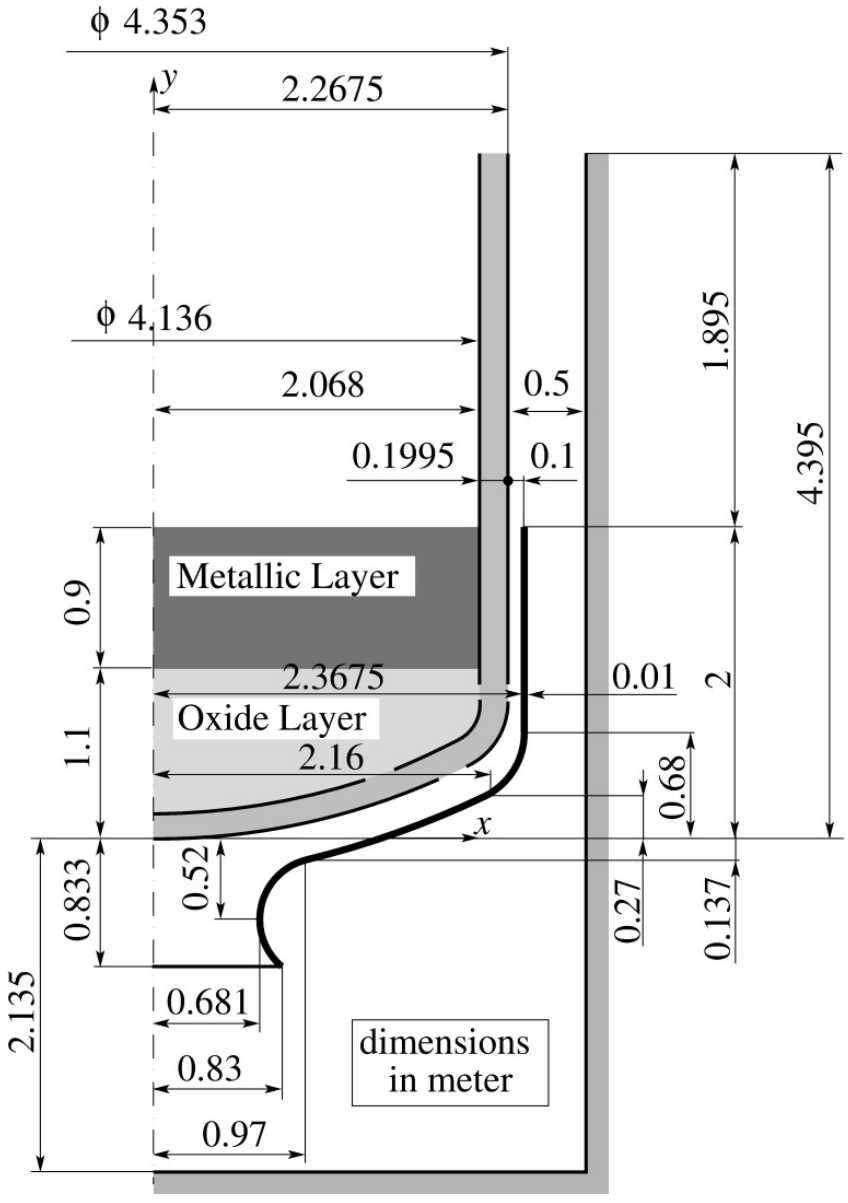

Figure 6: Geometrical properties of the modelling of the reactor pressure vessel, of the corium in two layers of melt and of the coolant domain with the deflector along outer side of the wall.

A.11.2 Results

The behaviour of the residual heat source is shown in Figure 7. The residual heat production is assumed to be equally distributed within the corium and decreases with time. Furthermore, the heat transfer at the inner and outer surface of the reactor vessel wall is shown in Figure 7. Due to the high temperatures, high buoyancy effects and low viscosity the recirculation in the corium melt is high. This can be seen buy the pronounced unsteady behaviour of the heat flux at the inner wall surface in Figure 7. The corresponding heat flux at the outer wall surface is of the same magnitude, but due to the damping effect of the thermal inertia of the wall the outer heat flux oscillates at significantly lower amplitudes. The heat flux at the outer wall side corresponds to the evaporation heat of the coolant.

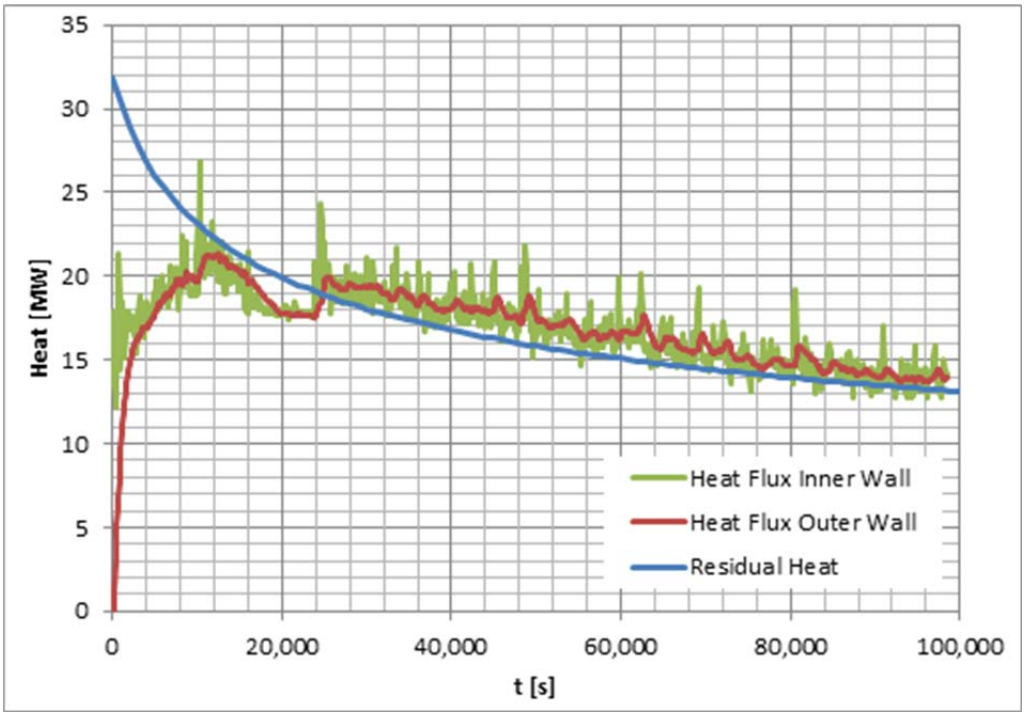

Figure 7: Residual heat production inside the RPV and the resulting heat flux through both faces of the vessel wall.

The local minimum of the heat fluxes after ca. 15,000 seconds is assumed to be caused by a numerical instability which occurred at this point of time. To be able to restart the calculation, the discretization scheme (the approximation of the derivatives for the advection) had to be changed from the highly accurate "centred differences scheme" to the less accurate but more robust "upwind scheme". The effect might be a numerical artefact produced by the instability and of the change of discretization scheme and needs to be evaluated.

Figure 8 gives an overview of the results at 60,000 s for the boiling coolant (outside the reactor pressure vessel), for the wall of the reactor pressure vessel, and for the corium (inside). Shown are the volume fraction of the coolant, the temperature fields for the vessel wall and for the corium, and the velocity fields for the coolant and for the corium. The wall temperatures above the assumed melting temperature of the wall (1500 K) are clipped away by means of post processing, showing the estimated ablation of the reactor pressure vessel wall. The melting of the wall is not actually modelled and for the computation the solid wall remains in place. Consequently, this approximation is not conservative. The corresponding estimated remaining wall thickness is shown on Figure 9. The nominal wall thickness is 199,5 mm. Due to the CFD computation ca. 65 mm of the wall remain below the melting temperature (minimum at ca. 25,000 s).

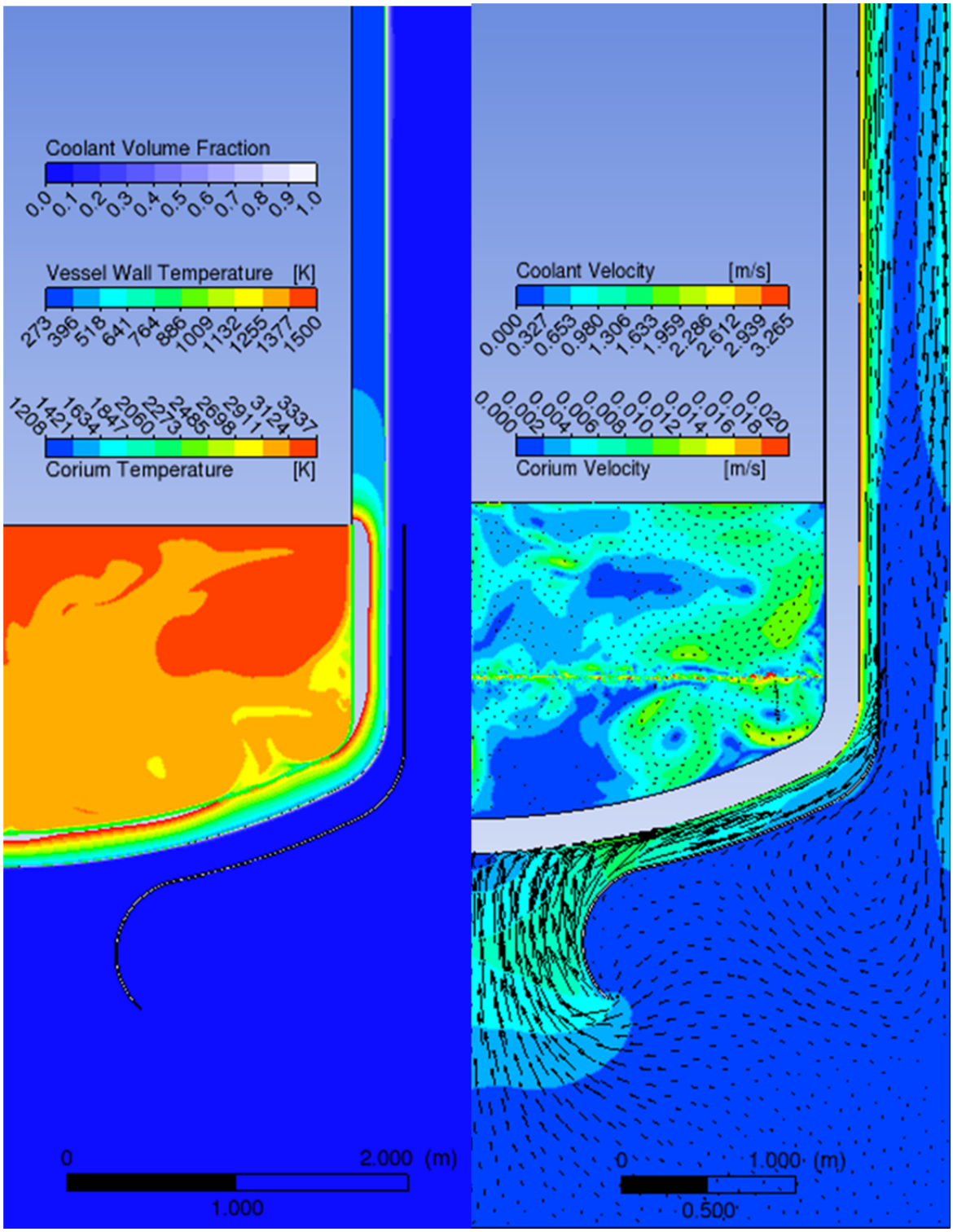

Figure 8: Results for the boiling coolant (outside of the vessel), for the wall of the vessel, and for the corium (inside) at 60,000 s. Left-hand side: volume fraction in the coolant domain (1.0 corresponds to 100 % vapour), temperature in the vessel wall (clipped away above melting temperature), and the corium temperature. Right-hand side: velocity fields for the coolant and for the corium. The stratification of the melt can be seen by velocity effects at the interface between the layers.

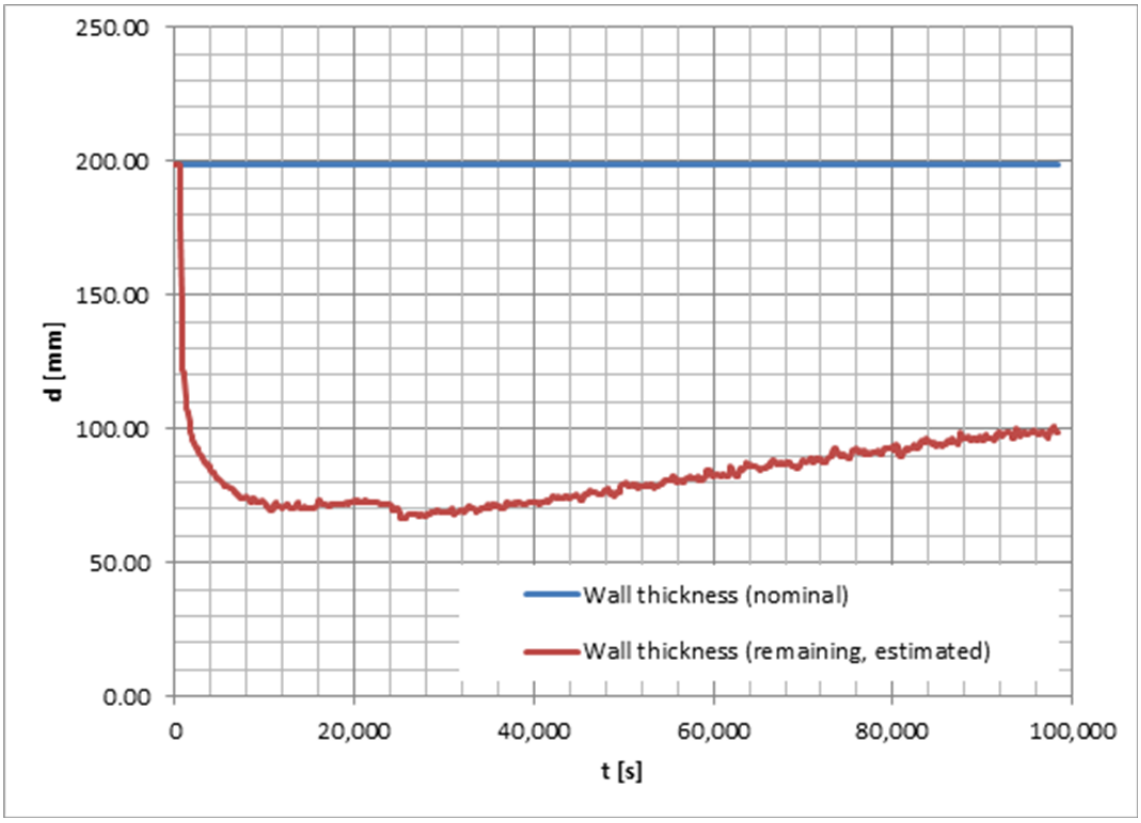

Figure 9: Estimated remaining wall thickness at a height of y =1 m (y = 0 is at the lower end of the cylindrical part of the wall). The ablation is estimated by the reached melting temperature inside the wall.

The maximum temperatures in the model are shown on Figure 10 for the molten corium, at the vicinity of the inner side of the reactor pressure wall and at its outer surface. The maximum temperatures of the molten corium are in the magnitude of 4,000 K and at the wall they reach ca. 3,300 K. The outer side of the wall remains at ca 400 K which is close to the assumed saturation temperature of the coolant of ca. 393 K. Hence, the cooling seems to be sufficient to prevent a boiling crisis and a local dry out. The peak and local minimum at ca 20,000 s are related to the numerical effect discussed above. Furthermore, the melt overheat ~500K seems to bequite large. That indicates that heat transfer in a pool or in its boundary is modelled inadequately. Consequently, it has to be investigated if the Nusselt number might be too small.

Figure 11 displays the maximum velocities occurring within of the coolant domain and at the outflow at the top of the domain. The coolant domain velocity maximum establishes around 3.2 m/s (also shown on the right-hand side of Figure 8). The maximum velocities occur at the outlet (at the top of the domain) where the velocities peak at 7.2 m/s. The highly transitory behaviour of the velocities at ca 10,000 s is assumed to be related to the discussed instability.

In Figure 12 the heat flux density for the inner surface and for the outer surface of the wall is given. Again, the high amplitudes of the inner heat flux density demonstrate pronounced unsteady behaviour of the melt within the vessel. The maximum (for a smoothed curve) can be assumed close to 3 MW/m^2 at ca 25,000 s (see discussion for Figure 13). The maximum heat flux density is significantly lower at the outer surface of the vessel. This can be explained by the high level of lateral heat conduction within the wall which decreases local hot spots along the way of heat transfer through the wall. The maximum value for the outer heat flux density can be observed at ca. 25,000 s and reaches values close to 0.8 MW/m^2.

The heat flux densities along the height at both sides of the wall are given on Figure 13 and on Figure 14, at different points of time. At the inner side of the wall the het flux density varies a lot over the height which demonstrates the high degree of recirculation inside the molten corium. Local peaks might not be physical (the maximum value of 3 MW/m^2 discussed for Figure 12 seems to be too high).

Generally, the inner heat flux density is about three times higher for the upper layer (metal with high heat conduction of 45 W/mK) than for the lower layer (oxide with low heat conduction of 2 W/mK). A similar (but much smoother) picture can be seen for the outer vessel wall where the highest value for the heat flow density of ca. 0.77 MW/m^2 can be seen at ca 25,000 s.

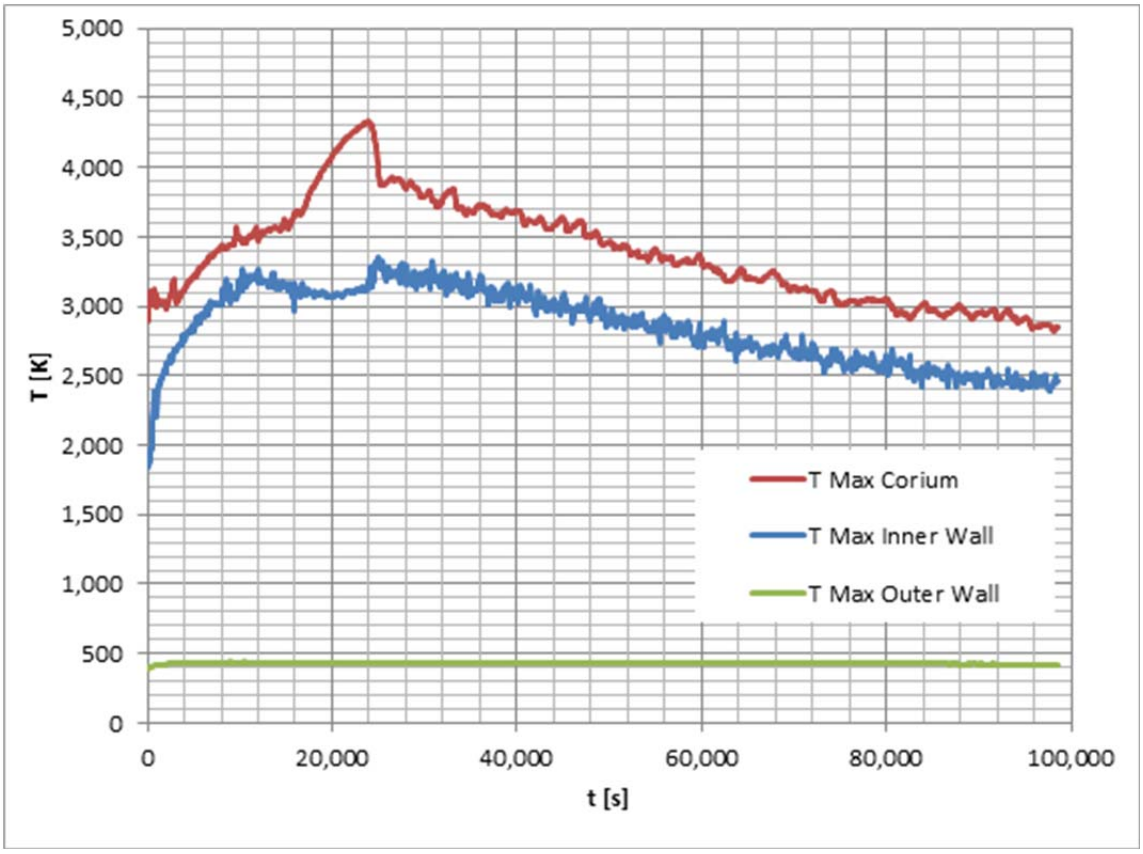

Figure 10: Maximum temperature in the molten corium, maximum temperature in the vicinity of the inner side of the wall and the temperature of the cooled outer wall surface.

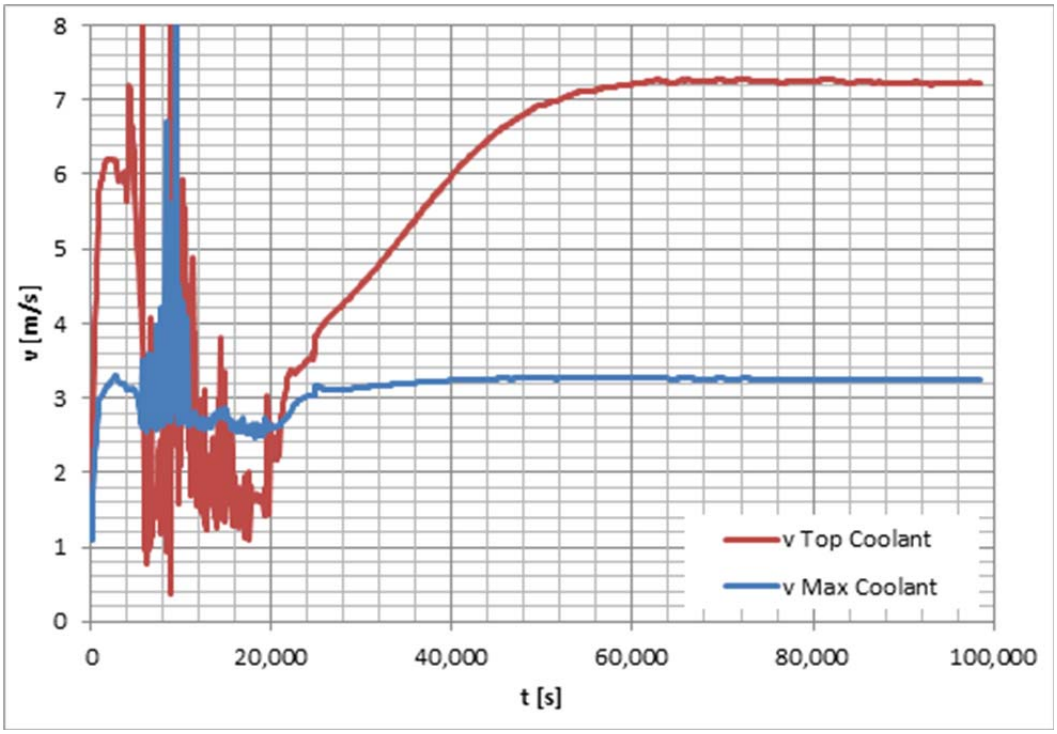

Figure 11: Maximum velocities in the coolant domain are typically in the order of 3 m/s except for the outlet at the top where velocities of 7 m/s are reached.

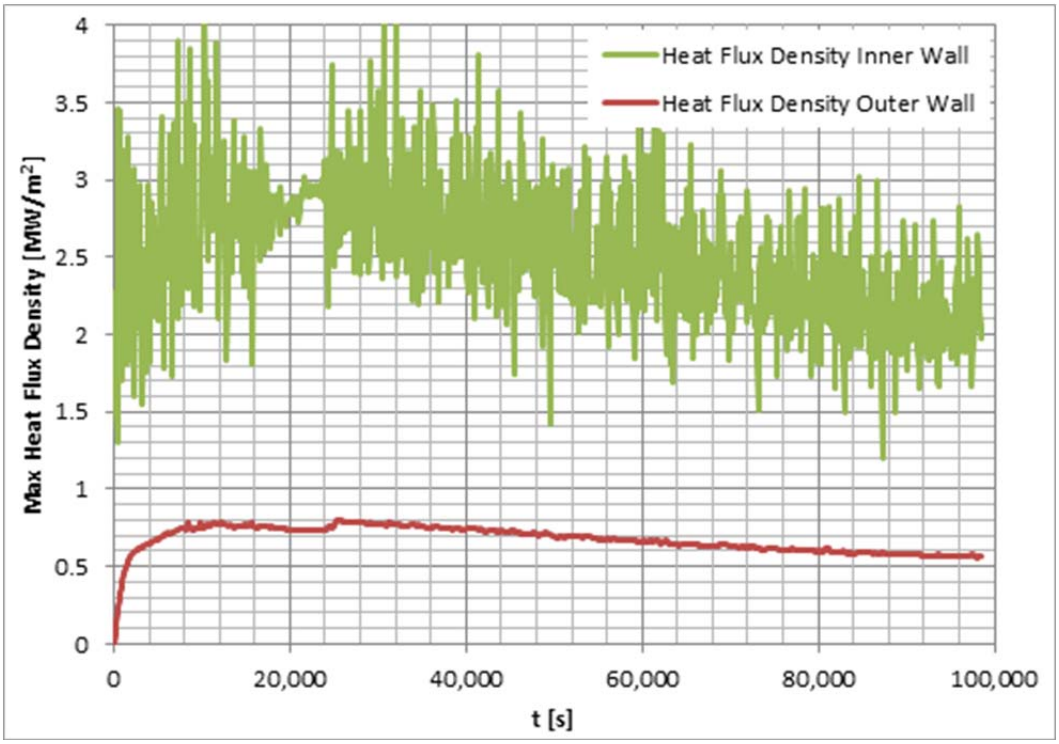

Figure 12: Maximum heat flux density at the inner side of the vessel wall (highly unsteady due to recirculation in the melt) and the heat flux density at the cooled outer face of the wall.

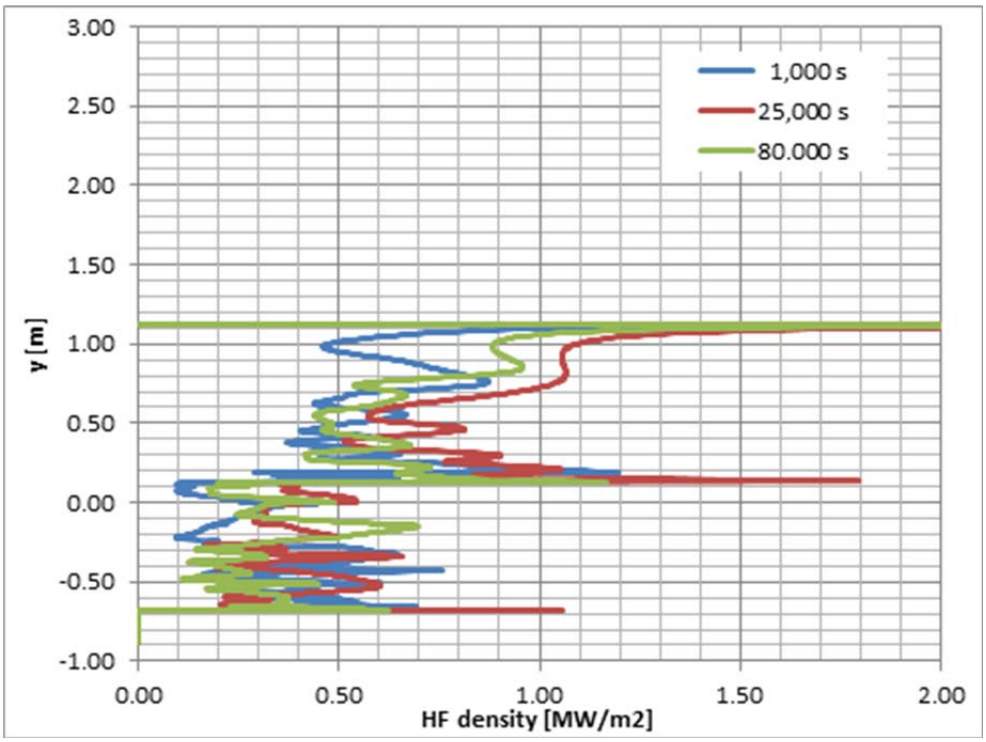

Figure 13: Heat flux density along the height at the inner side of the vessel wall.

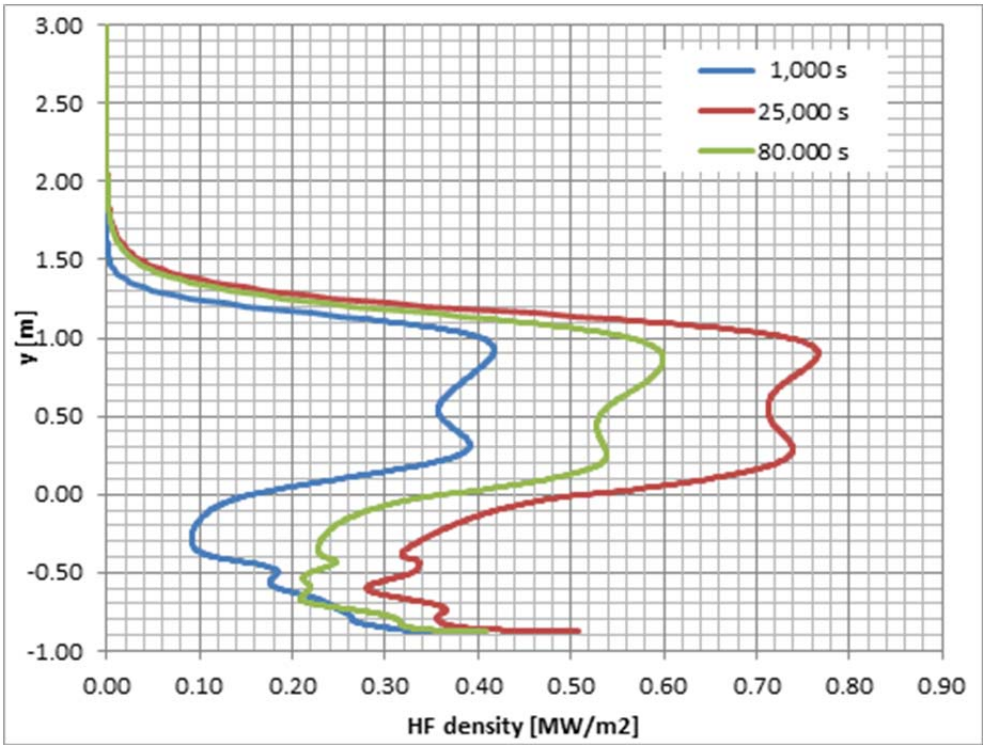

Figure 14: Heat flux density along the height at the outer side of the vessel wall. The peak at the lowest point is probably a numerical effect and not physical.

A.12 EDF CFD with NEPTUNE_CFD

A.12.1 Setup

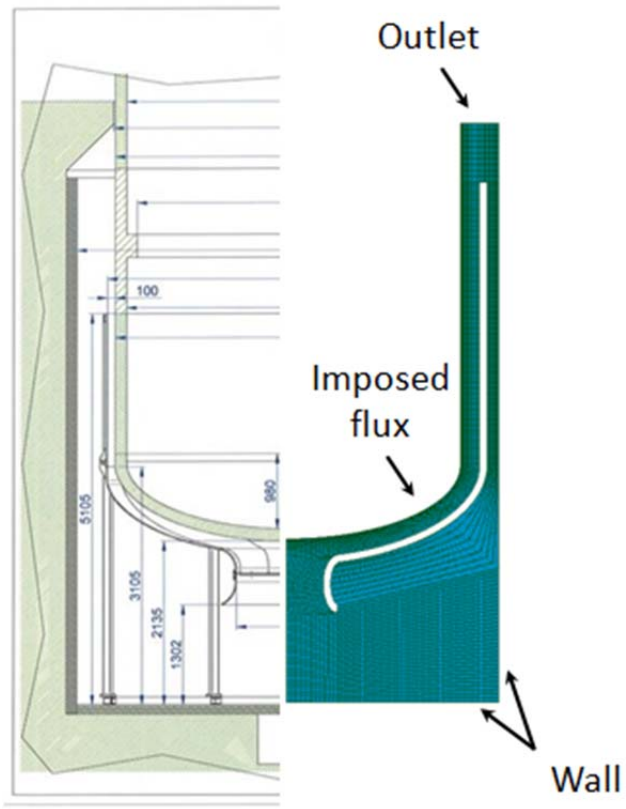

Figure 1 UJV's outline, Salomé mesh and boundary conditions

The calculation is based on:

- a CAD and structured 3D hexahedral mesh (about 50000 cells) realized with Salomé using UJV's reactor pit outline. The computational domain is a 15 cm-thick slice.
- NEPTUNE_CFD's recommended setup for boiling flows;
- an imposed heat flux boundary condition, with an input profile obtained from KI's SOCRAT calculation for the 2nd bench. The water inventory is regulated from the top (steam flows out and liquid water trickles back in). The other boundary conditions are all considered to be adiabatic walls.

The original UJV outline, mesh and boundary conditions are shown in Figure .

This is a steady incompressible calculation, with a physical computation time of 5000 s.

A.12.2 Results

Figure 2 shows the liquid velocity in the loop as computed by NEPTUNE_CFD, and the liquid velocity along the vertical axis. The maximum velocities (around 7.5 m/s) are found at the top of the mesh, while the velocities along the heated wall are about 2 to 4 m/s – a range consistent with the ULPU results as well as the other CFD computations presented at the benchmark.

The natural circulation loop is clearly established, with downwards velocities about 1 m/s in the downcomer; however, the deflector geometry leads to a sizeable eddy in the lower part of the computational domain, indicating that some optimization of this geometry might be needed in the future.

Figure 3 shows the void fraction in the loop as computed by NEPTUNE_CFD. While the main regime along the heated wall is nucleate boiling, there is a hot spot corresponding to the peak in the input flux profile with very high void fraction (this will require a correction of the mesh). Steam recondensation can be observed above the heated zone, with void fractions dropping to zero, followed by intense flashing in the upper part of the riser as the hydrostatic pressure decreases.

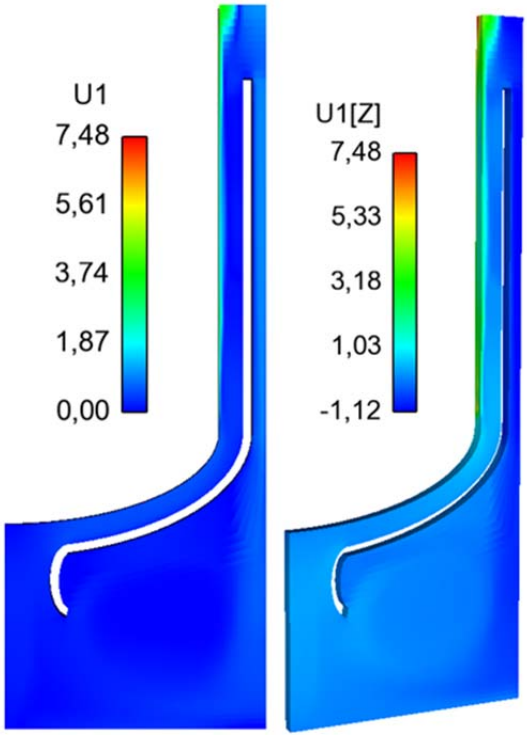

Figure 2 Liquid velocity

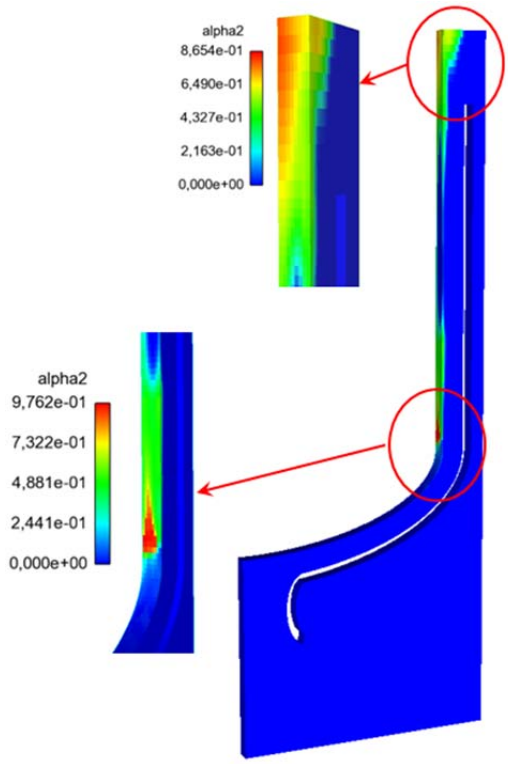

Figure 3 Void fraction

Figure 4 shows the results of the post-processing with the SULTAN CHF correlation (which computes the critical heat flux as a function of the pressure, the thermodynamic quality, the mass flux, the gap width and the inclination angle). As expected for this mild input flux, there are still significant margins. Nonetheless, these results have to be investigated further: the SULTAN correlation has been established for gap widths up to 15 cm, and its validity when extrapolated to larger gap widths (25 cm here) needs to be verified.

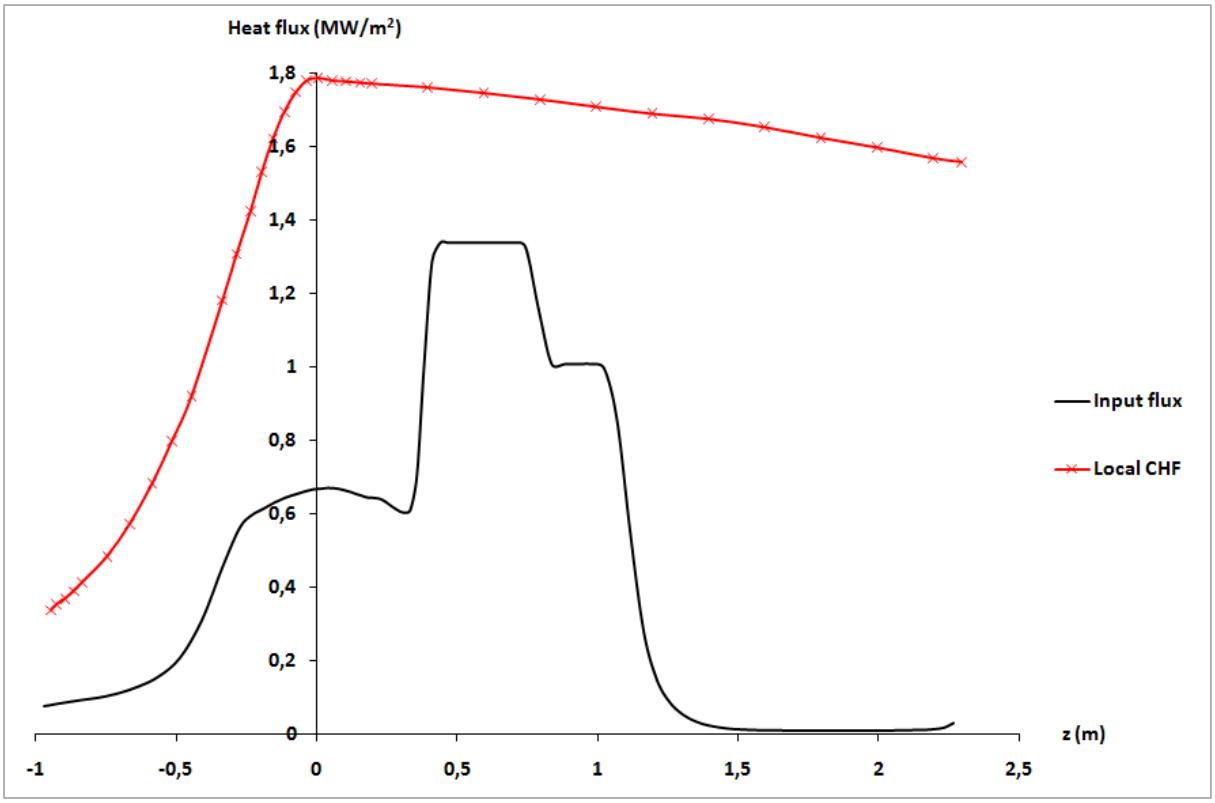

Figure 4 Evaluation of the CHF with SULTAN

These results can only be considered as temporary. The calculation is at the limits of NEPTUNE_CFD's current models for boiling flows (which assume a continuous liquid phase carrying a dispersed steam phase), which led to marked instabilities. Several improvements are under study to reduce these instabilities. However, the results are globally consistent with those obtained for ULPU, as well as those obtained with CFX and RELAP3D.

A.13 UJV FLUENT and RELAP-3D

A.13.1 Heat transfer in the melt inside the VVER-1000 RPV bottom

The goal of this work was simulate heat transfer in melt inside VVER-1000 reactor pressure vessel (RPV) during severe accident and determine wall heat flux. Simulation was performed with the Ansys FLUENT 13 CFD code. Simulated scenario was initiated by a large break LOCA (2x850mm) and loss of active core cooling systems. Two immiscible phases were assumed: 101 t oxide phase and 42 t metallic phase. Thermal power released in the oxide phase was 31 MW. 18 MW of the total power was transferred into RPV bottom wall and the remaining power was discharged through the top surface of the metallic phase. It was assumed that no thermal power is released in the metallic phase. Physical properties of melted materials were used from paper by (Bechta et al., 2008) and are summarized in Table 1.

Table 1: Physical properties of melted materials

	oxide phase	metallic phase
solidus temperature [K]	2500	1400
liquidus temperature [K]	2720	2000
density [kg/m^3]	7400	7245
thermal expansion coefficient [1/K]	6.5e-5	3.2e-5
dynamic viscosity [Pa.s]	4.5e-3	3.3e-3
thermal conductivity [W/m/K]	4	40
heat capacity [J/kg/K]	600	660

Because the phases are only partially melted, solidification and melting cannot be neglected. "Solidification/melting" model in FLUENT 13 was used in the simulations. So as to account for turbulence, standard k-epsilon model was used. The following simplifying assumptions were made: (1) oxide and metallic phases are completely immiscible, (2) the case is 2D rotationally symmetric and (3) there is no unsteady melting of RPV wall, i.e. the geometry of computational domain is fixed.

Computational domain can be seen in Figure 1. Boundary conditions are as follows: constant temperature boundary condition is used at the inner surface of RPV wall, temperature of 1700 K (melting point of steel) is set there. Constant heat flux is adjusted at the top surface of the metallic phase so that the total released thermal power is 13 MW. The computational mesh was refined in the vicinity of RPV wall, top surface and phasic interface (see Figure 1).

Simulation with solidification/melting was time-consuming. It was necessary to perform simulation of 20,000 s of transient to get a quasi-steady solution in which energy is conserved (i.e. energy source in volume is equal to energy released through boundaries). Another 8,000 s of transient was used for results time-averaging. Numerical time step was 0.5 s. Simulation took more than one day on one core.

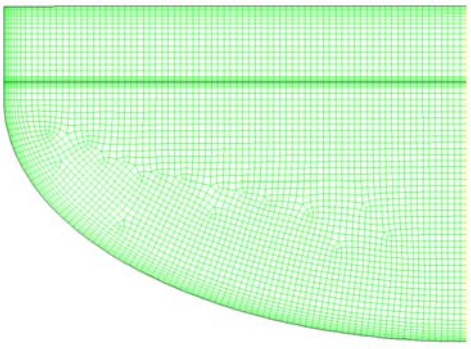

Figure 1 CFD simulation of melt: Computational domain and mesh

Calculation results from the base case (13 MW released through top surface) are shown in Figure 2 and Figure 3. Metallic (i.e. upper) phase has lower solidus temperature, hence it has higher liquid fraction. Velocities in the metallic phase are considerably higher than in the oxide phase because of the higher liquid fraction in the metallic phase. Velocity field in the oxide phase is markedly unsteady. Partially melted material is "tumbling". Velocity field in the metallic phase is almost steady.

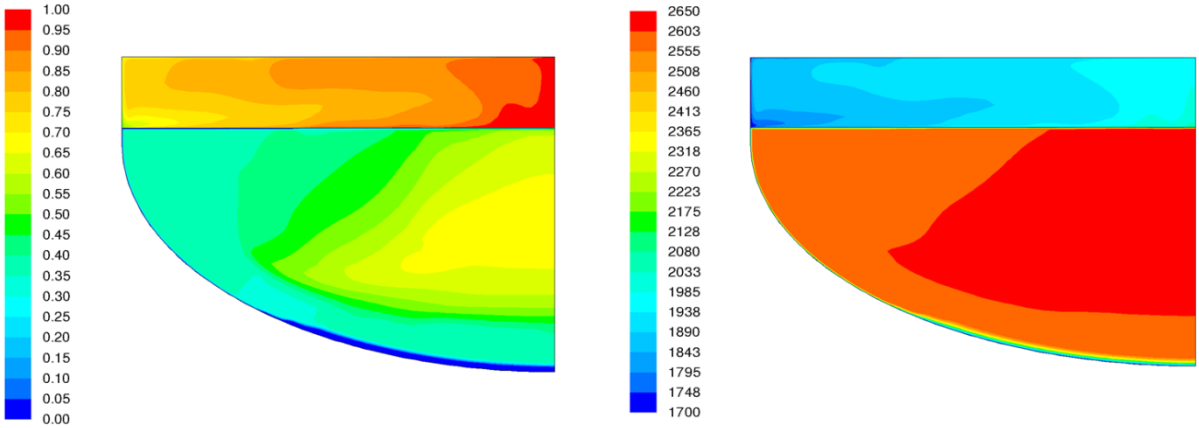

Figure 2 CFD simulation of melt: Calculation results (13 MW released through top surface): liquid fraction [-] on the left, temperature [K] on the right

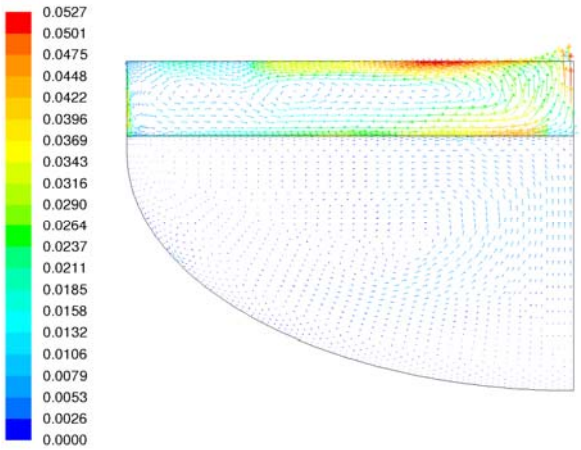

Figure 3 CFD simulation of melt: Calculation results (13 MW released through top surface): velocity vectors [m/s]

Calculated RPV wall heat fluxes are presented in Figure 4. Blue line in Figure 4 is the base calculation with 13 MW discharged through the top surface of metallic phase. These results serve as an input for the simulation of external cooling with the RELAP-3D code (see below). Yellow line is for the case with heat removal from the melt top surface decreased to approx. 10 MW. Green line is for the case with heat removal from the melt top surface is increased to 17 MW. Red line is critical heat flux limit for the case without deflector and with zero water subcooling (hypothetical worst case).

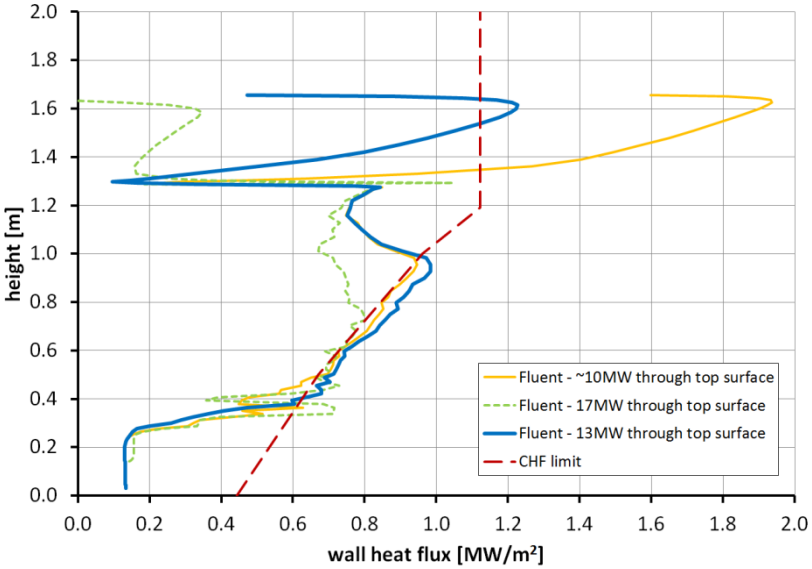

Figure 4 CFD simulation of melt: Calculated RPV wall heat fluxes, comparison of results for 3 cases with different power released from the melt top surface.

A.13.2 External RPV cooling performed with RELAP-3D code

The goal of this effort was to simulate flow and heat transfer in reactor cavity filled by water during severe accident. Heat from RPV is removed by natural circulation. Simulations were carried out with RELAP5-3D thermal hydraulic code. Heat fluxes on RPV surface are taken from FLUENT (see above) and or from SOCRAT/HEFEST simulations. Influence of deflector and water level position was studied.

One-dimensional model of reactor cavity with cross-flows was created (see Figure 5). Model options reducing numerical oscillations in two-phase flow at low pressure were used. Alternative 3D model suffered from numerical oscillations and could not be used. Heat transfer at RPV elliptical bottom was modelled as “boiling on the wall above liquid” (geometry 130 in RELAP-3D). Heat transfer at RPV cylindrical wall was modelled as “standard cylindrical geometry” (geometry 101 in RELAP-3D).

The following cases were analysed:

Case 1: deflector, wall heat flux from SOCRAT/HEFEST code, reactor cavity completely filled with water

Case 2: deflector, wall heat flux from SOCRAT/HEFEST code, water level in reactor cavity about 1 m above deflector outlet.

Case 3: deflector, wall heat flux from FLUENT code, reactor cavity completely filled with water.

Case 4: without deflector, wall heat flux from SOCRAT/HEFEST code, reactor cavity completely filled with water.

Sensitivity studies on position of water level, deflector height and pressure in containment were also performed. Major results from these simulations are presented in Figure 6 to Figure 10.

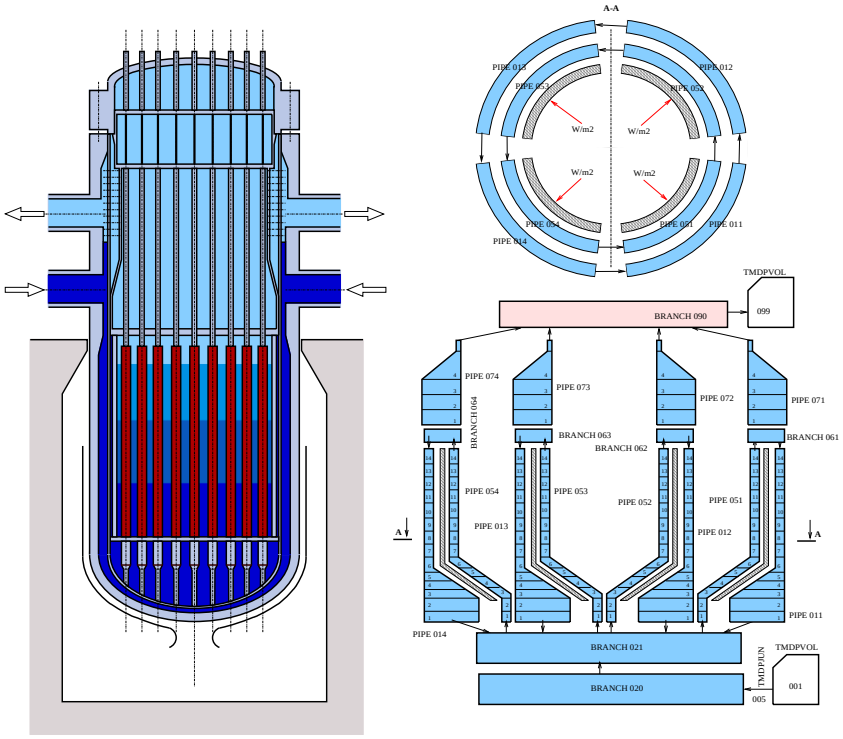

Figure 5 Model of reactor cavity, actual geometry on the left and RELAP-3D model on the right. Model version with deflector is shown.

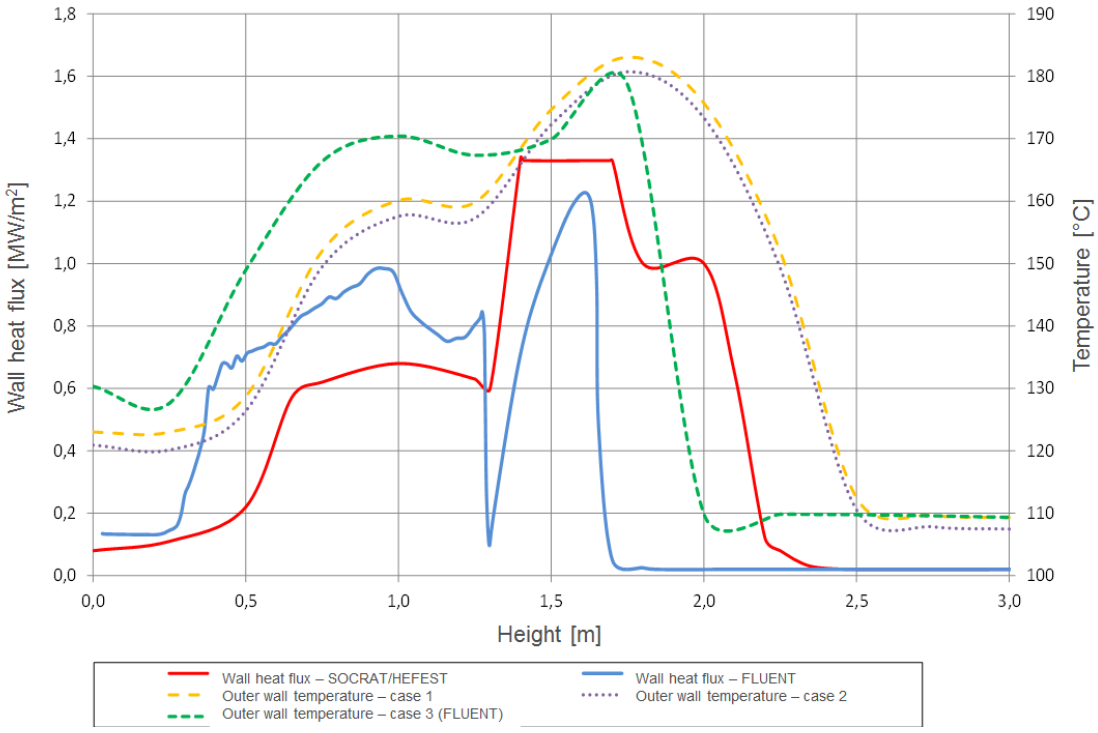

Figure 6 External cooling, RELAP-3D: Temperatures of RPV outer surface, with deflector

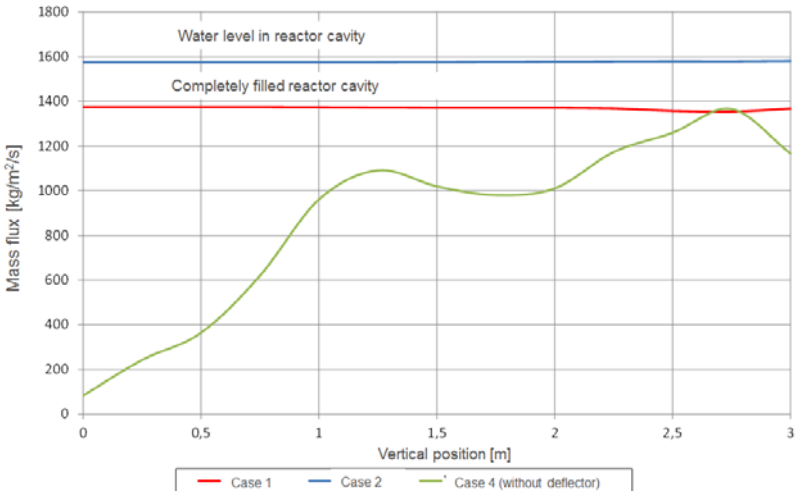

Figure 7 External cooling, RELAP-3D: Influence of deflector and position of water level in reactor cavity

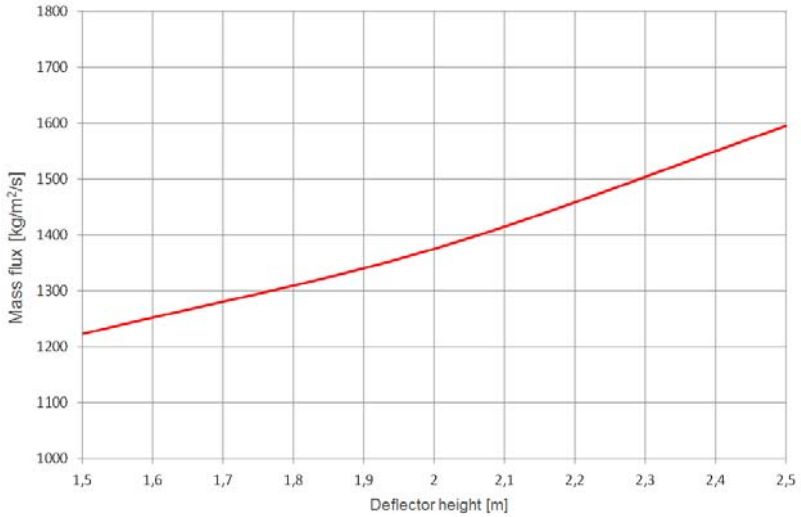

Figure 8 External cooling, RELAP-3D: Influence of deflector height

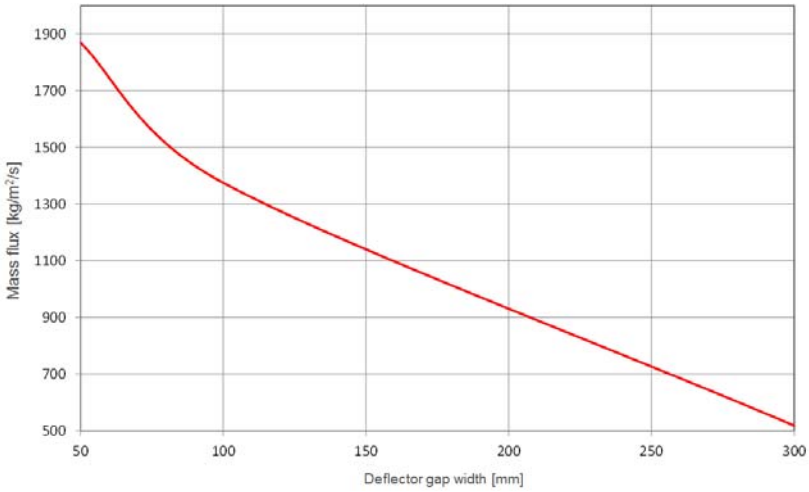

Figure 9 External cooling, RELAP-3D: Influence of deflector gap width

A.13.3 Critical heat flux evaluation

Several methods of critical heat flux (CHF) evaluation were used.

(a) Groeneveld CHF tables AECL-UO (1986): These tables are implemented in the RELAP-3D code and provide CHF limit for vertical tube as a function of local pressure, mass flux and steam

quality/subcooling. CHF limit from tables is then modified for given geometry and type of the flow. For elliptical bottom, correction is applied to account for flow below the heated wall.

(b) CHF correlation created by INL for Korean APR1400 reactor (with spherical bottom): CHF depends on inlet subcooling and angular position on the reactor bottom. Type 1 correlation is for the case without deflector, Type 3 correlation is for the case with deflector.

(c) CHF correlation derived from the KAIST experiments for APR-1400 reactor: The correlation is valid for mass flux lower than 300 kg/s/m^2.

(d) CHF correlation derived from the SULTAN experiments.

Comparison of wall heat fluxes calculated with FLUENT and SOCRAT/HEFEST codes with critical heat flux evaluated by the above described methods is shown in Figure 10. The correlations were extrapolated on VVER-1000 RPV geometry (elliptical bottom). Water subcooling of 6°C was assumed. Note the favourable influence of the deflector on the CHF limit and also the wide spread of CHF limits.

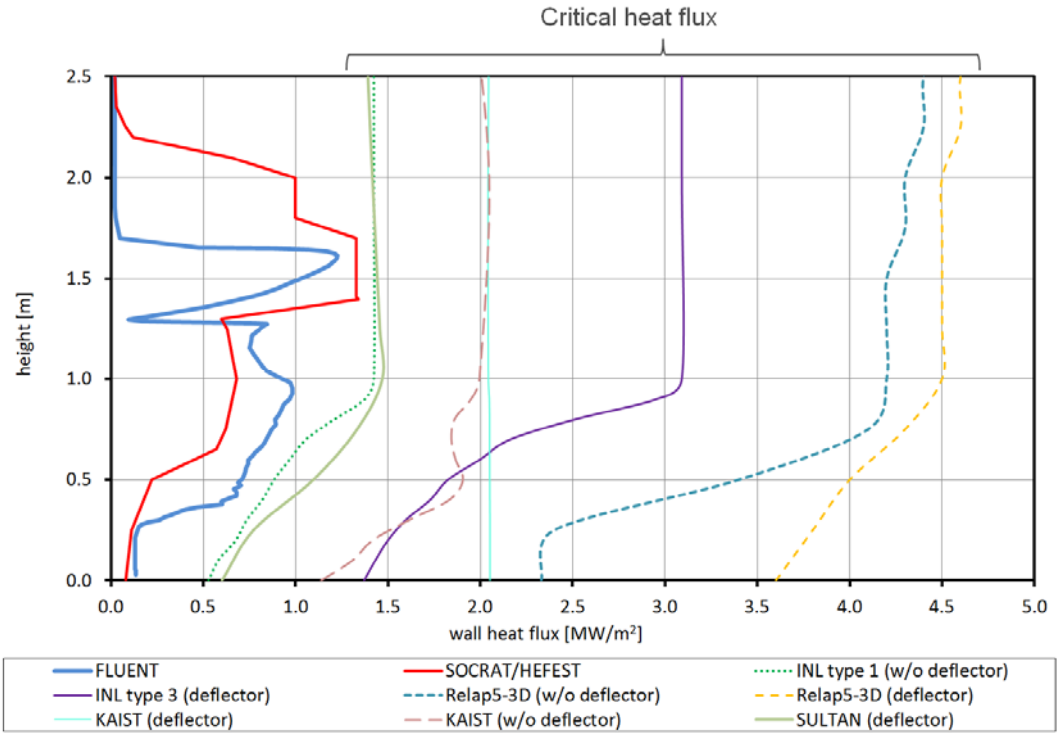

Figure 10 Comparison of calculated RPV wall heat fluxes with various CHF criteria

A.13.4 Feedback from external RPV cooling on heat transfer in melt

In the original FLUENT simulation, it was assumed that inner surface of RPV wall has a constant temperature of 1700 K everywhere (melting point of steel). Wall heat flux calculated by FLUENT at the lowest part of the RPV bottom is not enough for melting of RPV wall, so the constant temperature assumption is not exactly valid (see Figure 11). A new FLUENT simulation was performed with wall temperature boundary condition calculated from RELAP-3D temperature of RPV outer surface (constant) and FLUENT wall heat flux (variable). This was implemented into FLUENT using a user-defined function (UDF). Wall heat fluxes from this simulation are presented in Figure 12.

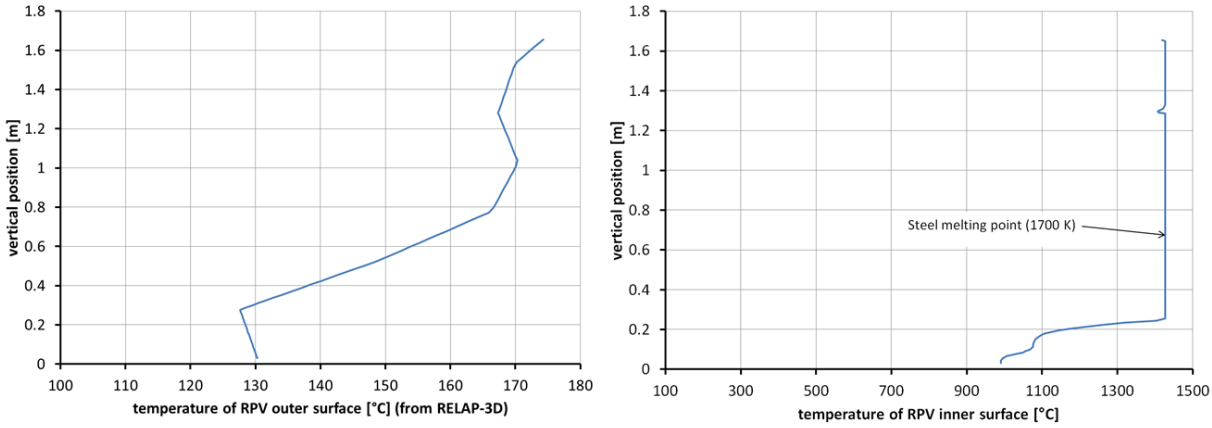

Figure 11 Calculated temperatures at RPV inner and outer surface

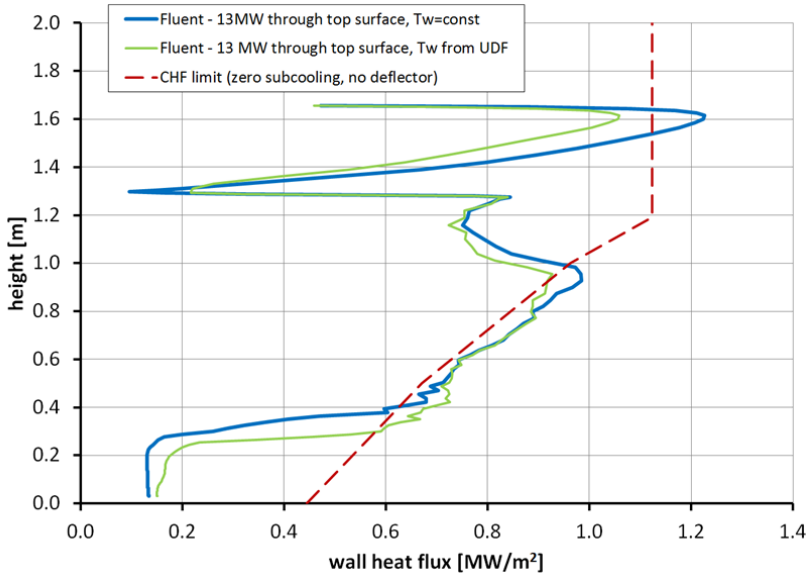

Figure 12 CFD simulation of melt: Calculated RPV wall heat flux, comparison of results from standalone FLUENT simulation (blue line) and from offline-coupling of FLUENT and RELAP-3D (green line).

A.13.5 Concluding remarks

Heat removal from the melt top surface has a significant impact on wall heat flux from the metallic phase. Influence on the on wall heat flux from the oxide phase is not so marked. In our case, if the heat removal from the melt top surface was decreased from 13 MW to 10 MW, the maximum wall heat flux in metallic phase increased from approx. 1.2 MW/m^2 to 1.9 MW/m^2. Wall heat flux in the oxide phase did not change much.

Higher liquid fraction and higher velocities in the metallic phase lead to a better heat transfer in this phase and also to a better wall heat transfer. Maximum of wall heat flux into RPV occurs at the metallic phase. This observation is not valid in the case of very intense cooling of melt top surface.

Deflector has a positive influence on external vessel cooling. Flow around wall surface gets more intense with deflector. The longer the deflector is the better cooling.

There is an influence of external vessel cooling on heat transfer inside the melt. Offline coupling of RELAP-3D and FLUENT was needed to account for this phenomenon.

FLUENT results can be viewed only as qualitative ones. Physical properties of melted phases are only approximate. Complete numerical model was not validated due to the lack of experimental data. Solidification-melting model and k-epsilon turbulence model implemented in FLUENT could be validated or possibly improved in the future using data from COPO II-Lo and BALI experiments.

A.13.6 Some references

Bechta S.V. et al.:	VVER steel corrosion during in-vessel retention of corium melt. The 3rd European Review Meeting on Severe Accident Research (ERMSAR-2008)
Groeneveld D.C., Shan J.Q., Vasic A.Z., Leung L.K.H., Durmayaz A., Yang J., Cheng S.C., Tanase A.:	The 2006 CHF look-up table. Nuclear Engineering and Design 237, 2007, pp. 1909-1922
Groeneveld D.C., Leung L.K.H., Guo Y., Vasic A., Nakla M.El, Peng S. W., Yang J., Cheng S.C.:	Lookup tables for predicting CHF and film-boiling heat transfer: past, present, and future. Nuclear Technology 152, 2005, pp. 87-104
Yang. J., Cheung F.B., Rempe J.L., Suh K.Y., Kim S.B:	Correlations Of Nucleate Boiling Heat Transfer And Critical Heat Flux For External Reactor Vessel Cooling. INEEL/CON-05-02604, 2005 ASME Summer Heat Transfer Conference
Jeong Y.H., Chang S.H., Baek W.-P.:	Critical heat flux experiments on the reactor vessel wall using 2-D slice test section. Nuclear Technology 152, 2005, pp. 162-169.
Jeong Y.H., Baek W.-P., Chang S.H.:	CHF Experiments for IVMR-EVC using 2-D Slice Test Section. Proceedings of the Korean Nuclear Society Spring Meeting, Kwangju, Korea, May 2002.
Rougé S.:	SULTAN test facility for large-scale vessel coolability in natural convection at low pressure. Nuclear Engineering and Design 169, 1997, pp. 185 – 195.

A.14 EDF CFD with ULPU calculations

ULPU-V (Dinh et al., 2003) is a full-height representation of the whole flow path between the reactor vessel and reflecting thermal insulation. The geometry is the one of the Westinghouse AP1000 reactor, with one-slice geometry and a ratio for the periphery equal to 1/84. Embedded cartridges in copper blocks enable to reach CHF since the maximum local heat flux is around 2.4 $MW.m^{-2}$. Two runs of the ULPU-V series have been simulated with NEPTUNE_CFD, a 3D-local CFD code, with a usual set of models for bubbly flows.

Figure 1 shows the void fraction in the loop as computed by NEPTUNE_CFD with maximum heat flux (experimental CHF value). It shows that the natural circulation is correctly established. Subcooled boiling is the dominant regime near the heated wall. Indeed, the increase of saturation temperature induced by significant water-column pressure is not compensated by the power that is provided by the heaters. Beyond the upper boundary of heaters, steam rapidly condenses and coolant flow in the riser becomes essentially single-phase liquid. The coolant boil-off re-emerges at higher elevations, near the nozzle by flashing phenomenon. Because of the nozzle that introduces a singular pressure drop, and the progressive decrease of pressure head, the void fraction increases suddenly in the inclined duct, reaching values very close to one.

Figure 2 shows the comparison between the velocity measured in the downcomer and the one computed by NEPTUNE_CFD with a steady algorithm. The velocity is quite well predicted since the maximum difference between calculated and experimental values is lower than 10%, except for one point in run #4. The heat flux indicated on the x-axis is the maximum heat flux imposed on the wall.

Figure 3 presents the spectrum obtained as a Fast Fourier Transform of the pressure measured at the bottom of the heated block with maximum heat flux. For this calculation, an unsteady algorithm has been used. A few peaks clearly appear between 1 and 4 Hz, as found experimentally.

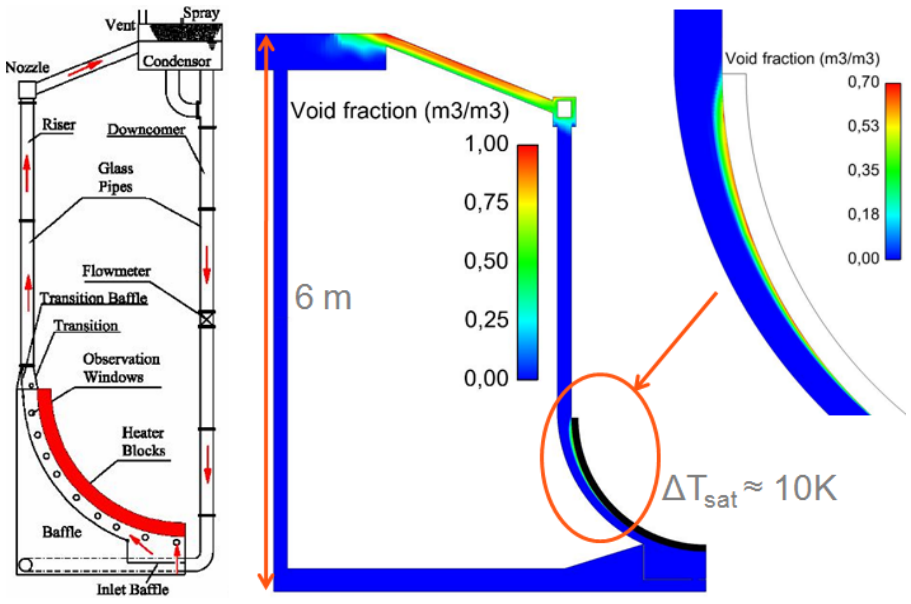

Figure 1: Void fraction profile in the loop

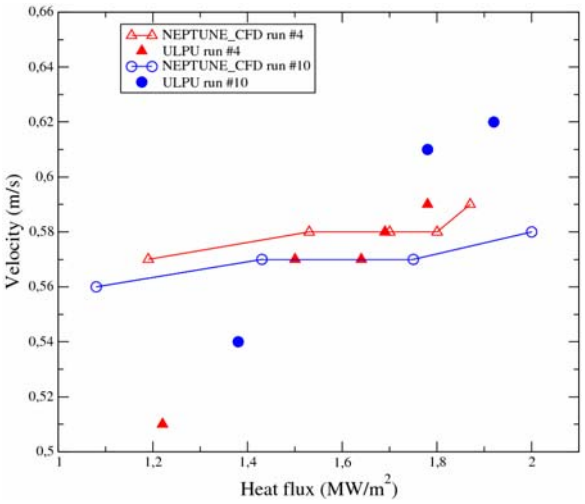

Figure 2: Comparison of measured and computed velocity for runs #4 and #10

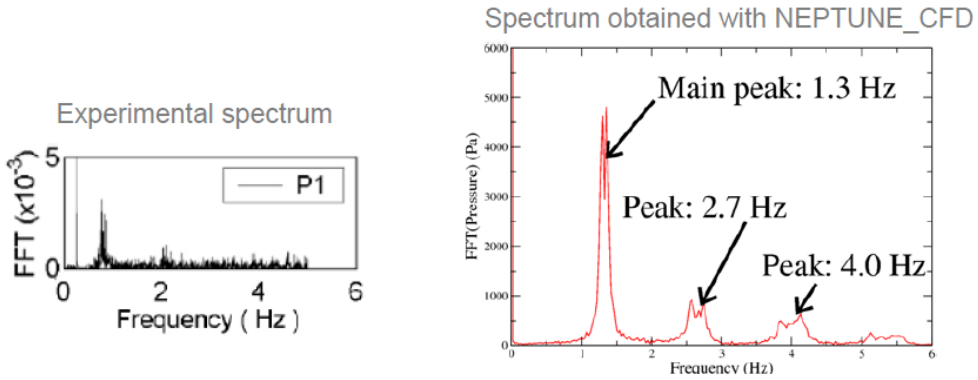

Figure 3: Comparison of pressure spectra for run #10

A.14.1 Some references

Dinh, T-N., Tu, J.P., Salmassi, T., Theofanous, T.G., 2003. Limits of Coolability in the AP1000-Related ULPU-2400 Configuration V Facility, CRSS Technical Report 0306

B First calculations

Based on the existing integral input deck for the LBLOCA calculation with ASTEC provided by KI, IRSN developed a first simplified ASTEC/ICARE stand-alone input deck, focusing mainly on the corium melt modelling.
Nevertheless some participants decided to use their own input decks based on their specific plant knowledge.
The codes used by the participants are specified in Table 10.

Table 10: Participants to the first calculations

	ASTEC integral	ASTEC stand-alone	SOCRAT	MAAP	PROCOR	MELCOR
EDF				x		
CEA					x	
UJV						
KI			x			
INRNE		x				
TUS		x				
JRC		x				
IVS	x	x				

The initial conditions to run ASTEC/ICARE stand-alone calculations were extracted from the SOCRAT integral calculation and distributed to all participants. These initial conditions included:

- Melt history: mass, temperature and composition of corium arriving into elliptical part of the barrel
- Decay heat

Table 11 Corium history provided by KI for the 1st calculations

Time, s	Mass of UO_2, t	Mass of ZrO_2, t	Mass of Zr, t	Mass of SS, t	Total mass, t	Temperature, °K
3251.5	0	0	0	0.1108	0.1108	1851
3280.5	0	0	0	1.0426	1.0426	1874
3509.6	0.7874	0.2769	0.694	1.0527	2.811	2745
3531.5	15.643	6.0004	8.8717	3.0852	33.6003	2787
3540.5	77.5435	12.434	8.9465	9.5945	108.519	2846
3548	81.4016	12.518	8.9469	10.7901	113.657	2853
3954.4	81.6538	13.0472	10.5921	14.6109	119.904	2960
3957.4	81.7304	13.218	11.179	15.9999	122.127	2964
4703.3	81.7304	13.218	11.179	16.1732	122.301	2885
4709	82.7726	13.5081	11.786	20.3003	128.367	2891

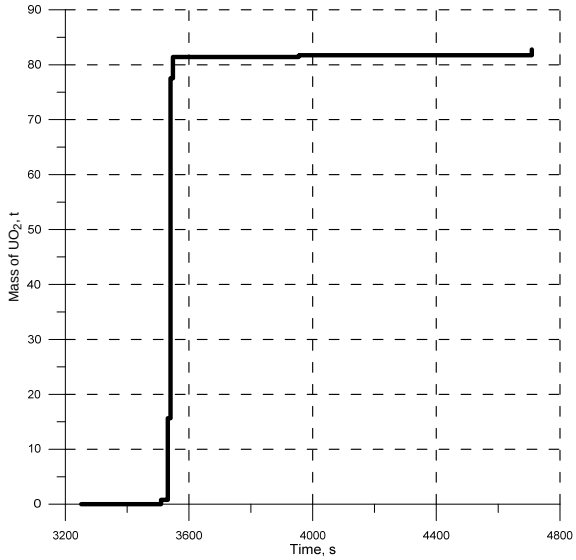

Figure 1-15: UO_2 accumulation in lower plenum

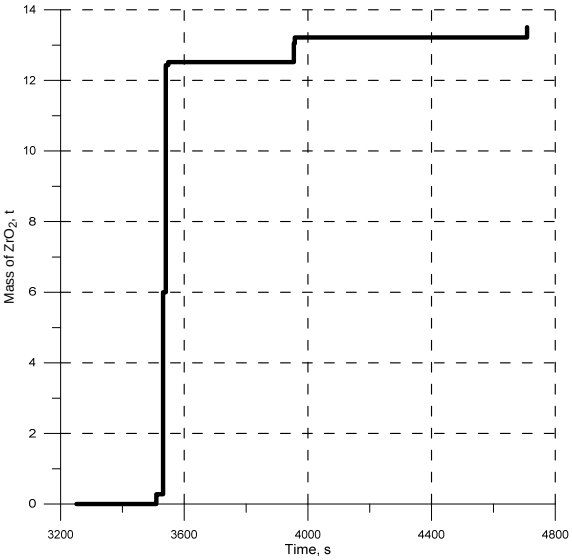

Figure 1-16: ZrO_2 accumulation in lower plenum

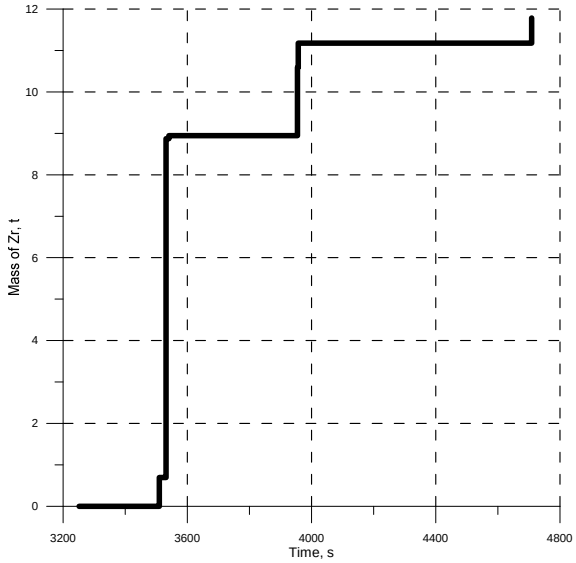

Figure 1-17: Zr accumulation in lower plenum

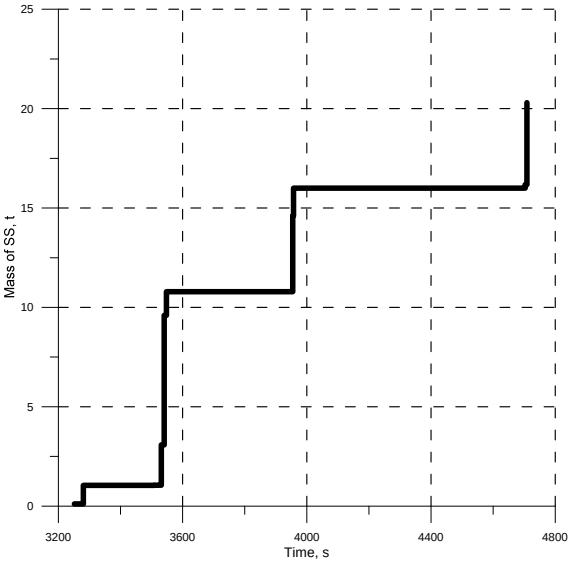

Figure 1-18: SS accumulation in lower plenum

Decay heat time dependence, which was used in calculation

Time, s	Decay heat, Wt (per 1 kg of UO_2)
1000	731.6
2000	609.4
3000	542.4
4000	497.1
5000	463.8
6000	437.5
7000	416.6
8000	398.9
9000	384.4
10000	371.6
20000	300.1
30000	268.9
40000	250.5
50000	237.7
60000	227.8
70000	218.9
80000	211.2
90000	203
100000	194.9
200000	166.5
300000	146.3
400000	128.6

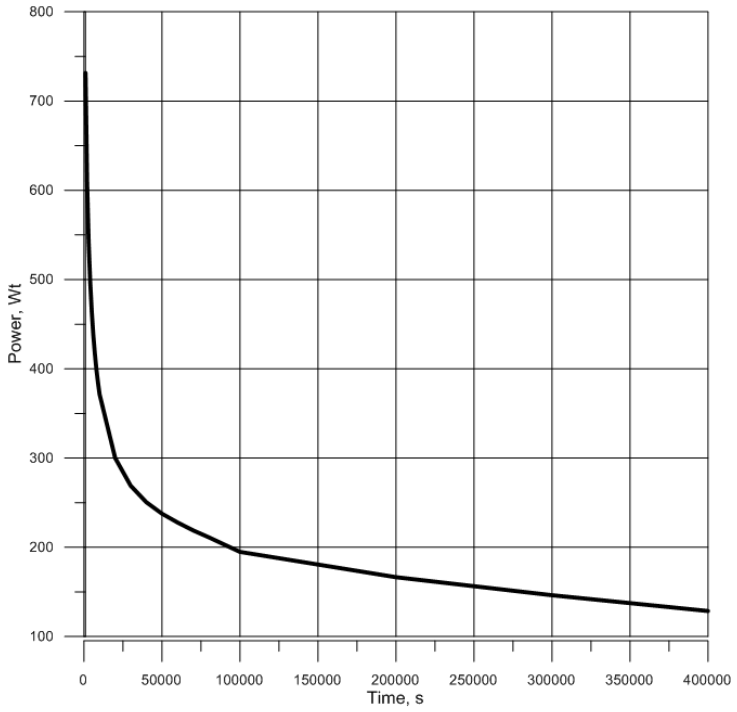

Figure 1-19: Decay heat time dependence

The first results to be provided by participants were:

- *Max of max*: the maximum HF axial profile given looking at each external and internal nodes occurring during the whole calculation. This plot is therefore time independent.
- *Shape at peak one and two*: according to the peaks of «max of max», these plots show the HF profile at the time when the peaks occurred, representing the most critical situations
- *Stabilized profile*: the HF profile at the stabilized state

Max_of_max

This comparison is a bit confusing because the plotted HF on the internal side of the LH is very high even if the duration of the peak is for a very short time, and the energy transferred from the corium to the lower head is not as much as it seems from the plot; in fact only the first nodes of the lower head are melt. The HF plotted on the external side of the lower head is smoother and the results are more comparable to each other's.

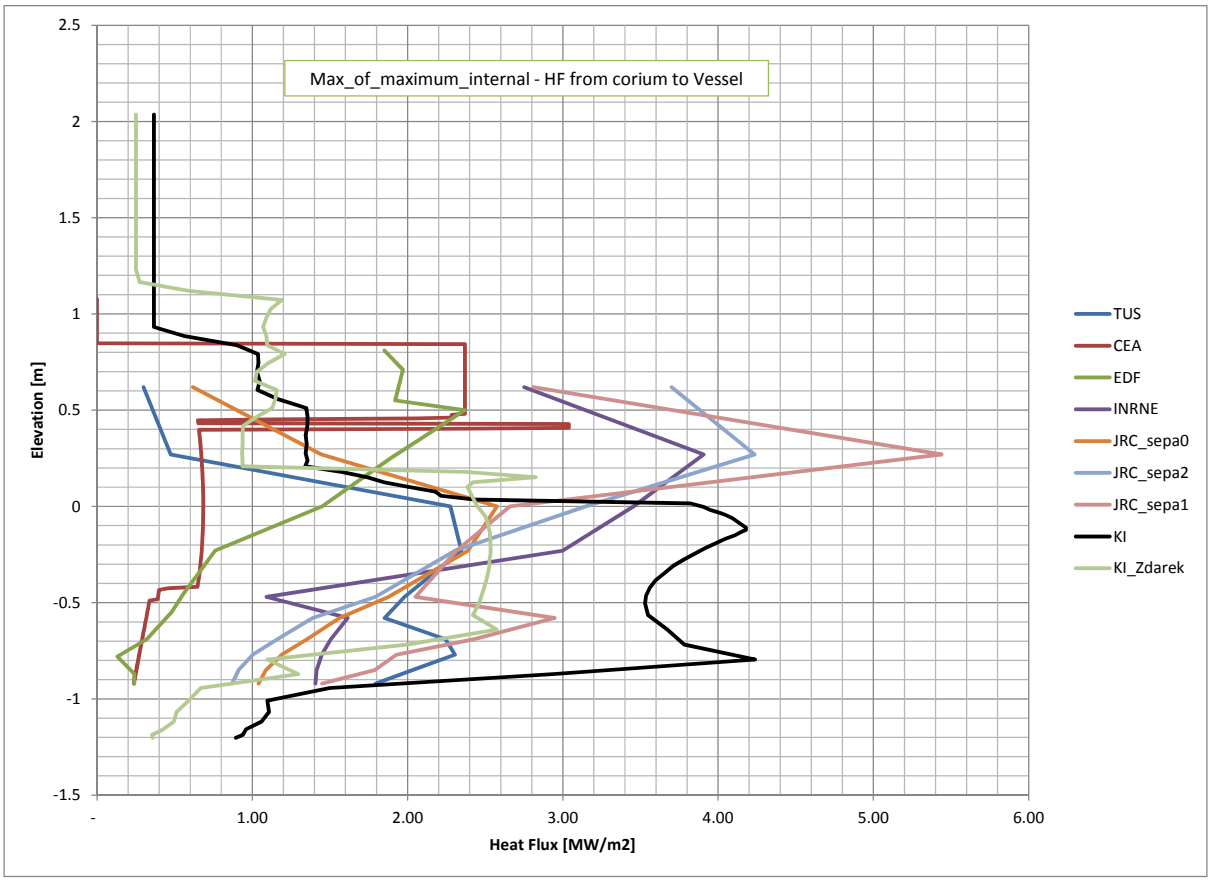

Figure 1-20: Max_of_max internal HF

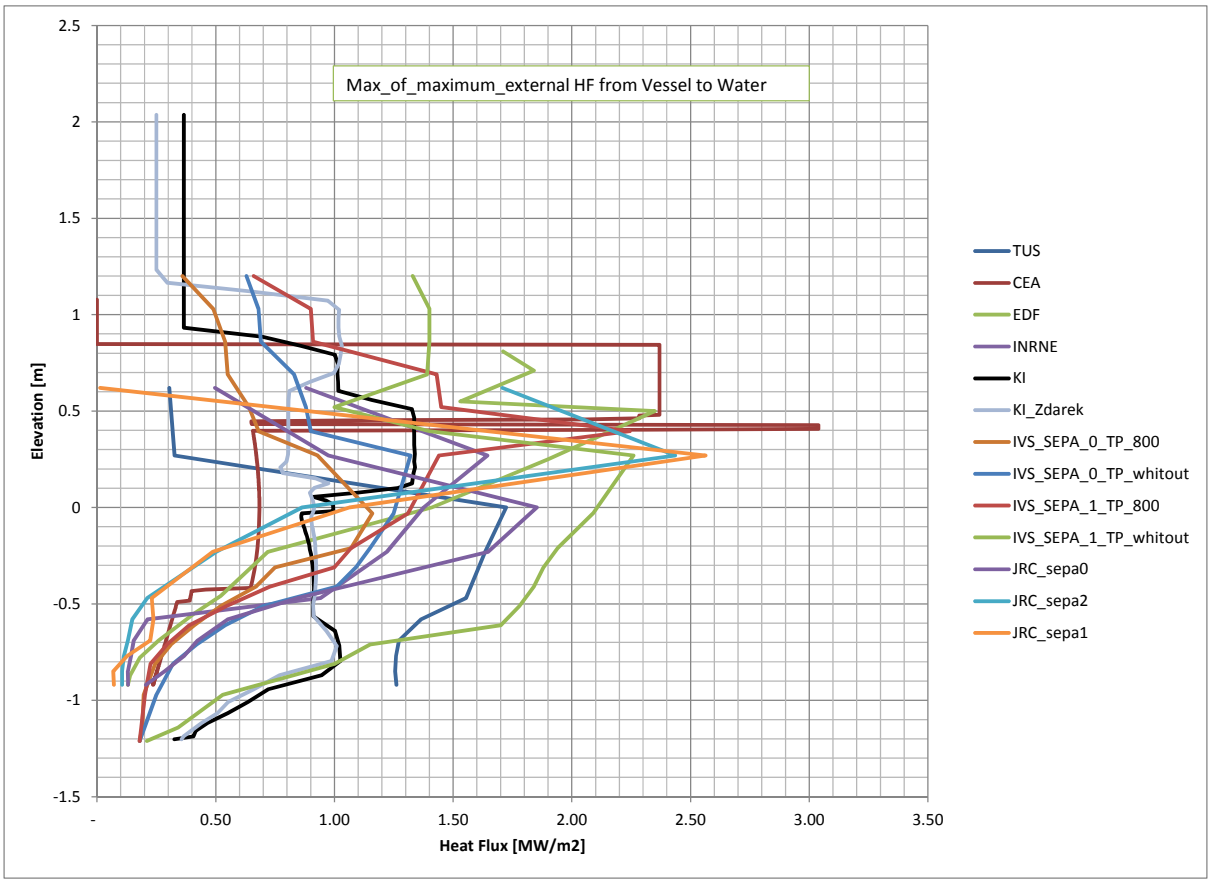

Figure 1-21: Max_of_max external HF

The results were quite spread, and for that reason JRC decided to create an additional plot just with the external HF calculated with ASTEC in stand-alone mode, where the results were a bit more coherent between each other's.

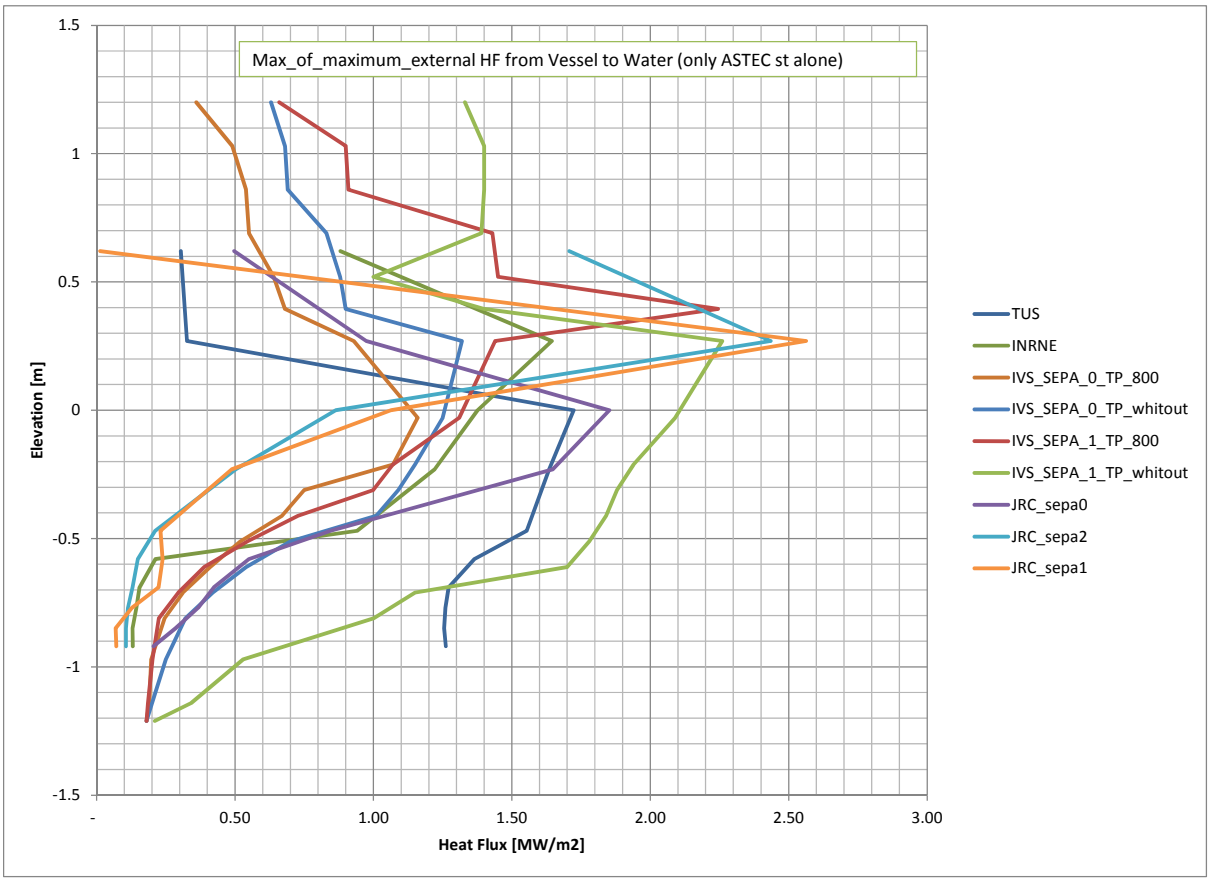

Figure 1-22: Max_of_max external HF, ASTEC stand-alone

JRC also created a histogram for the external HF with some of the calculations in order to obtain the frequency of the HF. The bins of the frequency are 0.5 MW/m^2 each, so the first column of the histogram indicates how many times the HF was [0 ÷ 0.5] MW/m^2, the second column indicates how many times the HF was [0.5 ÷1.0] MW/m^2, and so on…. This is just a proposal for analysing the results; in order to have a proper histogram we need to use the same nodalization. It is possible to create a histogram for every node with HF, residual thickness, temperature, etc…

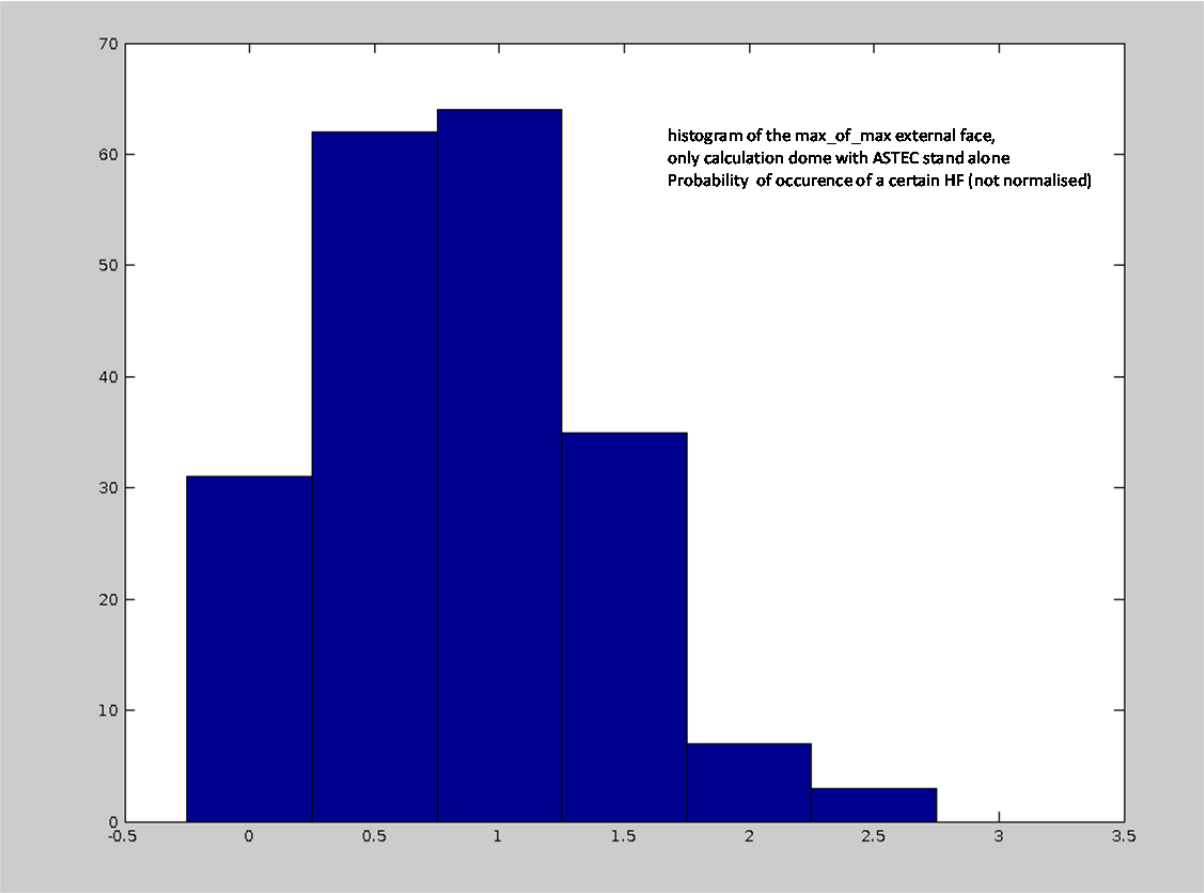

Figure 1-23: Max_of_max external HF histogram based on some calculations

Shape at peak one

The results were a bit misleading: we asked the participants to provide the HF axial profile corresponding to the highest HF and the highest HF is always on the INTERNAL side of the lower head (corium/vessel). IVS didn't provide internal HF, so their results cannot be compared here: we created an additional file in which we compare the axial profile corresponding to the highest HF on the EXTERNAL side of the lower head (vessel/water) for JRC and IVS calculation and this is probably more interesting.

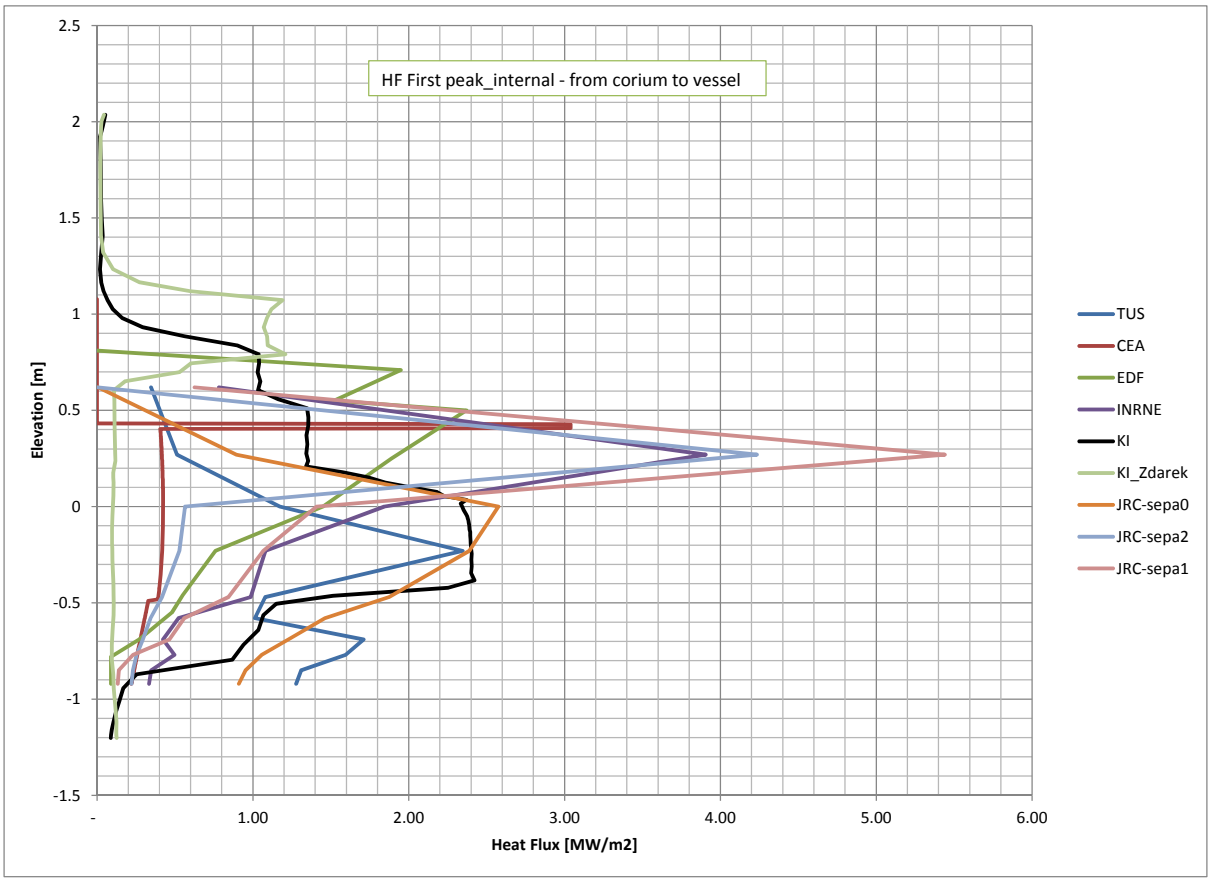

Figure 1-24: shape at internal peak one, internal HF

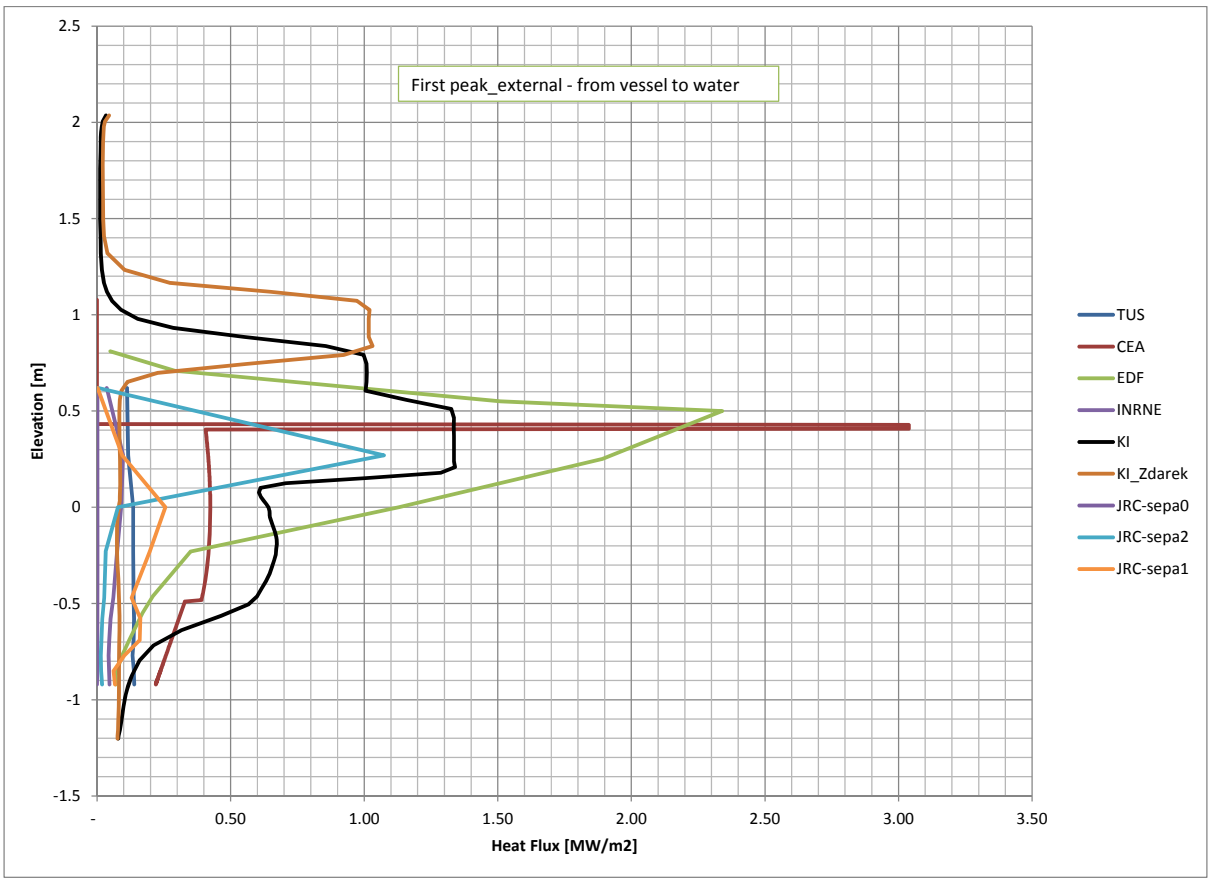

Figure 1-25: shape at internal peak one, external HF

The time when the HF peaked varies between participants, therefore the comparison is a bit confused, but if we focus just on ASTEC stand-alone calculations we can see that the HF is maximum during the

second corium slump (the biggest one) and at that time the heat transfer between the lower head and the external water was still very low excluding any boiling crisis.
According to the data provided the peak calculated by KI occurs very late in time when the corium was almost stabilized (KI could you please confirm that).
MAAP predicted also a peak later in time and the internal and external HF were very similar, indicating a quasi-stabilized configuration.

HF Stabilized

JRC predicted lower head failure in two calculations out of three, therefore only one calculation is plotted.
The results are still spread but not as much as in the max_of_max, and JRC decided anyway to create an additional plot just with ASTEC stand-alone calculations that are a bit more coherent between them.

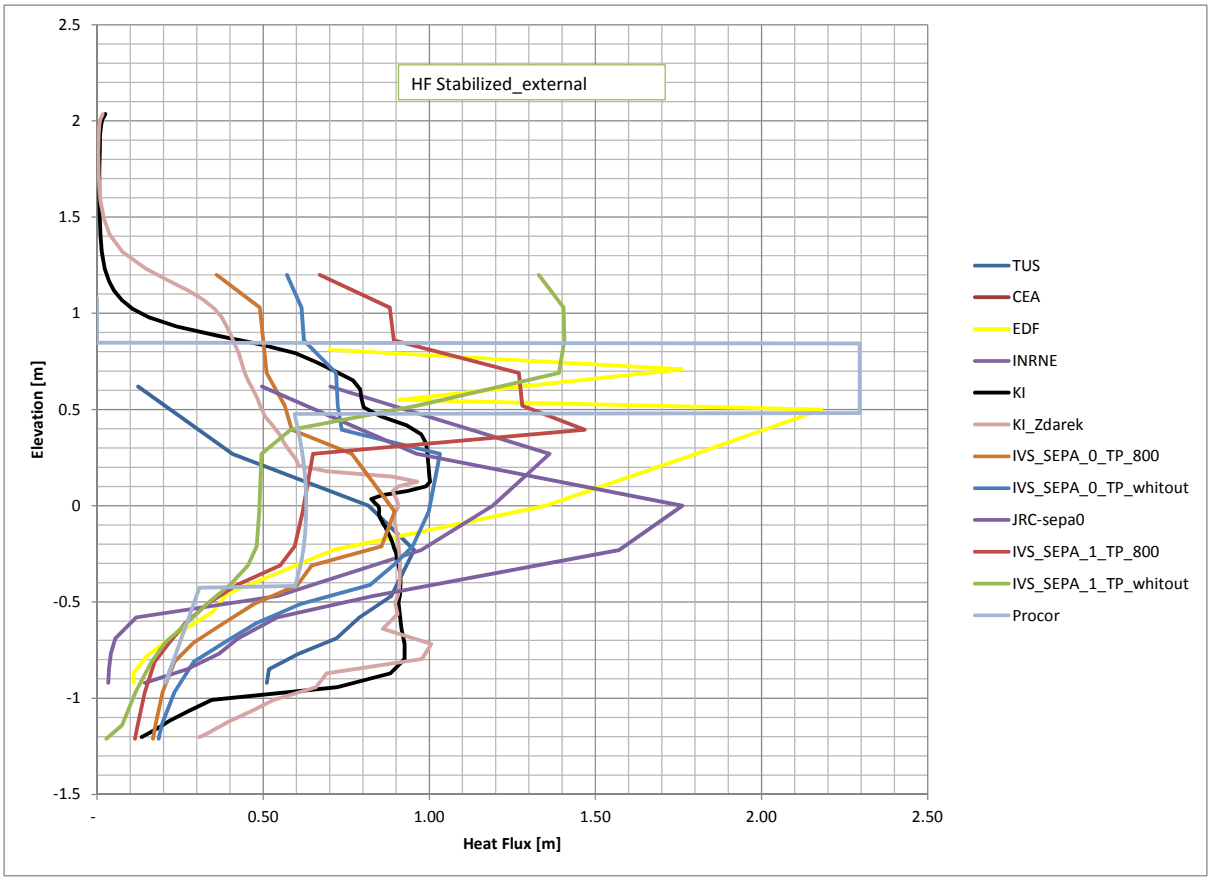

Figure 1-26: stabilized heat flux, external profile

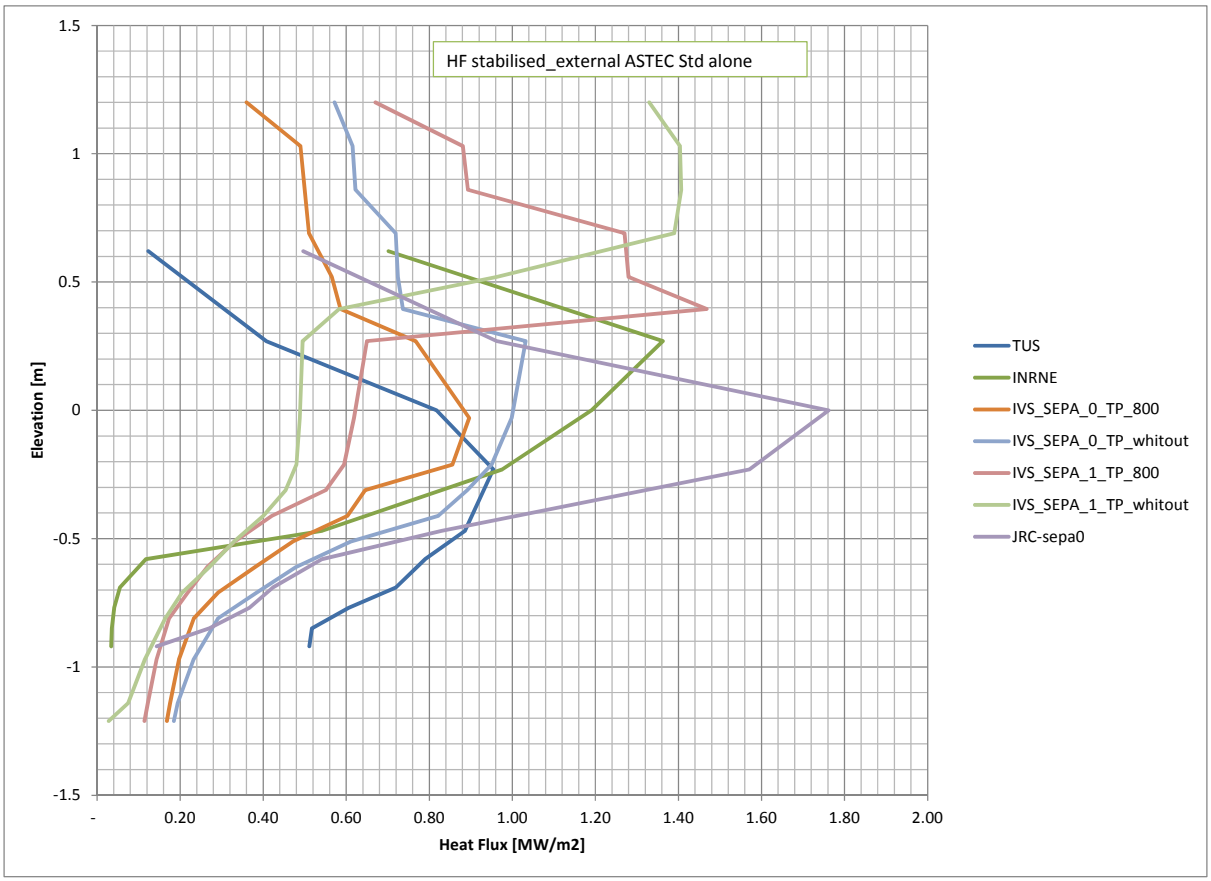

Figure 1-27: stabilized heat flux, external profile, ASTEC stand-alone calculations

IVS predicted layer inversion when simulating the corium with the detailed phase separation model including thermochemical equations (SEPA_1 in the plots), therefore the oxide layer is on the top of the metallic layer and the HF is higher at the top. Please note that the layer inversion is very sensitive to the eutectic temperature and probably also on the melt composition, so a sensitivity study should be performed to address this issue.

JRC also created a histogram for the external HF with just the ASTEC stand-alone calculations in order to obtain the frequency of the HF. The beans of the frequency are 0.5 MW/m^2 each, so the first column of the histogram indicates how many times the HF was [0 ÷ 0.5] MW/m^2, the second column indicates how many times the HF was [0.5 ÷1.0] MW/m^2, and so on….. We can see that the biggest spread in the results is where the oxide and metallic layers separate, the results are very consistent at the bottom of the lower head.

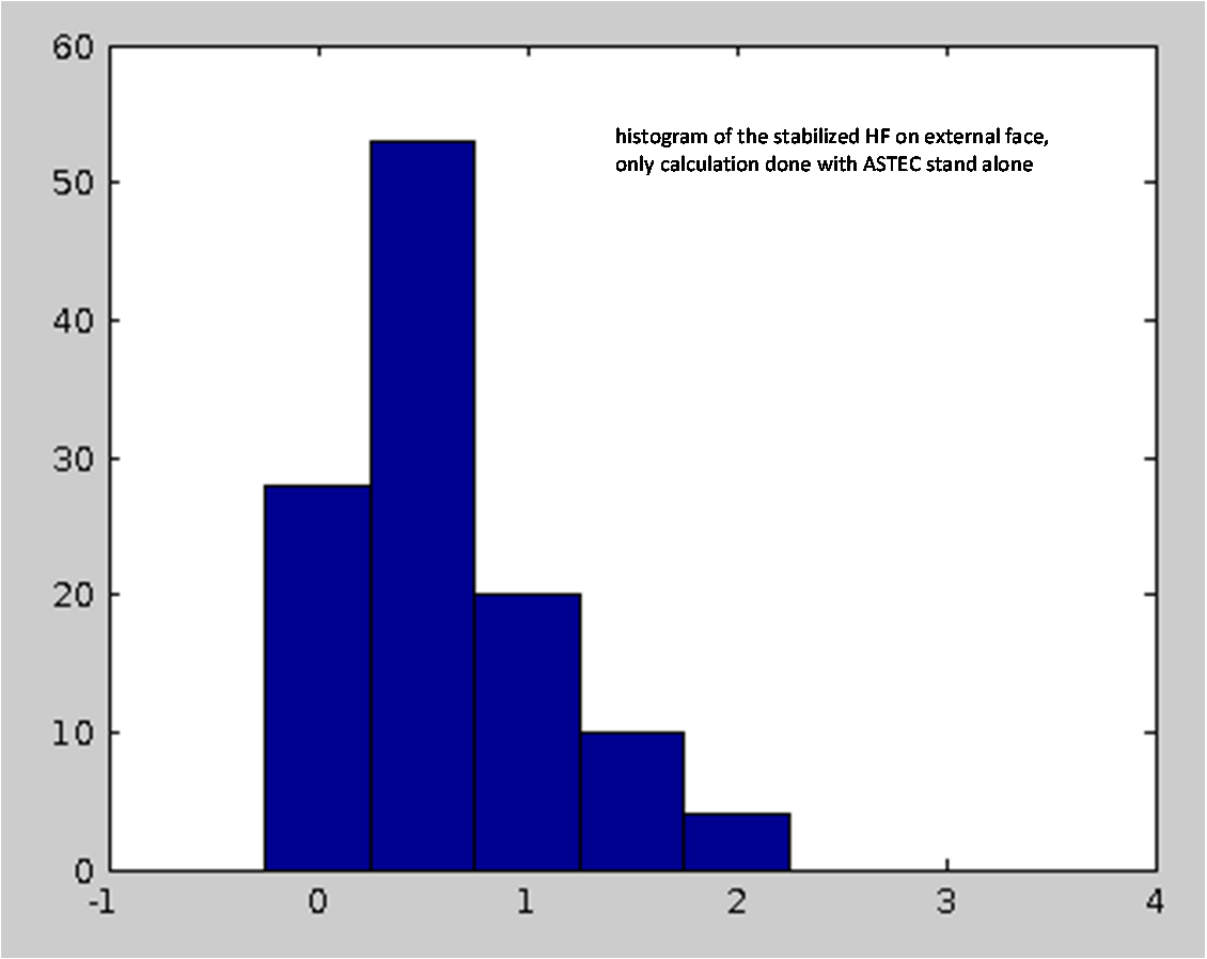

Figure 1-28: histogram of the stabilized HF, external profile, ASTEC stand-alone calculations

Shape at external peak

This is an additional comparison of the axial profile corresponding to the highest HF on the EXTERNAL side of the lower head (vessel/water). We could use only data from IVS and JRC, but the results are interesting. When the external HF peaks the corium is almost stabilized.

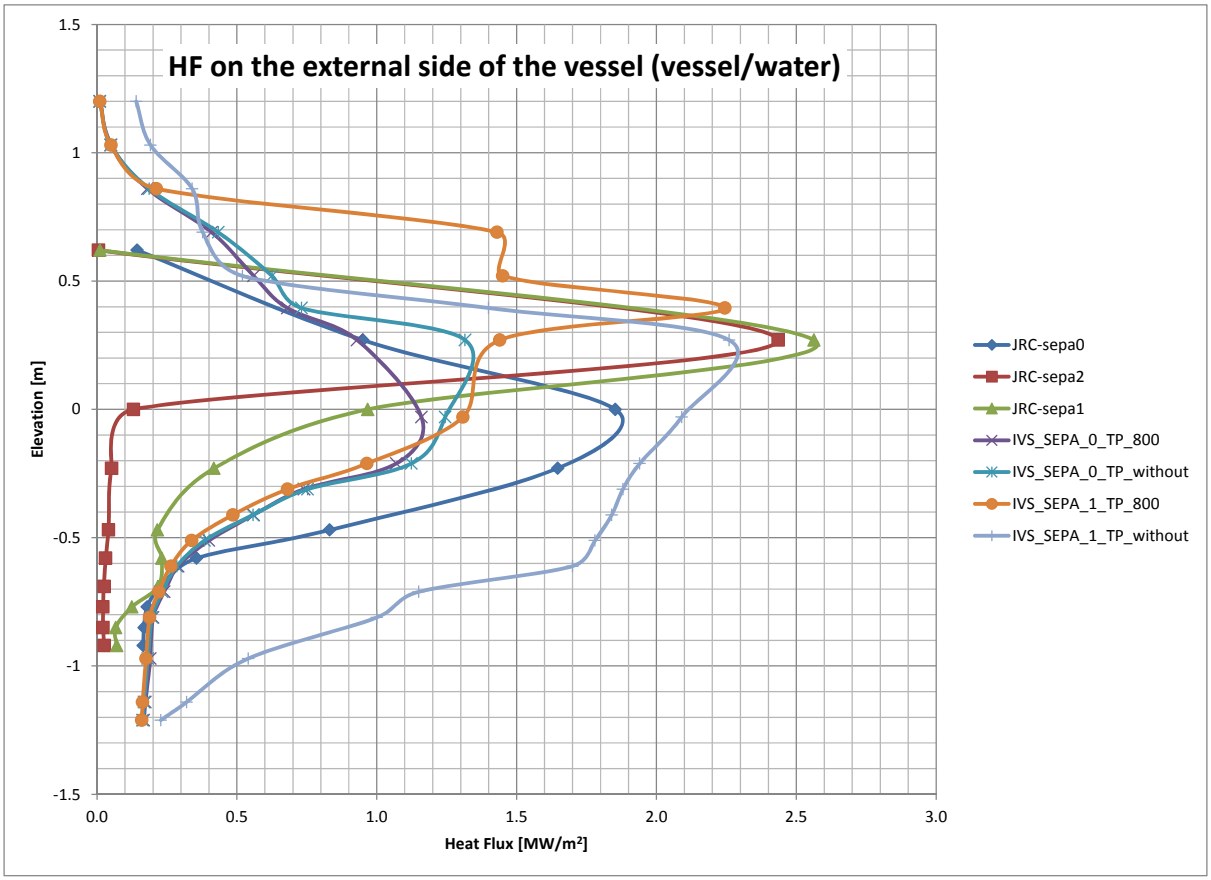

Figure 1-29: HF on the external side of the vessel (IVS and JRC only)

First screening of the uncertainties that most affect the results

During the first round of calculations it was observed that the results could be affected by the uncertainty of some parameters, and some of these parameters were more important than others. It was decided that in the next round of calculations the following uncertainties should be investigated:

- Steel mass (30 t, 80 t)
- Corium (zirconium) oxidation degree (30%, 70%)
- Account of heat yielded by the metallic layer (15%)

Two layers stratification model for corium pool was recommended; composition of metal layer based on MASCA experiments and includes metal Uranium and ZrO_2. The recommended value for the heat transfer coefficient is $H=10^4$ for reactor vessel surface.

C Description of the main models

Based on the existing integral input deck for the LBLOCA calculation with ASTEC provided by KI, IRSN developed a first simplified ASTEC/ICARE stand-alone input deck, focusing mainly on the corium melt modelling.

C.1 SOCRAT description

SOCRAT – best-estimated software (code) – was jointly developed by several Russian organizations. This software package allows realistic analysis of VVER reactor facilities in cases of severe loss-of-coolant accidents (LOCA) by simulating physical processes throughout all the accident development stages, with account of VVER design-specific features. Physical and mathematical models, as well as improved-precision computation modules, allow a coordinated description of a variety of thermohydraulic, physical, chemical and thermomechanical phenomena. SOCRAT verifications performed on the basis of data obtained from Russian and foreign experimental studies of individual phenomena and from integral experiments confirm this code's capability to properly describe the totality of processes and phenomena associated with beyond-design-basis accidents (BDBA) in VVER reactor facilities.

SOCRAT code solves the following basic tasks:

- realistic assessment of steam and hydrogen sources to assure fire and explosion safety of the reactor containment;
- realistic assessment of the reactor status; analysis of reactor response to possible accident-control measures;
- realistic assessment of mass and energy of corium to be released from the RPV in case its floor gets destroyed.

The code enables appropriate mathematical simulation of the following thermophysical, physical and chemical processes, which have the strongest impact on the severe accident course:

- zirconium oxidation, suppression of oxidation reactions in steam-starvation conditions;
- oxidation of steel components of the core and in-vessel devices;
- rupture of fuel cladding, with possible start of cladding oxidation on both sides;
- oxidation of absorber rod material;
- melting of steel structures in the core, protective tubing and baffle; eutectic interactions; melting of fuel cladding metal;
- heat-up of lower areas by downflowing molten core and in-vessel structures to temperatures, at which intensive oxidation starts;
- possible core re-flooding, with hydrogen generation accelerated by corium oxidation and by bare metallic surfaces having no surface oxide layer anymore;
- failure of fuel assembly tail-pieces; corium propagation to fuel assembly supports followed by their collapse; corium penetration into the lower plenum;
- molten material interaction with water; its dispersion and full oxidation; additional steam ingress to the core; intensified oxidation;
- re-heating and re-melting of core and in-vessel structures; heat-up and melting of lower plenum structures; formation of corium pool in the lower plenum;
- disintegration of in-vessel barrel bottom with formation of corium pool on the RPV floor;
- melt stratification including inversion ("MASCA configuration"); convective heat transfer in the melt layers; effect of heat flow "focusing" in the metallic layer;

– melt penetration of the RPV and gradual erosion of the remained bottom wall;

– melt retention in externally cooled RPV.

For numerical simulation of all the above physical phenomena and processes, SOCRAT applies the following software modules, which are its basic components:

- RATEG – full-circuit two-fluid thermohydraulics and heat transfer in solids (developed by VNIIEF);
- SVECHA – in-core physical and chemical processes (up to total core disintegration) taking place in case of severe accident (developed in IBRAE);
- HEFEST – processes in the lower plenum, concrete barrel or core catcher; behaviour of materials in case of core-meltdown accidents; RPV melt-through (developed in IBRAE).

HEFEST also simulates the processes of corium retention and cooldown in the lower regions of the RPV. It may function as as built-in and stand-alone modes.

C.2 HEFEST description

C.2.1 Main assumptions of HEFEST code in the model of stratified melt

HEFEST model of stratified molten pool is based on several assumptions. Most of them are common for evaluation of melt-structure interaction:

– Core melt is stratified on two immiscible phases, metallic and oxide;

– The compositions of the phases is close to thermodynamically equilibrium; they are defined from the results of MASCA experiments;

– Having different densities (difference is larger than some accepted tolerance) the phases are rather quickly separated due to gravity, and form two layers of the melt having the horizontal interlayer boundary;

– Decay heat power is distributed among the layers in accordance with the solute fractions of decay products and their heat generation. It may be estimated in accordance with the model;

– In case of metallic layer lying atop the oxide layer (“normal stratification”) the interlayer boundary is a kind of relatively stable transition zone. Its properties are defined by the difference between the compositions and liquidus temperatures of metal and oxide phases and intensive cooling of upper metal layer caused by heat transfer from its other boundaries; in particular, the interlayer boundary may be the solid crust as it is commonly assumed;

– In case of interlayer crust, it is supposed that its composition and liquidus temperature is close to that of oxide phase with the same liquidus temperature. Then heat transfer between the layers may be treated on the base of existing experimental data of single phase experiments with isothermal boundaries as it is described lower;

– in opposite case of absence the solid crust in interlayer boundary heat transfer between the layers is controlled by additional assumptions through definite coefficient.

In HEFEST, solid crust on interlayer boundary is not modelled as a specific region or structure and is accounted for by only assumptions made about heat transfer. In case of solid crust and congruent melting/solidification of all oxide melt, the oxide and metallic layers may be considered as separated pools coupled by interlayer heat transfer. The overall temperature on a solid boundary of the oxide layer is the same, and for consideration of convective heat transfer it should be set to oxide liquidus temperature. Then, the flow pattern and boundary heat flux for oxide melt may be studied separately in one phase experiments. The same may be referred to the metallic layer.

The full model of heat transfer in a normally stratified melt may be, therefore, split on the models of:

1) Molten pool with internal heat generation having a spherical (PWR) or torispherical (VVER) bottom;
2) Metallic layer uniformly heated on its lower boundary by definite heat flux and internal heat generation;
3) Interlayer heat transfer.

Seemingly, the approach of such kind is adopted in most of codes dealing with stratified oxide-metal molten pool.

The integrated heat transfer in case (1) may be taken from the experimental data (COPO II Lo for torispherical bottom of VVER, BALI – for spherical segments approximately presenting torispherical bottoms of different kinds).

The second item is a matter of consideration in "focusing effect" theory, which actually treats metallic layer as a bulk point. Note that such a treatment allows to sum the existing internal heat generation in the metallic layer and to change the heat flux from oxide layer by an equivalent volumetric heat source.

Third item may be treated as follows. In supposition of solid crust the heat flux from oxide to metallic layer is the same as in heat generating molten pool with the boundary and volumetric heat source corresponding to that in the oxide layer. Hence, the integrated heat flux through the upper horizontal boundary observed in the experiment with heat generating pool having isothermal boundaries (like BALI or COPO) may be taken as the good estimation for interlayer heat transfer in that case.

If the interlayer boundary does not contain solid crust the heat transfer from the oxide to metallic layer may be some more intensive and is undefined additional parameter of the model. This case needs special consideration but now is treated in the considered methodology as an intrinsic uncertainty of the model of stratified molten pool.

C.2.2 Some common uncertainties of the pool physical behaviour affecting its modelling and obtained results

The following really existing uncertainties in phenomenology and numerical characteristics should be resolved in computer code by means of proper assumptions. The ways of solution may be different in different computer codes that would affect the results obtained. The appropriate adjustments may be the subject of a detailed consideration in code comparisons.

- Stratification of the initially uniform melt is a complicated process depending on actual physical state of the melt and requiring a row of additional assumptions (local separation and solidification of phases? physical reason of existence of the uniform initial state in calculations – these reasons define subsequent evolution of the melt; the process of stratification and its characteristic time scales?). Realistic models are impossible now, and parameters of the used phenomenological approaches may differ in different codes. All this may essentially affect a transient behaviour and absolute maximum of HF in calculations;
- Compositions of melt phases, which are not in global thermodynamical equilibrium. Its dependence on temperature: the used MASCA results were obtained in small facilities being in equilibrium. The composition was measured after melt cooling and solidification. This defines the thickness of a metallic layer and focusing effect;
- Densities of melt layers – affect a kind of stratification – normal or inverse (in VVER normal type is most likely but this should be checked in each case). The details of the used procedure of density evaluation may be essential for stratification criteria;
- Actual physical state of interlayer boundary that influence on interlayer heat transfer and sidewall heat flux distribution. (In HEFEST this is controlled by separate parameter ζ);

C.2.3 Some references

Bolshov L., Strizhov V. SOCRAT – The System of Codes for Realistic Analysis of Severe Accidents. Proc. of Int. Congress on Advances in Nuclear Power Plants (ICAPP '06), Reno, NV, USA, June 4-8, 2006, Paper 6439.

N.A. Mosunova, V.F. Strizhov, A.S. Filippov. Corium pool simulation for VVER by SOCRAT/HEFEST. RAS news. Energy, 3, 2010, pp. 43-63

V.D. Ozrin, V.I. Tarasov, V.F. Strizhov, A.S. Filippov. Model for calculation of the corium composition and density during a severe accident on VVER. RAS news. Energy, 3, 2010, pp. 25-42

V.D. Ozrin, V.I. Tarasov, A.S. Filippov, E.V. Moiseenko, O.V. Tarasov. Distribution of fission product residual decay heat in stratified core melt of LWR and its influence on sidewall heat flux. // Nucl. Eng. Des. – 261 (2013) 107-115

Maria Helle, Oui Kymalainen and Harri Tuomisto (1998) Experimental Data on Heat Flux Distribution from a Volumetrically Heated Pool with Frozen Boundaries. *OECD/CSNI Workshop on In-Vessel Core Debris Retention and Coolability*, Garching, Germany, 3–6 March

Bonnet J.M. and Seiler J.M. (1999) Thermal Hydraulic Phenomena in Corium Pools: the BALI Experiment, ICONE–7, Tokyo, Japan, April 19-23, Paper-7057

A.S.Filippov, D.D.Kamenskaya, E.V. Moiseenko. The development of the heat transfer model in a stratified corium pool for simulation of severe accidents at NPP by SOCRAT/HEFEST. // RAS news. Energy, 5, 2013 pp.108–128.

A.S.Filippov, V.I. Tarasov. Simulation of COPO II Lo experiments on natural convection of heat generating liquid at high Rayleigh numbers // Journal of Engineering Thermophysics – 2 (2014)

C.3 PROCOR description

- The corium pool is always considered to be composed of two parts: a **set of layers** that are embedded in a refractory **crust** and a **steel layer** above the crust.

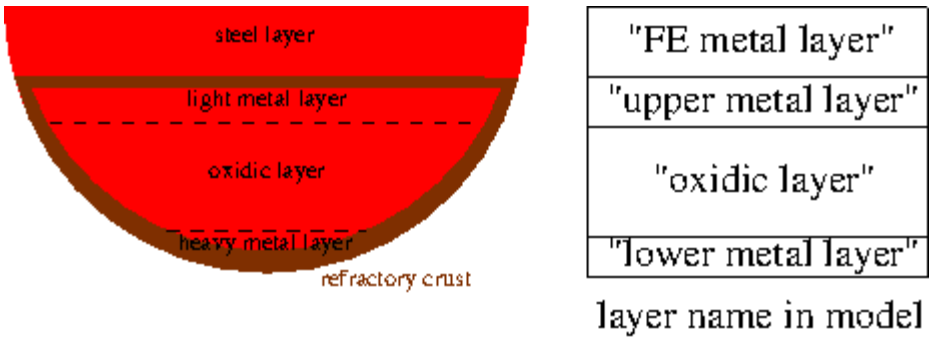

Figure 1: Corium pool stratification

- Note that the crust is not modelled; it only acts as a boundary condition for the layer thermal models and a potential solid barrier in the inter-layer mass transfer calculation. The pool-crust interface temperature is taken equals to $T_{liquidus}$, the liquidus temperature of the system, which is set constant throughout the transient. The thermal balance associated with the corium pool layers **below the crust** is independent of the its surrounding (the crust imposes the boundary condition in terms of temperature).
- Thermal models for light metal **above the crust**: because of the crust, the thermal balance associated to the steel layer can be computed after the calculation of the pool below the crust; it takes the heat flux coming from the pool; the interface temperature with the vessel wall is equal to T_{steel_fusion}. An **upward radiation** is modelled between this steel layer and an upper gray body with a temperature $T^{\infty} = T_{steel\_fusion}$. The Stefan-Boltzmann law for grey bodies is used.

- **OD mass and energy balance** conservation equations are solved for each layer of the corium pool.

- In the case of convection in liquid, the associated heat flux terms are based on a Nusselt number with :
  - Internal Rayleigh correlations used for internally heated fluids (BALI & COPO, ACOPO, Fieg & Werle, etc.),
  - External Rayleigh correlations for a liquid without internal power (Globe & Dropkin, Churchill & Chu, Chawla & Chan, etc.).
- For the corium pool, a **kinetic stratification model** computes the inter-layer mass transfers. Considering a corium pool composed of one oxidic layer and possibly two metallic layers (one heavier, one lighter), this transient stratification model is a generalization of the OD mass transfer model obtained from a phenomenological analysis of the MASCA-RCW experiment and is based on the thermodynamic equilibrium associated to the corium pool inventory that gives the stationary state that the corium pool will eventually reach.

This model makes use of a thermodynamic equilibrium model that uses the pseudo ternary diagrams based on MASCA experiments. The mass transfer coefficient is obtained through a heat-mass transfer analogy that relates the thickness of the mass transfer boundary layer δ_m to the thermal boundary layer δ_t.

- Wall ablation model: the lower head vessel wall is discretized into independent meshes treated as 1D slabs. A heat transfer coefficient (constant in time and all over the wall height) is defined for the external side of the wall. An external temperature (also constant) is defined for the external water.

- **The critical heat flux** correlation used in the vessel ablation model is based on the ULPU profile. In the calculation for the VVER1000 benchmark, the ULPU values are multiplied by a factor large enough for the vessel not to fail. As a matter of fact :
    - The ULPU correlation is valid for spherical lower head and specific conditions. It may not be directly extrapolated to a semi-elliptical lower head.
    - The aim of the "VVER1000 calculation" is to evaluate a "penalizing" heat flux profile on the vessel.

In PROCOR, a critical value ϕ_i^{crit} (based on the experimental program ULPU) is associated to each mesh i of the vessel wall (see Figure 2). The ULPU heat flux profile is multiplied by 1.45, so the maximum value (on the cylindrical part) is equal to 2.175 MW/m^2 instead of 1.5 MW/m^2 (ULPU value).

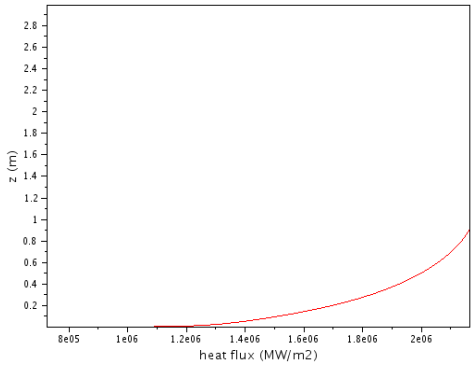

Figure 2: Critical heat flux profile on the vessel wall

At each time step of the PROCOR calculation, the internal heat flux ϕ_i^{in} (transmitted by the internal layers of the corium pool to the vessel wall) is compared to this critical value:

- While $\phi_i^{in} < \phi_i^{crit}$, the plane fusion equation, with an established conduction heat flux in the solid wall, is solved.
- When $\phi_i^{in} \geq \phi_i^{crit}$, the conduction in the wall is supposed to be zero and $\phi_i^{out} = 0$, with ϕ_i^{out} = external heat flux going out from the vessel wall, on the "wet" side. In this case, all the internal heat flux is used for the vessel wall fusion.

- An analytical and normalized **heat flux profile** (which can be constant, linear or based on MAAP4 heat flux profile) is applied to the mean lateral heat flux (calculated with the 0D model of mass and energy conservation) of each corium pool layer.

- The residual power is "attached" to the element U.

Weaknesses of PROCOR:

- There is no axial conduction modelled in the vessel wall.

- There is no limitation on the HF value associated to a very thin layer thickness (lack of knowledge in this field area).

Strong points of PROCOR:

- The code is “bounding”, concerning the “focusing effect”.
- Sensitivity analyses can easily be carried out with the PROCOR platform, using a Monte-Carlo method. To do so, a C++ application constructed with the URANIE library (based on the ROOT framework) has been built. It can be used to drive the PROCOR-based calculations.

Some references

G. Ratel et al., "Considerations on mass transfer kinetics for layer inversion and layer oxidation: from MASCA program to the reactor situation," in Proc. of MASCA-2 seminar. Cadarache, France, 2007

M. Salay and F. Fichot, "Modelling of metal-oxide corium stratification in the lower plenum of a reactor vessel," in Proc. of int. topical meeting on nuclear thermal-hydraulics (nureth-11). Avignon, France, 2005

T.N. Dinh, J.P. Tu, and T.G. Theofanous, “Two-Phase Natural Circulation Flow in AP-1000 In-Vessel Retention-Related ULPU-V Facility Experiments”, in: Proceedings of ICAPP ’04 Pittsburgh, PA USA, June 13-17, 2004 - Paper 4242

F. Gaudier. URANIE: the CEA/DEN uncertainty and sensitivity platform. Procedia – Social and Behavioural Sciences, 2(6):7660–7661, 2010

I. Antcheva, M. Ballintijn, B. Bellenot, M. Biskup, R. Brun, N. Buncic, Ph. Canal, D. Casadei, O. Couet, V. Fine, L. Franco, G. Ganis, A. Gheata, D. Gonzalez Maline, M. Goto, J. Iwaszkiewicz, A. Kreshuk, D. Marcos Segura, R. Maunder, L. Moneta, A. Naumann, E. Offermann, V. Onuchin, S. Panacek, F. Rademakers, P. Russo, and M. Tadel. ROOT - a C++ framework for petabyte data storage, statistical analysis and visualization. Computer Physics Communications, 180(12):2499–2512, 2009

C.4 MELCOR description

Modelling approach related to the application of the IVMR strategy in the MELCOR 1.8.6 code is very complicated as this is the integral code with taking into account all possible phenomena, but at variant level of detail and mechanical vs. parametric modelling. Very detailed description is included in the Reference Manual of the MELCOR code itself (Chapter 1.4 Molten Pool Heat Transfer with 20 pages, 5.1 Lower Head Model – Heat Transfer with additional 10 pages, but with many relations to other parts of Reference Manual), so it is impossible to describe all models and correlations in the simplified manner. So here the only basic information about modelling approach is presented, for details of the correlations used the RM is needed.

The MELCOR code, and its COR package, which solves the core and corium/debris behaviour, distinguish different COR components, concerning degraded core three components are the most important – particulate debris (PD), oxidic molten pool (MP1) and metallic molten pool (MP2) (see figure 1 below). Some other components can play some role during relocation process, mainly supporting structures (SS) which are used for modelling of the internals of the lower plenum of the VVER-1000/320 reactor. Figure 2 shows the nodalization used for the modelling of the lower plenum in the analysis of the LBLOCA with loss of all ECCs and implemented IVMR strategy (reflooding of cavity and application of deflector structure). Figure shows (from bottom) modelling of the lower head wall, lower plenum internals (core barrel lower head and columns – hollow upper part and solid lower part) and core support plate. The boxes with black border line represent intact components – so it is well visible that lower head is axially subdivided into 12 axial levels, the axial level 13 models lower nozzles of fuel assemblies – this is necessary as the level of total amount of corium (level of upper metallic pool) exceeds axially to this axial level no. 13 – so also the RPV lower head wall is modelled to that level within COR package (grey colour of cylindrical par means that that part is modelled as heat structure, which can't be melted). Grey thin line outside of the RPV vessel head represents deflector. Coloured boxes inside of the RPV without black border line represent corium/debris, so figure 2 shows situation with some debris on and inside of the core support plate and also some small amount relocated to the lower plenum.

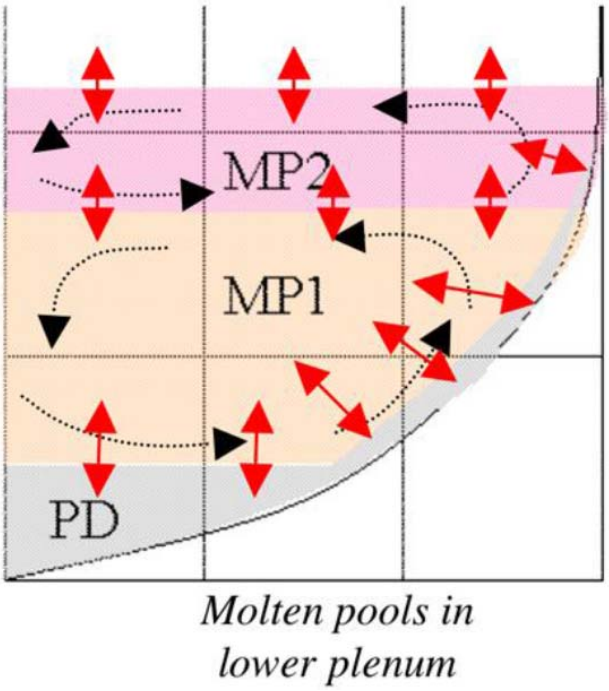

Figure 1 Configuration of corium/debris in lower plenum in MELCOR 1.8.6 (fig. 1.12 of MELCOR manual)

The important issue of the modelling is shown on figure 3 and it represents an overview of the heat transfers taken into account in the energy balance. The situation in the VVER-1000 case is a little simpler as the penetrations are not present for the lower head of this type of reactor. The modelling capability of the MELCOR code of lower head allows to user to select between a hemispherical bottom

head and a truncated hemispherical head, but the real case of the VVER-1000 is the semi-elliptical lower head. In the modelling of this case, the truncated hemisphere option is used with preserving of the internal volume of lower plenum in the input model to be identical as in the real case.

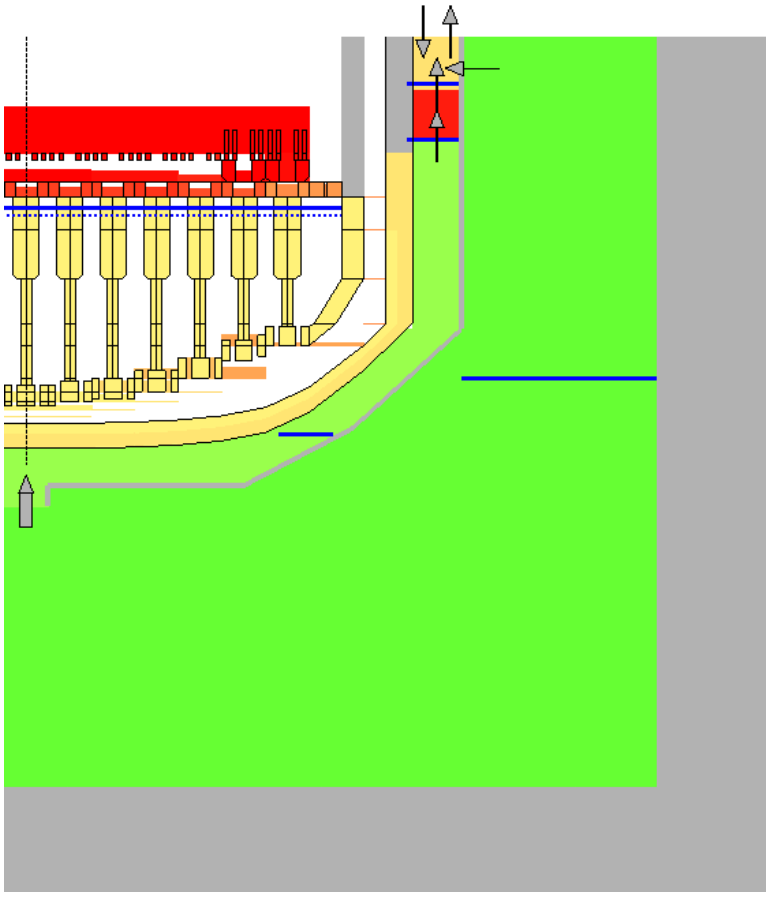

Figure 2 Nodalization of lower plenum in the integral model of VVER-1000/320 in UJV model for the MELCOR 1.8.6

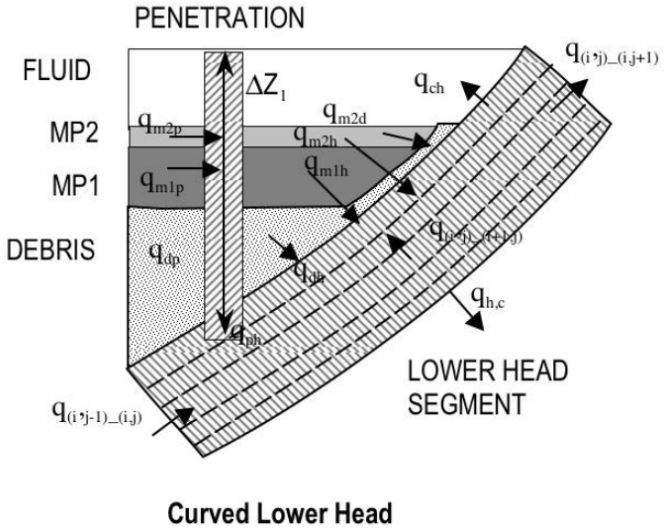

Figure 3 Heat transfers taken into account in the energy balance of the lower plenum solution in MELCOR code (figure 5.28 of MELCOR manual)

Very important and complicated is treatment of particulate debris and molten pools. Contiguous volumes containing molten pool components constitute coherent molten pools that are assumed to be uniformly mixed by convection so as to have uniform material composition, radionuclide composition, and temperature. Two distinct molten pools (oxide and metallic) are allowed in the lower plenum, and

potentially four molten pools can be modelled in the upper core (oxide and metallic in the channel and oxide and metallic in the bypass volume). A search is made in the core and the lower plenum to find the largest contiguous molten pools (by volume), which are then modelled as convecting molten pools. This requirement for contiguity ensures that isolated cells containing molten materials are not mixed with the convecting pools. These convecting molten pools will transfer heat to the lower head (or the lower plenum pools); the fluids (water or steam); the substrate material; and the structural components, such as the shroud (PWR). In addition, the transfer of heat and radionuclides will occur between stratified molten pools. New models in the version MELCOR 1.8.6 have been added to predict the heat transfer coefficients to the substrate supporting the molten pool, the heat transfer between pools, and the heat transfer to surroundings. Note that isolated volumes of molten pool material are not part of these contiguous molten pools and are not included in the convective mix.

The estimation of the heat transfer coefficients is done either by internal model for molten pool, or the user can calculate it via control functions, or the constant value can be used, depends on user definition in the input data. Heat transfer for solid debris is defined in the input as constant value with default value of 1000 W/m^2K, which is for the VVER-1000 modified to 100 W/m^2K.

Concerning the cooling of the lower head, the heat transfer coefficient (HTC) to the atmosphere is constant value (default is 10 $W/m^2/K$) in the MELCOR code, but the HTC to water is calculated using correlations depending on flow conditions outside of the lower head. The downward-facing saturated pool boiling model treats three heat transfer regimes:

1. fully-developed nucleate boiling with no dependence on the orientation of the boiling surface;
2. transition boiling between the fully developed and film boiling regimes, in which the heat flux is obtained by logarithmic interpolation between the critical heat flux and the minimum heat flux, based upon the temperature difference between the surface and saturation; and
3. stable film boiling, which depends upon the orientation of the boiling surface.

The boundaries between the heat transfer regimes are determined by a correlation for the critical heat flux, which separates fully developed and transition boiling, and a correlation for the minimum-stable-film-boiling heat flux, which separates transition and stable film boiling.

Some references

R.O. Gaunt et al., MELCOR Computer Code Manuals, Vol.2 Reference Manuals, Version 1.8.6 September 2005, NUREG/CR6119, SAND 2005-5713, September 2005

Kyle Ross, Jesse Phillips, Randall O. Gauntt, Kenneth C. Wagner: MELCOR Best Practices as Applied in the State-of-the-Art Reactor Consequence Analyses (SOARCA) Project, NUREG-7008, August 2014

C.5 ASTEC description

ASTEC is an integral code jointly developed by IRSN (France) and GRS (Germany) to simulate the whole sequence of a severe accident in nuclear power plants, from the initiating event up to the fission products releases and their behaviour in the containment, and finally to estimate radioactive releases out of the containment. The “lower plenum” models implemented in ASTEC deal with the corium behaviour in the reactor vessel after its collapse from the core, its possible fragmentation and solidification in water present in the lower plenum, up to the possible failure of the vessel lower head, taking into account the corium stratification (separation of non-miscible phases) and heat transfers with the vessel lower head wall. If there is no external cooling of the vessel (or if this cooling is insufficient) ASTEC predicts the time of vessel rupture and the characteristics (temperature, composition…) of corium which would flow subsequently in the reactor pit, leading to direct containment heating (DCH) or interaction with water (with possible steam explosion) and molten-core-concrete-interaction (MCCI).

If there is external cooling, ASTEC predicts the distribution of heat flux along the vessel wall, in order to compare with estimated critical heat flux (CHF) values on the external side of the vessel. It has to be noted that ASTEC is not able to predict the CHF profile outside the vessel. It has to be estimated from correlations or experimental results and provided to ASTEC as boundary conditions applied to the external vessel wall.

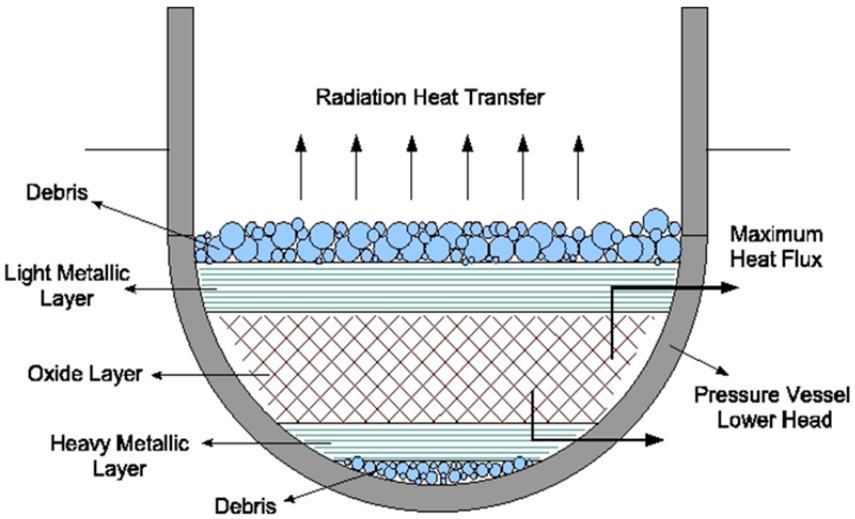

Fig.1: Schematic representation of the corium in the vessel lower plenum, as implemented in the ASTEC code

When the molten corium relocates from the core down to the lower plenum, the melt jets interact with water and may be totally or partially fragmented depending on the level of water inside the vessel. The code evaluates the jet break-up length and deduces the fragmentation rate and the associated water vaporization. Accurate evaluation of this steam production is important in order to be able to predict the associated pressurisation. If the melt jet is totally fragmented, a debris bed is created at the bottom of the lower plenum, but if it is only partially fragmented, a corium layer is formed at the bottom, covered by the debris bed (Fig. 1). Models are implemented to take into account the possible melting of the debris layers, which then feed the corium layers, and the sinking of debris into corium layers or conversely, depending on their relative densities.

ASTEC evaluates the separation of non-miscible liquid oxide and metal phases and the stratification of those phases up to 3 corium layers. The phase separation model was developed for situations involving

a U-Zr-O-Fe molten pool in agreement with MASCA results. This model is the same as in the earlier ICARE/CATHARE code.

Heat transfers are evaluated between all the layers in the lower plenum as well as between corium and the vessel wall and the internal structures. A specific model is also available to take into account the focusing effect related to the formation of a thin metallic layer (in case the layer thickness is small compared to the vessel mesh size in contact). The boundary condition for the oxide layer corresponds to the liquidus temperature of the oxide mixture. The boundary conditions for the metal layers correspond to the melting temperature of the vessel wall. Radiative heat transfer from the top of the pool may be taken into account.

The vessel wall is represented by a 2D meshing and 2D heat conduction is calculated. The melting of the vessel wall is computed and molten steel is added to the material layers (oxide or metal depending on the position of the melting wall).

When the vessel wall heats up, its mechanical deformation and progressive melting are calculated until its possible failure. A specific model for mechanical deformation of semi-elliptical vessels is also available.

Most of the models used in ASTEC were validated against experimental results. The tests chosen for validation described in the table below. More details about the validation may be found in (Carenini et al., 2013).

Table 12: Validation matrix for lower plenum models of ASTEC

Experiment		Main phenomena
FARO	L14	Corium fragmentation
	L28	
LIVE	L1	Thermal exchanges between the corium molten pool and the vessel
	L6	
MASCA (STFM/MA series)		Oxide/metal layers stratification
OLHF-1		Vessel lower head failure

Some references

M. Salay and F. Fichot, "Modelling of metal-oxide corium stratification in the lower plenum of a reactor vessel," in Proc. of int. topical meeting on nuclear thermal-hydraulics (NURETH-11). Avignon, France, 2005

Fichot F., Marchand O., Drai P., Chatelard P., Zabiégo M. and Fleurot J. : "Multi-dimensional approaches in severe accident modelling and analyses", Nuclear Engineering and Technology, Vol. 38, 8, pp. 733-752, 2006.

Koundy V., Fichot F., Willshuetz H.G., Altstadt E., Nicolas L., Lamy J.S. and Flandi L. : "Progress on PWR lower head failure predictive models", Nuclear Engineering and Design, Vol. 238, pp. 2420-2429, 2008

L. Carénini, F. Fichot, J. Fleurot : Validation of ASTEC V2 models for the behaviour of corium in the vessel lower head, Nuclear Engineering and Design, Vol. 272, pp. 152-162, 2013.

C.6 MAAP description

The EDF proprietary corium-in-vessel model has been developed in collaboration with CEA. As a consequence, the key features are similar to those of the PROCOR code. They encompass:

- chemically reacting metal and oxide layers;
- a kinetic inter-layer mass transfer model based on a simplified representation of the miscibility gap in oxide-metal corium systems and controlled by the Uranium diffusion in the oxide phase;
- 0D mass and energy conservation equations of the immiscible layers.

The heavy metal, oxide and light metal layers are enclosed by the oxide crust and supposed to be close to the equilibrium state. The boundary condition for these layers is the $T_{liquidus}$ of the mix. Under certain conditions, the current in-equilibrium position of the layers can change, producing an inversion of stratification (so called MASCA effect). This phenomenon is linked to the current chemical composition of the pool.

The out-of-equilibrium metal layer is located above the crust in direct contact to the vessel. This layer is supposed to be the cause of the focusing effect.

The external vessel-water heat flux is computed using the Rohsenow correlation for the heat transfer coefficient h_{nuc} 0, which is based on experiments of flat plate pool boiling:

$$h_{nuc} = \left[\frac{\mu_l \, h_{fg}}{\Delta T \left(\frac{g_c \, \sigma}{g(\rho_f - \rho_g)} \right)^{1/2}} \right] \left[\frac{c_{pl} \, \Delta T}{0.013 \, h_{fg} \, Pr^{1.7}} \right]^3$$

where ΔT = $T_{wall} - T_{sat}$,

μ_R = viscosity of water,

h_{fg} = latent heat,

g_c = gravity constant,

g = gravitational acceleration,

ρ_f = density of water,

ρ_g = density of steam,

c_{pR} = specific heat of water, and

Pr = Prandtl number.

The 2D temperature field in the vessel wall is used to compute the ablated steel mass. Typical meshes for vessel modelling are illustrated in Figure 1 0.

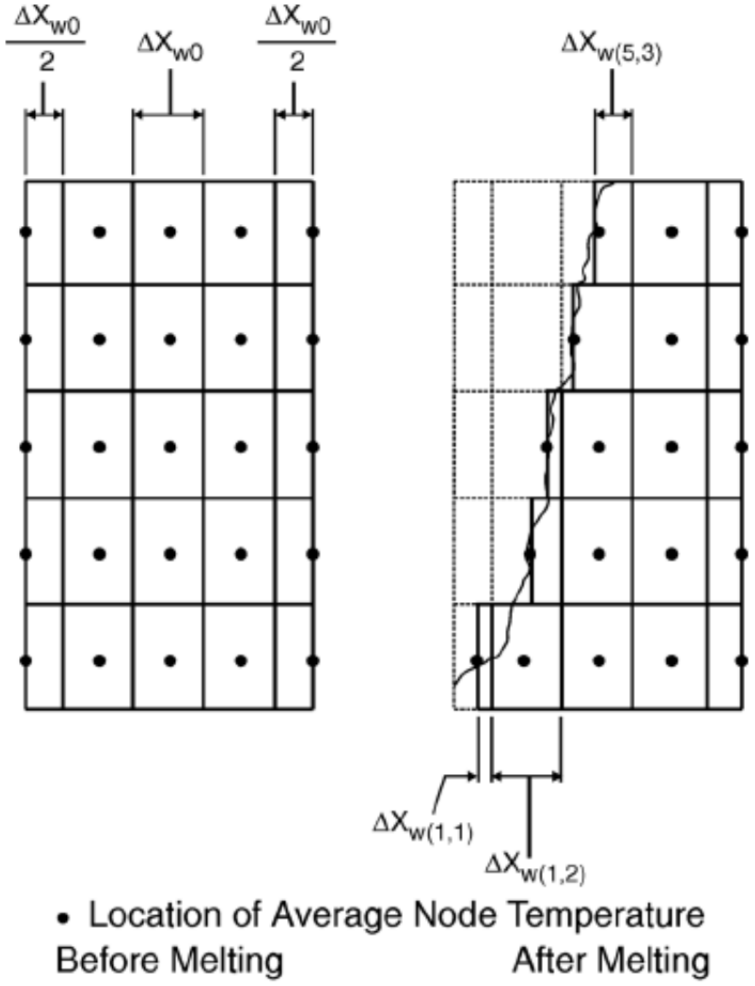

Figure 1 Nodalization Scheme Accounting for Melting of Vessel 0

In case of melting, the radial sizes of the nodes in which the melting front is located are proportional to the current mass in the node:

$$\Delta X_{ji} = \Delta X^{0}_{ji} \frac{M_{ji}}{M^{0}_{ji}}, j = 1 \div 5$$

Where: ΔX_{ji}, M_{ji} and ΔX^{0}_{ji}, M^{0}_{ji} are respectively the current and the initial size and mass in node (j,i). The current mass M_{ji} is computed taking into account the molten mass Ml_{ji} which in turn depends from the node current internal energy U_{ji}:

$$Ml_{ji} = M_{ji} \frac{U_{ji} - U_s}{U_l - U_s}, j = 1 \div 5$$

Where: U_s and U_l are the internal energies of solid and liquid steel respectively.

U_{ji} can be obtained by resolving an energy balance on each mesh.

The subsequent treatment of the ablated steel is one of the model's major causes of uncertainty. The current MAAP model considers that the ablated vessel steel relocates on top of the pool (above the crust). This is caused by the weight of the pool, which weighs down on the crust and pushes the steel upward (this mechanism is illustrated in Figure 2).

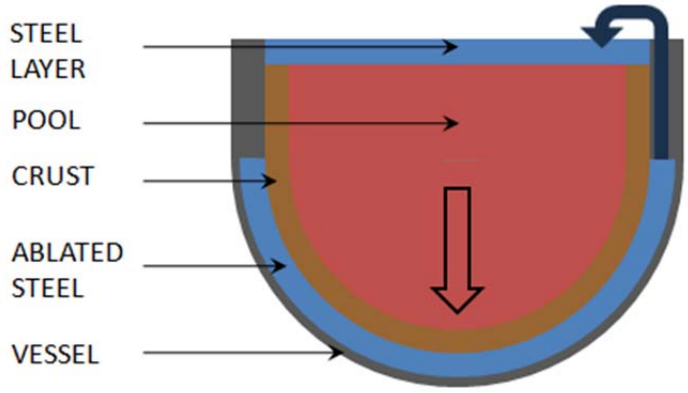

Figure 2 Default assumption: steel relocation

However, the METCOR experiments tend to suggest that chemical interaction could take place between the steel and the oxidic crust. This would lead to the formation of heavier, uranium-enriched steel that would move downward and ultimately percolate through the crust to be added to the pool. This mechanism is depicted in Figure 3.

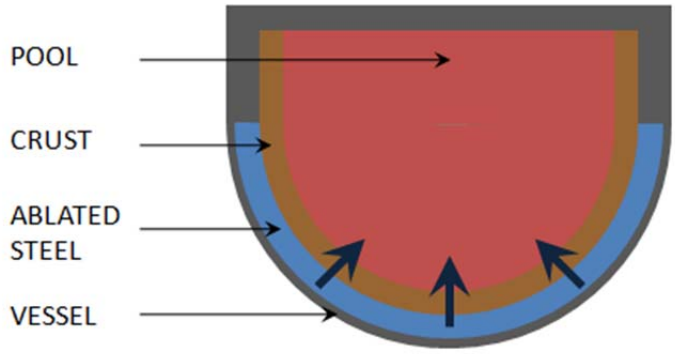

Figure 3 Alternate model: steel percolation

Since the behaviour of the ablated steel has a direct influence on the formation of a thin, out-of-equilibrium metallic layer on top of the pool, and on the occurrence of the focusing effect, we decided to add this case to our sensitivity analysis.

Results

To showcase the impact of this model, we choose to simultaneously present the results of two calculations:

- the best estimate calculation, with steel relocation;
- the calculation with our alternative model, with uranium enrichment in the ablated steel.

Best-estimate calculation: all ablated steel is pushed-up by the pool in the gap between crust and vessel.

<table>
<tr>
<td> 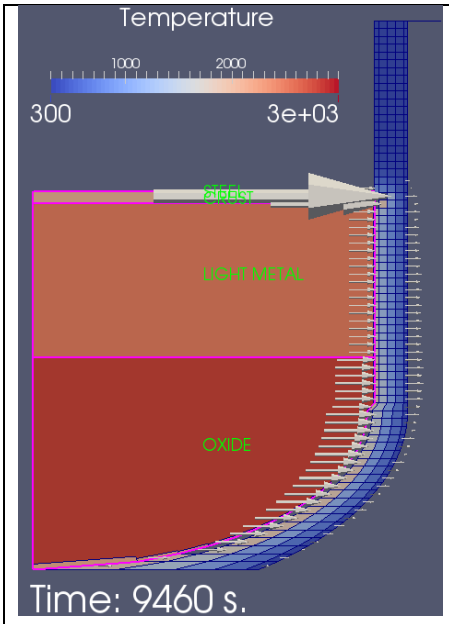

The ablation starts at 8760 s. The ablated steel relocates above the axial crust and forms a top layer. The max. corium-to-vessel flux value 2.88 MW/m^2 is reached at 9460 s.</td>
<td> 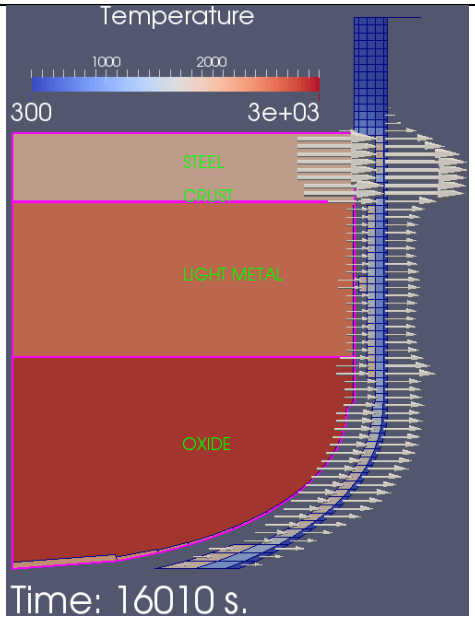

The quasi-steady state is reached at 16000 s with both fluxes maximum about 1 MW/m^2.</td>
</tr>
<tr>
<td colspan="2">Ablated steel weight is increased due to U. Steel goes to the lowest layer.</td>
</tr>
<tr>
<td> 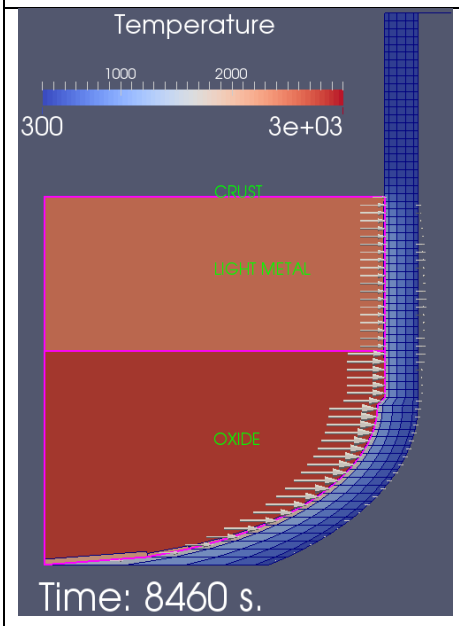

The ablation starts at 8460 s. The ablated steel relocates to the oxide layer. The max. corium-to-vessel flux value 0.62 MW/m^2 is reached at 8460 s.</td>
<td> 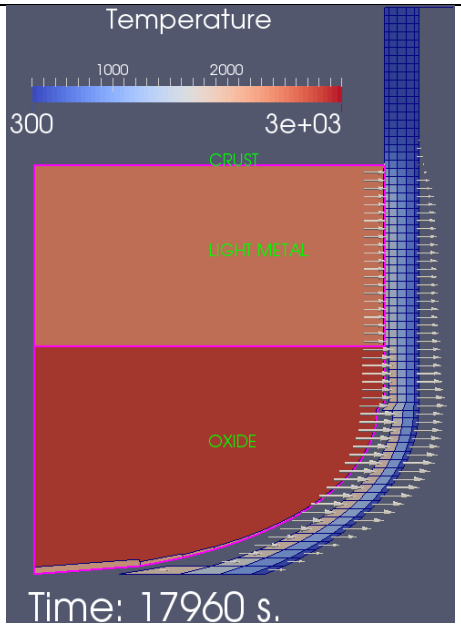

The quasi-steady state is reached at 18000 s with both fluxes maximum about 0.4 MW/m^2.</td>
</tr>
</table>

The stabilized state parameters are the following:

- fluxes about 0.4 MW/m^2;
- the ablated steel mass is 18.1 t;
- the minimum residual thickness is 11 cm (the initial wall thickness was 20 cm);
- the maximum vessel-to-water heat exchange coefficient is H = 4.2 kW/m^2/K.

While this configuration leads to much lower heat flux, it is important to note that we are not certain that the METCOR results can be considered as representative enough of the reactor case to be directly

used. As a result, **we choose to keep MAAP's current, more conservative modelling** until we obtain sufficient experimental evidence.

Some references

Rohsenow, W. M., and Choi, H., 1961, Heat, Mass, and Momentum Transfer, Prentice-Hall.

Fauske & Associates Inc., MAAP – modular accident analysis program for LWR power plants, in: User's Manual, PSHS subroutine, Electric Power Research Institute, 2008.

Europe Direct is a service to help you find answers to your questions about the European Union
Free phone number (*): 00 800 6 7 8 9 10 11
(*) Certain mobile telephone operators do not allow access to 00 800 numbers or these calls may be billed.

A great deal of additional information on the European Union is available on the Internet.
It can be accessed through the Europa server http://europa.eu

How to obtain EU publications

Our publications are available from EU Bookshop (http://bookshop.europa.eu),
where you can place an order with the sales agent of your choice.

The Publications Office has a worldwide network of sales agents.
You can obtain their contact details by sending a fax to (352) 29 29-42758.

LD-NA-27951-EN-N

JRC Mission

As the Commission's in-house science service, the Joint Research Centre's mission is to provide EU policies with independent, evidence-based scientific and technical support throughout the whole policy cycle.

Working in close cooperation with policy Directorates-General, the JRC addresses key societal challenges while stimulating innovation through developing new methods, tools and standards, and sharing its know-how with the Member States, the scientific community and international partners.

Serving society
Stimulating innovation
Supporting legislation

Publications Office

doi:10.2790/62596
ISBN 978-92-79-58899-0